UC Santa Barbara

UC Santa Barbara Electronic Theses and Dissertations

Title

Unraveling Quantum Gravity through the Gravitational Path Integral: Geometries, Entropies, and Algebras

Permalink

https://escholarship.org/uc/item/2c4651jd

Author

Wang, Zhencheng

Publication Date

2023

Peer reviewed|Thesis/dissertation

eScholarship.org Powered by the California Digital Library
University of California

University of California
Santa Barbara

Unraveling Quantum Gravity through the Gravitational Path Integral: Geometries, Entropies, and Algebras

A dissertation submitted in partial satisfaction
of the requirements for the degree

Doctor of Philosophy
in
Physics

by

Zhencheng Wang

Committee in charge:

Professor Donald Marolf, Chair
Professor Xi Dong
Professor David Stuart

September 2023

The Dissertation of Zhencheng Wang is approved.

Professor Xi Dong

Professor David Stuart

Professor Donald Marolf, Committee Chair

July 2023

Unraveling Quantum Gravity through the Gravitational Path Integral: Geometries, Entropies, and Algebras

Copyright © 2023

by

Zhencheng Wang

Acknowledgements

First of all, I would like to thank my advisor, Don Marolf, for his guidance over the years, and his deep physical insights that constantly inspire me. Every research meeting with Don is like a small lecture, as I can always learn a lot about physics and how to think about it. I really appreciate Don being very patient and very clear in explaining physics to me every time, and you know he's again ready to talk about physics when you hear his signature laughter on the 6th floor of Broida.

I would also like to thank Xi Dong, Mukund Rangamani, and Henry Maxfield, who I learned a lot from as a young graduate student through collaborating with them. How they think about physics problems and handling technicalities have really influenced me. I would like to also thank all my other collaborators (including upcoming work), my research work couldn't be pushed forward so well without you: Abdulrahim Al Balushi, Eugenia Colafransceschi, Sean Colin-Ellerin, Jesse Held, Maciej Kolanowski, Xiaoyi Liu, Pratik Rath, Amir Tajdini, Aron Wall, Shannon Wang.

I would like to thank all my other physics friends whether on or not on the 6th floor of Broida who I have spent wonderful times discussing physics with: Zicao Fu, Brianna Grado-White, David Grabovsky, Sergio Hernandez Cuenca, Adolfo Holguin, Jesse Held, Molly Kaplan, Sean McBride, Robinson Macilla, Alexey Milekhin, Gabriel Trevino, Ziyue Wang, Xuyang Yu, Jiuci Xu, Chih-Hung Wu, Jie-qiang Wu, Misha Usatyuk, Wayne Weng, Zixia Wei.

I would also like to thank Diandian Wang and Yiting Li for the fun times we had during my first and second years. However, there are also bad times in life. During the past five years, the Covid-19 pandemic was the biggest event that everyone suffered from. I would like to thank my therapist Yu-shan Huang, for talking with me, and curing my depression condition that I developed during that time. I would like to thank my friends

outside physics, Lingxiao Chen, Zijian Song, Alexa (Qingyi) Wang, and Luqi Wang, for constantly talking to me and supporting me. I would also like to pay my condolences to people who lost their lives either directly due to the virus, or because of authoritarian policies.

Finally, I would like to especially thank my family for their belief in me, and Xiaoyi Liu for her constant care and support.

Curriculum Vitæ

Zhencheng Wang

Education

2023	Ph.D. in Physics (Expected), University of California, Santa Barbara.
2021	M.A. in Physics, University of California, Santa Barbara.
2018	B.Sc in Physics, Nankai University

Publications

1. X. Dong, D. Marolf, P. Rath, A. Tajdini, and Z. Wang,
   "The Spacetime Geometry of Fixed-Area States in Gravitational Systems",
   Journal of High Energy Physics 08 (2022) 158 [arXiv: 2203.04973] [1]
2. H. Maxfield and Z. Wang,
   "Gravitating spinning strings in AdS_3",
   Journal of High Energy Physics 07 (2022) 075 [arXiv: 2203.02492] [2]
3. D. Marolf and Z. Wang,
   "Time-independence of gravitational Rényi entropies and unitarity in quantum gravity",
   Journal of High Energy Physics 10 (2021) 196 [arXiv: 2106.07835] [3]
4. S. Colin-Ellerin, X. Dong, D. Marolf, M. Rangamani, and Z. Wang,
   "Real-time gravitational replicas: Low dimensional examples",
   Journal of High Energy Physics 08 (2021) 171 [arXiv: 2105.07002] [4]
5. A. Al Balushi, Z. Wang, and D. Marolf,
   "Traversability of Multi- Boundary Wormholes",
   Journal of High Energy Physics 04 (2021) 083 [arXiv: 2012.04635][5]
6. S. Colin-Ellerin, X. Dong, D. Marolf, M. Rangamani, and Z. Wang,
   "Real-time gravitational replicas: Formalism and a variational principle",
   Journal of High Energy Physics 05 (2021) 117 [arXiv: 2012.00828][6]
7. D. Marolf, S. Wang, and Z. Wang,
   "Probing phase transitions of holographic entanglement entropy with fixed area states",
   Journal of High Energy Physics 12 (2020) 084 [arXiv: 2006.10089][7]
8. D. Marolf, A. Wall, and Z. Wang,
   "Restricted Maximin surfaces and HRT in generic black hole spacetimes",
   Journal of High Energy Physics 1805 (2019) 127 [arXiv: 1901.03879][8]
9. Z. Fu, A. Maloney, D. Marolf, H. Maxfield, and Z. Wang,
   "Holographic complexity is nonlocal",
   Journal of High Energy Physics 1802 (2018) 072 [arXiv: 1801.01137][9]

Abstract

Unraveling Quantum Gravity through the Gravitational Path Integral: Geometries, Entropies, and Algebras

by

Zhencheng Wang

The gravitational path integral has long served as a crucial tool in deciphering mysteries within quantum gravity. In recent years, studies of the Anti-de Sitter/Conformal Field Theory (AdS/CFT) correspondence have offered many valuable insights into comprehending those mysteries, and many fruitful results have been yielded from utilizing the gravitational path integral within the framework of AdS/CFT.

This dissertation is devoted to studying certain aspects of the gravitational path integral, discussing its relation with gravitational entropies, spacetime geometries, and its algebraic aspects. We explore contexts from Euclidean to Lorentz signature, from holographic theories to general theories, with a goal of understanding quantum gravity in the real world.

In Part I, we discuss the fixed-(HRT)-area states in the gravitational path integral. The fixed-area states are holographic states where the area of the Hubeny-Rangamani-Takayanagi (HRT) surface, the holographic dual of entanglement entropy for a region in the boundary CFT, is constrained to a small window when prepared by the gravitational path integral. The study of those fixed-area states helps understand quantum gravity beyond the leading semiclassical order. We first show that by decomposing a general holographic state into fixed-area states, an important subleading correction appears to the entanglement entropy near phase transitions. Then we explore the intrinsic spacetime geometries of fixed-area states under Lorentz-signature time evolution.

In Part II, we study saddle-point geometries of the real-time gravitational path integral, in the context of computing holographic Rényi entropies. Unlike their Euclidean counterparts, these real-time saddles necessarily have complex metrics, giving an example where the saddle point is off the original contour of integration. We first present the formalism of this setup, illustrating the relevant variational problem, and features of the complex saddles. Then we demonstrate explicitly the structure of those saddles by showing examples in low dimensions by direct calculation. We also find that it is possible to deform the original integration contour to pass through saddles of this kind constructed in two-dimensional Jackiw-Teitelboim gravity. Finally, we show that the existence of these saddles results in a consequence which is necessary for unitarity to hold in quantum gravity.

In Part III, we take a step towards explaining the origin of gravitational entropies, by utilizing the mathematical tool of von Neumann algebras. In particular, we give an explanation of the HRT formula purely from the bulk perspective, without making any reference to holography. This is done by constructing Hilbert spaces and von Neumann algebras from boundary conditions of the gravitational path integral with several natural axioms. The von Neumann algebras we find from this construction allows us to define a notion of entropy, which matches the HRT formula in the semiclassical limit. One of the axioms we assume which is crucial for the construction of von Neumann algebras – the trace inequality, is proven in the semiclassical limit, and it leads to novel positivity conjectures for the gravitational action.

Contents

Chapter 1

Introduction

The pursuit of quantum gravity represents a profound endeavor to unify two pillars of modern physics: quantum mechanics and general relativity. Despite the remarkably deep understanding of each theory, combining them into a consistent framework remains a significant challenge. In deciphering mysteries of quantum gravity, the gravitational path integral has played a crucial role. In modern studies, the gravitational path integral is often utilized as a tool in the context of holographic duality and has brought us many insightful results.

In this Introduction, we first briefly review the holographic duality and its concrete realization, known as the AdS/CFT correspondence. We then discuss the gravitational path integral from various perspectives, each providing a unique insight into quantum gravity. These perspectives are closely related to the notion of entropy in quantum gravity, in particular within the context of holography. Finally, we give a brief introduction to the von Neumann algebra, explaining the importance of this mathematical tool in the study of quantum gravity, and this sets the stage for constructing von Neumann algebras from the gravitational path integral.

1.1 Quantum gravity through holography

Gravity is holographic in nature. The first hint of this can be traced back to Arnowitt, Deser, and Misner that conserved charges (for example, mass) in general relativity can only be defined at the boundary [10]. The Bekenstein-Hawking entropy of black holes provides further evidence: the entropy of a black hole is proportional to its horizon area, not volume [11, 12],

$$S_{BH} = \frac{A_{hor}}{4G}, \tag{1.1}$$

where G is Newton's constant. However, it was not until 't Hooft and Susskind [13, 14] that the holographic principle has been started to be taken seriously.

The first concrete realization of the holographic principle is Maldacena's Anti-de Sitter/Conformal Field Theory (AdS/CFT) correspondence [15], where a Type IIB string theory in $\mathrm{AdS}_5 \times S^5$ (the bulk theory) is dual to the $\mathcal{N} = 4$ $SU(N)$ super Yang-Mills theory living on the conformal boundary in 4 dimensions (the boundary theory) [15, 16, 17, 18]. Later, people found more concrete constructions for dualities of this kind in various contexts, and now it is widely believed that the $\mathrm{AdS}_{d+1}/\mathrm{CFT}_d$ duality should hold for general dimension d (or at least for $d \leq 9$). This correspondence gives a non-perturbative formulation of quantum gravity.

Importantly, parameters on both sides are related: the 't Hooft coupling of the gauge theory $\lambda \equiv g_{YM}^2 N$ is related to the string length ℓ_s by $\lambda \sim \left(\frac{\ell_{Ads}}{\ell_s}\right)^4$, where ℓ_{AdS} is the AdS length scale; N can be related to the Planck scale ℓ_P in the bulk by $N^2 \sim \left(\frac{\ell_{AdS}}{\ell_P}\right)^{d-1} \sim \frac{\ell_{AdS}^{d-1}}{G_N}$. Both sides also enjoy the same symmetries: the isometry group of AdS_{d+1} is $SO(d,2)$, the same as the conformal group in d dimensions.

The correspondence between parameters shows that this is a strong/weak duality: the strong coupling regime on the boundary corresponds to the weak coupling regime in the bulk, and vice versa. Although the original correspondence was established in the

large N limit, this duality is generally believed true for general parameter ranges. From a modern perspective, the dual CFT provides the UV completion of the gravity theory in AdS since CFTs are themselves UV-complete quantum theories.

The most studied regime for this duality is the limit of large N (so the bulk Newton's constant $G \to 0$; gravity is weakly coupled) and large λ (so $\ell_s/\ell_{AdS} \to 0$; stringy effects can be neglected). In this limit, the bulk theory can be well approximated by semiclassical (super)gravity. Even in this semiclassical limit, a lot of phenomena of quantum gravity can be revealed.

This duality connects bulk and boundary via "dictionaries", through which many quantities can be matched on the two sides. The most fundamental dictionary is that the partition functions on the two sides should be equal:

$$Z_{AdS} = Z_{CFT}, \tag{1.2}$$

where the right-hand side is computed from the CFT path integral, while the left-hand side is computed from some kind of "gravitational path integral", which will be reviewed in section 1.2[1]. Furthermore, if the two sides indeed describe the same theory, the Hilbert spaces should also match:

$$\mathcal{H}_{AdS} = \mathcal{H}_{CFT}. \tag{1.3}$$

Some examples of matching between states include that the pure AdS spacetimes correspond to the CFT vacuum; the two-sided black hole corresponds to the thermofield double state [19].

Other famous examples of dictionaries are the extrapolate dictionary and the differentiate dictionaries, where correlation functions on two sides are related [16, 17, 20];

[1] As we will also see in section 1.2, when non-perturbative contributions are included, this relation is interpreted in the sense of ensemble averages.

the causal wedge/entanglement wedge reconstruction, where bulk local operators are reconstructed from the CFT [21, 22, 23, 24, 25].

This duality has also found a correspondence of the entanglement entropy in the boundary CFT. This is first proposed by Ryu and Takayanagi (RT) [26] that for a CFT region R, its von Neumann entropy $S_R = -\operatorname{Tr}\rho_R \log \rho_R$ is given in the bulk by the area of the minimal surface that is homologous to the boundary region R divided by $4G$. The RT formula can only be applied for static spacetimes or time slices of reflection symmetry, but later it is generalized to generic spacetimes by Hubeny-Rangamani-Takayanagi (HRT) [27]. When quantum corrections are included, it is generalized to the Faulkner-Lewkowycz-Maldacena (FLM) [28] formula to $O(1)$ and later to the quantum extremal surface (QES) formula [29] to all orders in G. The QES formula can be expressed in the following form,

$$S_R = \operatorname{ext}_\gamma \left(\frac{A_\gamma}{4G} + S_{bulk} \right), \tag{1.4}$$

where S_{bulk} is the entanglement entropy of the bulk region bounded by the QES and the boundary region R. If we apply this formula to a two-sided black hole and choose the region R to be the entirety of one boundary, the quantum extremal surface coincides with the bifurcation surface, and we see the generalized entropy $S_{gen} = \frac{A_{hor}}{4G} + S_{out}$ [30, 31] reproduced from QES as a special case. A proof of the above formulae involves the gravitational path integral, which will be reviewed in section 1.2.

1.2 The gravitational path integral

The gravitational path integral, is the path integral over all configurations of metrics and fields that satisfy given boundary conditions. It has been a very powerful tool in producing profound results, even just at the level of saddle-point approximation, and

many of the results are related to gravitational entropies.

Despite the successes, the exact rules for the gravitational path integral need to be clarified: What set of metrics should we integrate over, and what spacetime topologies should we include? Answers to these questions largely affect our understanding of quantum gravity.

1.2.1 From black hole entropy to holographic entanglement entropy

The Bekenstein-Hawking entropy, established through black hole thermodynamics, is later computed by Gibbons and Hawking using the technique of Euclidean gravitational path integrals [32]. The Bekenstein-Hawking entropy is derived from the thermal partition function, whose dominant saddle is the Euclidean black hole.

Regarding the RT formula as a generalization of the Bekenstein-Hawking formula, one might imagine also deriving RT from the gravitational path integral. This has been done by Lewkowycz and Maldacena [33]. In their proof, they first use the replica trick on the boundary CFT – a standard trick to express the entanglement entropy in terms of a limit of Rényi entropies $\frac{1}{1-n}\log \mathrm{Tr}\,\rho^n$, quantities that are easier to be represented using path integrals on some replicated manifold. Then the gravitational path integral is computed with this replicated manifold as the boundary condition. The RT formula is reproduced from the saddle-point approximation of this calculation in the semiclassical limit. Later, this proof is generalized to the time-dependent case [34], and to the case with quantum corrections [35].

In recent years, the quantum extremal surface formula has brought us many remarkable results, one of which is providing a resolution to the black hole information problem [36, 37, 38, 39]. If we apply the QES formula to an evaporating black hole to compute

the entanglement entropy of the Hawking radiation, we find a Page curve: the entropy of radiation first goes up and then goes down, always bounded by the Bekenstein-Hawking entropy of the black hole. This calculation resolves the issue raised by Hawking's original calculation [11], where the entropy of radiation keeps increasing as the black hole evaporates, causing a violation of unitarity of quantum mechanics. This transition of entropy from increasing to decreasing at the Page time results from a phase transition of the quantum extremal surface. This transition is because different saddles in the gravitational path integral dominate at different stages of the black hole evaporation. If we do a Lewkowycz-Maldacena style replica calculation, the disconnected saddle dominates before the Page time, while the connected "replica wormhole" saddle dominates after the Page time.

1.2.2 Euclidean vs. Lorentzian, and contours of integration

In the above discussion of the gravitational path integral, we did not specify the contour of integration, which should be part of the definition of a path integral, but is sometimes obscure. There are two natural choices for the integration contour: integrating over real Euclidean metrics (Euclidean path integral) or integrating over real Lorentzian metrics (Lorentzian path integral). But in general, the integration contour could be over some family of complex metrics, and there is no first principle to determine which contour is most fundamental.

However, some contours are problematic. It is first noted by Gibbons, Hawking, and Perry [40] that the Euclidean gravitational action is unbounded below, and it causes the path integral to be divergent. This indefiniteness is due to the conformal mode, and is usually referred to as the "conformal factor problem". The hypothesized solution by these authors is to rotate the integration contour of the conformal mode by 90 degrees

in the complex plane, and the resulting action is bounded below. Despite its success in reproducing many physically satisfying results [41, 42, 43], it has yet to be known why this is the right thing to do. In fact, there are examples where this contour-rotating procedure is not applicable, and new contour-rotating prescriptions are needed [44, 45].

For this dissertation, we take the point of view that integrating over real Lorentzian metrics gives the fundamental definition of the contour of the gravitational path integral. The reason for this viewpoint is that the Lorentzian path integral is free from the conformal factor problem, and suitable for calculations in real time with non-analytic sources, where it is hard to use Euclidean techniques. Furthermore, the Lorentzian path integral may provide us a guide on how to rotate the integration contours for Euclidean path integrals.

For any given contour of integration, when we use the saddle-point approximation, the saddles could in general be anywhere in the complex metric space. Thus, it is important to check what are the right saddles to include by first checking whether they give the expected answer, and importantly, whether the original contour can be deformed smoothly to the contour that passes through the saddle points.

1.2.3 The fixed-area states

Although the full gravitational path integral is hard to do, there exists strong evidence [38, 46, 1, 7] that in the semiclassical limit, the full gravitational path integral can be done by integrating over "fixed-area" saddles [47, 48] where the areas of certain codimension-2 surfaces are fixed:

$$Z = \int dA\, e^{-I(s_A)}, \tag{1.5}$$

where $I(s_A)$ is the (Euclidean) action of the fixed-area saddle s_A.

The codimension-2 surfaces are usually chosen to be the extremal surfaces, as it is easy

to be specified in a diffeomorphism-invariant way. In general, these fixed-area saddles have conical defects at the positions where the area is held fixed, and the strengths of the defects are determined by the values the areas are fixed at. Each of the fixed-area saddles defines a fixed-area state [47, 48], which resembles simple tensor network models of gravity in terms of entanglement properties. Superposing fixed-area states gives us detailed information about gravity beyond the leading semiclassical order.

1.2.4 Non-perturbative effects, baby universes, and ensemble of theories

Non-perturbative contributions to the gravitational path integral are usually due to including spacetime configurations with different topologies. Sometimes including them gives us a drastic change in results. As alluded to above, in calculating the entropy of radiation for black hole evaporation, we get an entropy that is bounded, by including the replica wormhole saddle which dominates at late times. The boundedness of entropy is necessary for unitarity to hold. Meanwhile, these non-perturbative effects seem to demonstrate that gravity behaves differently from what we expect from the CFT in the standard AdS/CFT context. On the CFT side, partition functions factorize between disconnected boundaries. However, due to the existence of wormholes, this is no longer the case:

$$\langle Z_1 Z_2 \rangle \neq \langle Z_1 \rangle \langle Z_2 \rangle, \tag{1.6}$$

where $\langle \cdot \rangle$ denotes results from the gravitational path integral. This inconsistency is usually referred to as the "factorization problem" [49][2]. One solution to this is to interpret the result from the gravitational path integral as the averaged result over an ensemble of

[2]Not to be confused with a related but different factorization problem about the quantum gravity Hilbert space.

CFTs [50, 51, 38, 52, 53].

In fact, just from the perspective of gravitational path integral, there is a similar structure of ensembles due to baby universes [54, 55]. Baby universes are spatially compact spacetimes without boundaries, and baby-universe-creating operators commute with any other operators. So we can diagonalize any operators in the basis of baby-universe-creating operators: α states. α states give rise to a structure of superselection sectors for the quantum gravity Hilbert space. Within an α sector, the dimension of the Hilbert space is definite, so entropy is bounded; besides, partition functions factorize between different connected boundaries. Entropy computed by the QES formula should be interpreted as the expectation value of entropy in the Hartle-Hawking state – a coherent state of α states, and this expectation value represents the entropy in a typical α state [54, 55].

1.3 The von Neumann algebra and quantum gravity

The von Neumann algebra is a very useful mathematical tool for studying quantum systems and quantum field theories, and can also help us have deeper understanding of problems in quantum gravity. In recent years, the application of von Neumann algebras, especially of the Tomita-Takesaki theory [56], has been applied to prove many results related to quantum field theory and quantum gravity. For example, the proof of the averaged null energy condition and the quantum null energy condition [57, 58].

Very recently, using von Neumann algebras, people have gained more understanding about the emergence of bulk spacetimes and gravitational entropies. Particularly, Leutheusser and Liu found that there is an emergent Type III von Neumann algebra[3]

[3]To briefly summarize the type classification of von Neumann algebras: Type III von Neumann algebras are the type of algebras for subregions in quantum field theory, where no notion of density matrix or entropy can be defined; for Type II von Neumann algebras, we can define a notion of density

from single-trace operators of the large N Yang-Mills theories [59, 60]. Later on, it is found that this Type III algebra can be modified to Type II after taking the crossed product, a standard construction in von Neumann algebra, with operators like the ADM Hamiltonian [61, 62, 63]. Similar constructions also exist for de Sitter space, when observers are included [64].

Since the notion of entropy can be defined for Type II von Neumann algebras, these constructions provide us with more information about the origin of gravitational entropies. And indeed, the entropies defined in the aforementioned constructions match with the usual notion of gravitational entropies up to additive constants. However, the above construction is perturbative in N (or $1/G$). For finite N, we should expect Type I algebras to arise, possibly from non-perturbative effects, to match the Type I-ness of the von Neumann algebras of the CFT[4].

1.4 Outline and Summary

The content of this dissertation is strongly related to the topics reviewed above. It contains three parts: The HRT Surface and the Fixed-Area States, Real-Time Replica Wormholes, and Algebras from the Gravitational Path Integral.

Part I is devoted to studying some interesting properties of the fixed-area states, which give us a handle on studying quantum gravity beyond the leading semiclassical order.

In Chapter 2, we show that under certain "diagonal approximation", near phase transitions of the holographic entanglement entropy (where the RT surface jumps from one

matrix and entropy, but pure states do not exist; Type I von Neumann algebras are the algebras for ordinary quantum mechanics, where there exist pure states, density matrices and entanglement entropies.

[4]In this case, Type I algebras are expected because we are considering the CFT living on an entire asymptotically AdS boundary. The algebras for CFT subregions are of Type III, and we should also expect Type III von Neumann algebras to arise from gravity.

homotopy class to another), there is an enhanced correction of order $1/\sqrt{G}$ coming from superposition of fixed-area states, which is larger than generic corrections from the entanglement of bulk quantum fields (which are $O(1)$). This correction decays exponentially away from the transition; thus it makes the holographic entanglement entropy a smooth function of the size of the boundary region. We illustrate this effect with explicit calculations for boundary regions given by a pair of disconnected intervals on the boundary of the AdS_3 vacuum and for a single interval on the boundary of the BTZ black hole. The latter case has an analog in the large-volume limit for chaotic many-body systems that satisfies the Eigenstate Thermalization Hypothesis [65].

In Chapter 3, we explore the Lorentz-signature spacetime geometry intrinsic to fixed-area states. This contrasts with previous treatments which focused instead on Euclidean-signature saddles for path integrals that prepare such states. The Lorentzian spacetime metrics are real at real times and have no conical singularities. With enough symmetry, the classical metrics are smooth, though more generally their curvatures feature power-law divergences along null congruences launched orthogonally from the fixed-area surface. While we argue that such divergences are not problematic at the classical level, quantum fields in fixed-area states feature stronger divergences. At the quantum level, we thus expect fixed-area states to be well-defined only when the fixed-area surface is appropriately smeared.

Part II of this dissertation studies the Lorentzian gravitational path integral, in the context of computing holographic Rényi entropies. When using the saddle-point approximation in the semiclassical limit, we find that interestingly, the saddles necessarily have complex metrics. This gives us an example where the saddles are not on the original contour of integration.

In Chapter 4, we set up the problem, studying the real-time gravitational path integral and constructing the variational principle that will define its saddle points. We also

describe the general structure of the resulting real-time replica wormhole saddles, arguing that a certain set of complex saddles should be dominant, and thus are accessed by deforming the original real contour of integration. The construction of these saddles need not rely on analytic continuation, and our formulation can be used even in the presence of non-analytic boundary sources. Furthermore, at least for replica- and CPT-symmetric saddles we show that the metrics may be taken to be real in regions spacelike separated from a so-called 'splitting surface', and this feature is an important hallmark of unitarity in a field theory dual.

In Chapter 5, we do direct computations for examples in two and three spacetime dimensions, finding the exact complex saddle-point solutions, and checking that they give the expected Rényi entropies. The examples we examined include JT gravity, and connected and disconnected intervals for holographic 2d CFTs.

However, in general, it is very difficult to check whether these complex saddles can be accessed by contour deformations, due to our lack of control over this infinite-dimensional path integral and the gauge invariances. Nevertheless, in Chapter 6, we directly check that in the simple case of two-dimensional JT gravity, where the relevant path integral is finite-dimensional, the original contour can be deformed smoothly to a contour that passes through this complex saddle.

Chapter 7 demonstrates an important consequence we find from the existence of these complex saddles. It is known that the HRT surface computing the entropy of a domain of dependence D on an asymptotically AdS boundary is causally inaccessible from D. The result we find is a generalization of this fact to the case of Rényi number $n > 1$, that in the aforementioned complex saddles, the replica-symmetric surface (the splitting surface) is causally inaccessible from the boundary domain of dependence D. This result is crucial for the unitarity in the dual field theory.

Part III focuses on understanding the origin of the gravitational entropy, by con-

structing von Neumann algebras from gravitational path integrals.

Before the detailed construction of algebras, Chapter 8 presents a proof of a new dictionary of AdS/CFT, for which we provide evidence to be true more generally, and it will be a very important axiom for the gravitational path integral in Chapter 9. On the CFT side of the correspondence, any two positive operators A, B will satisfy the trace inequality $\mathrm{Tr}(AB) \leq \mathrm{Tr}(A)\,\mathrm{Tr}(B)$. This relation holds on any Hilbert space $\mathcal{H}$ and is deeply associated with the fact that the algebra $B(\mathcal{H})$ of bounded operators on $\mathcal{H}$ is a Type I von Neumann factor. Holographic bulk theories must thus satisfy a corresponding result. In particular, we argue that the Euclidean gravitational path integral should satisfy a corresponding condition at all orders in the semi- classical expansion and with arbitrary higher-derivative corrections. The argument relies on a conjectured property of the classical gravitational action, which in particular implies a positive action conjecture for quantum gravity wavefunctions. We prove for Jackiw-Teitelboim gravity and also motivate it for more general theories.

In Chapter 9, we study the von Neumann algebras defined by the gravitational path integral, without taking the semiclassical limit. In general, it is extremely difficult to compute the full gravitational path integral without such a limit, however, we deal with this problem by constructing the algebras purely from boundary conditions, and only specify a few axioms that the full gravitational path integral should naturally satisfy, including the trace inequality. Our main result is that, for each compact asymptotic boundary B, the quantum gravity path integral defines both a von Neumann algebra $\mathcal{A}_B$ of observables acting at B and an entropy on $\mathcal{A}_B$. The fact that operators in the von Neumann algebras are bounded is closely related the trace inequality. In an appropriate semiclassical limit this entropy is computed by the RT formula with quantum corrections. Our result is also closely related to the fact that, in similar semiclassical limits, one may argue that the so-called island formula computes the standard entropy of non-

gravitational quantum systems entangled with a gravitational bulk without assuming that the bulk admits a holographic dual. Since our axioms do not restrict ultra-violet bulk structures, they may be expected to hold equally well for successful formulations of string field theory, spin-foam models, or any other approach to constructing a UV-complete theory of gravity.

In summary, this dissertation studies various aspects of the gravitational path integral, focusing on its relation with gravitational entropies, spacetime geometries, and its algebraic aspects. We study in detail some properties of the fixed-area states, the real-time replica wormholes – novel complex saddle-point geometries, and von Neumann algebras defined by gravitational path integrals with natural axioms. While the full gravitational path integral is a subtle and involved object to study, we find that a considerable amount of progress can still be made perturbatively in the semiclassical limit, with the crutch of the holographic duality. Some of the lessons we learned from this convenient setup can actually motivate us to study more general scenarios. In this dissertation, we also make efforts to understand quantum gravity in Lorenzian signature, and in general theories without assuming holography, to approach the goal of understanding quantum gravity in the real world.

1.5 Permissions and Attributions

1. The content of Chapter 2 and Appendix A is the result of a collaboration with Donald Marolf and Shannon Wang, and has previously appeared in the Journal of High Energy Physics [7]. It is reproduced here with the permission of the International School of Advanced Studies (SISSA): `http://jhep.sissa.it/jhep/help/JHEP/CR_OA.pdf`.

2. The content of Chapter 3 and Appendix B is the result of a collaboration with Xi

Dong, Donald Marolf, Pratik Rath, and Amirhossein Tajdini, and has previously appeared in the Journal of High Energy Physics [1]. It is reproduced here with the permission of the International School of Advanced Studies (SISSA): `http://jhep.sissa.it/jhep/help/JHEP/CR_OA.pdf`.

3. The content of Chapter 4 and Appendix C is the result of a collaboration with Sean Colin-Ellerin, Xi Dong, Donald Marolf, and Mukund Rangamani, and has previously appeared in the Journal of High Energy Physics [6]. It is reproduced here with the permission of the International School of Advanced Studies (SISSA): `http://jhep.sissa.it/jhep/help/JHEP/CR_OA.pdf`.

4. The content of Chapter 5 and Appendix D is the result of a collaboration with Sean Colin-Ellerin, Xi Dong, Donald Marolf, and Mukund Rangamani, and has previously appeared in the Journal of High Energy Physics [4]. It is reproduced here with the permission of the International School of Advanced Studies (SISSA): `http://jhep.sissa.it/jhep/help/JHEP/CR_OA.pdf`.

5. The content of Chapter 6 and Appendix E is the result of a collaboration with Jesse Held, Xiaoyi Liu, and Donald Marolf.

6. The content of Chapter 7 and Appendix F is the result of a collaboration with Donald Marolf, and has previously appeared in the Journal of High Energy Physics [3]. It is reproduced here with the permission of the International School of Advanced Studies (SISSA): `http://jhep.sissa.it/jhep/help/JHEP/CR_OA.pdf`.

7. The content of Chapter 8 and Appendix G is the result of a collaboration with Eugenia Colafranceschi and Donald Marolf.

8. The content of Chapter 9 and Appendix H is the result of a collaboration with Eugenia Colafranceschi and Donald Marolf.

Part I

The HRT Surface and the Fixed-Area States

Chapter 2

Probing phase transitions of holographic entanglement entropy with fixed-area states

2.1 Introduction

The Ryu-Takayanagi (RT) [26, 66] prescription, or more generally that of Hubeny-Rangamani-Takayanagi (HRT) [27], computes the entanglement entropy in some region R of a holographic CFT at leading order in the dual bulk Newton constant G. To this order, the entropy is given by $A/4G$ in terms of the area A of an extremal surface homologous to R [33]. In addition, a well-known correction at order G^0 is given by the entanglement of bulk fields [28].

However, in the context of chaotic many-body systems it was recently noted that entanglement entropy can have extra correction terms near entanglement phase transitions [67, 65]. In particular, motivated by [67], Murthy and Srednicki studied energy eigenstates in systems satisfying the eigenstate thermalization hypothesis (ETH) [65]. Dividing the

system into two spatial regions of volume V_1 and V_2 then yields a nontrivial entanglement entropy $S_{ent}(E)$. Taking a large-volume limit and ignoring terms that scale no faster than the area of the interface between V_1 and V_2 allows one to define a corresponding partition of the total energy, $E = E_1 + E_2$, between the two regions. In this context, for generic V_1, V_2, they show the entanglement entropy $S_{ent}(E)$ to be approximated to exponential accuracy by the lesser of the microcanonical entropies $S_1(E_1), S_2(E_2)$ determined by the associated partition of the total energy $E = E_1 + E_2$ between the two regions. But there is a larger correction of order $\sqrt{S_1} = \sqrt{S_2}$ near the transition where $S_1(E_1) = S_2(E_2)$. Furthermore, the net effect of this correction is to make the entanglement a smooth function of all parameters, so that the apparent 'phase transition' in fact becomes a crossover already at this level of analysis[1].

Closely related physical settings have been considered in the holographic context for some time. For example, one may consider a pure-state black hole, divide the boundary into regions V_1, V_2, and compute the HRT entropy; see e.g. [68, 69]. One then finds that the leading-order bulk RT/HRT computation describes a sharp RT/HRT phase transition with no analogue of the corrections described in [67, 65]. This should not be a surprise as RT/HRT entropy is of order $1/G$ so the above $\sqrt{S}$ correction is only of order $G^{-1/2}$. But such a correction should appear in a more complete study, and one might expect similar $O(G^{-1/2})$ corrections to arise near more general RT/HRT transitions as well. These corrections are too large to arise from the entropy of bulk fields, and so must arise from some other aspect of the semiclassical approximation in the bulk. A related $O(G^{-1/2})$ correction was recently discussed in [38] for an analogous quantum RT transition.

Our goal below is to provide a general description of such corrections near RT/HRT phase transitions using properties of the bulk fixed-area states introduced in [47] (see also

[1] In the strict limit of large volume the crossover occurs very quickly and one recovers the expected sharp phase transition.

[48]). For simplicity, we focus on the time-symmetric (RT) case below where one may use real Euclidean path integrals. However, we expect that the essential argument can be generalized to the more general HRT context using the Schwinger-Keldysh techniques of [34]. In particular, we decompose a general bulk into states in which we have simultaneously fixed the areas of all extremal surfaces satisfying the homology constraint (i.e., we have fixed the areas of all candidate RT surfaces). For simplicity, we assume below that there are precisely two such extremal surfaces in a given such fixed-area state, and that their areas have been fixed to A_1 and A_2. We then argue that the entanglement $S(A_1, A_2)$ in the associated fixed-area state $|A_1, A_2\rangle$ is given by RT up to corrections of order G^0, so that

$$S(A_1, A_2) = \frac{1}{4G} \min(A_1, A_2) + O(G^0). \tag{2.1}$$

We also conjecture that – again up to corrections of order G^0 – the entanglement in a more general holographic state $|\psi\rangle = \int dA_1 dA_2 \psi(A_1, A_2)|A_1, A_2\rangle$ can be computed using a certain 'diagonal approximation.' When this conjecture holds, we show to leading order in G that the von Neumann entropy is just the expectation value of $S(A_1, A_2)$ in the natural ensemble defined by the (normalized) state $|\psi\rangle$; i.e.

$$S = \int dA_1 dA_2 |\psi(A_1, A_2)|^2 S(A_1, A_2) + O(G^0). \tag{2.2}$$

Evaluating this expression then gives the desired contribution at order $G^{-1/2}$, and with properties directly analogous to the correction of [65]. Finally, we provide some evidence in support of our diagonal approximation by demonstrating agreement with the results of both [65] and [38].

We begin in section 2.2 with a brief review of fixed-area states. General arguments for (2.2) and a statement of our diagonal-approximation conjecture are then given in

section 2.3. The rest of the paper is devoted to more detailed computations of the effect, and to showing that our diagonal approximation reproduces results from [65] and [38]. Section 2.4 consists of a warm-up exercise in which we study fixed-area states associated with a single interval in vacuum AdS_3. While there is no phase transition in this context, results from this simple context will be useful studying examples of the above phase transition in section 2.5. The first example concerns a pair of intervals on the boundary of vacuum AdS_3, while the second involves a single interval on the boundary of the Bañados-Teitelboim-Zanelli (BTZ) black hole [70, 71]. After taking a natural large volume limit, the latter context allows us to demonstrate explicit agreement between our BTZ results and the predictions of [65]. A final part of section 2.5 shows that we can also reproduce the $O(1/\sqrt{G})$ correction found in [38] for an analogous quantum RT transition. We close with some final comments in section 2.6, and in particular discuss the cutoff dependence of fluctuations in RT-areas.

Closely related work has been done independently by Xi Dong and Huajia Wang [72]. We have arranged with them to coordinate simultaneous postings of the original versions of the papers to the arxiv.

2.2 Review of fixed-area states

We now briefly review some basic properties of fixed-area states following [47]. In particular, after defining the fixed-area states, we will review their connection with the probability distribution $P(A_*)$ for a holographic state to have RT-area A_*, features of the semiclassical approximation for such states, and the simple form of their Renyi entropies. All of these features will play important roles in the analysis of section 2.3.

We consider a CFT state $|\psi\rangle$ prepared by a Euclidean path integral over a manifold M_{CFT} with boundary ∂M_{CFT}. It is thus natural to think of $|\psi\rangle$ as a state on the surface

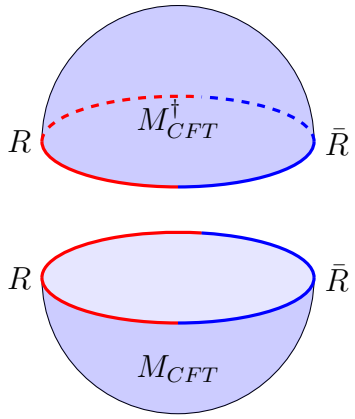

Figure 2.1: The manifold M_{CFT} (bottom) that we use in the Euclidean path integral to prepare our holographic state $|\psi\rangle$ and the CPT-conjugate manifold $M^\dagger_{CFT}$ (top). Sewing the two together along their boundaries defines the manifold $M_{double} := M^\dagger_{CFT} M_{CFT}$. If the state is time-symmetric, then $M^\dagger_{CFT}$ is equivalent to M_{CFT}, the two manifolds are exchanged by the relevant notion of time-reversal, and this symmetry leaves invariant the boundary $\partial M_{CFT} = \partial M^\dagger_{CFT}$ of $M_{CFT}, \partial M^\dagger_{CFT}$. The surface ∂M_{CFT} is partitioned into regions R (red) and $\bar{R}$ (blue).

∂M_{CFT}.

We suppose that ∂M_{CFT} is partitioned into regions R and $\bar{R}$. For simplicity, we take the state to be invariant under a time-reflection symmetry that leaves fixed the surface ∂M_{CFT}. Under the AdS/CFT correspondence, we may identify M_{CFT} with the boundary of a bulk system, and we may similarly identify ∂M_{CFT}, R, $\bar{R}$ with corresponding (partial) surfaces in that boundary. We will use ∂R to denote the boundary between R and $\bar{R}$ within ∂M_{CFT}. The correspondence also tells us that the norm $\langle\psi|\psi\rangle$ can be computed using a Euclidean bulk path integral with boundary conditions defined by the closed manifold $M_{double} := M^\dagger_{CFT} M_{CFT}$ defined by sewing together M_{CFT} and its CPT-conjugate $M^\dagger_{CFT}$ along the common boundary ∂M_{CFT}; see figure 2.1. The assumption of time-symmetry requires $M^\dagger_{CFT}$ to be equivalent to M_{CFT}, so that ∂M_{CFT} is a surface of time-symmetry in M_{double}.

Roughly speaking, given a state $|\psi\rangle$ defined as above, we wish to define associated states $|\psi\rangle_{A_*}$ of fixed RT area by restricting the domain of integration to metrics for which

the area A_{γ_R} of the RT surface[2] γ_R takes on a definite value A_*, and by thus projecting $|\psi\rangle$ onto the subspace with area A_*. In this sense, the norm of a fixed-area state is calculated by the path integral

$$\begin{aligned} {}_{[]}\langle\psi|\psi\rangle_{A_*} &= \int \mathcal{D}g|_{A_{\gamma_R}=A_*} e^{-I[g]} \\ &= \int \mathcal{D}g d\mu e^{-I[g]-i\mu(A_{\gamma_R}[g]-A_*)}. \end{aligned} \tag{2.3}$$

In the second line we have introduced a Lagrange multiplier μ to enforce the constraint on the area of γ_R. In practice, we will wish to restrict A_{γ_R} to some window around A_* where the width of the window is small compared to other scales of interest, but where the window still contains many area-eigenvalues. As a result, one should think of the measure $d\mu$ as being a broad Gaussian measure instead of being precisely flat. However, we will take this measure to be sufficiently flat that its Gaussian nature can be ignored in the saddle-point approximation used below.

Due to our projection, the path integral (2.3) is closely associated with the probability $P(A_*)$ for the holographic state $|\psi\rangle$ to have an RT area in the above window about A_*. In particular, we have

$$P(A_*) = \frac{{}_{A_*}\langle\psi|\psi\rangle_{A_*}}{\langle\psi|\psi\rangle}. \tag{2.4}$$

Since we will study (2.3) in the saddle-point approximation, our task will be to find on-shell solutions to the Euclidean equations of motion. As is well known[3], at this level the integral over μ and the term $-i\mu A_{\gamma_R}[g]$ in the exponent allow the insertion of an arbitrary conical defect (aka 'cosmic brane') at the location of the RT surface. The defect angle is to be chosen so that the saddle-point geometry g_* satisfies the constraint

[2]A better approach which avoids the need to define an RT surface for off-shell metrics may be to build a path integral using the fixed-area action of [73]. This action singles out a preferred surface whose area is to be fixed and then finds that the equations of motion require it to be an RT surface modulo imposition of the homology constraint.

[3]Though see appendix A of [73] for a more complete justification.

$A_{\gamma_R} = A_*$. In the stationary phase approximation we thus find

$$ {}_{A_*}\langle\psi|\psi\rangle_{A_*} \approx e^{-I[g_*]}. \tag{2.5}$$

Note that $I[g_*]$ is the full gravitational action for g_* and in particular includes a contribution from the delta-function curvature scalar on the conical singularity.

A priori, the form of (2.3) suggests an imaginary conical defect angle $i\mu$, but as always the relevant saddles may not lie on the original contour of integration. As a result, real defect angles (with imaginary values of our μ) are allowed, and may arise with either sign. Note that real $\mu_E = i\mu$ is in fact generally required for the stationary point g_* to satisfy real Euclidean boundary conditions. Thus g_* is typically a real Euclidean metric, though it may contain either a conical deficit or a conical excess. As discussed in [47, 73], the location of the conical deficit should be thought of as the RT surface in the conical geometry. We will thus refer to it as such below.

Since the classical actions $I(A_*) = I(g_*)$ are proportional to $1/G$, in the semiclassical limit $G \to 0$ the distribution $P(A_*)$ becomes sharply peaked about the most likely value $\bar{A}$. This mostly likely values can be found by maximizing $P(A_*)$, or equivalently by minimizing the on-shell action with respect to A_*. But minimizing the action in this way imposes the remaining Einstein equations on γ_R, and thus forbids any cosmic brane sources. As a result, the most likely value $\bar{A}$ is just the area of γ_R in the dominant bulk saddle g_0 associated with the path integral that computes the norm $\langle\psi|\psi\rangle$ [47, 73] without any a priori specification of areas.

Finally, we turn to considerations of entropy. Let us consider the normalized density matrix ρ_{A_*} on R defined by the CFT dual to the bulk fixed-area state $|\psi\rangle_{A_*}$. This density

matrix may be written in the form

$$\rho_{A_*} = \frac{\mathrm{Tr}_{\bar{R}} \left(|\psi\rangle_{A_* A_*} \langle\psi| \right)}{{}_{A_*}\langle\psi|\psi\rangle_{A_*}}, \tag{2.6}$$

where in (2.6) we have used $|\psi\rangle_{A_*}$ to also denote the CFT dual to the bulk fixed-area state $|\psi\rangle_{A_*}$. In the above semiclassical approximation, the freedom to tune the conical defect angle to enforce the constraint makes it straightforward to compute Renyi entropies $S_n(A_*) = \frac{1}{1-n} \ln \mathrm{Tr}_R \rho_{A_*}^n$. In particular, the associated saddles $g_n(A_*)$ are just n-sheeted branched covers of the saddle g_* used in (2.5). A straightforward computation [74] then finds $I[g_n(A_*)] = nI[g_*] + (n-1)\frac{A_*}{4G}$, and thus $S_n = \frac{A_*}{4G}$. In particular, the Renyi entropies $S_n(A_*)$ are independent of n . However, as usual, if $\partial R \neq \emptyset$ the Renyis diverge and require either a cutoff (say, defined using a certain boundary conformal frame) or renormalization to give finite results.

In general, one expects the RT area A_{γ_R} to define superselection sectors of the quantum error correcting code associated with CFT reconstruction of the bulk entanglement wedges of R and $\bar{R}$ [25]. When this is the case, the density matrix on R of a CFT state $|\psi\rangle$ is block-diagonal A_{γ_R}, so that

$$\rho = \oplus_{A_*} P(A_*) \rho_{A_*}, \tag{2.7}$$

with ρ_{A_*} given by (2.6) in terms of the corresponding fixed-area state. The representation (2.7) motivates the idea that fixed-area states may be useful in studying the entropy of $|\psi\rangle$. However, the arguments for (2.7) (see [25]) are based (in part via [75, 24]) on the Faulkner-Lewkowycz-Maldacena result [28] that the leading correction to $A/4G$ is of order G^0 and is given by bulk entanglement. As described above, we expect this to fail

near an RT phase transition[4]. So while (2.7) may provide some motivation, we should take care not to rely on it to hold exactly in the regime of interest.

We conclude this section with a remark about notation. Most of the explicit computations in sections 2.4 and 2.5 will be for 3-dimensional bulk spacetimes. In such cases codimension-2 extremal surfaces are geodesics and the associated 'areas' are in fact lengths. We will thus introduce $L_* = A_*$ and write all equations in those sections in terms of L_*, referring to it as the fixed length of the RT surface. Once the reader is aware of this convention, it should create no confusion. We will also generally drop the subscript $*$ below.

2.3 Corrections to holographic entanglement entropy near phase transitions

We now turn to our main task of studying entropies of holographic states near RT phase transitions. In particular, let us suppose our holographic state $|\psi\rangle$ is associated with a semi-classical geometry g having two candidate RT surfaces γ_1, γ_2 associated with some partial Cauchy surface R of the boundary spacetime. Thus γ_1, γ_2 are both extremal surfaces anchored to the boundary ∂R of R, and both are homologous to R in the sense of [77]. Since our state is assumed to be pure, the surfaces γ_1, γ_2 are homologous to $\bar{R}$ as well.

We will proceed by considering a holographic state $|\psi\rangle$ and fixing the areas of both γ_1 and γ_2. The probabilities $P(A_1, A_2)$ to obtain areas A_1 and A_2 can then be computed in

[4]Such a failure is natural as [28] builds on the semi-classical Lewkowycz-Maldacena argument [33], which assumes a single RT surface to dominate. This assumption clearly breaks down at an RT phase transition, and it is known that a proper treatment of cases with multiple extremal surfaces will be subtle; see e.g. comments in [76] based on a talk by Matt Headrick, which was in turn based on private remarks by Rob Myers.

direct analogy to the method described in section 2.2 for fixing the area of an RT surface. In particular, we have

$$P(A_1, A_2) = \frac{{}_{A_1,A_2}\langle\psi|\psi\rangle_{A_1,A_2}}{\langle\psi|\psi\rangle}, \tag{2.8}$$

with $\langle\psi|\psi\rangle = e^{I+O(G^0)}$ and ${}_{A_1,A_2}\langle\psi|\psi\rangle_{A_1,A_2} = e^{I(A_1,A_2)+O(G^0)}$ in terms of the Euclidean actions I, $I(A_1, A_2)$ of the leading saddles defined respectively by the path integral for $\langle\psi|\psi\rangle$ and by the corresponding path integral with the areas of γ_1, γ_2 fixed to take the values A_1, A_2. Recall that in the latter case the action generally includes a delta-function curvature contribution from both surfaces γ_1 and γ_2. As before, the most likely values $\bar{A}_1, \bar{A}_2$ for our areas are just the values in the smooth saddle g_0 that dominates the path integral for the norm $\langle\psi|\psi\rangle$ (and with no a priori fixing of areas).

Below, we first describe some of the topological details of our setup that will prove useful in the main argument. We then discuss and motivate our diagonal approximation before computing the resulting $O(G^{-1/2})$ correction in section 2.3.3.

2.3.1 Topological remarks

For convenience we will assume that while γ_1 and γ_2 are homologous, the two surfaces lie in distinct *homotopy* classes[5], and that each is the minimal-area such extremal surface within its homotopy class. Having a topological distinction between the surfaces provides a natural definition of what we mean by the corresponding extremal surfaces γ_1, γ_2 in the conically-singular spacetimes associated with fixing the area of these extremal surfaces[6]. Furthermore, we will assume that – at least for small defect angles and near the phase transition – in all other homotopy classes the minimal surface γ has area strictly greater

[5]Recall that homotopy is a more fine-grained equivalence relation than homology.

[6]This is merely a matter of convenience. One could alternatively simply consider all saddle-points of the fixed-area action described in [73], which describe spacetimes with what one may call extremal codimension-2 conical defects anchored to ∂R. It is not strictly necessary to label such conical defects as being associated with one of the extremal surfaces γ_1, γ_2 in the original smooth spacetime.

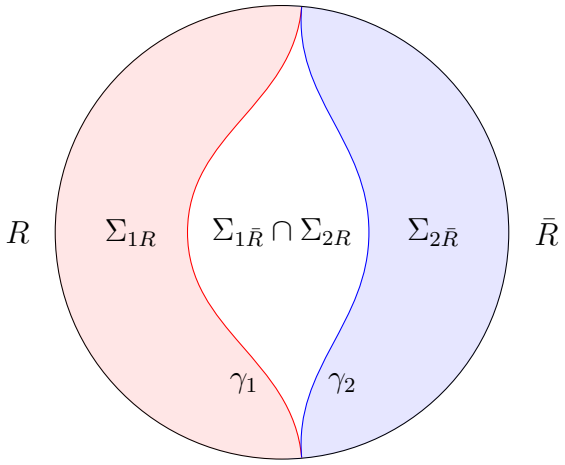

Figure 2.2: An illustration of two competing RT surfaces γ_1 and γ_2 near a phase transition. In our convention, we always let $\Sigma_{1R} \subset \Sigma_{2R}$, as a result Σ_{1R} and $\Sigma_{2\bar{R}}$ are non-overlapping.

than either γ_1 or γ_2. This allows us to neglect such additional candidate RT surfaces in the semi-classical approximation.

Even in Lorentz signature, two extremal surfaces anchored on the same boundary set ∂R are spacelike separated in the bulk and lie on a common Cauchy surface Σ [78]. We note that this is the case even when $\partial R = \emptyset$. As a result, the associated RT area operators $\hat{A}_1$, $\hat{A}_2$ for γ_1, γ_2 commute at all orders in the semi-classical expansion and – at least at this level – can be simultaneously diagonalized. In particular, the possible obstruction described in [79] does not arise. We may thus consider the doubly-fixed-area states $|\psi\rangle_{A_1,A_2}$ in which the area of γ_1 is A_1 and the area of γ_2 is A_2. Here we introduce an appropriate UV cutoff in the boundary to render A_1, A_2 finite. Since both are anchored on the same set ∂R, we use the same cutoff to define both A_1 and A_2.

The homology constraint means that each surface γ_i ($i \in \{1, 2\}$) must partition Σ into two (non-overlapping) parts $\Sigma_{iR}, \Sigma_{i\bar{R}}$ where $\partial\Sigma_{iR} = \gamma_i \cup R$ and similarly for $\partial\Sigma_{i\bar{R}}$; see figure 2.2. We will further assume that Σ_{1R} is contained in Σ_{2R}. At least in the time-symmetric case, this assumption can be made without loss of generality. To see this, note that we must have either $\Sigma_{1R} \subset \Sigma_{2R}$, $\Sigma_{2R} \subset \Sigma_{1R}$, or that γ_2 enters both Σ_{1R}

and $\Sigma_{1\bar{R}}$. The first case fulfills our assumption, and in the second case the assumption can be fulfilled by simply exchanging the labels $1 \leftrightarrow 2$.

In the third case, the intersection $\gamma_{int} = \gamma_1 \cup \gamma_2$ partitions γ_2 into two parts $\gamma_{2R} \subset \Sigma_{1R}$ and $\gamma_{2\bar{R}} \subset \Sigma_{1\bar{R}}$. Similarly, we must also find that γ_1 enters both Σ_{2R} and $\Sigma_{2\bar{R}}$, so γ_{int} also partitions γ_1 into two parts $\gamma_{1R} \subset \Sigma_{2R}$ and $\gamma_{1\bar{R}} \subset \Sigma_{2\bar{R}}$. Note that γ_{1R} and $\gamma_{2\bar{R}}$ must be homologous but cannot be homotopic. Similarly, γ_{2R} and $\gamma_{1\bar{R}}$ must be homologous but cannot be homotopic.

For this case, let us choose the labels 1 and 2 so that γ_{2R} has smaller area than $\gamma_{1\bar{R}}$ and define a new surface $\gamma_3 = \gamma_{1R} \cup \gamma_{2R}$. Note that γ_3 also satisfies the homology constraint, but that it cannot be homotopic to either γ_1 or γ_2. While γ_3 is not extremal, it has area A_3 satisfying $A_3 < A_1$. So the minimal surface within its homotopy class also has area less than A_1. But this contradicts the earlier assumption that the least-area extremal surface in any other homotopy class must have area strictly greater than either A_1 or A_2. Thus our 3rd case cannot exist in the time-symmetric case, and we can take $\Sigma_{1R} \subset \Sigma_{2R}$ without loss of generality[7].

2.3.2 The diagonal approximation

Because the states $|\psi\rangle_{A_1,A_2}$ are at least approximate eigenstates of $\hat{A}_1, \hat{A}_2$, any two such states are semi-classically orthogonal unless they have fixed the same values for the areas of both γ_1 and γ_2. The fixed-area states thus naturally define a decomposition of $|\psi\rangle$ according to

$$|\psi\rangle = \sum_{A_1,A_2} \sqrt{\frac{P(A_1,A_2)}{\langle\psi|\psi\rangle}} |\psi\rangle_{A_1,A_2}. \tag{2.9}$$

[7]It would be interesting to understand if this result continues to hold without time symmetry. If it does, the rest of the argument generalizes in a straightforward way to the HRT case using the Schwinger-Keldysh techniques of [34].

As in section 2.2, we take the states $|\psi\rangle_{A_1,A_2}$ to be associated with finite intervals of A_1, A_2 that are small with respect to the semiclassical width of $P(A_1, A_2)$ but large compared with the spacing between adjacent area eigenstates. We thus take the intervals to be polynomially small in G, but not exponentially small.

It now remains to compute the density matrix ρ_R on the region R by tracing $|\psi\rangle\langle\psi|$ over the complementary region $\bar{R}$:

$$\rho_R = \sum_{A_1,A_2,A_1{}',A_2{}'} \sqrt{P(A_1,A_2)}\sqrt{P(A_1{}',A_2{}')}\mathrm{Tr}_{\bar{\mathrm{R}}}\left(\frac{|\psi\rangle_{\mathrm{A_1,A_2A_1{}',A_2{}'}}\langle\psi|}{\langle\psi|\psi\rangle}\right). \tag{2.10}$$

In doing so, one must consider contributions from both diagonal terms (with $A_1 = A_1{}'$ and $A_2 = A_2{}'$) as well as contributions from off-diagonal terms (where either $A_1 \neq A_1{}'$ or $A_2 \neq A_2{}'$).

The diagonal terms give the average over the distribution $P(A_1, A_2)$ of the (normalized) density matrices $\rho_R(A_1, A_2)$ defined by the normalized fixed-area states. Let us therefore write

$$\rho_R = \sum_{A_1,A_2} P(A_1, A_2)\rho_R(A_1, A_2) + OD_R, \tag{2.11}$$

where OD_R is the result of summing all off-diagonal contributions.

Since A_1 defines a Hermitian operator that can be reconstructed on R, we must have $\rho_R(A_1, A_2)\rho_R(A_1{}', A_2{}') = 0$ for $A_1 \neq A_1{}'$. Note that the same need not always hold for A_2 since it can be reconstructed on R only for $A_2 < A_1$. However, if we instead considered the density matrices on $\bar{R}$ that result from tracing over R, this would interchange the roles of A_1 and A_2, suggesting that the full problem exhibits a greater symmetry. We will therefore treat the $\rho_R(A_1, A_2)$ below as if they live in orthogonal subspaces[8].

Let us first discuss the contributions of the diagonal terms. In particular, we introduce

[8]We emphasize that this is an additional assumption and thank Geoffrey Penington for conversations related to this point.

the von Neumann entropies

$$S_D = -\mathrm{Tr}\left(\rho_D \ln \rho_D\right) \quad \text{for} \quad \rho_D := \oplus_{A_1,A_2} P(A_1,A_2)\rho_R(A_1,A_2), \tag{2.12}$$

$$S(A_1,A_2) = -\mathrm{Tr}\left(\rho_R(A_1,A_2)\ln \rho_R(A_1,A_2)\right). \tag{2.13}$$

Treating the diagonal terms as living in orthogonal subspaces, a standard computation shows these quantities to be related by

$$S_D = \sum_{A_1,A_2} \left(P(A_1,A_2)S(A_1,A_2) - P(A_1,A_2)\ln P(A_1,A_2)\right)\right), \tag{2.14}$$

where the 2nd term is often called the entropy of mixing. The entropy of mixing is bounded by the logarithm of the number of values that the pair (A_1, A_2) can take. Since each value (A_1, A_2) labels an interval that is only polynomially small in G, this bound is of the form $C \ln G + s(\psi)$ where C is an order-one constant and dependence on the state ψ appears only through the order-one function $s(\psi)$. We will thus neglect the entropy of mixing below since it is parametrically smaller than the $O(G^{-1/2})$ term we wish to study.

Now, before returning to the off-diagonal terms OD_R, we also wish to compute $S(A_1, A_2)$. As reviewed in section 2.2, the fact that fixed-area states allow arbitrary conical singularities at the associated extremal surfaces means that the semiclassical Renyi entropies of such states are straightforward to compute. In particular, every n-sheeted branched cover of the original Euclidean geometry defines a saddle for the nth Renyi problem. Furthermore, comparison with tensor networks suggests that all Renyi saddles are of this form.

In our present case, the branching can occur at either surface γ_1 or γ_2, or on any of their Renyi copies. Note that the surfaces γ_1, γ_2 partition the time-symmetric surface Σ into 3 parts according to $\Sigma = \Sigma_{1R} \cup \Sigma_{int} \cup \Sigma_{2\bar{R}}$ where $\Sigma_{int} = \Sigma_{1\bar{R}} \cap \Sigma_{2R}$ lies between γ_1

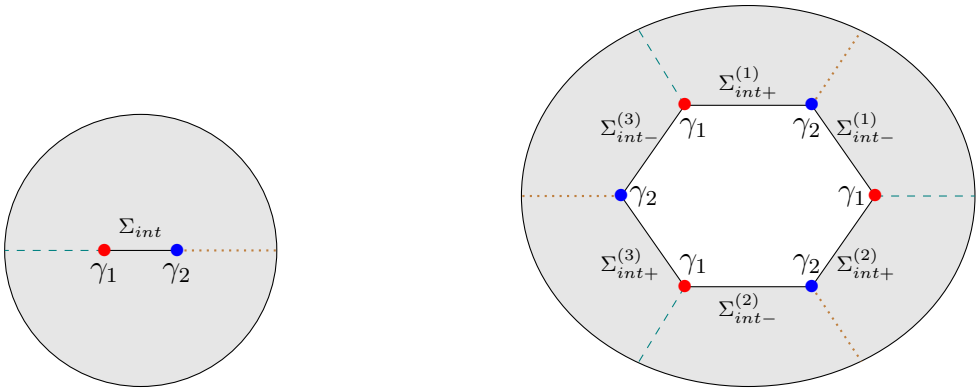

Figure 2.3: **Left:** A two-dimensional projection of an $n = 1$ solution with two extremal surfaces γ_1, γ_2 (having areas A_1 and A_2) and a surface Σ_{int} stretching between them. **Right:** An n-fold cover of the figure at left for the case $n = 3$ after cutting open a slit along Σ_{int}. The $2n$ copies of Σ_{int} are labeled $\Sigma^{(i)}_{int\pm}$, where $i = 1, \ldots, n$. Saddles for the Rényi entropy are formed by identifying $\Sigma^{(i)}_{int+}$ with $\Sigma^{(\pi(i))}_{int-}$ for some permutation π. After making such identifications, the number $N_2 = n - n_2$ of copies of γ_2 that remain is the number $C(\pi)$ of cycles generated by π, while the corresponding $N_1 = n - n_1$ is $C(\tau \circ \pi)$ where τ is the counterclockwise cyclic permutation. The asymmetry is due to the numbering of replicas, which breaks the natural symmetry between the dashed lines (separating replicas) and dotted lines (separating the two halves of each replica).

and γ_2. The possible saddles can then be constructed by the following procedure. First, cut a slit along Σ_{int} in the original spacetime g_0 to define a spacetime with an internal boundary $\Sigma_{int+} \cup \Sigma_{int-}$, where $\Sigma_{int\pm}$ are the two sides of the newly-opened slit along Σ_{int}. Next consider the n-fold cover of the result that winds n times around this slit; see figure 2.3. Finally, sew the up the slit by making identifications between the n copies of Σ_{int+} and the n copies of Σ_{int-}. Since there are $n! = \Gamma(n+1)$ ways to pair up the copies of Σ_{int+} and Σ_{int-}, this results in $\Gamma(n+1)$ saddles.

However, as shown in [47] the fixed-area action of a branched cover depends only on the action of the spacetime $g_{0,0}$ that dominates the fixed-area path integral for ${}_{A_1,A_2}\langle\psi|\psi\rangle_{A_1,A_2}$ and on the conical defects and areas of the branching surfaces. As a result, for a given branched-cover the Euclidean action depends only on the numbers n_1, n_2 of times that it branches over each of γ_1, γ_2, irrespective of the order in which

those branchings occur. In more detail, we take $2\pi n_1$ to be the sum of the conical excesses around all copies of γ_1, and similarly for n_2.

The action for these saddles follows from the analysis of [47], which yields

$$I[g_{n_1,n_2}] = nI[g_0] + \frac{n_1 A_1 + n_2 A_2}{4G}. \tag{2.15}$$

Here[9] $n_1 + n_2 \geq n - 1$, consistent with the fact that no branching occurs for $n = 1$. To minimize the action, we will be interested in saddles that saturate this inequality (so that $n_1 + n_2 = n - 1$). To understand these saddles, we may describe the above sewing by a permutation π of the copies of Σ_{int-} relative to the copies of Σ_{int+}. As shown in figure 2.3, any numbering of the copies of $\Sigma_{int\pm}$ breaks a natural symmetry between γ_1 and γ_2. As a result, with the conventions of figure 2.3, the number N_2 of copies of γ_2 that remain after these identifications is given by the number $C(\pi)$ of closed cycles associated with the permutation π (e.g., the permutation (12)(3) on 3 objects has $C = 2$), while the corresponding N_1 is given by the number $C(\tau \circ \pi)$ where τ is the cyclic permutation that maps copy i to copy $i - 1$). Since the winding numbers n_1, n_2 defined above are $n_1 = n - N_1$, $n_2 = n - N_2$, we have $N_1 + N_2 = 2n - (n_1 + n_2) \leq n + 1$ and we wish to saturate this bound. As described in appendix E of [38], the number of permutations on n objects that do so (and thus which have $N_1 + N_2 = C(\pi) + C(\pi \circ \tau) = n + 1$) is given by the nth Catalan number $C_n = \frac{1}{n+1}\binom{2n}{n} = \frac{\Gamma(2n+1)}{(n+1)[\Gamma(n+1)]^2}$.

When A_1 and A_2 differ significantly, the nth Renyi is clearly dominated by a saddle with action $I = nI[g_0] + \frac{n-1}{4G}\min(\mathrm{A}_1, \mathrm{A}_2)$ and we find $S(A_1, A_2) = \frac{\min(\mathrm{A}_1, \mathrm{A}_2)}{4G}$ in direct analogy with the case studied in [47] where only one area is fixed. On the other hand, when $A_1 = A_2$ all of the C_n saddles with $n_1 + n_2 = n - 1$ have the same action[10] $I[g_{n-1,0}]$

[9] We thank Geoffrey Penington for pointing out an error in a previous draft and for conversations related to the comments below.

[10] Because the number $\Gamma(n + 1) - C_n$ of other saddles vanishes at $n = 1$, the other saddles can contribute at most an $O(1)$ correction to the von Neumann entropy. That is enough for us to drop

and we find

$$S_n = \frac{1}{1-n}\ln\frac{Z_n}{Z_1^n} \approx \frac{\ln C_n + I[g_{n-1,0}] - nI[g_0]}{1-n} = \frac{A_1}{4G} - \frac{1}{n-1}\ln\left(\frac{\Gamma(2n+1)}{(n+1)[\Gamma(n+1)]^2}\right). \tag{2.16}$$

in terms of the nth Renyi partitions functions Z_n. Note that the final term is of order G^0 and has a finite limit $-2\frac{\Gamma'(3)}{\Gamma(3)} + \frac{1}{2} + 2\frac{\Gamma'(2)}{\Gamma(2)} = -\frac{1}{2}$ as $n \to 1$. Since it is clear that the largest correction will occur for $A_1 = A_2$, we may thus write $S(A_1, A_2) = \frac{\min(A_1, A_2)}{4G} + O(G^0)$ for all A_1, A_2.

We now return to the off-diagonal term OD_R in (2.11) and its contributions to the Renyi entropies $S_n(\rho_R)$. While we leave full consideration of such terms to future work, we will give a plausibility argument suggesting that these contributions can be ignored for our current purposes. To begin this plausibility argument note that, in the semiclassical approximation, each such contribution can be written as e^{-I} where I is the action of a branched cover of g_0 similar to those described above, but where the areas of the various Renyi copies of γ_1 can differ from each other[11], and similarly for the Renyi copies of γ_2. See figure 2.4. In particular, at least at the leading semiclassical order discussed here, such contributions are associated with the possibility of breaking replica symmetry. Since a strict breaking of replica symmetry is impossible at $n = 1$, it is plausible that their contribution will be subleading in the limit where the replica number n is taken to 1. In particular, since for any normalized ρ_R the diagonal terms yield $S_{n,\text{diag}} = O(n-1)$, it is plausible that off diagonal contributions will be of order $O\left((n-1)^2\right)$ or of order G^0 (from corrections to the leading semiclassical terms). For now, we simply assume that this is the case and follow up by checking consistency with results from [65] and [38] in

such contributions. But the interested reader can find more discussion in [38], and it appears that the contribution of such saddles to the von Neumann entropy is in fact non-perturbatively small, being proportional to $e^{-\frac{A_{1,2}}{4G}}$ and thus vanishing exactly when $\gamma_{1,2}$ reach the boundary and $A_{1,2}$ diverge.

[11] We thank Xi Dong, Geoffrey Penington, Xiaoliang Qi, and Douglas Stanford for discussions of this point.

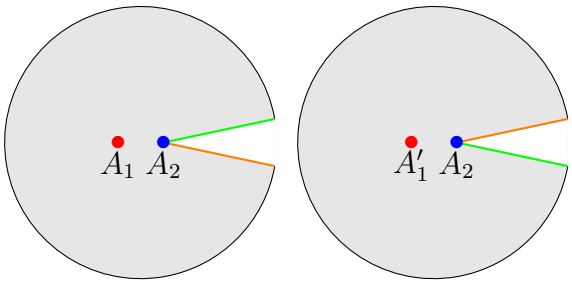

Figure 2.4: Using the same projection as for the $n = 1$ figure at left in figure 2.3, we show two pieces of a corresponding saddle that for $A_1 \neq A_1'$ describes an off-diagonal contribution to the second Rényi entropy S_2. The full saddle is constructed by sewing the two pieces together along edges of the same color; i.e., we may first identify the two green edges and then identify the two orange edges. Note that this particular saddle contains only one copy of the surface γ_2 and so cannot be 'off-diagonal' in A_2.

section 2.5.

With the above assumption, the von Neumann entropy $S(\rho_R)$ is given by just the diagonal contributions $S_D(\rho_R)$ up to corrections of order G^0 and, introducing a normalization factor N, we write

$$\begin{aligned} S(\rho_R) := S_D + O(G^0) &= \sum_{A_1,A_2} \frac{\min(\mathrm{A}_1, \mathrm{A}_2)}{4G} P(A_1, A_2) + O(G^0) \\ &= \sum_{A_1,A_2} \frac{\min(\mathrm{A}_1, \mathrm{A}_2)}{4G} N e^{-(I(A_1,A_2)-I(\bar{A}_1,\bar{A}_2))} + O(G^0) \\ &= \int dA_1 dA_2 \frac{\min(\mathrm{A}_1, \mathrm{A}_2)}{4G} N e^{-(I(A_1,A_2)-I(\bar{A}_1,\bar{A}_2))} + O(G^0), \end{aligned} \quad (2.17)$$

where in the last step we may approximate the sum by an integral with error smaller than $O(G^0)$ since the spacings between values of A_1, A_2 included in the sum were taken to be small compared with the natural scale of variation of $I(A_1, A_2)$.

2.3.3 The general form of corrections

The above section motivated the diagonal approximation (2.17) $S(\rho_R) := S_D + O(G^0)$ (with S_D given by (2.14)) and derived the resulting simple form (2.17) for $S(\rho_R)$ in terms of the fixed-area actions. We will now show how this form gives an $O(G^{-1/2})$ correction to the RT entropy. This merely requires evaluating the final integral in (2.17) in the semiclassical limit $G \to 0$.

Since the action I is proportional to $1/G$, taking $G \to 0$ concentrates the integral near the areas $\bar{A}_1, \bar{A}_2$ that minimize the action. As usual, we can approximate I near that minimum as quadratic:

$$I(A_1, A_2) = I(\bar{A}_1, \bar{A}_2) + \frac{1}{2} \sum_{i,j=1}^{2} \left(\frac{\partial^2 I}{\partial A_i \partial A_j}\Big|_{\bar{A}_i} \right) (A_i - \bar{A}_i)(A_j - \bar{A}_j) + O\left((A - \bar{A})^3\right), \quad (2.18)$$

where the cubic and higher terms in (2.18) will contribute to (2.17) only at order G^0. We may neglect all such terms since our goal is to study corrections at order $G^{-1/2}$. It will prove useful in analyzing the examples of section 2.5 that (2.18) involves only configurations infinitesimally close to the smooth saddle $g_{0,0}$ that dominates the path integral for $\langle \psi | \psi \rangle$, and in particular which has vanishing cosmic brane tension (and thus vanishing conical defect) on both γ_1 and γ_2.

For later reference, we introduce the covariance matrix C with components

$$C_{ij} = \begin{bmatrix} \sigma_1^2 & r\sigma_1\sigma_2 \\ r\sigma_1\sigma_2 & \sigma_2^2 \end{bmatrix} = G \begin{bmatrix} \tilde{\sigma}_1^2 & r\tilde{\sigma}_1\tilde{\sigma}_2 \\ r\tilde{\sigma}_1\tilde{\sigma}_2 & \tilde{\sigma}_2^2 \end{bmatrix} \quad (2.19)$$

defined by $(C^{-1})_{ij} = \frac{\partial^2 I}{\partial A_i \partial A_j}\Big|_{\bar{A}_i}$. Note that since $\frac{\partial^2 I}{\partial A_i \partial A_j}$ is of order $1/G$, the covariance matrix is of order G. The final form in (2.19) displays this G-dependence explicitly, and the parameters $\tilde{\sigma}_1, \tilde{\sigma}_2, r$ are all of order G^0.

The integral defined by using (2.18) in (2.17) is naturally studied in terms of the variables $A_\pm = \frac{A_1 \pm A_2}{2}$ for which we have $\min(A_1, A_2) = A_+ - |A_-|$ and the most likely values are $\bar{A}_\pm := \frac{\bar{A}_1 \pm \bar{A}_2}{2}$. The integral over A_+ is straightforward and gives

$$S_D = \int_{-\infty}^{\infty} dA_- \frac{(A_- - \bar{A}_-)(\tilde{\sigma}_1^2 - \tilde{\sigma}_2^2) + 4(\bar{A}_+ - |A_-|)\tilde{\sigma}_-^2}{16 G^{3/2}\sqrt{2\pi}\tilde{\sigma}_-^3} \exp\left\{\left(-\frac{(A_- - \bar{A}_-)^2}{2G\tilde{\sigma}_-^2}\right)\right\} + O(G^0), \tag{2.20}$$

where $4\tilde{\sigma}_-^2 = \tilde{\sigma}_1^2 - 2r\tilde{\sigma}_1\tilde{\sigma}_2 + \tilde{\sigma}_2^2$. We will also use $\sigma_-^2 = G\tilde{\sigma}_-^2$ below.

The term linear in $(A_- - \bar{A}_-)$ integrates to zero by symmetry. The remaining integral can be written in terms of the error function $\operatorname{erf} x := \frac{2}{\sqrt{\pi}} \int_0^x dt e^{-t^2}$ as

$$\begin{aligned} S(\rho) &= \frac{\bar{A}_+}{4G} - \frac{\bar{A}_-}{4G} \operatorname{erf}\left(\frac{\bar{A}_-}{\sqrt{2G}\tilde{\sigma}_-}\right) - \frac{\tilde{\sigma}_-}{2\sqrt{2\pi G}} \exp\left\{\left(-\frac{\bar{A}_-^2}{2G\tilde{\sigma}_-^2}\right)\right\} + O(G^0) \\ &= \frac{\min\left(\bar{A}_1, \bar{A}_2\right)}{4G} - \frac{\tilde{\sigma}_-}{2\sqrt{2\pi G}} \Phi\left(\frac{\bar{A}_1 - \bar{A}_2}{2\tilde{\sigma}_-\sqrt{2G}}\right) + O(G^0), \end{aligned} \tag{2.21}$$

where we have introduced

$$\Phi(x) := e^{-x^2} + \sqrt{\pi}|x|(\operatorname{erf}|x| - 1) \tag{2.22}$$

following the notation of [65]. Note that $\Phi(x)$ is bounded by a constant of order G^0, The final expression in (2.21) thus makes manifest that we find a correction of order $G^{-1/2}$ at the transition where $\bar{A}_1 = \bar{A}_2$, but that the correction is exponentially small at large $|A_1 - A_2|/\tilde{\sigma}_-\sqrt{G} = |A_1 - A_2|/\sigma_-$. On the other hand, the first line in (2.21) shows that the entropy at this order is a smooth function of $\bar{A}_1 - \bar{A}_2$; the supposed RT 'phase transition' is in fact already a crossover at this level of analysis.

2.4 Fixed length states for a single interval in the AdS_3 vacuum

We now wish to perform explicit computations illustrating the above $O(G^{-1/2})$ correction and exploring the size of fluctuations in RT-areas in various examples. However, before doing so it is useful to analyze fixed-area states associated with a simple case in which phase transition do *not* arise. We do so here, studying the particularly simple case where we choose our boundary region R to be a single interval on the $t = 0$ slice of the boundary of empty global AdS_3. Since two of our examples in section 2.5 below will also involve intervals on the boundary of either AdS_3 or a BTZ quotient, we will be able to use results obtained below to simplify the analysis of those phase transitions.

As usual, in order to find the probability that the RT surface for our single-interval R has some fixed length L_*, we will use the saddle-point approximation and study the action for the appropriate classical Euclidean solution. As discussed above, this solution will have a conical defect (which in AdS_3 takes the form of a spacelike cosmic string). For pure Einstein-Hilbert AdS_3 gravity, the fact that all solutions are locally equivalent to AdS_3 means that the solution with fixed length L_* may be constructed from global AdS_3 by inserting a conical singularity along the associated RT surface and tuning the conical angle so that the length becomes L_* as defined by using an appropriate cutoff with respect to the desired conformal frame at infinity.

We thus begin by recalling that the Euclidean AdS_3 vacuum can be described as the Poincaré ball with metric

$$ds^2 = \frac{dr^2 + r^2 d\theta^2 + r^2 \sin^2\theta d\phi^2}{(1 - r^2/4)^2}. \tag{2.23}$$

In (2.23), the coordinate ranges are $\theta \in [0, \pi]$, $\phi \in [0, 2\pi)$, and $r \in [0, 2)$. The AdS

boundary lies at $r = 2$ and we have set the bulk AdS length scale ℓ to 1.

It is then straightforward to address the case where the boundary region R is half of a great circle on the boundary S^2. With an appropriate Wick rotation, we may thus think of this as half of the boundary circle at Lorentzian time $t = 0$. However, for our current purposes it will be convenient to take this interval to be the half-circle $\theta \in [0, \pi]$ at $\phi = 0$; i.e., we take it to be the prime meridian instead of half of the equator.

By symmetry, the corresponding RT surface is then just the ϕ-axis. Fixed length states for R will then be associated with similar Euclidean solutions in which this axis is a conical singularity. General such solutions are then described by inserting a positive factor α into (2.23) to yield

$$ds^2 = \frac{dr^2 + r^2 d\theta^2 + \alpha^2 r^2 \sin^2\theta d\phi^2}{(1 - r^2/4)^2}. \tag{2.24}$$

Note that we may also write (2.24) in terms of a rescaled angular coordinate $\tilde{\phi} = \alpha\phi$ with $\tilde{\phi} \in [0, 2\pi\alpha)$ to give a perhaps-more-familiar description of this conical metric. The cases $\alpha < 1$ describe conical deficits, while $\alpha > 1$ is a conical excess. Using the Einstein equations to interpret this conical defect as a (Euclidean) cosmic string, one finds that the string has a tension μ such that

$$\alpha = 1 - 4\mu G. \tag{2.25}$$

In particular, the string tension is negative for geometries with a conical excess.

We wish to fix the length of our defect cosmic string. Of course, the actual length of the ϕ-axis diverges but, as mentioned above we in fact wish to specify an appropriately regularized notion of its length. We will do so by introducing a UV cutoff in the dual CFT, which then defines a radial cutoff in the bulk. This requires specifying a conformal

frame, and it is natural to take this to be the frame in which the boundary geometry is given by the round metric on the unit-radius S^2.

For $\alpha \neq 1$ this round conformal frame differs from the conformal frame naturally associated with the bulk metric (2.24). In particular, for $\alpha \neq 1$ multiplying (2.24) by $(1 - r^2/4)^2$ and setting $r = 2$ would give a boundary metric with conical singularities at both poles. Of course, this conical metric is related to the round metric by a conformal (aka Weyl) rescaling of the metric. Both the associated conformal factor Ω and the polar coordinate $\tilde{\theta}$ associated with the standard presentation of the round metric can be found by writing

$$d\theta^2 + \alpha^2 \sin^2\theta d\phi^2 = \Omega^2 (d\tilde{\theta}^2 + \sin^2\tilde{\theta} d\phi^2). \tag{2.26}$$

Solving for Ω^2 and θ gives

$$\Omega^2 = \left(\frac{\alpha \sin\theta (1 + (\tan\frac{\theta}{2})^{2/\alpha})}{2(\tan\frac{\theta}{2})^{1/\alpha}} \right)^2 \tag{2.27}$$

and

$$\theta = 2\tan^{-1}\left[\left(\tan\frac{\tilde{\theta}}{2} \right)^{\alpha} \right]. \tag{2.28}$$

We take our UV cutoff to be given by a distance δ in the boundary as defined in the round unit-sphere conformal frame. The associated bulk radial cutoff would then be at $z = \delta$ where z is the Fefferman-Graham coordinate associated with the same round conformal frame. However, for $\alpha \neq 1$ the conical singularity in (2.24) makes it non-trivial to write our metric in such coordinates. So instead of explicitly computing the transformation between r, θ, ϕ and the desired Fefferman-Graham coordinates, we will use the well-known fact that (to leading order in δ) the desired cutoff $z = \delta$ can be identified as the greatest depth to which minimal surface anchored on a circle of size δ (as defined in the desired conformal frame) hangs down into the bulk. In particular,

since our conical singularity lies on the ϕ-axis, it should be cutoff where it intersects the minimal surface anchored to a circle of round-frame radius δ about the pole $\tilde{\theta} = 0$. Note that the bulk conical singularity will prevent the minimal surface from being smooth, but that – as is most easily seen for the case $\delta = \pi/4$ – symmetry requires the surface to be invariant under an appropriate $\mathbb{Z}_2$ reflection. This condition implies that the minimal surface must still intersect the axis orthogonally.

In the conical boundary-conformal frame, we see from (2.28) that the surface is anchored at $\theta = \delta_\alpha \equiv \tan^{-1}\left[\left(\tan\frac{\delta}{2}\right)^\alpha\right]$. A short computation shows that the desired minimal surface satisfies

$$\frac{1}{r} + \frac{r}{4} = \frac{\cos\theta}{\cos\delta_\alpha}. \tag{2.29}$$

The intersection with the $\theta = 0$ axis occurs at $r_\alpha = 2(\sec\delta_\alpha - \tan\delta_\alpha)$, so the cutoff RT surface (i.e., the cutoff cosmic string) has length

$$\begin{aligned} L &= 2\int_0^{r_\alpha} \frac{dr}{1 - r^2/4} \\ &= 2\ln\frac{1}{\tan(\delta_\alpha/2)} \\ &= 2\alpha\ln\frac{1}{\tan(\delta/2)} \\ &\approx 2\alpha\ln\frac{2}{\delta}. \end{aligned} \tag{2.30}$$

To study a fixed-length state with prescribed length L_*, we then use (2.25) and (2.30) to determine the required tension μ of the cosmic string. Below, from (2.30) we keep only the leading order term at small δ .

We may also use the above results to compute the (cutoff) length of a RT surface defined by an interval R of any angular size 2λ . The point here is that the isometries of global AdS_3 act as conformal transformations on the boundary S^2 and can be used to map the interval $[0, \pi]$ to the interval $[0, 2\lambda]$. Such isometries are easy to describe by

embedding Euclidean AdS_3 into four-dimensional Minkowski space. In our coordinates this embedding takes the form:

$$\begin{aligned} T &= \frac{4+r^2}{4-r^2}, \\ X &= \frac{4r}{4-r^2}\sin\tilde{\theta}\sin\phi, \\ Y &= \frac{4r}{4-r^2}\cos\tilde{\theta}, \\ Z &= \frac{4r}{4-r^2}\sin\tilde{\theta}\cos\phi. \end{aligned} \tag{2.31}$$

While the above embedding holds only for the case $\alpha = 1$ (where $\tilde{\theta} = \theta$), we have chosen to write the embedding in terms of $\tilde{\theta}$ as we will eventually apply the boundary conformal transformation to cases with general α using the round conformal frame.

It will be convenient to take the new interval R to also lie along the boundary great circle defined by $\phi = 0$ and $\phi = \pi$. Note that such intervals all lie at $X = 0$ in the embedding coordinates, and that they are thus invariant under the $\mathbb{Z}_2$ isometry $(T, X, Y, Z) \to (T, -X, Y, Z)$. We refer to this isometry as reflection in X.

Note that boosts in the Z, T plane preserve this $\mathbb{Z}_2$ symmetry while acting non-trivially on the desired boundary great circle. In particular, a boost in the negative Z direction with rapidity η acts on this circle as $\sin\tilde{\theta} \to \frac{\sin\tilde{\theta}-\eta}{1-\eta\sin\tilde{\theta}}$. So to map the angular interval $\tilde{\theta} \in [\pi/2 - \lambda, \pi/2 + \lambda]$ at $\phi = 0$ to the interval $\tilde{\theta} \in [0, \pi]$ at $\phi = 0$ we need only choose $\eta = \sin\lambda$.

Such a boost also acts on our cutoff, taking a cutoff δ associated with $\tilde{\theta} \in [\pi/2 -$

$\lambda, \pi/2 + \lambda]$ to a new cutoff associated with $\tilde{\theta} \in [0, \pi]$ given by

$$\begin{aligned}\delta_b &= \frac{1}{2}\left(\sin^{-1}\frac{\sin\left(\frac{\pi}{2}-\lambda+\delta\right)-\sin\left(\frac{\pi}{2}-\lambda\right)}{1-\sin\left(\frac{\pi}{2}-\lambda+\delta\right)\sin\left(\frac{\pi}{2}-\lambda\right)} - \sin^{-1}\frac{\sin\left(\frac{\pi}{2}-\lambda-\delta\right)-\sin\left(\frac{\pi}{2}-\lambda\right)}{1-\sin\left(\frac{\pi}{2}-\lambda-\delta\right)\sin\left(\frac{\pi}{2}-\lambda\right)}\right) \\ &= \frac{\delta}{\sin\lambda} + O(\delta^2).\end{aligned} \tag{2.32}$$

Applying the associated boundary conformal transformation to the general case $\alpha \neq 1$, we then find that boundary intervals of angular size λ are associated with bulk cosmic strings of length given by (2.30) with δ replaced by (2.32) to yield

$$L = 2\alpha \ln \frac{2\sin\lambda}{\delta} =: \alpha L_0(\lambda). \tag{2.33}$$

where $L_0(\lambda)$ is the cutoff length of this same geodesic when there is no cosmic string.

In section 2.5 below, we will also find it useful to allow different cutoffs δ_L and δ_R at the two ends of the cosmic string. Generalizing the above arguments then yields

$$L = \alpha \ln \frac{4\sin^2\lambda}{\delta_L \delta_R}, \tag{2.34}$$

where α again describes the defect on this string.

It is now straightforward to compute the Euclidean action I of our solutions as a function of λ, δ, and $L = L_* = \alpha L_0$. Since this computation is somewhat of an aside from the main thrust of this work we have relegated the details to appendix A.1. Up to an α-independent constant (which depends on the choice of boundary conformal frame, and thus in a fixed frame may depend on δ and λ), the action can be written in terms of just α and L_0:

$$I = \frac{\alpha(\alpha-2)L_0}{8G}. \tag{2.35}$$

Since there is no RT phase transition for single intervals, we can use the results of

[25] to write the density matrix of the dual CFT on our interval in the block-diagonal form

$$\rho = \oplus_\alpha P(\alpha)\rho_\alpha, \tag{2.36}$$

where $P(\alpha)$ is the probability for the RT surface to have length αL_0. As explained in section 2.2, in the semiclassical approximation this probability is

$$P(\alpha) = N\exp(-I) = \sqrt{\frac{L_0}{8\pi G}}\exp\left(-\frac{(\alpha-1)^2 L_0}{8G}\right), \tag{2.37}$$

where in the last step we have computed the appropriate normalization coefficient N so that[12] $\int_0^\infty P(\alpha)d\alpha = 1$. Furthermore, in this approximation reference [47] finds each ρ_α to be a maximally mixed state in a subspace whose dimension agrees with the RT entropy $L_0/4G$. Thus we may write

$$\rho_\alpha = e^{-\frac{\alpha L_0}{4G}}\mathbb{I}_{\exp\left(\frac{\alpha L_0}{4G}\right)}, \tag{2.38}$$

where $\mathbb{I}_{\exp(S)}$ is the identity matrix in a Hilbert space of dimension e^S.

The physics of the result (2.38) is most easily seen as follows. Let us focus on the case $\lambda = \pi/2$ for simplicity, and let us then identify the cutoff surface near $\tilde{\theta} = 0$ with the one near $\tilde{\theta} = \pi$. Except for the conical singularity, the resulting spacetime is a Euclidean BTZ black hole with horizon length $L_* = \alpha L$ and energy $E_{BTZ} = \frac{r_+^2}{8G} = \frac{L^2}{32\pi^2 G}$ as defined in the standard BTZ conformal frame. If we treat α (and thus E) as a discrete index, we may then write the density matrix (2.36) as

$$\rho = N_E\left(\oplus_E e^{-\beta E}\mathbb{I}_{\exp(S_{BTZ}(E))}\right), \tag{2.39}$$

[12] In fact, we have used the value of N for which $1 = \int_{-\infty}^{\infty} P(\alpha)d\alpha = \int_0^\infty P(\alpha)d\alpha + O\left(e^{-\frac{L_0}{8G}}\right)$. The associated error is negligible in the semiclassical limit.

where $\beta_{BTZ} = 4\pi^2/L_0$ and $S_{BTZ}(E) = \sqrt{2\pi^2 E/G}$ is the entropy of a BTZ black hole with energy E. The normalization coefficient N_E is $N_E = \sqrt{\frac{L_0}{8\pi G}} e^{-L_0/8G}$. In other words, the density matrix coincides with a canonical ensemble of BTZ microstates at inverse temperature β. This is precisely what one expects from the general discussion of fixed-area states in section 5 of [47].

Using the above results, it is of course straightforward to compute Rényi entropies. We find

$$\begin{aligned} \operatorname{Tr}\rho^n &= \int P(\alpha)^n e^{-n\frac{\alpha L_0}{4G}} e^{\frac{\alpha L_0}{4G}} d\alpha \\ &= \sqrt{\frac{8\pi G}{nL_0}} \left(\frac{L_0}{8\pi G}\right)^{n/2} \exp\left(-\frac{L_0}{8G}(n-\frac{1}{n})\right), \end{aligned} \tag{2.40}$$

and thus

$$\begin{aligned} S_n &:= \frac{1}{1-n} \ln \operatorname{Tr}\rho^n \\ &= \frac{L_0}{8G}\left(1+\frac{1}{n}\right) + O(\ln(G)) \\ &= \frac{c}{6}\left(1+\frac{1}{n}\right) \ln \frac{2\sin\lambda}{\delta} + O(\ln(c)), \end{aligned} \tag{2.41}$$

where we used the Brown-Henneaux relation $c = \frac{3\ell}{2G}$ [80], with $\ell = 1$. Of course, this precisely matches the well-known results of [81, 82] for the dual CFT.

2.5 Examples

We now we consider several examples of the general framework discussed above. The first two cases concern AdS_3 and its BTZ quotients. In those cases we compute the covariance matrix (2.19) by treating the conical defect as a small perturbation, working to linear order in the (Euclidean) tension μ of the associated (spacelike) cosmic strings. As a result, the effect of multiple such cosmic strings satisfy linear superposition, and results for general configurations of strings can be computed from the one-interval results of section 2.4. In practice, instead of the fixed-area action I, we find it convenient to study

the action $I_{def} = I_{defect}$ for fixed tensions μ_1, μ_2 of the cosmic strings along the two RT surfaces. However, the two are related by a Legendre transform $I = I_{def} - \mu_1 A_1 - \mu_2 A_2$ (see e.g. [47, 73]). As a result, the matrix $\frac{\partial^2 I}{\partial A_i \partial A_j}$ is the inverse of $\frac{\partial^2 I}{\partial \mu_i \partial \mu_j}$ and we have

$$C_{ij} = \frac{\partial^2 I_{def}}{\partial \mu_i \partial \mu_j} = -\frac{\partial}{\partial \mu_i} \langle A_j \rangle_{\mu_1,\mu_2} \Big|_{\mu_1=\mu_2=0} = -\frac{\partial}{\partial \mu_j} \langle A_i \rangle_{\mu_1,\mu_2} \Big|_{\mu_1=\mu_2=0}, \tag{2.42}$$

where $\langle A_i \rangle_{\mu_1,\mu_2}$ is the most likely value of A_i in the presence of cosmic strings with tensions μ_1, μ_2. Here we have used the standard Legendre transform relation $\frac{\partial I_{def}}{\partial \mu_i} = -\langle A_i \rangle_{\mu_1,\mu_2}$.

2.5.1 Example 1: Two intervals in the AdS_3 vacuum

Our first example concerns the Euclidean global AdS_3 vacuum as in section 2.4. However, we now take the boundary region R to be given by a pair of non-overlapping intervals on the great circle of the boundary S^2 associated with $\phi = 0$ and $\phi = \pi$. For simplicity, we choose the two intervals to be related by a π rotation. In particular, they are each of the same angular size $2\lambda < \pi$. We take both to be given by $\theta \in [\pi/2 - \lambda, \pi/2 + \lambda]$ and to respectively lie at $\phi = 0$ and $\phi = \pi$.

As is well known, there are two locally-minimal surfaces that satisfy the required boundary conditions. While both are homologous to the pair of boundary intervals R, only one of them is homotopic to R. For reasons that will shortly become clear, we denote this homotopic surface by $\gamma_d = \gamma_{diagonal}$ while the other will be denoted $\gamma_o = \gamma_{off-diagonal}$. Since the RT surfaces are one-dimensional, we will again use the terms length and area interchangeably as in section 2.4. In particular, the total lengths of the above RT surfaces are L_d and L_o.

Each of the above RT surfaces is disconnected, and in fact consists of two geodesics. We label the four relevant geodesics $\gamma_{11}, \gamma_{12}, \gamma_{21}, \gamma_{22}$, with $\gamma_d = \gamma_{11} \cup \gamma_{22}$ and $\gamma_o = \gamma_{12} \cup \gamma_{21}$ as shown in figure 2.5. The corresponding lengths are $L_{11} = L_{22}$, and $L_{12} = L_{21}$. The

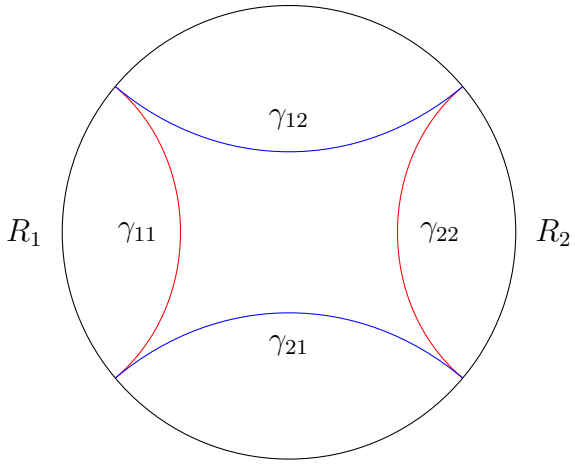

Figure 2.5: Two competing extremal surfaces when $R = R_1 \cup R_2$ is a pair of intervals on the boundary of the AdS_3 vacuum. The homotopic RT surface $\gamma_d = \gamma_{11} \cup \gamma_{22}$ and the non-homotopic RT surface $\gamma_o = \gamma_{12} \cup \gamma_{21}$ are shown respectively in red and blue. The case shown sits precisely at the RT phase transition, where γ_d and γ_o are related by a $\pi/2$ rotation.

system undergoes an RT phase transition at $\lambda = \pi/4$, when γ_d and γ_o are related by a $\pi/2$ rotation. For vanishing cosmic-string tensions the solution is just global Euclidean AdS_3 and the lengths of the RT surfaces are

$$\bar{L}_d = 2\bar{L}_{11} = 2\bar{L}_{22} = 4 \ln \frac{2 \sin \lambda}{\delta} \tag{2.43}$$

$$\bar{L}_o = 2\bar{L}_{21} = 2\bar{L}_{12} = 4 \ln \frac{2 \cos \lambda}{\delta}. \tag{2.44}$$

Due to the superposition principle mentioned in the introduction to this section, it will be convenient to allow independent cosmic string tensions μ_{ij} for all $i, j \in \{1, 2\}$. To compute (2.42), we need only find the response functions $\Delta_{mn} L_{ij}$ that describe how the lengths L_{ij} of the geodesics in figure 2.5 change at linear order under the addition of the sources μ_{mn}. Of the 16 response functions $\Delta_{mn} L_{ij}$, the four terms $\Delta_{ij} L_{ij}$ where we study the change in length L_{ij} along the same defect (with tension μ_{ij}) are just the linearization of the single-interval result (2.33) from section 2.4. Furthermore, the 8 terms

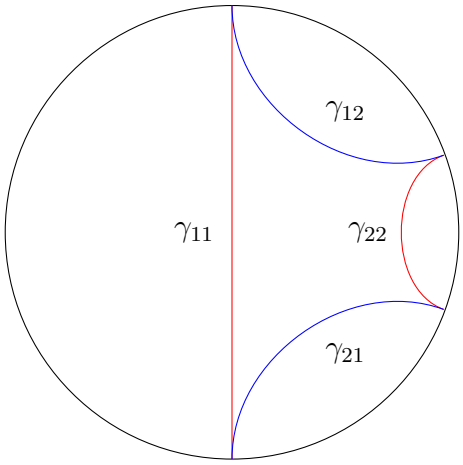

Figure 2.6: The same geodesics as in figure 2.5 after applying an AdS_3 isometry to move the boundary-anchors γ_{11} to the poles $\theta = 0, \pi$. This configuration allows us to compute changes in length by applying results from section 2.4.

$\Delta_{mn} L_{ij}$ where (m, n, i, j) are permutations of $(1, 1, 1, 2)$ and $(2, 2, 2, 1)$ (i.e., where 3 of the 4 indices m, n, i, j coincide but the last is different) are all related to each other by symmetry (and perhaps interchanging $\lambda \to \pi/2 - \lambda$). Finally, the last 4 terms $\Delta_{ij} L_{\bar{i}\bar{j}}$ (with $\bar{i} \neq i$ and $\bar{j} \neq j$) involve diametrically opposite geodesics. As representatives of these 3 classes of terms, we will compute $\Delta_{11} L_{11}$, $\Delta_{11} L_{12}$, and $\Delta_{11} L_{22}$.

Let us begin by computing $\Delta_{11} L_{12}$, the first-order change in the length L_{12} due to the source μ_{11}. As in section 2.4, this is straightforward if we act with an AdS isometry to move the boundary-anchors of γ_{11} to the poles $\theta = 0, \pi$, so that γ_{11} runs along the ϕ-axis; see figure 2.6 below. After this transformation, the two anchors of γ_{12} lie at the pole $\theta = 0$ and at $\theta = \vartheta$ with

$$\vartheta = \sin^{-1} \frac{2 \cos \lambda}{1 + \cos^2 \lambda}. \tag{2.45}$$

In the resulting (round) conformal frame, the cutoffs at the two ends of L_{12} will differ. This occurs because the boundary conformal transformation associated with the above AdS_3 isometry fails to preserve the original symmetry between the endpoints. In the new

conformal frame the cutoffs are given by

$$\delta_L \approx \frac{\delta}{\sin\lambda} \tag{2.46}$$

$$\begin{aligned}\delta_R &= \frac{1}{2}\left(\sin^{-1}\frac{\sin\left(\frac{\pi}{2}-\lambda+\delta\right)+\sin\left(\frac{\pi}{2}-\lambda\right)}{1+\sin\left(\frac{\pi}{2}-\lambda+\delta\right)\sin\left(\frac{\pi}{2}-\lambda\right)} - \sin^{-1}\frac{\sin\left(\frac{\pi}{2}-\lambda-\delta\right)+\sin\left(\frac{\pi}{2}-\lambda\right)}{1+\sin\left(\frac{\pi}{2}-\lambda-\delta\right)\sin\left(\frac{\pi}{2}-\lambda\right)}\right) \\ &\approx \frac{2\sin\lambda}{3+\cos 2\lambda}\delta,\end{aligned} \tag{2.47}$$

with δ_L being the cutoff at left end in figure 2.6, where γ_{12} meets γ_{11}.

Now, the length of a geodesic in the position of γ_{12} with cutoffs δ_L, δ_R in pure AdS_3 was studied in section 2.4. It was found there to be given by (2.34), where one should insert the value $\alpha = 1$ since there is no defect on γ_{12}. And since the local metric near γ_{12} in coordinates (r, θ, ϕ) does not change when we insert a string of tension $\mu_{11} = \frac{1-\alpha_{11}}{4G}$ on L_{11}, the length L_{12} in the presence of this defect can again be obtained from (2.34) with $\alpha = 1$. However, after the addition of the defect the coordinates (r, θ, ϕ) are associated with the conical conformal frame on the boundary. As a result, we must insert into (2.34) the θ-locations $0, \hat{\vartheta}$ of the γ_{12} anchors and the cutoffs $\hat{\delta}_L, \hat{\delta}_R$ as described in the conical conformal frame. Using again the conformal transformation (2.28), we find

$$\hat{\vartheta} = 2\tan^{-1}\left(\tan^{\alpha_{11}}\frac{\vartheta}{2}\right), \tag{2.48}$$

$$\hat{\delta}_L = 2\tan^{-1}\left(\tan^{\alpha_{11}}\frac{\delta_L}{2}\right) \approx 2\left(\frac{\delta_L}{2}\right)^{\alpha_{11}}, \tag{2.49}$$

and

$$\begin{aligned}\hat{\delta}_R &= \tan^{-1}\left(\tan^{\alpha_{11}}\frac{\vartheta+\delta_R}{2}\right) - \tan^{-1}\left(\tan^{\alpha_{11}}\frac{\vartheta-\delta_R}{2}\right) \\ &\approx \frac{\alpha_{11}(3+\cos 2\lambda)\sin^{\alpha_{11}-1}\lambda}{2(1+\cos^{2\alpha_{11}}\lambda)}\delta_R.\end{aligned} \tag{2.50}$$

Here the symbol $\approx$ indicates that we have dropped higher order terms in the original

cutoff δ. The first-order change in length is thus

$$\begin{aligned}\Delta_{11} L_{12} &= \ln \frac{4 \sin^2 \frac{\hat{\vartheta}}{2}}{\hat{\delta}_L \hat{\delta}_R} - \ln \frac{4 \sin^2 \frac{\vartheta}{2}}{\delta_L \delta_R} \\ &\approx 4 \mu_{11} G \left(1 - \ln \frac{\sin 2\lambda}{\delta} \right).\end{aligned} \tag{2.51}$$

We now address the diametrically opposite case. In particular, we compute the change $\Delta_{11} L_{22}$ in L_{22} when we add tension μ_{11} on γ_{11}. As above, we apply an AdS_3 isometry to move the anchors of γ_{11} to the poles as shown in figure 2.6. Since this figure is symmetric under exchange of the two ends of γ_{22}, and since the left end of γ_{22} coincides with the right end of γ_{12}, after the transformation the cutoff at either end of γ_{22} becomes $\delta' = \delta_R$ as given by (2.47) and the angular size of γ_{22} becomes $2\lambda' = 2(\frac{\pi}{2} - \vartheta)$ in terms of (2.45).

Once again, we wish to hold fixed the locations and cutoffs in the round conformal frame when we insert the cosmic string on γ_{11}. And again we wish to apply formulae from section 2.4 that apply in the conical-frame coordinates r, θ, ϕ. We will thus need the associated conical frame cutoff $\hat{\delta} = \hat{\delta}_R$ and angular size $2\hat{\lambda} = 2(\frac{\pi}{2} - \hat{\vartheta})$. The length change is thus

$$\begin{aligned}\Delta_{11} L_{22} &= 2 \ln \frac{2 \sin \hat{\lambda}}{\hat{\delta}} - 2 \ln \frac{2 \sin \lambda}{\delta'} \\ &\approx 8 \mu_{11} G \left(1 + \left(\frac{2}{\sin^2 \lambda} - 1 \right) \ln \cos \lambda \right).\end{aligned} \tag{2.52}$$

To complete our study of the 3 possible classes of changes we need only compute $\Delta_{11} L_{11}$. From (2.33) we immediately find

$$\Delta_{11} L_{11} = -8 \mu_{11} G \ln \frac{2 \sin \lambda}{\delta}. \tag{2.53}$$

We are now ready to assemble the above results into complete expressions for the first order changes in our lengths. As described above, our three representatives $\Delta_{11} L_{11}$,

$\Delta_{11}L_{12}$, and $\Delta_{11}L_{22}$ can be used to obtain all other $\Delta_{mn}L_{ij}$ by acting with appropriate symmetries and/or replacing λ by $\frac{\pi}{2}-\lambda$. After doing so, we wish to set the tension to be constant along each of γ_d, γ_o. I.e., we impose $\mu_{11}=\mu_{22}=\mu_d$, $\mu_{12}=\mu_{21}=\mu_o$. Using the notation $\langle L_d\rangle_{\mu_o,\mu_d}$ for the expectation value of L_d in the presence of sources, we have

$$\langle L_d\rangle_{\mu_o,\mu_d} = 2\langle L_{11}\rangle_{\mu_o,\mu_d} = 2\left(\langle L_{11}\rangle_{0,0} + \Delta_{11}L_{11} + \Delta_{12}L_{11} + \Delta_{21}L_{11} + \Delta_{22}L_{11}\right) + O(\mu^2). \tag{2.54}$$

Thus we find

$$\begin{aligned}\langle L_d\rangle_{\mu_o,\mu_d} = 4\ln\frac{2\sin\lambda}{\delta} &+ 16\mu_d G(1-\ln\sin 2\lambda + \frac{2\ln\cos\lambda}{\sin^2\lambda} + \ln\delta)\\ &+ 16\mu_o G(1-\ln\sin 2\lambda+\ln\delta) + O(\mu^2).\end{aligned} \tag{2.55}$$

The corresponding expression for L_o is obtained from (2.55) by exchanging μ_d with μ_o and replacing λ by $\pi/2-\lambda$. This yields

$$\begin{aligned}\langle L_o\rangle_{\mu_o,\mu_d} = 4\ln\frac{2\cos\lambda}{\delta} &+ 16\mu_d G(1-\ln\sin 2\lambda+\ln\delta)\\ &+ 16\mu_o G(1-\ln\sin 2\lambda + \frac{2\ln\sin\lambda}{\cos^2\lambda} + \ln\delta) + O(\mu^2).\end{aligned} \tag{2.56}$$

The two point functions are thus

$$\langle L_d^2\rangle_{0,0} - \langle L_d\rangle_{0,0}^2 = -\frac{\partial}{\partial\mu_d}\langle L_d\rangle_{\mu_o,\mu_d}\Big|_{\mu_o=0,\mu_d=0} = -16G(1-\ln\sin 2\lambda + \frac{2\ln\cos\lambda}{\sin^2\lambda} + \ln\delta), \tag{2.57}$$

$$\langle L_o^2\rangle_{0,0} - \langle L_o\rangle_{0,0}^2 = -\frac{\partial}{\partial\mu_o}\langle L_o\rangle_{\mu_o,\mu_d}\Big|_{\mu_o=0,\mu_d=0} = -16G(1-\ln\sin 2\lambda + \frac{2\ln\sin\lambda}{\cos^2\lambda} + \ln\delta), \tag{2.58}$$

and

$$\langle L_dL_o\rangle_{0,0} - \langle L_d\rangle\langle L_o\rangle_{0,0} = -\frac{\partial}{\partial\mu_d}\langle_{\mu_o,\mu_d}L_o\rangle\Big|_{\mu_o=0,\mu_d=0} = -16G(1-\ln\sin 2\lambda+\ln\delta). \tag{2.59}$$

Combining these to find the variance of $(L_1 - L_2)$ yields

$$\begin{aligned} 4\sigma_-^2 &= \langle (L_d - L_o)^2 \rangle_{0,0} - \langle L_d - L_o \rangle_{0,0}^2 \\ &= \left(\langle L_d^2 \rangle - \langle L_d \rangle_{0,0}^2 \right) + \left(\langle L_o^2 \rangle_{0,0} - \langle L_o \rangle_{0,0}^2 \right) - 2 \left(\langle L_d L_o \rangle_{0,0} - \langle L_d \rangle_{0,0} \langle L_o \rangle_{0,0} \right) \\ &= -32G \left(\frac{\ln \sin \lambda}{\cos^2 \lambda} + \frac{\ln \cos \lambda}{\sin^2 \lambda} \right) \end{aligned} \tag{2.60}$$

Note that σ_-^2 is positive as required since $\cos \lambda$ and $\sin \lambda$ are less than or equal to one. From (2.21), the $O(G^{-1/2})$ correction to the entropy at the transition is thus

$$\Delta_{-1/2} S = \sqrt{\frac{\tilde{\sigma}_-^2}{8\pi G}} = \frac{\sigma_-}{\sqrt{8\pi} G} = 2\sqrt{\frac{\ln 2}{2\pi G}}. \tag{2.61}$$

The most interesting feature of (2.61) is that it is independent of the cutoff δ. This was a direct result of the fact that, while the cutoff appeared in each of (2.57), (2.58), and (2.59), it cancelled in the computation of $\tilde{\sigma}_-$. A related observation is that σ_-^2 takes on its minimal value $16G \ln 2$ at the phase transition point $\lambda = \pi/4$, though it diverges in the degenerate limits $\lambda \to 0$ or $\lambda \to \pi/2$.

Such results are in fact very natural. Since γ_o and γ_d have the same boundary anchors, the two curves will largely coincide near infinity. Contributions to the length of these curves from the asymptotic region will thus be highly correlated and will tend to cancel in computations of $L_d - L_o$. The results above show that the divergent parts of the fluctuations cancel entirely. Thus σ_- is determined by the regions of γ_d and γ_o that are widely separated. Since the length of such regions diverges in the limits $\lambda \to 0$ or $\lambda \to \pi/2$ (where one curve or the other degenerates), it is no surprise that σ_- diverges in those limits as well. Further discussion of divergences in RT-area fluctuations will be provided in section 2.6.

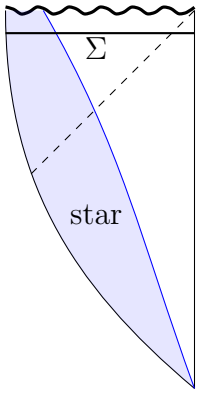

Figure 2.7: The Penrose diagram of a pure-state geometry in which matter (a 'star') collapses to become a BTZ black hole. On the surface Σ the geometry displays a long 'throat' region where the metric is *very* well-approximated by exact BTZ. On Σ, all details of the original star that collapsed to form the black hole are hidden at the bottom of this throat.

2.5.2 Example 2: BTZ black hole

Our next example is a generic pure microstate of a one-sided non-rotating BTZ black hole. The RT phase transition in this context was previously studied in e.g. [83, 68, 69]. Since the bulk spacetime has dimension 3, our RT surfaces will again be spacelike geodesics.

In the region outside the horizon, the corresponding bulk geometry should well-described by the BTZ metric

$$ds^2 = -(r_{BTZ}^2 - r_+^2)dt^2 + \frac{dr_{BTZ}^2}{r_{BTZ}^2 - r_+^2} + r_{BTZ}^2 d\varphi^2, \tag{2.62}$$

where r_+ is the horizon radius and the black hole has total energy $E = \frac{r_+^2}{8G}$ as in section 2.4. Inside the horizon the geometry may reflect the details of the microstate. But as shown in figure 2.7, any classical interior solution will evolve to have the same long throat at late times, with any microstate-dependence hidden at the bottom of the throat. One thus expects such a long throat to be common to generic microstates. Noting that this throat also appears in the two-sided eternal BTZ black hole, and that in the eternal

BTZ case spacelike geodesics starting and ending in the same boundary region never pass behind the horizon (see e.g. [84]), it follows that all relevant geodesics will lie in the exterior region. We thus restrict attention to the geometry described by (2.62).

By analytic continuation $t \to i\tau$, the associated Euclidean solution will also contain a region described by the metric

$$ds^2 = (r_{BTZ}^2 - r_+^2)d\tau^2 + \frac{dr_{BTZ}^2}{r_{BTZ}^2 - r_+^2} + r_{BTZ}^2 d\varphi^2, \tag{2.63}$$

though this will not cover the entire spacetime. In particular, the metric (2.63) will generally hold only in some range $\tau \in (-\tau_-, \tau_+)$ where τ_- and τ_+ are *not* to be identified[13]. We will consider single intervals R in the boundary at $t = 0 = \tau$, for which the RT surfaces will also lie in the bulk surface $t = \tau = 0$ that appears in both the Lorentzian and Euclidean sections.

As shown in figure 2.8, we take γ_1 to be the minimal curve in the $t = \tau = 0$ surface that is homotopic to R, and γ_2 to be the corresponding minimal curve homotopic to $\bar{R}$. Note that both γ_1 and γ_2 are homolologous to both intervals $R, \bar{R}$. Denoting the angular sizes of $R, \bar{R}$ respectively by $\pi + \eta$ and $\pi - \eta$, symmetry dictates that there will be an RT phase transition at $\eta = 0$. As in section 2.5.1, we will insert cosmic strings on γ_1, γ_2 and compute the induced changes in their lengths L_1, L_2. And just as in sections 2.4 and 2.5.1, we will again use a UV regulator defined by a scale δ on the boundary in the conformal frame where the boundary metric is $d\tau^2 + d\varphi^2$.

To compute the desired response functions $\frac{\partial}{\partial \mu_i}\langle L_j \rangle_{\mu_1,\mu_2}$, we must gain control not only over the original BTZ metric (2.63), but also over solutions deformed by the addition of cosmic strings. If we were to strictly confine our analysis to the region $-\tau_- < \tau < \tau$ where the metric (2.63) applies, this would require a choice of boundary condition at

[13]See e.g. [85, 86, 87] for discussions of particular such Euclidean geometries.

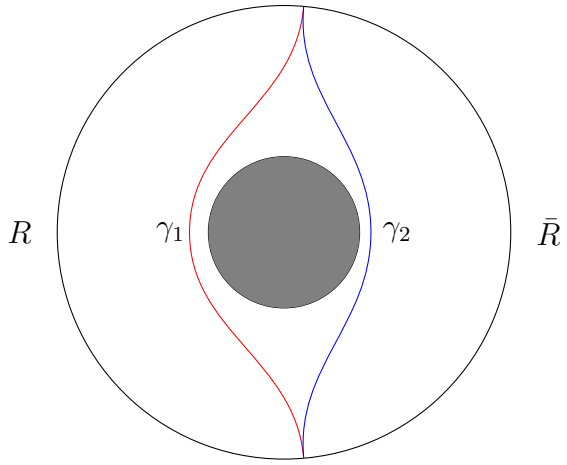

Figure 2.8: Two competing candidate RT surfaces in the BTZ black hole spacetime.

$\tau = \tau_{\pm}$. We do not wish to rely on an ad hoc such choice. But as noted above, in the relevant region of the geometry one expects our spacetime to agree precisely with the eternal *two*-sided BTZ black hole. We will therefore assume that this remains true after the addition of at least weak-tension cosmic strings. As a result, we simply compute $\frac{\partial}{\partial \mu_i}\langle L_j \rangle_{\mu_1,\mu_2}$ in the full Euclidean BTZ geometry given by (2.63) and by taking τ to have the appropriate period $\beta_{BTZ} = \frac{2\pi}{r_+}$.

As in well-known, the BTZ geometry is a quotient of global AdS_3 [71]. Lifting the geodesics γ_1, γ_2 to the AdS_3 cover will allow us to directly apply our previous results from section 2.4. In practice, this lift is accomplished by simply ignoring the fact that ϕ is periodic identified in the BTZ metric[14]. Taking the anchors of both geodesics γ_1, γ_2 to be at $\varphi = \pm\left(\frac{\pi+\eta}{2}\right)$, we see that γ_1 lifts to an infinite set of geodesics $\gamma_{1,k}$ anchored at $\varphi = \pm\left(\frac{\pi+\eta}{2}\right) + 2\pi k$, while γ_2 lifts to geodesics $\gamma_{2,k}$ anchored at $\varphi = \left(\frac{\pi+\eta}{2}\right) + 2\pi k$ and $\varphi = -\left(\frac{\pi+\eta}{2}\right) + 2\pi(k+1)$. Note that the geodesics $\gamma_{2,-1}, \gamma_{2,0}$ lie on either side of $\gamma_{1,0}$.

The results of section 2.4 were written in terms of a different set of coordinates on Euclidean AdS_3. Taking the angular coordinate τ above to be proportional to ϕ of section

[14]Since the τ-circle is contractible in BTZ, the coordinate τ remains periodic with period β_{BTZ} in the AdS_3 cover.

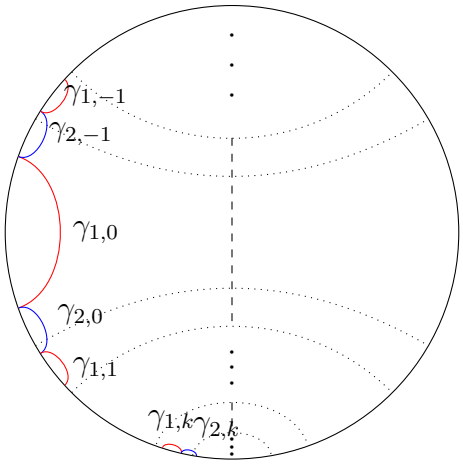

Figure 2.9: RT surfaces in the AdS_3 covering space of a BTZ black hole. One RT surface in BTZ corresponds to infinitely many ones in the covering space. The dashed lines denote the horizon. Since we are studying a one-sided black hole, only half of the space (we take it to be the left half) is relevant to us.

2.4, one may solve for the relation between our (r_{BTZ}, φ) and the (r, θ) of section 2.4. In particular, on the AdS boundary one finds

$$\theta(\varphi) = \tan^{-1}\left(\sinh(r_+\varphi)\right) + \frac{\pi}{2}. \tag{2.64}$$

Thus if R is the interval $-\frac{\pi}{2} - \frac{\eta}{2} < \varphi < \frac{\pi}{2} + \frac{\eta}{2}$ at $\tau = 0$, it also corresponds to the infinite set of intervals $\frac{\pi}{2} - \theta_k < \theta < \frac{\pi}{2} + \theta_k$ with

$$\theta_k = \tan^{-1}\left(\sinh\left((\frac{\pi}{2} + \frac{\eta}{2} + 2\pi k)r_+\right)\right). \tag{2.65}$$

For simplicity, we begin by focusing on the case $k = 0$. For this case, a cutoff δ defined in terms of the angle φ at the endpoints of R maps to a cutoff

$$\begin{aligned} \delta_0 &= \frac{1}{2}\left(\theta(\frac{\pi}{2} + \frac{\eta}{2} + \delta) - \theta(\frac{\pi}{2} + \frac{\eta}{2} - \delta)\right) \\ &\approx \frac{r_+ \cosh\left((\frac{\pi}{2} + \frac{\eta}{2})r_+\right)}{1 + \sinh\left((\frac{\pi}{2} + \frac{\eta}{2})r_+\right)}\delta \end{aligned} \tag{2.66}$$

in terms of the angle θ. With vanishing cosmic string tension the length of γ_1 is thus

$$\bar{L}_1 := \langle L_1 \rangle_{\mu_1=0,\mu_2=0} = 2 \ln \frac{2 \sin \theta_0}{\delta_0} = 2 \ln \frac{2 \sinh \left((\frac{\pi}{2} + \frac{\eta}{2}) r_+ \right)}{r_+ \delta}. \tag{2.67}$$

Since interchanging R and $\bar{R}$ changes the sign of η, applying this transformation to (2.67) yields the length of γ_2:

$$\bar{L}_2 := \langle L_1 \rangle_{\mu_1=0,\mu_2=0} = 2 \ln \frac{2 \sinh \left((\frac{\pi}{2} - \frac{\eta}{2}) r_+ \right)}{r_+ \delta}. \tag{2.68}$$

We now compute the first-order changes $\Delta_i L_j$ $(i, j \in \{1, 2\})$ in the length change of γ_j due to adding a cosmic string with tension μ_i on γ_i. In the covering space description, we could compute the change in length of any of the geodesics $\gamma_{j,n}$. However, the covering space description of inserting a cosmic string of tension μ_i on γ_i is to in fact insert cosmic strings of this same tension μ_i on *each* of the geodesics $\gamma_{i,k}$. At linear order in μ_i we may compute the effect of each such cosmic string separately and then simply sum the change induced in our given $\gamma_{j,k}$.

However, performing the above sum is equivalent to inserting a cosmic string on a given geodesic (say, $\gamma_{1,0}$ or $\gamma_{2,0}$), computing the first order change in length for each $\gamma_{1,n}$ or each $\gamma_{2,n}$, and again summing the results. We will find this perspective to be more convenient in making use of our results from section 2.4. We will thus study the first-order changes $\Delta_1 L_{1,k}$, $\Delta_1 L_{2,k}$ in the lengths of $\gamma_{1,k}, \gamma_{2,k}$ associated with putting a cosmic string on $\gamma_{1,0}$. We can then later then obtain results for strings on $\gamma_{2,0}$ by changing the sign of η.

We begin with $\Delta_1 L_{1,k}$. As in section 2.4, we apply an AdS_3 isometry to move the anchors of $\gamma_{1,0}$ to the $\theta = 0$ and $\theta = \pi$ so that $\gamma_{1,0}$ now lies along the ϕ-axis; see figure 2.10. Before applying this transformation, the angular coordinates θ of the endpoints of

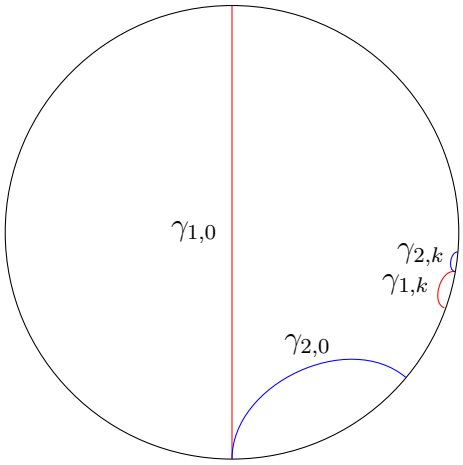

Figure 2.10: The representative geodesics $\gamma_{1,0}$, $\gamma_{2,0}$, $\gamma_{1,k}$ and $\gamma_{2,k}$ from figure 2.9 are shown after applying an AdS_3 isometry to move $\gamma_{1,0}$ into the standard position along the ϕ-axis.

$\gamma_{1,k}$ are

$$\theta^{(k)}_{L/R} = \tan^{-1}\left(\sinh[r_+(\mp\frac{\pi}{2} \mp \frac{\eta}{2} + 2\pi k)]\right) + \frac{\pi}{2} \tag{2.69}$$

with $\phi = 0$. After the transformation, they become

$$\tilde{\theta}^{(k)}_{L/R} = \pi - \sin^{-1}\frac{-\sin\left(\pi - \theta^{(k)}_{L/R}\right) + \cos\theta_1}{1 - \sin\left(\pi - \theta^{(k)}_{L/R}\right)\cos\theta_1}, \tag{2.70}$$

with $\phi = \pi$. The cutoffs will again become some $\tilde{\delta}^{(k)}_L$ and $\tilde{\delta}^{(k)}_R$.

We now wish to add a cosmic string of tension $\mu_1 = \frac{1-\alpha_1}{4G}$ on the ϕ axis, holding fixed both the cutoffs and the anchors for the geodesics in the round conformal frame. But we will also need the values of these parameters in the conical frame, which by (2.28) are the 'hatted' values

$$\hat{\theta}^{(k)}_{L/R} = 2\tan^{-1}\left(\tan^{\alpha_1}\frac{\tilde{\theta}^{(k)}_{L/R}}{2}\right) \tag{2.71}$$

$$\hat{\delta}^{(k)}_{L/R} \approx \frac{2\alpha_1\cot^{\alpha_1}\frac{\tilde{\theta}^{(k)}_{L/R}}{2}}{\sin\tilde{\theta}^{(k)}_{L/R}(1+\cot^{2\alpha_1}\frac{\tilde{\theta}^{(k)}_{L/R}}{2})}\tilde{\delta}^{(k)}_{L/R}. \tag{2.72}$$

The above results allow us to read off the change in length by making appropriate use of (2.34). This is most straightforward for the case $k = 0$ where geodesic $\gamma_{1,0}$ of interest lies on the conical singularity. That was the setting considered in the derivation of (2.33), so we need only recall that our conical parameter is $\alpha_1 = 1 - 4\mu_1 G$ and that at $\alpha_1 = 1$ the length is $\bar{L}_1$ as given by (2.67). Eq. (2.33) then gives $L_{1,0} = \alpha_1 \bar{L}_1$ from which we find

$$\Delta_1 L_{1,0} = -8\mu_1 G \ln \frac{2\sinh\left((\frac{\pi}{2} + \frac{\eta}{2})r_+\right)}{r_+ \delta}. \tag{2.73}$$

In contrast, for $k \neq 1$ we study geodesics $\gamma_{1,k}$ with no conical singularity. In vacuum AdS_3, the length of such geodesics is given by (2.34) with $\alpha = 1$ and cutoffs $\delta_R = \tilde{\delta}_R$ and $\delta_L = \tilde{\delta}_L$ defined in the round frame. We wish to hold fixed these round-frame cutoffs when computing $\Delta_1 L_{1,k}$. But when we add a conical singularity elsewhere in the spacetime, the length of $\gamma_{1,k}$ is given by (2.34) (still with $\alpha = 1$ in that expression) if we insert the cutoffs $\delta_R = \hat{\delta}_R^{(k)}, \delta_L = \hat{\delta}_L^{(k)}$ and the angular size $\lambda = \hat{\lambda}^{(k)} := \frac{\hat{\theta}_L^{(k)} - \hat{\theta}_R^{(k)}}{2}$ associated with the *conical* frame. As a result, for $k \neq 0$ we find

$$\begin{aligned}
\Delta_1 L_{1,k} &= \ln \frac{4\sin^2 \frac{\hat{\theta}_L^{(k)} - \hat{\theta}_R^{(k)}}{2}}{\hat{\delta}_L^{(k)} \hat{\delta}_R^{(k)}} - \ln \frac{4\sin^2 \frac{\tilde{\theta}_L^{(k)} - \tilde{\theta}_R^{(k)}}{2}}{\tilde{\delta}_L^{(k)} \tilde{\delta}_R^{(k)}} \\
&= 4\mu_1 G \left(2 + \frac{\sin \frac{\tilde{\theta}_L^{(k)} + \tilde{\theta}_R^{(k)}}{2}}{\sin \frac{\tilde{\theta}_L^{(k)} - \tilde{\theta}_R^{(k)}}{2}} \ln \frac{\tan \frac{\tilde{\theta}_L^{(k)}}{2}}{\tan \frac{\tilde{\theta}_R^{(k)}}{2}} + O(\mu_1^2) \right) \\
&= 4\mu_1 G f(k, \eta) + O(\mu_1^2),
\end{aligned} \tag{2.74}$$

where $f(k, \eta)$ is

$$\begin{aligned}
f(k, \eta) =& 2 - \frac{1 - 2\cosh[2kr_+\pi] + \cosh[r_+(\pi + \eta)]}{2\sinh^2[(\pi + \eta)\frac{r_+}{2}]} \\
& \ln \frac{\left(\cosh[(\pi + \eta)\frac{r_+}{2}] - \cosh[((4k-1)\pi - \eta)\frac{r_+}{2}]\right) \sinh^2[((2k+1)\pi + \eta)\frac{r_+}{2}]}{\left(\cosh[(\pi + \eta)\frac{r_+}{2}] - \cosh[((4k+1)\pi + \eta)\frac{r_+}{2}]\right) \sinh^2[kr_+\pi]}.
\end{aligned} \tag{2.75}$$

Note that $f(k,\eta)$ vanishes exponentially as $k \to \infty$. In particular, $\lim_{k\to\infty} |\frac{f(k+1,\eta)}{f(k,\eta)}| < 1$, so the sum $\sum_{k=1}^{\infty} f(k,\eta)$ converges. Furthermore, (2.74) is completely independent of the choice of cutoffs.

For $k \neq -1, 0$ the computation of $\Delta_1 L_{2,k}$ proceeds in precisely the same way. Indeed, it is identical to the computation of (2.74) with k replaced by $k + 1/2$ in all expressions and with η replaced by $-\eta$ in the expressions for $\theta^{(k)}_{L/R}$ and the associated cutoffs (but with η unchanged in the expressions for θ_1 and δ_1). As a result, we find

$$\Delta_1 L_{2,k} = 4\mu_1 G g(k,\eta) + O(\mu_1^2), \tag{2.76}$$

with

$$\begin{aligned} g(k,\eta) = 2 - \frac{\cosh[r_+\pi] - 2\cosh[(1+2k)r_+\pi] + \cosh[r_+\eta]}{\cosh[r_+\pi] - \cosh[r_+\eta]} \\ \ln \frac{e^{r_+\eta}(e^{2kr_+\pi} - 1)(e^{2(1+k)r_+\pi} - 1)}{(e^{(1+2k)r_+\pi} - e^{r_+\eta})(e^{r_+(1+2k)\pi + r_+\eta} - 1)}. \end{aligned} \tag{2.77}$$

Note that $g(k,\eta)$ is an even function of η as required by the symmetry of figure 2.9.

The remaining cases $\Delta_1 L_{2,0}$ and $\Delta_1 L_{2,-1}$ are identical by symmetry; see again figure 2.9. Let us concentrate on $\Delta_1 L_{2,0}$. This case differs from the above in that $\gamma_{2,0}$ meets the conical singularity at the boundary. After using an AdS isometry to place the conical singularity on the ϕ-axis as usual, the left anchor of $\gamma_{2,0}$ becomes $\tilde{\theta}_L = \pi$ and the right anchor becomes $\tilde{\theta}_R = \tilde{\theta}^{(1)}_L$. The transformed cutoffs are $\tilde{\delta}_L = \frac{\delta}{\sin\theta_0}$ (with θ_0 again given by (2.65) with $k = 0$) and $\tilde{\delta}_R = \tilde{\delta}^{(1)}_L$. As usual, we hold these quantities fixed in the round conformal frame, but we will need to insert the conical frame values into (2.33). After

inserting the cosmic string on $\gamma_1^{(0)}$, the conical frame parameters become

$$\begin{aligned} &\hat{\theta}_L = \pi, \quad \hat{\theta}_R = \hat{\theta}_L^{(1)}, \\ &\hat{\delta}_L = 2\left(\frac{\tilde{\delta}_L}{2}\right)^{\alpha_1} = 2\left(\frac{\delta}{2\sin\theta_0}\right)^{\alpha_1} \\ \text{and} \quad &\hat{\delta}_R = \hat{\delta}_L^{(1)}. \end{aligned} \tag{2.78}$$

We thus find

$$\Delta_1 L_{2,0} = 4\mu_1 G\left(1 - \ln\frac{\cosh r_+\pi - \cosh r_+\eta}{r_+\delta\sinh r_+\pi}\right). \tag{2.79}$$

Combing these results and applying symmetries as needed to obtain changes not directly computed above yields a complete first-order expression for the length of γ_1:

$$\begin{aligned} \langle L_1\rangle_{\mu_1,\mu_2} =&\bar{L}_1 + \Delta_1 L_{1,0} + 2\Delta_2 L_{1,0} + 2\sum_{k=1}^{\infty}\Delta_{1,k}L_{1,0} + 2\sum_{k=1}^{\infty}\Delta_{2,k}L_{1,0} + O(\mu^2) \\ =&(2-8\mu_1 G)\ln\frac{2\sinh\left((\frac{\pi}{2}+\frac{\eta}{2})r_+\right)}{r_+\delta} + 8\mu_2 G\left(1 - \ln\frac{\cosh r_+\pi - \cosh r_+\eta}{r_+\delta\sinh r_+\pi}\right) \\ &+ 8\mu_1 G\sum_{k=1}^{\infty} f(k,\eta) + 8\mu_2 G\sum_{k=1}^{\infty} g(k,\eta) + O(\mu^2) \end{aligned} \tag{2.80}$$

Since L_2 can be obtained from L_1 by changing the sign of η and exchanging μ_1 and μ_2, we also find

$$\begin{aligned} \langle L_2\rangle_{\mu_1,\mu_2} =&(2-8\mu_2 G)\ln\frac{2\sinh\left((\frac{\pi}{2}-\frac{\eta}{2})r_+\right)}{r_+\delta} + 8\mu_1 G\left(1 - \ln\frac{\cosh r_+\pi - \cosh r_+\eta}{r_+\delta\sinh r_+\pi}\right) \\ &+ 8\mu_2 G\sum_{k=1}^{\infty} f(k,-\eta) + 8\mu_1 G\sum_{k=1}^{\infty} g(k,\eta) + O(\mu^2) \end{aligned} \tag{2.81}$$

It is now straightforward to compute the desired two-point functions:

$$\langle L_1^2\rangle_{0,0} - \langle L_1\rangle_{0.0}^2 = -\frac{\partial}{\partial\mu_1}\langle L_1\rangle_{\mu_1,\mu_2}\Big|_{\mu_1=\mu_2=0} = 8G\left(\ln\frac{2\sinh\left((\frac{\pi}{2}+\frac{\eta}{2})r_+\right)}{r_+\delta} - \sum_{k=1}^{\infty} f(k,\eta)\right) \tag{2.82}$$

$$\langle L_2^2\rangle_{0,0} - \langle L_2\rangle_{0,0}^2 = -\frac{\partial}{\partial\mu_2}\langle L_2\rangle_{\mu_1,\mu_2}\Big|_{\mu_1=\mu_2=0} = 8G\left(\ln\frac{2\sinh\left((\frac{\pi}{2}-\frac{\eta}{2})r_+\right)}{r_+\delta} - \sum_{k=1}^{\infty} f(k,-\eta)\right) \tag{2.83}$$

$$\begin{aligned}\langle L_1L_2\rangle_{0,0} - \langle L_1\rangle_{0,0}\langle L_2\rangle_{0,0} &= -\frac{\partial}{\partial\mu_1}\langle L_2\rangle_{\mu_1,\mu_2}\Big|_{\mu_1=\mu_2=0} \\ &= 8G\left(\ln\frac{\cosh(r_+\pi)-\cosh(r_+\eta)}{r_+\delta\sinh(r_+\pi)} - 1 - \sum_{k=1}^{\infty} g(k,\eta)\right).\end{aligned} \tag{2.84}$$

In particular, the variance of $L_- = (L_1 - L_2)/2$ is

$$\begin{aligned}\sigma_-^2 =& 2G\left(\ln\frac{4\sinh^2(r_+\pi)\sinh\left(\left(\frac{\pi}{2}+\frac{\eta}{2}\right)r_+\right)\sinh\left(\left(\frac{\pi}{2}-\frac{\eta}{2}\right)r_+\right)}{\left(\cosh(r_+\pi)-\cosh(r_+\eta)\right)^2} + 2\right. \\ &\left. - \sum_{k=1}^{\infty}\left(f(k,\eta)+f(k,-\eta)-2g(k,\eta)\right)\right).\end{aligned} \tag{2.85}$$

While the full expressions above are somewhat complicated, one should recall that both f and g fall off exponentially. As a result, at large r_+ one can ignore the sum over images. In particular, in that limit σ_-^2 is given by just the first line in (2.85). As in section 2.5.1, the variance σ_-^2 is independent of the cutoff δ, though δ appears linearly in $\langle L_1^2\rangle_{0,0} - \langle L_1\rangle_{0.0}^2$, $\langle L_2^2\rangle_{0,0} - \langle L_2\rangle_{0.0}^2$, and $\langle L_1L_2\rangle_{0,0} - \langle L_1\rangle_{0,0}\langle L_2\rangle_{0,0}$.

2.5.3 Agreement with ETH

As described in section 2.5.2, we may think of the analysis performed there as applying to a generic microstate of the BTZ black hole with some given energy E. From the perspective of the dual CFT this is just a generic state with the given energy. Furthermore, as noted in the introduction, when the volume of the CFT becomes large this

reduces to the setting analyzed by Murthy and Srednicki [65] using the eigenstate thermolization hypothesis (ETH). We now confirm that our results coincide with theirs in the desired limit.

In particular, [65] considered a system of total volume V partitioned into two parts with volumes $V_1 + V_2 = V$. In the limit where V_1, V_2 are both large, and ignoring terms that scale with subleading powers of V, we may also identify separate energies E_1, E_2 and density-of-states functions[15] $S_1(E_1), S_2(E_2)$ for the two parts that satisfy $E \approx E_1 + E_2$ and $S(E_1, E_2) \approx S_1(E_1) + S_2(E_2)$. Here $S(E_1, E_2)$ is the logarithm of the total number of states with the given partition of the energy E, and we use the symbol $\approx$ to make explicit that we have kept only terms that are extensive in the sense that they proportional to one of the volumes V_1 or V_2. As in section 2.5.2, we take subsystem 1 to be associated with the boundary interval R and subsystem 2 to be associated with $\bar{R}$.

Typical microstates with energy E will have subsystem energies $\bar{E}_1, \bar{E}_2$ determined by the constraint $E = \bar{E}_1 + \bar{E}_2$ and the usual thermodynamic equilibrium condition

$$\frac{1}{T_1} := \frac{dS_1}{dE_1}|_{\bar{E}_1} = \frac{dS_2}{dE_2}|_{\bar{E}_2} =: \frac{1}{T_2}, \tag{2.86}$$

which allows us to define a temperature $T = T_1 = T_2$. The analysis of [65] found such states to have entanglement

$$S_{ent}(E) = \min\left(S_1(\bar{E}_1), S_2(\bar{E}_2)\right) - \sqrt{\frac{2K}{\pi}}\Phi\left(\frac{S_2(E - \bar{E}_1) - S_1(\bar{E}_1)}{\sqrt{8K}}\right), \tag{2.87}$$

where Φ is again given by (2.22) and

$$\frac{1}{K} := T^2\left(\frac{d^2S_1}{dE_1^2}|_{\bar{E}_1} + \frac{d^2S_2}{dE_2^2}|_{\bar{E}_2}\right). \tag{2.88}$$

[15]These are the usual thermodynamic entropies defined as the logarithm of the number of states of each subsystem with the given energies.

Comparing (2.87) with our expression (2.21), we see that they agree if

$$S_1(\bar{E}_1) = \frac{\bar{L}_1}{4G}, \quad S_2(\bar{E}_2) = \frac{\bar{L}_2}{4G}, \quad K = \frac{\tilde{\sigma}_-^2}{32G}. \tag{2.89}$$

Our main task is thus to identify the functions $S_1(E_1), S_2(E_2)$ for the relevant limit of the BTZ system studied in section 2.5.2. Doing so requires an understanding of black hole geometries that have independent energies E_1, E_2 in regions R and $\bar{R}$ at the given time $t = 0$ (though energy will flow between these regions under time evolution due to the intrinsic couplings between the two). In particular, we must allow the energy densities at $t = 0$ to differ between R and $\bar{R}$.

The limit studied by [65] involves taking a large volume. But since our system is to be thought of as dual to a conformal field theory, any large volume limit is equivalent to the limit of high temperatures (or, perhaps better, the limit of large energy densities) taken with the volume V held fixed. We may then define the energy E_1 of region R by integrating the CFT energy density over R, and similarly for the energy E_2 of $\bar{R}$. To define a good operator in the CFT we should also apply an appropriate smoothing at the boundary ∂R between R and $\bar{R}$, though this is often not needed if we simply discuss expectation values. In either case, we find $E \approx E_1 + E_2$ in the desired limit.

To leading order in the limit of large volumes or high temperatures, we can study the thermodynamics of each region R and $\bar{R}$ by treating the regions as homogeneous independent CFTs. The density of states of each region is then given by the thermal entropy of the CFT at energy E_i on a space of volume V_i; i.e.

$$S_i(E_i) \approx 2\pi \sqrt{\frac{cE_iV_i}{6}}, \tag{2.90}$$

where we have used the Cardy approximation appropriate to our high temperature limit

and $c = \frac{3}{2G}$ is the CFT central charge since we have set the bulk AdS scale ℓ to one[16].

It is now manifest that we will find $S_1(\bar{E}_1) = \frac{\bar{A}_1}{4G}$ and $S_2(\bar{E}_2) = \frac{\bar{A}_2}{4G}$, though this can also be verified by direction computation using (2.67) and (2.68) in the limit of large $E = \frac{r_+^2}{8G}$. Furthermore, the standard deviation $\tilde{\sigma}_-$ of our fixed-area discussion is easily extracted from the two-point functions (2.82), (2.83), and (2.84). At leading order in large r_+ we find

$$\frac{\tilde{\sigma}_-^2}{32G} \approx \frac{(\pi^2 - \eta^2) r_+}{8G\pi}. \tag{2.91}$$

It thus remains only to compute (2.88) and compare with (2.91). In terms of the parameter η from 2.5.2 and the bulk Newton constant G and the energy E_1, Cardy's formula (2.90) becomes

$$S(\bar{E}_1) = \frac{\pi + \eta}{4G} \sqrt{\frac{2\pi}{\pi + \eta} E_1}, \quad \text{and} \tag{2.92}$$

$$S(\bar{E}_2) = \frac{\pi - \eta}{4G} \sqrt{\frac{2\pi}{\pi - \eta} (E - E_1)}. \tag{2.93}$$

Using (2.88) then gives

$$K = \frac{(\pi^2 - \eta^2) r_+}{8G\pi}, \tag{2.94}$$

which agrees with (2.91) as desired. So in the relevant limit our analysis does indeed reproduce the results of [65].

[16]One can of course also derive this result from the AdS_3 bulk. To do so, one notes that a general solution to Einstein-Hilbert AdS_3 gravity is just a BTZ black hole with some choice of conformal frame. As we are interested in thermal entropies, so that the full CFT can be in a mixed state, one then computes the RT entropies for R and $\bar{R}$ using surfaces that are *homotopic* to R, $\bar{R}$ as a function of the BTZ parameters and this conformal transformation. Holding the UV cutoff fixed, at leading order in large energy density maximizing the RT areas at fixed energies E_1, E_2 will give the desired result. Indeed, in a general theory of gravity one should expect the generic high energy-density state with energies E_1, E_2 at $t = 0$ to strongly resemble a black hole of total energy $\frac{E_1 V}{V_1}$ in region R but to also strongly resemble a black hole of total energy $\frac{E_2 V}{V_2}$ in region $\bar{R}$. This can be seen, for example, by considering the thermofield-double-like state defined by a Euclidean path integral where the period of Euclidean time is tuned independently in R and $\bar{R}$ to obtain the desired energies and using a Euclidean version [88] of the fluid-gravity correspondence [89, 90, 91]. The corresponding Renyi problem was recently discussed in [47].

2.5.4 Comparison with a simple quantum RT transition

In the above sections we have examined corrections to the RT entropy near RT phase transitions. However, such phase transitions are very similar to the phase transitions associated with quantum extremal surfaces discussed in e.g. [37, 36, 38, 39]. Let us in particular consider the simple model described in section 2 of [38], which considers a black hole in Jackiw-Teitelboim gravity with an end-of-the-world brane behind the horizon. The end-of-the-world-brane can appear in any of k flavors. There is then a *quantum* RT phase transition associated with whether the entropy $\ln k$ of the state on the end-of-the-world brane exceeds the Bekenstein-Hawking entropy S_{BH} of the black hole. When S_{BH} is the larger of the two, the (quantum) RT surface is the emptyset and the entire spacetime lies in the entanglement wedge of the boundary. In contrast, if the end-of-the-world brane entropy is larger, the quantum RT surface lies instead at the black hole horizon and an 'island' [92] forms inside.

Although this is technically a quantum-RT transition, quantum mechanics plays very little role in the discussion. In particular, for the non-trivial extremal surface the entropy is well approximated by $A/4G$. And for the trivial extremal surface, the (generalized) entropy is effectively a constant determined by the choice of end-of-the-world brane state. It may thus be reasonable to expect that our arguments above would apply to this case as well. We confirm this below, though we leave a full discussion of quantum phase transitions for future work.

In particular, in the semiclassical limit of large temperature $1/(\beta G) \gg 1$ and with large end-of-the-world brane tension $\mu_{EOW} \gg 1/(\beta G)$, the details of their phase transition are studied in appendix F of [38] via a careful computation using the replica trick. At the phase transition, the actual entropy is again found to be smaller than $A/4G$ by a

correction

$$\Delta_{-1/2}S = \sqrt{\frac{2\pi}{\beta G}}. \tag{2.95}$$

We wish to verify that this result also follows from (2.21) if we simply set $A_2 = \ln k$ (without fluctuations). As a result, $4\sigma_-^2 = \sigma_1^2$ and it remains only to determine the width of fluctuations in the horizon area A_1.

This width can be extracted from their n-replica partition functions

$$Z_n = e^{S_0} \int ds \rho(s) y(s)^n, \tag{2.96}$$

where

$$\rho(s) = \frac{s}{2\pi^2} \sinh(2\pi s), \tag{2.97}$$

$$y(s) = e^{-\frac{\beta G s^2}{2}} 2^{1-2\mu_{EOW}} \left| \Gamma\left(\mu_{EOW} - \frac{1}{2} + is\right) \right|^2. \tag{2.98}$$

In the limit $\mu_{EOW} \gg 1/\beta G$, the integrand can be approximated by

$$\rho(s) y(s)^n \sim \frac{s}{2\pi^2} y(0)^n e^{2\pi s - n\beta G s^2/2}. \tag{2.99}$$

The saddle point is

$$s^{(n)} = \frac{2\pi}{n\beta G}. \tag{2.100}$$

We may thus define an on-shell action I_n by inserting $s^{(n)}$ into the exponent of (2.99) to find

$$I_n = \frac{2\pi^2}{n\beta G}. \tag{2.101}$$

The n-replica saddle-points should represent smooth geometries, but taking a $\mathbb{Z}_n$ quotient of such geometries should give spacetimes with a single boundary and a $\mathbb{Z}_n$ conical defect. The fixed-defect-angle action $I_1(n)$ in such cases is generally I_n/n (see [33] and also [73]

for further details of such actions). We thus find

$$I_1(n) := \frac{I_n}{n} = \frac{2\pi^2}{n^2 \beta G}, \tag{2.102}$$

where the conical defect tension μ satisfies

$$n = \frac{1}{1 - 4\mu G}. \tag{2.103}$$

It now straightforward to analytically continue the result (2.102) to all real μ. As in section 2.3, the variance of the RT area A_1 can be obtained by taking the second derivative of I_1 with respect to μ:

$$\sigma_1^2 = \left(\frac{\partial^2 I_1}{\partial \mu^2} \right)_{T \to 0} = \frac{64\pi^2 G}{\beta}. \tag{2.104}$$

Inserting (2.104) into (2.21) gives (2.95) in agreement with [38]

2.6 Discussion

Our work above studied corrections to the Ryu-Takayanagi entropy of holographic systems near an RT-phase transition in the semiclassical limit. Using a decomposition into fixed-area states we found that, when a so-called diagonal approximation holds, the result can be written in the form (2.21). In particular, at the phase transition where the mean value $\bar{A}_1 - \bar{A}_2$ vanishes, we find a correction of order $G^{-1/2}$ controlled by the width $\sigma_- = G^{1/2}\tilde{\sigma}_-$ of the fluctuations in $(A_1 - A_2)/2$. This correction is parametrically larger than corrections associated with the entropy of bulk quantum fields.

However, it also decays exponentially in $|A_1 - A_2|$ as one moves away from the transition. In particular, just as in [65], with this correction the entanglement becomes a

smooth function of all parameters. The RT 'phase transition' has thus become a crossover already at this level of analysis, though in the limit $G \to 0$ the crossover happens very quickly and one recovers the sharp transition of the standard classical RT-surfaces.

This behavior is very different from the $O(N)$ corrections described in [93] for 2d Yang-Mills. Although that theory admits a 'bulk' closed string expansion, the strings are light. As a result, they give rise to D-brane-like (and thus $O(N)$) contributions to general entropies [94, 95], regardless of proximity to a phase transition. In contrast, stringy modes appear to play no role in our effect.

The interesting question that we have not addressed is just when this diagonal approximation should hold. We conjecture that it holds for arbitrary holographic states, but this remains to be verified. What we have done in this regard is to compare our (2.21) with the exact results at this order that are known in two cases. The first was the large mass limit of (pure microstates of) BTZ black holes. If we take the black hole to be in an energy eigenstate, then since the dual theory is conformal this limit is equivalent to the large volume limit studied by Murthy and Srednicki in [65]. We found in section 2.5.3 that our results coincide with theirs in the desired limit.

Now, one might ask if the condition that the black hole is an energy eigenstate might enforce our diagonal approximation even if the approximation were to fail more generally. And indeed, for classical saddles that contribute to holographic Renyi computations, one expects the areas A_1, A_2 to be functions of the energies E_1, E_2 of the two parts of the system (R and $\bar{R}$). As a result, since $E_1 + E_2 = E$ is fixed, given two pairs of areas, (A_1, A_2) and (A_1', A_2') either the pairs coincide ($A_1 = A_1'$ and $A_2 = A_2'$), or both areas differ ($A_1 \neq A_1'$ *and also* $A_2 \neq A_2'$). But as described in section 2.3.2, the saddles that give possible off-diagonal contributions require at least one area in each Renyi copy to coincide with one area in the next. So there are no off-diagonal contributions with $A_1 \neq A_1'$ *and also* $A_2 \neq A_2'$ and the diagonal approximation should hold.

On the other hand, one can give a state-counting argument that generalizes the argument of [65] to generic states with a given expectation value of the energy, but which leaves the result unchanged[17]. This removes the above constraint and allows off-diagonal saddles to contribute. Yet we continue to find agreement with the computations of section 2.5.2. Indeed, our analysis made no use of any assumption regarding the width of fluctuations in the total energy of the black hole.

We take this as encouraging evidence in favor of our conjecture. However, one can expect the diagonal approximation to fail for carefully chosen non-generic states, and there remains the possibility that at least some holographic states are non-generic in just the required way – though this cannot be the case for pure microstates of BTZ.

We also performed what appears to be an independent check on our conjecture by comparing (2.21) with the results of [38] for their quantum RT-transition. While we have not analyzed quantum transitions in detail, one would expect analogous results to hold, and especially so for the special case considered in [38] where the quantum contributions are fixed and do not fluctuate. And indeed we find our (2.21) to exactly reproduce the $G^{-1/2}$ correction of [38].

A by-product of the computations in our examples was to investigate the cutoff dependence of fluctuations in RT-areas. In AdS_3, we found RT-surfaces anchored to the boundary to have fluctuations whose variance is of order $-\ln\delta$, and thus whose width is of order $\sqrt{-\ln\delta}$. They thus diverge as $\delta \to 0$, but do so more slowly than the RT-lengths themselves (which are of order $\ln\delta$). Furthermore, given two extremal surfaces γ_1, γ_2 anchored at the same boundary points, the *difference* in their lengths $L_1 - L_2$ has finite (cutoff-independent) fluctuations as $\delta \to 0$.

It is straightforward to see that similar results must hold in complete generality and in all dimensions. First, recall from section 2.5 that fluctuations are related to expected

[17]We thank Chaitanya Murthy and Mark Srednicki for sharing their notes on this point.

RT-areas via

$$\langle A_i A_j \rangle_{0,0} - \langle A_i \rangle_{0,0} \langle A_j \rangle_{0,0} = -\frac{\partial}{\partial \mu_i} \langle A_j \rangle_{\mu_1,\mu_2} \Big|_{\mu_1=\mu_2=0}. \tag{2.105}$$

In general, the divergences (or cutoff-dependences) of the variance RT-area fluctuations will agree with those of RT-areas A at general tensions μ, so that the width of such fluctuations scales like $A^{1/2}$. This result is also to be expected physically, as the fluctuations should be local. Since uncorrelated fluctuations add in quadrature, summing such fluctuations over all area elements of the RT-surface must again give fluctuations in the total area A that scale like $A^{1/2}$.

In contrast, the cancellation of divergences that occurs in fluctuations of $A_1 - A_2$ occurs precisely because the surfaces γ_1, γ_2 largely coincide near the AdS boundary, so that correlations between their area-fluctuations are naturally strong. That fluctuations of $A_1 - A_2$ will always be finite can be seen by recalling that any two extremal surfaces γ_1, γ_2 with the same boundary anchor set ∂R in fact coincide near the boundary to all orders in the Fefferman-Graham expansion that give divergent contributions to A_1 and A_2 [96]. Since this is the case for all smooth geometries with arbitrary matter sources, it will remain true in the conical limit where the sources become cosmic branes. Thus $A_1 - A_2$ is manifestly finite at general tensions μ_1, μ_2. Using (2.105) to write

$$\langle (A_1 - A_2)^2 \rangle_{0,0} - \langle A_1 - A_2 \rangle_{0,0}^2 = \left(\frac{\partial}{\partial \mu_2} - \frac{\partial}{\partial \mu_1} \right) \langle A_1 - A_2 \rangle_{\mu_1,\mu_2} \Big|_{\mu_1=\mu_2=0}, \tag{2.106}$$

we see immediately that the desired fluctuations are finite as well. The same argument indicates that one should be able to construct a holographically-renormalized bulk action for spacetimes with finite-tension cosmic branes anchored on the boundary, and similarly for spacetimes with boundary-anchored fixed-area surfaces. We hope to return to the explicit construction of such actions in subsequent work.

It would also be interesting to explore other properties of fluctuations about holographic bulk saddles. In particular, we saw above that fluctuations smooth out the classically-sharp RT phase transition of the entanglement entropy into a smooth crossover. But in addition to this entropy, RT phase transitions also control the size and shape of the bulk entanglement wedge that can be recovered from a given boundary region R. Fluctuations in bulk geometry should thus play a key role in smoothing out such transitions in the bulk reconstruction map. Indeed, a natural extrapolation of our use of the diagonal approximation in section 2.3 would be to *also* assume that we may approximate the bulk reconstruction map at any $\bar{A}_1 - \bar{A}_2$ by using ρ_D from (2.12), and taking the map to be the standard one determined by $\min(A_1, A_2)$ for each term in the sum over fixed-areas A_1, A_2. This seems like to follow from the diagonal conjecture for entropy via a suitable generalization of the arguments in [75] and [24], though we leave exploration of the implications this conjecture and full justification for future work.

Chapter 3

The spacetime geometry of fixed-area states in gravitational systems

3.1 Introduction

The study of entropy and quantum entanglement is a central focus of modern treatments of the AdS/CFT correspondence and its possible generalizations. In general, for a given boundary region R, the Hubeny-Rangamani-Takayanagi (HRT) [27] generalization of the Ryu-Takayanagi formula [66] tells us that the entropy of region R in the dual CFT is given by $\frac{A[\gamma_R]}{4G}$ where G is the bulk Newton constant and $A[\gamma_R]$ is the area of the smallest extremal surface γ_R satisfying both $\partial\gamma_R = \partial R$ and the requirement that R and γ_R be homologous within some Cauchy surface [77, 78]. The proof of this relation [34] generalizes the Lewkowycz-Maldacena argument [33] for the time-symmetric case.

As a result, the area $A[\gamma_R]$ of the HRT surface γ_R plays a critical role in many discussions of AdS/CFT. It is thus natural to study bulk states in which the distribution

of $A[\gamma_R]$ is sharply peaked with only very small fluctuations. Such 'fixed-area' states were introduced in Refs. [48, 47] to reproduce the entanglement properties of simple tensor network models of quantum error correction[1] [98, 99] and have since proved to be useful for a variety of constructions and analyses; see e.g. [79, 73, 100, 38, 7, 72, 101]. This is in part due to the fact that the replica trick is particularly straightforward to apply to fixed-area states, as there is a sense in which the usual back-reaction associated with replica numbers $n \neq 1$ vanishes for fixed-area states [48, 47].

Our goal here is to explore and elucidate the spacetime geometries associated with such states. While the original works [48, 47] observed that saddles for Euclidean path integrals *preparing* such states will generally feature conical singularities at the fixed-area surface, the spacetime geometry *intrinsic to* fixed-area states has received relatively little attention. This has led to some confusion in the literature, especially with regard to the relation between fixed-area states and the microcanonical thermofield-double in the presence of a time-translation symmetry [102]. We now discuss this apparent puzzle as an appetizer to our general treatment of the spacetime geometry of fixed-area states.

A possible confusion: the Microcanonical TFD vs Fixed-area states

Fixed-area states may be constructed by starting from a seed state $|\psi\rangle$ and applying a quasi-projection operator that, for a given boundary region R, restricts the probability distribution of the HRT area to be sharply peaked around a particular value A_0. From Refs. [48, 47], it is also known that the entanglement spectrum of a fixed-area state is quite flat, so that the eigenvalues of the modular Hamiltonian $\hat{K}_R$ are also sharply peaked.

[1] Though one may also construct similar tensor network models with more general entanglement properties by adding additional degrees of freedom to the tensor network [97].

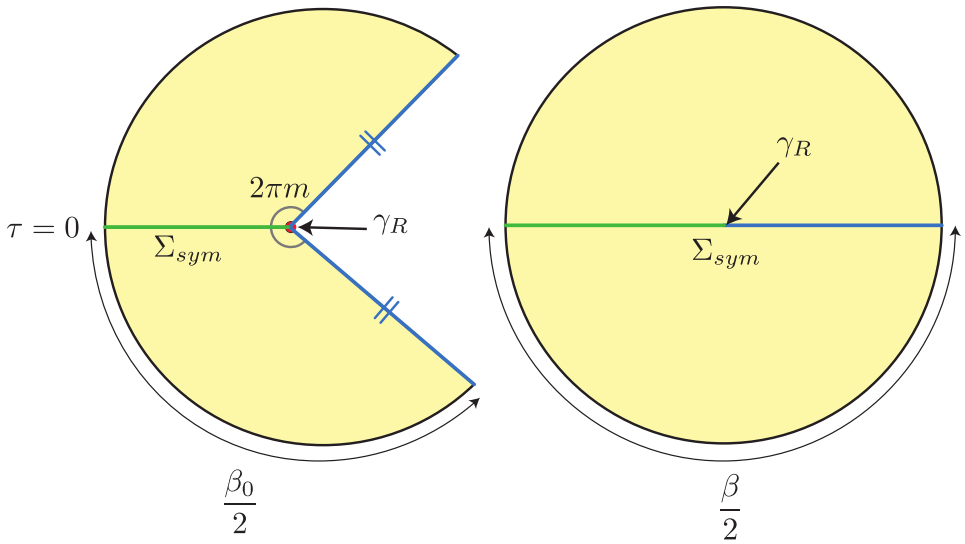

Figure 3.1: Left: Starting from a TFD state with inverse temperature β_0, fixing the area of the HRT surface γ_R, corresponding to the time slice $\tau = 0$, results in a Euclidean saddle with a conical singularity (red) with opening angle $2\pi m$, where $m = \frac{\beta_0}{\beta}$. Right: The same state prepared as a microcanonical TFD state by imposing asymptotic fixed energy boundary conditions. This results in a smooth Euclidean saddle with boundary length β. The $\mathbb{Z}_2$ symmetric Cauchy slice Σ_{sym} (green and blue) on both saddles has identical data and thus, results in identical Lorentzian spacetimes upon time evolution.

A particularly simple case is one in which the seed-state $|\psi\rangle$ is a thermofield-double (TFD) state for which the bulk geometry has a static Killing field with bifurcate horizon; i.e., in the bulk $|\psi\rangle$ describes a standard 2-sided black hole. Since $|\psi\rangle$ is the TFD state, the norm $\langle\psi|\psi\rangle$ is computed by a Euclidean thermal path integral with boundary $S^1 \times X$ for some X, where the metric on this boundary is also a product. It is easiest to visualize the associated bulk saddles when the bulk is 2-dimensional as in the case of Jackiw-Teitelboim gravity (where by 'area' we mean the value of the dilaton). In that case, a bulk saddle can be represented as a disk in which there is a preferred point that represents the Euclidean horizon, see Fig. 3.1.

We wish to consider the state constructed from $|\psi\rangle$ by fixing the area of the Euclidean horizon. In this case, the Euclidean horizon coincides with the HRT surface for the region defined by taking all of X at some point (which we may call $\tau = 0$) on the S^1. As described in Ref. [47], the corresponding fixed-area state is defined by the path integral with the same asymptotically AdS boundary conditions as the one that defines $|\psi\rangle$, but where the area of this HRT surface is also fixed to some A_0 as a boundary condition. Since we do not integrate over that area, saddles for this path integral need not satisfy the corresponding equation of motion at the HRT-surface. In particular, such saddles need not be smooth, and can instead have a conical singularity of arbitrary (constant) strength along the HRT surface.

If we consider saddles that preserve all symmetries, then in many cases there will be an analogue of Birkhoff's theorem which states that, at least locally, the possible bulk solutions are just the set of appropriately-symmetric (Euclidean) black holes. Fixing $A[\gamma_R]$ to some A_0 will then select precisely one such solution. But the period β of the smooth Euclidean black hole with horizon area A_0 will not generally match the period β_0 of the S^1 at infinity. Nevertheless, we can use the freedom to introduce a conical

singularity at γ_R (in this case with deficit angle $2\pi\left(1-\frac{\beta_0}{\beta}\right)$) to change the period of this solution to match β_0; see Fig. 3.1.

On the other hand, as discussed in Ref. [47], one expects that in the leading semiclassical approximation the above fixed-area state will be equivalent to the microcanonical thermofield double so long as the area A_0 chosen above is not too small (so that the microcanonical ensemble is dominated by AdS-Schwarzschild black holes). The point here is that the seed state $|\psi\rangle$ above was chosen to be the usual (canonical) thermofield double, and so has modular Hamiltonian

$$\hat{K}_R = \beta H + \log Z, \tag{3.1}$$

where H is the boundary Hamiltonian and the second term makes up the normalization. Furthermore, for each energy E (again chosen to not be too small), the entropy is maximized by states that are well-described by an AdS-Schwarzschild black hole with horizon area A determined by E. As a result, restricting the canonical TFD to a narrow band of energies is essentially the same as restricting to a narrow band of areas.

The interesting point then is that the restriction on energies can be implemented by performing an inverse Laplace transform. This can be done semiclassically by integrating over boundary length β to find a saddle with definite energy. Unlike the above fixed-area saddle, the corresponding Euclidean geometry is just a smooth disk with period β at infinity determined as usual by the energy, or equivalently by the horizon area. See e.g. [103, 45]. Note also that in this case the period at infinity was *not* fixed as a boundary condition, but was determined dynamically by the saddle-point conditions.

Naively, it may appear that the conical defect appearing in the fixed-area state description might leave some singular imprint on the Lorentzian spacetime described by that state. In contrast, it is clear that no such issue arises for the microcanonical TFD.

Nevertheless, we will argue that these indeed lead to the same smooth Lorentzian classical solution.

Note in particular that the fixed-area Euclidean solution has a $\mathbb{Z}_2$ symmetry that leaves invariant a particular slice, Σ_{sym}. The $\mathbb{Z}_2$ symmetry implies that Σ_{sym} has vanishing extrinsic curvature[2] $K_{ij} = 0$, so the data on Σ_{sym} also provides Cauchy data for a Lorentzian solution. Furthermore, the $U(1)$ symmetry of the Euclidean solution means that the induced metric h_{ij} on Σ_{sym} is just the usual induced metric on the surface of time-symmetry associated with the black hole of area A_0. In particular, the conical singularity leaves no imprint on either h_{ij} or K_{ij}. Thus, the resulting Lorentzian spacetime is completely smooth until one reaches the usual black hole singularities. In particular, this Lorentzian spacetime is completely smooth at the HRT surface of interest. And since the corresponding Σ_{sym} in the microcanonical TFD saddle has precisely the same h_{ij} and K_{ij}, it defines precisely the same Lorentzian solution.

Now, the above setting is not generic, and it turns out that the Lorentzian solutions generally become singular when the U(1) symmetry is broken. but these are power law singularities, not conical singularities or strict shockwaves. We will describe the details of these singularities in Sec. 3.4.4 below.

Overview

Our treatment begins in Sec. 3.2 with a brief review of fixed-area states and their preparation via path integrals. As mentioned above, a common algorithm [48, 47, 73] for constructing fixed-area states involves first using a standard Euclidean (or, more generally, complex) path integral to construct a more familiar semiclassical bulk state and then modifying this prescription to fix the area of $A[\gamma_R]$. This then allows us to

[2]Subtleties in this argument associated with the fact that Σ_{sym} passes through the defect will be discussed in Sec. 3.2.1 below.

study the spacetime geometry of the fixed-area state in terms of the boundary conditions imposed on the above Euclidean path integral. Sec. 3.2 extends previous such discussions by using Schwinger-Keldysh-like constructions to study the spacetime geometry intrinsic to the fixed-area state itself and to cleanly separate this geometry from that associated with sources used to prepare the state.

While fixed-area states can be of use in constructing replica saddles, and while real-time replica saddles require complex metrics [6, 4], we will show that the spacetime metrics in fixed-area states are generally real at real times. Furthermore, they have no conical singularities.

As emphasized earlier, a $U(1)$ symmetric Euclidean solution results in a smooth Lorentzian spacetime. We thus analyze various examples where this $U(1)$ symmetry is broken to demonstrate the features of generic fixed-area states. Our main analyses will be performed at the classical level, though we will comment on quantum effects at the end.

We first discuss a warmup example in Sec. 3.3 where we consider a non-gravitational scalar field theory in $1+1$ dimensions. This highlights the prominent features that we expect from fixed-area states such as the existence of power law divergences in the scalar field on the lightcone of the fixed-area surface.

We then move on to a general discussion of the structure of the Lorentzian spacetimes of fixed-area states in gravitational theories. We propose a general ansatz for the form of the classical solution in Sec. 3.4.1. We then construct detailed examples in Jackiw-Teitelboim (JT) gravity and $\mathrm{AdS}_3 \times X$ for compact X in Sec. 3.4.2 and Sec. 3.4.3 demonstrating the validity of our ansatz. The general structure of the above-mentioned singularities on the light cone of the fixed-area surface are analyzed in Sec. 3.4.4. We close with some final discussion in Sec. 3.5 including comments on higher derivative and quantum corrections.

3.2 Schwinger-Keldysh path integrals for fixed-area states

As described in Sec. 3.1, fixed-area states are simply states of gravitational systems in which the distribution of some HRT-area operator $A[\gamma_R]$ is sharply peaked, i.e. the width ΔA is small. Let us first discuss precisely what we mean by sharply peaked. As anticipated in Ref. [104] and as established in Refs. [105, 106], in the semiclassical approximation the action of $\frac{A[\gamma_R]}{4G}$ is given by a so-called boundary-condition-preserving kink transform, which in particular induces a relative boost between the two entanglement wedges of some rapidity s. From the uncertainty relation, we have

$$\Delta A \Delta s \gtrsim O(G), \tag{3.2}$$

where s is the relative boost between the two entanglement wedges on either side of the HRT surface. Depending on the value of ΔA, we can classify fixed-area states into two types: pseudo-eigenstates and squeezed states.

Pseudo-eigenstates are very sharply peaked and have $\Delta A \sim O(G^\alpha)$ with $\alpha \geq 1$. This leads to $\Delta s \to \infty$ in the semiclassical limit. As a result, we do not expect a single geometry to describe such states. On the other hand, squeezed states have $\Delta A \sim O(G^\alpha)$ with $\alpha \in (\frac{1}{2}, 1)$. Such states are expected to have a semiclassical description, and yet have ΔA parametrically smaller than states usually constructed by Euclidean path integrals [103]. Here we shall focus on such squeezed states and describe their associated Lorentzian spacetimes.

Now, fixed-area geometries must of course have a specified value of $A[\gamma_R]$. But as noted above, so long as we consider the squeezed state case (so that $A[\gamma_R]$ is not specified too precisely), we expect that the state can remain semiclassical. And since there are no

other constraints, one further expects that all other aspects of the semiclassical spacetime geometry can be chosen arbitrarily (so long as they solve the equations of motion). However, as described in Refs. [48, 47, 73], one is typically interested in starting with some semiclassical bulk state $|\psi\rangle$, perhaps constructed using a gravitational path integral, and then applying a projection-like operator[3] Π_R that restricts this state to a range of $A[\gamma_R]$-eigenvalues of some small width ΔA about a central value A_0. We will thus investigate the spacetime geometries of fixed-area states that arise from such constructions and in particular their relation to the path integral boundary conditions used to define $|\psi\rangle$.

Recall that the squeezed state regime $\alpha \in (\frac{1}{2}, 1)$ described above suffices to fix the value of A in the semiclassical limit $G \to 0$. In particular, in that limit we may use the recipe described in Refs. [47, 73] for studying $|\psi\rangle_{A_0} := \Pi_R|\psi\rangle$. The recipe begins by supposing that we have already constructed a gravitational path integral that computes the original state $|\psi\rangle$, which in particular means that we are given boundary conditions for that path integral. From the bulk point of view we can think of the new state $|\psi\rangle_{A_0}$ as being created from $|\psi\rangle$ by the insertion of additional sources on γ_R, though of course the location of γ_R must be determined dynamically in a manner that takes into account the back-reaction from those sources. As explained in Refs. [47, 73], in the saddle-point approximation this means that saddles for $|\psi\rangle_{A_0}$ can be taken to satisfy the same asymptotic AdS boundary conditions as $|\psi\rangle$ (with precisely the same sources at the asymptotic boundary), so long as we also 1) impose the usual equations of motion away from γ_R, 2) allow the bulk to have a codimension-2 conical singularity of arbitrary strength on a locus γ_R homologous to R and satisfying $\partial\gamma_R = \partial R$, 3) choose the strength of the conical singularity so that $A[\gamma_R] = A_0$, and 4) impose appropriate boundary conditions at γ_R.

[3]We use the term "projection-like operator" to mean a Hermitian operator for which the variance of $A[\gamma_R]$ is small in the state $|\psi\rangle_{A_0} := \Pi_R|\psi\rangle$. We do *not* require $\Pi_R^2 = \Pi_R$. In particular, we might consider a Gaussian $\Pi_R = e^{-\frac{(A[\gamma_R]-A_0)^2}{2\sigma^2}}$ with some small width σ.

In particular, in Euclidean signature, Appendix A of Ref. [73] shows that the Euclidean Einstein-Hilbert action (including the delta-function term in the Ricci scalar associated with the conical singularity at γ_R) defines a good variational principle for this problem when the metric near γ_R takes the following form:

$$ds^2 = dzd\bar{z} + T\frac{(\bar{z}dz - zd\bar{z})^2}{z\bar{z}} + h_{ij}dy^i dy^j + 2iW_j dy^j(\bar{z}dz - zd\bar{z}), \tag{3.3}$$

$$T = \hat{o}(1), \quad \partial_r T = \frac{\hat{o}(1)}{r}, \quad \partial_r h_{ij} = \frac{\hat{o}(1)}{r}, \quad \partial_r W_j = \frac{\hat{o}(1)}{r}, \tag{3.4}$$

where z is defined as $z = re^{im\theta}$ with $\theta \sim \theta + 2\pi$, and T, h_{ij}, and W_j are functions of all coordinates $(z, \bar{z}, y^i)$. Furthermore, $\hat{o}(1)$ denotes terms that vanish in the $r \to 0$ limit at least as fast as some power law r^η with $\eta > 0$.[4] We refer to the conditions imposed by Eq. (3.3), (3.4) as boundary conditions to be imposed on Euclidean metrics at γ_R.

We emphasize that the conical singularities on the surfaces γ_R are associated with insertions of the operator Π_R and, as such, they represent features of the way that the state $|\psi\rangle_{A_0}$ is being prepared rather than a feature intrinsic to the state itself. Indeed, if we can find another state $|\tilde{\psi}\rangle$ described by a smooth bulk saddle which yields the same fixed-area state up to quantum corrections

$$|\tilde{\psi}\rangle_{A_0} = \Pi_R|\tilde{\psi}\rangle \approx \Pi_R|\psi\rangle = |\psi\rangle_{A_0}, \tag{3.5}$$

but where the saddle-point value of $A[\gamma_R]$ in the state $|\tilde{\psi}\rangle$ is already A_0, then the fixed-area saddle with asymptotically-AdS boundary conditions associated with the state $|\tilde{\psi}\rangle$ will be smooth regardless of the strength of the conical singularity in the original saddle defined by the asymptotically-AdS boundary conditions associated with $|\psi\rangle$.

To study the geometry intrinsic to the state $|\psi\rangle_{A_0}$, we should instead compute corre-

[4] This fixes a typo in v1 of Ref. [73].

lation functions in this state (which in the semiclassical limit should then factorize into a product of one-point functions). We thus consider

$$ {}_{A_0}\langle\psi|g_{\mu_1\nu_1}(x_1)\dots g_{\mu_n\nu_n}(x_n)|\psi\rangle_{A_0} = \langle\psi|\Pi_R g_{\mu_1\nu_1}(x_1)\dots g_{\mu_n\nu_n}(x_n)\Pi_R|\psi\rangle, \tag{3.6} $$

where issues related to the gauge-dependence of the $g_{\mu_i\nu_i}(x_i)$ will not affect our discussion and will thus be ignored. Note that it is critical that there are two insertions of the operator Π_R in Eq. (3.6). In particular, even if Π_R were an exact projector, the fact that Π_R will generally not commute with $g_{\mu_i\nu_i}(x_i)$ would make it difficult to use such a property to remove either copy of Π_R. Note also that the operators that sample the desired geometry naturally live *between* the two projectors.

We may thus construct a path integral that computes Eq. (3.6) by first constructing path integrals for the bra and ket wavefunctions ${}_{A_0}\langle\psi| = \langle\psi|\Pi_R$ and $|\psi\rangle_{A_0} = \Pi_R|\psi\rangle$ and then using these wavefunctions as boundary conditions for a path integral that computes correlators of the $g_{\mu_i\nu_i}(x_i)$. The first step above is identical to constructing path integrals for the unconstrained bra and ket states $\langle\psi|$ and $|\psi\rangle$, except for the insertion of a constraint on the area of γ_R. Thus the final path integral involves constraints on two such surfaces γ_R (though these surfaces may sometimes coincide).

We should of course add suitable sources $T^{\mu_i\nu_i}(x_i)$ to the action with respect to which we can vary to obtain the desired insertions of $g_{\mu_i\nu_i}(x_i)$. However, we see that in an appropriate sense we will make such variations only in the region between the two surfaces γ_R. Saddles for this problem will thus have two codimension-2 conical singularities, and it is only the region of the spacetime that in some sense lies between those singularities[5] that can be directly interpreted as the geometry intrinsic to the fixed-area state $|\psi\rangle_{A_0}$. In particular, in the leading saddle-point approximation we can simply set the sources

[5]We will explain the correct sense in more detail shortly. This sense will be clearest in Lorentz signature where the Cauchy problem is well-posed.

$T^{\mu_i\nu_i}(x_i)$ to zero and take the insertions of $g_{\mu_i\nu_i}(x_i)$ to report the saddle-point value of the metric at the point x_i. In that sense it is in fact sufficient to study the path integral that computes the norm

$$ {}_{A_0}\langle\psi|\psi\rangle_{A_0} = \langle\psi|\Pi_R^2|\psi\rangle. \tag{3.7}$$

3.2.1 Saddle points for fixed-area path integrals

We now wish to describe the saddle points of this path integral. The constraints on the areas of the γ_R surfaces mean that we do not integrate over these areas and, as a result, two of the Einstein equations need not be satisfied by our saddles, one at each of the two γ_R surfaces. As explained in Refs. [48, 47, 73], this extra freedom allows conical singularities of arbitrary strength on each γ_R-surface. While the conical deficit or excess must be constant along each such surface, the fact that the constraints remove *two* Einstein equations means that the strengths of the singularities on the two γ_R surfaces may be chosen independently. Furthermore, the idea that our path integral may be thought of as computing matrix elements associated with the bra and ket states ${}_{A_0}\langle\psi|$, $|\psi\rangle_{A_0}$, and that each contributes one of the conical singularities, suggests that one should be able to cut the saddle $\mathcal{M}$ into two pieces $\mathcal{M}_1, \mathcal{M}_2$ along some codimension-1 surface Σ_{cut} (so that $\partial\mathcal{M}_1 \supset \Sigma_{cut} \subset \partial\mathcal{M}_2$) such that $\mathcal{M}_1, \mathcal{M}_2$ each contain only one of the γ_R surfaces, see Fig. 3.2. We will thus impose this requirement below, with the understanding that we think of each piece as being closed so that $\Sigma_{cut} \subset \mathcal{M}_1, \mathcal{M}_2$. Thus, this condition can be satisfied in the degenerate case where the two γ_R surfaces at least coincide (in part or in whole) by taking Σ_{cut} to pass through the locus of this coincidence. Note that this restriction requires the tangent spaces of the surfaces γ_R to coincide at any point where the two surfaces intersect.

Now, in many cases the state $|\psi\rangle$ will have been constructed by specifying boundary

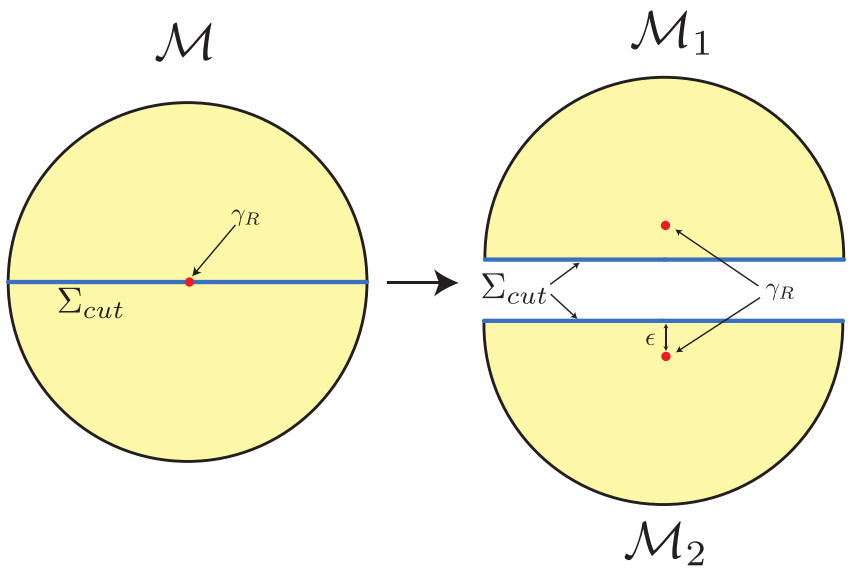

Figure 3.2: The saddle point manifold $\mathcal{M}$ for $\langle\psi|\Pi_R^2|\psi\rangle$ can be split into two parts $\mathcal{M}_1$ and $\mathcal{M}_2$ along a slice Σ_{cut} such that there are two conical defects (red) at γ_R, with one on the bra side of the cut and the other on the ket side. On the right, we have added a regulator ϵ that moves each of the resulting singularities away from the cut. The original $\mathcal{M}$ should be understood as the limit $\epsilon \to 0$ where the two γ_R surfaces coincide.

conditions on a Euclidean asymptotically-AdS boundary. But we may nevertheless be interested in the metric $g_{\mu_i\nu_i}(x_i)$ at real times t_i. In this case our path integral will integrate over spacetimes which follow a Schwinger-Keldysh-like contour through the plane of complex times. Nevertheless, since Π_R is Hermitian the expression Eq. (3.7) is manifestly real. As a result, the path integral will have a $\mathbb{Z}_2$ symmetry that exchanges the parts of the boundary associated with boundary conditions for $\langle\psi|$ and for $|\psi\rangle$ and which simultaneously acts by complex-conjugation. Since this symmetry acts as a reflection (and conjugation) on the asymptotically AdS boundary, any bulk saddle $\mathcal{M}$ that preserves this conjugation symmetry must have a codimension-1 surface Σ_{sym} that is invariant under the action of this $\mathbb{Z}_2$ symmetry[6] as shown in Fig. 3.3. We will consider only such

[6]The argument uses the fact that our asymptotically AdS boundary conditions require $\mathcal{M}$ to have a C^1 conformal compactification so that at each point on the boundary the conformally rescaled spactime can be approximated by a Euclidean half-space. One may then show the existence of Σ_{sym} by exhaustively studying the symmetries of the Euclidean plane.

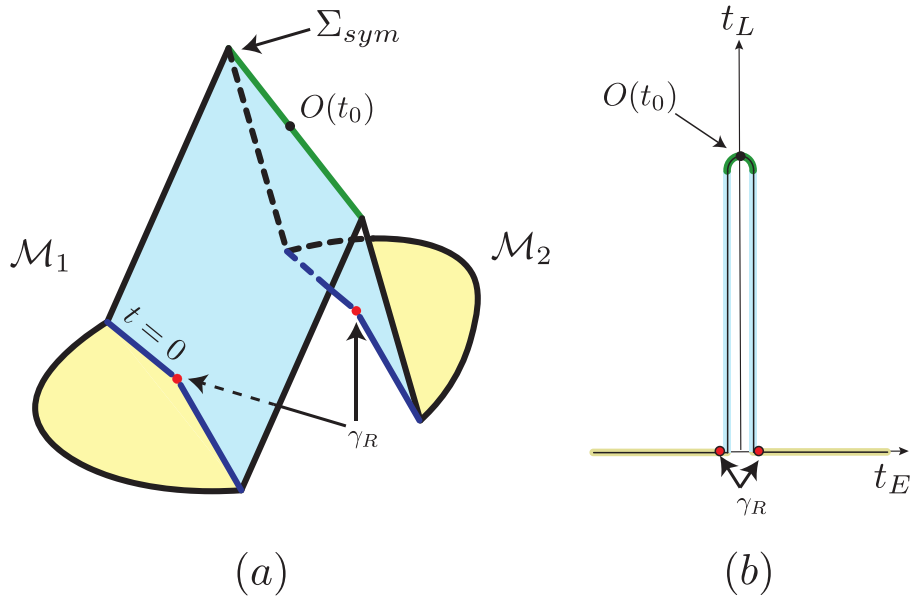

Figure 3.3: (a) The saddle point for $\langle\psi|\Pi_R(0)O(t_0)\Pi_R(0)|\psi\rangle$ has two conical defects (red) at γ_R on the bra and ket side respectively. It has a $\mathbb{Z}_2$ symmetry that leaves invariant the Cauchy slice Σ_{sym} (green). This slice splits the saddle into two parts $\mathcal{M}_1$ and $\mathcal{M}_2$. The region of the saddle point shaded light blue can be thought of as the spacetime inherent to the fixed-area state, while the yellow portion is involved in the preparation of the state. We may take the blue portion to lie at real Lorentzian times and the yellow portion to lie at real Euclidean times. In that sense, the two blue portions each involve the same interval of real Lorentzian times and should perhaps be drawn as being degenerate with each other, but we have separated the pieces for ease of visualization. (b) The corresponding Schwinger-Keldysh contour in the complex-time plane.

saddles below.

For the moment, let us assume Σ_{sym} does not intersect either surface γ_R so that it lies in a smooth region of the saddle-point spacetime. In this case, Σ_{sym} has a well-defined induced metric h_{ij} and extrinsic curvature. We will use the symbol K^E_{ij} to denote the extrinsic curvature defined using Euclidean conventions, and we will use $K^L_{ij} = iK^E_{ij}$ to denote the extrinsic curvature defined using Lorentz-signature conventions. Since all equations of motion are satisfied on Σ_{sym}, the data h_{ij}, K^E_{ij} (or h_{ij}, K^L_{ij}), i.e., the metric and extrinsic curvature will clearly satisfy the relevant constraint equations. Furthermore, the invariance of Σ_{sym} under the conjugation symmetry means that h_{ij} must be real

and the real part of K^E_{ij} must vanish. This of course simply means that K^E_{ij} is purely imaginary, or equivalently that K^L_{ij} is real. In other words, just as in the analysis of real-time replica wormholes in Ref. [6], symmetry requires Σ_{sym} to define Cauchy data appropriate to the Lorentz-signature initial value problem.

Let us now consider the case where Σ_{sym} intersects some γ_R at some point x. In this case one might worry that the extrinsic curvature of Σ_{sym} at x is not well-defined. In particular, consider surfaces $\Sigma_\pm$ on either side of Σ_{sym}, where we take the conjugation symmetry to interchange Σ_+ and Σ_-. When there is a conical singularity at x, the surfaces $\Sigma_\pm$ will have different extrinsic curvatures at x even in the limit where $\Sigma_\pm \to \Sigma_{sym}$. Indeed, with Euclidean signature conventions the real parts of their extrinsic curvatures will have delta-functions along γ_R of opposite signs. In contrast, the conjugation symmetry requires that the imaginary parts of their K^E_{ij} tensors match, so this imaginary part is continuous and unambiguous.

Since the two surfaces γ_R are in principle independent, the case where they intersect is just a degenerate limit of the more general case where they do not. As noted above, when they do not intersect the conjugation symmetry requires the real part of the extrinsic curvature of Σ_{sym} to vanish. We will thus define this to also be the case when the γ_R intersect. In effect, this is the statement that we should define the extrinsic curvature on Σ_{sym} by first regulating the problem in a manner that separates the γ_R surfaces (with Σ_{sym} lying between them) as shown in Fig. 3.2. We then take a limit where the regulator is removed.[7] But in practice it suffices to simply compute the (well-defined) imaginary part of K^E_{ij} and to take the real part of K^E_{ij} to vanish.

Now, when γ_R intersects Σ_{sym} at x, the conical singularity on γ_R also means that

[7]Similar reasoning tells us that we can always take the conical singularities to lie inside the Euclidean region. This means that the boundary conditions described by Eqs. (3.3) and (3.4) suffice to treat them. The case where the conical singularities lies at the boundary between the Euclidean and Lorentzian region is to be regarded as a limit of the case where the singularities lie entirely in the Euclidean region of the contour.

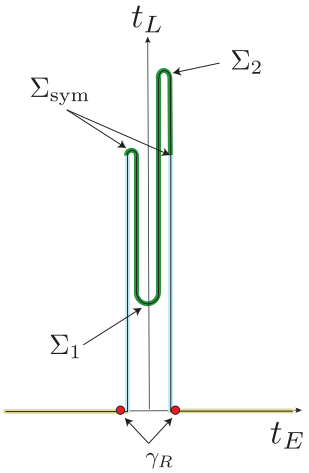

Figure 3.4: The saddle can be extended in the real time direction by evolving using the data on Cauchy slice $\Sigma_{\rm sym}$. As an example, we depict the Schwinger-Keldysh contour for forward evolution up to surface Σ_2 and backward evolution up to surface Σ_1.

some equations of motion are not satisfied at x. However, the fact that we required the existence of Σ_{cut} means that the conjugation symmetry must exchange the two surfaces γ_R. As a result, each point of the fixed-point set Σ_{sym} that intersects one copy of γ_R must in fact intersect both copies. Furthermore, as noted in Ref. [73] (see footnote 15), conical singularities can be thought of as arising from spacelike cosmic-brane sources that lie along γ_R. The effective stress tensor of such branes has non-zero components only tangent to γ_R, and in particular tangent to Σ_{sym} at any point of intersection. But the constraints on initial data on Σ_{sym} are associated with components of the equations of motion *normal* to Σ_{sym}, so they receive no contributions from such sources – i.e., even when γ_R intersects Σ_{sym} the initial data on Σ_{sym} satisfies the constraints that guarantee the initial value problem of the desired theory to be well-posed.

As a result, given any conjugation-symmetric saddle for the path integral that computes Eq. (3.7), we are free to extend it in the real time direction by evolving forward in time from Σ_{sym} up to some new Cauchy surface Σ_2 and then backwards from Σ_2 back to Σ_{sym}. Indeed, we could just as well evolve backward in time from Σ_{sym} to some Σ_1

and then forwards again from Σ_1 to Σ_{sym} as shown in Fig. 3.4, or we could even insert additional timefolds and evolve forwards and backwards in any manner that we like. The new piece of this spacetime corresponding to our excursion along the real-time axis will be real and Lorentz signature, and will satisfy all of the equations of motion. In particular, it will be free of conical singularities. Futhermore, extending the saddle in this way leaves the action of the saddle unchanged because the factors of e^{iS} associated with the forward-in-time parts of this evolution will precisely cancel the factors of e^{-iS} associated with the backwards-in-time evolution. It is the geometry along this real-time excursion that we explore in more detail below. As a final remark we note that this part of the spacetime lies between the two surfaces γ_R in the sense that it lies between two copies of the Cauchy surface Σ_{sym}, while the copies of γ_R lie in the two regions between the copies of Σ_{sym} and the Euclidean asymptotically AdS boundary.

3.3 Warmup: Scalar Field Theory in 1+1 dimensions

We would like to understand fixed-area states in the absence of a $U(1)$ symmetry. In order to do so, we first discuss a related-but-simpler problem involving a free scalar field ϕ in 1+1 dimensions on a fixed conical background. Due to the fixed background, this example cannot be directly interpreted as involving a fixed-area state. Nevertheless, the analysis will highlight the key ideas needed for our discussion of dynamical gravity in Sec. 3.4. There we will analyze the general structure of fixed-area states and illustrate it with various examples.

As discussed in Sec. 3.2, saddles for Euclidean path integrals preparing fixed-area states typically contain conical singularities. Here we study a toy model of the influence of such singularities on solutions to equations of motion by considering saddles for a scalar field path integral on a fixed conical background. We can choose the time-contour

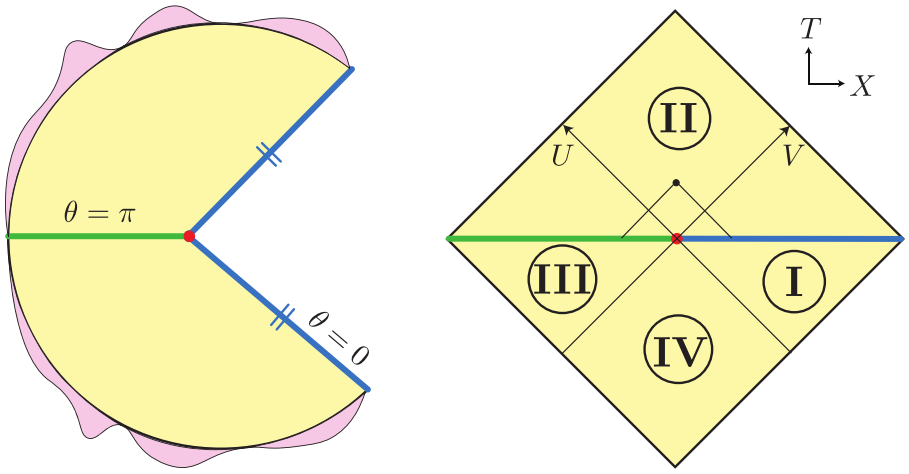

Figure 3.5: **Left:** Euclidean preparation of the state of a scalar field on a conical background of opening angle $2\pi m$. A source for the scalar field (pink) is present at the asymptotic boundary and which breaks the $U(1)$ symmetry of the geometry. This prepares initial data for Lorentzian evolution on the $\mathbb{Z}_2$ symmetric slice defined by the union of the blue half-line at $\theta = 0$ line and the green half-line at $\theta = \pi$. Note that there is really only a single blue half-line; the marks on the diagram indicate that the two copies are to be identified. **Right:** The initial data prepared by the Euclidean solution is used to generate the Lorentzian solution in Minkowski space by solving the equation of motion as described in the main text. The solution at the small black dot in region II is obtained by propagating the data along left and right-moving light rays (for a free massless field).

of the background so that the saddle is purely Euclidean, or we can choose a contour for which the saddle contains pieces that evolve in real Lorentzian time.

We take the background Euclidean geometry to be the simple $U(1)$-symmetric cone. However, we will impose boundary conditions for the scalar field that break this $U(1)$ symmetry as shown in Fig. 3.5. In particular, the boundary conditions will preserve a $\mathbb{Z}_2$ conjugation symmetry. Although the geometry in this example is flat, we will sometimes refer to these boundary conditions as 'sources' using the terminology common in the AdS/CFT context.

Any scalar field saddle on the Euclidean cone determines values of the scalar field ϕ on the $\mathbb{Z}_2$ symmetric Cauchy slice. Assuming that the saddle respects this $\mathbb{Z}_2$ symmetry, the real part of the normal derivative of ϕ must vanish.

As a result, the data on this slice gives Cauchy data for a real solution to the equations of motion for our scalar in $1 + 1$-dimensional Minkowski spacetime (with no conical singularity). We will see that such solutions have power-law singularities on the past and future lightcones of the point $x = 0$. We present the analysis for a massless scalar field in Sec. 3.3.1 and for a massive scalar field in Sec. 3.3.2, both of which have qualitatively similar properties.

Since gravity is non-dynamical in this example, at some level we have simply chosen the Lorentzian spacetime by hand to be a singularity-free Minkowski space. But one may view this choice as arising from a natural analogue of the discussion surrounding Fig. 3.3. If a regulator was introduced to split the original Euclidean conical singularity (say, with conical deficit δ) into two singularities (both with deficits $\delta/2$) while preserving $\mathbb{Z}_2$ symmetry, then the symmetric slice would have vanishing extrinsic curvature and induced metric dx^2. This is precisely the data for the $t = 0$ slice of Minkowski space. One may also think of the Lorentz-signature Minkowski space as being generated by analytically-continuing the geometry from the Euclidean region between the singularities.

3.3.1 Massless Field

Consider a free massless real scalar field on a fixed conical background. The Euclidean action is given by

$$S_{\text{massless}} = \frac{1}{2}\int d^2x\sqrt{g}(\partial\phi)^2, \tag{3.8}$$

with the standard metric given by

$$ds^2 = dr^2 + m^2r^2d\theta^2, \qquad \theta \in [0, 2\pi). \tag{3.9}$$

In this coordinate system, the time-reflection symmetric slice corresponds to $\theta = 0$ and $\theta = \pi$ as shown in Fig. 3.5.

In order to have a non-trivial classical solution, we turn on sources for the scalar field at some large distance cutoff boundary, $r = r_c$, and solve the equations for $r \leq r_c$. A simple source we consider which breaks the $U(1)$ symmetry is the boundary condition

$$\phi_b(\theta) \equiv \phi(r_c, \theta) = 2r_c^{k/m}\cos(k\theta) \tag{3.10}$$

with some positive integer k. This source satisfies $\partial_\theta\phi_b|_{\theta=0,\pi} = 0$, as would any real source that preserves the $\mathbb{Z}_2$ symmetry $\theta \to -\theta$. As a result, the slice defined by $\theta = 0, \pi$ provides initial data for a real Lorentzian solution. Solving the equation of motion associated with Eq. (3.8) is straightforward. Furthermore, in order for our action to yield a well-defined variational principle for the scalar field, we require the solution to be finite at $r = 0$. This uniquely determines the solution to be

$$\phi(r, \theta) = 2r^{k/m}\cos(k\theta). \tag{3.11}$$

The desired Lorentzian initial data is found simply by setting $\theta = 0, \pi$ in Eq. (3.11). Defining the coordinate $X = r$ when $\theta = 0$ and $X = -r$ when $\theta = \pi$, we can write the full initial value of ϕ in the form

$$\phi_0(X) = 2X^{k/m}\Theta(X) + 2(-1)^k(-X)^{k/m}\Theta(-X). \tag{3.12}$$

When combined with the condition $\partial_T\phi(T,X)|_{T=0} = 0$, the data $\phi(T = 0, X) = \phi_0(X)$ determines a unique Lorentzian solution on Minkowski space (which we take to have the standard metric $ds^2 = -dT^2 + dX^2$).

While this example is simple enough that we could explicitly solve for $\phi(T,X)$ everywhere, it will be instructive to first find the corresponding solutions in the left and right Rindler wedges marked as regions I and III in Fig. 3.5. The point here is that, by causality, the analytic continuation $\theta \to \theta + it$ of Eq. (3.11) is guaranteed to coincide in regions I and III with the Lorentzian solutions constructed above. This follows from the fact that the analytic continuation gives a Lorentzian solution with the correct initial data on both the positive and negative X-axes at $t = 0$, together with the fact that such data defines a unique solution in each Rindler wedge[8]. More explicitly, the above analytic continuation will give $\phi(X,T)$ in e.g. region I using $X = r\cosh(mt), T = r\sinh(mt)$. The solutions in regions I, III are thus given by

$$\phi(U,V) = V^{k/m} + (-U)^{k/m}, \qquad \text{(Region I)} : V > 0 \text{ and } U < 0, \tag{3.13}$$

$$\phi(U,V) = (-1)^k\left((-V)^{k/m} + U^{k/m}\right), \qquad \text{(Region III)} : V < 0 \text{ and } U > 0, \tag{3.14}$$

[8] Simple attempts to extend the argument to include the origin $X = T = 0$ will fail for the simple reason that the background Euclidean cone is not analytic at this point due to the delta-function Ricci scalar supported at the tip of the cone. However, we describe a more sophisticated such extension in Appendix B.2.

where U, V are the null coordinates

$$V = T + X, \qquad U = T - X. \tag{3.15}$$

The key issue is then to find the solutions in regions II and IV. Since the initial data is real, on general grounds we must find a real solution everywhere in the Lorentzian manifold. On the other hand, starting from Eq. (3.13) and Eq. (3.14), one might naively expect to find a complex solution when k/m is not an integer, as this is certainly the result of e.g. analytically continuing V across the horizon at $V = 0$.

Luckily, the massless field is simple enough to allow us to clarify this issue by finding the explicit solutions in the past and future wedges. As is well-known, the most general solution to the massless $1 + 1$ Klein-Gordon equation is given by

$$\phi(U, V) = f(V) + g(U) \tag{3.16}$$

for arbitrary functions f, g. Since the data in the left and right Rindler wedges fully determines both f and g, the full solution must be

$$\phi(U, V) = V^{k/m} + (-1)^k (U)^{k/m}, \qquad \text{(Region II)} : V > 0 \text{ and } U > 0, \tag{3.17}$$

$$\phi(U, V) = (-1)^k (-V)^{k/m} + (-U)^{k/m}, \qquad \text{(Region IV)} : V < 0 \text{ and } U < 0. \tag{3.18}$$

Eqs. (3.17) and (3.18) are clearly real, solve the equation of motion, and induce the correct initial data on the surface $T = 0$. Thus they give the desired solutions. We also describe an alternate construction of the same solution in Appendix B.1.1 by using a plane-wave basis.

The important feature of Eqs. (3.17), (3.18) is that they display power law behaviour near the horizons. Furthermore, for generic values of m, sufficiently high derivatives of

$\phi(U,V)$ diverge. This can already be seen from the initial data at $T=0$ in Eq. (3.12), which due to the time-symmetry of our solutions is closely related to the data on the horizons $U=0$ and $V=0$. A similar feature will be true of the metric in the fixed-area states studied in Sec. 3.4.4, where it will lead to divergent tidal forces.

3.3.2 Massive Field

We now consider the case of a real massive scalar with a mass μ in a "fixed-area" state in 1+1 dimensional Minkowski space. This example will play a key role in understanding higher dimensional examples in the presence of gravity. In particular, as we will see later, the equations near the horizon for a scalar field coupled to gravity in AdS behave similar to the example studied below. Here the various coordinates and both the Euclidean and Lorentzian metrics are chosen to be the same as in Sec. 3.3.1.

The equation of motion for the massive field is given by

$$(\nabla^2 - \mu^2)\phi = 0. \tag{3.19}$$

In Euclidean signature, we impose the following boundary conditions at $r = r_c$,

$$\phi(r_c, \theta) = 2I_{k/m}(\mu r_c)\cos(k\theta). \tag{3.20}$$

The regular solution at the origin consistent with this boundary condition is

$$\phi(r, \theta) = 2I_{k/m}(\mu r)\cos(k\theta). \tag{3.21}$$

In much the same way as in the massless case, by changing coordinates to (U,V) and performing an analytic continuation one may show the Lorentzian solution in the Rindler

wedges to be given by

$$\phi(U,V) = I_{k/m}(\mu\sqrt{-UV})\left((-V/U)^{\frac{k}{2m}} + (-U/V)^{\frac{k}{2m}}\right), \qquad V \geq 0, U \leq 0,$$
$$\phi(U,V) = (-1)^k I_{k/m}(\mu\sqrt{-UV})\left((-V/U)^{\frac{k}{2m}} + (-U/V)^{\frac{k}{2m}}\right), \quad U \geq 0, V \leq 0, \quad (3.22)$$

where $I_\nu(x)$ is the modified Bessel function of the first kind. Note that as $\mu \to 0$, these solutions approach the massless solutions Eq. (3.13) and Eq. (3.14) (up to a multiplicative constant associated with the different normalizations of Eq. (3.10) and Eq. (3.20)).

Given the solutions in the Rindler wedges, we can solve the equations of motion to extend the solution into regions II and IV. In fact, this example is simple enough that we can simply guess the solution. This is what we do below. But the interested reader may consult Appendix B.1.2 for a derivation of the result along the line $X = 0$ performed by expanding the solution in terms of plane waves.

If we guess that solutions in regions II and IV have the form $(V/U)^{\frac{k}{2m}} G(\sqrt{UV})$, then the equation of motion sets the function G to be a linear combination of Bessel functions $J_{k/m}(\mu\sqrt{UV})$ and $Y_{k/m}(\mu\sqrt{UV})$. One can check that only $J_{k/m}(\mu\sqrt{UV})$ is consistent with continuity of the solution across the horizons (as $U, V \to 0$), and thus with the absence of delta-function sources in the equations of motion. The solution is thus given by

$$\phi(U,V) = J_{k/m}(\mu\sqrt{UV})\left((V/U)^{\frac{k}{2m}} + (-1)^k (U/V)^{\frac{k}{2m}}\right) \qquad U \geq 0, V \geq 0, \quad (3.23)$$
$$\phi(U,V) = J_{k/m}(\mu\sqrt{UV})\left((U/V)^{\frac{k}{2m}} + (-1)^k (V/U)^{\frac{k}{2m}}\right) \qquad U \leq 0, V \leq 0. \quad (3.24)$$

Note that in (for example) region II, the limit $UV \to 0$ gives $\phi(U,V) \sim V^{k/m} + (-1)^k U^{k/m}$ which coincides with Eq. (3.17). So for the types of sources we have considered, the leading behaviour of the solution near the lightcone is determined by the

massless solution. In particular, the power law divergences found in Sec. 3.3.1 are not tied to the massless nature of that example, but are generic for all masses. We will find a similar feature to be true in arbitrary theories of gravity coupled to matter.

3.4 Fixed-area states in gravity

We now turn our attention to the Lorentzian geometry of fixed-area states in the presence of dynamical gravity. We will show how to obtain the Lorentzian metric from the Euclidean path integral which prepares the fixed-area state. In Sec. 3.4.1, we begin with a discussion of the general structure of fields as power series expansions near the HRT surface in both Euclidean and Lorentzian signature. Then, we illustrate the prescription for constructing the Lorentz-signature fixed-area state solutions in two simple examples. In Sec. 3.4.2, we construct exact fixed-area solutions in JT gravity coupled to a scalar field. In Sec. 3.4.3, we construct fixed-area solutions in AdS_3 gravity coupled to a scalar field by including the effects of backreaction perturbatively. This example illustrates the generic features of fixed-area states in higher dimensional gravity since it arises from dimensional reduction. Thus, it complements the example in JT gravity. Finally, Sec. 3.4.4 discusses singularities on the horizons of fixed-area states in the presence of arbitrary boundary sources.

3.4.1 General Lorentzian solutions

Before discussing the structure of the Lorentzian solutions, let us first review the structure of Euclidean conical solutions as analyzed in Ref. [73]. The metric near the

codimension-2 defect at the HRT surface γ_R takes the form

$$ds^2 = dzd\bar{z} + T\frac{(\bar{z}dz - zd\bar{z})^2}{z\bar{z}} + h_{ij}dy^i dy^j + 2iW_j dy^j(\bar{z}dz - zd\bar{z}), \tag{3.25}$$

where y^i denotes the transverse directions and $(z, \bar{z})$ represent the normal directions to γ_R. Note z may be written as $z = re^{im\theta}$ with $\theta \sim \theta + 2\pi$. The quantities T, h_{ij} and W_j are functions of all the coordinates $(z, \bar{z}, y^i)$. For Einstein gravity minimally coupled to scalar matter with standard two-derivative actions, the metric components in general have the following power series expansion in terms of powers of $z, \bar{z}$ in a neighbourhood of γ_R:

$$T = \sum_{\substack{p,q,s=0 \\ pq>0 \text{ or } s>0}}^{\infty} T_{pqs}(y^i) z^{p/m} \bar{z}^{q/m} (z\bar{z})^s, \tag{3.26}$$

$$W_i = \sum_{p,q,s=0}^{\infty} W_{i,pqs}(y^i) z^{p/m} \bar{z}^{q/m} (z\bar{z})^s, \tag{3.27}$$

$$h_{ij} = \sum_{p,q,s=0}^{\infty} h_{ij,pqs}(y^i) z^{p/m} \bar{z}^{q/m} (z\bar{z})^s, \tag{3.28}$$

where $2\pi m$ is the opening angle of the conical defect at γ_R. Any scalar matter field ϕ has a similar series expansion near the conical defect:

$$\phi = \sum_{p,q,s=0}^{\infty} \phi_{pqs}(y^i) z^{p/m} \bar{z}^{q/m} (z\bar{z})^s. \tag{3.29}$$

In particular, it was demonstrated in Ref. [73] that such a power series expansion near γ_R provides a good variational ansatz for finding Euclidean conical solutions with specified asymptotic boundary conditions.

As discussed previously, the Euclidean solution can be analytically continued to obtain a solution in each of the Rindler wedges defined by the HRT surface γ_R. We promote

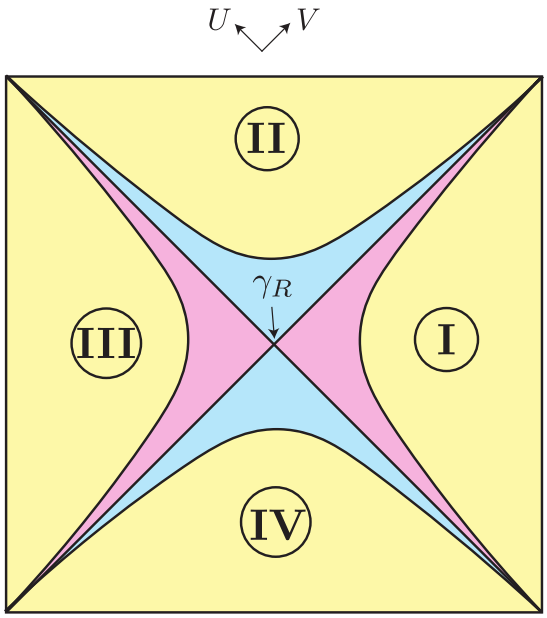

Figure 3.6: The Lorentzian spacetime can be divided into four wedges with respect to the HRT surface γ_R labelled I-IV. The power series expansion we propose is valid in the regions shaded pink and blue. The solution in the pink region is obtained by analytically continuing the Euclidean solution. The solution in the blue region is obtained by a simple transformation of the analytically continued solution.

the complex coordinates $z, \bar{z}$ to lightcone coordinates U, V and assuming that the power series expansion is valid in a tubular neighbourhood $|z\bar{z}| \leq r_0^2$ around γ_R, we obtain a Lorentzian solution in a corresponding hyperboloidal region $-r_0^2 \leq UV < 0$ as shown in Fig. 3.6 (shaded pink). For any field $\phi(U, V)$, we obtain a power-series expansion in the Rindler wedges of the form

$$\begin{aligned} \phi(U,V) &= \sum_{p,q,s} \phi_{pqs} V^{p/m} (-U)^{q/m} (-UV)^s, && U \leq 0, V \geq 0, \\ \phi(U,V) &= \sum_{p,q,s} (-1)^{p+q} \phi_{pqs} (-V)^{p/m} U^{q/m} (-UV)^s, && U \geq 0, V \leq 0, \end{aligned} \tag{3.30}$$

In order to construct the solution in the future and past wedges, we first demonstrate a simple procedure for generating new solutions to the equations of motion. Given a solution for a field $\phi(U, V)$ in terms of the coefficients ϕ_{pqs}, another solution is given by

the set of coefficients $\tilde{\phi}_{pqs} = e^{i\alpha_1 p} e^{i\alpha_2 q} \phi_{pqs}$, where $\alpha_{1,2}$ are arbitrary constants. This can be easily seen in the case when m is chosen to be irrational, since terms of the form $V^{p/m} U^{q/m}$ are linearly independent for different values of p, q. In this case, at any given order the equations of motion generate a relation for the coefficient ϕ_{pqs} in terms of a combination of homogenous product of coefficients such as $\phi_{p_1 q_1 s_1} \phi_{p_2 q_2 s_2}$ with $p_1 + p_2 = p$ and $q_1 + q_2 = q$. This makes it clear that multiplying the coefficients by a phase that linearly depends on p or q doesn't alter the defining relation arising from the equation of motion. Thus, the new set of coefficients $\tilde{\phi}_{pqs}$ also solves the equation of motion.

For rational values of m, one can take the limit from irrational m and the limit is well-behaved as demonstrated in Ref. [73]. Since the Lorentzian equations of motion we are analyzing here are Wick-rotated versions of the Euclidean equations of motion analyzed there, the same arguments go through in our case.

In general, this new solution would not be as useful since it is complex while one is usually interested in a real solution given real initial data. However, in our problem, this transformation will turn out to be useful in generating real solutions in the past and future wedges. In particular, we propose that the solution in these regions take the form:

$$\begin{aligned} \phi(U,V) &= \sum_{p,q,s} (-1)^{s+q} \phi_{pqs} V^{p/m} U^{q/m} (UV)^s, && U \geq 0, V \geq 0, \\ \phi(U,V) &= \sum_{p,q,s} (-1)^{p+s} \phi_{pqs} (-V)^{p/m} (-U)^{q/m} (UV)^s, && U \leq 0, V \leq 0, \end{aligned} \tag{3.31}$$

The above power series can be obtained from Eq. (3.30) by applying a phase rotation to the coefficients that is linear in p, q as described above. This ensures that it solves the equations of motion. It is also easy to check that this ansatz agrees with Eq. (3.30) on all horizons, and so satisfies the desired initial data on these null surfaces. Uniqueness of the null initial value problem then guarantees that the correct solution will be of this

form. Indeed, one can directly check that the solutions in Sec. 3.3 take this form. We now demonstrate this procedure in more detail in various explicit examples in JT gravity and AdS_3.

3.4.2 Example 1: JT Gravity + Matter

We begin with an example involving JT gravity minimally coupled to a massless real scalar field. We use Φ to represent the dilaton in order to distinguish it from the matter field ϕ. This case is sufficiently simple that the equations of motion can be solved exactly with arbitrary boundary sources [107]. We first solve for the dilaton profile in Euclidean signature, and then obtain the Lorentzian solution using the initial value formulation.

The Euclidean metric for a fixed-area state in AdS_2 is

$$ds^2 = \frac{dzd\bar{z}}{(1 - z\bar{z}/4)^2}, \tag{3.32}$$

where $z = re^{im\theta}$ and $\bar{z} = re^{-im\theta}$ with m chosen to satisfy boundary conditions at Euclidean infinity. On the cutoff surface $z\bar{z} = r_c^2 = 4(1 - m\epsilon)^2$ where ϵ is small, we impose a boundary condition on the matter field ϕ,

$$\phi = 2r_c^{k/m}\cos(k\theta). \tag{3.33}$$

The equation of motion for the massless scalar field is invariant under conformal transformations and thus, the solution is the same as the solution on a flat cone in Sec. 3.3.1. Thus, we obtain the solution

$$\phi = z^{k/m} + \bar{z}^{k/m}. \tag{3.34}$$

The stress tensor for this solution is

$$T_{zz}(z) = (k/m)^2 z^{2(k/m-1)}, \quad T_{\bar{z}\bar{z}}(\bar{z}) = (k/m)^2 \bar{z}^{2(k/m-1)}, \quad T_{z\bar{z}} = 0, \tag{3.35}$$

and the dilaton equation of motion is [107]

$$-(1 - z\bar{z}/4)^{-2}\partial_\mu \left((1 - z\bar{z}/4)^2 \partial_\nu \Phi\right) = T_{\mu\nu}. \tag{3.36}$$

We thus find

$$\begin{aligned}\Phi &= \int^z dx \frac{(1 - \bar{z}x/4)(x - z)}{(1 - z\bar{z}/4)} T_{zz}(x) + \int^{\bar{z}} dx \frac{(1 - zx/4)(x - \bar{z})}{(1 - z\bar{z}/4)} T_{\bar{z}\bar{z}}(x) + \Phi_0 \\ &= (z^{2k/m} + \bar{z}^{2k/m}) \frac{(k/m)\left((1 + 2k/m) + (1 - 2k/m)z\bar{z}/4\right)}{2(1 - 4k^2/m^2)(1 - z\bar{z}/4)} + \Phi_0,\end{aligned} \tag{3.37}$$

where Φ_0 can be any solution to pure JT gravity without matter, i.e.,

$$\Phi_0 = \frac{a + dz\bar{z}}{1 - z\bar{z}}, \tag{3.38}$$

for any constants a and d. Note that the ambiguity in choosing the lower limits of the integrals can be absorbed into Φ_0, and possible linear terms of the form $bz + c\bar{z}$ in the numerator of Φ_0 are discarded since they do not respect the $\mathbb{Z}_2$ symmetry and periodicity $\theta \to \theta + 2\pi$.

We choose to study an example where the pure gravity solution is the fixed-area state defined by a Euclidean black hole at inverse temperature β, so that [107]

$$\Phi_0 = m\Phi_b \frac{1 + z\bar{z}/4}{1 - z\bar{z}/4}, \tag{3.39}$$

with β/ϵ the length of the boundary curve and Φ_b/ϵ the boundary dilaton value.[9]

The next step is to inspect the initial value for the dilaton on the $T = 0$ surface, which will then be used to construct the Lorentzian solution. The $\mathbb{Z}_2$ symmetric slice is given by the union of the surfaces $\theta = 0$ and $\theta = \pi$. For $0 < X < 2$ we take $X = r$, and for $-2 < X < 0$ we take $X = -r$. The initial value for Φ is thus

$$\Phi|_{T=0}(X) = \left(X^{2k/m}\Theta(X) + (-X)^{2k/m}\Theta(-X)\right) \frac{(k/m)\left((1+2k/m) + (1-2k/m)X^2/4\right)}{(1-4k^2/m^2)(1-X^2/4)} + m\Phi_b \frac{1+X^2/4}{1-X^2/4}. \tag{3.40}$$

In the Lorentzian spacetime, the metric may always be written in the form

$$ds^2 = -\frac{dUdV}{(1+UV/4)^2}, \tag{3.41}$$

with the asymptotic boundaries being located at $UV = -4$.

We start by finding the solution for the scalar field. Since this field satisfies the massless wave equation, and since this wave equation is conformally invariant, the result is identical to that in the non-gravitational example in Sec. 3.3.1, i.e.,

$$\phi(U,V) = V^{k/m} + (-U)^{k/m}, \qquad \text{(Region I)} \ : V > 0 \text{ and } U < 0, \tag{3.42}$$

$$\phi(U,V) = V^{k/m} + (-1)^k (U)^{k/m}, \qquad \text{(Region II)} \ : V > 0 \text{ and } U > 0, \tag{3.43}$$

$$\phi(U,V) = (-1)^k \left((-V)^{k/m} + U^{k/m}\right), \qquad \text{(Region III)} \ : V < 0 \text{ and } U > 0, \tag{3.44}$$

$$\phi(U,V) = (-1)^k (-V)^{k/m} + (-U)^{k/m}, \qquad \text{(Region IV)} \ : V < 0 \text{ and } U < 0. \tag{3.45}$$

[9] One may observe that, in our full solution (3.37), as we approach the cutoff surface $z\bar{z} \to r_c$, the dilaton Φ does not approach a constant. This may appear inconsistent with the usual boundary condition $\Phi|_{r=r_c} = const$ in JT gravity. However, we can instead choose to reformulate the boundary conditions by finding a surface on which the dilaton is in fact constant in our solution and then using the scalar field profile on the given surface as the boundary condition we impose for the scalar field. We simply choose the above formulation for convenience.

This yields the stress tensor

$$T_{UU}(U) = (k/m)^2 \left(U^{2(k/m-1)}\Theta(U) + (-U)^{2(k/m-1)}\Theta(-U)\right), \tag{3.46}$$

$$T_{VV}(V) = (k/m)^2 \left(V^{2(k/m-1)}\Theta(V) + (-V)^{2(k/m-1)}\Theta(-V)\right), \tag{3.47}$$

$$T_{UV} = 0. \tag{3.48}$$

Following Ref. [107], the dilaton solution in the Lorentzian spacetime can then be computed as

$$\Phi = \int^U dx \frac{(1+Vx/4)(U-x)}{(1+UV/4)} T_{UU}(x) + \int^V dx \frac{(1+Ux/4)(V-x)}{(1+UV/4)} T_{VV}(x) + \tilde{\Phi}_0, \tag{3.49}$$

where

$$\tilde{\Phi}_0 = \frac{A + BU + CV + DUV}{1 + UV/4}. \tag{3.50}$$

The full Lorentzian solution can then be constructed by performing the integrals in Eq. (3.49) and choosing integration constants to the prescribed initial values from Eq. (3.40). Doing so leads us to the result

$$\Phi = f(U,V)\frac{(k/m)\left((1+2k/m) - (1-2k/m)UV/4\right)}{2(1-4k^2/m^2)(1+UV/4)} + m\Phi_b \frac{1-UV/4}{1+UV/4}, \tag{3.51}$$

where

$$f(U,V) = V^{2k/m} + (-U)^{2k/m}, \qquad \text{(Region I): } U<0, V>0 \tag{3.52}$$

$$f(U,V) = V^{2k/m} + U^{2k/m}, \qquad \text{(Region II): } U>0, V>0 \tag{3.53}$$

$$f(U,V) = (-V)^{2k/m} + U^{2k/m}, \qquad \text{(Region III): } U>0, V<0 \tag{3.54}$$

$$f(U,V) = (-V)^{2k/m} + (-U)^{2k/m}, \qquad \text{(Region IV): } U<0, V<0. \tag{3.55}$$

One can then verify that the above expressions solve the equations of motion, and one can also check that the solution satisfies the general power series expansion described in Sec. 3.4.1. Importantly, despite the appearance of singularities on the lightcone of the HRT surface, the solution is smooth in the interior of both the past and future wedges.

3.4.3 Example 2: AdS_3 coupled to a massless scalar field

We now consider an example of a fixed-area state geometry for AdS_3 gravity minimally coupled to a real scalar field. The corresponding Euclidean problem was analyzed in detail in Ref. [33] for the case $m = 1/n$ with $n \in \mathbb{Z}^+$ where it was interpreted as a Euclidean replica geometry. Here we extend the calculation in Ref. [33] to conical defects with arbitrary strength m and focus on the Lorentzian solution whose initial data agrees with the Euclidean solution on the surface of time-symmetry.

An interesting feature of this example is the connection to gravity in higher dimensions. As mentioned in Ref. [33], solutions of the form $AdS_3 \times S^3 \times T^4$ give rise to three dimensional gravity coupled to two massless real scalar fields. One obtains scalar fields ϕ_1 and ϕ_2 from the metric components of T^4 when parametrized in the form

$$ds^2_{T^4} = e^{2\phi_1} dy_1^2 + e^{2\phi_2} dy_2^2 + e^{-2\phi_1} dy_3^2 + e^{-2\phi_2} dy_4^2. \tag{3.56}$$

Studying the fixed-area state solution of the scalar field and metric components in this example is thus directly related to fixed-area states in pure gravity in higher dimensions. In particular, as we will discuss, the Lorentz-signature singularities of the scalar field that arise from the presence of the conical defect in the Euclidean preparation correspond to geometric singularities (and generally to Weyl curvature singularities) of the higher-dimensional gravity theories. For simplicity and clarity, we will set $\phi_2 = 0$ and denote $\phi = \phi_1$ as the only relevant scalar field.

We now turn to the actual preparation of our fixed-area state solution. As usual, we start in Euclidean signature and use the result to determine the initial data for the Lorentzian scalar field and metric. Following Ref. [33], we solve the Euclidean equation of motion for the massless real scalar field and the metric perturbatively by assuming that the source for the scalar field is small. To zeroth order, the metric of Euclidean AdS_3 with a conical defect of strength m is given by

$$ds^2 = \frac{dr^2}{r^2+1} + m^2 r^2 d\theta^2 + m^2(r^2+1)dy^2, \tag{3.57}$$

where $\theta \in [0, 2\pi)$. Here we set $l_{AdS} = 1$. The transverse coordinate y does not play a role for the class of solutions considered here and can be chosen to be either compact or non-compact. The factor of m^2 in the last term in Eq. (3.57) is chosen to ensure that when y is compact with fixed period, the conformal structure of the boundary torus is independent of m.

We turn on a non-trivial source for the scalar field by imposing the following boundary condition at a cutoff surface $r = r_c$,

$$\phi|_{r=r_c} = 2\eta \cos(k\theta). \tag{3.58}$$

The equation we are solving is

$$\nabla_\mu \nabla^\mu \phi = 0, \tag{3.59}$$

and the solution is then given by

$$\phi = 2\eta \cos(k\theta) \frac{f_{m,k}(r)}{f_{m,k}(r_c)}, \qquad f_{m,k}(r) = r^{k/m} {}_2F_1\left(\frac{k}{2m}, \frac{k}{2m}+1, \frac{k}{m}+1, -r^2\right). \tag{3.60}$$

Using the solution for the scalar field, the stress tensor can be decomposed in terms of Fourier modes,

$$T_{\mu\nu} = \nabla_\mu \phi \nabla_\nu \phi - \frac{g_{\mu\nu}}{2}(\nabla\phi)^2 \tag{3.61}$$

$$= T^0_{\mu\nu} + T^+_{\mu\nu} e^{2ik\theta} + T^-_{\mu\nu} e^{-2ik\theta}. \tag{3.62}$$

We can then use the above result to solve the metric equations at leading order in η. Following the ansatz in Ref. [33], we write the perturbed metric as

$$ds^2 = \frac{dr^2}{r^2 + 1 + g(r,\theta)} + m^2 r^2 d\theta^2 + m^2(r^2+1)(1+v(r,\theta))dy^2, \tag{3.63}$$

where $g(r,\theta), v(r,\theta)$ consist of three fourier modes in the angular direction, e.g.,

$$g(r,\theta) = g_0(r) + g^+(r)e^{2ik\theta} + g^-(r)e^{-2ik\theta}. \tag{3.64}$$

The Einstein equations after dimensional reduction are then given by,

$$R_{\mu\nu} - \frac{g_{\mu\nu}}{2}(R+2) = 8\pi G T_{\mu\nu}, \qquad T_{\mu\nu} = \nabla_\mu\phi\nabla_\nu\phi - \frac{g_{\mu\nu}}{2}(\nabla\phi)^2. \tag{3.65}$$

By using the ansatz in Eq. (3.63), one can find integral expressions for $g(r,\theta)$ and $v(r,\theta)$. However, the closed form solutions for $v(r,\theta)$ or $g(r,\theta)$ will not be important for the discussion of the Lorentzian evolution. The interested reader may refer to Appendix B.3 for more details.

So far, we have considered the equations and solution in Euclidean signature. In order to write down the Lorentzian solution, we follow identical steps to Sec. 3.3. Let us first discuss the undeformed metric in the Lorentzian signature. The initial slice is given by the union of the slices $\theta = 0$ and $\theta = \pi$. By continuing $\theta \to \theta + it$, on the $\theta = 0, \pi$ slices we find

$$ds_L^2 = -m^2 r^2 dt^2 + \frac{dr^2}{r^2+1} + m^2(r^2+1)dy^2. \tag{3.66}$$

By rescaling the coordinates, the metric can be written in the more suggestive form

$$ds_L^2 = -r^2 d\tilde{t}^2 + \frac{dr^2}{r^2+1} + (r^2+1)d\tilde{y}^2, \qquad \tilde{t} = mt, \qquad \tilde{y} = my, \tag{3.67}$$

which is just the familiar Lorentz signature AdS_3 metric with a rescaled transverse coordinate $y \to my$. In particular, the geometry in Eq. (3.67) is manifestly smooth in Lorentz signature.

In order to make the Lorentzian solution more explicit, let us write the undeformed metric (3.66) in global coordinates

$$ds_L^2 = -\frac{4dUdV}{(1+UV)^2} + m^2\left(\frac{1-UV}{1+UV}\right)^2 dy^2, \tag{3.68}$$

where

$$U = -\frac{r}{1+\sqrt{1+r^2}}e^{-mt},\ V = \frac{r}{1+\sqrt{1+r^2}}e^{mt}, \tag{3.69}$$

are the global null coordinates. As in the discussion of Sec. 3.3, the Lorentzian solution for the scalar field inside the "Rindler" wedges is straightforward to obtain by analytically continuing Eq. (3.60) to find

$$\begin{aligned}
\phi &= \frac{\eta}{f_{m,k}(r_c)}\,\frac{(-2U)^{k/m}+(2V)^{k/m}}{(1+UV)^{k/m}}\,{}_2F_1\left(\frac{k}{2m},\frac{k}{2m}+1,\frac{k}{m}+1,\frac{4UV}{(1+UV)^2}\right), \\
&\qquad\qquad U<0,\ V>0, \\
\phi &= \frac{\eta}{f_{m,k}(r_c)}\,(-1)^k\frac{(2U)^{k/m}+(-2V)^{k/m}}{(1+UV)^{k/m}}\,{}_2F_1\left(\frac{k}{2m},\frac{k}{2m}+1,\frac{k}{m}+1,\frac{4UV}{(1+UV)^2}\right), \\
&\qquad\qquad U>0,\ V<0.
\end{aligned} \tag{3.70}$$

We can now obtain the solution in the past and future wedges by solving the equations of motion and ensuring continuity of the fields across the horizons. Doing so yields

$$\begin{aligned}
\phi &= \frac{\eta}{f_{m,k}(r_c)}\,\frac{(-2U)^{k/m}+(-1)^k(-2V)^{k/m}}{(1+UV)^{k/m}}\,{}_2F_1\left(\frac{k}{2m},\frac{k}{2m}+1,\frac{k}{m}+1,\frac{4UV}{(1+UV)^2}\right), \\
&\qquad\qquad U<0,\ V<0, \\
\phi &= \frac{\eta}{f_{m,k}(r_c)}\,\frac{(-1)^k(2U)^{k/m}+(2V)^{k/m}}{(1+UV)^{k/m}}\,{}_2F_1\left(\frac{k}{2m},\frac{k}{2m}+1,\frac{k}{m}+1,\frac{4UV}{(1+UV)^2}\right), \\
&\qquad\qquad U>0,\ V>0.
\end{aligned} \tag{3.71}$$

One can check that the above expressions are consistent with the general power series expansion described in Sec. 3.4.1. Again, in generic situations, we find power law

divergences on the lightcones.

One can also analyze the behaviour of the Euclidean metric components $g(r,\theta), v(r,\theta)$ near $r = 0$ based on the analysis in Appendix B.3. The dependence on r, θ immediately gives us the dependence on U, V in a near-horizon region of the Rindler wedges ($UV < 0$) by analytic continuation. We find power-series expansions of the form

$$g^{\pm}(U,V) = (-UV)^{k/m} \sum_{n=1}^{\infty} g_n^{\pm} (-UV)^n, \qquad g^0(U,V) = (-UV)^{k/m} \sum_{n=0}^{\infty} g_n^0 (-UV)^n \quad (3.72)$$

$$v^{\pm}(U,V) = (-UV)^{k/m} \sum_{n=0}^{\infty} v_n^{\pm} (-UV)^n, \qquad v^0(U,V) = (-UV)^{k/m} \sum_{n=1}^{\infty} v_n^0 (-UV)^n \quad (3.73)$$

where $g_n^{\pm,0}, v_n^{\pm,0}$ are coefficients found by solving the Euclidean equations of motion, Eq. (B.37) – Eq. (B.42), in a power series expansion near $r = 0$. Given these solutions in the Rindler wedges, the by-now-familiar ansatz defined by Eq. (3.30) and Eq. (3.31) gives the solutions in the past and future wedges. In particular, when $UV > 0$ we find the solutions have the following form

$$g^{\pm}(U,V) = (UV)^{k/m} \sum_{n=1}^{\infty} g_n^{\pm} (-UV)^n, \qquad g^0(U,V) = (UV)^{k/m} \sum_{n=0}^{\infty} g_n^0 (-UV)^n \quad (3.74)$$

$$v^{\pm}(U,V) = (UV)^{k/m} \sum_{n=0}^{\infty} v_n^{\pm} (-UV)^n, \qquad v^0(U,V) = (UV)^{k/m} \sum_{n=1}^{\infty} v_n^0 (-UV)^n \quad (3.75)$$

We can check this by plugging the stress tensor inside the horizon regions and solving for the metric components directly in Lorentzian signature.

3.4.4 Divergence structure of fixed-area states

As we saw in the examples above, for general sources at the Euclidean boundary, fixed-area states lead to power-law divergences on the codimension-2 conical defects. Similar divergences then also appear on the lightcones emanating from the HRT surface

in the Lorentzian spacetime. We now generalize these results to arbitrary dimension and study the divergence structure of the general solution.

Euclidean signature

As usual, we begin by studying the divergence structure in Euclidean signature. We consider Einstein-Hilbert gravity coupled to classical scalar fields. We expect other classical matter fields to give similar results.

In quasi-cylindrical coordinates the metric near the codimension-2 defect can be always be written as Eq. (3.25),

$$ds^2 = dzd\bar{z}+T\frac{(\bar{z}dz - zd\bar{z})^2}{z\bar{z}} + h_{ij}dy^i dy^j + 2iW_j dy^j(\bar{z}dz - zd\bar{z}), \tag{3.76}$$

where T, h_{ij}, W_j are functions of all coordinates $(z, \bar{z}, y^i)$. The metric components have series expansions in terms of powers of $z^{1/m}$, $\bar{z}^{1/m}$ and $z\bar{z}$ near $r = 0$ as given in Eq. (3.26)-(3.29).

As noted before, in the presence of a $U(1)$ symmetry, all fields are smooth near $r = 0$ and there is no singularity in any derivative of the fields. Furthermore, when $m = \frac{1}{n}$ for integer n there is a smooth n-fold cover (as in the Lewkowycz-Maldacena discussion of gravitational Renyi entropies [33]), so again there are no power law divergences (even in the quotient). But more generally we will find divergences. Thus, in the following discussion, we consider a generic situation where $\frac{1}{m}$ is not an integer and where every coefficient in the power-series expansion of any metric component and matter field is non-zero.

Analyzing the Christoffel symbols we find

$$\Gamma^{\rho}_{\mu\nu} \sim r^{1/m-1}, \tag{3.77}$$

where we use the $\sim$ notation to keep track of the leading, non-smooth term appearing in various quantities like metric components, derivatives of the matter field, etc. In the case $m > 1$, the explicit $r^{1/m-1}$ term in fact represents the most singular term in the Christoffel symbols. For the Riemann tensor, there are terms involving the square of Christoffel symbols and terms involving the second derivatives of the metric. From Eq. (3.77), it is easy to see that the former terms at most are of order $r^{2/m-2}$. It turns out that the latter terms give the most singular terms in the Riemann tensor. In order to see this, let us define

$$A_{\mu\nu\rho\sigma} \equiv R_{\mu\nu\rho\sigma} - \Gamma_{\lambda\mu\sigma}\Gamma^{\lambda}_{\nu\rho} + \Gamma_{\lambda\mu\rho}\Gamma^{\lambda}_{\nu\sigma}. \tag{3.78}$$

We find

$$A_{z\bar{z}z\bar{z}} = T_{,z\bar{z}} + \frac{1}{2}\left(T\frac{z}{\bar{z}}\right)_{,zz} + \frac{1}{2}\left(T\frac{\bar{z}}{z}\right)_{,\bar{z}\bar{z}} \sim r^{\frac{2}{m}-2}, \tag{3.79}$$

where we have used

$$T = T_{110}(z\bar{z})^{1/m} + T_{101}\bar{z}z^{1/m+1} + T_{011}\bar{z}^{1/m+1}z + \cdots . \tag{3.80}$$

Similarly we find

$$A_{z\bar{z}zj} = \frac{1}{2}\left(i(W_j\bar{z})_{,z\bar{z}} + i(W_jz)_{,zz} - T_{,zi} - \left(T\frac{\bar{z}}{z}\right)_{,\bar{z}i}\right) \sim r^{1/m-1}, \tag{3.81}$$

and

$$A_{z\bar{z}ij}, A_{ijkl} \sim r^{1/m}, \tag{3.82}$$

while

$$A_{aijk} \sim r^{1/m-1}, \tag{3.83}$$

where $a = z, \bar{z}$. The most singular term comes from $h_{ij,ab}$ and is given by

$$A_{aibj} = \frac{1}{2}\left(g_{aj,ib} + g_{ib,aj} - g_{ab,ij} - g_{ij,ab}\right) \sim r^{1/m-2}. \tag{3.84}$$

So in this case the most singular component of the Riemann tensor is

$$R_{aibj} \sim \frac{r^{1/m}}{r^2}. \tag{3.85}$$

This behavior can be confirmed for the ten-dimensional Riemann tensor in the example of $AdS_3 \times S^3 \times T^4$ discussed in Sec. 3.4.3. In that case, the coefficient of Eq. (3.85) contains $(\frac{1}{m} - 1)$ and therefore when $m = 1$ there is no singularity.

The degree of singularity in Eq. (3.85) naively implies that the Ricci tensor has similar singularities. For instance R_{zz} contains terms like $h^{ij}\partial_z^2 h_{ij}$ which naively can be as singular as $r^{1/m-2}$. However, it was shown in Ref. [73] for pure gravity with a cosmological constant that solving the Einstein equations sets

$$h^{ij}_{,000}h_{ij,100} = h^{ij}_{,000}h_{ij,010} = 0. \tag{3.86}$$

This means that due to the equation of motion, the leading term for the Ricci tensor must be of form $r^{2/m-2}$ which are less singular than terms in R_{zizj}. If the matter coupled to gravity is classical, we expect that $R_{\mu\nu} \sim T_{\mu\nu}$ and $T_{\mu\nu} \sim \partial_\mu\psi\partial_\nu\psi$ where $\psi \sim r^{1/m}$ near $r = 0$. Therefore in this case, the most singular terms that scale as $r^{1/m-2}$ must be in the Weyl tensor and not the Ricci tensor.

Lorentzian signature

Generalizing the analysis of divergences to Lorentzian signature is now straightforward. Continuing $z \to V, \bar{z} \to -U$, the Lorentzian metric takes the form

$$ds^2 = -dUdV - T\frac{(VdU - UdV)^2}{UV} + h_{ij}dy^i dy^j + 2iW_j dy^j (VdU - UdV), \tag{3.87}$$

where since T vanishes on the horizons $V = 0$ and $U = 0$, we see that U and V asymptotically become affine parameters as one approaches either horizon. We now repeat the analysis of the components of the Riemann tensor. The main difference from the Euclidean analysis is that U, V are independent. As a result, we consider the derivative of the metric as $U \to 0$ for a fixed V (and similarly $V \to 0$ for fixed U). Note that Eq. (3.25) was originally an expansion for the metric in $r = \sqrt{z\bar{z}}$. A point with a fixed V and $U \to 0$ eventually ends up in the small UV region where Eq. (3.25) is a valid expansion. We use this expansion in the Lorentzian signature to find the leading singularity as $U \to 0$. However, the dependence on V at fixed V can be arbitrary and we only keep track of powers of U.

We find:

$$\begin{aligned}
&A_{VUVU} \sim U^{1/m-1}, \qquad A_{VUVj} \sim U^{1/m}, \qquad A_{VUUj} \sim U^{1/m-1}, \\
&A_{UVij} \sim U^{1/m}, \qquad A_{ijkl} \sim U^{1/m}, \qquad A_{Vijk} \sim U^{1/m}, \qquad A_{Uijk} \sim U^{1/m-1} \\
&A_{UiUj} \sim U^{1/m-2}, \qquad A_{UiVj} \sim U^{1/m-1}, \qquad A_{ViVj} \sim U^{1/m}.
\end{aligned} \tag{3.88}$$

Therefore, the most singular components of the Riemann tensor are $R_{UiUj} \sim U^{1/m-2}$.[10]

Although the Riemann tensor itself can be divergent at the horizon (depending on m), the displacement of nearby geodesics passing through the horizon will be negligible.

[10] As discussed previously, if $m = 1/n$ for integer n, the singular terms in the Riemann tensor vanish.

This can be seen if we integrate the geodesic deviation equation near $U = 0$ twice to find the tidal displacement for nearby geodesics. The most singular term in the displacement goes as $U^{1/m}$ which vanishes for $U = 0$. Thus, we see that fixed-area states have relatively mild divergences when working in the classical limit.

3.5 Summary and Discussion

Our work above studied the spacetime geometry intrinsic to fixed-area states at leading order in the bulk Newton constant G. While the saddle point geometries typically used to prepare such states contain conical singularities, they represent sources involved in the preparation and are not part of the fixed-area spacetime itself. Instead, the fixed-area spacetimes satisfy the usual equations of motion without conical singularities.

With either fine-tuning or enough symmetry, the fixed-area spacetimes can be completely smooth at leading order in G. More generally, however, derivatives of fields may diverge on null congruences fired orthogonally from the fixed-area surface. In particular, as described in Sec. 3.4.4, for states defined by cutting open Euclidean path integrals without a $U(1)$ symmetry, one typically finds the curvature tensor to diverge as $U^{1/m-2}$ as these null congruences are approached, where U is the affine null parameter orthogonal to the null congruence and $2\pi m$ is the opening angle of the Euclidean saddle that prepares the fixed-area state. The singularities are integrable, meaning that the total tidal distortion experienced by freely-falling particles crossing the null congruence is finite. Thus such singularities need not necessarily destroy infalling observers and, in fact, so long as the coefficients of such singularities are small the effect on such observers can be negligible.

Importantly, in our example in Sec. 3.4.2 we found that the equations of motion could be solved in a manner that continues the solution beyond the power-law divergences on

the lightcones of the HRT surface. The resulting solution then had a large smooth region in both the past and future wedges. While these regions are harder to analyze in higher dimensional contexts, as in the three-dimensional analysis of section 3.4.3 they will remain amenable to study via both standard perturbation theory and a near-horizon power series expansion. This provides strong evidence that a large smooth region will continue to exist in both the past and future wedges.[11] Furthermore, while the singularities we find at the horizons do in principle raise concerns regarding our control over the effect of any UV corrections on solutions in the past and future wedges, these concerns can be tamed by smearing out the HRT surface in the transverse directions and thus effectively introducing a UV cutoff.

Such singularities can be strong enough that they remove the spacetime from the realm in which the initial value problem for the Einstein-Hilbert gravity is well-posed. For example, in 3+1 dimensions standard such results require the curvature to be appropriately square-integrable [108, 109]. This is clearly violated for sufficiently large m. However, in our context this may not be a problem as we impose additional boundary conditions at the fixed-area surface (and, in effect, on the orthogonal null congruences) adapted from the Euclidean analysis of Ref. [73]. These conditions are chosen to make the Einstein-Hilbert variational principle well-defined, and one may hope that they similarly repair the initial value problem. However, we leave the detailed study of such issues for future work.

Additional singularities will arise once we consider quantum corrections. One way to see this is to recall the example of a bifurcate Killing horizon in which the Euclidean saddle had a $U(1)$ symmetry. Such saddles were just familiar Euclidean black holes with conical singularities inserted at the horizon so that they could match boundary conditions

[11] Though a spacelike singularity may develop after some proper time since, even before fixing the area, we might consider a state that describes a black hole.

with some period β_0 unrelated to the usual inverse temperature β of the Lorentz-signature fixed-area geometry. At the quantum level, this clearly prepares quantum fields around this black hole in a state of inverse temperature β_0 which differs from the inverse Hawking temperature β. This is well-known to give a singular stress tensor at the black hole horizon, and in fact the special case $\beta_0 = \infty$ corresponds to the Boulware vacuum state for the black hole. The Boulware vacuum is much like the Rindler vacuum on Rindler space, for which the stress tensor features a quadratic divergence at the horizon [110]. The associated back-reaction on the metric would then force the Ricci-tensor to be quadratically divergent as well, so that general integrated tidal distortions diverge logarithmically. This suggests that using fixed-area states beyond leading order in G will require taming this divergence by smearing out the fixed-area surface along the orthogonal two spacetime dimensions; see also related comments in Ref. [73]. This may also be related to issues regarding quantum corrections to HRT-areas seen in Ref. [61]. We hope to return to further study of such quantum corrections in the future.

It would also be useful to generalize our results to include perturbative higher-derivative corrections and non-minimal couplings. In this context, the area is replaced by a more general geometric entropy functional [111, 112]. Nevertheless, in the leading semi-classical approximation, states of fixed geometric-entropy states are again constructed by using Euclidean saddles with conical defects [73]. The general arguments described here should thus go through in a similar fashion. In particular, there is a similar power-series expansion for metric quantities in a conical defect spacetime in higher-derivative theories [73]. This will again give power-series solutions in the past and future wedges just as described in Sec. 3.4.1. However, an important difference in this case is that the power series expansion involves more singular terms. To resolve this, one may again consider a smeared version of the fixed geometric-entropy state in order to obtain reasonable initial data for Lorentzian evolution. It would be interesting to understand such solutions in

greater detail in future.

A final open question involves the states where we fix the area of an HRT surface γ_R that is anchored to an asymptotically AdS boundary (say, at the edges of a boundary subregion R). In this case, the area is divergent. While one can renormalize the HRT-area by subtracting its expectation value, fluctuations of this renormalized area remain divergent; see e.g. [7]. As a result, projecting onto a small window of HRT-area eigenvalues would remove the state from the CFT Hilbert space.[12] A useful notion of fixed-area state in this context will thus require the introduction of an appropriate boundary UV cutoff.

This then raises the question of how such UV issues will manifest themselves in the boundary-anchored versions of the calculations described in this work. One possibility is that, in the absence of a UV regulator, a singular shock will arise at the boundary anchors and will propagate into the bulk toward both past and future. On the other hand, related UV concerns arise in the study of the flow by taking Poisson brackets with the HRT area operator [104, 105, 106]. But in that context, at least in AdS_3, the behavior turns out to be milder. Indeed, in that context Ref. [105] showed that the bulk itself remains smooth, and that the CFT singularity is dual only to a singularity in the manner that the bulk and boundary are attached. It thus seems likely that boundary-anchored fixed-area geometries will be similar. A better understanding of the area operator from the CFT perspective, perhaps along the lines of Ref. [113], may also be useful for understanding such issues.

[12] The situation is much like that for the operator $:\phi^2(x):$ in the theory of a free scalar field.

Part II

Real-Time Replica Wormholes

Chapter 4

Real-time gravitational replicas: Formalism and a variational principle

4.1 Introduction

The path integral formulation of quantum theories has inherent advantages in Euclidean signature. In particular, the fact that the Euclidean action is non-negative in stable quantum field theories allows for a straightforward saddle point analysis. The presence of non-trivial saddles provides important insights into non-perturbative dynamics of the theory, as illustrated by the instanton solutions in non-abelian gauge theories. A direct first-principles Lorentzian path integral perspective on some of these issues is not as well developed for the simple reason that the rules for carrying out the stationary phase approximation have not been satisfactorily clarified.

However, despite a corresponding possible lack of rigor, path integrals may still be used to compute real-time correlation functions. To this end one often uses the Schwinger-

Keldysh formalism [114, 115] (involving a mixture of Euclidean and Lorentzian path integrals) or one of its out-of-time-order generalizations [116, 117, 118]. A purely Lorentz-signature path integral may also be used if one explicitly specifies the relevant quantum state.

Similar prescriptions also exist for computing the Rényi or von Neumann entropies that capture fine-grained notions of quantum information. To illustrate the point, consider the computation of such entropies in a quantum field theory in some time-dependent state $\rho(t)$. The state may be obtained from some past initial condition followed by evolution $\rho(t) = \mathcal{U}(t;t_0)\,\rho_0(t_0)\,\mathcal{U}(t;t_0)^\dagger$ in Lorentzian time t, potentially with a time-dependent Hamiltonian. The quantities of interest depend only on the information at the prescribed time t, and require no knowledge of the state at any future instant of time. The Rényi entropies which capture moments of the spectrum of the density operator $\mathrm{Tr}(\rho(t)^n)$ are naturally described using an n-fold replication of the system along with n-copies each of the forward and backward time evolution. Thus we can view the quantities as being defined on a suitable timefolded contour, see fig. 4.1.

Analogous statements also hold when computing spectral moments $\mathrm{Tr}(\rho_{\mathcal{A}}^n)$ of reduced density matrices restricted to some spatial domain $\mathcal{A}$ of the constant t time-slice. The main difference is that this case involves a non-trivial gluing of the timefolds due to implementing the partial trace over the complement $\mathcal{A}^c$ of $\mathcal{A}$. In the path integral, this partial trace requires sewing together along $\mathcal{A}^c$ the $\mathcal{U}(t;t_0)^\dagger$ and $\mathcal{U}(t;t_0)$ parts of each copy of the time-evolved state (i.e., of each copy of the piece shown at left in fig. 4.1). The remaining $\mathcal{A}$ regions of the $\mathcal{U}(t;t_0)^\dagger$ and $\mathcal{U}(t;t_0)$ parts of each copy are then connected cyclically as before (see again the right panel of fig. 4.1). Readers seeking more detailed reviews may consult e.g. [34, 119].

Note that nowhere in the above discussion were we required to invoke a Euclidean formulation of the theory. However, in practice it is sometimes efficacious to perform

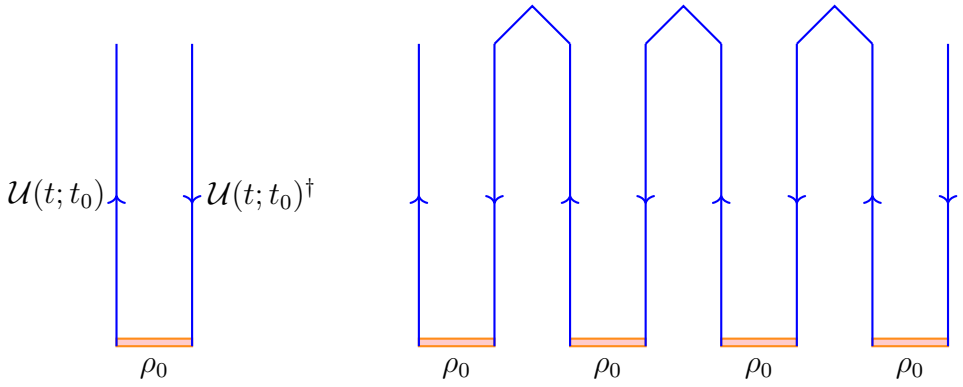

Figure 4.1: A schematic illustration of the real-time (Schwinger-Keldysh) contours for the computation of the density matrix $\rho(t)$ (left) and its powers (right). The past boundary condition is supplied by the prescribed initial state ρ_0 and the direction of time evolution is explicitly indicated by the arrows. Forward evolution corresponds to the ket part of the state while backward evolution corresponds to the bra part. The reduced density matrix $\rho_{\mathcal{A}}(t)$ associated with some spatial domain at $t = 0$ is obtained by sewing together the $\mathcal{U}(t;t_0)$ and $\mathcal{U}(t;t_0)^\dagger$ parts of the left panel along the complementary $t = 0$ domain $\mathcal{A}^c$, while leaving open the parts along $\mathcal{A}$. It's powers thus involve similar contractions between the two parts of any given copy, while the $\mathcal{A}$ parts are again contracted with neighboring copies as shown at right.

computations entirely in Euclidean space. This is particularly so if the quantity is being computed at a moment of time reflection symmetry. But analytic continuation can also be employed even in certain circumstances with explicit time dependence. Classic examples of the latter include computations of the growth of entanglement entropy in two dimensional CFTs following a global [120] or local [121] quantum quench. In such cases, one may proceed by identifying related Euclidean configurations and computing the entropies therein as a function of Euclidean time t_{E}. At the end of the day, the result of the Euclidean computation is then analytically continued to non-trivial Lorentzian times t by Wick rotating $t_{\text{E}} \to i\,t$. This allows one to obtain the desired real-time evolution of the entropies.

The reasons for employing the Euclidean crutch are two-fold. Firstly, at a technical level one can exploit the fact that the replication is geometrically easy to understand as the construction of a branched cover geometry, and in particular one that is branched

over a codimension-2 locus. The spectral moments of the density matrix are then given by partition functions on the branched cover. Secondly, one can evaluate such partition functions in a semiclassical approximation using a saddle-point analysis which, as for the instantons, is facilitated in the field theory context by the boundedness of the Euclidean action. A key fact that will play a crucial role below is that the resulting entropies are manifestly real in this computational scheme since they are written in terms of real Euclidean configurations.

The Euclidean perspective can thus be an efficient technical tool to eke out the answer for real-time quantities of interest. Unfortunately, it also has some major disadvantages. The first is that it is not obviously useful in contexts with general smooth-but-nonanalytic sources. And for related reasons, it can be difficult to use when Lorentzian sources are only approximately known (perhaps because they have been computed numerically). But from the conceptual point of view the main issue with a Euclidean approach is that the real-time dynamics lies obscured. While this lacuna is not particular to entropic quantities – the real-time dynamics of instantons is also not well understood – it ends up being striking in this context, especially when we also allow gravity to be dynamical, as for instance in the duals of holographic field theories.

To illustrate this, recall that holographic entanglement entropy prescriptions [66, 27] posit that the von Neumann entropy is computed by the area of a bulk codimension-2 extremal surface at leading (planar) order in an expansion at large central charge c_{eff}, or equivalently at small bulk Newton constant G_N with the bulk AdS scale ℓ_{AdS} held fixed.[1] The time-reflection symmetric RT prescription [66] is justified by a gravitational version of the replica construction [33] (following earlier such constructions [122, 123, 124, 125, 126]). The construction proceeds by noting that the standard AdS/CFT dictionary requires the

[1]It is convenient to define $c_{\text{eff}} = \frac{\ell_{\text{AdS}}^{d-1}}{16\pi G_N}$ as the effective central charge of a CFT_d dual to gravity in AdS_{d+1}.

dual gravitational spacetime to be the lowest action saddle-point solution to the Euclidean quantum gravity path integral whose boundary is the branched cover geometry described earlier.[2] The analysis of [33], which at its core is a generalization of the Gibbons-Hawking prescription for computing partition functions in Euclidean quantum gravity [32], focused on recovering the von Neumann entropy by noting that the gravitational replica construction takes a particularly simple form when analytically continued to replica numbers n close to 1. But this prescription also helps one understand the gravity dual of Rényi entropy [74].

This Euclidean quantum gravity perspective has been enormously helpful in clarifying various aspects of the holographic entanglement. For instance, it was used to establish that subleading corrections are given in terms of bulk entanglement across the homology surface[3] [28]. More generally, the quantum extremal surface prescription of [29] argues that, to all orders in a perturbative expansion at large central charge, the von Neumann entropy is given by extremizing the generalized entropy which is the combination of the leading order classical area term and the subleading bulk entanglement entropy. And this stronger result is likewise justified by an analogous variational argument in the Euclidean path integral [35, 38, 39].

While the standard derivation of the quantum extremal surface proposal stems from the Euclidean path integral, its physical implications are most striking in the realm of real-time evolution in the context of the black hole information paradox. As argued

[2]Technically, one has to worry about the fact that in gravitational theories (in contrast to quantum field theories) the Euclidean action is of indefinite sign owing to the conformal mode. The standard prescription [40] is to analytically continue the conformal mode to a presumed steepest-descent contour (which involves purely imaginary scale factors at 2^{nd} order about familiar solutions). We will assume that such a prescription has been employed to render the semiclassical Euclidean quantum gravity path integral sensible.

[3]The homology surface is a partial Cauchy surface of the bulk geometry whose boundaries are the extremal surface and the subregion of interest on the asymptotic boundary of the spacetime. The entanglement wedge is the bulk domain of dependence of this region cf., [127]. The notion of homology surface was originally introduced in [77] in contexts restricted to time-reflection symmetry.

originally by [37, 36] the quantum extremal surface associated with the entire boundary in an evaporating black hole undergoes a dynamical phase transition after which the entanglement wedge of the boundary no longer includes a portion of the black hole interior (called a quantum extremal 'island' in [92, 128]). This in particular reproduces the expected Page curve [129] of the evaporating black hole. A summary of these developments from the past year can be found in the review [130].

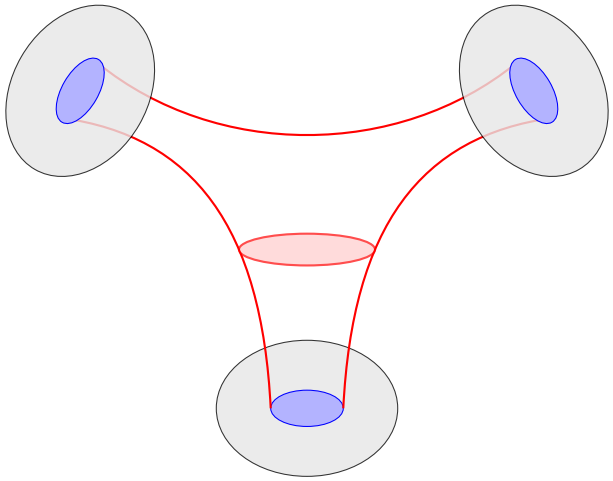

Figure 4.2: A replica wormhole spacetime that contributes in to the Euclidean path integral for the computation of spectral traces of density matrices.

As described above, the justification in most of the literature for the use of these quantum extremal surfaces has been based on Euclidean gravitational replica saddle-point geometries. Given the boundary replica spacetime, the presence of dynamical gravity in the bulk allows non-trivial replica symmetric configurations that connect different replica copies, leading to replica wormholes [38, 39]; see the schematic illustration in fig. 4.2. Such configurations are allowed because the quantum gravity path integral instructs us to sum over all geometries which can connect the given boundaries. In general there may be several different ways to do so respecting the boundary conditions and symmetries, perhaps allowing several different topologies for the Euclidean bulk. These geometries can, and often do, exchange dominance as one varies parameters. In particular, [38, 39]

argued that this leads to the aforementioned phase transition associated with the Page curve.

While replica wormholes define sensible Euclidean manifolds, the real-time dynamics of the above phase transition remains obscure. And while the technical construction in [38, 39] exploited specific features of low dimensional gravity models, as emphasized in [54] the basic lesson is that one should expect non-trivial replica wormhole contributions to general Euclidean path integrals.[4]

These developments thus suggest an important link between gravitational entropy and spacetime wormholes. But while this connection has been well fleshed out in the Euclidean context, the corresponding real-time story remains more obscure. Indeed, it is a classic result that replica-wormhole-like topologies do not admit smooth Lorentz-signature metrics. This is particularly clear if we assume replica symmetry, which for an n-fold replica would require the replica-invariant surface to have $2n$ distinct timelike normals with the property that no such normal can be deformed to any other while remaining timelike. Such surfaces cannot occur in smooth Lorentz-signature manifolds when $n \geq 2$. So one may ask what form any corresponding real-time saddles might take. Since black hole evaporation involves dynamical time-dependent geometries, a clearer understanding of the real-time description is imperative if we are to fully fathom the impact of spacetime wormholes on black hole information.

With these motivations in mind, let us revisit the real-time setup for computing entropies in gravitational theories.[5] Given a timefold replica contour at the boundary, our task is to ascertain the stationary points of the bulk Lorentzian Einstein-Hilbert

[4]Although we have couched our discussion in the holographic setting (in which the bulk spacetime is asymptotically AdS), the democratic nature of gravity makes it clear that similar statements apply in other contexts. See [131, 132, 133, 134, 135, 136, 137, 138, 55] for analyses of replica wormholes with other asymptotic boundary conditions.

[5]As argued in [55], this prescription is properly taken to compute 'swap entropies.'

action.[6] In the AdS/CFT context this problem was examined in [34] for use in deriving the covariant holographic entanglement entropy proposal. The authors of that work used the real-time AdS/CFT prescription of [139, 140] to motivate the resulting bulk spacetimes, primarily focusing on the von Neumann entropy ($n \to 1$). In the latter limit one has the advantage that the field equations may be analyzed perturbatively in the replica parameter $(n-1)$, which allows for considerable simplification. While the construction is in no way restricted to this regime, the analysis for $n > 1$ was not hitherto carried out in detail (though see Appendix A of [34]).

We will undertake a careful examination below of real-time gravitational replica saddles at finite $n-1$, arguing that the Einstein-Hilbert action does in fact admit stationary points but that the associated spacetimes have complex-valued metrics. In particular, in our formalism the time coordinate will remain real but the metric will take complex values in the spacetime interior (though boundary conditions will require the induced metric to remain real on e.g. timelike asymptotically-AdS boundaries). In simple cases the complex nature of the bulk can be encapsulated in an appropriate $i\varepsilon$ condition.

The appearance of complex solutions should come as no surprise. From the Schwinger-Keldysh point of view, it is natural to construct the quantum state ρ_0 of fig. 4.1 from an imaginary-time path integral, so that real spacetimes cannot describe the full timefolded field theory contour. More generally, while one may expect the real-time equations of motion governing stationary points to be real, there is no reason to expect this for the boundary conditions imposed by attaching any particular quantum state. Indeed, vacuum states for harmonic oscillators famously tend to impose positive-frequency boundary conditions which render any associated solutions intrinsically complex.[7] See e.g., section

[6] While the discussion here can be generalized to other gravitational theories to include higher derivative couplings or matter fields, for the sake of simplicity we will focus on just Einstein-Hilbert dynamics.

[7] Real-time correlation functions in thermal states of holographic field theories have also been argued to be computed on complex gravitational Schwinger-Keldysh geometries [141]. But while detailed analysis of observables shows consistency with field theory expectations [142, 143], a first-principles argument

4.3 of [144] for a discussion in language closely connected to that used here. In particular, it is the complex nature of such real-time stationary points that allows them to contribute anything other than a pure phase, and thus to reproduce Euclidean results in appropriate contexts.[8] Indeed, any stationary point that is invariant under the natural CPT-conjugation symmetry of any Rényi calculation (associated with exchanging the bra and ket parts in fig. 4.1) must contribute a real *amplitude* e^{iS_L}, thus necessitating an imaginary Lorentzian action S_L. This is in fact a manifestation of the general phenomenon noted some time ago [145] that singularities in the Lorentz-signature causal structure are associated with imaginary contributions to the Lorentzian action.

The goal of this work is to set up the variational problem for the determination of the gravitational replica saddle which computes the n^{th} (swap) Rényi entropy of an appropriate density matrix ρ_0. This sets the stage for constructing examples of such saddles in the companion paper [4]. Lorentz-signature replica wormholes and the associated Lorentzian path integrals were also recently discussed in [55], though the form of the saddle-point geometries was not analyzed in detail.

We begin in section 4.2 with a discussion of the relevant Lorentzian path integrals, emphasizing the space of bulk configurations over which we choose to sum. With replica boundary conditions, the bulk configurations are naturally called Lorentz-signature replica wormholes. We then set up an associated variational problem in section 4.3. In particular, the Einstein-Hilbert action extends naturally to our somewhat-singular Lorentzian configurations using ideas from [145] associated with the complex generalization of the Gauss-Bonnet theorem. And borrowing from the Euclidean discussion of [73] allows us

that they are unique saddle point of the gravitational path integral does not yet exist. Nevertheless, we will argue in appendix C.2 that these geometries do provide an useful arena to illustrate some of the ideas we discuss.

[8] In many cases this again leads to an $i\varepsilon$ prescription. Thus the above comment is then largely equivalent to noting that one might regularize the sewing of bra spacetimes to ket spacetimes by including a small Euclidean piece of spacetime, and that doing so would then require excursions into complex time. This one again suggests that the final solution is complex.

to introduce boundary conditions that make the associated variational principle well-defined. In the process we will elaborate on the symmetries of the replicas and general expectations for the saddle-point spacetimes. For completeness, we also present a brief discussion of initial conditions for our path integrals in section 4.4. Elements of these discussions are already present in [34] (see also [55]); our aim here is to elaborate on certain aspects for clarity, and to describe in detail the real-time variational problem for replica wormhole saddles. We close with a summary and discussion of future directions in section 4.5. The appendices contain some additional details of corner term contributions and an example with smooth complex valued metrics.

4.2 Path integrals for the density matrix and replicas

As described above, we would like to compute entropies (or, more precisely, swap entropies [55]) in holographic field theories without employing analytic continuation. To do so, let us first discuss the situation for standard quantum mechanical theories on a fixed spacetime (and thus without dynamical gravity) in section 4.2.1. We then address the case of dynamical gravity in section 4.2.2.

4.2.1 Replica path integrals in standard quantum theories

We begin by discussing the path integral that computes matrix elements of $\rho(t)$. Given an initial state ρ_0 at time t_0,[9] we can construct the density matrix $\rho(t)$ on a Cauchy slice Σ_t by applying time-dependent Hamiltonian evolution to write $\rho(t) = \mathcal{U}(t;t_0)\,\rho_0\,\mathcal{U}(t;t_0)^\dagger$. Taking a partial trace $\rho_{\mathcal{A}}(t) = \mathrm{Tr}_{\mathcal{A}^c}(\rho(t))$ then gives its restriction to a subregion $\rho_{\mathcal{A}}(t)$, where $\mathcal{A}$ and $\mathcal{A}^c$ are complementary to each other at time t. Here $\mathcal{U}(t;t_0)$ includes any explicit sources that may be introduced in the course of the evolution. Note that the path

[9] We will discuss initial states in section 4.4 below.

integral constructing the elements of the density matrix ρ involves a piece implementing $\mathcal{U}(t;t_0)$ for the forward evolution of its 'ket' $|\psi\rangle$ as well as another implementing $\mathcal{U}(t;t_0)^\dagger$ for the backward evolution for its 'bra' $\langle\psi|$. One may think of the former as integrating over fields in a 'ket spacetime' and the latter as integrating over fields in a 'bra spacetime,' with configurations weighted by $e^{i(S^{\rm k}-S^{\rm b})}$, with $S^{\rm k}, S^{\rm b}$ being the standard actions for fields on the ket and bra spacetimes respectively.

To construct the reduced density matrix $\rho_{\mathcal{A}}$, one traces $\rho(t)$ over the Hilbert space associated with the region $\mathcal{A}^c$. This is implemented in the path integral by identifying the associated ket and bra spacetimes at the final time along $\mathcal{A}^c$.[10] The result of this sewing is a time-folded (Schwinger-Keldysh) spacetime $\mathcal{B}$ over which the path integral is to be performed, see fig. 4.3.

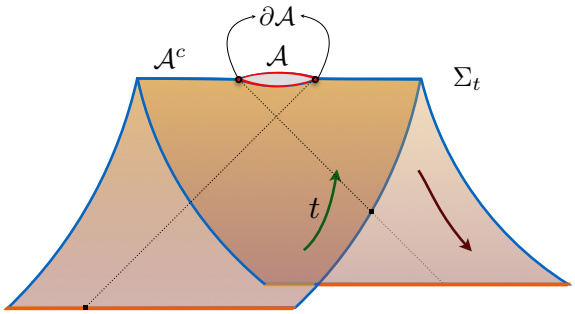

Figure 4.3: The timefolded Schwinger-Keldysh geometry $\mathcal{B}$ computing the matrix elements of $\rho_{\mathcal{A}}$ for a quantum theory on a fixed background. The forward and backward evolutions are glued together on the partial Cauchy slice Σ_t, except for a cut around $\mathcal{A}$. We have also indicated the past light-cones from the entangling surfaces which serve to demarcate the Milne and the Rindler wedges defined in the main text. In the gravitational context, the boundary geometries will be of this form.

The time-folded spacetime $\mathcal{B}$ has three causal domains of interest. Focusing on the ket piece of the contour we have:

1. The set $J^-[\partial\mathcal{A}]$ describing the causal past of $\partial\mathcal{A}$. We will refer to $J^-[\partial\mathcal{A}]$ as the

[10] One can equivalently project ρ against the maximally entangled state supported on two copies of $\mathcal{A}^c$, though this requires a notion of CPT conjugation to turn kets into bras.

Milne wedge.

2. The past domain of dependence $D^-[\mathcal{A}]$ of $\mathcal{A}$. We will refer to this region as the *Rindler wedge* of $\mathcal{A}$.

3. The analogous Rindler wedge of $\mathcal{A}^c$ defined as past domain of dependence $D^-[\mathcal{A}^c]$ of $\mathcal{A}^c$.

These regions are separated by 'Rindler horizons' defined by the past-directed null congruences orthogonal to $\partial\mathcal{A}$. The same regions are present on the bra piece of the contour. In particular, note that the causal nature of the Schwinger-Keldysh construction ensures that we consider only regions to the *past* of $\mathcal{A}$ and $\mathcal{A}^c$ on both bra and ket pieces of the contour, since we have not evolved the system beyond the Cauchy surface at time Σ_t.

4.2.2 Replica path integrals with dynamical gravity

We now discuss contexts with dynamical gravity, following the same basic approach as in section 4.2.1. For simplicity, we assume the system to be asymptotically AdS, and thus to have a well-defined notion of a boundary spacetime (at least in some given conformal frame). It is also convenient to assume some notion of AdS/CFT duality (though perhaps involving an ensemble of dual field theories as in [51], and as suggested by general discussions in [146, 147, 148, 54, 55]) so that we can motivate our bulk construction using the dual CFT.

In particular, we first describe a bulk path integral that may be said to compute the bulk description of matrix elements of the dual field theory restricted density matrix $\rho_{\mathcal{A}}(t)$. The boundary conditions for this path integral will be defined by the Schwinger-Keldysh contour $\mathcal{B}$ associated with matrix elements of $\rho_{\mathcal{A}}(t)$ described in section 4.2.1 above. Here $\mathcal{A}$, $\mathcal{A}^c$ are complementary regions within some boundary Cauchy slice Σ_t.

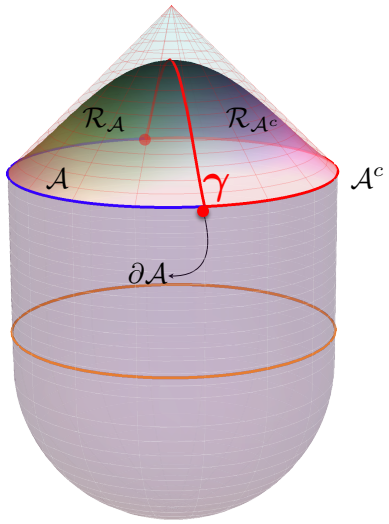

Figure 4.4: The bulk domains of interest in the Lorentzian construction for either the ket or the bra spacetime. Given a partition of Σ_t into regions $\mathcal{A}$ and $\mathcal{A}^c$, any bulk Cauchy surface $\tilde{\Sigma}_t$ with $\partial\tilde{\Sigma}_t = \Sigma_t$ admits a decomposition $\tilde{\Sigma}_t = \mathcal{R}_{\mathcal{A}} \cup \mathcal{R}_{\mathcal{A}^c}$. These domains are separated by a bulk codimension-2 surface $\boldsymbol{\gamma}$, which is anchored on the entangling surface. On saddle point solutions this surface approaches the extremal surface as $n \to 1$.

We will also need some further elements to describe the bulk geometries $\mathcal{M}$ (with $\partial\mathcal{M} = \mathcal{B}$) over which our path integral will sum. As in the boundary, the bulk spacetimes $\mathcal{M}$ will consist of bra and ket parts. Focusing first on the ket part, we imagine that we can use a standard bulk path integral to evolve the initial state wavefunction of the bulk forward (in the usual ADM sense) up to a bulk Cauchy slice $\tilde{\Sigma}_t$ with $\partial\tilde{\Sigma}_t = \Sigma_t$. The slice $\tilde{\Sigma}_t$ is not uniquely determined given Σ_t, but since Cauchy surfaces are achronal the surface $\tilde{\Sigma}_t$ must be everywhere spacelike separated from Σ_t; see fig. 4.4. At an extreme, we can take $\tilde{\Sigma}_t$ to be null, straddling the past boundary of the bulk domain of influence of Σ_t.

We now partition $\tilde{\Sigma}_t$ into two regions by introducing a bulk codimension-2 surface $\boldsymbol{\gamma}$ lying in $\tilde{\Sigma}_t$ (and thus which is codimension-1 in $\tilde{\Sigma}_t$). Following [55], we will call $\boldsymbol{\gamma}$ the splitting surface, though we will sometimes also refer to $\boldsymbol{\gamma}$ as the cosmic brane.[11] The

[11]It is perhaps natural to reserve the term 'cosmic brane' for the case where $\boldsymbol{\gamma}$ is associated with a

location of $\boldsymbol{\gamma}$ in a saddle-point geometry may eventually be determined dynamically from the variational principle, though for the moment we simply sum over all possible choices of $\boldsymbol{\gamma}$ (and also over all inequivalent choices of $\tilde{\Sigma}_t$, see further discussion below). The two resulting parts of $\tilde{\Sigma}_t$ will be called the homology surfaces $\mathcal{R}_{\mathcal{A}}$ and $\mathcal{R}_{\mathcal{A}^c}$ respectively of $\mathcal{A}$ and $\mathcal{A}^c$, with $\partial\mathcal{R}_{\mathcal{A}} = \mathcal{A} \cup \boldsymbol{\gamma}$ and $\partial\mathcal{R}_{\mathcal{A}^c} = \mathcal{A}^c \cup \boldsymbol{\gamma}$. This partition will also endow the bulk with three distinguished causal domains: the causal past $\tilde{J}^-[\boldsymbol{\gamma}]$ of the separatrix cosmic brane $\boldsymbol{\gamma}$, and the past domains of dependence $\tilde{D}^-[\mathcal{R}_{\mathcal{A}}]$ and $\tilde{D}^-[\mathcal{R}_{\mathcal{A}^c}]$ of the two homology surfaces. We will refer to the latter domains as the past homology wedges. We illustrate these bulk regions in fig. 4.4.

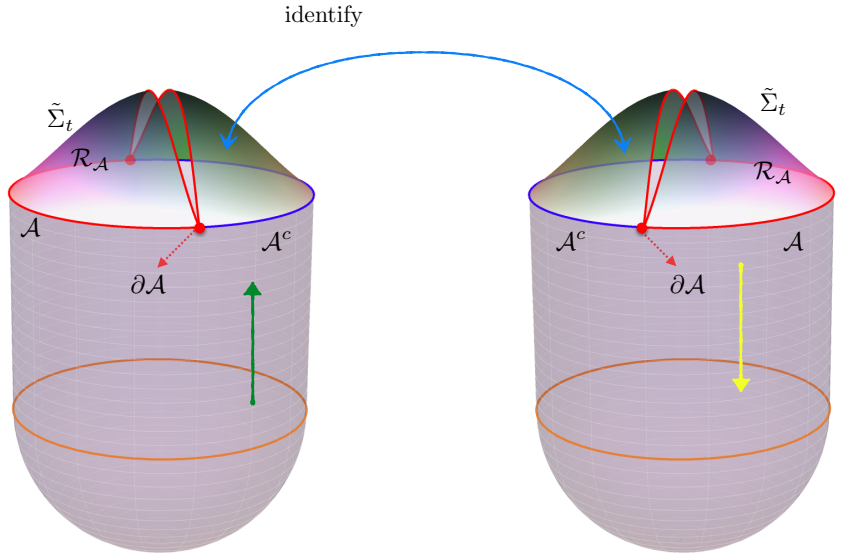

Figure 4.5: Bulk configurations relevant to computing the bulk dual of the boundary density matrix $\rho_{\mathcal{A}}(t)$. The forward evolution for $|\Psi\rangle$ (left) proceeds up to $\tilde{\Sigma}_t$, while the backwards evolution for $\langle\Psi|$ starts there (right). We have identified the bra and ket spacetime along $\mathcal{R}_{\mathcal{A}^c}$ in accord with the prescription for the bulk dual of $\rho_{\mathcal{A}}(t)$. Further gluing the two spacetimes together along $\mathcal{R}_{\mathcal{A}}$ and summing over all metrics would compute the trace of $\rho_{\mathcal{A}}(t)$.

The bra part of the geometry is constructed similarly, except that one now evolves

non-trivial delta-function in the Ricci scalar while using 'splitting surface' to include the case where the coefficient of this delta-function vanishes.

back to the initial state wavefunction. At the AdS boundary, the gluing between the bra and ket spacetimes is determined by the regions $\mathcal{A}$ and $\mathcal{A}^c$ on the boundary. It is natural to extend this gluing into the bulk by identifying the bra and ket spacetimes along $\mathcal{R}_{\mathcal{A}^c}$ and summing over bulk geometries to obtain the bulk dual of the reduced density matrix $\rho_{\mathcal{A}}$. Note that this sum over geometries can be said to implicitly sum over all inequivalent choices of $\tilde{\Sigma}_t$ and $\boldsymbol{\gamma}$, or alternatively to implicitly sum over all inequivalent choices of the resulting $\mathcal{R}_{\mathcal{A}}$ and $\mathcal{R}_{\mathcal{A}^c}$.

In the above, we have basically chosen the bulk configurations over which we sum to mimic the boundary contour $\mathcal{B}$, replacing the sewing across the boundary region $\mathcal{A}^c$ with sewing across the homology surface $\mathcal{R}_{\mathcal{A}^c}$. One can attempt to motivate this in a neighborhood of the boundary by the usual Fefferman-Graham expansion. And one can further motivate this prescription by cutting open bulk path integral computations of traces of powers of the density matrix in familiar cases as in [47] (in the discussion surrounding its figure 3). But for the present work we will simply declare the above to be our recipe, leaving for the future any attempt to upgrade the above naturalness arguments into a complete derivation. This will then lead to an ansatz for a bulk path integral that compute boundary (swap) Rényi entropies by summing over what we call Lorentz-signature replica wormholes. As we show in section 4.3, the key point will then be that such replica wormholes lead to a well-defined Einstein-Hilbert variational problem. Furthermore, when appropriately complexified, such real-time replica wormholes can provide stationary points that allow our path integral to be studied semiclassically.

To summarize, bulk configurations of the path integral associated with matrix elements of $\rho_{\mathcal{A}}$ have the following ingredients:

- An initial state wavefunction (or an Euclidean end-cap geometry, see section 4.4), prescribing the state ρ_0 from which we evolve.

- Lorentzian sections of the geometry for the ket and bra parts, with the flow of time dictated by the evolution direction specified at the boundary.

- A gluing condition across a homology surface $\mathcal{R}_{\mathcal{A}^c}$, with the flow of time reversing as we cross the gluing surface.

We now have the ingredients in place to set up the replica computation and define the bulk path integral for $\mathrm{Tr}(\rho_{\mathcal{A}}^n)$. To define the boundary conditions for the bulk path integral, we begin with n-copies of the bra and ket boundary geometries, each constructed in section 4.2.1 above. Labeling the boundary ket spacetimes as $\mathsf{B}_i^{\mathrm{k}}$ and the boundary bra spacetimes as $\mathsf{B}_i^{\mathrm{b}}$ (with $i = 1, 2, \cdots, n$), we sew these geometries into a Rényi boundary spacetime $\mathcal{B}_n$ by gluing $\mathsf{B}_i^{\mathrm{k}}$ onto $\mathsf{B}_i^{\mathrm{b}}$ along $\mathcal{A}^c$, and onto $\mathsf{B}_{i-1}^{\mathrm{b}}$ along $\mathcal{A}$. Here additions involving the index i are performed modulo n.

Turning now to the bulk, each path integral configuration will be formed from n bulk ket pieces $\mathsf{M}_i^{\mathrm{k}}$ and n bulk bra pieces $\mathsf{M}_i^{\mathrm{b}}$, with $i = 1, 2, \cdots, n$. We will sew these geometries into a bulk Rényi configuration by gluing $\mathsf{M}_i^{\mathrm{k}}$ onto $\mathsf{M}_i^{\mathrm{b}}$ along $\mathcal{R}_{\mathcal{A}^c}$, and onto $\mathsf{M}_{i-1}^{\mathrm{b}}$ along $\mathcal{R}_{\mathcal{A}}$. As in [55], we use the term Lorentz-signature replica wormholes to refer to any bulk spacetime of the above form, regardless of whether or not it is a stationary point of a variational principle. We depict such a configuration for $n = 2$ in fig. 4.6.

Note that above-described space of configurations for the bulk replica path integral has the following discrete symmetries:

- A cyclic $\mathbb{Z}_n$ replica symmetry that acts by shifting the bra and ket spacetimes by $i \to i + 1, \mod (n)$.

- For each copy i of the density matrix we have a $\mathbb{Z}_2$ involution associated with the CPT map (which involves anti-linear complex conjugation). This map exchanges corresponding bras and kets, with the i^{th} such CPT map acting as $\mathsf{M}_j^{\mathrm{k}} \leftrightarrow \mathsf{M}_{i-j}^{\mathrm{b}}$ (using addition modulo n).

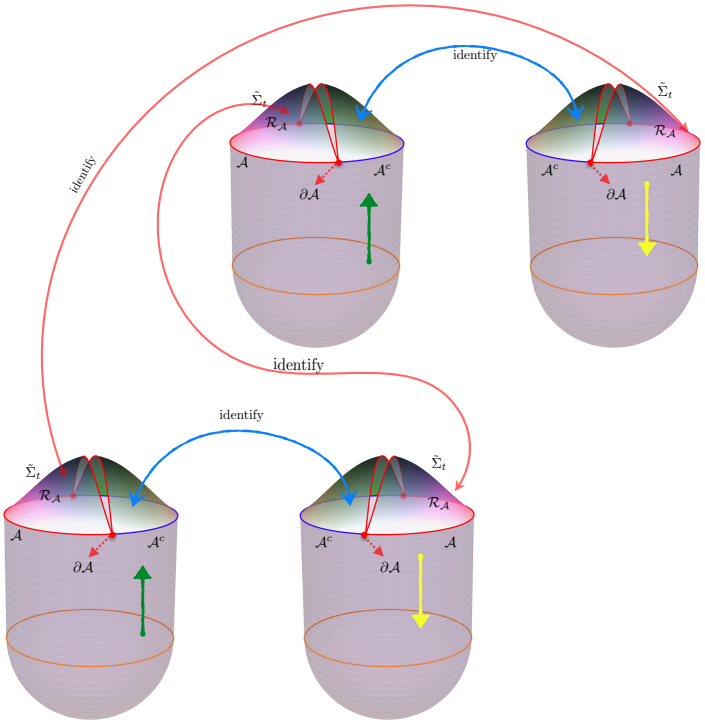

Figure 4.6: The form of configurations over which we sum in the bulk path integral for $\mathrm{Tr}(\rho_\mathcal{A}^2(t))$. We again use the conventions described in fig. 4.5.

By definition, our path integral sums over real such Lorentz-signature replica wormholes. However, in looking for saddle points $\mathcal{M}_n$ we will wish to deform the contour of integration to allow complex metrics. Indeed, it is familiar from standard quantum mechanics that processes forbidden by standard classical evolution are dominated by a complex saddle-point, as in the use of Euclidean paths to compute quantum tunneling. And in the gravitational Rényi context, it is clear that smooth Lorentz-signature metrics cannot yield saddles since for $n > 1$ the causal structure at $\boldsymbol{\gamma}$ is ill-defined. But we may hope to find complex saddles when the time coordinate remains real by allowing the metric to be complex.

It will thus be of interest below to study the action of the above symmetries on complex saddles. In doing so, in order to preserve the reality of $\mathrm{Tr}(\rho^n)$, the CPT maps should be extended so that they complex-conjugate the metric as well. Note that complex spacetimes which are symmetric under all of these symmetries remain real on the gluing surfaces (i.e., along $\mathcal{R}_{\mathcal{A}}$ and $\mathcal{R}_{\mathcal{A}^c}$ on each of the $2n$ copies of the spacetime), and this will in particular be true of symmetric saddles.[12] Furthermore, we expect deformations (of the location) of the homology surfaces $\mathcal{R}_{\mathcal{A}}$ and $\mathcal{R}_{\mathcal{A}^c}$ that do not affect $\boldsymbol{\gamma}$ to describe unitary evolution of the bulk that will cancel exactly between the bra and ket spacetimes on either side of the surface. We thus correspondingly expect that while the saddle-point dynamics may in some sense determine $\boldsymbol{\gamma}$, it should not lead to preferred choices for $\mathcal{R}_{\mathcal{A}}, \mathcal{R}_{\mathcal{A}^c}$. Symmetric saddle-points should thus remain real and Lorentz-signature within the entire homology wedges of $\mathcal{R}_{\mathcal{A}}, \mathcal{R}_{\mathcal{A}^c}$ so that the actions for these regions cancel between the bra and ket spacetimes for all choices of $\mathcal{R}_{\mathcal{A}}, \mathcal{R}_{\mathcal{A}^c}$. We will justify this expectation more fully when we study the variational principle below, but the upshot is that for symmetric saddles the homology wedges $\tilde{D}^-[\mathcal{R}_{\mathcal{A}}]$ and $\tilde{D}^-[\mathcal{R}_{\mathcal{A}^c}]$ will remain

[12] We will focus below on the solutions that preserve replica symmetry: it would be interesting to understand whether solutions that break the aforementioned symmetries could play a role analogous to replica symmetry breaking saddles; see e.g., [38, 72, 7, 101].

well-defined, and that such saddles will be complex only outside these homology wedges (in a region that we may still call the past Milne wedge $\tilde{J}^-[\boldsymbol{\gamma}]$ of $\boldsymbol{\gamma}$).

4.3 The variational problem

Section 4.2 described the branched and time-folded bulk spacetimes over which our replica path integral will sum, but we have not yet addressed the bulk dynamics in detail. Of course, we wish to take this to be described by the Einstein-Hilbert action. But while this action is familiar when evaluated on smooth Lorentz-signature spacetimes, it may not be immediately clear how to define contributions to this action from the region near $\boldsymbol{\gamma}$. Furthermore, the choice of action is intimately tied to the construction of a good variational problem. In particular, to ensure a good semiclassical limit we must show that varying our action within the class of allowed variations leads precisely to an appropriate formulation of the Einstein equations (without extra constraints).

We address these issues below. We begin in section 4.3.1 by quickly discussing the spacetime away from $\boldsymbol{\gamma}$. We then define contributions to our Einstein-Hilbert action from the region near $\boldsymbol{\gamma}$ in section 4.3.2 and discuss boundary conditions to be imposed at $\boldsymbol{\gamma}$ in sections section 4.3.3 and section 4.3.4. Together, these yield a well-defined variational principle as desired. All of this treats the full n-fold replica geometry $\mathcal{M}_n$ with boundary $\mathcal{B}_n$. section 4.3.5 then briefly describes the implications when one imposes replica symmetry and describes the bulk using the geometry $\widehat{\mathcal{M}}_n = \mathcal{M}_n/\mathbb{Z}_n$ associated with a single fundamental domain.

4.3.1 The action and variations away from the splitting surface

Heuristically, we define the gravitational dynamics by the real-time path integral:

$$Z[\mathcal{B}_n] := \int_n [Dg]\, e^{i\,S}, \tag{4.1}$$

with the subscript n reminding us that we are computing the path integral over bulk replica wormholes with the gluing conditions specified above and with boundary conditions defined by $\mathcal{B}_n$. We will take

$$S = S^k_{\rm gr} - S^b_{\rm gr} + S_{\boldsymbol{\gamma}}, \tag{4.2}$$

where $S^k_{\rm gr}$ is the standard gravitational action for the ket parts of the spacetime, $S^b_{\rm gr}$ is the standard gravitational action for the bra parts of the spacetime, and $S_{\boldsymbol{\gamma}}$ is a contribution to S from the splitting surface $\boldsymbol{\gamma}$ that we will address more carefully below. If we can define and solve the variational problem for the bulk geometry $\mathcal{M}_n$, the Rényi entropies will be obtained from the standard formula

$$S^{(n)}_{\mathcal{A}} = \frac{1}{1-n}\,\log\left(\frac{Z[\mathcal{B}_n]}{Z[\mathcal{B}]^n}\right) = \frac{1}{n-1}\,(I_n - n\,I_1)\ , \tag{4.3}$$

where $I_n := -\log Z[\mathcal{B}_n] \approx -i\,S[\mathcal{M}_n]$.

The gravitational action with which we work is the Einstein-Hilbert action, supplemented with the usual Gibbons-Hawking term at any boundaries. We also include additional counter-terms $S_{\rm ct}$ at the asymptotic boundary as required. For any bra or ket

piece $\mathcal{M}$ of $\mathcal{M}_n$ we thus have

$$S_{\rm gr}[\mathcal{M}] = \frac{1}{16\pi G_N}\int_{\mathcal{M}} d^{d+1}x\,\sqrt{-g}\left[R+\frac{d(d-1)}{\ell^2_{\rm AdS}}\right] + \frac{1}{8\pi G_N}\int_{\mathcal{B}} d^dx\,\sqrt{|\gamma|}\,K \\ + \frac{1}{8\pi G_N}\int_{\mathcal{R}_{\mathcal{A}}\cup\mathcal{R}_{\mathcal{A}^c}} d^dx\,\sqrt{h}\,K + S_{\rm ct}\,, \tag{4.4}$$

where $\mathcal{B}$ is the asymptotic boundary $\mathcal{M}$. Note in particular that we include a Gibbons-Hawking term on the gluing surfaces $\mathcal{R}_{\mathcal{A}}, \mathcal{R}_{\mathcal{A}^c}$. If the metric and extrinsic curvature are continuous, these Gibbons-Hawking terms will cancel between the bra and ket parts of the spacetime when computing $S_{\rm gr} = S^k_{\rm gr} - S^b_{\rm gr}$. Continuity of the metric is required by the sewing along $\mathcal{R}_{\mathcal{A}} \cup \mathcal{R}_{\mathcal{A}^c}$, but continuity of the extrinsic curvature should not be assumed a priori. For future reference our notation is as follows: g_{AB} denotes the metric in the bulk spacetime $\mathcal{M}$, $\gamma_{\mu\nu}$ that on the asymptotic boundary $\mathcal{B}$, and h_{ij} the metric induced on the homology surfaces $\mathcal{R}_{\mathcal{A}} \cup \mathcal{R}_{\mathcal{A}^c}$. We will later also introduce a metric q_{IJ} on $\boldsymbol{\gamma}$.

Varying the exponent of (4.1) with respect to the metric at generic points results in the standard Einstein-Hilbert equations of motion. However, we should more carefully consider variations at the various copies of $\tilde{\Sigma}_t$ where different branches of the spacetime join. This is especially true in the vicinity of the splitting surface which, in the limit $n \to 1$, will give us the Hubeny-Rangamani-Takayanagi (HRT) surface [27]. Nevertheless, we begin by addressing the simpler cases of $\mathcal{R}_{\mathcal{A}}, \mathcal{R}_{\mathcal{A}^c} \subset \tilde{\Sigma}_t$, saving consideration of the region near $\boldsymbol{\gamma}$ for sections section 4.3.2-4.3.4.

Recall then that our action (4.4) included Gibbons-Hawking terms at $\mathcal{R}_{\mathcal{A}}, \mathcal{R}_{\mathcal{A}^c}$ for both the bra and ket parts of the spacetime. The gluing conditions at $\mathcal{R}_{\mathcal{A}}, \mathcal{R}_{\mathcal{A}^c}$ require continuity of the metric, so such terms will cancel between the bra and ket parts if the extrinsic curvature is also continuous. But, recognizing that the support of the gravitational path integral may include rather wild non-smooth geometries, we should use

the variational principle to derive any conditions on the extrinsic curvature at $\mathcal{R}_{\mathcal{A}}, \mathcal{R}_{\mathcal{A}^c}$.

Having included these Gibbons-Hawking terms, it is straightforward to do so. As is well-known, working about a spacetime that satisfies the Einstein equations away from $\mathcal{R}_{\mathcal{A}}, \mathcal{R}_{\mathcal{A}^c}$, and $\boldsymbol{\gamma}$, variations that preserve boundary conditions on $\mathcal{B}_n$ give

$$\delta S_{\rm gr}[\mathcal{M}] = \frac{1}{16\pi G_N} \int_{\mathcal{R}_{\mathcal{A}} \cup \mathcal{R}_{\mathcal{A}^c}} \sqrt{h}\, \pi_{ij}\, \delta h^{ij}\,, \qquad \pi_{ij} = K_{ij} - K\, h_{ij}\,, \tag{4.5}$$

where h_{ij} is again the induced metric on $\mathcal{R}_{\mathcal{A}} \cup \mathcal{R}_{\mathcal{A}^c}$ and now π_{ij} is its the conjugate momentum. Variations of $S_{\rm gr} = S^k_{\rm gr} - S^b_{\rm gr}$ thus involve the change $\Delta\pi_{ij}$ in π_{ij} when passing from a bra to a ket spacetime across $\mathcal{R}_{\mathcal{A}}$ or $\mathcal{R}_{\mathcal{A}^c}$. Stationarity of $S_{\rm gr}$ implies $\Delta\pi_{ij} = 0$. Since the gluing already requires continuity of the induced metric, we see that the extrinsic curvature must be continuous as well.

This fact has important consequences for the causal structure of saddles with replica and CPT symmetry. As noted at the end of section 4.2, imposing both symmetries forces the induced metric to be real on $\mathcal{R}_{\mathcal{A}}$ and $\mathcal{R}_{\mathcal{A}^c}$. Moreover, it requires the extrinsic curvature defined there from the bra side to be the complex conjugate of that defined from the ket side. But we have seen that stationarity also compels these complex conjugate extrinsic curvatures to agree, so saddle-point geometries must have real extrinsic curvatures on $\mathcal{R}_{\mathcal{A}}$ and $\mathcal{R}_{\mathcal{A}^c}$. Since the saddle-point geometry will satisfy the usual hyperbolic equations of Einstein-Hilbert gravity away from $\tilde{\Sigma}_t$, Cauchy evolution toward the past from $\mathcal{R}_{\mathcal{A}}, \mathcal{R}_{\mathcal{A}^c}$ obliges the metric to remain real throughout the homology wedges of $\mathcal{R}_{\mathcal{A}}, \mathcal{R}_{\mathcal{A}^c}$ in saddles preserving both replica and CPT symmetries. This completes the previously advertised argument that symmetric saddles have well-defined homology wedges as expected from more general considerations mentioned above.

As in the Euclidean discussion of [33], there are two ways to proceed with specifying the remainder of the variational problem:

1. We could work with the full n-fold geometry $\mathcal{M}_n$ which defines a stationary point of the variational principle satisfying the full asymptotic boundary conditions $\mathcal{B}_n$. For reasons that will be clear below, we henceforce refer to $\mathcal{M}_n$ as the *covering space* geometry. If desired, we may attempt to simplify the problem of solving the equations of motion by imposing on $\mathcal{M}_n$ any of the symmetries described above.

2. Alternately, if we are interested only in symmetric saddles we can impose $\mathbb{Z}_n$ replica symmetry from the outset and consider the quotient spacetime $\widehat{\mathcal{M}}_n = \mathcal{M}_n/\mathbb{Z}_n$. Clearly, $\mathcal{M}_n$ is an n-fold cover of $\widehat{\mathcal{M}}_n$. We will refer to $\widehat{\mathcal{M}}_n$ as a single *fundamental domain* below following the terminology of [149]. The fundamental domain will include a single bra branch and a single ket branch. Note that there is only one splitting surface $\boldsymbol{\gamma}$ in $\mathcal{M}_n$, so it must remain fixed under the action of the replica symmetry group. As a result, one expects the quotient spacetime to have an explicit source of curvature (a cosmic brane) localized along $\boldsymbol{\gamma}$. As in [33], the fundamental domain description is particularly useful in analytically continuing to non-integer n (when effects that break replica symmetry can be ignored).

Note that the covering space perspective is the more general of the two, in that it also allows discussion of saddles that break replica symmetry. Such saddles have recently been shown to be important near phase transitions [38, 72, 101]. Furthermore, working in the covering space provides the cleaner description of the physics as it avoids introducing artificial singularities at $\boldsymbol{\gamma}$. We therefore focus on this perspective through section 4.3.4 below. However, we will return to the quotient $\widehat{\mathcal{M}}_n = \mathcal{M}_n/\mathbb{Z}_n$ in section 4.3.5 since (as in [33]) in simple cases this perspective greatly simplifies analytic continuation to non-integer n.

4.3.2 Contributions to the action from the splitting surface

It remains to discuss contributions to S in (4.2) from the region near the cosmic brane $\boldsymbol{\gamma}$. We focus here on defining such contributions, postponing to sections section 4.3.3 and section 4.3.4 the description of boundary conditions at $\boldsymbol{\gamma}$ that make the variational principle well-defined. In particular, here we wish to understand whether there are delta-function-like contributions to the Ricci scalar at $\boldsymbol{\gamma}$ that should be taken to give finite contributions $S_{\boldsymbol{\gamma}}$ to $S_{\rm gr}$.[13] At first sight, the situation may appear especially confusing due to the fact that $\boldsymbol{\gamma}$ lies at the boundary between the bra and ket parts of the spacetime, and thus at the locus where the action changes sign.

However, things are simpler than they appear. Since we expect no strong curvatures from the directions along the brane, any such delta-functions contributions will be associated with the metric transverse to the brane. The problem thus becomes effectively two-dimensional in the plane normal to $\boldsymbol{\gamma}$, which we recall has Lorentz signature. We may thus *define* the contribution $S_{\boldsymbol{\gamma}}$ from a small tubular region $\mathcal{U}_\epsilon$ containing $\boldsymbol{\gamma}$ by using a generalization of the Gauss-Bonnet theorem. Topologically, we require $\mathcal{U}_\epsilon$ to be the product $\tilde{\mathcal{U}}_\epsilon \times \boldsymbol{\gamma}$ for an appropriate two-dimensional space $\tilde{\mathcal{U}}_\epsilon$, so that we may apply our Gauss-Bonnet theorem to the latter.

The idea of using a generalization of the Gauss-Bonnet theorem was suggested in e.g., [145]. However, we use a slightly different generalization due to the fact that $\boldsymbol{\gamma}$ lies on a timefold. The required generalization may be motivated by analytically continuing a Euclidean metric as $t_{\rm E} \to i t_{\rm L}$ in the ket parts of the spacetime, but using the complex conjugate $t_{\rm E} \to -i t_{\rm L}$ in the bra parts of the spacetime. This is the same change of sign that creates the timefold as it gives $t_{\rm L} < 0$ in both the bra and ket parts (though we

[13] We should emphasize here that our preceeding discussion makes clear that there are no singularities along the past light-cone of $\boldsymbol{\gamma}$. The delta function curvature singularities are localized solely on the codimension-2 fixed point locus.

think of the bra parts as coming from $t_{\rm E} > 0$). It is then associated with particular signs in our Gauss-Bonnet theorem. As in [145], the resulting Gauss-Bonnet theorem will also involve various factors of $i = \sqrt{-1}$.

To describe the relevant signs, it is useful to introduce $\eta = \pm 1$ taking the positive sign on the ket parts of the spacetime and taking the negative sign on the bra parts of the spacetime. This allows us to define the action contribution from $\mathcal{U}_\epsilon$ by

$$\begin{aligned} iS_{\boldsymbol{\gamma}} &:= \lim_{\epsilon\to 0} \frac{i}{16\pi G_N} \int_{\mathcal{U}_\epsilon} d^{d+1}x\ \eta\sqrt{-g}R \\ &:= \lim_{\epsilon\to 0} \frac{-i}{8\pi G_N} \int_{\partial\mathcal{U}_\epsilon} d^d x\ \eta\sqrt{|h|}\,K + \frac{1}{4G_N}\,\chi(\tilde{\mathcal{U}}_\epsilon)\,A_{\boldsymbol{\gamma}}. \end{aligned} \tag{4.6}$$

The extrinsic curvature term in (4.6) is subtle and requires detailed comment. First, in Lorentz signature it receives imaginary delta-function-like contributions from submanifolds of $\partial\mathcal{U}_\epsilon$ where $\partial\mathcal{U}_\epsilon$ changes from spacetime to timelike (or vice versa). This is most easily seen in the $1+1$ case where K can be written as the derivative of the boost parameter θ (aka rapidity) describing the tangent to $\partial\mathcal{U}_\epsilon$. Since null tangents have $\theta = \infty$, the boost parameter θ has a pole at such transitions. Furthermore, in the ket part of the spacetime and when a timelike portion of $\partial\mathcal{U}_\epsilon$ is attached to a spacelike portion of $\partial\mathcal{U}_\epsilon$ that lies to its past, the above analytic continuation recipe makes θ real on the timelike portions (where the normal is spacelike) but yields $\theta \in i\frac{\pi}{2} + \mathbb{R}$ on spacelike portions (where the normal is timelike). Integrating through the transition in a ket part of the spacetime thus yields a finite contribution $i\frac{\pi}{2}$, or $-i\frac{\pi}{2}$ in the alternate case where the timelike portion of $\partial\mathcal{U}_\epsilon$ is attached to a spacelike portion of $\partial\mathcal{U}_\epsilon$ that lies to its future. In higher dimensions the contribution is similarly $\pm i\frac{\pi}{2}A_\parallel$, where the longitudinal area $A_\parallel$ becomes $A_{\boldsymbol{\gamma}}$ in the limit $\epsilon \to 0$. Contributions from the bra parts of the spacetime take the complex-conjugate form. These localized contributions (from both the ket and bra parts) are shown explicitly as the last term in (4.6) and are therefore no longer included

in the extrinsic curvature term there.

The other subtlety involves the possibility of explicit corner contributions to the extrinsic curvature term when $\partial\mathcal{U}_\epsilon$ is not smooth. In particular, such terms arise if $\mathcal{U}_\epsilon$ fails to have orthogonal intersection with $\mathcal{R}_\mathcal{A} \cup \mathcal{R}_{\mathcal{A}^c}$ so that there is an abrupt change in the normal to $\partial\tilde{\mathcal{U}}_\epsilon$ when crossing from a ket spacetime to the attached bra spacetime.[14] The interested reader can find a discussion of such terms in appendix C.1, but for the moment we simply choose $\partial\mathcal{U}_\epsilon$ smooth to avoid such terms.[15] In particular, we take $\partial\mathcal{U}_\epsilon$ to be of the form depicted by the blue surface in fig. 4.7.

The extrinsic curvature thus gives both real and imaginary contributions to (4.6). However, for spacetimes that are symmetric under both the $\mathbb{Z}_n$ cyclic symmetry and the conjugation symmetry, the imaginary contributions from the extrinsic curvature term cancel between the bra and ket parts of the spacetime. Such spacetimes thus have real weight e^{iS} as required by the conjugation symmetry. As discussed in appendix C.2, the spacetime of [143] realizes the framework described here in an $n = 1$ Schwinger-Keldysh example that illustrates the reality of e^{iS} in a particularly explicit manner.

Before proceeding, we emphasize that (4.6) is to define the action in the full region $\tilde{\mathcal{U}}_\epsilon$. Thus while the Gibbons-Hawking term in (4.4) was written as an integral over $\mathcal{R}_\mathcal{A} \cup \mathcal{R}_{\mathcal{A}^c}$, for consistency it should be understood as being defined by integrating only over the parts $\mathcal{R}^\epsilon_\mathcal{A} \cup \mathcal{R}^\epsilon_{\mathcal{A}^c}$ of $\mathcal{R}_\mathcal{A} \cup \mathcal{R}_{\mathcal{A}^c}$ that lie outside $\mathcal{U}_\epsilon$ and then taking the limit $\epsilon \to 0$.

Due to the above subtleties, in calculating the path integral weight for a conjugation-symmetric saddle it will often be simplest to compute just the ket contributions to S (including the ket contributions to (4.6)), and then to use the conjugation symmetry to

[14] This can happen with the surface $\partial\tilde{\mathcal{U}}_\epsilon$ either remaining entirely spacelike, or having both spacelike and timelike pieces. In the latter case, there are the contributions from the change in the signature described above. In addition one also encounters corner terms from the intersection of the timelike part of $\partial\tilde{\mathcal{U}}_\epsilon$ with $\mathcal{R}_\mathcal{A} \cup \mathcal{R}_{\mathcal{A}^c}$. These however give a real contribution and thus cancel out in between the ket and the bra.

[15] A good general discussion can be found in [150] though such contributions have been considered various earlier discussions eg., [151, 152, 34].

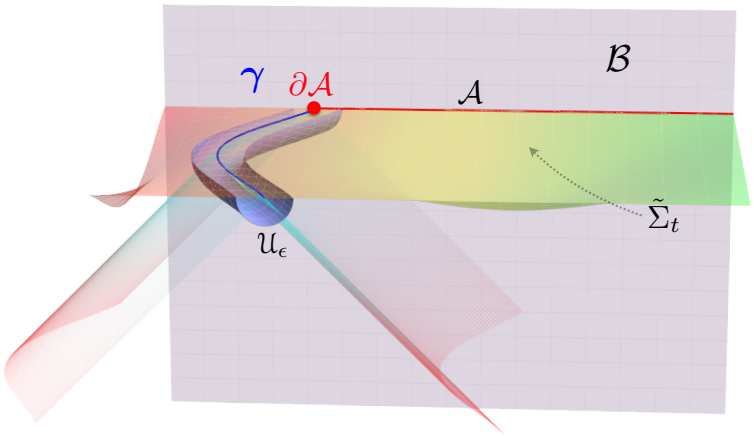

Figure 4.7: Regulating the fixed point locus in the spacetime by excising a tubular neighbourhood around it. fig. 4.8 displays a slice through this at fixed y^I for ease of visualization.

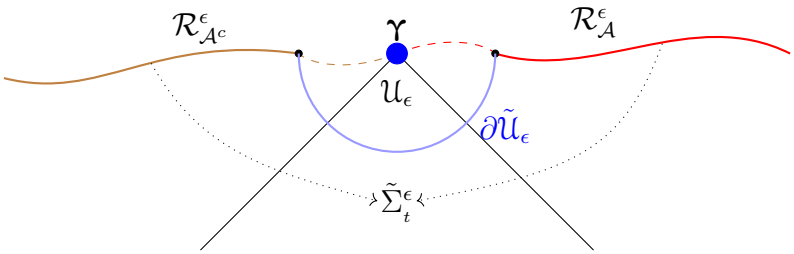

Figure 4.8: The local geometry in the cosmic brane excised spacetime shown at fixed y^I. The inner boundary consists of half of $\partial\tilde{\mathcal{U}}_\epsilon$ (blue), along with two regions we call $\mathcal{R}^\epsilon_{\mathcal{A}}, \mathcal{R}^\epsilon_{\mathcal{A}^c}$ (solid red and brown lines). The latter are regulated versions of $\mathcal{R}_{\mathcal{A}}, \mathcal{R}_{\mathcal{A}^c}$ with the differences indicated by dashed lines. The Gibbons-Hawking term associated with $\mathcal{R}_{\mathcal{A}} \cup \mathcal{R}_{\mathcal{A}^c}$ in (4.4) should understood as the $\epsilon \to 0$ limit of the integral over $\mathcal{R}^\epsilon_{\mathcal{A}} \cup \mathcal{R}^\epsilon_{\mathcal{A}^c}$.

Figure 4.9: The local geometry near the cosmic brane and the boundary conditions in Lorentz signature. We have exhibited here the regulated ket spacetime $\mathsf{M}^{\mathrm{k}}_\epsilon$ which is obtained from M^{k} by excising a topological half-disc ribbon around the fixed point locus $\boldsymbol{\gamma}$ (i.e., half of the exicison domain $\mathcal{U}_\epsilon$).

write the bra contributions as the complex conjugates. In doing so, one may wish to employ an alternate accounting scheme in which the splitting surface contribution (4.6) is absorbed into the contributions from the ket and bra parts of the spacetime. This alternate scheme is described in appendix C.1. We also discuss there the inclusion of explicit corner terms that necessarily arise if one wishes to avoid the presence of timelike pieces of $\partial\mathcal{U}_\epsilon$.

It now remains to evaluate (4.6) on interesting configurations and to understand the implications for our variational principle. Our approach will be to use previous work on the Euclidean replica problem to motivate a useful ansatz for the metric near $\boldsymbol{\gamma}$, and then to check that this ansatz allows for stationary points of the full action S under variations of the metric near $\boldsymbol{\gamma}$.

4.3.3 Imaginary-time boundary conditions at the splitting surface

As stated above, we will first review the boundary conditions at $\boldsymbol{\gamma}$ associated with the analogous variational problem in Euclidean signature. Although we are interested here in the covering space perspective, and while the covering space is smooth in Euclidean signature, it will nevertheless be useful to allow a localized delta-function source of curvature at $\boldsymbol{\gamma}$ in the (generally off-shell) metric configurations that we consider. As is well known, this gives a conical defect, though the condition that the defect should vanish on-shell can be recovered from an equation of motion associated with variations with respect to the area $A_{\boldsymbol{\gamma}}$ of $\boldsymbol{\gamma}$. This perspective will be useful in the real-time context where the real Lorentz-signature replica wormholes require causal singularities so that, with replica boundary conditions, there are simply no smooth Lorentz-signature metrics on which to base a discussion of the real-time variational problem. Interpreting the vanishing-defect condition as an equation of motion rather than a boundary condition will thus allow us to formulate a variational principle on the original contour of integration defined by real Lorentz-signature metrics, even if the final stationary points can be accessed only by deforming this contour into the complex plane.

We parameterize the Euclidean conical defect by using $2\pi m$ to denote the full angle around the cone, by which we mean that small circles of radius r about the defect have

circumference $2\pi mr$. Thus the case $m = 1$ is smooth. For later use, we allow m to be independent of the replica number n.

As discussed in [153], a convenient set of quasi-cylindrical coordinates generalizing the notion of Gaussian or Riemann normal coordinates can be constructed using geodesics launched orthogonally from the conical defect. We pick $(r, t_{\scriptscriptstyle \rm E})$ to parameterize the normal plane and y^I to be longitudinal along the cosmic brane. In such coordinates, with the cosmic brane located at $r = 0$, the metric can be taken to have the form

$$ds^2 = dr^2 + \big(m^2 + \mathcal{O}(r^\alpha)\big)\, r^2\, dt_{\scriptscriptstyle \rm E}^2 + \mathcal{O}(r^0)\, dy^I dy^J + \mathcal{O}(r^2)\, dt_{\scriptscriptstyle \rm E} dy^I\,. \tag{4.7}$$

Here $t_{\scriptscriptstyle \rm E}$ is an angular coordinate taking values in $[0, 2\pi)$ and the y^I denote an arbitrary set of coordinates on the conical defect. We take the rates of radial fall-off to be as prescribed in (4.7) with the constraint $\alpha > 1$. The metric coefficients may contain arbitrary functions of $(r, t_{\scriptscriptstyle \rm E}, y^I)$ subject to periodicity under $t_{\scriptscriptstyle \rm E} \to t_{\scriptscriptstyle \rm E} + 2\pi$. As a result, all the functions can be expanded in a Fourier series involving only integral powers of $e^{it_{\scriptscriptstyle \rm E}}$.

It will be useful below to pass to complex coordinates. If this is an n-replica calculation, it will be useful to choose coordinates $v, \bar{v}$ adapted to a single replica in the sense that $v, \bar{v}$ are periodic in $t_{\scriptscriptstyle \rm E}$ with period $\frac{2\pi}{n}$, and also such that $v, \bar{v}$ are real on the CPT-invariant surfaces.[16] In particular, we take $v = r^{\frac{1}{\hat{m}}}\, e^{int_{\scriptscriptstyle \rm E}}$ with $\hat{m} := \frac{m}{n}$. In terms of this $v, \bar{v}$, the metric (4.7) becomes

$$\begin{aligned} ds^2 &= \hat{m}^2 (v\bar{v})^{\hat{m}-1}\, dv d\bar{v} + T\, \frac{(\bar{v}\, dv - v\, d\bar{v})^2}{(v\bar{v})^{2-\hat{m}}} + q_{IJ}\, dy^I dy^J + 2i\, W_J\, dy^J\, \frac{\bar{v} dv - v d\bar{v}}{v\bar{v}}, \\ T &= \mathcal{O}(r^\alpha) = \mathcal{O}(v\bar{v})^{\frac{\alpha m}{2n}} = \mathcal{O}(v\bar{v})^{\frac{\alpha \hat{m}}{2}}\,, \quad q_{IJ} = \mathcal{O}(r^0) = \mathcal{O}(v\bar{v})^0\,, \\ W_J &= \mathcal{O}(r^2) = \mathcal{O}(v\bar{v})^{\frac{m}{n}} = \mathcal{O}(v\bar{v})^{\hat{m}}\,. \end{aligned} \tag{4.8}$$

[16] Thus our $v, \bar{v}$ are not the $z, \bar{z}$ of [73].

Since $v\bar{v}$ is real and positive, we may define fractional powers (e.g., $(v\bar{v})^{\hat{m}}$) to be real and positive as well. Note that periodicity in t_{E} requires the metric functions T, q_{IJ}, W_J to contain only integer powers of $v^{1/n}$ and $\bar{v}^{1/n}$, except where they appear in the manifestly real combination $v\bar{v}$. Furthermore, replica symmetry solutions will involve only integer powers of $v, \bar{v}$ (except in the combination $v\bar{v}$).

Having specified the local geometry (4.8) in the vicinity of the splitting surface, we can proceed to show that Einstein-Hilbert variational problem is well-defined. To this end, let us first focus on the modified variational problem defined as in [33] by using the Einstein-Hilbert action but removing the delta-function curvature contribution normally associated with the conical singularity. We denote the resulting brane-excised Euclidean action by $\check{I}_{m,n}$. One may think of $\check{I}_{m,n}$ as being defined by simply dropping the $S_{\boldsymbol{\gamma}}$ term from (4.2) without changing the definition of the other terms.[17] Although the parameters m, n play very different roles – with m controlling the conical singularity and n controlling only our description of the spacetime through the definition of the coordinates $v, \bar{v}$ – it will be useful to keep both labels in $\check{I}_{m,n}$ for comparison with the real-time discussion below.

The analysis of [73] then shows that, for fixed m and n, requiring the behavior (4.8) suffices to make $\check{I}_{m,n}$ a good variational principle for the Einstein equations.[18] Indeed, although different coordinates were used to describe the covering spacetime, our $\check{I}_{m,n}$ agrees precisely with the object called $\tilde{I}_m$ in [73]. We also recall from their analysis that the Hamilton-Jacobi variation of the brane-excised Einstein-Hilbert action with respect

[17] In particular, at finite regulator ϵ there will still be no Gibbons-Hawking term at $\partial\mathcal{U}_\epsilon$.

[18] This was understood much earlier in many contexts (see e.g. [154, 33]), though we are not aware of a fully general prior study of the case $m > 1$. We also comment that this variational principle provides what one may call an equation of motion for the splitting surface given by equation (A.66) of [73], that in some sense determines the location of $\boldsymbol{\gamma}$ relative to other features of the spacetime. For example, in the limit $n \to 1$, this condition requires $\boldsymbol{\gamma}$ to be extremal.

to m is just $-\frac{A_{\boldsymbol{\gamma}}}{4G_N}$, where $A_{\boldsymbol{\gamma}}$ is the area of the cosmic brane $\boldsymbol{\gamma}$

$$-\frac{\delta \check{I}_{m,n}}{\delta m} = \frac{A_{\boldsymbol{\gamma}}}{4G_N}. \tag{4.9}$$

In particular, this holds for arbitrary real m.

As a result, if one happened to be interested in a related problem that fixed the area $A_{\boldsymbol{\gamma}}$ of $\boldsymbol{\gamma}$ but left the opening angle $2\pi m$ of the conical singularity unconstrained, one could construct a good variational principle I_A for that problem via the Legendre transform

$$I_A = \check{I}_{m,n} + (m-1)\,\frac{A_{\boldsymbol{\gamma}}}{4G_N}\,. \tag{4.10}$$

The ambiguity in the Legendre transform (associated with adding an arbitrary m-independent function of $A_{\boldsymbol{\gamma}}$) has been fixed by requiring the value of (4.10) to agree with that of the standard Einstein-Hilbert action in the case $m = 1$ (when there is no conical singularity). This then has the consequence that (4.10) in fact agrees with the standard Einstein-Hilbert action for all m. In particular, for any m the term $(m-1)\,A_{\boldsymbol{\gamma}}$ in (4.10) precisely restores the contribution $S_{\boldsymbol{\gamma}}$ associated with a possible conical defect.

The above argument provides an especially clean way to see that, if one uses the standard Einstein-Hilbert action, requiring stationarity under constrained variations that fix $A_{\boldsymbol{\gamma}}$ imposes the equations of motion away from $\boldsymbol{\gamma}$ but allows a general conical singularity at $\boldsymbol{\gamma}$. If one further also requires stationarity under variations of $A_{\boldsymbol{\gamma}}$ (which then amount to Hamilton-Jacobi variations of (4.10) with respect to $A_{\boldsymbol{\gamma}}$), one obtains the condition $m = 1$ that requires the spacetime to be smooth.

In summary, we see that an alternate way to impose the condition that the full n-replica geometry be smooth at $\boldsymbol{\gamma}$ is simply to require that it provide a stationary point of the Einstein-Hilbert action ((4.10)) with respect to variations of $A_{\boldsymbol{\gamma}}$. In particular, from

(4.9) we see that the action (4.10) is also stationary under variations of m so that we may consistently treat the smoothness condition $m = 1$ as an equation of motion that follows from the gravitational dynamics rather than as an a priori boundary condition. Indeed, since the support of any path integral measure will not be concentrated on smooth configurations, it is natural to take the equation-of-motion perspective to be more fundamental than simply imposing smoothness as a boundary condition.

4.3.4 Real-time boundary conditions at the splitting surface

With this understanding we can now turn to the real-time context. While we wish to avoid analytic continuation of our physical metric, its boundary conditions, or any relevant real-time sources, we are nevertheless free to use the Euclidean analysis as *motivation* for a choice of real-time boundary conditions at $\boldsymbol{\gamma}$. As in the imaginary time case, we will first discuss a brane-excised variational principle which in some sense allows an arbitrary fixed 'defect' at $\boldsymbol{\gamma}$. We will then use this brane-excised action to show that similar boundary conditions promote the S of (4.2) to a well-defined variational principle that can be formulated on real Lorentz-signature replica wormhole spacetimes. In this latter variational principle, the defect parameter m is free to vary, but is then determined on-shell by an equation of motion associated with varying the area $A_{\boldsymbol{\gamma}}$ of the splitting surface. Furthermore, while real replica wormholes cannot make the action stationary at $\boldsymbol{\gamma}$, we will see that complex replica wormholes can do so, and that they are also compatible with the full set of stationarity conditions at the level of counting the relevant equations. This sets the stage for the construction of examples in the companion paper [4], which will demonstrate that the desired complex saddles do in fact exist (at least in the contexts studied there).

To begin our real-time analysis, we remind the reader that we consider here the real-

time covering-space description of the n-replica saddle, which thus has n bra spacetime pieces and n ket spacetime pieces glued together along appropriate surfaces $\mathcal{R}_{\mathcal{A}}, \mathcal{R}_{\mathcal{A}^c}$. For the moment, we do not require any particular symmetries of this spacetime.

Let us first focus on one of the ket spacetimes (which is associated with the more familiar $e^{iS^k_{\rm gr}}$ in the path integral), with the understanding that the complex-conjugate boundary conditions will hold on the bra spacetimes. As stated above, our Lorentzian approach will be motivated by Wick-rotation of the Euclidean results discussed in section 4.3.3. In particular, it is natural to associate any particular pair of bra and ket spacetimes with a single fundamental domain of some replica-symmetric Euclidean solution under the $\mathbb{Z}_n$ cyclic symmetry. Recall that the Euclidean metric near $\boldsymbol{\gamma}$ in any such fundamental domain can be described by (4.8). Now, note that taking the above Euclidean complex coordinates $v, \bar{v}$ to be $x + i\, t_e, x - i\, t_e$ and Wick-rotating $t_e \to it$ would define 'light-cone' coordinates[19] $\tilde{x}^{\pm} = x \pm t$. Applying this transformation $v \to \tilde{x}^-$ and $\bar{v} \to \tilde{x}^+$ to (4.8) yields the metric (with $\hat{m} \equiv \frac{m}{n}$)

$$\begin{aligned} ds^2 = \sigma(\tilde{x}^+, \tilde{x}^-)\, d\tilde{x}^+ d\tilde{x}^- + T\, \frac{(\tilde{x}^+\, d\tilde{x}^- - \tilde{x}^-\, d\tilde{x}^+)^2}{(\tilde{x}^+\tilde{x}^-)^{2-\hat{m}}} \\ + q_{IJ}\, dy^I dy^J + 2\, W_J\, dy^J\, \frac{\tilde{x}^+ d\tilde{x}^- - \tilde{x}^- d\tilde{x}^+}{\tilde{x}^+\tilde{x}^-}, \end{aligned}$$

with

$$\begin{aligned} &\sigma(\tilde{x}^+, \tilde{x}^-) \equiv \hat{m}^2 (\tilde{x}^+\tilde{x}^-)^{\hat{m}-1}\,, \\ &T = \mathcal{O}(r^\alpha) = \mathcal{O}(\tilde{x}^+\tilde{x}^-)^{\frac{\alpha m}{2n}} = \mathcal{O}(\tilde{x}^+\tilde{x}^-)^{\frac{\alpha \hat{m}}{2}}\,, \\ &q_{IJ} = \mathcal{O}(r^0) = \mathcal{O}(\tilde{x}^+\tilde{x}^-)^0\,, \\ &W_J = \mathcal{O}(r^2) = \mathcal{O}(\tilde{x}^+\tilde{x}^-)^{\frac{m}{n}} = \mathcal{O}(\tilde{x}^+\tilde{x}^-)^{\hat{m}}\,. \end{aligned} \tag{4.11}$$

[19] This choice differs by signs from the standard null coordinates $x^{\pm} \equiv t \pm x = \pm\tilde{x}^{\pm}$. It is also worth noting that the Euclidean time coordinate t_e here is a Cartesian coordinate, in contrast to the angular coordinate $t_{\rm E}$ used in (4.7).

Furthermore, the analogue of the Euclidean metric being periodic in $t_{\rm E}$ with period 2π is to require that the metric functions T, q_{IJ}, W_J involve only integer powers of $(\tilde{x}^{\pm})^{\frac{1}{n}}$, except perhaps in the combination $\tilde{x}^+\tilde{x}^-$. In other words, we require these coefficients to be functions of the triple $((\tilde{x}^+)^{\frac{1}{n}}, (\tilde{x}^-)^{\frac{1}{n}}, \tilde{x}^+\tilde{x}^-)$ that are analytic in the first two arguments in some neighborhood of the origin $\tilde{x}^+ = 0 = \tilde{x}^-$. Note that such local analyticity is to be expected at any source-free regular point of the equations of motion and does not restrict the use of non-analytic sources at the asymptotic boundary. (Replica-symmetric solutions will involve only integer powers of $\tilde{x}^{\pm}$, again with the possible exception of appearance in the combination $\tilde{x}^+\tilde{x}^-$.)

Let us first consider the case where $\hat{m}$ is a positive integer, and in particular the case $\hat{m} = 1$ (where $m = n$). For appropriate T, q_{IJ}, and W_J, the metric (4.11) can then be both real and completely smooth away from the timefold. In particular, this case includes real Lorentz-signature replica wormhole spacetimes of the sort that define the domain of integration for the Lorentz-signature path integral described in section 4.2.

On the other hand, for more general values of $\hat{m}$ (or for more general choices of T, q_{IJ}, and W_J), metrics satisfying (4.11) are at best a complex deformation of the above real Lorentz-signature replica wormholes. This deformation will be of interest below, though it has several subtleties that require comment.

(a). The first subtlety is that (4.11) can involve negative powers of $\tilde{x}^+\tilde{x}^-$, in which case it is singular when either $\tilde{x}^+$ or $\tilde{x}^-$ vanish. More generally, we should expect a solution to the Einstein equations that behaves like (4.11) near $\boldsymbol{\gamma}$ to be singular on the past light cone of $\boldsymbol{\gamma}$. This is an interesting difference from the Euclidean case, where the metric is smooth away from the tip of the cone. Note that for $m = 1$ (and thus for $\hat{m} = \frac{1}{n}$) the singularity was obtained by making a complex coordinate transformation and analytically continuing a smooth Euclidean solution, so in that

case this appears to be a form of coordinate singularity. It should thus be harmless for $m = 1$, though see further discussion in section 4.5. Note that for $n > 1$ the choice $m = 1$ forbids taking $\hat{m} = \frac{m}{n}$ to be a positive integer, and is thus intrinsically complex.

(b). The second subtlety is that, since $\tilde{x}^+$ and $\tilde{x}^-$ can be negative (and in particular since $\tilde{x}^+\tilde{x}^-$ is negative in the Milne wedge), fractional powers can be complex and require appropriate definition.

In fact, motivated by the Euclidean description, we will deal with both issues in much the same way, choosing our ket spacetime definitions for general $\hat{m}$, T, q_{IJ}, W_J to match what would be obtained by analytically continuing t through the upper half-plane (since $t_E \to it$ and the ket part of the spacetime comes from $t_E < 0$.). This amounts to introducing the $i\varepsilon$ prescriptions $\tilde{x}^\pm \to \tilde{x}^\pm \mp i\varepsilon$ (with $\varepsilon > 0$) and taking the powers of $\tilde{x}^\pm$ appearing in (4.11) to be analytic functions. Thus for negative $\tilde{x}^+$ we have $(\tilde{x}^+)^{\frac{1}{n}} = e^{-\frac{i\pi}{n}} |\tilde{x}^+|^{\frac{1}{n}}$ and for negative $\tilde{x}^-$ we find $(\tilde{x}^-)^{\frac{1}{n}} = e^{+\frac{i\pi}{n}} |\tilde{x}^-|^{\frac{1}{n}}$. In particular, $(\tilde{x}^+\tilde{x}^-)^{\frac{1}{n}}$ remains real at positive at $t = 0$, so that (4.11) is compatible with the previously advertised requirement that the metric and its extrinsic curvature be real and positive on $\mathcal{R}_{\mathcal{A}}$ and $\mathcal{R}_{\mathcal{A}^c}$. Nevertheless, it is forced to be complex in the Milne wedge to the 'past' of $\boldsymbol{\gamma}$.

We take the above specifications to be part of the boundary conditions at $\boldsymbol{\gamma}$ for our real-time variational problem. In particular, this refines the definition of the real Lorentz-signature replica wormhole configurations that specify the original domain of integration for our Lorentz-signature path integral. As noted above, reality generally requires $\hat{m}$ to be an integer. Metrics with other values of $\hat{m}$ simply do not lie in the original domain of integration.

Nevertheless, metrics with general $\hat{m}$ are allowed to appear in complex deformations

of that domain. In particular, the $i\varepsilon$ prescription included in our proposal for general $\hat{m}$ turns out to be very useful. For any fixed m, n it will imply that the above are indeed a valid set of boundary conditions for a variational problem associated with the brane-excised Einstein-Hilbert action $\check{S}_{m,n} := S - S_{\boldsymbol{\gamma}}$ on the timefolded bulk spacetime. This timefolded spacetime only retains the $t \leq 0$ regions in both the ket and bra spacetimes, and we may think of the excision as removing a small disk-shaped region of size[20] ϵ around the origin $\tilde{x}^{\pm} = 0$, though we eventually take $\epsilon \to 0$ at the end of the computation.[21]

The fact that $\check{S}_{m,n}$ gives a valid variational principle for fixed m, n can be read directly from the Euclidean analysis of [73]. Since the arguments of that reference simply manipulated power series expansions in their $z^{\frac{1}{n}}, (\bar{z})^{\frac{1}{n}}$, it is immediate that every step of can be 'Wick rotated' and rewritten in terms of $\tilde{x}^{\pm}$ to yield an equally-valid treatment of the real-time boundary conditions above. And as in footnote 18, this in a certain sense provides an equation of motion for the splitting surface $\boldsymbol{\gamma}$. Furthermore, by the same argument we can read from [73] that the Hamiltonian-Jacobi variation of $\check{S}_{n,m}$ with respect to m yields

$$\frac{\delta \check{S}_{n,m}}{\delta m} = -i \frac{A_{\boldsymbol{\gamma}}}{4G_N} \ . \tag{4.12}$$

Now, we in fact wish to show that metrics of the form (4.11) promote the full 'Einstein-Hilbert action' $S = \check{S}_{m,n} + S_{\boldsymbol{\gamma}}$ to a well-defined variational principle. And as in the imaginary-time context, we will now allow m to vary as well. We thus need to consider the piece $S_{\boldsymbol{\gamma}}$ associated with the region near $\boldsymbol{\gamma}$. To this end, in some ket part of our spacetime, let us consider a small semicircle $\mathcal{C}_\epsilon$ about the origin in the lower half of the (real) $\tilde{x}^{\pm}$ plane (i.e., of the form described by the orange curve in fig. 4.8). In particular, we take the curve to have orthogonal intersection with $\mathcal{R}_{\mathcal{A}}, \mathcal{R}_{\mathcal{A}^c}$ so that there is no delta-

[20] Since we are Lorentz signature, this 'size' does not in any way measure proper distance from $\boldsymbol{\gamma}$.

[21] The reader might find it helpful to recall our definition $I = -iS$ below (4.3), which makes it natural to talk about I for the Euclidean computation, but stick to S for the Lorentzian on-shell action.

function contribution to the right-hand-side of (4.6) from 'corners' where the normal to $\mathcal{C}_\epsilon$ changes when crossing from a ket to a bra spacetime across $\mathcal{R}_{\mathcal{A}}, \mathcal{R}_{\mathcal{A}^c}$.

In the limit of small ϵ, non-vanishing contributions to the integrated extrinsic curvature will come only from the explicit terms in (4.11); terms associated with T, q_{IJ}, and W_J decay too quickly to contribute. By inspection, one sees that the explicit terms in (4.11) are invariant under both replica and conjugation symmetry. This means that their contributions to the real part of the integrated extrinsic curvature must cancel between the bra and ket parts of our spacetimes. We may thus focus on the imaginary parts.

Now, as noted below (4.6), there are in fact two kinds of contributions to $\mathrm{Im} \int_{\mathcal{C}_\epsilon} d^d x \sqrt{h}\, K$, which is to be computed using the outward pointing unit normal. The first comes from computing the extrinsic curvature in the past Milne region where the metric can be complex. But the second is associated with loci where the spacetime metric is real and of Lorentz signature but $\mathcal{C}_\epsilon$ transitions from being spacelike to being timelike (or vice versa). Noting that the relevant terms in (4.11) are real outside the past Milne region, we choose $\mathcal{C}_\epsilon$ to coincide with the surface $\tilde{x}^- - \tilde{x}^+ = \epsilon$ in the past Milne region (and a bit outside) but to otherwise be an arbitrary smooth curve that meets the timefold orthogonally. This in particular requires $\mathcal{C}_\epsilon$ to be spacelike just outside the past Milne wedge (and on either side) but timelike where it meets the timefold. Since we currently focus on a ket part of the spacetime, the contribution to $\mathrm{Im} \int_{\mathcal{C}_\epsilon} d^d x \sqrt{h}\, K$ from outside the past Milne wedge is thus

$$- \mathrm{Im} \int_{\mathcal{C}_\epsilon} d^d x \sqrt{h}\, K \Big|_{\text{outside past Milne wedge}} = 2 \times \frac{\pi}{2} \times A_{\boldsymbol{\gamma}} = \pi A_{\boldsymbol{\gamma}} \tag{4.13}$$

from the associated transitions.

The contribution to $\mathrm{Im} \int_{\mathcal{C}_\epsilon} d^d x \sqrt{h}\, K$ from the past Milne wedge is also straightforward to compute. Since $\sqrt{h}K$ is real for any spacelike surface outside the Milne wedge

(again restricting to contributions from the explicit terms in (4.11) both here and below), we may in fact integrate $\sqrt{h}\,K$ over any surface cutting across the Milne wedge that becomes spacelike in the Rindler wedges. For simplicity, we choose this to be the surface $\tilde{x}^- - \tilde{x}^+ = -2t = \epsilon$. The explicit terms in the metric (4.11) then give

$$\begin{aligned} -\operatorname{Im}\int_{t=-\frac{\epsilon}{2}} d^d x\,\sqrt{h}\,K &= \operatorname{Im}\int_{t=-\frac{\epsilon}{2}} dx\,d^{d-1}y\,\sqrt{q(y)}\,\frac{\partial}{\partial t}\log\sqrt{\sigma(\tilde{x}^+,\tilde{x}^-)} \\ &= \frac{\hat{m}-1}{2}\operatorname{Im}\int_{t=-\frac{\epsilon}{2}} dx\,\partial_t \log\big(\tilde{x}^+\tilde{x}^-\big)\times\int d^{d-1}y\,\sqrt{q(y)} \\ &= \frac{\hat{m}-1}{2}\operatorname{Im}\int_{t=-\frac{\epsilon}{2}} dx\,\partial_x\left(\log\tilde{x}^+ - \log\tilde{x}^-\right)\times A_{\boldsymbol{\gamma}} \\ &= 2\pi\frac{\hat{m}-1}{2}A_{\boldsymbol{\gamma}} = (\hat{m}-1)\pi A_{\boldsymbol{\gamma}}\,. \end{aligned} \tag{4.14}$$

The factor of $A_{\boldsymbol{\gamma}}$ comes from integrating $\sqrt{q}$ over the longitudinal coordinates y^I as indicated. In passing from the third to the fourth line we have used the fact that $\tilde{x}^\pm$ have opposite $i\varepsilon$ pole prescriptions so that their logarithms give oppositely-signed imaginary parts (which then reinforce each other due to the explicit minus sign in the $\tilde{x}^-$ term in line three).

Summing the two contributions above in (4.13) and (4.14) gives

$$\operatorname{Im}\int_{\mathcal{C}_\epsilon} d^d x\,\sqrt{h}\,K = -\pi\,\hat{m}\,A_{\boldsymbol{\gamma}}. \tag{4.15}$$

But since the full replica geometry involves n copies of M^{k} ket spacetimes and n copies of M^{b} bra spacetimes, we must include such a semicircle through each in order to form the boundary of a disk around the origin. Comparing with (4.6) and setting $\chi(\tilde{\mathcal{U}}_\epsilon) = 1$ yields

$$iS_{\boldsymbol{\gamma}} = \frac{i}{16\pi G_N}\int_{\mathcal{U}_\epsilon}\eta\sqrt{-g}\,R = -\frac{(n\,\hat{m}-1)\,A_{\boldsymbol{\gamma}}}{4G_N} = -\frac{(m-1)\,A_{\boldsymbol{\gamma}}}{4G_N}\,. \tag{4.16}$$

We now conclude our argument by making several observations. The first is simply

that comparing (4.12) and (4.16) shows – again in parallel with the Euclidean case – that for any n the full action S is a Legendre transform of $\check{S}_{m,n}$ with respect to m. So by the usual argument S yields a well-defined variational principle with the 'conjugate' boundary conditions still defined by (4.11) but where we fix $A_{\boldsymbol{\gamma}}$ and instead allow m to vary (still holding n fixed). In particular, we see that any stationary point of $\check{S}_{m,n}$ will automatically make S stationary with respect to variations of m.

Second, we note that we may consider boundary conditions defined by (4.11) for fixed n but with *both* $A_{\boldsymbol{\gamma}}$ and m free to vary. Given the observation above, to investigate the status of S for such boundary conditions we need only compute

$$\frac{\delta S}{\delta A_{\boldsymbol{\gamma}}} = \frac{\delta S_{\boldsymbol{\gamma}}}{\delta A_{\boldsymbol{\gamma}}} = i\frac{m-1}{4G_N}, \tag{4.17}$$

where in the first step we have again assumed that we evaluate the result on a stationary point of $\check{S}_{m,n}$. We see from (4.17) that stationary points of $\check{S}_{m,n}$ with $m = 1$ are also stationary points of S. We have thus shown by direct computation that S does indeed yield a well-defined variational principle with boundary conditions defined by (4.11) and with n fixed but with m free to vary. And we have also shown that stationarity with respect to $A_{\boldsymbol{\gamma}}$ is equivalent to $m = 1$, and thus to $\hat{m} = 1/n$. In particular, this is the real-time analogue of the stationarity condition that requires the metric to be smooth in the purely Euclidean context and in any single replica real-time context (i.e., for which $n = 1$).

Let us conclude this section with a summary of the requirements for a covering space description of a replica wormhole spacetime to yield a saddle point of our variational principle associated with the full action S for some n. First, it must satisfy the usual Einstein equations away from the timefold surfaces $\mathcal{R}_{\mathcal{A}}$, $\mathcal{R}_{\mathcal{A}^c}$, and $\boldsymbol{\gamma}$. Second, the extrinsic curvatures at $\mathcal{R}_{\mathcal{A}}$, $\mathcal{R}_{\mathcal{A}^c}$ must be continuous when passing from any bra part of the

spacetime to any ket part. Third, near $\boldsymbol{\gamma}$ it must take the form (4.11) with $\hat{m} = 1/n$ and with the $i\varepsilon$ prescriptions given above.[22] Finally, it must be consistent with whatever initial conditions are used to specify the quantum state. This last requirement will be discussed further in section 4.4, though we first briefly address the fundamental domain description of our saddles in section 4.3.5.

4.3.5 The view from a single fundamental domain

Despite the elegance of the above covering space description, imposing replica symmetry allows one to reconstruct the full solution from a single fundamental domain. It is thus often useful to formulate the entire problem in terms of one such domain $\widehat{\mathcal{M}}_n$, containing only a single bra spacetime and a single ket spacetime sewn together along $\mathcal{R}_{\mathcal{A}}$ and $\mathcal{R}_{\mathcal{A}^c}$. As in [33], this can be particularly useful for analytically continuing to non-integer n as the parameter n now only appears in the metric through the combination $\hat{m} = \frac{m}{n}$, which is already allowed to be an arbitrary positive real number. Below, we also require the spacetime to be invariant under CPT conjugation.

The desired variational principle follows immediately from our discussion above. We simply define the allowed fundamental domains $\widehat{\mathcal{M}}_n$ to be quotients $\widehat{\mathcal{M}}_n = \mathcal{M}_n/\mathbb{Z}_n$ of the replica- and conjugation-symmetric covering spaces $\mathcal{M}_n$ satisfying the boundary

[22] It would be interesting to attempt to strengthen the above argument and show that the full $\hat{m} = 1/n$ 'boundary conditions' associated with (4.11) – and in particular the $i\varepsilon$ prescription associated with the poles and branch cuts – are in fact consequences of the equation of motion associated with stationarity of the action under varying the area of $\boldsymbol{\gamma}$. In particular, the $i\varepsilon$ prescription is precisely the condition that powers of $\tilde{x}^{\pm}$ define positive frequency functions. And as noted in section 4.4 below, for the case where we compute Rényi entropies of the vacuum state, we expect this state to enforce boundary conditions on the ket spacetime that in some sense require positive frequency solutions. Furthermore, since the $i\varepsilon$ prescription is needed only on the past light cone of $\boldsymbol{\gamma}$, it is a UV issue that one expects to be independent of the choice of state. We thus suspect that a full analysis of the equations of motion and the initial conditions for good quantum states could derive this condition from an entirely real-time point of view.

conditions of section 4.3.4. We then define the action

$$S_n^{\text{fund}}\left(\widehat{\mathcal{M}}_n\right) = \frac{1}{n} S_n\left(\mathcal{M}_n\right) = 2i\,\text{Im}\left(S^k_{\text{gr},n}\right) - i\left(\frac{(\hat{m}-\frac{1}{n})A_{\boldsymbol{\gamma}}}{4G_N}\right), \tag{4.18}$$

where $S^k_{\text{gr},n}$ is the action (4.4) evaluated on the ket part of $\widehat{\mathcal{M}}_n$, and where in the last step we have used (4.16). This Lorentz-signature action is always purely imaginary so that the associated weights in the path integral are real. In particular, since saddles will again have $\hat{m} = 1/n$, the Rényi entropies (4.3) computed by any given such saddle take the form

$$S^{(n)}_{\mathcal{A}} = 2\frac{n}{n-1}\,\text{Im}\left(S^k_{\text{gr},n} - S^k_{\text{gr},1}\right). \tag{4.19}$$

This is manifestly real, and coincides with the Euclidean answer when analytic continuation can be performed. This will be verified explicitly in [4] for the examples studied there.

4.4 State preparation

Thus far we have imagined starting from an initial (perhaps mixed) state ρ_0 at some t_0 and evolving it to the time t of interest taking into account any real-time sources between t_0 and t. By 'time' t, we in fact mean that we choose some Cauchy surface Σ_t, and similarly for t_0. To be definite, we take t to lie to the future of t_0. In the holographic context these will refer to boundary Cauchy surfaces, and we will allow boundary sources which will affect the quantum state of the bulk within their causal future.[23]

While this setting is natural, it raises the question of precisely how the state ρ_0 is

[23]The effects of such sources on the saddle-point geometries used to calculate Rényi entropies need not be confined to this causal future. The point here is that such solutions are not constructed by solving a Cauchy problem with initial data in the past. Instead, they involve timefolded spacetimes with boundary conditions on both sides. Furthermore, the equations of motion may fail to be hyperbolic in any complex parts of the spacetime.

to be specified. In the discussion above, we have generally supposed that we have been given the explicit matrix elements of ρ_0 in a basis defined by field eigenstates at the time t_0. However, at least in field theoretic contexts, we should admit that it can be difficult to obtain such a description for interesting states. Let us therefore briefly remark on other methods that can be used to specify ρ_0, and which are also readily incorporated into our discussion.

One strategy is to choose a familiar state that allows for a particularly simple treatment and then to construct more complicated states by adding sources between t_0 and t. For example, one might take the initial state to be the vacuum, and perhaps also taking t_0 to lie in the far past. This has several advantages. In the free field limit, the vacuum initial conditions require positive-frequency boundary conditions at the initial time, cf., [144] for a discussion in language similar to that used here. Similarly, for vacuum gravity in AdS_3 the geometry in the far past should be diffeomorphic to global AdS_3 with all boundary gravitons being of positive frequency. In higher dimensions or when matter fields are coupled to gravity, we still expect an analog of the positive-frequency boundary condition to hold, though making it precise might require employing a suitable '$i\varepsilon$' prescription.[24]

Alternately, it may be useful to consider states that can be prepared by slicing open a Euclidean path integral. One can then implement the past boundary condition by simply attaching this Euclidean path integral. At the semiclassical level, this will then require the bulk spacetime to satisfy appropriate Euclidean boundary conditions in the far past. The vacuum can of course be treated in this way, as can the thermofield double state, or deformations of these states by operator insertions in the Euclidean section; see e.g. related discussions in [155, 156, 157, 158].

[24]In an asymptotically flat spacetime it will suffice to ensure that the linearized gravitational solutions in the far past only have support on positive frequency incoming radiative modes.

It can thus be useful to allow Euclidean sections of an a priori real-time path integral for use in preparing states. However, we emphasize that this is a not matter of necessity, but is only a matter of expedience. Such Euclidean sections are a useful technical simplification to enable us exploit known features of the Euclidean path integral to give a geometric picture of the initial condition. In particular, the use of such Euclidean sections will not restrict in any way the possible presence of non-analytic sources between t_0 to t.

A particularly simple example is provided by the gravitational Schwinger-Keldysh geometries discussed in [141, 142, 143] which capture the real-time evolution of the thermal density matrix of the boundary CFT (see also [159]) in the absence of any sources in the Lorentzian evolution. This example is described in appendix C.2, where it is used to illustrate some of the general features discussed above.

4.5 Discussion

Our work above provides a framework for discussing replica wormholes within a real-time formalism, and in particular in contexts that may include non-analytic sources. We described a Lorentz-signature bulk gravitational path integral with boundary conditions associated with computing (swap) Rényi entropies in a dual field theory, and which allows configurations with the topology of replica wormholes. Real Lorentz-signature configurations of this type contain timefolds and a cosmic brane 'splitting surface.' We carefully formulated a variational principle for such spacetimes that yields the Einstein-Hilbert equations of motion away from the timefolds and the splitting surface, and which imposes natural constraints at these surfaces. In particular, stationarity at the splitting surface forbids having a delta-function contribution to the scalar curvature as defined by a Lorentz-signature (or more generally, complex) generalization of the $2d$ Gauss-Bonnet

theorem. Explicit examples of such real-time replica wormhole saddles will be presented in a companion paper [4]. And while we focused here on bulk gravity described by an Einstein-Hilbert action, the generalization to include perturbative higher curvature terms is straightforward using results from appendix B of [73].

The fundamental formulation of our real-time path integral involved only real Lorentz-signature configurations. However, solutions to the above stationarity conditions are necessarily complex. Accessing the associated saddles thus requires deforming the original real contour of integration. This should not be a surprise. While real-time equations of motion must be real, this need not be true of the boundary conditions imposed by any particular quantum state. Indeed, instantons that describe gravitational tunneling are famously associated with Euclidean stationary points that again can be accessed only by deforming the original contour of integration specified by a Lorentzian path integral.

Importantly, however, at least for replica-symmetric saddles (preserving both a $\mathbb{Z}_n$ cyclic symmetry and conjugation symmetry) we found that the metrics to be real in the region spacelike separated from the splitting surface. As a result, contributions of such spacelike-separated regions to S cancel between the bra and ket parts of the spacetime. In particular, so long as they remain spacelike separated from the splitting surface, we can move the bulk timefold along $\mathcal{R}_{\mathcal{A}}, \mathcal{R}_{\mathcal{A}^c}$ forward or backward in time as we please without changing the path integral weight of our replica-wormhole. This remains true even if we move $\mathcal{R}_{\mathcal{A}}, \mathcal{R}_{\mathcal{A}^c}$ at the AdS boundary, where such deformations correspond to changing the time t at which our (swap) Rényi is computed. This feature is an important hallmark of unitarity in a dual field theory interpretation, which would indeed require such Rényi's to be time-independent.

The above argument suffices to show critical features of unitarity at boundary times that are spacelike separated from the splitting surface, and in contexts where the bulk computation is controlled by a single replica- and conjugation-symmetric saddle. But it

is clearly of interest to understand whether and how bulk replica wormholes implement the expected unitarity more generally. In particular, since the formal $n \to 1$ limit of an on-shell splitting surface is an extremal surface, and since extremal surfaces must be spacelike separated from any part of the AdS boundary not causally related to their boundary anchors [78, 127], it is natural to ask whether general on-shell splitting surfaces with any $n > 1$ must also be spacelike separated from corresponding regions of AdS boundary. And it is also clearly important to understand the possible effect of saddles in which replica symmetry is broken.

Now, as a matter of principle, an inherently real-time prescription for constructing saddle-point geometries of gravitational replica path integrals is critical to describing physics in the presence of non-analytic sources. However, in some contexts it will in practice be convenient to proceed by studying a related Euclidean problem and analytically continuing the resulting Euclidean saddle. This may in particular be useful when the initial state can be prepared using a Euclidean path integral and when any sources are analytic functions of time. In that context, one may imagine computing entropies associated with general Euclidean choices of the region $\mathcal{A}$ and then analytically continuing parameters to obtain entropies for general Lorentzian regions as in [39, 134, 160]. Analytically continuing the Euclidean replica geometry in this way must give a solution to the variational problem described in section 4.2. Indeed, if the analytic continuation is performed using the prescription described below (4.8) then it is manifest that the result will satisfy the conditions at the real-time splitting surface associated with (4.11). And it is also manifest that analytic continuation of a Euclidean saddle will solve the standard Einstein equations away from $\boldsymbol{\gamma}$.

Of particular interest may be the way that such analytic continuations glue together the bra and ket parts of the resulting Lorentz-signature spacetime. This gluing is naturally described by a smooth excursion into the space of complex metrics, which then

becomes our $i\varepsilon$ prescription in the limit where the curve connecting the Lorentz-signature bra and ket branches becomes very tight.

A particularly clean example was described in [143] based on earlier work of [141] for the case of replica number $n = 1$. The context there involved computing boundary correlation functions of light fields in a thermal state in the limit of vanishing bulk Newton constant G_N with a bulk theory described by pure AdS gravity. As this example may provide inspiration for future work, we recall it briefly in appendix C.2, commenting briefly on the extension to general n and emphasizing the way that it displays the reality of the weight e^{iS} and the associated facets of unitarity described above.

Let us now conclude with a few further brief comments on future directions. First, while it sufficed for our current purposes, there is admittedly something unsatisfying about using an $i\varepsilon$ prescription to define the boundary conditions at $\boldsymbol{\gamma}$ for general $\hat{m}$. It would thus be interesting to understand whether the allowed configurations could be generalized in some natural way so that our $i\varepsilon$ prescription arose from solving the Einstein equations subject to boundary conditions imposed by natural quantum states. Indeed, the latter are naturally complex. One can certainly imagine that such a prescription would follow for vacuum states (as it does in the free field case, see e.g. section 4.3 of [144]), and since the $i\varepsilon$ prescription controls a UV singularity on a lightcone one may hope that it in fact follows for more general states due to the requirement that they agree with the vacuum in the UV.

Second, it is clearly of interest to extend our analysis beyond leading order in the bulk Newton constant G_N to include one-loop back-reaction from quantum fields. Here one would like to understand the relationship to classic discussions [161, 162] of back-reaction in the presence of Lorentz-signature topology change. But the extension to include one-loop back-reaction is also important for many applications to black hole evaporation (where one expects the relevant replicas to be saddles only for the one-loop-corrected

effective action [37, 36]. In particular, if one can extend the above discussion of dual field theory unitarity to the bulk one-loop level, it should provide a bulk argument that black hole evaporation not only yields a Page curve as in [39, 38] but that it implements fully unitary evolution as expected for a field theory dual.

Chapter 5

Real-time gravitational replicas: Low dimensional examples

5.1 Introduction

Real-time computation of correlation functions, both time-ordered and out-of-time-order, as well as density operator matrix elements and their moments, in any quantum system either with or without dynamical gravity, requires the use of a suitable timefolded contour, with segments of forward and backward evolution. One often however eschews the use of such contours, relying instead on computations in the Euclidean domain, and then analytically continuing the answers thus obtained into the real-time domain (see e.g., [120, 121] for non-gravitational theories as well as the more recent analysis in gravitational context in [160]), a strategy that works well when the quantum evolution is not subject to non-analytic sources. While this is strategy is efficient in extracting information about the non-perturbative aspects of the theory, it does not lend insight into the physical dynamical evolution directly.

These issues have been well appreciated in the context of quantum field theory for

many decades, but have come to fore with recent analyses of new semiclassical configurations that address the black hole information problem. Inspired by the Euclidean path integral arguments [33, 28, 74, 35] that helped derive the static holographic entanglement entropy formula [66] and its quantum generalization [29], recent investigations in low-dimensional gravity theories have argued for the contribution of replica wormhole saddles [38, 39] in the gravitational path integral. For a review of these developments in the context of the black hole information problem, see [130]. Furthermore, as argued for in [54] such replica wormhole configurations are quite generic in the Euclidean formalism.

Motivated by these developments, and by earlier efforts [34] to derive the covariant holographic entanglement entropy prescription of [27], in a companion paper [6] we outlined the general formalism for understanding the stationary phase approximation of the real-time gravitational functional integral. In addition, connections to the black hole information problem and baby universes have also been discussed recently in [55]. Our goal in this current paper is to exemplify the formal discussion in [6] with some concrete examples. For technical reasons our examples will rely on gravitational dynamics in low dimensions, especially in 2 and 3 spacetime dimensions, where one can write down explicit geometries that provide the appropriate stationary points. It should however be clear from our discussion that the construction can in principle be carried out, at least numerically, in higher-dimensions with dynamical gravitational degrees of freedom.

The specific class of problems we study herein are those that correspond to computation of Rényi entropies in holographic field theories in low dimensions, specifically AdS_2 and AdS_3. We recall that in the field theory one is instructed to consider path integral contours of the form illustrated in fig. 5.1. Reduced density matrices $\rho_{\mathcal{A}}(t)$ associated with spatial subregions $\mathcal{A}$ on a Cauchy slice Σ_t are obtained by sewing together the ket and bra parts along the complementary domain $\mathcal{A}^c$, leaving open the parts along $\mathcal{A}$. Traces of powers of $\rho_{\mathcal{A}}(t)$ are computed by taking n-copies of the geometry and cyclically

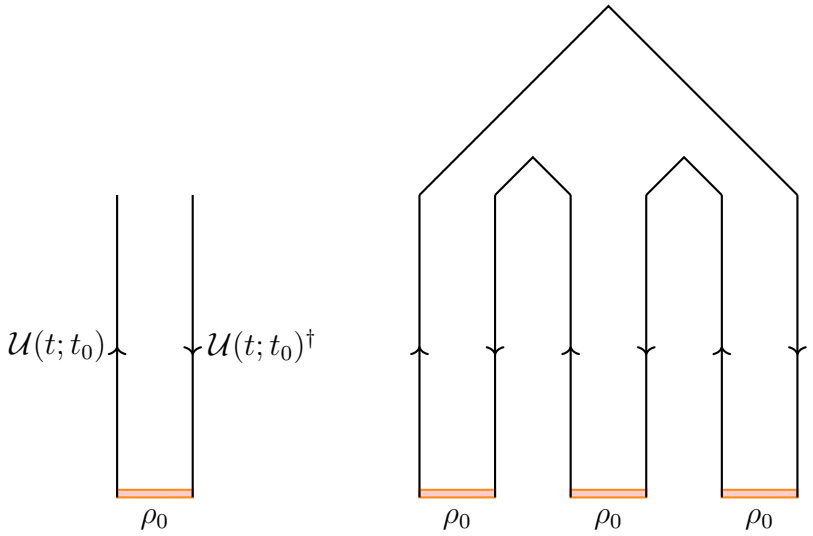

Figure 5.1: An illustration of the real-time contours for the computation of the density matrix $\rho(t)$ (left) and traces of its powers ($\mathrm{Tr}(\rho(t)^3)$ on right) . The past boundary condition is supplied by the prescribed initial state ρ_0 and the direction of time evolution is explicitly indicated by the arrows.

gluing the parts associated with $\mathcal{A}$ across the copies in a replica $\mathbb{Z}_n$ symmetric manner. This boundary geometry provides the asymptotic boundary conditions for our AdS gravity dual, which we seek to determine. In what follows we will adhere to the terminology of [6] referring to the n-fold replica boundary geometry as the branched cover spacetime $\mathcal{B}_n$, its dual bulk gravity stationary phase solution as the covering space geometry, $\mathcal{M}_n$, and the quotient of the bulk geometry by the $\mathbb{Z}_n$ replica symmetry as the fundamental domain, $\widehat{\mathcal{M}}_n = \mathcal{M}_n/\mathbb{Z}_n$.

The boundary and bulk spacetimes are composed of elementary building blocks which are the ket (B^{k} and M^{k}) and bra components (B^{b} and M^{b}), which we indicate with k and b superscripts, respectively. We will be interested in computing the Rényi (or swap) entropy, which will be obtained from the stationary phase evaluation of the gravitational

path integral. The n^{th} Rényi entropy will be given by

$$S^{(n)} = \frac{1}{1-n}\,\log\left(\frac{\mathcal{Z}[\mathcal{B}_n]}{\mathcal{Z}[\mathcal{B}]^n}\right) = \frac{1}{n-1}(I_n - n\,I_1)\,,$$
$$I_n := -\log\mathcal{Z}[\mathcal{B}_n] = \begin{cases} S^E_{\rm gr}[\mathcal{M}_n]\,, & \text{Eulidean} \\ -i\,S_{\rm gr}[\mathcal{M}_n]\,, & \text{Lorentzian} \end{cases} \tag{5.1}$$

where $\mathcal{B} = \mathcal{B}_1$. The Lorentzian action with the general time-ordering necessary to compute replica path integrals takes a Schwinger-Keldysh form:

$$S_{\rm gr}[\mathcal{M}_n] = S^k_{\rm gr}[\mathcal{M}_n] - S^b_{\rm gr}[\mathcal{M}_n]\,, \tag{5.2}$$

where we have forward evolution for the 'kets' (k) and backward evolution for the 'bras' (b), resulting in the relative sign above. As argued in [6] (and earlier in [34, 55]), the on-shell action I_n in the Lorentzian context is real, and is given by

$$I_n = 2\,\text{Im}(S^k_{\rm gr}[\mathcal{M}_n]) \implies S^{(n)} = \frac{2}{n-1}\left[\text{Im}(S^k_{\rm gr}[\mathcal{M}_n]) - n\,\text{Im}(S^k_{\rm gr}[\mathcal{M}])\right], \tag{5.3}$$

where $\mathcal{M} = \mathcal{M}_1$. While the general arguments for these statements were presented in our companion paper [6], we will verify these statements explicitly in some specific contents herein.

The examples we discuss in the bulk of the paper are the following. In section 5.2 we examine the computation of Rényi entropy in an excited state with a localized dilaton excitation in Jackiw-Teitelboim (JT) gravity [163, 164]. This provides a concrete context to contextualize the general discussion of [6] and understand the geometry in some detail. To orient the reader we present both the Euclidean approach as well as the real-time computation, for the state we consider will be time-reversal symmetric, thereby providing

a further check on the results we obtain. In section 5.3 and section 5.4 we then turn to examples in 2d CFTs starting first with the case of a single-interval in section 5.3. This example has been well studied both in field theory and gravity and we again use it to provide an illustration of the geometry of the real-time gravitational solution. In section 5.4 we then turn to a more interesting case, that of two disjoint intervals in a CFT on $\mathbb{R}^{1,1}$. We first begin by illustrating the geometry and the computation of the second Rényi entropy when the two intervals lie on a fixed time slice, and subsequently generalize to the case when the intervals are relatively boosted with respect to each other. We conclude with a brief discussion of other interesting avenues to explore in section 5.5.

We include in the appendices various technical details that enter into our calculations. appendix D.1 computes the Lorentzian on-shell action for a semi-infinite interval in a 2d CFT using a Rindler regulator to contrast with the discussion in the main text. In appendix D.2 we give further details for the evaluation of the Lorentzian on-shell action for disjoint intervals supplementing the discussion in section 5.4.2. appendix D.3 is a quick overview of the Schottky construction of the covering space geometry (both on the boundary and in the bulk) for the computation of second Rényi entropy for 2 disjoint intervals. For this case we present an explicit evaluation of the Euclidean action from the bulk solution in appendix D.4 (as far as we are aware this computation has not hitherto been reported in the literature). Finally, appendix D.5 summarizes some familiar sign conventions and useful identities that we employ in the course of our calculation.

5.2 A toy model in 2d gravity

As our first example, we will consider a two dimensional scenario and examine the real-time contours for computing moments of the density matrix. The particular example we pick is the ground state of JT gravity. In Euclidean signature one may prepare this

state by considering the thermal AdS_2 geometry with the Euclidean time identified with period β and taking $\beta \to \infty$. For finite β we may also slice open this geometry to expose the thermofield double (or Hartle-Hawking) state $|\text{TFD}(\beta)\rangle$ at temperature $T = \beta^{-1}$ at time $t = 0$ (which we can think of as a pure entangled state of two quantum systems, one on each asymptotic boundary of the Lorentzian geometry). If we focus on one of the boundaries we end up with a thermal density matrix $\rho_\beta(t = 0)$ at temperature β by the usual thermofield double construction. The entropy we compute may be viewed as the thermal entropy of this density matrix in the limit $\beta \to \infty$ or equivalently as the entanglement entropy between the two boundaries [165, 166, 167]. For earlier investigations of entanglement entropy in JT gravity see [168, 169] and [170] which computes the subleading corrections and discusses a Lorentzian interpretation of the Euclidean replica trick.

We will focus on computing the moments $\text{Tr}(\rho_\beta^n(t = 0))$ at $\beta = \infty$. The geometry computing this is obtained by stringing together n-copies of that preparing $\rho_\beta(t = 0)$ cyclically and gluing them together. Once again in Euclidean signature we know the resulting spacetime: the n-fold replica geometry is thermal AdS_2, albeit now with a thermal circle that is n times larger [33].

As described in [6] once one has the ansatz for the geometry $\mathcal{M}_n$ which is dual to the n-fold replica, we can either work in the covering space, or take a replica $\mathbb{Z}_n$ quotient and work in a single fundamental domain $\widehat{\mathcal{M}}_n = \mathcal{M}_n/\mathbb{Z}_n$. In the present example the covering spacetime $\mathcal{M}_n$ is simply AdS_2. When we take the $\mathbb{Z}_n$ quotient we will obtain the fundamental domain $\widehat{\mathcal{M}}_n$ which has a fixed point of the $\mathbb{Z}_n$ action at the locus $\boldsymbol{\gamma} = \{x = t = 0\}$. We will describe below the real-time geometry, delineating the various domains of interest, and then proceed to compute the on-shell action. To help orient the reader given that the configuration is time-reversal symmetric about $t = 0$ (in fact it is globally static), we will describe both the Euclidean and the Lorentzian constructions

and computations therein.

Before proceeding, it is worth recording the actual answer for the moments of the ground state density operator are not all that illuminating. The ground state entropy in JT gravity is set by the value of the dilaton, and since there is a finite large β limit it gives $\mathrm{Tr}(\rho(t)^n) = \mathrm{Tr}(\rho(t))$. Nevertheless, the example is instructive to consider, as it provides for useful illustration of the general issues encountered in real-time replica geometries which are easy to discern and intuit.

5.2.1 The Hartle-Hawking state in JT gravity

The two-dimensional JT gravity is a dilaton-gravity theory with the following action in Lorentz signature:[1]

$$\begin{aligned} S_{\rm gr}^{JT} &= \frac{\phi_0}{16\pi G_N}\left[\int_{\mathcal{M}} d^2x\,\sqrt{-g}\,R + 2\int_{\mathcal{B}} dx\,\sqrt{-\gamma}K\right] \\ &\quad + \frac{1}{16\pi G_N}\left[\int_{\mathcal{M}} d^2x\,\sqrt{-g}\,\phi\,(R+2) + 2\int_{\mathcal{B}}\sqrt{-\gamma}\,\phi\,(K-1)\right], \\ &\equiv S_0 + S_\phi\,, \end{aligned} \tag{5.4}$$

where S_0 is the topological 2d gravity action and S_ϕ the dilatonic contribution. The classical equations of motion obtained by varying the dilaton and metric demand

$$R + 2 = 0\,, \qquad (\nabla_\mu\nabla_\nu - g_{\mu\nu})\,\phi = 0\,, \tag{5.5}$$

respectively. We now proceed to solve these in Euclidean signature where the geometries are familiar and thence explain the Lorentz counterparts.

[1]We will only quote explicitly the Lorentz signature action for the gravitational dynamics. The Euclidean action is given by $S_{\rm gr}^E = -S_{\rm gr}$ with the Lagrangian density evaluated on the appropriate signature metric in both cases; see appendix D.5.1. The overall negative sign is consistent with the general intuition the Euclidean action is the Hamiltonian for imaginary time evolution.

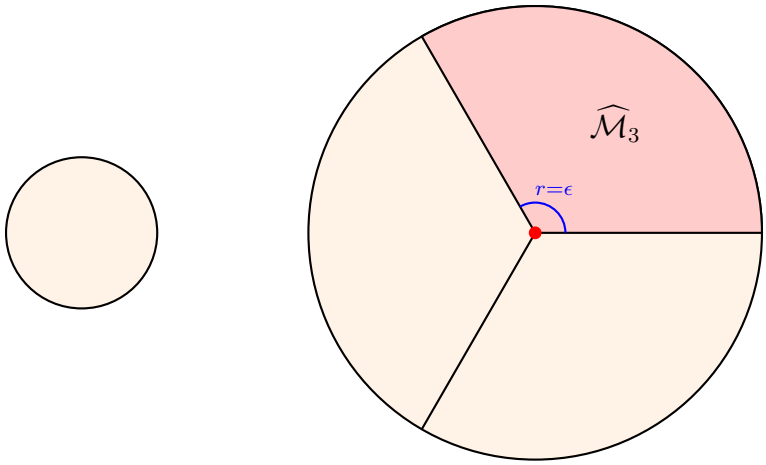

Figure 5.2: The Poincaré disc geometry dual to the thermofield double (or Hartle-Hawking) state of JT gravity and its n-fold replica depicted here for $n = 3$. We have shaded the single fundamental domain obtained by taking the replica quotient and indicated the interior boundary at $r = \epsilon$ one introduces while computing the on-shell Euclidean action contribution from a single fundamental domain.

Replicas in Euclidean signature

The thermofield double state where the Euclidean time coordinate t_{E} has period β is simply thermal AdS_2 by virtue of the first equation in (5.5). The n-fold replica is likewise the same geometry albeit now with the thermal circle being n-times larger.

Covering space: It is useful to write down the geometry using the Poincaré disc model, and parameterize the Euclidean covering space $\mathcal{M}_n$ by complex coordinates $z, \bar{z}$ as

$$ds^2 = \frac{4\, dz\, d\bar{z}}{(1 - z\,\bar{z})^2} = 4\, \frac{dr^2 + \frac{1}{n^2}\, r^2\, d\tau^2}{(1 - r^2)^2}\,, \qquad z = r\, e^{i\,\tau/n}\,, \tag{5.6}$$

with the identification $\tau \sim \tau + 2\pi\, n$ on the Poincaré disc to account for the n-fold cover.

A general solution for the dilaton can be easily written down:[2]

$$\phi = \frac{1}{1-z\bar{z}}\big[\alpha_-(1+z\bar{z}) - i\,\alpha_0\,(z-\bar{z}) + \alpha_+\,(z+\bar{z})\big]. \tag{5.7}$$

The covering space is an n-fold branched cover over a single Euclidean-AdS_2 geometry; we will require that the fields respect the replica $\mathbb{Z}_n$ symmetry which acts by $\tau \to \tau + 2\pi$. The dilaton solution (5.7) will be admissible only it is invariant under $z \to z\,e^{2\pi i/n}$. This forces $\alpha_+ = \alpha_0 = 0$ and thus the solution for the dilaton in covering space AdS_2 is simply

$$\phi = \alpha\,\frac{1+z\bar{z}}{1-z\bar{z}}\,, \tag{5.8}$$

where we have renamed $\alpha_- \to \alpha$ for simplicity.

A single fundamental domain: The $\mathbb{Z}_n$ replica symmetry acts on this geometry by $\tau \to \tau + 2\pi$, or equivalently as $z \to z\,e^{2\pi i/n}$. Consequently, we can let $v = z^n$ be coordinates on a single fundamental domain $AdS_2/\mathbb{Z}_n$. On the quotient space the metric and dilaton are then given by

$$ds^2 = \frac{4\,(v\bar{v})^{\frac{1-n}{n}}}{n^2\left(1-(v\bar{v})^{\frac{1}{n}}\right)^2}dvd\bar{v} = 4\,\frac{n^2\,dr^2 + r^2\,d\tau^2}{n^2(1-r^2)^2}\,, \tag{5.9a}$$

$$\phi = \alpha\frac{1+(v\bar{v})^{\frac{1}{n}}}{1-(v\bar{v})^{\frac{1}{n}}}\,. \tag{5.9b}$$

[2]The easiest way to obtain the solution is to view Euclidean-AdS_2 as a hyperboloid embedded in $\mathbb{R}^{2,1}$. The embedding coordinates are $\{X_0, X_{\pm 1}\}$ with the mapping

$$X_0 = -i\,\frac{z-\bar{z}}{1-z\bar{z}}\,, \qquad X_{-1} = \frac{1+z\bar{z}}{1-z\bar{z}}\,, \qquad X_1 = \frac{z+\bar{z}}{1-z\bar{z}}$$

to the Poincaré model. It is easy to see that (5.5) requires $\phi = \alpha_-\,X_{-1} + \alpha_0\,X_0 + \alpha_+\,X_1$.

We have depicted the replica geometries of interest in Euclidean signature in fig. 5.2. In what follows we will find it more convenient to use a Cartesian chart for the fundamental domain, so will let $\{v, \bar{v}\} \equiv \{x + i\, t_{\rm E}, x - i\, t_{\rm E}\}$.

Lorentz signature replicas

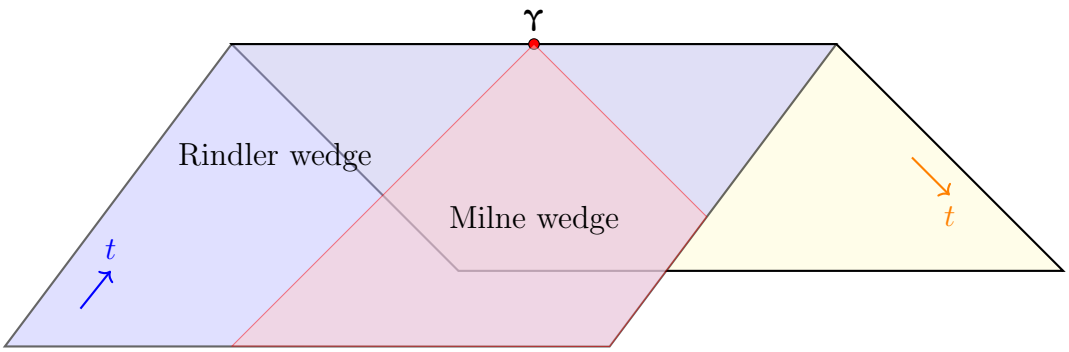

Figure 5.3: The domains in the Lorentzian geometry dual to a single fundamental domain $\widehat{\mathcal{M}}_n$. We have indicated both the 'ket' and 'bra' components of the spacetime M^k and M^b which are each a copy of the AdS_2 geometry past of the Cauchy slice at $t = 0$. The geometry $\widehat{\mathcal{M}}_n$ has a fixed point locus of the replica $\mathbb{Z}_n$ action at the splitting surface $\boldsymbol{\gamma}$. The ket and bra geometries are real in the Rindler wedges, regions spacelike separated from $\boldsymbol{\gamma}$, but are complex in the Milne wedge, the causal past of $\boldsymbol{\gamma}$.

In Lorentz signature we work with coordinates $\{t, x\}$ with light-cone like combinations $\tilde{x}^{\pm} = x \pm t$ which are adapted to be positive in the spacelike domain as they will be natural analytic continuations of Euclidean variables. The metric in the covering space is that of AdS_2 itself, with no identifications. It is more interesting to examine the geometry in a single fundamental domain. Owing to the time translational symmetry of the background, we may analytically continue and obtain the metric and dilaton profiles

on $\widehat{\mathcal{M}}_n$ to be:

$$ds^2 = \frac{4\left(\tilde{x}^+\tilde{x}^-\right)^{\frac{1-n}{n}}}{n^2\left(1-\left(\tilde{x}^+\tilde{x}^-\right)^{\frac{1}{n}}\right)^2}\, d\tilde{x}^+ d\tilde{x}^- \,, \tag{5.10a}$$

$$\phi = \alpha\, \frac{1+\left(\tilde{x}^+\tilde{x}^-\right)^{\frac{1}{n}}}{1-\left(\tilde{x}^+\tilde{x}^-\right)^{\frac{1}{n}}} \,. \tag{5.10b}$$

The metric and dilaton profile in (5.10) clearly solves (5.5). However, it remains to fix the value of α. Since we wish to model the ground state, we should impose a positive frequency condition as described in [6]. But (5.10) is not positive frequency, so the only allowed solution is $\alpha = 0$ for which $\phi = 0$ everywhere. This is somewhat degenerate in our description, but we can certainly study the limit $\alpha \to 0$ for all replica numbers n. Note that this is in fact precisely the way in which our Euclidean analysis was performed.

One can add excitations to this state by allowing for time-dependent sources to be turned on in the real-time evolution. In this example one can give a clear picture of the positive-frequency boundary conditions necessary to define the initial state ρ_0. Let us consider this for finite α, after which we can again take the limit $\alpha \to 0$. A massless scalar field Φ, by virtue of its conformal invariance satisfies the standard wave equation $(-\partial_t^2 + \partial_x^2)\Phi = \delta(t - t_0, x)$ in the AdS_2 geometry. The solution in the presence of the source term will be given by

$$\Phi(t,x) = \frac{1}{2\pi}\int \frac{-e^{-i\omega(t-t_0)-ikx}}{-\omega^2+k^2} d\omega dk \,. \tag{5.11}$$

The positive frequency mode here can be isolated by an $i\varepsilon$ prescription; we pick the $\omega = -|k|$ pole when integrating over ω. The result is the familiar retarded solution for

the scalar field (γ is the Euler-Mascheroni constant)

$$\Phi(t,x) = i\,\mathrm{sgn}(t-t_0)\left(\frac{1}{2}\log\left((t-t_0)^2 - x^2\right) + \gamma\right). \tag{5.12}$$

We will not be considering excitations of the thermofield double state for simplicity, but the above analysis makes clear that we can easily add additional fields coupled gravitationally and study their effects.

Let us examine the Lorentzian geometry: the metric (5.10a) describes the metric on the 'ket' part of a single fundamental domain which we denote as M^k, see fig. 5.3. As described in [6] the cyclic $\mathbb{Z}_n$ replica symmetry together with the CPT symmetry that exchanges the bra and ket $\mathsf{M}^k \leftrightarrow \mathsf{M}^b$ requires that the geometric configurations be real in the homology wedge which is the region of spacetime spacelike separated from the fixed point locus $\boldsymbol{\gamma}$, also referred to as the *splitting surface* [6]. Since the fixed point locus $\boldsymbol{\gamma}$ in the present case is at $x = t = 0$, the homology wedges are the past Rindler wedges $|x| > |t|$ with $t \leq 0$. This is ensured in (5.10) by the choice of analytic continuation: $\tilde{x}^{\pm}$ are both positive in the right Rindler wedge, and both negative in the left Rindler wedge. However, the solution is complex in the Milne wedge, the causal past of $\boldsymbol{\gamma}$ where $\tilde{x}^- > 0$ and $\tilde{x}^+ < 0$. Additionally, we need to choose α to be real owing to the $\mathbb{Z}_2$ symmetry at $t = 0$. This may be achieved by our choice of the initial state.

We can exhibit a manifestly real form of the configuration in the right Rindler wedge by the following coordinate transformation:

$$t = (n\,\rho)^n \sinh \mathsf{t}_{_R}, \quad x = (n\,\rho)^n \cosh \mathsf{t}_{_R}\,, \qquad \rho \in \mathbb{R}_{\geq 0} \text{ and } \mathsf{t}_{_R} < 0\,. \tag{5.13}$$

which maps (5.10) into

$$ds^2 = 4\,\frac{n^2\,d\rho^2 - \rho^2\,d\mathtt{t}_{_R}^2}{(1-n^2\rho^2)^2}\,, \qquad \phi = \alpha\frac{1+n^2\,\rho^2}{1-n^2\,\rho^2}. \tag{5.14}$$

One can pass to the other wedges by effectively rotating $\mathtt{t}_{_R}$ by a phase as we cross the past horizon of $\boldsymbol{\gamma}$, with the result,

$$\begin{aligned}
&\text{left Rindler wedge}: \quad t = (n\rho)^n\,\sinh\mathtt{t}_{_L}\,, \qquad x = -(n\rho)^n\,\cosh\mathtt{t}_{_L}\,, \quad \rho\in\mathbb{R}_{\geq 0}\text{ and }\mathtt{t}_{_L}<0\,,\\
&\text{lower Milne wedge}: \quad t = -(i\,n\rho)^n\,\cosh\mathtt{t}_{_M}\,, \quad x = (i\,n\rho)^n\,\sinh\mathtt{t}_{_M}\,, \quad \rho\in\mathbb{R}_{\geq 0}\text{ and }\mathtt{t}_{_M}\in\mathbb{R}\,.
\end{aligned} \tag{5.15}$$

5.2.2 The Rényi entropy computation

Now that we have our replica spacetime we need to evaluate the on-shell action. We will first do so in the Euclidean setting just to remind ourselves of the expected answer, and then proceed with the real-time computation.

Euclidean action calculation

The on-shell Euclidean action we need to evaluate is

$$\mathscr{Z} = e^{-I} = e^{-S^E_{\rm gr}}\big|_{\text{on-shell}} = e^{-S_0-S_\phi}\big|_{\text{on-shell}}\,. \tag{5.16}$$

Recall that the counter-terms are designed to make the action finite, and recall also that our limit $\alpha\to 0$ sends $\phi\to 0$ everywhere. Thus $\lim_{\alpha\to 0} S_\phi = 0$. It thus remains only to evaluate the contribution from S_0.

The boundary conditions we need are that the radial coordinate is cut-off at $r = r_c$ and the proper length of the boundary thermal circle is β/ϵ with the boundary value of the dilaton being $\phi_b = \phi_c/\epsilon$.

In this example it is simplest to work in the covering space, where S_0 can be trivially evaluated. One simply notes that the Gauss-Bonnet theorem gives us the gravitational contribution to be the Euler character of a disc, and hence

$$S_0\big|_{\text{on-shell}} = -\frac{\phi_0}{16\pi G_N} \times 4\pi = -\frac{\phi_0}{4\,G_N}\,. \tag{5.17}$$

One can also directly verify this result by computing the Einstein-Hilbert and Gibbons-Hawking terms in S_0 separately with a radial cut-off at r_c and the thermal periodicity as required. One has the extrinsic curvature $K = \frac{1+r_c^2}{2\,r_c}$ for the constant $r = r_c$ slice and thus

$$\begin{aligned} S_0\big|_{\text{on-shell}} &= -\frac{\phi_0}{16\pi G_N}\left[\int_{\mathcal{M}_n} d^2x\,\sqrt{g}\,R + 2\int_{\mathcal{B}_n} dx\,\sqrt{\gamma}\,K\right] \\ &= -\frac{\phi_0}{16\pi G_N} \times \left[\int_0^{r_c} \frac{4r\,dr}{n\,(1-r^2)^2} \times (-2) + 2\,\frac{2r_c}{1-r_c^2}\frac{1+r_c^2}{2\,n\,r_c}\right] \times \int_0^{2\pi n} d\tau \\ &= -\frac{\phi_0}{4\,G_N}\,. \end{aligned} \tag{5.18}$$

In principle there is a further contribution from the dilaton action (the Schwarzian term). For the thermofield double state at $\beta \to \infty$ however this can be checked to vanish at tree level (Schwarzian fluctuations will give the near-extremal result [167]).

Let us also check the result directly by working in a single fundamental domain. We will again use the Gauss-Bonnet theorem, but we will be careful to excise the contribution from the cosmic brane, the singular codimension-2 locus of the replica $\mathbb{Z}_n$ symmetry fixed point at $r = 0$. The fastest way to proceed is to excise a disc $\mathcal{D}_\epsilon$ of radius $r = \epsilon$ around the origin. One then computes S_0 in terms of the Euler character of the resulting annulus and the contribution from the inner boundary term at $r = \epsilon$ which is another copy of the

Gibbons-Hawking term now on a circle of radius ϵ. To wit,

$$\begin{aligned} S_0\big|_{\text{on-shell}} &= -n\,(S_0)_{\text{fund}} \\ &= -n\,\frac{\phi_0}{16\pi G_N}\left(\int_{\widehat{\mathcal{M}}_n} d^2x\,\sqrt{g}\,R + 2\int_{\mathcal{B}} dx\,\sqrt{\gamma}\,K - 2\int_{r=\epsilon} dx\,\sqrt{h}\,K\right) \\ &= -\frac{n\,\phi_0}{16\pi G_N}\left(0 - 2\left(\frac{2\epsilon}{1-n^2\epsilon^2}\right)\left(-\frac{1+n^2\epsilon^2}{2\,n\,\epsilon}\right)\int_0^{2\pi} d\tau\right) \\ &= -\frac{\phi_0}{4\,G_N}\,. \end{aligned} \tag{5.19}$$

where we used the fact that the Euler characteristic of the annulus vanishes and $K = -\frac{1+n^2\epsilon^2}{2\,n\,\epsilon}$ on the regulating surface at $r = \epsilon$ (note the change in orientation of the normal gives us an extra negative sign).

With the on-shell action at hand we can compute the n^{th} Rényi entropy for the thermofield double (Hartle-Hawking) state. Since $I_n = I_1$ it immediately follows from (5.1) that

$$S^{(n)} = \frac{\phi_0}{4\,G_N}\,. \tag{5.20}$$

which is the promised temperature independent answer.

Lorentzian action calculation

Let us now compute the result for the on-shell action in Lorentz signature. Again, the limit $\alpha \to 0$ sends $\phi \to 0$ at all points, so we should understand S_ϕ as vanishing in the limit. To compute the gravitational contributions, we will work in a single fundamental domain. Recall that the metric on $\widehat{\mathcal{M}}_n$ is given by (5.10). We will organize the computation as follows: $\widehat{\mathcal{M}}_n$ has two components M^k corresponding to the forward evolution of the ket and M^b corresponding to the backward evolution of the bra. The direction of

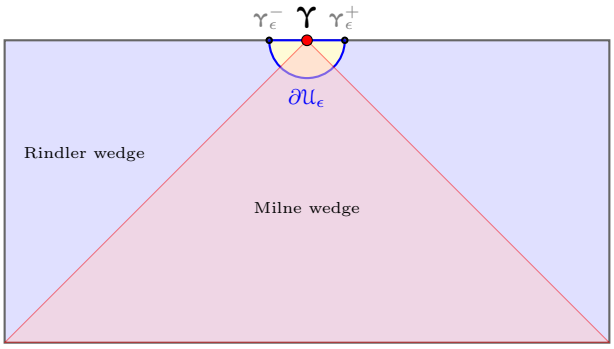

Figure 5.4: The geometry in the vicinity of the splitting surface $\boldsymbol{\gamma}$ in the Lorentzian geometry dual to a single fundamental domain $\widehat{\mathcal{M}}_n$. We have excised a neighbourhood $\mathcal{U}_\epsilon$ of $\boldsymbol{\gamma}$ with boundary $\partial\mathcal{U}_\epsilon$ to regulate the contribution from the fixed point locus. We take $\partial\mathcal{U}_\epsilon$ to be parametrized by an arbitrary curve $\tilde{x}^+ = U(\tilde{x}^-)$ in the $\tilde{x}^\pm$ plane.

time evolution being reversed in the two, one needs to compute as described in (5.3)

$$S_n^{\rm fund}(\widehat{\mathcal{M}}_n) = \frac{1}{n}\left[S^k_{{\rm gr},n} - S^b_{{\rm gr},n}\right] \implies I_n = -i\,n\,S_n^{\rm fund} = 2\,n\,{\rm Im}(S^k_{\rm gr,fund})\,. \tag{5.21}$$

We can thus focus on computing the imaginary part of $S^k_{\rm gr,fund}$ from the ket. In implementing this computation, we will organize the pieces in the following manner: we first excise a region $\mathcal{U}_\epsilon$ around $\tilde{x}^\pm = 0$, the fixed point locus $\boldsymbol{\gamma}$ with boundary $\partial\mathcal{U}_\epsilon$. This cut-off region with the topology of a disc, intersects the Cauchy slice at $t = 0$ on two corners $\boldsymbol{\gamma}_\epsilon^\pm$, respectively, as depicted in fig. 5.4. We will take $\partial\mathcal{U}_\epsilon$ to be parameterized by a function $\tilde{x}^+ = U(\tilde{x}^-)$. We can implement the Gauss-Bonnet theorem on the lower-half plane after excising $\mathcal{U}_\epsilon$, provided we include a boundary term at the excision surface $\partial\mathcal{U}_\epsilon$ and the corner terms where this cut-off region meets the Cauchy surface at $t = 0$. Specifically, focusing on the gravitational contribution of the JT action (5.4) we have

$$\begin{aligned} S_0 &= \frac{\phi_0}{16\pi G_N}\left[\int_{\mathcal{M}} d^2x\,\sqrt{-g}\,R + 2\int_{\mathcal{B}} dx\,\sqrt{-\gamma}K\right] \\ &= \frac{\phi_0}{16\pi G_N}\left[4\pi\,\chi - 2\int_{\partial\mathcal{U}_\epsilon} dx\,\sqrt{h}\,K - S_{\rm corner}\right], \end{aligned} \tag{5.22}$$

with χ being the Euler character. The bulk term encoded in χ does not give any imaginary contribution – these are completely subsumed into the Gibbons-Hawking term on the Cauchy slice and the corner term. We will evaluate these in turn.

To facilitate the computation for the metric (5.10a) let us write the prefactor as $\sigma(\tilde{x}^+, \tilde{x}^-)$ and compute the extrinsic curvature of the surface $\partial\mathcal{U}_\epsilon$. Given the normal vector

$$n^\mu \partial_\mu = \sqrt{\frac{U'(\tilde{x}^-)}{\sigma}}\,\frac{\partial}{\partial \tilde{x}^+} - \sqrt{\frac{1}{\sigma\, U'(\tilde{x}^-)}}\,\frac{\partial}{\partial \tilde{x}^-}\,, \tag{5.23}$$

one finds:

$$K = \frac{1}{2\,(U'\,\sigma)^{\frac{3}{2}}}\left[\sigma\, U'' - U'\left(\frac{\partial \sigma}{\partial \tilde{x}^-} - U'\,\frac{\partial \sigma}{\partial \tilde{x}^+}\right)\right]. \tag{5.24}$$

Factoring in the induced measure $\sqrt{h} = \sqrt{\sigma\, U'}$ we end up with the Gibbons-Hawking contribution evaluating to

$$2\int_{\mathcal{U}_\epsilon} dx\,\sqrt{h}\,K = \int d\tilde{x}^-\,\left(\frac{U''}{U'} - \frac{\partial \log\sigma}{\partial \tilde{x}^-} + U'\,\frac{\partial \log\sigma}{\partial \tilde{x}^+}\right) \equiv T_0 + T_- + T_+\,, \tag{5.25}$$

where we have chosen to split the integrand and label the three integrals as $T_{0,\pm}$ for convenience. We now note the following T_0, which is an integral of our cut-off function $U(\tilde{x}^-)$ alone, can be seen to be purely real. We can pick for instance a smooth function and realize that the integral is over some domain of the form: $\tilde{x}^- \in [-\delta, x_* + \delta]$ with x_* being a zero locus of $U(x)$ and $\delta > 0$. Important to this argument is the fact that the integrand can be made a regular function of $\tilde{x}^-$. Furthermore,

$$T_+ = \int dx^+\,\frac{\partial \log\sigma}{\partial \tilde{x}^+}\,, \tag{5.26}$$

which is obtained by a $\tilde{x}^- \leftrightarrow \tilde{x}^+$ swap from T_- and we record that $\sigma(\tilde{x}^-, \tilde{x}^+))$ is a symmetric function. We will see below that $\mathrm{Im}(T_- + T_+) = 2\,\mathrm{Im}(T_-)$, so we will simply

focus on its evaluation for now.

Plugging in the conformal factor σ from (5.10a) we have

$$T_- = -\int d\tilde{x}^- \frac{\partial \log \sigma}{\partial \tilde{x}^-} = \int \frac{d\tilde{x}^-}{n\,\tilde{x}^-} \left(1 + n - \frac{2}{1-(\tilde{x}^+\tilde{x}^-)^{\frac{1}{n}}}\right). \tag{5.27}$$

We see that the integral over $\tilde{x}^-$ has a pole at the origin which needs to be accounted for. We will do so using an $i\epsilon$ regulator and defining the integrand by a principal value prescription. Recall,

$$\frac{1}{x \pm i\epsilon} = \mathcal{P}\frac{1}{x} \mp i\,\pi\delta(x)\,. \tag{5.28}$$

The natural choice of the contours is such that $\tilde{x}^- \to \tilde{x}^- + i\epsilon$ [6]. We then have

$$\begin{aligned} T_- &= \frac{1}{n}\int d\tilde{x}^- \left[\mathcal{P}\frac{1}{\tilde{x}^-} \mp i\,\pi\delta(\tilde{x}^-)\right]\left(1 + n - \frac{2}{1-(U(\tilde{x}^-)\,\tilde{x}^-)^{\frac{1}{n}}}\right), \\ \implies \quad \mathrm{Im}(T_-) &= -\frac{1}{n}(n-1)\,\pi\,. \end{aligned} \tag{5.29}$$

In evaluating the integral we have finally restricted to the cut-off surface and used the smoothness of $U(x)$ to obtain the final result. The evaluation of T_+ proceeds similarly with the $i\epsilon$ prescription reading now $\tilde{x}^+ \to \tilde{x}^+ - i\epsilon$. The relative sign of the $i\epsilon$ implies that the imaginary part from T_- is doubled, so that

$$\mathrm{Im}\left[2\int_{\partial\mathcal{U}_\epsilon} dx\,\sqrt{h}\,K\right] = 2\pi\left(\frac{1}{n} - 1\right). \tag{5.30}$$

The final piece we need is the corner term where the spacelike Cauchy surface $\tilde{\Sigma}_t$ intersects with the chosen cut-off $\partial\mathcal{U}_\epsilon$. As explained in [6] this contribution arises when the regulator surface $\partial\mathcal{U}_\epsilon$ does not intersect the Cauchy surface orthogonally.[3] For our

[3]We pause to note here that these contributions have been discussed earlier in [152] (in the context of applications to black hole entropy computations) and were treated in full generality quite elegantly in [150]. We also note its use in the holographic entanglement entropy computations in [34].

purposes we simply need to know that the integral of the extrinsic curvature along the boundary in two dimensions is the same as adding up the infinitesimal rotation angles of the normal n^μ. At the corner the boost angle associated with the normal vector jumps by a factor $i\,\frac{\pi}{2}$ as originally computed in [151]. Specifically, at each corner $\boldsymbol{\gamma}^{\pm}$ we get a contribution from the relative boost that arises in going from the ket to the bra component M^{k} of $\widehat{\mathcal{M}}_n$[4]

$$\int \sqrt{-h}K = \cosh^{-1}\left(n_\epsilon^{\mathsf{k}} \cdot n_\epsilon^{\mathsf{b}}\right) = i\,\frac{\pi}{2}\,. \tag{5.31}$$

We have two corners $\boldsymbol{\gamma}_\epsilon^{\pm}$ with opposing orientations and hence

$$\mathrm{Im}(S_{\mathrm{corner}}) = \mathrm{Im}\left(2\int_{\boldsymbol{\gamma}_\epsilon^+}\sqrt{-h}\,K + 2\int_{\boldsymbol{\gamma}_\epsilon^-}\sqrt{-h}\,K\right) = 2\pi\,. \tag{5.32}$$

Adding all the contributions from (5.30) and (5.32), we get the full Lorentzian action,

$$I_n = -2\,n\,\frac{\phi_0}{16\pi\,G_N}\,\mathrm{Im}\left[2\int_{\partial\mathcal{U}_\epsilon}\sqrt{h}\,K + S_{\mathrm{corner}}\right] = -\frac{\phi_0}{4\,G_N}\,. \tag{5.33}$$

This indeed is the expected answer for one immediately recovers from the above the result for the n^{th} Rényi entropy obtained from the Euclidean computation (5.20).

5.3 Rényi entropies in 2d CFTs: A single interval

As our next example we will examine the much studied example of a single-interval Rényi entropy in the vacuum state of a two dimensional conformal field theory on the

[4]There is a useful heuristic for this calculation which underlies the complex Gauss-Bonnet theorem employed in [145] – the cut-off surface has to pass from the timelike Milne region to the spacelike Rindler region and each crossing involves a $i\frac{\pi}{2}$ jump in the normal (see also [152]). This is the piece we pick up in the corner contribution if we have a non-orthogonal intersection at the Cauchy slice; see Appendix A of [6] for a brief discussion.

plane. This computation which was first carried out in [171] and re-examined in [81] exploits the fact that the computation of the Rényi entropies can either be viewed as the computation of the partition function on a n-folded branch cover, or equivalently as the correlation function of $\mathbb{Z}_n$ twist operators. The key point is that the n-fold branched cover of the complex plane is a genus-zero Riemann surface which can be uniformized by a simple map.

To be concrete let us consider the CFT_2 on $\mathbb{R}^{1,1}$ and let $\mathcal{A}$ be a codimension-1 spacelike region on some Cauchy surface with $\partial\mathcal{A}$ comprising of two-points $a_1 = (0,0)$ and $a_2 = (t_0, x_0)$ with $t_0 < x_0$. The CFT computation gives (δ is a UV regulator)

$$\begin{aligned} S_{\mathcal{A}}^{(n)} &= \frac{1}{1-n}\,\log\,\text{Tr}(\rho_{\mathcal{A}}^n) = \frac{1}{1-n}\,\log\,\langle \mathcal{T}_n(a_1)\,\mathcal{T}_{-n}(a_2)\rangle \\ &= \frac{c}{12}\left(1+\frac{1}{n}\right)\log\left(\frac{|a_2-a_1|^2}{\delta^2}\right) = \frac{c}{12}\left(1+\frac{1}{n}\right)\log\left(\frac{x_0^2-t_0^2}{\delta^2}\right). \end{aligned} \tag{5.34}$$

Here $\mathcal{T}_n$, $\mathcal{T}_{-n}$ are the $\mathbb{Z}_n$ twist operators and we have exploited the fact that the partition function on the n-fold cover $\mathcal{B}_n$ can be mapped to a two-point function of these twist operators.

We would like to reproduce this answer from a gravity computation. We will take the bulk theory to be Einstein-Hilbert gravity in AdS_3 which has by the classic analysis of [80] an asymptotic Virasoro symmetry with central charge $c = \frac{3\ell_{\text{AdS}}}{2G_N}$. We will use this relation explicitly and rewrite the strength of the gravitation interaction $\frac{\ell_{\text{AdS}}}{16\pi G_N} = \frac{1}{24\pi}\,c$.[5]

[5]We will set $\ell_{\text{AdS}} = 1$ in most of our analysis below, but will quote the result in terms of the dimensionless CFT central charge.

5.3.1 The boundary replica geometry

Let us first examine the boundary replica geometry in Euclidean signature obtained by Wick rotating $t \to -i\,t_{\rm E}$.[6] The original geometry $\mathcal{B}$ is the complex plane with coordinates $\{v = x + i\,t_{\rm E}, \bar{v} = x - i\,t_{\rm E}\}$, and hence the branched cover replica space $\mathcal{B}_n$ is topologically a sphere, with branch points at a_1 and a_2 where it has a conical excess given by $2\pi(n-1)$. Let z be the complex coordinate on the covering space. The complex structure on $\mathcal{B}_n$, $\frac{v-a_1}{v-a_2}$, defines a uniformization map to the smooth covering space, which itself is a complex plane with coordinate z defined by

$$z = \left(\frac{v-a_1}{v-a_2}\right)^{\frac{1}{n}} \tag{5.35}$$

In the z-plane the n-sheets of the branched cover are mapped to n wedges with opening angle $\frac{2\pi}{n}$ as depicted in fig. 5.2. The uniformization map can be viewed as a conformal transformation since

$$dz d\bar{z} = \Omega^2\, dv\, d\bar{v}\,, \qquad \Omega^2 \equiv \frac{1}{n^2}\,\frac{|a_2-a_1|^2}{\left|(v-a_1)^{1-\frac{1}{n}}\,(v-a_2)^{1+\frac{1}{n}}\right|^2}\,. \tag{5.36}$$

The passage to Lorentz signature can be achieved by the inverse Wick rotation and in terms of our light-cone coordinates $\tilde{x}^{\pm} = x \pm t$, the metric is

$$ds^2 = \frac{|a_2-a_1|^2}{n^2}\,\frac{d\tilde{x}^+\,d\tilde{x}^-}{(\tilde{x}^- - a_1)^{\frac{1}{2}-\frac{1}{2n}}(\tilde{x}^- - a_2)^{\frac{1}{2}+\frac{1}{2n}}\,(\tilde{x}^+ - a_1)^{\frac{1}{2}-\frac{1}{2n}}(\tilde{x}^+ - a_2)^{\frac{1}{2}+\frac{1}{2n}}}. \tag{5.37}$$

Note that the Wick rotation is carried out with respect to the time-coordinate on the base space $\mathcal{B}$ where the physical quantum fields reside. The Lorentzian metric on $\mathcal{B}_n/\mathbb{Z}_n$

[6]For any $t_0 < x_0$ we can pick a Cauchy surface of $\mathbb{R}^{1,1}$ to be defined by $\frac{x}{x_0} = \frac{t}{t_0}$ – its normal is a timelike vector: $x_0\,\frac{\partial}{\partial t} + t_0\,\frac{\partial}{\partial x}$. We can Wick rotate this vector and obtain the Euclidean spacetime of interest. It is simpler to visualize the case when $t_0 = 0$. However, for the SL(2) invariant CFT_2 vacuum, all foliations by slices of constant $-\frac{x}{x_0} + \frac{t}{t_0}$ are equivalent by the underlying boost invariance.

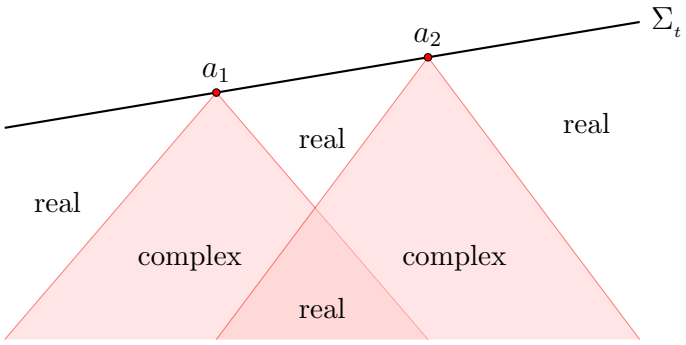

Figure 5.5: Causal domains on the boundary ket spacetime B^k for a two dimensional field theory with the region $\mathcal{A}$ taken to be a spacelike segment of a boosted Cauchy slice. We indicate the regions where the resulting metric is real and complex, respectively. In general the metric is not guaranteed to be real in regions that are in the causal past of the entangling surface $\partial\mathcal{A}$ which here comprises of the two points a_1 and a_2.

is not real everywhere: it is complex in regions that lie in the causal past of $\partial\mathcal{A}$. For the present example this is the domain that is timelike separated from one endpoint, but spacelike separated from the other as depicted in fig. 5.5.[7]

In arriving at this answer we have used the Euclidean construction of the branched cover as a crutch, but one can verify this directly by taking n-copies of the ket and bra spacetimes with the replica gluing conditions. A simple way to see this is to consider a conformal transformation which makes $\mathcal{A}$ a semi-infinite interval, mapping in the process its past domain of dependence to a Rindler wedge of the resulting Minkowski spacetime (on $\mathcal{B}$) [124]. The n-fold cover is obtained by gluing the Rindler wedges of $\mathcal{A}$ cyclically across the replica bras and kets (while those of $\mathcal{A}^c$ are glued together within the bra-ket combination of each replica copy). The combination of $\mathbb{Z}_n$ replica symmetry and the $\mathbb{Z}_2$ CPT-conjugation swapping bras and kets, ensures that the resulting spacetime has a real

[7]As noted in [6] the boundary conditions at the asymptotic AdS boundary are specified by a real boundary metric (with conical singularities at the entangling surface). The reason for the complex metric in (5.37) is because we have made a specific choice for the boundary conformal frame which is related to the real boundary metric by a complex Weyl factor. We have analytically continued the Euclidean boundary geometry (5.36) obtained via the uniformization and it is this choice that is responsible for the complex Weyl factor.

Lorentz signature geometry in the Rindler wedges, but not necessarily so in the Milne wedges [6]. The example above makes this manifest.

5.3.2 The bulk Rényi geometries

Given the boundary geometry $\mathcal{B}_n$ we are tasked with constructing the bulk dual $\mathcal{M}_n$. We will first describe the geometry in Euclidean signature and then outline the Lorentzian description. The covering space geometry $\mathcal{M}_n$ is simply AdS_3, since the z-plane is a copy of $\mathbb{C}$. It is more interesting to examine the geometry of the fundamental domain $\widehat{\mathcal{M}}_n$ where the boundary has the conical singularities associated with the branch points.

We will proceed by exploiting the fact that the Fefferman-Graham expansion converges in AdS_3 (since all geometries are locally diffeomorphic to AdS_3). Using the general results of [172] one can write the metric dual to the state of interest in terms of the boundary stress tensor data (this was used by [173] to compute holographic Rényi entropies in AdS_3). The physical state we are considering on one fundamental domain of the CFT is the state obtained by acting on the vacuum with the twist operators (which thence create the appropriate monodromy around the branch points).

The standard Fefferman-Graham expansion in AdS_3 with boundary metric γ_{ij} and ρ being the Fefferman-Graham radial coordinate, is given as [172]

$$ds^2 = \frac{d\rho^2}{4\,\rho^2} + \frac{1}{\rho}\left[\left(1-\frac{\rho}{4}\,\mathrm{Tr}(T)\right)\delta_i{}^k + \frac{\rho}{4}\,T_i{}^k\right]\gamma_{kl}\left[\left(1-\frac{\rho}{4}\,\mathrm{Tr}(T)\right)\delta^l{}_j + \frac{\rho}{4}\,T^l{}_j\right]\,dx^i\,dx^j\,. \tag{5.38}$$

Working in the complex coordinates $v, \bar{v}$ the geometry takes the form:

$$\begin{aligned} ds^2 = \frac{d\rho^2}{4\,\rho^2} + \frac{dv\,d\bar{v}}{\rho} - \frac{1}{2}\left[T_{v\bar{v}}\,dvd\bar{v} - T_{vv}\,dv^2 - T_{\bar{v}\bar{v}}\,d\bar{v}^2\right] \\ + \frac{\rho}{8}\left[\left(T_{vv}\,T_{\bar{v}\bar{v}} + T_{v\bar{v}}^2\right)dvd\bar{v} - 2\,T_{v\bar{v}}\left(T_{vv}\,dv^2 + T_{\bar{v}\bar{v}}\,d\bar{v}^2\right)\right]. \end{aligned} \tag{5.39}$$

For the case of interest we need to know the boundary stress tensor, which is easily obtained by the conformal map (5.35). One has the result given in terms of the Schwarzian map for the diagonal components, viz.,

$$\begin{aligned} T_{vv} &= \mathrm{Sch}(z, v) = \frac{1}{2}\left(1 - \frac{1}{n^2}\right) \frac{|a_2 - a_1|^2}{(v - a_1)^2 (v - a_2)^2}, \\ T_{\bar{v}\bar{v}} &= \mathrm{Sch}(\bar{z}, \bar{v}) = \frac{1}{2}\left(1 - \frac{1}{n^2}\right) \frac{|a_2 - a_1|^2}{(\bar{v} - a_1)^2 (\bar{v} - a_2)^2}\,. \end{aligned} \tag{5.40}$$

The off-diagonal term is instead given by the conformal anomaly term:

$$T_{v\bar{v}} = -2\,\partial_v \partial \bar{v}\, \log \Omega = \pi \left[\left(1 - \frac{1}{n}\right) \delta(|v - a_1|) + \left(1 + \frac{1}{n}\right) \delta(|v - a_2|)\right]. \tag{5.41}$$

Plugging in these expressions into (5.39) we obtain the metric on a single fundamental domain $\widehat{M}_n$ in Euclidean signature.

One can exhibit the fact that the Euclidean geometry on $\mathcal{M}_n$ is smooth by constructing an explicit diffeomorphism (see [174]) from the $(\rho, v, \bar{v})$ coordinates above to a new set of coordinates $(\xi, y, \bar{y})$. All we need is for this diffeomorphism to act as the desired conformal transformation implementing the uniformization. Explicitly, we have

$$\xi = \frac{\sqrt{\rho}\,\Omega}{1 + \rho\,\Omega^2\,|\partial_z \log \Omega|^2}\,, \qquad y = z + \frac{\rho\,\Omega^2\,\partial_{\bar{z}} \log \Omega}{1 + \rho\,\Omega^2\,|\partial_z \log \Omega|^2}\,, \tag{5.42}$$

which maps the metric on the covering space to the standard Poincaré metric:

$$ds^2 = \frac{d\xi^2 + dy d\bar{y}}{\xi^2}\,. \tag{5.43}$$

On this covering space the replica $\mathbb{Z}_n$ symmetry acts as $z \to e^{\frac{2\pi i}{n}}\, z$ or equivalently $y \to e^{\frac{2\pi i}{n}}\, y$. The fixed points of the symmetry are the branch points $v = a_1$ and $v = a_2$ on the boundary, and a bulk locus $\boldsymbol{\gamma}$ which in this particular case is a geodesic that connects

the two boundary points. In the regular $(\xi, y, \bar{y})$ coordinates this is the geodesic that connects the north and south poles of the boundary Riemann sphere.

The Lorentzian geometry on the ket part, M^k, of a single fundamental domain $\widehat{M}_n$ can be obtained from the above. One might naively think this is simply an analytic continuation of the $(v, \bar{v})$ coordinates. However, we should exercise some care since the naive analytic continuation of the $T_{v\bar{v}}$ component of the stress tensor which has delta function sources would indicate that we have shockwaves propagating along the past-light cones of the branch points. This is incorrect and inconsistent with the boundary conditions of the variational problem described in [6]. The single fundamental domain has a fixed point locus from the replica $\mathbb{Z}_n$ action, and a complex metric in the causal past of $\partial\mathcal{A}$, but no singularities along the light-cone. Instead the correct metric in real-time is one where we Wick rotate $T_{vv} \to T_{\tilde{x}^-\tilde{x}^-}$ and $T_{\bar{v}\bar{v}} \to T_{\tilde{x}^+\tilde{x}^+}$ but define the analytic continuation of $T_{v\bar{v}} \to T_{\tilde{x}^-\tilde{x}^+}$ to only have delta function singularities at the fixed point locus. To wit, (with $T_{-+} \equiv T_{\tilde{x}^-\tilde{x}^+}$ etc)

$$\begin{aligned}
T_{-+} &= 2\pi i \left[\left(1 - \frac{1}{n}\right) \delta(\tilde{x}^- - a_1)\, \delta(\tilde{x}^+ - a_1) + \left(1 + \frac{1}{n}\right) \delta(\tilde{x}^- - a_2)\, \delta(\tilde{x}^+ - a_2) \right], \\
T_{--} &= \frac{1}{2}\left(1 - \frac{1}{n^2}\right) \frac{|a_2 - a_1|^2}{(\tilde{x}^- - a_1)^2\,(\tilde{x}^- - a_2)^2}, \\
T_{++} &= \frac{1}{2}\left(1 - \frac{1}{n^2}\right) \frac{|a_2 - a_1|^2}{(\tilde{x}^+ - a_1)^2\,(\tilde{x}^+ - a_2)^2},
\end{aligned} \tag{5.44}$$

in terms of which we can parameterize the bulk real-time metric on M^k as

$$\begin{aligned}
ds^2 = \frac{d\rho^2}{4\rho^2} + \frac{d\tilde{x}^+\, d\tilde{x}^-}{\rho} + \frac{1}{2}\left(-T_{-+}\, d\tilde{x}^-\, d\tilde{x}^+ + T_{--}\,(d\tilde{x}^-)^2 + T_{++}\,(d\tilde{x}^+)^2\right) \\
+ \frac{\rho}{8}\left[\left(T_{--}T_{++} + T_{-+}^2\right) d\tilde{x}^+ d\tilde{x}^- - 2\,T_{-+}\left(T_{--}\,(d\tilde{x}^-)^2 + T_{++}\,(d\tilde{x}^+)^2\right)\right].
\end{aligned} \tag{5.45}$$

The choice of analytic continuation made in (5.44) is really a question of correctly

interpreting the codimension-2 delta functions therein. One can justify this by an integral representation in momentum space. We recall that the T_{-+} component is determined by the conformal factor Ω since

$$\begin{aligned} T_{-+} &= 2\,\partial_-\partial_+ \log\Omega(\tilde{x}^+,\tilde{x}^-) \\ &= 2\left(1-\frac{1}{n}\right)\partial_-\partial_+\log\sqrt{(\tilde{x}^- - a_1)(\tilde{x}^+ - a_1)} \\ &\qquad + 2\left(1+\frac{1}{n}\right)\partial_-\partial_+\log\sqrt{(\tilde{x}^- - a_2)(\tilde{x}^+ - a_2)}. \end{aligned} \tag{5.46}$$

We need to define the argument of the logarithm by analytic continuation, which we do by using a Fourier transform trick. Consider the following regulated integral which in Euclidean space, $\mathbf{x} \equiv (x, t_{\scriptscriptstyle \rm E})$, provides the standard integral representation of the modified Bessel function of the second kind $K_0(\mathbf{x}) = -\log(|\mathbf{x}|) + \text{constant}$:[8]

$$\begin{aligned} \log(|\mathbf{x}|) &= -\lim_{m\to 0}\frac{1}{2\pi}\int d^2\mathbf{p}\,\frac{e^{i\mathbf{p}\cdot\mathbf{x}}}{|\mathbf{p}|^2+m^2} \\ &\to -\lim_{m\to 0}\frac{i}{2\pi}\int d^2p\,\frac{e^{ip\cdot x}}{p^2+m^2-i\tilde{\epsilon}} \\ &= -\lim_{m\to 0}\frac{i}{4\pi}\int dp^+dp^-\,\frac{e^{-\frac{i}{2}(p^+\tilde{x}^- + p^-\tilde{x}^+)}}{p^+p^- - m^2 - i\tilde{\epsilon}}\,. \end{aligned} \tag{5.47}$$

Using the last line of the expression above it can be checked that one does recover (5.44) from (5.46).

5.3.3 Rényi entropies from gravity

We will now outline the computation of the Rényi entropies from the bulk geometries constructed in section 5.3.2. We will first revisit the computation in Euclidean signature as before just to set the stage and then proceed to describe how the Lorentzian com-

[8]The Pauli-Villars mass term here is introduced to remove the IR divergence. We are also allowing for a constant shift which will not affect the analysis.

putation works. The logic we follow will roughly parallel the discussion in section 5.2.2 though we now have to deal with the fact that the geometry in a single fundamental domain is more complicated.

Euclidean on-shell action in a fundamental domain

We will compute the Rényi entropies using (5.1). As remarked above, we carry out the computation of I_n in a single fundamental domain and then scale it up to the covering space. In evaluating the fundamental domain action, as explained in [33], we need to ensure that we do not include the contribution from the cosmic-brane, i.e., from the delta-function singularities arising as a result of taking the quotient. We thus want to evaluate

$$I_n = S^E_{\rm gr}[\mathcal{M}_n] = n\,\hat{I}_n \equiv n\,S^E_{\rm gr}[\widehat{\mathcal{M}}_n]\Big|_{\text{cosmic brane excised}} . \tag{5.48}$$

We will start by outlining the contributions to $S^E_{\rm gr}[\widehat{\mathcal{M}}_n]$ and then note the pieces that we need to remove to excise the cosmic brane contribution.

The on-shell action in gravity has three distinct contributions: a bulk term from the Einstein-Hilbert action, a boundary Gibbons-Hawking term, and finally boundary counterterms necessary to regulate the divergences. For definiteness we will regulate the spacetime by cutting-off the radial coordinate at $\rho = \rho_c$ and thence take the limit $\rho_c \to 0$ at the end of the computation. Denoting the induced metric on the cut-off timelike boundary $\mathcal{B}_c$ by $\gamma_{\mu\nu}$ we have the action as the sum of the aforementioned three contributions:

$$S^E_{\rm gr}[\widehat{\mathcal{M}}_n] = -\frac{1}{16\pi G_N}\left[\int_{\widehat{\mathcal{M}}_n} d^3x\,\sqrt{g}\,(R+2) + 2\int_{\mathcal{B}_c}\sqrt{\gamma}\,K - \int_{\mathcal{B}_c}\sqrt{\gamma}\,(2+{}^{\gamma}R\,\log\rho_c)\right] . \tag{5.49}$$

We can evaluate each of these in turn. Firstly, since $R=-6$ it follows that the bulk

contribution can be evaluated explicitly to be

$$\begin{aligned}\int_{\widehat{\mathcal{M}}_n} d^3x\,\sqrt{g}\,(R+2) &= -4\int_{\widehat{\mathcal{M}}_n}\sqrt{g}\\ &= -\int dvd\bar{v}\int_{\rho_c}^{\rho_*} d\rho\left[\frac{1}{\rho^2}+\frac{\mathrm{Tr}(T)}{4\rho}+\frac{\det(T)}{16}\right]\\ &= -\int dvd\bar{v}\left[\frac{1}{\rho_c}-\frac{\mathrm{Tr}(T)}{4}\,\log\frac{\rho_*}{\rho_c}-\sqrt{|T_{vv}|^2}\right].\end{aligned} \tag{5.50}$$

In this expression ρ_* is the value of ρ at the origin of AdS_3. In the Fefferman-Graham chart this is the point where the determinant of the metric vanishes. Explicitly one finds

$$\rho_* = \frac{8}{\mathrm{Tr}(T)+\sqrt{\mathrm{Tr}(T)^2-4\,\det(T)}}\,. \tag{5.51}$$

The boundary terms follow easily once we note that $K=-\frac{2}{\sqrt{g}}\,\rho\,\frac{\partial\sqrt{g}}{\partial\rho}+2$ evaluated at $\rho=\rho_c$ and that the curvatures of the induced metric on the cut-off boundary are related to the stress tensor. One has

$$\begin{aligned}2\int_{\mathcal{B}_c}\sqrt{\gamma}\,K &= -4\int_{\mathcal{B}_c} d^2x\,\sqrt{\gamma}\,\left(\frac{1}{\sqrt{g}}\,\rho\,\frac{\partial\sqrt{g}}{\partial\rho}-1\right)\\ &= 2\int_{\mathcal{B}_c} dvd\bar{v}\,\frac{1}{\rho_c}\,.\end{aligned} \tag{5.52}$$

The counterterm piece evaluates to

$$\int_{\mathcal{B}_c} d^2x\,\sqrt{\gamma}\,(2+{}^{\gamma}R\,\log\rho_c) = \int dvd\bar{v}\left(\frac{1}{\rho_c}-\frac{\mathrm{Tr}(T)}{4}\,(1+\log\rho_c)\right)\,. \tag{5.53}$$

Putting the pieces together we find

$$S^E_{\mathrm{gr}}[\widehat{\mathcal{M}}_n] = -\frac{c}{24\pi}\int dvd\bar{v}\,\left[\frac{\mathrm{Tr}(T)}{4}\,(1+\log\rho_*)+\sqrt{|T_{vv}|^2}\right]. \tag{5.54}$$

Now as remarked we need to exclude the contribution from the cosmic brane. In

the form written above in (5.54) this term is completely isolated in the contribution to $\mathrm{Tr}(T)$. Dropping these terms will in fact suffice to extract for us the part that is the cosmic-brane excised action. As a result:

$$\hat{I}_n = -\frac{c}{24\pi}\int dv d\bar{v}\,\sqrt{|T_{vv}|^2}\,. \tag{5.55}$$

We can evaluate this integral using the explicit form of the stress tensor quoted in (5.40). One has

$$\begin{aligned}
\hat{I}_n &= -\frac{c}{48\pi}\left(1-\frac{1}{n^2}\right)\int dv d\bar{v}\,\frac{(a_2-a_1)^2}{|v-a_1|^2\,|v-a_2|^2} \\
&= -\frac{c}{48\pi}\left(1-\frac{1}{n^2}\right)\int dv d\bar{v}\,\partial_v\,\mathcal{Q}\,\partial_{\bar{v}}\,\mathcal{Q}\,, \qquad\qquad \mathcal{Q}(v,\bar{v})\equiv\log\left|\frac{v-a_1}{v-a_2}\right|^2 \\
&= -\frac{c\,\delta}{96\pi}\left(1-\frac{1}{n^2}\right)\left[\oint_{a_1}\mathcal{Q}\partial_{|v|}\mathcal{Q}+\oint_{a_2}\mathcal{Q}\partial_{|v|}\mathcal{Q}\right] \\
&= \frac{c}{6}\left(1-\frac{1}{n^2}\right)\log\frac{|a_2-a_1|}{\delta}\,.
\end{aligned} \tag{5.56}$$

This integral has been evaluated by using the fact that $\mathcal{Q}(v,\bar{v})$ is a Green's function on the plane with sources at a_1 and a_2. Massaging the integral and integrating by parts, we find source δ-function contributions and the above boundary terms. We discard the former since the conical singularities on $\mathcal{B}_n/\mathbb{Z}_n$ also ought not be included in the cosmic-brane excised action. This leaves us with a contour integral around each branch point which we have evaluated with a UV regulator δ. Finally, from (5.1) and (5.48) we obtain on using $I_1=0$, the expected answer (5.34) of the n^{th} Rényi entropy, viz.,

$$S_{\mathcal{A}}^{(n)} = \frac{n}{n-1}\,\Big[\,\hat{I}_n - I_1\Big] = \frac{c}{6}\left(1+\frac{1}{n}\right)\log\frac{|a_2-a_1|}{\delta}\,. \tag{5.57}$$

Lorentzian on-shell action in a fundamental domain

Let us now turn to the computation of the on-shell action for the real-time geometry (5.45). The on-shell Lorentzian action we need is given by (5.21) which we rewrite here for convenience as

$$\begin{aligned} I_n &= -i\, S^L_{\rm gr}[\mathcal{M}_n] = -i\, n\, \left[S^k_{\rm gr}[\widehat{\mathcal{M}}_n] - S^b_{\rm gr}[\widehat{\mathcal{M}}_n]\right]_{\text{cosmic-brane excised}} \\ &= 2\, n\, \text{Im}\left(S^k_{\rm gr,fund}\right). \end{aligned} \tag{5.58}$$

We will as before focus on the ket part of the geometry and try to directly isolate the imaginary part of the on-shell Lorentzian action. In fact, we have already computed the various pieces hitherto in the Euclidean context and we can simply take the contributions from (5.50), (5.52), and (5.53) and continue $\{v, \bar{v}\} \to \{\tilde{x}^-, \tilde{x}^+\}$. We would now find prior to excising the cosmic-brane contribution the following integral to evaluate:

$$S^k_{\rm gr}[\widehat{\mathcal{M}}_n] = \frac{c}{24\pi} \int d\tilde{x}^-\, d\tilde{x}^+ \left[-\frac{\text{Tr}(T)}{4}\left(1 + \log \rho_*\right) + \sqrt{T_{++}\, T_{--}}\right]. \tag{5.59}$$

where the stress tensor components are given in (5.44). In writing this expression we have performed the radial integral and converted the computation of the on-shell action into an integral over the boundary directions alone. This is somewhat different from the basic philosophy outlined in [6], so let us pause a moment to record them.

The evaluation of the on-shell action with a neighbourhood of the cosmic brane excised is easiest to implement in coordinates which are adapted to the brane. In the present case the locus is a curve in three dimensions. We pick coordinates y^i tangent to the brane and a Gaussian normal chart in the normal plane (which is locally $\mathbb{R}^{1,1}$). The regulator around the brane then is a simple matter of excising a disc shaped domain in the normal plane.

However, this coordinate chart which is adapted to $\boldsymbol{\gamma}$ is not the Fefferman-Graham chart used in (5.45). This may a-priori seem surprising since the normal plane for each fixed ρ is parameterized by $\tilde{x}^{\pm}$ and the cosmic brane is located at the same coordinate positions in this Minkowski plane. This is misleading, since the range of ρ is constrained to lie within the interval $\rho \in [\rho_c, \rho_*]$ and the right-end point ρ_* is a non-trivial function of $\tilde{x}^{\pm}$ from (5.51). In our coordinates, the radial direction in the normal $\mathbb{R}^{1,1}$ plane is an admixture of the Fefferman-Graham radial coordinate ρ and a timelike combination made up from $\tilde{x}^{\pm}$. Adapting coordinates to the cosmic brane locus is in principle possible, but quite messy, since the stress tensor is a non-trivial function of $\tilde{x}^{\pm}$.[9]

Rather than attempt to convert this to the Gaussian normal chart in the neighbourhood of $\boldsymbol{\gamma}$, we will instead demonstrate a direct way to compute the on-shell action in Lorentz signature. Our starting point is the integral in (5.59) and we first excise a neighbourhood of the cosmic brane. This removes the piece $\mathrm{Tr}(T)$ which only has delta function support on $\boldsymbol{\gamma}$ owing to (5.44). Dropping this piece in the excised geometry we have

$$\begin{aligned} S^k_{\rm gr,fund} &= \frac{c}{24\pi} \int_{t<0} d\tilde{x}^- \, d\tilde{x}^+ \, \sqrt{T_{++}\, T_{--}} \\ &= \frac{c}{48\pi} \left(1 - \frac{1}{n^2}\right) (a_2 - a_1)^2 \, \mathfrak{I}(a_1, a_2) \,, \\ \mathfrak{I}(a_1, a_2) &\equiv \int_{t<0} \frac{d\tilde{x}^- \, d\tilde{x}^+}{(\tilde{x}^- - a_1)(\tilde{x}^+ - a_1)(\tilde{x}^- - a_2)(\tilde{x}^+ - a_2)} \,. \end{aligned} \tag{5.60}$$

We need to evaluate thus the integral $\mathfrak{I}$ defined above and extract an imaginary piece from it. As a warm up consider first the simpler case of a semi-infinite interval, where

[9] If the boundary stress tensor is constant, then the transformation is straightforward, and can be inferred from the BTZ solution.

$a_2 \to \infty$ and $a_1 = 0$ which will serve to exemplify the general case. We have then

$$\mathfrak{I}_{\text{half-line}} = \lim_{a_2 \to \infty} a_2^2 \, \mathfrak{I}(0, a_2) = \int_{t<0} \frac{d\tilde{x}^+ \, d\tilde{x}^-}{\tilde{x}^+ \, \tilde{x}^-} \tag{5.61}$$

which the reader will recognize bears a close resemblance to the integral we computed in section 5.2.2. We will proceed similarly here using an $i\varepsilon$ prescription to pick out the projection onto the vacuum state of the CFT. It will be convenient to introduce an IR cut-off L which will enter the answer for the semi-infinite interval. We integrate up on M^{k} up to a UV cut-off restricting $|\tilde{x}^+| > \delta$ and obtain

$$\mathfrak{I}_{\text{half-line}} = \lim_{\delta \to 0} \lim_{L \to \infty} \left[\mathfrak{I}_{\text{left}} + \mathfrak{I}_{\text{strip}} + \mathfrak{I}_{\text{right}} \right]$$

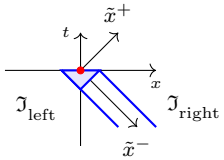

$$\begin{aligned}
\mathfrak{I}_{\text{left}} &= \int_{-L}^{-\delta} \frac{d\tilde{x}^+}{\tilde{x}^+} \int_{\tilde{x}^+}^{L} \frac{d\tilde{x}^-}{\tilde{x}^-} = \left[-\log \frac{L}{\delta} \right] \left[-i\pi + \mathcal{P} \int_{L}^{\tilde{x}^+} \frac{d\tilde{x}-}{\tilde{x}^-} \right] \\
\mathfrak{I}_{\text{right}} &= \int_{\delta}^{L} \frac{d\tilde{x}^+}{\tilde{x}^+} \int_{\tilde{x}^+}^{L} \frac{d\tilde{x}^-}{\tilde{x}^-} = \int_{\delta}^{L} \frac{d\tilde{x}^+}{\tilde{x}^+} \log \left(\frac{\tilde{x}^+}{L} \right) \\
\mathfrak{I}_{\text{strip}} &= \int_{\delta}^{L} \frac{d\tilde{x}^-}{\tilde{x}^-} \int_{-\delta}^{\delta} \frac{d\tilde{x}^+}{\tilde{x}^+} = \left[\log \frac{L}{\delta} \right] \left[i\pi + \mathcal{P} \int_{-\delta}^{\delta} \frac{d\tilde{x}+}{\tilde{x}^+} \right]
\end{aligned} \tag{5.62}$$

where we have used (5.28) and as before analytically continued $\tilde{x}^- \to \tilde{x}^- + i\epsilon$ while $\tilde{x}^+ \to \tilde{x}^+ - i\epsilon$. We see then that the imaginary parts as before add from the first and third integrals which leads to the final result

$$I_n\big|_{\text{half-line}} = 2\, n \, \text{Im}(S^k_{\text{gr,fund}}) = \frac{c}{48\pi} \left(1 - \frac{1}{n^2} \right) 4\pi \, n \log \frac{L}{\delta} = \frac{c}{12} \left(n - \frac{1}{n} \right) \log \frac{L}{\delta} \tag{5.63}$$

which one can check leads to the correct Rényi entropy (5.34).[10]

[10]Note that the result appears to be missing a factor of 2, but this is consistent since in the limit of a semi-infinite interval we only pick up the contribution from one branch point. We evaluate the integral

Armed with this understanding it is now clear how to evaluate the integral $\mathfrak{I}(a_1, a_2)$. We again introduce UV and IR regulators δ and L, respectively, and break up the integration range $t < 0$ into five domains

$$\mathfrak{D} = \mathfrak{D}_1 \cup \mathfrak{D}_2 \cup \mathfrak{D}_3 \cup \mathfrak{D}_{\text{strips}} \,, \tag{5.64}$$

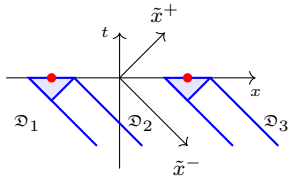

Three of the domains are analogous to the regions to the left and right of the fixed point in the half-line case considered above. They are demarcated by constant $\tilde{x}^+$ lines: $\mathfrak{D}_1 : \tilde{x}^+ \in (-L, a_1 - \delta)$, $\mathfrak{D}_2 : \tilde{x}^+ \in (a_1 + \delta, a_2 - \delta)$ and $\mathfrak{D}_3 : \tilde{x}^+ \in (a_2 + \delta, L)$ and $\tilde{x}^-$ runs up from $\tilde{x}^+$ to some IR cut-off value L. We also now have two strips $\mathfrak{D}_{\text{strips}}$ once we excise the triangular domains around the fixed points at a_1 and a_2. We will as before consider the contributions from each region separately. Writing $\mathfrak{I} = \mathfrak{I}_1 + \mathfrak{I}_2 + \mathfrak{I}_3 + \mathfrak{I}_{\text{strips}}$ we have

$$\begin{aligned}
\mathfrak{I}_1 &= \int_{-L}^{a_1-\delta} \frac{d\tilde{x}^+}{(\tilde{x}^+ - a_1)(\tilde{x}^+ - a_2)} \int_{\tilde{x}^+}^{L} \frac{d\tilde{x}^-}{(\tilde{x}^- - a_1)(\tilde{x}^- - a_2)} \\
&= \frac{1}{|a_2 - a_1|} \int_{-L}^{a_1-\delta} \frac{d\tilde{x}^+}{(\tilde{x}^+ - a_1)(\tilde{x}^+ - a_2)} \left[-\mathcal{P} \int_{\tilde{x}^+ - a_1}^{L-a_1} \frac{d\tilde{x}_1^-}{\tilde{x}_1^-} + \mathcal{P} \int_{\tilde{x}^+ - a_2}^{L-a_2} \frac{d\tilde{x}_2^-}{\tilde{x}_2^-} \right]
\end{aligned} \tag{5.65}$$

where we have taken partial fractions introducing $\tilde{x}_i^- = \tilde{x}^- - a_i$ and used the principal value prescription. This term has no imaginary part as should be clear from the fact that we are in the left homology wedge in $\mathfrak{D}_1$. Similarly we can evaluate the contribution from $\mathfrak{D}_3$ to be purely real, for

$$\begin{aligned}
\mathfrak{I}_3 &= \int_{a_2+\delta}^{L} \frac{d\tilde{x}^+}{(\tilde{x}^+ - a_1)(\tilde{x}^+ - a_2)} \int_{\tilde{x}^+}^{L} \frac{d\tilde{x}^-}{(\tilde{x}^- - a_1)(\tilde{x}^- - a_2)} \\
&= \frac{1}{|a_2 - a_1|} \int_{a_2+\delta}^{L} \frac{d\tilde{x}^+}{(\tilde{x}^+ - a_1)(\tilde{x}^+ - a_2)} \log\left(\frac{\tilde{x}^+ - a_1}{\tilde{x}^+ - a_2} \right)
\end{aligned} \tag{5.66}$$

a different way in appendix D.1 to double check this factor.

where we have dropped terms that vanish as $L \to \infty$. We do pick up imaginary parts from the region $\mathfrak{D}_2$ and the strips. The region $\mathfrak{D}_2$ picks out the contribution from the right branch point at a_2 as

$$\begin{aligned}\mathfrak{I}_2 &= \int_{a_1+\delta}^{a_2-\delta} \frac{d\tilde{x}^+}{(\tilde{x}^+ - a_1)(\tilde{x}^+ - a_2)} \int_{\tilde{x}^+}^{L} \frac{d\tilde{x}^-}{(\tilde{x}^- - a_1)(\tilde{x}^- - a_2)} \\ &= \frac{2\pi i}{|a_2 - a_1|^2} \log \frac{|a_2 - a_1|}{\delta} \\ &\quad + \frac{1}{|a_2 - a_1|} \int_{a_1+\delta}^{a_2-\delta} \frac{d\tilde{x}^+}{(\tilde{x}^+ - a_1)(\tilde{x}^+ - a_2)} \left[\log \left(\frac{\tilde{x}^+ - a_1}{L - a_1} \right) + \mathcal{P} \int_{\tilde{x}^+ - a_2}^{L-a_2} \frac{d\tilde{x}_2^-}{\tilde{x}_2^-} \right]\end{aligned} \tag{5.67}$$

The final contribution comes from the strips which lie a distance $a_i + \delta$ around $\tilde{x}^- = 0$. These do give non-vanishing imaginary contributions as one of the strips captures the left branch point. To wit,

$$\begin{aligned}\mathfrak{I}_{\text{strips}} &= \int_{a_1-\delta}^{a_1+\delta} \frac{d\tilde{x}^+}{(\tilde{x}^+ - a_1)(\tilde{x}^+ - a_2)} \int_{a_1+\delta}^{L} \frac{d\tilde{x}^-}{(\tilde{x}^- - a_1)(\tilde{x}^- - a_2)} \\ &\quad + \int_{a_2-\delta}^{a_2+\delta} \frac{d\tilde{x}^+}{(\tilde{x}^+ - a_1)(\tilde{x}^+ - a_2)} \int_{a_2+\delta}^{L} \frac{d\tilde{x}^-}{(\tilde{x}^- - a_1)(\tilde{x}^- - a_2)} \\ &= \frac{2\pi i}{|a_2 - a_1|^2} \log \frac{|a_2 - a_1|}{\delta} \\ &\quad - \frac{1}{|a_2 - a_1|} \mathcal{P} \int_{-\delta}^{\delta} \frac{d\tilde{x}^+}{\tilde{x}^+} \left[\mathcal{P} \int_{a_1}^{a_2} \frac{d\tilde{x}^-}{\tilde{x}^- - a_2} - \log \frac{|a_2 - a_1|}{\delta} \right]\end{aligned} \tag{5.68}$$

Putting together all the contributions we find

$$\text{Im}(S^k_{\text{gr,fund}}) = 4\pi \log \frac{|a_2 - a_1|}{\delta}, \tag{5.69}$$

which as one can readily verify leads to the expected result for the Rényi entropy (5.34). At various points above we have taken the interval to lie on the $t = 0$ slice in $\mathbb{R}^{1,1}$ for illustrative purposes. This is however unnecessary, and the result holds for any boosted

slice, owing to the boost invariance of the vacuum state of the CFT.

5.4 Rényi entropies in 2d CFTs: Disjoint intervals

The examples we have discussed thus far comprise of situations where the entropies are computed at a moment of time symmetry. While we see that even in these examples the real-time computations require a careful analysis, we now turn to an example where time reflection symmetry is explicitly broken (in a controllable manner). We explore the Rényi entropy for a 2d CFT in its vacuum state on the plane, with the region $\mathcal{A}$ taken to be the disjoint union of N intervals.

In the Euclidean set-up the computation of the n^{th} Rényi entropy requires us to compute the CFT partition function on a n-sheeted branch cover of the plane with $2N$ branch points. This is a genus $(n-1)(N-1)$ surface, albeit one at a special point in moduli space since the moduli are specified by $2N-3$ parameters (using conformal invariance to fix 3 points). Unfortunately, one does not have readily available partition functions for generic 2d CFTs on higher genus Riemann surfaces.

Nevertheless one can make progress in certain circumstances. For instance, the problem was first analyzed using replica methods in CFT in [175] for free 2d CFTs for which the higher genus partition functions are available. One can likewise study large c holographic CFTs. In fact, the first non-trivial computations of holographic Rényi entropies were undertaken in [123], who analyzed the $N=2$ example for large c CFTs and explicitly demonstrated the holographic entanglement entropy phase transition. Subsequently, [126] analyzed the problem in detail in the gravitational context, constructing the dual gravitational solutions as handlebody geometries, and evaluated the on-shell action to extract the answer. A complementary CFT analysis using properties of Virasoro vacuum blocks was also concurrently given in [125]. We will adapt the discussion of [126] to the

real-time setting after reviewing the ingredients of Schottky uniformization that enter the computation in Euclidean signature. We will keep our discussion general in the main text, though for ease of presentation we will use the 2nd Rényi entropy $n = 2$ for $N = 2$ intervals to illustrate the general arguments.[11]

5.4.1 Rényi from Schottky uniformization

We give a quick overview of the Schottky uniformization exploited in [126] to compute the holographic Rényi entropies for disjoint intervals. For the vacuum entanglement entropy of N intervals $\mathcal{A} = \cup_{i=1}^{N} (a_{2i-1}, a_{2i})$, we must compute the partition function on the n-fold cover $\mathcal{B}_{n,N}$ branched over the N intervals. The manifold $\mathcal{B}_{n,N}$ is a compact Riemann surface of genus $(N-1)(n-1)$ with complex structure

$$z^n = \prod_{i=1}^{N} \left(\frac{v - a_{2i-1}}{v - a_{2i}} \right). \tag{5.70}$$

Following [126] we will assume that the dominant bulk saddles are replica $\mathbb{Z}_n$ symmetric handlebodies.

A Riemann surface of genus g can be constructed by starting with the Riemann sphere $\mathbb{C}$ and quotienting it by a Schottky group $\Gamma \subset \mathrm{PSL}(2, \mathbb{C})$, which is a discrete subgroup freely generated by g loxodromic elements, constrained such that the closure of the set of fixed points Δ of its action is not the entirety of $\mathbb{C}$. The Riemann surface is $\widetilde{\mathbb{C}}/\Gamma$ with $\widetilde{\mathbb{C}} = \mathbb{C} - \Delta$. Operationally, one picks $2g$ non-intersecting circles $\{\mathfrak{C}_i, \tilde{\mathfrak{C}}_i\}$, lets the generators γ_i of Γ act by mapping the interior of the disc bounded by $\mathfrak{C}_i$ to the exterior of the disc bounded by $\tilde{\mathfrak{C}}_i$, along with $\gamma_i(\mathfrak{C}_i) = \tilde{\mathfrak{C}}_i$. The quotient operation then cuts

[11] Details of the geometry for $N = n = 2$ are given in appendix D.3. In appendix D.4 we explicitly evaluate the on-shell action in Euclidean signature for this case. In the bulk of our discussion we will sidestep the evaluation of the Rényi entropies, concentrating on obtaining its variation with respect to one of the endpoints.

out the $2g$ discs to the interior of these circles and identifies the circles themselves, thus creating the handles.

This construction on the Riemann sphere extends to the bulk of Euclidean AdS_3 where the $PSL(2,\mathbb{C})$ map acts as on the coordinates $(\xi, y, \bar{y})$ as

$$y \to \frac{(a\,y+b)(\bar{c}\,\bar{y}+\ d)+a\bar{c}\,\xi^2}{|c\,y+d|^2+|c|^2\,\xi^2}, \qquad \xi \to \frac{\xi}{|c\,y+d|^2+|c|^2\,\xi^2}, \qquad \begin{pmatrix} a & b \\ c & d \end{pmatrix} \in \mathrm{PSL}(2,\mathbb{C})\,. \tag{5.71}$$

The quotient acts smoothly in the bulk (because Γ has loxodromic elements). However, given a choice of Γ which determines the Schottky uniformization of $\mathcal{B}_{n,N}$ there may be multiple bulk geometries. These are handlebodies where g commuting cycles of $\mathcal{B}_{n,N}$ smoothly pinch off in the bulk.

To determine all the bulk handlebodies that respect the replica $\mathbb{Z}_n$ symmetry, we need to decide which cycles are contractible. Around any single branch point, which is a localized source of stress-energy (see e.g., (5.40)), we know the inverse map $y = \pi^{-1}(v)$ of the quotient $\pi : \mathbb{C} \mapsto \widetilde{\mathbb{C}}/\Gamma$, has local solutions $(v-a_i)^{\frac{1}{2}\pm\frac{1}{2n}}$, where we coordinatize $\mathbb{C}$ with $\{v, \bar{v}\}$ as before. However, around a loop $\mathfrak{C}$ that contains two or more branch points one picks up a monodromy $M(\mathfrak{C}) \in \mathrm{PSL}(2,\mathbb{C})$.

For example with $N = 2$, the region $\mathcal{A} = \mathcal{A}_1 \cup \mathcal{A}_2 \equiv (a_1, a_2) \cup (a_3, a_4)$, the boundary manifold for $n = 2$ is a genus 1 Riemann surface, a torus. There are two distinct bulk geometries that should be considered as the dual handlebody – we either let the a-cycle of the torus shrink smoothly, or let the b-cycle shrink. The two choices can equivalently be characterized by the choice of cycles around which we impose trivial monodromy as depicted in fig. 5.6.

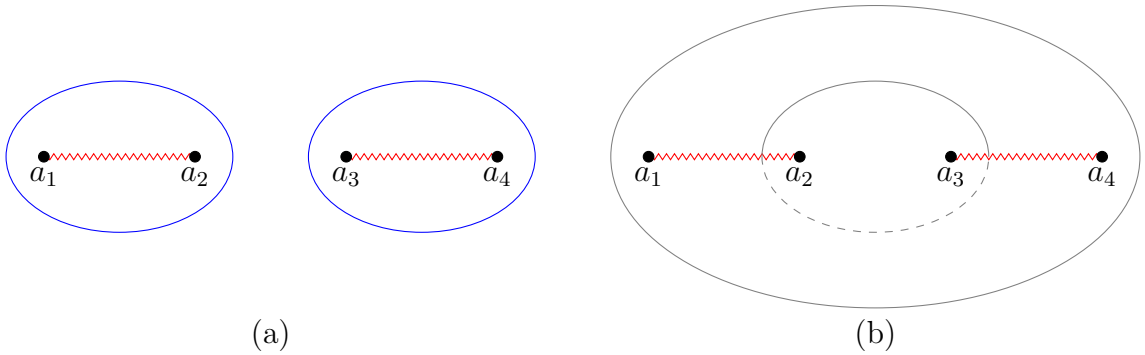

Figure 5.6: The choices of cycles around which we can impose trivial monodromy to construct the dual handlebody. (a) trivial monodromy around the two cycles that circle the branch cut, denoted by $\mathfrak{C}_d$, which corresponds to the disconnected RT surface in the limit $n \to 1$; (b) trivial monodromy around the cycle that circles around both branch cuts and the cycle that passes through the branch cuts and laces through all the n sheets, denoted by $\mathfrak{C}_c$, which corresponds to the connected RT surface in the limit $n \to 1$.

To solve the monodromy problem, we realize that the map $y(v)$ satisfies

$$\{y(v)), v\} = T(v)\,, \qquad T_{vv}(v) = \sum_{i=1}^{2N} \left[\frac{\Delta_n}{(v-a_i)^2} + \frac{p_i}{v-a_i} \right], \tag{5.72}$$

where $T(v)$ is the source of the stress-energy on a single sheet arising from the branch structure and Δ_n is the conformal weight of the defect

$$\Delta_n \equiv \frac{1}{2}\left(1 - \frac{1}{n^2}\right) \tag{5.73}$$

This stress-energy is yet to be fully determined, parameterized as it is by a set of accessory parameters, p_i, which carry information about the covering space topology. Once we solve for these parameters we should have the necessary information to determine the geometry.

One proceeds by solving an auxiliary homogeneous linear differential equation for a function $\psi(v)$, from whose linearly independent solutions, $\psi_{1,2}(v)$, one can recover $y(v)$,

viz.,

$$\psi''(v) + \frac{1}{2}\, T_{vv}(v)\, \psi(v) = 0\,, \qquad y(v) = \frac{\psi_1(v)}{\psi_2(v)}\,. \tag{5.74}$$

We have $2N$ accessory parameters p_i. To fix them, consider one sheet of the Riemann surface which is a copy of a sphere with $2N$ punctures. Let $\mathfrak{C} = \{\mathcal{C}_a, a = 1, \ldots N\}$ be the set of cycles which contain an even number of punctures. The accessory parameters are fixed by demanding that the solution has trivial monodromy around $v = \infty$ and around the remaining $N - 1$ independent cycles $\mathcal{C}_a$. The absence of monodromy around $v = \infty$ gives three relations:

$$\sum_{i=1}^{2N} p_i = 0\,, \qquad \sum_{i=1}^{2N} p_i a_i = -2N\,\Delta_n\,, \qquad \sum_{i=1}^{2N} p_i a_i^2 = -2\Delta_n \sum_{i=1}^{2N} a_i. \tag{5.75}$$

By replica symmetry one has actually specified the $(n-1)(N-1)$ cycles on $\mathcal{B}_{n,N}$ which have trivial monodromy. Demanding these cycles be contractible in the bulk we have completed the specification of a smooth handlebody.

Note that once we have specified the set of monodromies we fix the accessory parameters, since this suffices to characterize the covering space Riemann surface topology. This implies that $T(v)$ in (5.72) is now completely determined. This will be sufficient for us to understand the computation of the dual geometry, and in particular the on-shell action.

While the accessory parameters were introduced here to solve the uniformization problem, physically they specify the stress-energy source on a single sheet necessary to build up the Riemann surface. As a result, it should be no surprise to learn that they directly determine the on-shell action of gravity, and thus the Rényi entropies. For a given collection of cycles $\mathfrak{C}$ which are contractible one has the result (5.76) obtained in

[126] (using results of [176])

$$S^{(n)} = \min_{\mathfrak{C}}\{S^{(n)}_{\mathfrak{C}}\}\,, \qquad \frac{\partial}{\partial a_i} S^{(n)}_{\mathfrak{C}} = -\frac{c\,n}{6\,(n-1)}\,p^{\mathfrak{C}}_i\,. \tag{5.76}$$

where $\mathfrak{C}$ represents the different sets of choices of cycles which can be made contractible. We present the details for $N = n = 2$ in appendix D.3 where the branched cover is a torus.

We will broadly content ourselves with obtaining the variation of the Rényi entropy with respect to the endpoint, viz., the second expression in (5.76). There is one special case where $S^{(n)}_{\mathfrak{C}}$ itself is directly computable, which is the second Rényi entropy for two disjoint intervals $N = n = 2$. In appendix D.4 we evaluate the on-shell action of gravity (for the connected phase) to obtain $S^{(2)}$ directly, cf., (D.45). We will return to this issue in section 5.4.2.

5.4.2 The action from a single fundamental domain

Let us assume that one has solved the monodromy problem and thus determined the accessory parameters by picking a set of contractible cycles. Furthermore, recall that we can use the Fefferman-Graham expansion quite effectively to compute the bulk geometry, cf., (5.39) and (5.45) for the Euclidean and Lorentzian signature metrics, respectively. We also know that the computation of the on-shell action in these coordinates is straightforward and one obtains the final results quoted in (5.54) and (5.59), respectively.

Inspired by their simplicity we can address the problem as follows. Focus for the present on the Euclidean geometries where in the v-plane corresponding to a single sheet of the Riemann surface, we have a set of branch points, which are a source of stress-energy. The stress tensor is parameterized in terms of the accessory parameters p_i. Once we solve the monodromy problem and fix these p_i we have determined on a single sheet

the local sources of energy-momentum that we need to turn on to construct the Riemann surface. With this knowledge we can immediately compute the on-shell action using (5.54) in Euclidean signature.

As a quick check, let us look back at the single-interval case discussed in the main text. We have two branch points, and a single choice of cycle $\mathfrak{C}_1$ which encircles both branch points. It is trivial to check that $p_1 = -p_2 = 2\,\frac{\Delta_n}{a_2 - a_1}$ are fixed uniquely, and thus we recover $T(v)$ quoted in (5.40) which we used to compute the on-shell action in (5.56). In fact we will borrow extensively from the one-interval analysis for general n, N below.

The Euclidean computation

We start with the assumption that we have been given the stress tensor on a single fundamental domain (5.72). This stress tensor is localized on the branch points and excising the sources at these loci, we have to evaluate (5.55), i.e.,

$$\hat{I}_n = -\frac{c}{24\pi} \int_{\mathcal{R}_\epsilon} dv d\bar{v}\, \sqrt{T_{vv}\, T_{\bar{v}\bar{v}}}\,, \tag{5.77}$$

where $\mathcal{R}_\epsilon$ is a domain of the complex v-plane with infinitesimal discs $\mathcal{D}_i^\epsilon$ of size ϵ around each of the branch points $v = a_i$ excised. We will attempt to evaluate not this integral, but rather its derivative with respect to the branch point location, viz.,

$$\frac{\partial}{\partial a_i}\hat{I}_n = -\frac{c}{48\pi} \int_{\mathcal{R}_\epsilon} dv d\bar{v}\, \left[\sqrt{\frac{T_{\bar{v}\bar{v}}}{T_{vv}}}\,\frac{\partial T_{vv}}{\partial a_i} + \sqrt{\frac{T_{vv}}{T_{\bar{v}\bar{v}}}}\,\frac{\partial T_{\bar{v}\bar{v}}}{\partial a_i}\right] + \text{boundary term}\,, \tag{5.78}$$

where the boundary term arises from the variation of the discs $\mathcal{D}_i^\epsilon$ about $v = a_i$.

To evaluate the variation of $\hat{I}_n$ with respect to the location of the branch points we are going to employ a trick which will reduce the calculation as in the single-interval case to the evaluation of contour integrals on the boundaries of the discs about each branch

point, $\mathcal{C}_i^\epsilon = \partial\mathcal{D}_i^\epsilon$. To facilitate this analysis let us first introduce a function $\mathcal{T}$ which satisfies:

$$\partial_v \mathcal{T}(v,\bar{v}) = \sqrt{T_{vv}}\,, \qquad \partial_{\bar{v}} \mathcal{T}(v,\bar{v}) = \sqrt{T_{\bar{v}\bar{v}}}\,. \tag{5.79}$$

We can formally write it as a contour integral

$$\mathcal{T}(v,\bar{v}) \equiv \int_{\mathcal{C}} \sqrt{T_{vv}}\, dv + \int_{\mathcal{C}} \sqrt{T_{\bar{v}\bar{v}}}\, d\bar{v} = \mathfrak{t}(v) + \bar{\mathfrak{t}}(\bar{v})\,. \tag{5.80}$$

To define $\mathcal{T}$ completely we need to specify the integration contour $\mathcal{C}$. It will however transpire that we will only care about the fact that this contour gets close to the branch points at a_i.

By a local analysis in the neighbourhood of each branch point we may deduce that

$$\partial_v \mathcal{T} = s_i \left[\frac{\sqrt{\Delta_n}}{v - a_i} + \frac{p_i}{2\sqrt{\Delta_n}} + \mathcal{O}(v - a_i) \right], \tag{5.81}$$

and similarly for $\partial_{\bar{v}}\mathcal{T}$. Here $s_i = \pm 1$ is a sign, $s_i^2 = 1$, which will drop out in our final answer. Integrating these up we have the local behaviour near $v = a_i$

$$\mathcal{T}(v,\bar{v}) = s_i \left[\sqrt{\Delta_n} \log|v - a_i|^2 - C_i(\{a_j\}) + \frac{p_i}{2\sqrt{\Delta_n}}(v + \bar{v} - 2\,a_i) + \mathcal{O}\big(|v - a_i|^2\big) \right] \tag{5.82}$$

with undetermined constants $C_i(\{a_j\})$.

While the local analysis thus gives an estimate for the function $\mathcal{T}$, the function is as yet undetermined owing to the information hidden in the constants C_i which as indicated above depend on the locations of the branch points. It is this dependence that makes the explicit evaluation of $\hat{I}_n$ quite tricky to obtain (though see appendix D.4 for the $N = n = 2$ case). We will see that these constants will drop out in our evaluation of the derivatives $\frac{\partial}{\partial a_i}\hat{I}_n$. Given the estimate (5.82), we may immediately compute the

derivatives with respect to the branch point locations a_j obtaining

$$\frac{\partial \mathcal{T}}{\partial a_j} = -s_i \left[\sqrt{\Delta_n} \left(\frac{1}{v - a_i} + \frac{1}{\bar{v} - a_i} \right) + \frac{p_i}{\sqrt{\Delta_n}} \right] \delta_{ij} - s_i \ \frac{\partial C_i}{\partial a_j} + \mathcal{O}(|v - a_i|). \tag{5.83}$$

Note that the derivative of the accessory parameter with respect to the branch point has been ignored as it is of order $v - a_i$.

We will now argue that these local estimates will suffice to compute the variation of the on-shell action with respect to the branch points. One has under the variation of a branch point, a bulk and a boundary contribution that we will study independently, and write (cf., appendix D.5.2)

$$\begin{aligned} \frac{\partial \hat{I}_n}{\partial a_i} &= -\frac{c}{24\pi} \left[\mathcal{I}_i^{\text{bulk}} + \mathcal{I}_i^{\text{bdy}} \right] \\ \mathcal{I}_i^{\text{bulk}} &\equiv \int_{\mathcal{R}_\epsilon} dv \, d\bar{v} \frac{\partial}{\partial a_i} \left(\frac{\partial \mathcal{T}}{\partial v} \frac{\partial \mathcal{T}}{\partial \bar{v}} \right) \\ \mathcal{I}_i^{\text{bdy}} &\equiv -2i \oint_{\mathcal{C}_i^\epsilon} dv \frac{\partial \mathcal{T}}{\partial v} \frac{\partial \mathcal{T}}{\partial \bar{v}} \, . \end{aligned} \tag{5.84}$$

Consider first the bulk integral. Using the fact that by definition $\mathcal{T}$ is a sum of a holomorphic and an anti-holomorphic piece (5.80), we may rearrange the derivatives in the bulk integral, write it as an integral of a total divergence, and convert it to a boundary integral over the circles $\mathcal{C}_i^\epsilon$:

$$\begin{aligned} \mathcal{I}_i^{\text{bulk}} &= \int_{\mathcal{R}_\epsilon} dv \, d\bar{v} \left[\frac{\partial}{\partial v} \left(\frac{\partial \mathcal{T}}{\partial a_i} \frac{\partial \mathcal{T}}{\partial \bar{v}} \right) + \frac{\partial}{\partial \bar{v}} \left(\frac{\partial \mathcal{T}}{\partial a_i} \frac{\partial \mathcal{T}}{\partial v} \right) \right] \\ &= i \sum_{j=1}^{2N} \oint_{\mathcal{C}_j^\epsilon} \left[\frac{\partial \mathcal{T}}{\partial a_i} \frac{\partial \mathcal{T}}{\partial \bar{v}} \, d\bar{v} - \frac{\partial \mathcal{T}}{\partial a_i} \frac{\partial \mathcal{T}}{\partial v} \, dv \right] \end{aligned} \tag{5.85}$$

We may now deduce using (5.82) and (5.83) that

$$\oint_{\mathcal{C}_j^\epsilon} \frac{\partial \mathcal{T}}{\partial a_i}\frac{\partial \mathcal{T}}{\partial v}\,dv = -s_j^2 \oint_{\mathcal{C}_j^\epsilon} \left[\left(\frac{\sqrt{\Delta_n}}{v-a_i}+\frac{\sqrt{\Delta_n}}{\bar{v}-a_i}+\frac{p_i}{\sqrt{\Delta_n}}\right)\delta_{ij}+\ \frac{\partial C_j}{\partial a_i}+\cdots\right] \left[\frac{\sqrt{\Delta_n}}{v-a_j}+\frac{p_j}{2\sqrt{\Delta_n}}+\cdots\right] \tag{5.86}$$
$$= -2\pi i\,\left(\frac{3}{2}\,p_i\,\delta_{ij}+\sqrt{\Delta_n}\,\frac{\partial C_j}{\partial a_i}\right).$$

Putting together the complex conjugate contribution yields

$$\mathcal{I}_i^{\text{bulk}} = -4\pi\left(\frac{3}{2}\,p_i+\sqrt{\Delta_n}\sum_{j=1}^{2N}\frac{\partial C_j}{\partial a_i}\right). \tag{5.87}$$

The boundary term may be evaluated directly to give

$$\mathcal{I}_i^{\text{bdy}} = -2i\oint_{\mathcal{C}_i^\epsilon} dv\left[\frac{\sqrt{\Delta_n}}{v-a_i}+\frac{p_j}{2\sqrt{\Delta_n}}+\cdots\right]\left[\frac{\sqrt{\Delta_n}}{\bar{v}-a_i}+\frac{p_j}{2\sqrt{\Delta_n}}+\cdots\right] = 2\pi\,p_i. \tag{5.88}$$

Hence we have

$$\frac{\partial \hat{I}_n}{\partial a_i} = \frac{c}{6}\left(p_i+\sqrt{\Delta_n}\sum_{j=1}^{2N}\frac{\partial C_j}{\partial a_i}\right). \tag{5.89}$$

To complete the argument we need to deduce the value of $\sum_{j=1}^{2N}\frac{\partial C_j}{\partial a_i}$, which we may do by judiciously combining $\mathfrak{t}$ and $\mathcal{T}$. We use the fact that the product $\frac{\partial \mathfrak{t}}{\partial a_i}\,\partial_v \mathcal{T}$ dies off

as v^{-2} at large v to deduce

$$\begin{aligned} 0 &= \oint_{|v|=\Lambda} \frac{\partial \mathfrak{t}}{\partial a_i}\, \partial_v \mathcal{T} \\ &= -\sum_j \oint_{\mathcal{C}_j^\epsilon} \left[\left(\frac{\sqrt{\Delta_n}}{v-a_j} + \frac{p_j}{2\sqrt{\Delta_n}} \right) \delta_{ij} + \frac{1}{2}\, \frac{\partial C_j}{\partial a_i} \right] \left[\frac{\sqrt{\Delta_n}}{v-a_j} + \frac{p_j}{2\sqrt{\Delta_n}} \right] \\ &= -2\pi i \left(p_i + \frac{\sqrt{\Delta_n}}{2} \sum_{j=1}^{2N} \frac{\partial C_j}{\partial a_i} \right) \\ &\implies \sqrt{\Delta_n} \sum_{j=1}^{2N} \frac{\partial C_j}{\partial a_i} = -2\, p_i \,. \end{aligned} \tag{5.90}$$

The asymptotic behaviour thus constrains the derivatives of the constants C_j allowing us to evaluate the quantity we want without detailed knowledge of these constants themselves. Consequently, we have as our final result:

$$\frac{\partial \hat{I}_n}{\partial a_i} = -\frac{c}{6}\, p_i \tag{5.91}$$

This indeed reproduces the result quoted in (5.76) for

$$\frac{\partial}{\partial a_i}\, S^{(n)} = \frac{n}{n-1}\, \frac{\partial}{\partial a_i} [\hat{I}_n - I_1] = -\frac{n}{6(n-1)}\, c\, p_i \,. \tag{5.92}$$

The Lorentzian computation

One reason for our going over the Euclidean computation in some detail was to simplify the ingredients to obtain the result directly in Lorentz signature. We will continue with the computation in a single fundamental domain, and exploit the Fefferman-Graham form of the metric (5.45) and distill the computation of the action as in the one-interval case to evaluating an integral of the form (5.59). In making these observations we are assuming that the form of the boundary stress tensor on a single fundamental domain is

known, i.e., one has solved the corresponding monodromy problem. Note that the latter is strictly a non-gravitational computation and thus can be carried out in Euclidean signature, and the result used to set-up the boundary conditions for our Lorentzian gravitational analysis.

In the process of deriving (5.59) we have integrated over the bulk radial coordinate and thus have a purely boundary integral to evaluate. As explained earlier in section 5.3.3 this method is conceptually different from the way we set-up the computation of the action in [6] where we adapted coordinates to the cosmic-brane in the bulk. While that analysis makes it easier to see where the imaginary part of the Lorentzian action arises from (viz., from the normal bundle to the splitting surface), we found the chart adapted to the cosmic brane hard to relate to the coordinates induced by the Schottky construction. All told the final result for the stress tensor is a function of the location of the end-points of our regions a_i and the stress tensor is parameterized by both a_i and the accessory parameters $p_j(a_i)$. The contribution from the trace of the stress tensor in (5.59) is delta-function localized at the entangling surfaces (i.e., at $\tilde{x}^+ = \tilde{x}^- = a_i$ if the intervals are all at $t = 0$) and should be dropped in the computation of the cosmic-brane excised action. We are then left with evaluating

$$S^k_{\rm gr,fund} = \frac{c}{24\pi} \int_{\mathcal{R}} d\tilde{x}^- \, d\tilde{x}^+ \, \sqrt{T_{++}\, T_{--}} \tag{5.93}$$

with

$$\begin{aligned} T_{--}(\tilde{x}^-) &= \sum_{i=1}^{2N} \left[\frac{\Delta_n}{(\tilde{x}^- - a_i)^2} + \frac{p_i(a_j)}{\tilde{x}^- - a_i} \right], \\ T_{++}(\tilde{x}^+) &= \sum_{i=1}^{2N} \left[\frac{\Delta_n}{(\tilde{x}^+ - a_i)^2} + \frac{p_i(a_j)}{\tilde{x}^+ - a_i} \right]. \end{aligned} \tag{5.94}$$

Once again we refrain from evaluating (5.93) but will take inspiration from the Euclidean

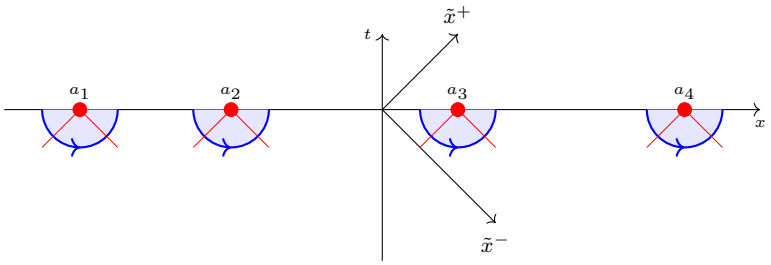

Figure 5.7: The domain of integration $\mathcal{R}$ for (5.95) is the lower half space $t < 0$ with half-discs $\mathcal{U}_i^\delta$ around each a_i removed. The imaginary contributions to $\frac{\partial}{\partial a_i}\,\mathrm{Im}(S^k_{\mathrm{gr,fund}})$ arise from the causal past of a_i.

computation and evaluate its variation of its imaginary part with respect to a_i, i.e.,

$$\frac{\partial}{\partial a_i}\,\mathrm{Im}(S^k_{\mathrm{gr,fund}}) = \frac{c}{24\pi}\,\mathrm{Im}\left(\frac{\partial}{\partial a_i}\int_{\mathcal{R}} d\tilde{x}^-\,d\tilde{x}^+\,\sqrt{T_{++}\,T_{--}}\right) \tag{5.95}$$

The region $\mathcal{R}$ is a part of the space with $t < 0$ with neighbourhoods $\mathcal{U}_i^\epsilon$ around each a_i excised.

Even before we set out to compute (5.95) let us convince ourselves that the general arguments of [6] suffice to give us the desired result. To infer this let us look back to the Euclidean computation described in section 5.4.2 and note that the final result (5.91) indicates that the variation of the stress tensor integral, $\frac{\partial}{\partial a_i}\int dv d\bar{v}\sqrt{T_{vv}\,T_{\bar{v}\bar{v}}}$, evaluates simply to $4\pi\,p_i$. We view this result as saying that the local contribution arises from the Euler character which changes because of the source of energy-momentum tensor at the branch points.

To motivate this interpretation we recall again that we have carried out the integral over the radial coordinate and are left with an integral along the boundary directions to evaluate in (5.77). On the contrary, [6] used a Gaussian normal chart adapted to the splitting surface to argue for the use of the complex Gauss-Bonnet theorem for the bulk Einstein-Hilbert action (supplemented by boundary terms). Continuing to carry out the integration as we have done, when we consider the variation of the bulk action

with respect to the parameter a_i we isolate the section of the splitting surface that is anchored at a_i on the boundary.

This can be understood as follows: variation with respect to a_i is a pure boundary term from the bulk perspective since one is evaluating the change of the on-shell action with respect to modified boundary conditions. Even if we had carried out the computation using the Gauss-Bonnet theorem adapting coordinates to the splitting surface, we would have only picked up the contribution from the vicinity of the boundary – there would have been no bulk integral to compute. The essential upshot of the Euclidean calculation is that the net variation is localized in the vicinity of the branch point at a_i. The simplicity of the result suggests a natural interpretation based on the above: there is a local contribution to the Euler character set by p_i.

Given this interpretation, we can deduce that one indeed obtains the expected result for $S^k_{\text{gr,fund}}$, viz.,

$$\frac{24\pi}{c}\,\frac{\partial}{\partial a_i}\,\text{Im}(S^k_{\text{gr,fund}}) = -2\pi\, p_i\,, \tag{5.96}$$

by invoking the complex version of Gauss-Bonnet theorem. Let us see this in a bit more detail. An imaginary contribution to (5.93) can arise because of the singularities at $\tilde{x}^+ = \tilde{x}^- = a_i$ which extend into the bulk along the splitting surface. The precise value of this imaginary part depends on the terms in the metric involving the accessory parameters p_i. These, by themselves, are hard to isolate in the on-shell action directly (see below). However, they can be straightforwardly extracted by considering the variation with respect to an endpoint a_i. In the process of taking the variation we effectively localize the computation to the neighbourhood of the branch point. In fact, in the Fefferman-Graham parameterization of the bulk geometry, the terms of interest are completely localized onto a neighbourhood of the branch point at the boundary of the spacetime.

With this picture in mind, one can trace the imaginary part to the contribution from

the cut-off surfaces around the a_i at the asymptotic boundary of the spacetime. Suppose, for example, we take the cut-offs to be half-discs $\mathcal{U}_i^\delta$ as illustrated in fig. 5.7. This choice (or indeed any other cut-off choice), will intersect the past light-cone from a_i. Indeed, the local structure is dictated completely by these light-cone crossings. The complex Gauss-Bonnet theorem would suggest that we pick up a factor of $-2\pi i$ from such crossings. For $\frac{\partial S^k_{\rm gr,fund}}{\partial a_i}$ using the Fefferman-Graham coordinate chart we can deduce that there is no bulk radial integral to perform along the splitting surface. However, from the earlier Euclidean analysis one learns that the contribution to the Euler characteristic is augmented by the local source of stress energy , which is captured by p_i. Putting these pieces together one is thus led to the final result quoted in (5.96).

One can understand the localized nature of the contribution by referring back to the one-interval computation in section 5.3.3 (which was also reduced to computing an integral along the boundary). There we had carried out the integral over the domain $\mathcal{R}$ directly after having used the fact that the accessory parameters p_1 and p_2 are fixed to be $p_1 = -p_2 = 2\,\frac{\Delta_n}{a_2-a_1}$. In that case we obtained imaginary contributions from light-cone crossings (using the principal value prescription) leading to (5.69). One can readily check that this result agrees with (5.96). In the evaluation of the gravity action itself we see parts where the imaginary parts cancel – for example in the domain $\mathfrak{D}_1$ in (5.65) which is crossed by the past directed light-rays from both a_1 and a_2. Such partial cancellations do not occur in the variation $\frac{\partial}{\partial a_i}\,\mathrm{Im}(S^k_{\rm gr,fund})$ which is another reason to consider it.

We emphasize the use of the complex Gauss-Bonnet theorem in the evaluation of the (5.95) as it illustrates quite generally the moral of the discussion in [6]. One can of course check that these statements hold by choosing an explicit regulator. For instance, in appendix D.2 we employ the light-cone regulators following the one-interval discussion.

At the end of the day we find indeed

$$\frac{\partial}{\partial a_i}\,\mathrm{Im}(S^k_{\mathrm{gr,fund}}) = -\frac{c}{12}\,p_i \quad \Longrightarrow \quad \frac{\partial}{\partial a_i} S^{(n)} = -\frac{n}{6(n-1)}\,c\,p_i\,. \tag{5.97}$$

Generalizations

We can use the mnemonic that the variation of the action with respect to the end-points gives an imaginary contribution to the Lorentz signature on-shell action as in (5.97) for more general configurations. For instance, while we have explicitly carried out the integrals when all the intervals are taken to lie at $t = 0$, we can more generally take the regions to be spacelike regions on an arbitrary boundary Cauchy slice. In this case the accessory parameters p_i are complex even in Euclidean signature. We expect that they should analytically continue to real accessory parameters in Lorentz signature and lead to real stress-energy sources, and real values for the entropies.

To see this in a particular example, consider the case of two intervals $N = 2$, one relatively boosted with respect to the other. In Euclidean signature, working with the invariant cross-ratio χ, the boost corresponds to rotating the finite interval $(0, \chi)$, allowing χ to have a non-zero imaginary part. For example, for $n = 2$, the branched cover geometry for the computation of the second Rényi entropy is a torus with a general complex structure and the dual geometry is the rotating BTZ black hole in a suitable conformal frame.[12] This rotation has no effect on the monodromy differential equation which did not require any assumption of the reality, nor does it affect our conditions to determine the accessory parameter by demanding trivial monodromy around certain cycles. The main difference is that with χ complex, the accessory parameter p_χ is likewise manifestly complex. The entropies are nevertheless real; this implies that we should integrate up

[12]This can be seen directly from the analysis in appendix D.3: the cross-ratio χ is complex if one of the end-points is displaced in real-time, and the complex structure $\tau(\chi)$ then is no longer purely imaginary.

(5.97) along a suitable contour choice to obtain the physically relevant real answers.

In the Lorentzian context, our analytic continuation $v \to \tilde{x}^-$ should be accompanied by $\chi \to \chi^-$ for χ being rotated in the Euclidean time direction (as usual we treat χ and $\bar{\chi}$ as independent in the analytic continuation). The restriction to spacelike intervals demands that $\chi_x > \chi_t > 0$. With this choice the accessory parameter p_χ is real in Lorentz signature, as is therefore the source of energy-momentum necessary to construct the branched cover geometry. The computation of the on-shell action proceeds as before, and the result for the variation of the entropies with respect to the accessory parameters is manifestly real. Integrating with respect to χ^- leads to the expected real answers for the entropies.

There is one limiting case to consider of our example, viz., the limit $\chi \to 1$ whence $\chi^- = x_\chi - t_\chi \to 1$. The interval $\mathcal{A}_1$ has left endpoint at $(t, x) = (0, 0)$ and right endpoint at $\left(\frac{\chi^+ - \chi^-}{2}, \frac{\chi^+ + \chi^-}{2}\right)$, while $\mathcal{A}_2$ runs from $(0, 1)$ to infinity. Now as $\chi^- \to -1$, the two intervals start to approach null separation. In the limit there is no spacelike surface containing both intervals and we should see this in the result, cf., [177]. Indeed, focusing on the $SL(2, \mathbb{C})$ invariant mutual Rényi information (MRI), cf., (D.17) which is a function of χ alone, purity of the global state demands that

$$I^{(n)}(\chi) = I^{(n)}(1 - \chi) + \frac{c}{6}\left(1 + \frac{1}{n}\right) \log\left(\frac{\chi}{1 - \chi}\right) \tag{5.98}$$

In Euclidean signature (5.98) implies that $I^{(n)}$ diverges as $\chi \to 1$, for using $I^{(n)}(0) = 0$ we have

$$I^{(n)}(\chi) \sim -\frac{c}{6}\left(1 + \frac{1}{n}\right) \log(1 - \chi)\,, \qquad 1 - \chi \ll 1 \tag{5.99}$$

Equivalently, this divergence can also be seen in the accessory parameter – from (D.25) we find that $p_\chi \sim \frac{1}{2(\chi - 1)}$ as $\chi \to 1$ in the connected phase (which dominates in this

regime). This holds under the analytic continuation $\chi \to \chi^-$ and is the signature of the intervals failing to be on a common Cauchy slice. We expect that the result of the two interval case generalizes to arbitrary intervals, with divergences encountered when the intervals enter into each other's causal domains.

One interesting generalization to consider is to directly evaluate the on-shell action $\mathrm{Im}(S^k_{\mathrm{gr,fund}})$ itself. As mentioned earlier, we have been able to carry out the evaluation of the bulk Euclidean action, S^E_{gr}, for the case $n = N = 2$. The reader can find a detailed account of the computation in appendix D.4. We work in the Fefferman-Graham gauge (in a suitable boundary conformal frame), evaluate the bulk action with a suitable cut-off of the radial coordinate (see fig. D.4), and exploit some useful incomplete elliptic function integral identities. The mechanics of this computation being highly adapted to the Euclidean setting, we were unable to translate it directly to the Lorentzian context, in particular, were unable to extract the desired imaginary pieces from the light-cone crossings. It should be possible to do better by working in a bulk coordinate chart adapted to the splitting surface as envisaged in [6].

Alternately, one could at least see how to integrate up (5.76) (the latter is blind to the spacetime signature, compare the Lorentzian (5.97) and Euclidean results (5.92)) to obtain the Rényi entropy $S^{(n)}$. As mentioned above for generic intervals with relative boosts this will require understanding an appropriate contour prescription. For two disjoint intervals with the intervals on a time symmetric slice (real cross-ratio χ) this was carried out numerically in [126], see Figure 5 of that paper. We note that the expressions for the accessory parameters themselves are quite simple when the intervals are far separated (for instance, for $N = n = 2$ from (D.25) we have $p_\chi \sim -\frac{3}{64}\,\chi$ for $\chi \ll 1$), but since the Rényi entropies are not invariant under change of conformal frame, one should pass again to working with the MRI $I^{(n)}$ which likewise has a simple variation, $\frac{\partial}{\partial\chi} I^{(2)}(\chi) \sim \frac{c}{64}\,\chi$ for small χ. If we consider relatively boosted intervals then χ becomes

complex. However, as we noted above, the accessory parameters are expected to be real in Lorentz signature and one should be able to obtain $\mathrm{Im}(S^k_{\mathrm{gr,fund}})$ without too much trouble. Moreover, this observation suggests that the contour prescription for computing the on-shell action with complex χ in Euclidean signature should be inherited from the Lorentzian geometry.

5.5 Discussion

We have exemplified the general discussion of [6] with some explicit low-dimensional examples, demonstrating a first-principles evaluation of stationary points of the real-time gravitational path integral. In particular, the on-shell action for these configurations was evaluated directly in Lorentz signature and shown to agree with the result obtained by analytically continuing the Euclidean saddle-point computations to real-time.

While our investigations were confined to analysis of the Rényi or swap entropies in simple states (thermofield double in JT-gravity and the vacuum state in AdS_3), it is clear that the principles outlined in [6] hold more generally. The essential point is that the contributions to the gravitational path integral are localized and isolated by suitable use of the complex Gauss-Bonnet theorem. In particular, entropies can be extracted by performing the analysis in Euclidean signature and thence analytically continuing the parameters to the real-time domain (say by moving the entangling surfaces appropriately). While this has been the modus operandi for computations of von Neumann and Rényi entropies both in field theory and gravity thus far, our results demonstrate the rationale behind the agreement. In particular, they lend support to the recent investigations in the gravitational context for the evolution of the fine-grained von Neumann entropy in the context of the black hole information problem.

There are several directions that would be interesting to pursue in the future. It would

for instance be helpful to understand the evolution of entropies following a quantum quench directly in Lorentz signature. These were first investigated in two dimensional CFTs in [120, 121] and studied in holography using properties of Virasoro conformal blocks in [68]. Reanalyzing the results of the latter discussion directly in real-time would pave the way for more general gravitational analysis such as the fine grained entropies in black hole collapse (which has been discussed in [178]).

Of direct relevance to the black hole information problem would be to construct the real-time replica wormholes relevant to obtaining the Page curve from an evaporating black hole (even in a simple model). This investigation will be aided by computation of the bulk quantum corrections to the entropies which we have not attempted to do here.

Ideally, it would be useful to extend the gravitational computations to higher dimensional scenarios with dynamical gravitational degrees of freedom. The non-trivial aspect here would be to deal with the gravitational backreaction. Developing numerical techniques to determine complex geometries for the class of real-time boundary value problems would greatly facilitate such explorations.

Chapter 6

Gravitational Renyi entropies from real-time path integrals: Complex saddles and contour deformations in JT gravity

6.1 Introduction

Studies of quantum gravity are often formulated using path integrals, after which computations are performed at the semiclassical level. Typically this involves the identification of interesting stationary points of the associated action, perhaps with some discussion of whether and when such saddles should dominate the computation.

Applying the saddle-point approximation to the Euclidean gravitational path integral has brought us many important results, with the thermal partition function as a classic example [32]. Recent applications include calculations of holographic entanglement entropy [33, 111, 28, 35], and of entropy of Hawking radiation for an evaporating black

hole [38, 39]. Nevertheless, Euclidean gravitational path integrals famously suffer from the conformal factor problem [40], where the (off-shell) action could be made arbitrarily negative by conformal transformations. The hypothesized solution in [40] is to rotate the integration contour of the conformal mode such that it is parallel to the imaginary axis. Despite its success in giving many physically satisfying results, this contour-rotating procedure is ad hoc in nature, and lacks justification from first principles. In fact, in cases where the conformal modes are coupled to other modes, this prescription fails and other kinds of contour-rotating prescription are needed [44, 45]. In this paper, we take the point of view that Lorentzian gravitational path integral is the most fundamental, where the integration contour is over all real Lorentz-signature metrics. This point of view has been argued in many previous works. The reason for us to take this point of view is that, first of all, there is no obvious reason to rule out the Lorentzian path integral; secondly, for computations in real time without analytic sources, it is hard to apply Euclidean techniques.

Furthermore, the Lorentzian gravitational path integral can in principle be taken as a guidance for choosing contours for the Euclidean gravitational path integral. This could be done by deforming properly the Lorentzian contour to include certain sets of real Euclidean configurations. This has been done for reproducing quantities related to black hole thermodynamics [46].

A first examination of Lorentzian path integral is to study its saddle points. In the discussion of saddle-point geometries, it appears that in certain scenarios they necessarily have complex spacetime metrics, and these complex saddles have produced many physically expected results [6, 4, 32, 145, 50][1]. Despite their existence and physical importance, it is still somewhat mysterious whether they are accessible by smoothly deforming the original integration contour.

[1]For a recent discussion of admissibility of complex metrics, see [179, 180].

In this paper, we verify this for one of the examples presented in [4], i.e. complex saddles in the computation of Rényi entropies of the Hartle-Hawking state in two-dimensional Jackiw-Teitelboim (JT) gravity. The general formalism of this setup has been discussed in a previous paper [6]. While it is hard to consider the path integral and contour deformation in standard Einstein gravity, the path integral greatly simplified in JT gravity, where after gauge-fixing, we are left with a only finite dimensional integral over the dilaton field.

We begin with a short introduction to the saddle-point approximation in section 6.2 and classical JT gravity in section 6.3. In section 6.4, we go into the semiclassical calculation of the wavefunction of the Hartle-Hawking state in a different basis to as our initial state for the replica calculation. Finally in section 6.5, we take replicas of the resulting semiclassical state, compute the Rényi entropies, and show the solutions match those found in [4].

6.2 Saddle-point Methods: A brief review

Consider an integral of the form

$$\int_\Gamma dz\, f(z) \exp[\lambda g(z)], \tag{6.1}$$

where λ is a constant, $f(z)$ and $g(z)$ are complex-valued functions, and Γ is an appropriate contour of integration through the complex plane. The saddle-point approximation is valid when λ is large. For many cases of interest, the contour Γ is the real axis. More generally, we need to properly choose Γ to avoid divergence at infinity.

In general, the saddles do not lie on original contour of integration, and we need to properly deform the original contour to pass through the saddle points for the approxi-

mation to hold. Luckily, there are theorems from either Morse theory or Picard-Lefshetz theory about saddle point approximation that can help us understand this and greatly simplify the analysis for the particular case to be studied below. We will review them, mainly following the results summarized in [181] and [46].

Suppose that the argument of the exponent in equation (6.1) has a stationary point p in $\mathbb{C}$ which in general could lie off of the original contour of integration Γ. There are two contours of interest associated with p: the steepest descent contour $\mathcal{J}_p$ (also called the downward flow) and the steepest ascent contour $\mathcal{K}_p$ (also called the upward flow). They are obtained by following from p upward or downward the gradient flow of the magnitude of the integrand. These gradient flows can be solved from the flow equations[2],

$$\frac{\mathrm{d}z}{\mathrm{d}t} = \pm\frac{\partial\overline{g}}{\partial\bar{z}}, \quad \frac{\mathrm{d}\bar{z}}{\mathrm{d}t} = \pm\frac{\partial g}{\partial z}. \tag{6.2}$$

where the positive and negative sign choices correspond to $\mathcal{K}_p$ and $\mathcal{J}_p$ respectively. From the flow equations, it follows that the phase of the integrand is constant along them,

$$\frac{\mathrm{d}\,\mathrm{Im}\,g}{\mathrm{d}t} = \frac{1}{2i}\frac{\mathrm{d}(g-\overline{g})}{\mathrm{d}t} = \frac{1}{2i}\left(\frac{\partial g}{\partial z}\frac{\mathrm{d}z}{\mathrm{d}t} - \frac{\partial\overline{g}}{\partial\bar{z}}\frac{\mathrm{d}\bar{z}}{\mathrm{d}t}\right) = 0. \tag{6.3}$$

This will be an important property in utilizing the saddle-point approximation.

Given the two contours $\mathcal{J}_p$ and $\mathcal{K}_p$, the relevant theorem states that, without changing the value of the integral, Γ can be deformed to a contour $\tilde{\Gamma}$ consisting of n_p copies of each $\mathcal{J}_p$, where n_p is the intersection number of $\mathcal{K}_p$ and Γ_R.

[2]To solve the flow equations, we first need to analyse the asymptotic behaviors of the flow lines as the parameter t in [181] goes to infinity, which is related to the eigenvalues of the Hessian matrix at the saddle point. Then we do a coordinate transformation $\tau = \tau(t)$ such that $\tau(\infty) = 0$. Finally we taylor expand the new differential equation with respect to τ near $\tau = 0$ so that we keep ourselves away from the singular point of the ODE. But in our case, since there is only one variable to be integrated, it turns out that solving contours of constant phase is much easier than solving the flow equation. As a result, in the following context, we find the flow lines by solving $\mathrm{Im}\,\lambda g(z) = \mathrm{Im}\,\lambda g(z_0)$ where z_0 is the saddle point of $\lambda g(z)$.

This theorem tells us that whether or not a stationary point of the action contributes to the semiclassical approximation of the path integral is diagnosed by whether or not $\mathcal{K}_p$ intersects the original contour Γ since, in the case we consider we have only cases $n_p = 0$ or $n_p = \pm 1$. After identifying the saddle points with $n_p \neq 0$, we can deform the contour of integration to a new one that is a combination of the steepest descent contours of the aforementioned saddles. We will illustrate this in an example in section 6.4.2. Saddle point approximation then tells us that we can approximate the original integral equation (6.1) by

$$\int_\Gamma dz\, f(z) \exp[\lambda g(z)] \sim \sum_p n_p \sqrt{\frac{2\pi}{\lambda |g''(z_p)|}} f(z_p) \exp[\lambda g(z_p)], \quad \lambda \to \infty, \tag{6.4}$$

where z_p is the relevant saddle point of the exponent in equation (6.1). Here since the factors in front of the exponential are $\mathcal{O}(1)$ correction and are only related to normalization, we will just drop them unless $f(z_0)$ is 0.

Similar results hold for higher-dimensional integrals. For a contour integral in the d-dimensional complex plane $\mathbb{C}^d$, the steepest ascent (descent) contour $\mathcal{K}_p$ ($\mathcal{J}_p$) which has the same real dimension as Γ is generated by the gradient flow from the stationary point p. Alternatively, it is always possible to write them as multiple one-dimensional integrals, and do them once at a time. For gravitational path integrals, d is technically infinite, but our analysis will not be significantly changed.

6.3 Preliminaries of JT Gravity

In this section, we will first give a brief introduction of classical JT gravity in Lorentz signature and the structure of its phase space, based on what has been studied in [182]. After this, we set up the stage for the path integral to be studied, by explaining variables

of integration, gauge fixing and boundary conditions.

6.3.1 Classical JT Gravity

In Lorentz signature, the action of JT Gravity is given by

$$S = S_g + S_\Phi, \tag{6.5}$$

where

$$S_g = \Phi_0 \left[\int_{\mathcal{M}} \sqrt{-g} R + 2 \int_{\partial \mathcal{M}} \sqrt{|\gamma|} K \right], \tag{6.6}$$

is the topological part of the action, with Φ_0 is a positive constant and

$$S_\Phi = \int_{\mathcal{M}} \sqrt{-g} \Phi (R+2) + 2 \int_{\mathcal{B}} \sqrt{-h} \Phi (K-1) + 2 \int_{\Gamma} \sqrt{|q|} \Phi K + S_{\text{corner}}, \tag{6.7}$$

is the dynamical dilaton part. In the above equations, $\partial\mathcal{M}$ is the entire boundary of the spacetime $\mathcal{M}$, $\mathcal{B}$ is the asymptotic timelike boundary, Γ is any finite boundary, with γ, h, and q the determinants of the induced metric on each respectively[3]. As commented in [6] and calculated in [152, 183], there are corner terms due to the extrinsic curvature being some delta function when the unit normal of the boundary changes direction discontinuously at some two surface or when the unit normal crosses a null line.

Varying this action gives the equations of motion

$$R = -2, \quad \big(\nabla_\alpha \nabla_\beta - g_{\alpha\beta}\big)\Phi = 0, \tag{6.8}$$

the first of which restricts the spacetime background to AdS_2. We also impose the usual

[3]The reason for the distinction between asymptotic and finite parts of the boundary is that the boundary terms require a counterterm $-\frac{1}{2}\int_{\mathcal{B}} \sqrt{-h}\Phi$ only on the asymptotic timelike pieces of the boundary.

asymptotic boundary conditions for the metric and dilaton

$$h_{tt}|_{\mathcal{B}} = 1/\epsilon^2, \quad \Phi|_{\mathcal{B}} = \phi_b/\epsilon. \tag{6.9}$$

To write down solutions of JT gravity, it is more convenient to use the embedding space, the (1+2)-dimensional Minkowski space $ds^2 = -d\mathcal{T}_1^2 - d\mathcal{T}_2^2 + d\mathcal{X}^2$, where AdS_2 spacetime can be viewed as a hyperboloid

$$\mathcal{T}_1^2 + \mathcal{T}_2^2 - \mathcal{X}^2 = 1, \tag{6.10}$$

and the dilaton solution is

$$\Phi = A\mathcal{T}_1 + B\mathcal{T}_2 + C\mathcal{X} \tag{6.11}$$

where A, B, C can be any real numbers. But our boundary condition is satisfied only when the vector $n^\mu = (-A, -B, C)$ is spacelike or null. Without loss of generality, we can perform an $SO(1,2)$ isometry and restrict the dilaton to take the form

$$\Phi = \Phi_h \mathcal{T}_1. \tag{6.12}$$

There are specific coordinate systems of interest. For global coordinates,

$$\mathcal{T}_1 = \sqrt{1+X^2}\cos T, \quad \mathcal{T}_2 = \sqrt{1+X^2}\sin T, \quad \mathcal{X} = X. \tag{6.13}$$

As a result, the metric and dilaton profile are given by

$$ds^2 = -(1+X^2)dT^2 + \frac{dX^2}{1+X^2}, \quad \Phi = \Phi_h\sqrt{1+X^2}\cos T. \tag{6.14}$$

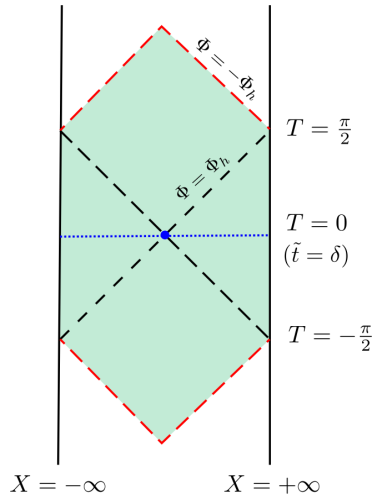

Figure 6.1: Two sided black hole solution in JT gravity (the shaded region). The spacetime is truncated at where $\Phi = -\Phi_h$, which we call the "inner horizon" (the red dashed lines) in Reissner-Nordstrom language. The dashed black lines are the "outer horizon" where $\Phi = \Phi_h$. The blue dot denotes the location of the bifurcation horizon.

We can also define "Schwarzschild" coordinates in the exterior region in figure 6.1 by

$$\mathcal{T}_1 = r/r_s, \quad \mathcal{T}_2 = \sqrt{(r/r_s)^2 - 1}\sinh(r_s t), \quad \mathcal{X} = \sqrt{(r/r_s)^2 - 1}\cosh(r_s t). \tag{6.15}$$

This gives us the metric and dilaton profile

$$ds^2 = -(r^2 - r_s^2)dt^2 + \frac{1}{r^2 - r_s^2}dr^2, \quad \Phi = \phi_b r, \quad r > r_s. \tag{6.16}$$

where r_s is the Schwarzschild radius and $\Phi_h = \phi_b r_s$ is the horizon dilaton value.

Since the boundary conditions (6.9) are not enough to determine the dynamics outsided the shaded region, the dynamical problem with such boundary conditions is only well-defined in this region, called the two-sided black hole solution, where the horizon dilaton value is $\Phi_h = \phi_b r_s$. The spacetime is truncated at the "inner horizons" where $\Phi = -\Phi_h$, c.f. figure 6.1. On both asymptotic boundaries the Schwarzschild time can take any real value, while the global time satisfies $-\pi/2 < T < \pi/2$.

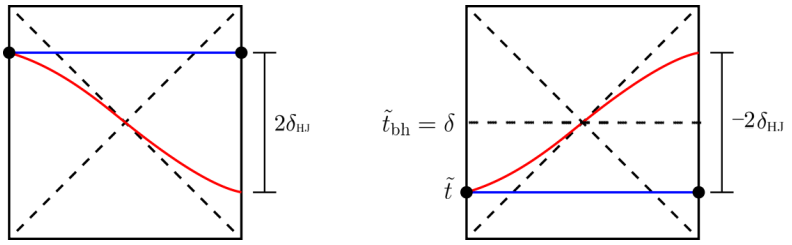

Figure 6.2: Comparison of different definitions of the time shift. **Left:** The time shift δ_{HJ} defined in [182]. **Right:** The time shift δ defined in this work. In both panels, the blue line represents a constant global time slice. The red line represents a geodesic that has the same left end point as the blue line and is orthogonal to the surface of constant dilaton. The left figure is adapted from [182]. The minus sign in the right panel comes from the fact that $\delta_{\rm HJ} < 0$ for this blue time slice but the length is positive.

6.3.2 Gauge Fixing and the Phase Space of JT Gravity

To perform the path integral, we need to fix a gauge and identify relevant physical degrees of freedom. First of all, since two-dimensional solutions in Einstein gravity are always locally AdS_2, we will gauge-fix the metric of the solutions to always take the form as in the first equation in (6.14). Here we assume that the spacetime is of trivial topology, leaving the higher topology discussion for future work. With this, the aforementioned boundary conditions tell us that the dilaton solution takes the form as in the second equation of (6.14). We also restrict our spacetime region to the two-sided black hole solution as shown in figure 6.1.

This solution has a symmetry of time evolution generated by $H_L - H_R$, where

$$H_L = H_R = \frac{\Phi_h^2}{\phi_b} \tag{6.17}$$

is the left and right boundary Hamiltonians. We identify configurations related by such symmetry, and as a result, we are left with one physical time evolution, which is generated by the full Hamiltonian

$$H = H_L + H_R = \frac{2\Phi_h^2}{\phi_b}. \tag{6.18}$$

As noted in [182], there is an additional degree of freedom which is needed to define a proper even-dimensional phase space for JT gravity. We will refer to this additional phase space variable as the "time shift" δ which is defined operationally in [182]. This time shift describes the difference between Schwarzschild times on the left and right boundaries connected by spacelike geodesics which are orthogonal to the surface of constant dilaton at the boundary; see the left panel in figure 6.2. In [182], δ is dynamic, in a sense that it is zero at global time $T = 0$, and evolves to non-zero at other times. We will refer to this time shift as δ_{HJ}.

In this work, we would like to adopt a different definition, such that δ is an overall shift of time, which is constant and uniquely labels different classical solutions to the JT gravity equations of motion.

As such, we define δ as a uniform translation of the boundary time. To account for this translation, we define a new time coordinate $\tilde{t}$ that is defined globally and approaches the Schwarzschild time (up to a sign) at the boundaries offset by some value δ. A constant $\tilde{t}$ slice corresponds to a constant T slice in the bulk. This new time coordinate is defined through[4]

$$\cos T = \operatorname{sech}\left[\frac{\Phi_h}{\phi_b}(\tilde{t} - \delta)\right]. \tag{6.19}$$

In this newly defined coordinate, the bifurcation surface is located at $\tilde{t} = \delta$, $X = 0$, as shown in the right panel in figure 6.2. Also from this figure we can see that $-2\delta_{\mathrm{HJ}} = 2(\delta - \tilde{t})$, i.e., $\delta_{\mathrm{HJ}} = -\delta + \tilde{t}$. This is to say, $\delta_{\mathrm{HJ}} = -\delta$ when $\tilde{t} = 0$. Here we note again that δ_{HJ} depends on the time coordinate while δ is a constant throughout the spacetime.

The time shift δ is the canonical conjugate of H [182], i.e.,

$$\{H, \delta\} = \{\frac{2\Phi_H^2}{\phi_b}, \delta\} = \frac{4\Phi_H}{\phi_b}\{\Phi_H, \delta\} = 1. \tag{6.20}$$

[4]As a comparison, we remind the reader that at the boundary $\cos T = \operatorname{sech}(r_s t)$.

For later convenience, we also define a new variable

$$Q_0 \equiv \frac{4\Phi_h}{\phi_b}\delta, \tag{6.21}$$

which is canonically conjugated to the extremal value of the dilaton Φ_h:

$$\{\Phi_h, Q_0\} = 4\frac{\Phi_h}{\phi_b}\{\Phi_h, \delta\} = 1. \tag{6.22}$$

We are also interested in studying the phase space on a constant $\tilde{t}$ slice. Thus we define a phase space variable

$$\Phi_{\tilde{t}} = \Phi_h \operatorname{sech}\left[\frac{\Phi_h}{\phi_b}\left(\tilde{t} - \delta\right)\right] \tag{6.23}$$

so that according to equation (6.14), on every constant $\tilde{t}$ slice, $\Phi = \Phi_{\tilde{t}}\sqrt{1+X^2}$. .

In the following context, we work in the semiclassical scheme. We promote the Hamiltonian H, the dilaton Φ_h and the time shift δ, as well as the quantities Q_0 and $\Phi_{\tilde{t}}$, to operators. Correspondingly, we have[5]

$$\hat{H} = \frac{2\hat{\Phi}_h^2}{\phi_b}, \quad \hat{Q}_0 = 4\frac{\hat{\Phi}_h}{\phi_b}\hat{\delta}, \tag{6.24}$$

as well as the commutation relation

$$[\hat{\Phi}_h, \hat{Q}_0] = i. \tag{6.25}$$

Denoting the time-evolution operator as $\mathcal{U} = e^{-i\hat{H}\tilde{t}}$, we can write down the time evolution

[5]Since Q_0 is a product of two variables that are conjugate to each other classically, there are many ways to promote it to an operator. Here we make one particular choice, but the choice does not affect our semi-classical calculation.

of the operator $\hat{Q}_0$ in the Heisenberg picture,

$$\hat{Q}_{\tilde{t}} = \mathcal{U}^\dagger \hat{Q}_0 \mathcal{U} = e^{i\hat{H}\tilde{t}} \hat{Q}_0 e^{-i\hat{H}\tilde{t}} = \frac{4\hat{\Phi}_h}{\phi_b}(\hat{\delta} - \tilde{t}), \tag{6.26}$$

where we have used the Baker–Campbell–Hausdorff formula and the fact that $[\hat{H}, \hat{Q}_0] = 4i\hat{\Phi}_h/\phi_b$ in the last step. We can see that $\hat{Q}_0 = \hat{Q}_{\tilde{t}=0}$. Furthermore,

$$[\hat{\Phi}_h, \hat{Q}_{\tilde{t}}] = [\hat{\Phi}_h, \hat{Q}_0] = i. \tag{6.27}$$

As we will see in section 6.4, the conjugate variable of $\Phi_{\tilde{t}}$ is actually $4\sinh\frac{Q_{\tilde{t}}}{4}$.

In section 6.4, we will study the eigenstates of operators Q_0 and $Q_{\tilde{t}}$. Suppose $\left|Q;\tilde{t}\right\rangle$ is the eigenstate of the operator $\hat{Q}_{\tilde{t}}$ with eigenvalue Q, whilde $|Q;0\rangle$ is the eigenstate of the operator $\hat{Q}_0$ with the same eigenvalue Q, i.e.,

$$\hat{Q}_0|Q;0\rangle = Q|Q;0\rangle, \quad \hat{Q}_{\tilde{t}}|Q;\tilde{t}\rangle = Q|Q;\tilde{t}\rangle. \tag{6.28}$$

The first equation yields

$$\mathcal{U}^\dagger \hat{Q}_0 \mathcal{U}\mathcal{U}^\dagger|Q;0\rangle = Q\mathcal{U}^\dagger|Q;0\rangle. \tag{6.29}$$

Comparing this with the second equation in equation (6.28), we get

$$|Q;\tilde{t}\rangle = \mathcal{U}^\dagger|Q;0\rangle. \tag{6.30}$$

6.3.3 Variational Principle, Boundary Conditions and Actions

In our later compution of path integrals, we are interested in a particular kind of boundary conditions for JT gravity. As shown in figure 6.3, besides the usual asymptotic timelike boundaries, we choose two Cauchy slices Σ_H and $\Sigma_{\tilde{t}}$ as our finite spacelike

boundaries with the following boundary conditions:

- On Σ_H, we fix the metric to be $ds^2_{\Sigma_H} = \frac{dx^2}{1+x^2}$ and extrinsic curvature $K = 0$ for $x \neq 0$. We fix $\Phi = \Phi_h$ and $n^\mu \nabla_\mu \Phi = 0$ [6] at $x = 0$;
- On $\Sigma_{\tilde{t}}$, we fix the induced metric to be $ds^2_{\Sigma_{\tilde{t}}} = \frac{dX^2}{1+X^2}$ and the dilaton profile to be $\Phi = \Phi_{\tilde{t}}\sqrt{1+X^2}$.

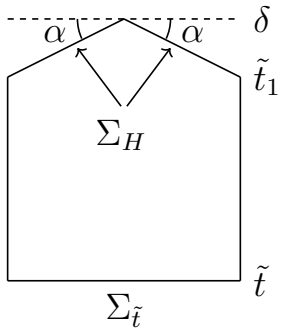

Figure 6.3: The classical spacetime configuration whose action is used to calculate the transition amplitude $\langle \Phi_{\tilde{t}} | \Phi_h \rangle$. In this figure, Σ_H and $\Sigma_{\tilde{t}}$ are Cauchy slices where we fix Φ_h and $\Phi_{\tilde{t}}$ respectively. Σ_H is one finite boundary passing through the bifurcation horizon and intersecting the asymptotic boundaries at time $\tilde{t}_1$, while $\Sigma_{\tilde{t}}$ is the other finite boundary with time $\tilde{t}$. α is the boost angle.

Since the extrinsic curvature is not fixed at one point on Σ_H, this results in the pentagon-shaped region in figure 6.3. One can check that for this kind of boundaty conditions, the usual Gibbons-Hawking boundary term in the action is still enough to give a good variational principle[7].

As we can see, the Cauchy surface $\Sigma_{\tilde{t}}$ is a geodesic, and $\Phi_{\tilde{t}} = \Phi_h \cos T$. The bifurcation surface $X = T = 0$ is also an extremal surface for the dilaton.

[6] Since the normal vector n^μ is not well-defined at $x = 0$, we should interpret n^μ in this equation as defined at some $x = \epsilon$ and take the limit $\epsilon \to 0$.

[7] With the Gibbons-Hawking term, variation of the action gives $\delta S \sim \int_{\partial M} \sqrt{\gamma} \left(2K\delta\Phi + (n^\nu \nabla_\nu \Phi)\, \gamma^{\alpha\beta} \delta\gamma_{\alpha\beta}\right)$. Although fixing $K = $ const. in general does not give a good variational principle, it does in the special case where we fix $K = 0$ and fix Φ on the part of boundary where K is not fixed.

Next we compute the action of the classical solution that satisfies the above boundary conditions. Without loss of generality, in this calculation we assume $\Sigma_{\tilde{t}}$ lies to the past of Σ_H ($\tilde{t} < 0$). Since $R = -2$ on shell, the Einstein-Hilbert term vanishes, and we only need to evaluate the remaining Gibbons-Hawking term. Since $K = 0$ on $\Sigma_{\tilde{t}}$ and Σ_H except for at the extremal surface, it only receives contribution from the center point, the asymptotic timelike boundaries and the corners where the spacelike and timelike boundaries meet.

Since K is not fixed at the extremal surface, in general there will be a "kink". Assuming the rapidity changes 2α (whose exact value will be determined later) as we move along Σ_H from right to left, the contribution to the action from the kink is

$$S_{\text{kink}} = 2\Phi_h(2\alpha), \tag{6.31}$$

since the spacetime there is locally flat and the integral of K is given by the change in rapidity in two-dimensional flat spacetimes [152].

Due to the left-right symmetry, the Cauchy slice Σ_H is composed of two semi-infinite geodesics which can be both conveniently expressed as $t = -\alpha/r_s$ in Schwarzschild coordinates on both sides. They touch the asymptotic boundaries at boundary time $\tilde{t}_1 = \delta - \alpha/r_s = \delta - \alpha\phi_b/\Phi_h$.

On the asymptotic boundaries $r = r_c$, we have

$$K = \frac{r_c}{\sqrt{r_c^2 - r_s^2}} = 1 + \frac{1}{2}\frac{r_s^2}{r_c^2} + \cdots . \tag{6.32}$$

As a result, its contribution to the Gibbons-Hawking term is

$$S_{\text{b}} = 2\int_{\mathcal{B}} \sqrt{h}\Phi(K-1) = 2\times 2\int_{\tilde{t}}^{\tilde{t}_1} d\tilde{t}\, \sqrt{r_c^2 - r_s^2}\,(\phi_b r_c)\left(\frac{1}{2}\frac{r_s^2}{r_c^2} + \dots\right) = \frac{2\Phi_h^2}{\phi_b}(\tilde{t}_1 - \tilde{t}), \tag{6.33}$$

where the extra prefactor 2 in the second step comes from the fact that there are two timelike boundaries in figure 6.3.

We still need to calculate the contribution from the four corners where spacelike and timelike boundaries meet. There is no real contribution from the two upper corners where a half geodesic (Schwarzschild time t = const.) is joined to the cutoff surface (Schwarzschild radius r = const.), since they are orthogonal to each other[8] [183]. At the lower two corners, the corner term is given by

$$S_{\rm c} = 4\phi_b r_s \sin T = 4\Phi_h \tanh\left(\frac{\Phi_h}{\phi_b}(\tilde{t}-\delta)\right). \tag{6.34}$$

The detailed calculation is given in Appendix E.1 for interested readers.

Now we are ready to write down the total Lorentzian action

$$S_L[\Phi_{\tilde{t}},\Phi_h,\tilde{t}] = S_{\rm kink}+S_{\rm b}+S_{\rm c} = 4\Phi_h\alpha + \frac{2\Phi_h^2}{\phi_b}\left(-\alpha\frac{\phi_b}{\Phi_h}+\delta-\tilde{t}\right)+4\Phi_h\tanh\left(\frac{\Phi_h}{\phi_b}(\tilde{t}-\delta)\right) \tag{6.35}$$

with δ related to Φ_h and $\Phi_{\tilde{t}}$ through (6.23). Note that for every set of $\Phi_t, \Phi_{\tilde{t}}, \tilde{t}$, there are two possible δ since $\cosh x$ is an even function on $\mathbb{R}$,

$$\delta = \tilde{t} \pm \frac{\phi_b}{\Phi_h}\cosh^{-1}\frac{\Phi_{\tilde{t}}}{\Phi_h}. \tag{6.36}$$

In our later discussion of path integral, this would mean that for any given Φ_h, $\Phi_{\tilde{t}}$ and $\tilde{t}$, there are two saddle point contributions that we need to consider. With the full action,

[8]There is still an imaginary part contribution $\int_{\rm corner} K = -i\frac{\pi}{2}$ from each corner; see e.g. [152] for details. We ignore this contribution since it is constant for any Φ_h, $\Phi_{\tilde{t}}$ and $\tilde{t}$, and can be absorbed into normalization. But as we will see in section xxx, this imaginary contribution is important in replica calculations.

we are able to determine α using Hamilton-Jacobi theory. For either choice of δ,

$$\frac{\partial S_L[\Phi_t, \Phi_h, \tilde{t}]}{\partial H} = \frac{\phi_b}{4\Phi_h} \frac{\partial S_L[\Phi_t, \Phi_h, \tilde{t}]}{\partial \Phi_h} = \delta. \tag{6.37}$$

Solving the ODE gives

$$\alpha = \frac{\Phi_h}{\phi_b}\delta, \tag{6.38}$$

where we have chosen the integration constant such that Σ_H joins the asymptotic boundaries at $\tilde{t} = 0$.

With this value of α, the full Lorentzian action is

$$S_L[\Phi_t, \Phi_h, \tilde{t}] = \frac{2\Phi_h^2}{\phi_b}\left(2\delta - \tilde{t}\right) + 4\Phi_h \tanh\left[\frac{\Phi_h}{\phi_b}(\tilde{t} - \delta)\right]. \tag{6.39}$$

6.4 The Hartle-Hawking Wavefunction

In this section, we use path integral to prepare the initial state for future calculation. In our following path integral of JT gravity, we always take the semiclassical limit $\phi_b \to \infty$, with $\frac{\Phi_0}{\phi_b}, \frac{\Phi_h}{\phi_b}, \frac{\Phi_{\tilde{t}}}{\phi_b}$ finite. Therefore our path integral is well approximated by saddle-point contributions.

6.4.1 Expression of the Hartle-Hawking Wavefunction

Before replica calculation, we would like to first prepare a state for us to use as the initial conditions for the Lorentzian path integral. This initial state is taken to be the Hartle-Hawking state that is evolved to the past or future of the bifurcation surface. We start from the Hartle-Hawking state in the basis of eigenstates of the $\hat{\Phi}_h$ operator

computed in [182] via semiclassical Euclidean path integral,

$$\Psi_{HH}[\Phi_h] = \langle \Phi_H | HH \rangle = \exp\left(2\pi\Phi_0 + 2\pi\Phi_h - \frac{\beta}{2}\frac{\Phi_h^2}{\phi_b}\right), \tag{6.40}$$

where the inverse temperature β defines the circumference of the thermal circle of the Euclidean manifold. We would like to evolve this wavefunction in Lorenztian time to some surface of constant $\tilde{t}$ and express it in the basis of eigenstates of the $\hat{\Phi}_{\tilde{t}}$ operator.

$$\Psi_{HH}[\Phi_{\tilde{t}}] = \langle \Phi_{\tilde{t}} | HH \rangle = \int d\Phi_h \, \langle \Phi_{\tilde{t}} | \Phi_h \rangle \langle \Phi_h | HH \rangle. \tag{6.41}$$

When computing $\langle \Phi_{\tilde{t}} | \Phi_h \rangle$, we use the semiclassical approximation to express it in terms of the action of some classical solution,

$$\langle \Phi_{\tilde{t}} | \Phi_h \rangle = \exp\left(-iS_L[\Phi_h, \Phi_{\tilde{t}}, \tilde{t}]\right). \tag{6.42}$$

Here, S_L is the Lorentzian JT action evaluated on-shell between a Cauchy slice of constant time $\tilde{t}$ and a constant Schwarzshild time slice which passes through the bifurcation surface, as described in section 6.3.3[9].

However, if we try to combine equations (6.41) and (6.42) and find its saddle point, the integrand has a branch cut that we need to integrate through. Besides, as mentioned before, there are always two saddle points for given Φ_h and $\Phi_{\tilde{t}}$. These issues bring us more subtleties to deal with.

To circumvent these issues, we can rewrite equation (6.41) by inserting a resolution of the identity $\mathbb{1} = \int dQ |Q; \tilde{t}\rangle\langle Q; \tilde{t}|$ to get

[9]The sign choice in the exponent is consistent with the action calculation in section 6.3.3, where in computing the integrals, we implicitly assume that the Cauchy slice where we fix $\Phi_{\tilde{t}}$ to be a constant lies to the past of the bifurcation surface.

$$\langle \Phi_{\tilde{t}}|HH\rangle = \int d\Phi_h dQ \langle \Phi_{\tilde{t}}|Q;\tilde{t}\rangle\langle Q;\tilde{t}|\Phi_h\rangle\langle \Phi_h|HH\rangle. \tag{6.43}$$

Since $\hat{Q}_{\tilde{t}}$ is defined in the way that it is the canonical conjugate of Φ_h, we know that

$$\langle Q;\tilde{t}|\Phi_h\rangle = \langle Q;\tilde{t}=0|\exp\left(-i\frac{2\hat{\Phi}_h^2}{\phi_b}\tilde{t}\right)|\Phi_h\rangle = \exp\left(-iQ\Phi_h - i\frac{2\Phi_h^2}{\phi_b}\tilde{t}\right), \tag{6.44}$$

where we have used equation (6.30) in the first step. Thus, equation (6.43) becomes

$$\langle \Phi_{\tilde{t}}|HH\rangle = \int d\Phi_h dQ \langle \Phi_{\tilde{t}}|Q;\tilde{t}\rangle \exp\left[-i\left(Q\Phi_h + \frac{2\Phi_h^2}{\phi_b}\tilde{t}\right)\right]\Psi_{HH}[\Phi_h], \tag{6.45}$$

where $\Psi_{HH}[\Phi_h]$ is given by equation (6.40). Now, similarly to equation (6.42), we identify the overlap between states of definite $\Phi_{\tilde{t}}$ and states of definite Q to the exponentiation of some action

$$\langle \Phi_{\tilde{t}}|Q;\tilde{t}\rangle = \exp\big(-iS_L[\Phi_{\tilde{t}},Q,\tilde{t}]\big). \tag{6.46}$$

It is not hard to get $S_L[\Phi_{\tilde{t}},Q,\tilde{t}]$ from the Lorentzian action equation (6.39). First, Since $\hat{Q}_{\tilde{t}}$ can be seen as the canonical momentum of Φ_h, the action $S_L[\Phi_{\tilde{t}},Q,\tilde{t}]$ is related to $S_L[\Phi_{\tilde{t}},\Phi_h,\tilde{t}]$ by a Legendre transformation, so we can simply add a boundary term $-Q\Phi_h$ to account for it. Besides, since Σ_H joins the asymptotic boundaries at $\tilde{t}=0$ while the state $|Q;\tilde{t}\rangle$ lives in a Cauchy slice with time $\tilde{t}$, we need to evolve the state $|\Phi_h\rangle$ to time $\tilde{t}$. With all these in mind, we finally have

$$S_L[\Phi_{\tilde{t}},Q,\tilde{t}] = S_L[\Phi_t,\Phi_h,\tilde{t}] - Q\Phi_h - \frac{2\Phi_h^2}{\phi_b}\tilde{t} = -4\Phi_{\tilde{t}}\sinh\frac{Q}{4}, \tag{6.47}$$

where we have used equation 6.39. Obviously, this action satisfies the Hamilton-Jacobi

equation with

$$\frac{\partial S_L[\Phi_{\tilde{t}}, Q, \tilde{t}]}{\partial Q} = -\Phi_h,$$

since $\Phi_h = \Phi_{\tilde{t}} \cosh Q/4$.

Finally, we get the path integral expression for the Hartle-Hawking wavefunction:

$$\begin{aligned}
\langle \Phi_{\tilde{t}} | HH \rangle &= \int d\Phi_h dQ \langle \Phi_{\tilde{t}} | Q; \tilde{t} \rangle \langle Q; \tilde{t} | \Phi_h \rangle \langle \Phi_h | HH \rangle \\
&= \int d\Phi_h dQ \exp\left(4i\Phi_{\tilde{t}} \sinh \frac{Q}{4}\right) \exp\left(-iQ\Phi_h - i\frac{2\Phi_h^2}{\phi_b}\tilde{t}\right) \Psi_{HH}[\Phi_h] \\
&= \int d\Phi_h dQ \exp\left[i\left(4\Phi_{\tilde{t}} \sinh \frac{Q}{4} - Q\Phi_h - \frac{2\Phi_h^2}{\phi_b}\tilde{t}\right) + \left(2\pi\Phi_0 + 2\pi\Phi_h - \frac{\beta}{2}\frac{\Phi_h^2}{\phi_b}\right)\right].
\end{aligned} \tag{6.48}$$

In the next subsection, we will evaluate this wavefunction using the saddle point approximation method.

However, rigorously speaking, the LHS and RHS of equation (6.46) always differ by an $\mathcal{O}(1)$ factor, which is related to normalization and is subleading in the semiclassical limit. In our case, this prefactor is indeed important since it eliminates a saddle that would otherwise have some finite contribution to the above integral. In order for the state $|Q; \tilde{t}\rangle$ to be delta-function normalized,

$$\langle Q; \tilde{t} | Q'; \tilde{t} \rangle = \int d\Phi_{\tilde{t}} \langle Q; \tilde{t} | \Phi_{\tilde{t}} \rangle \langle \Phi_{\tilde{t}} | Q'; \tilde{t} \rangle = \delta(Q - Q'), \tag{6.49}$$

we need to add an additional factor in equation (6.46) and thus (6.48),

$$\langle \Phi_{\tilde{t}} | Q; \tilde{t} \rangle = \sqrt{\cosh \frac{Q}{4}} \exp\big(-iS_L[\Phi_{\tilde{t}}, Q, \tilde{t}]\big). \tag{6.50}$$

The existence of this factor reflects the fact that in computing $\langle \Phi_{\tilde{t}} | Q; \tilde{t} \rangle$, the ket state is not exactly $|Q; \tilde{t}\rangle$, but $\sqrt{\cosh \frac{Q}{4}} |Q; \tilde{t}\rangle$.

6.4.2 Evaluating the Hartle-Hawking Wavefunction in the Saddle Point Approximation

We will begin by first doing the Φ_h integral in equation (6.48). This integral is of Gaussian form, so the saddle point contribution is exact. Taking a derivative of the logarithm of the integrand of equation (6.48) with respect to Φ_h and setting it equal to zero identifies the saddle point to be

$$\Phi_h^{\text{SP}} = -\phi_b \frac{2\pi i + Q}{4\tilde{t} - i\beta}. \tag{6.51}$$

So the result of the integral is

$$\langle \Phi_{\tilde{t}} | HH \rangle = \int dQ \sqrt{\cosh \frac{Q}{4}} \exp\left\{ \phi_b \left[2\pi \frac{\Phi_0}{\phi_b} + \frac{i}{2} \left(8 \frac{\Phi_{\tilde{t}}}{\phi_b} \sinh \frac{Q}{4} - \frac{\left(2\pi - iQ\right)^2}{4\tilde{t} - i\beta} \right) \right] \right\}. \tag{6.52}$$

Here we put ϕ_b in the front of the exponent in order to see the semiclassical limit directly. Similarly, the saddle points of the Q integral are the solutions to

$$\frac{2\pi - iQ}{-4\tilde{t} + i\beta} + i \frac{\Phi_{\tilde{t}}}{\phi_b} \cosh \frac{Q}{4} = 0, \tag{6.53}$$

where we took a derivative of the exponent in the integrand with respect to Q.

There is no analytic solution to this transcendental equation, thus we analyze the solutions numerically. Note that there is always a trivial saddle $Q = -2\pi i$ and that there are infinitely many solutions to the above equation when $\Phi_{\tilde{t}} \neq 0$. Here we focus on the case $\tilde{t} < 0$.

For each choice of $\beta, \tilde{t}, \Phi_{\tilde{t}}$, we first find the solutions to equation (6.53) in the complex Q plane, then find the contours of constant phase by equating the imaginary part of the exponent in equation (6.52) to that at each saddle point. Finally we determine whether

the contour is the steepest descent/ascent contour by comparing the real part of the exponent with that at the saddle point. As foreshadowed in section 6.2, whether the saddle point contributes to our gravitational integral or not depends on the intersection number n_p of the upward flow and the original contour of integration, the real line in our case. For instance, in the first panel in the first row of figure 6.4, for the trivial $Q = -2\pi i$ saddle, the red line is the steepest ascent contour and it intersects with the real line once, so this saddle contributes to our integral with factor 1. While for the upper two saddles, their corresponding upward flow lines do not intersect with the real line thus they do not contribute to our integral.

After checking numerically for a wide range in our parameter space $\{\beta, \tilde{t}, \Phi_{\tilde{t}}, \phi_b\}$, we find that only saddles with $-2\pi \leq \mathrm{Im}\, Q < 2\pi$ could contribute to our integral. Thus we restrict ourselves to this region in presenting our numerical results below. Besides, we found that for fixed $\{\beta, \tilde{t}, \phi_b\}$ and various $\Phi_{\tilde{t}}$, there is a general pattern of the position of the relevant saddles. Therefore, without loss of generality, we only present in figure 6.4 one parameter choice with $\beta = 5$, $\tilde{t} = -1$, $\phi_b = 10$. Although ϕ_b only appears as an overall factor in the action and its value does not affect our analysis, it is worth mentioning again that the semiclassical limit is characterized by $\phi_b \to \infty$.

As shown in figure 6.4, for $\Phi_{\tilde{t}} \leq 0$, only the saddle $Q = -2\pi i$ contributes to this integral. Since the normalization factor in 6.50 is exactly 0 at this saddle point, the transition amplitude vanishes in the semiclassical limit. This corresponds to the fact that there is no classical solution with $\Phi_{\tilde{t}} \leq 0$ since the boundary condition is $\phi_b > 0$. For $\Phi_{\tilde{t}} > 0$, there exists a threshold, below which there are two saddle contributing to the integral (6.52): the trivial saddle and the non-trivial saddle with $-2\pi < \mathrm{Im}\, Q < 2\pi$. Above this threshold, only the non-trivial saddle with $-2\pi < \mathrm{Im}\, Q < 2\pi$ contributes to the integral. At this threshold, the downward flow that starts at the non-trivial saddle ends at the trivial saddle. This situation is called the Stokes ray in [181]. In the next

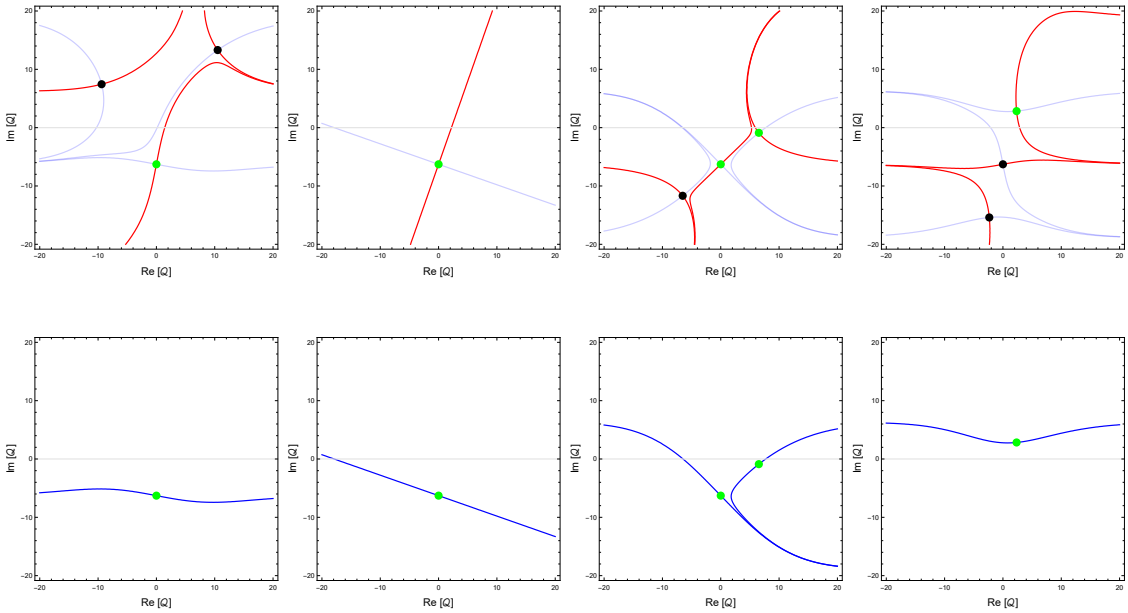

(a) $\Phi_{\tilde{t}} < 0$ (b) $\Phi_{\tilde{t}} = 0$ (c) $0 < \Phi_{\tilde{t}} <$ threshold (d) $\Phi_{\tilde{t}} >$ threshold

Figure 6.4: First row: saddle points (dots) and their steepest descent (light blue lines) and ascent (red lines) contours in the Q integral. The green dots are the saddles whose corresponding steepest ascent contour intersects with the original contour of integration — the gray contour. Second row: relevant saddle (green dots) and the corresponding deformed contours (blue lines). In each case, according to Cauchy–Goursat theorem and Morse theory, we can deform the original contour of integration to the steepest descent contour passing through the relevant saddle without changing the result of the integral. The third case is a bit tricky, we need to consider the union of the associated steepest descent contours. Obviously they cancel each other in the lower right part, so we can also think of deforming the original contour to the combination of the two half-branches on the top. Here the boundary conditions are given by $\tilde{t} = -1, \beta = 5, \phi_b = 10$. The values for $\Phi_{\tilde{t}}$ are $-5, 0, 5, 15$, respectively. The threshold occurs at $\Phi_{\tilde{t}} \simeq 5.1663$.

section, we will integrate over $\Phi_{\tilde{t}}$, so we do not need to analyze the saddle points in this case since it is of measure zero.

As a result, when $\Phi_{\tilde{t}} > 0$, the initial state is given by

$$\langle \Phi_{\tilde{t}} | HH \rangle = \exp\left\{ \phi_b \left[2\pi \frac{\Phi_0}{\phi_b} + \frac{i}{2}\left(8\frac{\Phi_{\tilde{t}}}{\phi_b} \sinh\frac{Q^{\mathrm{SP}}}{4} - \frac{\left(2\pi - iQ^{\mathrm{SP}}\right)^2}{4\tilde{t} - i\beta} \right) \right] \right\}, \tag{6.54}$$

where Q^{SP} is the non-trivial solution to equation (6.53) with $-2\pi < \mathrm{Im}\, Q^{\mathrm{SP}} < 2\pi$. When $\Phi_{\tilde{t}} \leq 0$, we have $\langle \Phi_{\tilde{t}} | HH \rangle = 0$ to leading order.

6.5 Complex saddles from Rényi Entropy calculation

In this section we compute the Rényi entropies S_n for the Hartle-Hawking state in JT gravity. As we will see, the saddle point geometry we find is complex, and can be matched with the the saddle found in [4].

6.5.1 Real-time replicas: formalism

To compute the Rényi entropy using the Schwinger-Keldysh contour, we need n copies of the ket state and n copies of the bra state, glued in a fashion as shown in Figure 6.5. As a result, all the kets and bras share the same dilaton value at the horizon, denoted as $\Phi_{h,n}$. If we take our initial state as the Hartle-Hawking state and express it in the $|\Phi_{\tilde{t}}\rangle$ basis, we need to integrate over $2n$ $\Phi_{\tilde{t}}$'s and one $\Phi_{h,n}$.

6.5.2 The fixed-area state wavefunction for one ket/bra

To start with, we focus on one ket/bra, computing the overlap between initial state and the fixed-area state $|\Phi_{h,n}\rangle$. Inserting two resolutions of identity $\mathbb{1} = \int d\Phi_{\tilde{t}} |\Phi_{\tilde{t}}\rangle\langle\Phi_{\tilde{t}}| =$

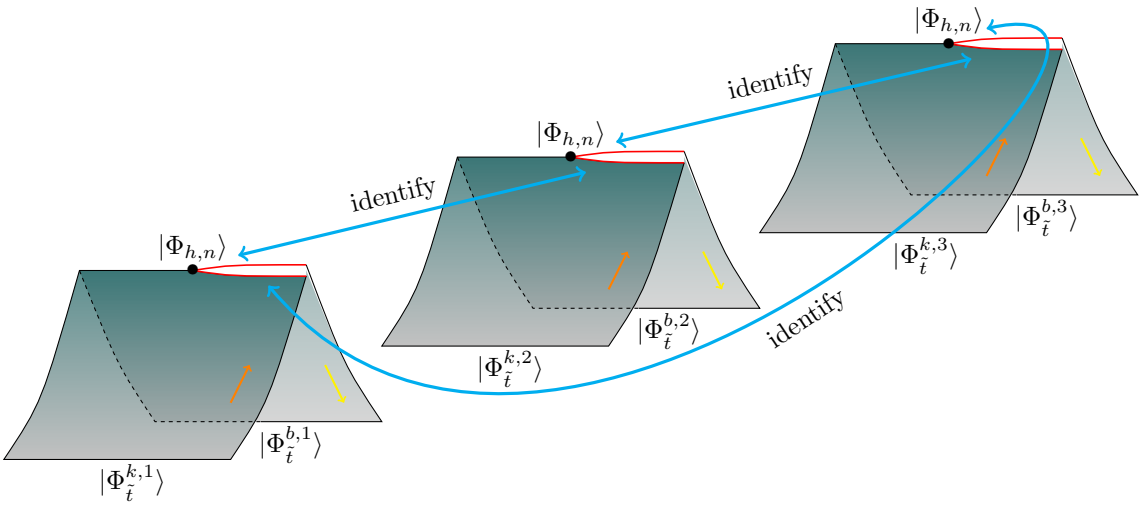

Figure 6.5: The bulk replica manifold $\mathcal{M}_n$ for computing the Rényi entropy when $n = 3$. The ket and bra spacetimes are identified in a manner as shown in the figure. As a result, there is only one splitting surface, where the dilaton value is fixed to be $\Phi_{h,n}$. The initial states for kets and bras are the Hartle-Hawking state expressed in different basis $|\Phi_{\tilde{t}}^{k,i}\rangle$ or $|\Phi_{\tilde{t}}^{b,i}\rangle$, as shown in the figure.

$\int dQ'|Q';\tilde{t}\rangle\langle Q';\tilde{t}|$, we have

$$\begin{aligned}
\langle\Phi_{h,n}|HH\rangle &= \int d\Phi_{\tilde{t}}dQ'\langle\Phi_{h,n}|Q';\tilde{t}\rangle\langle Q';\tilde{t}|\Phi_{\tilde{t}}\rangle\langle\Phi_{\tilde{t}}|HH\rangle \\
&= \int d\Phi_{\tilde{t}}dQ' \exp\left[i\left(Q'\Phi_{h,n} + \frac{2\Phi_h^2}{\phi_b}\tilde{t}\right)\right]\exp\left(iS_L\right) \\
&\qquad \exp\left[2\pi\Phi_0 + \frac{i}{2}\left(8\Phi_{\tilde{t}}\sinh\frac{Q^{\rm SP}}{4} - \phi_b\frac{\left(2\pi - iQ^{\rm SP}\right)^2}{4\tilde{t} - i\beta}\right)\right] \\
&= \int d\Phi_{\tilde{t}}dQ' \exp\left[2\pi\Phi_0 + i\left(Q'\Phi_{h,n} + \frac{2\Phi_h^2}{\phi_b}\tilde{t} - 4\Phi_{\tilde{t}}\sinh\frac{Q'}{4}\right.\right. \\
&\qquad \left.\left. -\frac{(2\pi - iQ^{\rm SP})^2\phi_b}{2(4\tilde{t} - i\beta)} + 4\Phi_{\tilde{t}}\sinh\frac{Q^{\rm SP}}{4}\right)\right],
\end{aligned} \tag{6.55}$$

where the state $|\Phi_{\tilde{t}}\rangle$ lives at past boundary at $\Sigma_{\tilde{t}}$, and the state $|\Phi_{h,n}\rangle$ lives at the future boundary anchored at $\tilde{t} = 0$ on $\mathcal{B}$. Again, here $Q^{\rm SP} = Q^{\rm SP}(\Phi_{\tilde{t}}, \tilde{t}, \phi_b, \beta)$ is the same as in equation (6.52) which is the saddle point for the Q integral.

We first do the integral over $\Phi_{\tilde{t}}$, which we remind the reader is from 0 to ∞. The saddle point occurs at

$$-4\sinh\frac{Q'}{4}+\frac{\phi_b(2i\pi+Q^{\rm SP})}{4\tilde{t}-i\beta}\frac{\partial Q^{\rm SP}}{\partial\Phi_{\tilde{t}}}+4\sinh\frac{Q^{\rm SP}}{4}+\Phi_{\tilde{t}}\cosh\frac{Q^{\rm SP}}{4}\cdot\frac{\partial Q^{\rm SP}}{\partial\Phi_{\tilde{t}}}=0. \tag{6.56}$$

The saddle point value of $\Phi_{\tilde{t}}$ turns out to be the one such that

$$Q^{\rm SP}(\Phi_{\tilde{t}}^{\rm SP},\tilde{t},\phi_b,\beta)=Q', \tag{6.57}$$

where we have used (6.53) to simplify the equation. Consequently, we get

$$\langle\Phi_{h,n}|HH\rangle=\int dQ'\exp\left[2\pi\Phi_0+i\left(Q'\Phi_{h,n}+\frac{2\Phi_{h,n}^2}{\phi_b}\tilde{t}+\frac{(2\pi-iQ')^2\phi_b}{2(-4\tilde{t}+i\beta)}\right)\right], \tag{6.58}$$

The saddle point for this integral is

$$(Q')^{\rm SP}=\frac{-4\tilde{t}\Phi_{h,n}+i(-2\pi\phi_b+\beta\Phi_{h,n})}{\phi_b}. \tag{6.59}$$

Using the definition equation (6.21), the corresponding time shift is

$$\delta=\frac{i(-2\pi\phi_b+\beta\Phi_{h,n})}{4\Phi_{h,n}}. \tag{6.60}$$

Note that this δ is purely imaginary, so time-reflection symmetry is preserved in this case. Finally, we have

$$\langle\Phi_{h,n}|HH\rangle=\exp\left(2\pi\Phi_0+2\pi\Phi_{h,n}-\frac{\beta\Phi_{h,n}^2}{2\phi_b}\right). \tag{6.61}$$

This is exactly the Hartle-Hawking wavefunction in the $\Phi_{h,n}$ basis.

In using the saddle point approximation for the $\Phi_{\tilde{t}}$ integral, we do not need to solve

equation (6.57), since terms involving $\Phi_{\tilde{t}}$ cancel out in the resulting action. However, we still need to verify the validity of saddle point approximation by solving for the saddle and analyzing the steepest descent and ascent of it like in section 6.4.2. Since the $\Phi_{\tilde{t}}$ integral is over the positive real half line, we change to a new variable $P = \log \Phi_{\tilde{t}} \in (-\infty, +\infty)$ for convenience. As a result, we must include a factor e^P in the integrand, but this will not change the position of the saddle point in the $\phi_b \to \infty$ limit.

Although we are not able to find analytic expressions, we are able to do the calculation numerically. For a wide range of parameter choices of $(\tilde{t}, \beta, Q')$, and for regions that are not too far from the real axis, there exist only one saddle point for the P integral. The saddle point is in general complex. We also find that the steepest ascent contour crosses the real P axis once, which means this saddle contributes to our path integral with factor 1.

One of the technical points of this calculation is to find Q^{SP} when $\Phi_{\tilde{t}}$ is complex. We choose Q^{SP} in this case to be the saddle point in the Q integral that, when tuning $\Phi_{\tilde{t}}$, is continuously connected to the Q saddle when $\Phi_{\tilde{t}}$ is real.

In figure 6.6, we show saddle points, the steepest and ascent contours for several different choices of parameters.

6.5.3 Contribution from the splitting surface

To compute the Rényi entropy, we sew the n bras and n kets together, and integrate over $\Phi_{h,n}$. However, the saddles when $n = 1$ are no longer saddles for general n since there is a difference in action, which is given by

$$\Delta I = -4\pi(n-1)\Phi_{h,n}. \tag{6.62}$$

This difference has appeared in previous replica calculations, e.g. [33, 34].

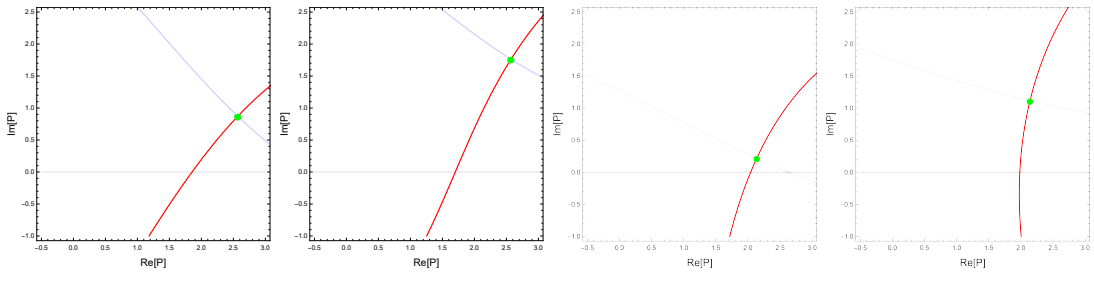

(a) $\tilde{t} = -1, \beta = 1, Q' = 3$ (b) $\tilde{t} = -1, \beta = 1, Q' = -3$ (c) $\tilde{t} = -1, \beta = 5, Q' = 3$ (d) $\tilde{t} = -1, \beta = 5, Q' = -3$

(e) $\tilde{t} = -5, \beta = 1, Q' = 3$ (f) $\tilde{t} = -5, \beta = 1, Q' = -3$ (g) $\tilde{t} = -5, \beta = 5, Q' = 3$ (h) $\tilde{t} = -5, \beta = 5, Q' = -3$

Figure 6.6: Saddle points (green dots) and their steepest descent (red lines) and ascent (light blue lines) contours in the P integral, where $P = \log \Phi_{\tilde{t}}$. The rest of our parameters do not affect our results, and we fix them to be $\phi_b = 10$, $\Phi_h = 3$. As we can see, in all eight panels, the steepest ascent contours cross the real axis (the original contour, gray colored), which means the saddle points contribute to our path integral.

To derive this difference, we use Gauss-Bonnet theorem following [6, 4]. In the replica manifold $\mathcal{M}_n$, we excise a small disk denoted $\mathcal{U}_\epsilon$ around the splitting surface; see figure 6.7. The contribution to the action from $\mathcal{U}_\epsilon$ is

$$\begin{aligned} iS_\Upsilon &= \lim_{\epsilon \to 0} \left[i \int_{\mathcal{U}_\epsilon} d^2x \, \eta \sqrt{-g} \Phi R \right] \\ &= \lim_{\epsilon \to 0} \left[-2i \int_{\partial \mathcal{U}_\epsilon} dx \, \eta \sqrt{|h|} \Phi K + 4\pi \chi(\tilde{\mathcal{U}}_\epsilon) \Phi_{h,n} \right] \end{aligned} \tag{6.63}$$

where $\eta = \pm 1$ taking the positive sign on the ket parts of the spacetime and taking the negative sign on the bra parts of the spacetime. We choose $\partial \mathcal{U}_\epsilon$ to be orthogonal to Σ_H, so it is smooth when passing from one copy to another one, and we don't receive any corner-term contribution from there.

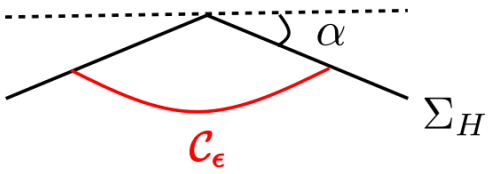

Figure 6.7: the region on one copy of the ket spacetime bounded by Σ_H and $\mathcal{C}_\epsilon$ (the part of $\partial\mathcal{U}_\epsilon$ in one ket)

To evaluate the first term in equation (6.63), we consider the region on one copy of the ket spacetime bounded by Σ_H and $\mathcal{C}_\epsilon$ (the part of $\partial\mathcal{U}_\epsilon$ in one ket, as shown in figure 6.7) and apply the Gauss-Bonnet theorem again. Since the spacetime is locally flat near the bifurcation surface, for each ket we have

$$2i\int_{\Sigma_H} dx\, K + 2i\int_{\mathcal{C}_\epsilon} dx\, K = iS_{\text{kink}} + 2i\int_{\mathcal{C}_\epsilon} dx\, K = 4\pi. \tag{6.64}$$

so

$$2i\int_{\mathcal{C}_\epsilon} dx\, K = 2i(-\pi i - 2\alpha). \tag{6.65}$$

Since $\chi(\tilde{\mathcal{U}}_\epsilon) = 1$, the full action from $\mathcal{U}_\epsilon$ is

$$\begin{aligned} iS_\Upsilon &= -2in\Phi_{h,n}\left[(-\pi i - 2\alpha) - (-\pi i - 2\alpha)^*\right] + 4\pi\Phi_{h,n} \\ &= 4\pi\Phi_{h,n} - 4n\Phi_{h,n}(\pi + 2\,\mathrm{Im}\,\alpha) \end{aligned} \tag{6.66}$$

Note that iS_Υ contains *all* the action contribution from the splitting surface, including the "kink terms" that we already computed. So we have another way to write iS_Υ:

$$\begin{aligned} iS_\Upsilon &= in(S_{\text{kink}} - S^*_{\text{kink}}) + \Delta I \\ &= in\Phi_{h,n}(4\alpha - 4\alpha^*) + \Delta I \\ &= -8n\Phi_{h,n}\,\mathrm{Im}\,\alpha + \Delta I. \end{aligned} \tag{6.67}$$

Comparing the above two equations we get $\Delta I = 4\pi(1-n)\Phi_{h,n}$.

6.5.4 Saddle point for replica calculation

The path integral for n replicas is

$$Z_n = \int d\Phi_{h,n} \langle \Phi_{h,n} | HH \rangle^{2n} e^{\Delta I} = \int d\Phi_{h,n} \exp\left(\Phi_{h,n} (4\pi - \frac{n\beta \Phi_{h,n}}{\phi_b}) \right), \tag{6.68}$$

whose saddle point is given by

$$(\Phi_{h,n})^{\text{SP}} = \frac{2\pi\phi_b}{n\beta}. \tag{6.69}$$

Plugging this back in the $\Phi_{\tilde{t}}$ saddle we find before, we get

$$\Phi_{\tilde{t}} = (\Phi_{h,n})^{\text{SP}} \operatorname{sech}\left[-\frac{\tilde{t}(\Phi_{h,n})^{\text{SP}}}{\phi_b} + i\frac{\beta(\Phi_{h,n})^{\text{SP}} - 2\pi\phi_b}{4\phi_b} \right] = \frac{2\pi\phi_b}{n\beta} \operatorname{sech}\left[-\frac{2\pi\tilde{t}}{n\beta} - \frac{i\pi}{2}\left(1 - \frac{1}{n}\right) \right]. \tag{6.70}$$

As we can see, $\Phi_{\tilde{t}}$ is real when $n = 1$, but complex for general values of n.

At the saddle point, we find that

$$I_n = \frac{4\pi^2\phi_b}{n\beta}, \tag{6.71}$$

which gives the Rényi entropy that matches the result found in:

$$S_n = \frac{1}{1-n}(I_n - nI_1) = \left(1 + \frac{1}{n}\right)\frac{4\pi^2\phi_b}{\beta}. \tag{6.72}$$

Next we will show that the saddle point we find (6.70) is exactly the same as the real-time replica wormhole solution found in [4]. The manifold has the same structure as

shown in Figure 6.5. On each sheet, the metric and dilaton are

$$\begin{aligned} ds^2 &= \frac{4\left(\tilde{x}^+\tilde{x}^-\right)^{\frac{1-n}{n}}}{n^2\left(1-\left(\tilde{x}^+\tilde{x}^-\right)^{\frac{1}{n}}\right)^2}d\tilde{x}^+d\tilde{x}^-, \\ \phi &= \alpha\frac{1+\left(\tilde{x}^+\tilde{x}^-\right)^{\frac{1}{n}}}{1-\left(\tilde{x}^+\tilde{x}^-\right)^{\frac{1}{n}}}, \end{aligned} \tag{6.73}$$

where $\tilde{x}^{\pm} = x_P \pm t_P$. The splitting surface is located at $\tilde{x}^+ = \tilde{x}^- = 0$, and each ket/bra piece of spacetime lie to the past of some Cauchy surface that passes through $t = 0$ on both boundaries and the splitting surface.

To compare solutions, we need to first figure out what our time shift δ corresponds to in the solution (6.73). It is easy to compute δ using the Euclidean path integral, which is shown in figure 6.8. There the periodicity for the Euclidean boundary time τ is $n\beta$. Following the procedure in [182], we shoot a geodesic from $\tau = 0$ on the boundary, we end up with $\tau = \frac{n\beta}{2}$. Since the time shift is defined in terms of the Lorentzian time $t = i\tau$, we get

$$\delta_{HJ} = \frac{i\Delta\tau - i\beta/2}{2} = \frac{i(n-1)\beta}{4} \tag{6.74}$$

where we subtracted $i\Delta\tau$ by $i\beta/2$ due to the KMS relation relating the time coordinates on left and right boundaries in Lorentzian signature. Since $\delta = -\delta_{HJ}$ at $t = 0$, this time shift is exactly the same as that in our current work

$$\delta = \frac{i(-2\pi\phi_b + \beta\Phi_{h,n})}{4\Phi_{h,n}} = -\frac{i(n-1)\beta}{4}. \tag{6.75}$$

We first define the global time coordinate T that lives on the m-th ket

$$\cos T = \operatorname{sech}\left(\frac{\Phi_h}{\phi_b}(\tilde{t} - \delta)\right). \tag{6.76}$$

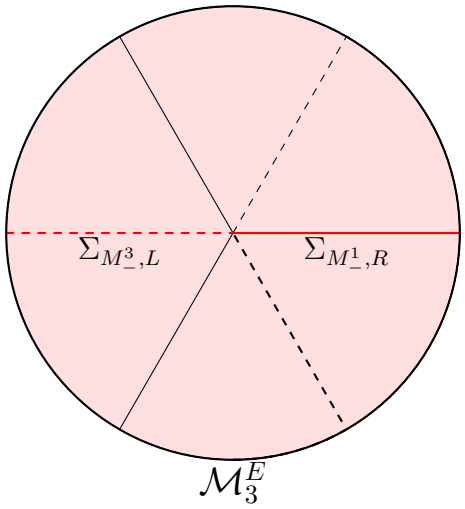

Figure 6.8: The replica manifold in Euclidean signature for $n = 3$.

and convert it to the $\tilde{x}^{\pm}$ coordinates

$$\tan T = \frac{(\tilde{x}^+)^{1/n} - (\tilde{x}^-)^{1/n}}{1 + (\tilde{x}^+\tilde{x}^-)^{1/n}} \tag{6.77}$$

$$X = \frac{(\tilde{x}^+)^{1/n} + (\tilde{x}^-)^{1/n}}{1 - (\tilde{x}^+\tilde{x}^+)^{1/n}}. \tag{6.78}$$

But note that in the saddle (6.73) the splitting surface can be approached in the real section of the metric, i.e. at $\tilde{x}^+ = \tilde{x}^- = 0$. In our solution, it is located at $\tilde{t} = \delta, X = 0$, which is no longer in the real section since δ is purely imaginary.

Chapter 7

Time-independence of gravitational Rényi entropies and unitarity in quantum gravity

7.1 Introduction

Many points of view have long motivated the idea that, in order to describe measurements of distant observers, black holes can be modeled as a quantum system with density of states $e^{S_{BH}}$ whose evolution is unitary up to possible interactions with other quantum systems; see e.g. [184, 185, 186] for reviews. Here S_{BH} is the Bekenstein-Hawking entropy of the black hole. Following [55], we refer to the above idea as Bekenstein-Hawking unitarity (or BH unitarity).[1] This property would in particular imply that Hawking radiation from evaporating black holes must carry information in a manner famously described by Page [129]. The recent replica wormhole derivations [39, 38] of the expected 'Page curve' for the entropy of this radiation thus provide strong evidence that there is

[1] It was instead called 'the central dogma' in [130] in analogy with the term's use in biology.

a sense in which BH unitarity holds.

Our goal here is to provide additional support for the idea that time evolution in quantum gravity is implemented by unitary operators on appropriate Hilbert spaces. For simplicity, we consider asymptotically AdS spacetimes. In that context one may think of this program as further verifying properties predicted by unitarity in some dual field theory description. But one may also take point of view that the bulk theory decomposes into superselection sectors defined by states in a so-called 'baby universe' sector of the theory, and that we verify predictions of the hypothesis that time evolution is unitary in each such superselection sector; see [146, 147, 148], related remarks in [50, 51, 38], and axiomatic arguments in [54, 55].

In this context, recall that a key hallmark of unitarity is the preservation of the eigenvalues of any density matrix in an isolated system.[2] This can be readily probed, and in some cases proven, by checking time-independence of the associated Rényi entropies $S_n = -\frac{1}{n-1}\log\left(\frac{\mathrm{Tr}[(\rho(D))^n]}{[\mathrm{Tr}(\rho(D))]^n}\right)$.

In the context of Einstein-Hilbert gravitational systems, an analogous result was established in [78, 127]. These works considered the Hubeny-Rangamani-Takayanagi (HRT) surface γ_{HRT} [27] associated with the entropy $S(D)$ of a domain of dependence D on an asymptotically AdS boundary. They then used the bulk Raychaudhuri equation to show that γ_{HRT} must be causally inaccessible from D when the Lorentzian bulk spacetime satisfies the null energy condition. As a result, no choice of boundary conditions on D can influence the HRT entropy determined by the area of γ_{HRT}. In other words, the

[2]In particular, this result (or even just preservation of von Neumann entropy) implies that time evolution maps pure states to pure states. If one also assumes time evolution to be a quantum channel, then the channel must in fact be unitary for this property to hold. This conclusion follows from the so-called Stinespring dilation theorem [187], which allows any quantum channel to be represented by tensoring the given system with some ancilla state, acting with a unitary on the joint system, and then tracing out the ancilla. If this procedure maps pure states to pure states, then the joint-system unitary cannot create entanglement with the ancilla and must thus define a unitary on the original system alone. We thank Geoffrey Penington for discussions regarding this point.

von Neumann entropy is invariant under any time evolution for which the system can be said to remain closed. But corresponding results remain to be established for $S_n(D)$ with $n > 1$.

This work begins to bridge this gap by studying saddle points of the real-time gravitational path integral for $S_n(D)$. In the context of an AdS bulk that is dual to a unique field theory, this $S_n(D)$ is the standard Rényi entropy. But in general the quantity $S_n(D)$ computed by these path integrals is more accurately described as a so-called swap Rényi entropy[3] [55]; see also [188].

Indeed, for reasons that we now describe, it would be even better to call the $S_n(D)$ we study an 'annealed swap Rényi entropy.' In a baby universe scenario for the bulk, this $S_n(D)$ is expected to closely approximate the average over superselection sectors of the corresponding Rényi entropy in each sector [54, 55]. However, it will differ from this average for two reasons: The first is that it is an 'annealed average,' meaning that we actually study the average $\exp(-S_n)$ and then take a logarithm. The second is a similar issue due to the fact that the normalization $Tr\rho$ can vary among members of the ensemble, but we normalize only by the average of $Tr\rho$. I.e., denoting averaging over superselection sectors by an overline, our gravitational Reńyi gives

$$S_n := -\frac{1}{n-1} \log \left(\frac{\overline{\mathrm{Tr}\left[(\rho(D))^n\right]}}{\left[\overline{\mathrm{Tr}\left(\rho(D)\right)}\right]^n} \right). \tag{7.1}$$

Expression (7.1) can also be used to relate our gravitational Reńyi to averages of $\mathrm{Tr}\left[(\rho(D))^n\right]$ over any ensemble of dual theories. In either context, we will use the term annealed swap Reńyi to refer to all of the complications of (7.1).

We consider contexts where the real-time (swap) replica path integral is dominated by

[3]From the purely bulk perspective, the term 'swap entropy' is physically most appropriate when we couple the AdS system to a non-gravitational bath and compute a (swap) entropy for some subset of the bath. We will nevertheless also use it in the above context where no bath is present.

a saddle that preserves both replica and conjugation symmetry. Examples of such real-time saddles were recently presented in [4]. Such path integrals and their saddles were described in [34, 55] and especially [6]. While parts of the saddle-point spacetime have a complex-valued metric, with the above symmetries there is a real Lorentz-signature metric on the regions spacelike separated from the replica-invariant surface $\boldsymbol{\gamma}$ (aka 'the splitting surface') [6]. And while the real-time saddles described in [6] are singular at $\boldsymbol{\gamma}$, we show that there is an appropriate sense in which $\boldsymbol{\gamma}$ remains extremal for $n > 1$.

For theories that satisfy the null energy condition on-shell, by making one assumption it will then follow from the results of [78, 127] that $\boldsymbol{\gamma}$ must again be causally inaccessible[4] from D. Although the argument is more subtle than in the HRT context, this will then again imply the Renyi entropies $S_n(D)$ to be independent of any choices within D. The key point is that our saddles will extend into the future only up to some surface Σ_{M_-} that is spacelike separated from $\boldsymbol{\gamma}$. In particular, much as in a Schwinger-Keldysh contour, our saddles will contain both future-directed pieces of spacetime and past-directed pieces of spacetime that meet in a timefold on Σ_{M_-}. The replica and conjugation symmetries require the solutions on future- and past-directed pieces to be related by complex conjugation, so that coincide in the region spacelike related to $\boldsymbol{\gamma}$ where the solution is real. Since the future- and past-directed pieces are weighted respectively by e^{iS} and e^{-iS} in the path integral, the contributions from the region spacelike separate from $\boldsymbol{\gamma}$ cancel, and the result is unchanged if we simply take Σ_{M_-} to lie along the past light cone of $\boldsymbol{\gamma}$. But doing so removes the entirety of D from the boundary so that the remaining saddle is manifestly independent of choices within D.

Furthermore, the reader may recall from [29] that one may use the generalized second law (GSL) to upgrade the arguments of [78, 127] to include quantum corrections. The

[4]Since only part of the spacetime is real and of Lorentz signature, this phrase remains to be properly defined. It will be discussed briefly in section 7.1.1 and in more detail in section 7.2.4.

same will again be true for our $n > 1$ Rényi problem. (One may of course consider the the generalized second law to follow from the quantum focussing condition of [189].)

Throughout this work we focus on the case of Einstein-Hilbert gravity with minimal couplings to any matter fields, though as noted in [6] the generalization to higher-derivative gravity is straightforward. For the interested reader, a brief summary of the argument for extremality of $\boldsymbol{\gamma}$ can be found in section 7.1.1 below. Other readers may prefer to proceed directly to the main discussion of sections 7.2-7.4.

The main text will begin with a brief review of the real-time gravitational path integral for $S_n(D)$ following [34, 55] and especially [6]. This material is presented in section 7.2, along with a description of the relevant saddle points. Section 7.2.4 then argues at the classical level that the splitting surface $\boldsymbol{\gamma}$ is extremal in saddles that preserve replica and conjugation symmetry. It also discusses the precise sense in which this requires $\boldsymbol{\gamma}$ to be causally inaccessible from D and in which it makes $S_n(D)$ independent of sources on D or choices of Cauchy surfaces Σ_D for D. Section 7.3 then follows with the upgraded argument that includes quantum corrections. As a supplement to the quantum argument, appendix F.1 illustrates the stationarity of S_{QFT} at $\boldsymbol{\gamma}$ an example in which the quantum corrections come from a bulk QFT that happens to be holographic; i.e., in which the matter entropy is described by an HRT surface in a higher-dimensional spacetime. We close with a broader discussion of unitarity in quantum gravity in section 7.4.

7.1.1 Summary of the extremality arguments

Let us briefly explain why $\boldsymbol{\gamma}$ should be extremal in our Rényi problem. As described in [6], in a saddle point geometry $\mathcal{M}_n$ for the real-time n-replica path integral, the metric near the splitting surface must have an asymptotic expansion of a certain form. This expansion appears singular as presented in [6], but as explained there it in fact

matches the form that would be obtained by applying a particular Wick rotation to a smooth Euclidean space $\mathcal{M}_n^E$, and in particular to a Euclidean space with no conical singularities. It is merely that the Wick rotation makes use of singular coordinates on the smooth geometry $\mathcal{M}_n^E$. Furthermore, the fact that the original real-time saddle $\mathcal{M}_n$ preserves replica symmetry requires $\mathcal{M}_n^E$ to have a $\mathbb{Z}_n$ symmetry that preserves the splitting surface $\boldsymbol{\gamma}$, but that rotates the tangent space at each point of $\boldsymbol{\gamma}$ in the plane orthogonal to $\boldsymbol{\gamma}$. Since the codimension-2 extrinsic curvature of $\boldsymbol{\gamma}$ must be invariant under this $\mathbb{Z}_n$ rotation, it must in fact vanish. In particular, the trace of the extrinsic curvature vanishes and $\boldsymbol{\gamma}$ is extremal in $\mathcal{M}_n^E$.

While the splitting surface $\boldsymbol{\gamma}$ is necessarily singular in the original real-time solution, the above facts imply that there is an arbitrarily smooth[5] spacetime $\hat{\mathcal{S}}_R$ (the 'right shadow of $\mathcal{M}_n$') with an extremal surface $\boldsymbol{\gamma}$ such that $\hat{\mathcal{S}}_R$ coincides with any single sheet of the original real saddle $\mathcal{M}_n$ in a connected region spacelike separated from $\boldsymbol{\gamma}$ that contains the boundary domain D. Furthermore, $\hat{\mathcal{S}}_R$ can be constructed by finding 'smoother' coordinates in the original real-time solution without reference to analytic continuation on $\mathcal{M}_n^E$. We will refer to this region of $\mathcal{M}_n$ as the 'right wedge[6]' of $\mathcal{M}_n$, which is why and we call $\hat{\mathcal{S}}_R$ the 'right shadow.' Although its geometry depends on n, we suppress the label n on $\hat{\mathcal{S}}_R$.

Finally, as noted in [6] the above symmetries require the metric to be real and Lorentz signature in the region spacelike separated from $\boldsymbol{\gamma}$. As a result, we may take $\hat{\mathcal{S}}_R$ to be both real and Lorentz-signature; indeed, this is what gives a well defined notion of 'the region spacelike separated from $\boldsymbol{\gamma}$' used above. In addition, since the null convergence condition holds where $\hat{\mathcal{S}}_R$ coincides with the original saddle $\mathcal{M}_n$, by taking limits it also holds on the closure of this region in $\hat{\mathcal{S}}_R$. But in real Lorentz-signature spacetimes

[5] I.e., $\hat{\mathcal{S}}_R$ can be chosen to be C^m for arbitrary m.

[6] As an n-replica geometry, $\mathcal{M}_n$ in fact contains n such regions, but we may choose any one to call the right wedge.

satisfying the null convergence condition, refs. [78, 127] showed any extremal surface anchored to the boundaries of Cauchy surfaces of D to be causally inacessible from D. The fact that $\hat{\mathcal{S}}_R$ and $\mathcal{M}_n$ coincide in the region spacelike separated from $\boldsymbol{\gamma}$ then provides a sense in which this conclusion also holds in $\mathcal{M}_n$; see section 7.2.4 for details.

The above perspective on the classical case now suggests a generalization that includes quantum corrections. If the splitting surface is also a stationary point of the generalized entropy $S_{gen}[\gamma] = \frac{A}{4G} + S_{QFT}$, then the quantum focussing condition of [189] (or, indeed, just the GSL as in [29]) will again allow us to conclude that $\boldsymbol{\gamma}$ must be causally separated from D [29].

One would thus like to argue as in the classical case that replica symmetry requires S_{gen} to be stationary on $\boldsymbol{\gamma}$. However, for any codimension-2 surface γ (which will generally differ from $\boldsymbol{\gamma}$), the bulk entropy $S_{QFT}[\gamma]$ refers to the entropy of quantum fields on a partial Cauchy surface stretching from γ to some boundary region. As shown in figure 7.5, this choice manifestly breaks replica symmetry and thus appears to invalidate the desired argument. Indeed, as shown in the same figure, the very requirement that γ can be connected to this boundary region by a partial Cauchy surface means if $S_{QFT}[\gamma]$ is defined at all, then $S_{QFT}[\gamma']$ will *not* be defined for any γ' related to γ by a non-trivial replica symmetry.

However, within the region where it is defined, S_{QFT} can be computed by considering the response of the partition function for bulk quantum fields to a change in boundary conditions that *does* respect replica symmetry.[7] As a result, one may extend the definition of S_{QFT} in a manner that preserves replica symmetry. We use this observation below to show that replica symmetry requires both A and S_{QFT} to be separately stationary on the splitting surface $\boldsymbol{\gamma}$, so that $S_{gen} = A/4G + S_{QFT}$ is stationary as well.

[7]This is just the usual replica trick applied to quantum fields propagating on the real-time replica wormhole geometry; see section 7.3.

7.2 Real-time path integrals with splitting surfaces

This section provides an extremely brief summary of the real-time gravitational path integral computation for $S_n(D)$ and the relevant saddles following [34, 55] and especially [6]. The general structure of such path integrals is described in section 7.2.1, while boundary conditions at a special 'splitting surface' are described in section 7.2.2. Saddles are further discussed in section 7.2.3. The reader may also wish to consult [4] for concrete examples.

7.2.1 Real-time Rényi path integrals

The boundary conditions for a gravitational path integral are typically chosen by first considering a corresponding non-gravitational problem. This long tradition is often justified by appealing to AdS/CFT or a broader holographic principle, but as described in [55], in many cases it also follows from a certain operational perspective associated with coupling non-gravitational systems to the gravitational system of interest.[8] But any of these perspectives motivates us to begin with a discussion of real-time Rényi path integrals for systems in which gravity is not dynamical.

To be specific, let us first consider the real-time path integral computation of $S_n(D)$ in a non-gravitating relativistic quantum field theory on some Lorentz signature spacetime $\mathcal{B}$. Recall that, given a (perhaps improperly normalized) density matrix $\rho(D)$ on a domain of dependence D, we define

$$S_n(D) := -\frac{1}{n-1} \log \left(\frac{\mathrm{Tr}\left[(\rho(D))^n\right]}{\left[\mathrm{Tr}\left(\rho(D)\right)\right]^n} \right). \tag{7.2}$$

Furthermore, given a pure state $|\psi\rangle$ on the entire system, one can define the density

[8] Though this may then be associated with refinements in the interpretation, such as replacing entropies by so-called swap entropies.

matrix $\rho(D)$ associated with some domain of dependence $D \subset \mathcal{B}$ by tracing $|\psi\rangle\langle\psi|$ over some Cauchy surface $\Sigma_{\bar{D}}$ for the region $\bar{D} \subset \mathcal{B}$ that is spacelike separated from D. Powers $(\rho(D))^n$ can then be computed by evaluating each copy of $\rho(D)$ on some cauchy surface Σ_D of D and performing appropriate index contractions. And we may similarly compute $\mathrm{Tr}[(\rho(D))^n]$ by contracting the final two free indices. Unitarity of the QFT then requires the result to be independent of the choices of $\Sigma_{\bar{D}}$ and Σ_D. It also requires the result to be unchanged by the addition of any sources on either D or $\bar{D}$.

As a result, if we are given a representation of $|\psi\rangle$ as a path integral over some manifold $\mathcal{B}_-$ with boundary $\partial\mathcal{B}_-$ containing $\Sigma_{\bar{D}} \cup \Sigma_D$, it is straightforward to construct a path integral for $\mathrm{Tr}[(\rho(D))^n]$. In general, the manifold $\mathcal{B}_-$ might be Euclidean, Lorentzian, complex, or a Schwinger-Keldysh-like combination of these options. However, the notation $\mathcal{B}_-$ reflects the fact that in many cases one would like to prepare some state in the past and then evolve it forward in time to $\Sigma_{\bar{D}} \cup \Sigma_D$. In such cases $\mathcal{B}_-$ will contain at least the (real and Lorentz-signature) region of $\mathcal{B}_-$ immediately to the past of $\Sigma_{\bar{D}} \cup \Sigma_D$.

As shown in figure 7.1, the path integral for $\mathrm{Tr}[(\rho(D))^n]$ is thus naturally represented as a path integral over a spacetime $\mathcal{B}_n$ constructed by cutting open n copies of $\mathcal{B}_-$ and n copies of an appropriate adjoint manifold[9] $\mathcal{B}_-^\dagger$ and pasting them together in a manner that – at least in simple cases – results in $\mathcal{B}_n$ having only a single connected component. However, even when $\mathcal{B}_-$ is real and Lorentz-signature near $\Sigma_{\bar{D}} \cup \Sigma_D$, the Rényi manifold $\mathcal{B}_n$ fails to have a standard causal structure on $\Sigma_{\bar{D}} \cup \Sigma_D$, and in particular at $\partial\Sigma_{\bar{D}} = \partial\Sigma_D$. But the path integral remains well-defined, since on these surfaces it merely implements the above contractions.

We now turn to the corresponding gravitational problem in which one defines Rényis

[9]The path integral weight for a region of in the adjoint $\mathcal{B}_-^\dagger$ is the complex conjugate that for the corresponding region of $\mathcal{B}_-$. In particular, sources in $\mathcal{B}_-^\dagger$ are the complex conjugates of sources in $\mathcal{B}_-$, and in terms of the Lorentz-signature action S_L regions of $\mathcal{B}_-^\dagger$ are weighted by e^{-iS_L} instead of e^{iS_L}.

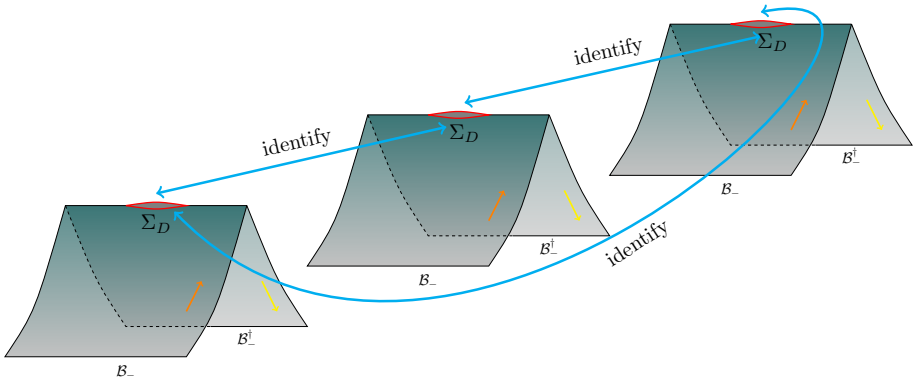

Figure 7.1: The manifold $\mathcal{B}_n$ used compute the path integral for $\mathrm{Tr}[(\rho(D))^n]$ in a non-gravitating QFT. Here Σ_D is a Cauchy surface of D and the figure shows $n = 3$.

via the standard formula

$$S_n(D) = \frac{1}{1-n} \log\left(\frac{Z[\mathcal{B}_n]}{Z[\mathcal{B}]^n}\right) = \frac{1}{n-1}\left(I_n - n\, I_1\right) , \tag{7.3}$$

where $Z[\mathcal{B}_n]$ is the gravitational path integral over spacetimes with a fixed asymptotically-AdS boundary $\mathcal{B}_n$ of the form constructed above. In particular, $\mathcal{B}_n$ has a $\mathbb{Z}_n$ replica symmetry that cyclicly permutes copies of $\mathcal{B}_- \cup \mathcal{B}_-^\dagger$, as well as a conjugation symmetry that exchanges each copy of $\mathcal{B}_-$ with an associated $\mathcal{B}_-^\dagger$ (and thus complex-conjugating all sources). However, the individual bulk configurations that contribute to $Z[\mathcal{B}_n]$ are allowed to break either or both symmetries. In the semiclassical limit, we can evaluate the above Rényis using $I_n := -\log Z[\mathcal{B}_n] \approx -i\, S_L[\mathcal{M}_n]$ for the appropriate saddles $\mathcal{M}_n$.

Now, the bulk spacetimes over which we integrate must be compatible with the structure of $\mathcal{B}_n$ near $\Sigma_{\bar{D}} \cup \Sigma_D$. Following [55, 6] we specify the desired bulk spacetimes by first considering the set M_- of bulk spacetimes M_- that contribute to the gravitational path integral with asymptotic boundary conditions $\mathcal{B}_-$, and thus which also end on some bulk surface Σ_{M_-} with boundary $\partial\Sigma_M = \Sigma_{\bar{D}} \cup \Sigma_D$ at which the induced metric is to be fixed as an additional boundary condition. The path integral $Z[\mathcal{B}_n]$ will then be defined to sum over bulk spacetimes $\mathcal{M}_n$ constructed by choosing $2n$ of the above spacetimes

$M_-^i, \tilde{M}_-^i \in \mathsf{M}_-$ for $i = 1, \ldots n$ and applying a cut-and-paste procedure to M_-^i and the adjoint manifolds $\tilde{M}_-^{\dagger i}$ analogous to that described for $\mathcal{B}_n$ above. Here, however, for each final bulk surface $\Sigma_{M_-^i}, \Sigma_{\tilde{M}_-^{\dagger i}}$ we may choose an arbitrary[10] 'splitting surface' $\boldsymbol{\gamma}_i, \tilde{\boldsymbol{\gamma}}_i$ that partitions $\Sigma_{M_-^i}, \Sigma_{\tilde{M}_-^{\dagger i}}$ into two pieces (in analogy with the way that $\partial\Sigma_D$ partitions $\Sigma_{\bar{D}} \cup \Sigma_D$ into $\Sigma_{\bar{D}}$ and Σ_D). Furthermore, since the bulk manifolds $\Sigma_{M_-^i}, \Sigma_{\tilde{M}_-^{\dagger i}}$ are generally distinct, the bulk metric generally fails to be continuous where two such surfaces are pasted together. When $\mathcal{M}_n$ is discontinuous in this way, we take it to have zero amplitude; i.e, the process of pasting together such surfaces leads to an appropriate delta-function that concentrates the path integral's integration measure on those $\mathcal{M}_n$ for which the bulk metric is continuous at each $\Sigma_{M_-^i}, \Sigma_{\tilde{M}_-^{\dagger i}}$. This will also result in various constraints relating the induced metrics on the splitting surfaces $\boldsymbol{\gamma}_i, \tilde{\boldsymbol{\gamma}}_i$, though the detailed form of such constraints depends on the particular pattern of cut-and-paste operations required to form a given $\mathcal{M}_n$.

It remains to further specify the path integral weight for $\mathcal{M}_n$. Since the action is local, we can specify the weight for each region of $\mathcal{M}_n$ independently. For regions away from $\Sigma_{M_-^i}, \Sigma_{\tilde{M}_-^{\dagger i}}$, this is just the relevant weight $e^{\pm iS_L}$ for the corresponding region of $M_-^i, \tilde{M}_-^{\dagger i}$. Indeed, we will use the same rule for regions that intersect $\Sigma_{M_-^i}, \Sigma_{\tilde{M}_-^{\dagger i}}$ but which remain away from all splitting surfaces $\boldsymbol{\gamma}_i, \tilde{\boldsymbol{\gamma}}_i$. In doing so, we should recall that the action S_L controlling the weight for $M_-^i, \tilde{M}_-^{\dagger i}$ must include a Gibbons-Hawking term since such pieces each individually describe contributions to a path integral with fixed induced metric on $\Sigma_{M_-^i}, \Sigma_{\tilde{M}_-^{\dagger i}}$. See figure 7.2 for an illustration of $\mathcal{M}_n$.

It now remains to specify the action for regions that include a splitting surface $\boldsymbol{\gamma}_i, \tilde{\boldsymbol{\gamma}}_i$. For Einstein-Hilbert gravity we may follow the guiding principle that, while the above cut-and-paste operations will introduce singularities at the codimension-2 surfaces $\boldsymbol{\gamma}_i, \tilde{\boldsymbol{\gamma}}_i$,

[10] In particular, such splitting surfaces may have multiple connected components. This allows for the Rényi equivalent of 'islands' [92].

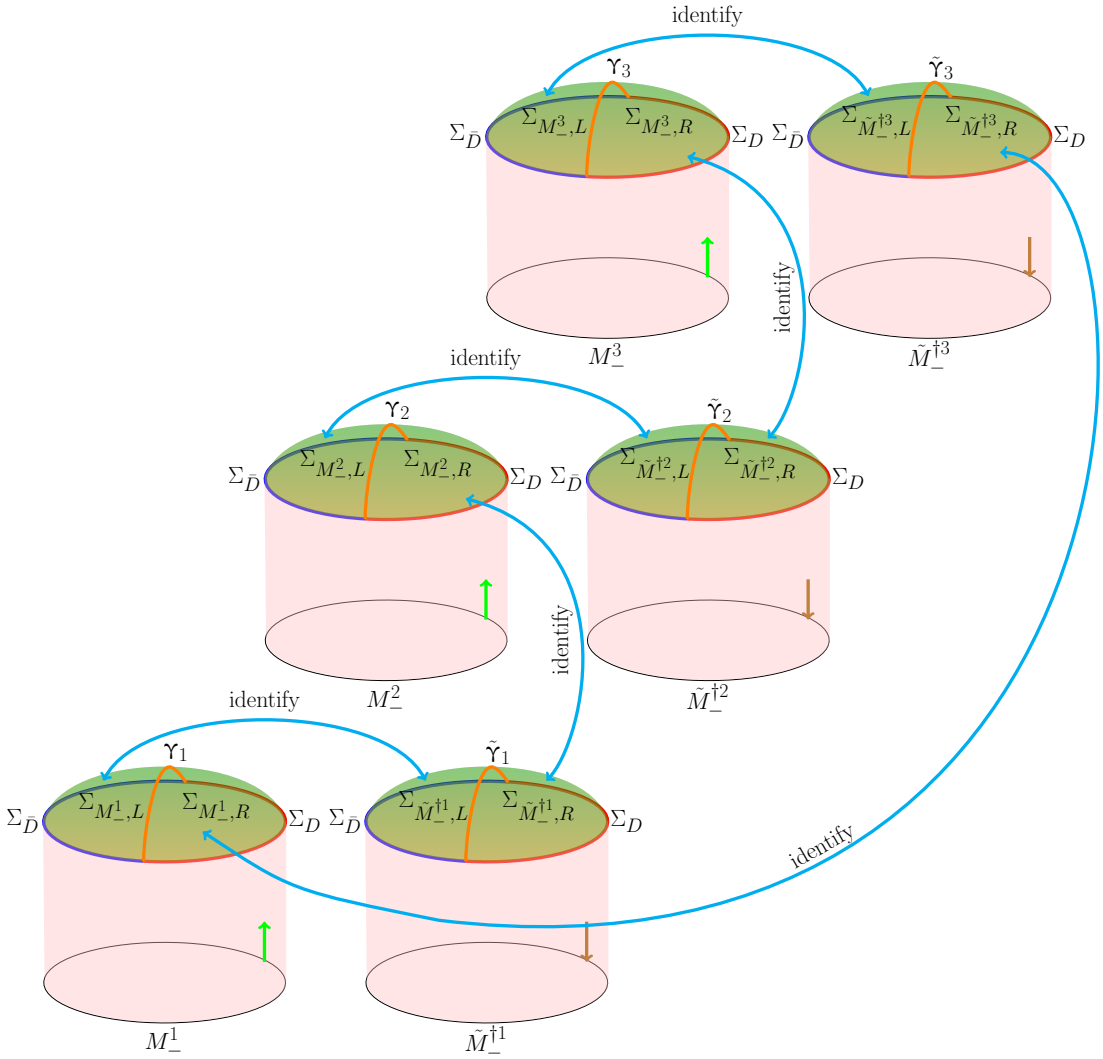

Figure 7.2: A typical bulk configuration of the gravitational path integral that computes $\mathrm{Tr}[(\rho(D))^n]$ for $n = 3$.

it is only the structure in the transverse two-planes to $\boldsymbol{\gamma}_i, \tilde{\boldsymbol{\gamma}}_i$ that will be singular. As a result, it suffices to understand the result for two-dimensional $\mathcal{M}_n$ in detail, and then to simply integrate that result along the $\boldsymbol{\gamma}_i, \tilde{\boldsymbol{\gamma}}_i$. Furthermore, in two dimensions one can use the Gauss-Bonnet theorem to write the integral of $\sqrt{-g}R$ over any region $\mathcal{U}$ in terms of the Euler character $\chi(\mathcal{U})$ and an integral of the extrinsic curvature over the surface $\partial\mathcal{U}$ (which by definition avoids the codimension-2 singularities at $\boldsymbol{\gamma}_i, \tilde{\boldsymbol{\gamma}}_i$). While the Gauss-Bonnet theorem is most familiar in the Euclidean context, there is a generalization to complex two-dimensional spacetimes that in particular includes the case relevant to small regions $\mathcal{U}$ around each $\boldsymbol{\gamma}_i, \tilde{\boldsymbol{\gamma}}_i$ where the metric is real and (at least at points away from $\mathcal{U}$) has Lorentz signature. See [6] for details and [145] for an earlier use of the complex Gauss-Bonnet theorem to evaluate the gravitational action at a related singularity; see also the examples in [4].[11]

In summary, we may follow [6] in writing the desired path integral as

$$Z[\mathcal{B}_n] := \int_n [Dg]\, e^{i\,S}, \tag{7.4}$$

where the subscript n is a reminder that we integrate over spacetimes $\mathcal{M}_n$ of the form described above satisfying boundary conditions defined by $\mathcal{B}_n$. In particular, the above action takes the form

$$S(\mathcal{M}_n) = \sum_{i=1}^{n} \left[S_L(M_-^i) - S_L(\tilde{M}_-^{\dagger i}) \right] + S_{\boldsymbol{\gamma}}, \tag{7.5}$$

where $\boldsymbol{\gamma}$ is the union of $\boldsymbol{\gamma}_i, \tilde{\boldsymbol{\gamma}}_i$ modulo the identifications induced by the manner in which the $M_-^i, \tilde{M}_-^{\dagger i}$ are pasted together to form $\mathcal{M}_n$. For Einstein-Hilbert gravity, the

[11] If one wishes to generalize this argument to include higher derivative corrections, the complex Gauss-Bonnet theorem may no longer suffice to determine the action completely. However, one may still follow the Lorentz-signature version of the minimal-subtraction prescription described in the appendices of [73], together with the Legendre transforms also described in [73].

contribution $S_{\boldsymbol{\gamma}}$ is defined by using the complex Gauss-Bonnet theorem and integrating along $\boldsymbol{\gamma}$ as outlined above; see [6] for details. As a reminder, for AdS Einstein-Hilbert gravity with AdS scale ℓ_{AdS} the Lorentzian action of each piece is

$$\begin{aligned} S_L[M_-] = \frac{1}{16\pi G_N}\int_{M_-} d^{d+1}x\,\sqrt{-g}\left[R+\frac{d(d-1)}{\ell_{AdS}^2}\right] + \frac{1}{8\pi G_N}\int_{\mathcal{B}_-} d^d x\,\sqrt{|\gamma|}\,K \\ + \frac{1}{8\pi G_N}\int_{\Sigma_{M_-}} d^d x\,\sqrt{h}\,K + S_{\rm ct}(\mathcal{B}_-)\,, \end{aligned} \tag{7.6}$$

where $\mathcal{B}_-$ is the asymptotic boundary of the piece M_- (including any Euclidean or complex-signature regions of this asymptotic boundary), $S_{\rm ct}$ denotes an appropriate set of counter-terms, and the full boundary of M_- is $\partial M_- = \mathcal{B}_- \cup \Sigma_{M_-}$.

7.2.2 Boundary Conditions at the Splitting Surface

In describing the bulk spacetimes $\mathcal{M}_n$ that contribute to our path integral, we have thus far glossed over one important detail. The issue is that we should require the $\mathcal{M}_n$ to satisfy boundary conditions at $\boldsymbol{\gamma}$ for which the above S defines a good variational principle. It was shown in [6] that this is indeed the case if, on each piece $M_-^i, \tilde{M}_-^{\dagger i}$ and near any component of $\boldsymbol{\gamma}$, one introduces coordinates y^I along $\boldsymbol{\gamma}$ and $\tilde{x}^\pm$ in the transverse space (with the component of $\boldsymbol{\gamma}$ lying at $\tilde{x}^\pm = 0$) and requires the metric in this region

to take the form

$$ds^2 = \sigma(\tilde{x}^+, \tilde{x}^-)\, d\tilde{x}^+ d\tilde{x}^- + T\, \frac{(\tilde{x}^+\, d\tilde{x}^- - \tilde{x}^-\, d\tilde{x}^+)^2}{(\tilde{x}^+\tilde{x}^-)^{2-\hat{m}}} + q_{IJ}\, dy^I dy^J + 2\, W_J\, dy^J\, \frac{\tilde{x}^+ d\tilde{x}^- - \tilde{x}^- d\tilde{x}^+}{(\tilde{x}^+\tilde{x}^-)^{1-\hat{m}}},$$

with

$$\begin{aligned} &\sigma(\tilde{x}^+, \tilde{x}^-) \equiv \hat{m}^2 (\tilde{x}^+\tilde{x}^-)^{\hat{m}-1}\,, \\ &T = \mathcal{O}\Big((\tilde{x}^+\tilde{x}^-)^{\frac{\alpha\hat{m}}{2}}\Big)\,, \\ &q_{IJ} = \mathcal{O}\big((\tilde{x}^+\tilde{x}^-)^0\big)\,, \\ &W_J = \mathcal{O}\big((\tilde{x}^+\tilde{x}^-)^{\hat{m}}\big)\,, \end{aligned} \tag{7.7}$$

for some $\alpha > 1$ and some $\hat{m} > 0$. The metric coefficients T, q_{IJ}, W_J depend smoothly on the y^I coordinates. Note that, following the conventions of [6], σ is positive for $\hat{m} = 1$. One should thus think of $\tilde{x}^\pm$ as analogues of the Minkowski-space coordinates $x \pm t$ as opposed to the more standard null coordinates $t \pm x$.

It remains to specify some further details. For positive $\tilde{x}^\pm$ the fractional powers above are defined by taking the positive real root. But for negative $\tilde{x}^+$ we take $(\tilde{x}^+)^{\hat{m}} = e^{-i\hat{m}\pi}\, |\tilde{x}^+|^{\hat{m}}$ and for negative $\tilde{x}^-$ we define $(\tilde{x}^-)^{\hat{m}} = e^{+i\hat{m}\pi}\, |\tilde{x}^-|^{\hat{m}}$.

In addition, the notation $\mathcal{O}((\tilde{x}^+\tilde{x}^-)^q)$ in principle allows terms of the form $(\tilde{x}^+\tilde{x}^-)^q f(\frac{\tilde{x}^+}{\tilde{x}^-})$ for any smooth f. However, if there are $2k$ pieces $M^i_-, \tilde{M}^{\dagger i}_-$ that meet at the relevant component of $\boldsymbol{\gamma}$ (so that this component is formed by identifying $2k$ splitting surfaces $\boldsymbol{\gamma}_i, \tilde{\boldsymbol{\gamma}}_i$), then we also require the metric functions T, q_{IJ}, W_J to involve only integer powers of $(\tilde{x}^\pm)^{\frac{1}{k}}$, except perhaps in the combination $\tilde{x}^+\tilde{x}^-$. In other words, we require these coefficients to be functions of the triple $((\tilde{x}^+)^{\frac{1}{k}}, (\tilde{x}^-)^{\frac{1}{k}}, \tilde{x}^+\tilde{x}^-)$ such that these functions are analytic in the first two arguments in some neighborhood of the origin $\tilde{x}^+ = 0 = \tilde{x}^-$. As remarked in [6], such local analyticity is to be expected at any source-free regular

point of the equations of motion and does not restrict the generality of any saddle points that we will find. (Configurations invariant under the local $\mathbb{Z}_n$ replica symmetry will have $k = n$ at each component of $\boldsymbol{\gamma}$ and will be further restricted by the condition that they involve only integer powers of $\tilde{x}^{\pm}$, again with the possible exception of their appearance in the combination $\tilde{x}^{+}\tilde{x}^{-}$.)

7.2.3 Real-time Rényi saddles

We now briefly review general features of the saddle points $\mathcal{M}_n$ of the gravitational Rényi path integral $Z[\mathcal{B}_n]$. The fact that [6] showed the definitions of the previous section to lead to a good variational principle means that $\mathcal{M}_n$ is a stationary point when it satisfies the standard (and, in our conventions, Lorentz signature) Einstein equations away from $\Sigma_{M_-^i}, \Sigma_{\tilde{M}_-^{\dagger i}}$ together with two simple additional conditions on $\Sigma_{M_-^i}, \Sigma_{\tilde{M}_-^{\dagger i}}$. The first condition is just that where $\Sigma_{M_-^i}$ is sewn to some $\Sigma_{\tilde{M}_-^{\dagger j}}$ (but away from $\boldsymbol{\gamma}$), the codimension-1 extrinsic curvatures of these surfaces must agree (e.g., when both are computed using future-pointing normals). The second condition is that for each component of $\boldsymbol{\gamma}$ we must impose $k\hat{m} = 1$, where $k, \hat{m}$ are the parameters defined in and below equation (7.7). The latter condition comes from varying the action with respect to the area element on $\boldsymbol{\gamma}$, and may be thought of as the condition that the Ricci scalar contain no delta-function at this surface. As a result, that despite the singular form of (7.7), there remains some physical sense in which we might think of the metric as being in some sense"smooth."

Recall that $k \in \mathbb{Z}^+$, and also that the case $k = 1$ describes a simpler construction for which splitting surfaces were not in fact required. In this sense we have $k \geq 2$ at a nontrivial component of $\boldsymbol{\gamma}$. So at a nontrivial such component, the saddle-point condition $k\hat{m} = 1$ forbids $\hat{m}$ from being an integer. Examination of (7.7) then shows

that the metrics for such saddles are always complex-valued. Following [6], we assume that the original real contour of integration can be deformed to pass through such complex saddles, though it would be useful to investigate this more carefully in the future.

We will focus below on saddles $\mathcal{M}_n$ that preserve both replica and conjugation symmetry. One consequence of replica symmetry is that all components of $\boldsymbol{\gamma}$ have $k = n$. Another is that, as noted below (7.7), there must be a region around $\boldsymbol{\gamma}$ where the functions T, q_{IJ}, W_I are analytic in $\tilde{x}^{\pm}$ up to functions of the product $\tilde{x}^+\tilde{x}^-$.

Finally, when combined with conjugation symmetry, replica symmetry imposes a further constraint where any $\Sigma_{M^i_-}$ is sewn to some $\Sigma_{\tilde{M}^{\dagger j}_-}$. At such loci, any quantity on $\Sigma_{M^i_-}$ must be the complex conjugate of the corresponding quantity on $\Sigma_{\tilde{M}^{\dagger j}_-}$. In particular, since our sewing conditions require the induced metrics on these surfaces to agree, it follows that the induced metrics on $\Sigma_{M^i_-}, \Sigma_{\tilde{M}^{\dagger j}_-}$ must be real. And since the above saddle-point conditions require the extrinsic curvatures to agree on the part of this seam away from $\boldsymbol{\gamma}$, such extrinsic curvatures must be real as well. We conclude that replica- and conjugation-invariant saddles have real initial data on each $\Sigma_{M^i_-} \setminus \boldsymbol{\gamma}_i, \Sigma_{\tilde{M}^{\dagger j}_-} \setminus \tilde{\boldsymbol{\gamma}}_j$. Since the relevant equations of motion are the Lorentz-signature Einstein equations, we expect that we can use this initial data to construct real Lorentz-signature spacetimes that we may call the domain of dependence of each $\Sigma_{M^i_-} \setminus \boldsymbol{\gamma}_i, \Sigma_{\tilde{M}^{\dagger j}_-} \setminus \tilde{\boldsymbol{\gamma}}_j$. This is clear when the induced metric on $\Sigma_{M^i_-} \setminus \boldsymbol{\gamma}_i, \Sigma_{\tilde{M}^{\dagger j}_-} \setminus \tilde{\boldsymbol{\gamma}}_j$ is positive definite, in which case we have defined good Cauchy data on this surface. Furthermore, in that case uniqueness of the initial value problem tells us that this is in fact the desired saddle in the stated region. In other words, replica- and conjugation-invariant saddles must be real in what we may call 'the region spacelike separated from $\boldsymbol{\gamma}$.'

However, it remains to consider the case where the induced metric on $\Sigma_{M^i_-} \setminus \boldsymbol{\gamma}_i, \Sigma_{\tilde{M}^{\dagger j}_-} \setminus \tilde{\boldsymbol{\gamma}}_j$ fails to be positive definite. Such cases are not at all pathological, and in fact are easily generated from the positive-definite cases above. In such cases, the fact that the saddle

is real in the region spacelike separates from $\boldsymbol{\gamma}$ means that a factor of e^{iS} from some part of this region in a ket spacetime will exactly cancel against the corresponding e^{-iS} factor from the corresponding region of a bra spacetime. As a result, without changing the action or the validity of the saddle we can deform the original $\Sigma_{M_-^i} \setminus \boldsymbol{\gamma}_i, \Sigma_{\tilde{M}_-^{\dagger j}} \setminus \tilde{\boldsymbol{\gamma}}_j$ to an *arbitrary* surface spacelike separated from $\boldsymbol{\gamma}$ that connects $\boldsymbol{\gamma}$ with Σ_D. In particular, the deformed surface may contain timelike or null regions, in which case the induced metric will fail to be positive definite. We will assume that all cases where the induced metric fails to be positive definite can be obtained in this way. This is the one assumption foreshadowed in the introduction. It was also implicit in [6].

7.2.4 Time independence of classical (annealed) swap entropies

Having reviewed real-time gravitational Rényi path integrals and their saddles in section 7.2, we are now ready to verify the claim that – in any saddle that preserves replica and conjugation symmetry – the splitting surface $\boldsymbol{\gamma}$ can be treated as an extremal surface in a real Lorentz signature spacetime. A critical point is the observation reviewed above that such saddles do in fact have real and Lorentz signature metrics in the domains of dependence of the surfaces $\Sigma_{M_-^i} \setminus \boldsymbol{\gamma}_i, \Sigma_{\tilde{M}_-^{\dagger j}} \setminus \tilde{\boldsymbol{\gamma}}_j$.

Indeed, we will now use this observation to introduce what we will call a real 'shadow' of the replica wormhole described above. To begin, recall that $\boldsymbol{\gamma}$ partitions each boundary $\Sigma_{M_-^i}, \Sigma_{\tilde{M}_-^{\dagger j}}$ into a piece that ends on Σ_D and a piece that ends on $\Sigma_{\bar{D}}$. Let us refer to the pieces ending on Σ_D as the 'right' pieces $\Sigma_{M_-^i,R}, \Sigma_{\tilde{M}_-^{\dagger j},R}$ and the pieces ending on Σ_D as the 'left' pieces $\Sigma_{M_-^i,L}, \Sigma_{\tilde{M}_-^{\dagger j},L}$. Note that the initial data sets on any two right pieces are related by replica and conjugation symmetry, and that the same is true of the initial data sets on any two left pieces.

Consider then the initial data on some $\Sigma_{M_-^i,R}$. Since this data is real, the fact that

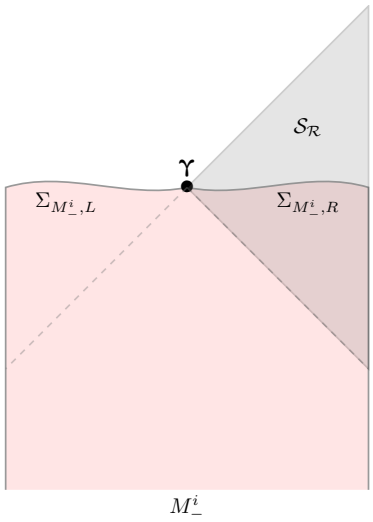

Figure 7.3: The 'right shadow' $\mathcal{S}_{\mathcal{R}}$ (shaded in gray) is the maximal AdS-Cauchy development of $\Sigma_{M^i_-,R}$. Note that $\mathcal{S}_{\mathcal{R}}$ includes regions both to the past and to the future of $\Sigma_{M^i_-,R}$. The region to the past also lies in M^i_- (shaded pink), while the region to the future does not. The intersection of $\mathcal{S}_{\mathcal{R}}$ and M^i_- has both shadings.

the Lorentz-signature Einstein equations have a good initial value problem allows us to construct a unique solution $\mathcal{S}_{\mathcal{R}}$ (the 'right shadow') describing the maximal AdS-Cauchy development[12] of $\Sigma_{M^i_-,R}$. Furthermore, $\mathcal{S}_{\mathcal{R}}$ must agree with the saddle point solution $\mathcal{M}_n$ on the domain of dependence of $\Sigma_{M^i_-,R}$ in M^i_-. In particular, near $\boldsymbol{\gamma}$ the shadow $\mathcal{S}_{\mathcal{R}}$ can be described by (7.7), where to be definite we choose $\tilde{x}^{\pm} > 0$ in $\mathcal{S}_{\mathcal{R}}$ (corresponding to our choice to think of this as the right wedge). However, since it lies in M^i_- the latter region exists only to the past of $\Sigma_{M^i_-,R}$, while $\mathcal{S}_{\mathcal{R}}$ includes a region to the future as well; see figure 7.3.

Now, in the region $\tilde{x}^{\pm} > 0$ we are free to introduce new coordinates $\tilde{X}^{\pm} = (\tilde{x}^{\pm})^{1/n}$.

[12]By an AdS-Cauchy development, we mean the analogue of a Cauchy development defined using the asymptotically AdS boundary conditions on D. In other words, the surface $\Sigma_{M^i_-,R}$ is allowed to be an AdS-Cauchy surface for this development in the sense of [78].

Recalling that $\hat{m} = 1/n$, in terms of such coordinates the metric (7.7) becomes just

$$\begin{aligned} ds^2 = d\tilde{X}^+ d\tilde{X}^- + n^2 T \frac{\left(\tilde{X}^+ d\tilde{X}^- - \tilde{X}^- d\tilde{X}^+\right)^2}{\tilde{X}^+\tilde{X}^-} \\ + q_{IJ}\, dy^I dy^J + 2n\, \tilde{W}_J\, dy^J \left(\tilde{X}^+ d\tilde{X}^- - \tilde{X}^- d\tilde{X}^+\right), \end{aligned}$$

with

$$\begin{aligned} T &= \mathcal{O}\Big((\tilde{X}^+\tilde{X}^-)^{\frac{\alpha}{2}}\Big), \\ q_{IJ} &= \mathcal{O}\Big((\tilde{X}^+\tilde{X}^-)^0\Big), \\ \tilde{W}_J &= \frac{W_J}{\tilde{X}^+\tilde{X}^-} = \mathcal{O}\Big((\tilde{X}^+\tilde{X}^-)^0\Big). \end{aligned} \tag{7.8}$$

Furthermore, the conditions on the coefficients T, q_{IJ}, W_I now state that they should be functions of the triple $\left((\tilde{X}^+)^n, (\tilde{X}^-)^n, \tilde{X}^+\tilde{X}^-\right)$ that are analytic in the first two arguments, at least in some neighborhood of $\tilde{X}^+ = \tilde{X}^- = 0$. As a result, the metric admits an extension $\hat{\mathcal{S}}_R$ to at least some negative values of both $\tilde{X}^+$ and $\tilde{X}^-$.

We would like to control the form of the extension $\hat{\mathcal{S}}_R$. The idea is to use the fact that we are interested in the saddle $\mathcal{M}_n$ which solves the Einstein equations for $\tilde{X}^\pm \neq 0$.

In particular, in the Euclidean context ref. [73] found a power series solution near the splitting surface which (at least at the level of function counting) had sufficient freedom to accommodate general smooth boundary conditions and which obeyed boundary conditions given by the Wick rotation of (7.7). Since the formal manipulation of power series is unchanged by Wick rotations, this immediately provides a similarly general solution to the Einstein equations in our context. We will thus now assume that any actual saddle $\mathcal{M}_n$ defined by sufficiently smooth boundary conditions can be described by such a power series. While it would be interesting to prove this statement rigorously, that task is beyond the scope of this work. We therefore leave it for appropriate mathematicians to investigate in the future.

In terms of $\tilde{X}^{\pm}$, and after the relevant Wick rotation and imposing replica symmetry and the condition $\hat{m} = 1/n$, the power series solution from [73] may be written as sums over integers p, q, s of the form

$$T \sim \sum_{\substack{p,q,s=0 \\ pq>0, \text{ or } s>0}}^{\infty} T_{pqs}(\tilde{X}^{+})^{pn}(\tilde{X}^{-})^{qn}(\tilde{X}^{+}\tilde{X}^{-})^{s}, \tag{7.9}$$

$$\tilde{W}_I \sim \sum_{p,q,s=0}^{\infty} W_{I,pqs}(\tilde{X}^{+})^{pn}(\tilde{X}^{-})^{qn}(\tilde{X}^{+}\tilde{X}^{-})^{s}, \tag{7.10}$$

$$q_{IJ} \sim \sum_{p,q,s=0}^{\infty} q_{IJ,pqs}(\tilde{X}^{+})^{pn}(\tilde{X}^{-})^{qn}(\tilde{X}^{+}\tilde{X}^{-})^{s}. \tag{7.11}$$

In particular, the restriction $pq > 0, \text{ or } s > 0$ in the sum for T means that for $n > 1$ the leading term will be $\tilde{X}^{+}\tilde{X}^{-}$. The coefficient $\frac{T}{\tilde{X}^{+}\tilde{X}^{-}}$ in (7.7) is thus smooth at $\tilde{X}^{\pm} = 0$.

Using the above power series expansion, we may choose the extension $\hat{\mathcal{S}}_R$ to negative $\tilde{X}^{\pm}$ to be arbitrarily smooth. And since it satisfies the Einstein equations on $\mathcal{S}_R$, we may choose the extension to satisfy the Einstein equations as well.[13] We also take $\hat{\mathcal{S}}_R$ to satisfy standard causality assumptions such as those used in [78, 127], perhaps at the cost of limiting the extension to negative values of $\tilde{X}^{\pm}$ that are very close to $\boldsymbol{\gamma}$. In particular, there is no need for the extension $\hat{\mathcal{S}}_R$ to be maximal in any sense.

By counting powers of $\tilde{X}^{\pm}$ is also easy to see that the codimension-2 extrinsic curvature of $\boldsymbol{\gamma}$ in $\hat{\mathcal{S}}_R$ must vanish in $\hat{\mathcal{S}}_R$.[14] Indeed, for even n comparing (7.7) with (7.9), (7.10), and (7.11) shows that every term in (7.7) is even under $\tilde{X}^{\pm} \to -\tilde{X}^{\pm}$, so we are free to take $\hat{\mathcal{S}}_R$ to have an exact $\mathbb{Z}_2$ symmetry about $\boldsymbol{\gamma}$ when n is even.[15]

[13] For this it suffices to first smoothly extend the initial data on some Cauchy surface and to then solve the Einstein equations.

[14] Aside from the terms independent of $\tilde{X}^{\pm}$, for integer $n > 1$ almost every term in (7.7) is at least quadratic in $\tilde{X}^{+}\tilde{X}^{-}$. The single exception is the leading contribution from W_J. But the term associated with the leading contribution from W_J is invariant under $\tilde{X}^{\pm} \to -\tilde{X}^{\pm}$ and so cannot contribute to the extrinsic curvature of the set $\boldsymbol{\gamma}$ at $\tilde{X}^{\pm} = 0$.

[15] For odd n, the fact that $\tilde{X}^{\pm} = (\tilde{x}^{\pm})^{1/n}$ maps positive real $\tilde{x}^{\pm}$ to positive real $\tilde{X}^{\pm}$ and also maps

For integer $n > 1$ we have now argued that $\boldsymbol{\gamma}$ has vanishing extrinsic curvature in an arbitrarily smooth spacetime $\hat{\mathcal{S}}_R$ which satisfies standard causality assumptions as well as the vacuum Einstein equations (and thus also the null convergence condition). In other words, the associated matter stress tensor vanishes identically and thus satisfied the null energy condition. Note that this result at $\tilde{X}^{\pm} = 0$ follows from smoothness and from the corresponding result at positive $\tilde{X}^{\pm}$. The results of [78, 127] then require D to be causally inaccessible from $\boldsymbol{\gamma}$.

This is essentially the desired result, though we should carefully state what this means for the original saddle $\mathcal{M}_n$ on which the metric in some regions is complex-valued. In order to do so, let us first return to $\hat{\mathcal{S}}_n$ and note that the boundary of the future of $\boldsymbol{\gamma}$ cannot intersect D, and neither can the boundary of the past. This is because D is an open set on the asymptotically AdS boundary, so such an intersection would require that D also intersect the interior of the causal past or future, contradicting the statement that it is causally inaccessible from $\boldsymbol{\gamma}$.

On the other hand, since the Cauchy surface $\Sigma_{M^i_-,R}$ intersects D, and since standard asymptotically AdS boundary conditions hold at D, the maximal AdS-Cauchy development $\mathcal{S}_{\mathcal{R}}$ of $\Sigma_{M^i_-,R}$ must contain part of D. In fact, since $\Sigma_{M^i_-,R}$ intersects D on a Cauchy surface for D, it intersects every connected component of D. Thus $\mathcal{S}_{\mathcal{R}}$ in fact contains at least part of every such connected component.

However, the boundary of the future of $\boldsymbol{\gamma}$ in $\hat{\mathcal{S}}_R$ is precisely the boundary of $\mathcal{S}_R$. Since this boundary cannot intersect D, it follows that any connected component of D

negative real $\tilde{x}^{\pm}$ to negative real $\tilde{X}^{\pm}$ means that in that case we can instead take the extension $\hat{\mathcal{S}}_R$ in the region where $\tilde{X}^{\pm}$ are both negative to coincide with the 'left shadow' $\mathcal{S}_L$ defined in analogy with $\mathcal{S}_R$ but using the maximal Cauchy development of $\Sigma_{M^i_-,L}$. Both properties are easy to see in the case where $\mathcal{M}_n$ is the Wick rotation of some $\mathcal{M}_n^E$, as comparison with [6] shows that $\hat{\mathcal{S}}_R$ can be defined by a different Wick-rotation of $\mathcal{M}_n^E$ that preserves smoothness. In effect, this is the Wick-rotation that would be obtained by interpreting the smooth $\mathcal{M}_n^E$ as an $n = 1$ geometry that computes the norm of some pure state by slicing it into two pieces, representing a single bra and a single ket, each of which contains $n/2$ replicas and such that the two pieces are related by a $\mathbb{Z}_2$ symmetry that complex-conjugates all sources. See figures in appendix F.2.

which intersects $\mathcal{S}_R$ is in fact fully contained in $\mathcal{S}_R$. And since this was the case for all such components, we in fact conclude that D is fully contained in the maximal Cauchy development of $\Sigma_{M^i_-,R}$.

This, then, is the desired result. For brevity, we will refer to it as stating that 'D is causally inaccessible from $\boldsymbol{\gamma}$ in $\mathcal{M}_n$'. This phrasing is motivated by the fact that, in any real Lorentz-signature globally-hyperbolic spacetime, any region R of a Cauchy surface Σ must be causally inaccessible from the maximal Cauchy development of the complementary region $\bar{R} = \Sigma \setminus R$.

However, the key point is that the solution is real on the maximal AdS Cauchy development of $\Sigma_{M^i_-,R}$, $\Sigma_{\tilde{M}^{\dagger j}_-,R}$. But our symmetries require the solution on any AdS-Cauchy development of $\Sigma_{M^i_-,R}$ to be the complex conjugate of that on the corresponding development of $\Sigma_{\tilde{M}^{\dagger j}_-,R}$. Thus the solutions on these developments agree and their contributions cancel in (7.5). Thus we obtain the same action if we choose $\Sigma_{M^i_-,R}$, $\Sigma_{\tilde{M}^{\dagger j}_-,R}$ to lie on the past light cone of $\boldsymbol{\gamma}$. But this has the effect of removing D entirely from the boundary $\mathcal{B}_n$ and thus makes manifest that the contribution of our saddle is independent of any choices within D. See figure 7.4.

7.2.5 Generalizations to include matter

The above arguments establish our result for vacuum Einstein-Hilbert gravity. Since we considered spacetimes of arbitrary dimension, we may then use Kaluza-Klein to deduce corresponding results for of Einstein-Hilbert gravity coupled to appropriate Kaluza-Klein matter, and in particular for the truncation of such theories to modes that preserve any symmetries of the internal manifold. Since non-linearities contribute only higher-order terms to our expansions above, this suggests that the exact form of the matter couplings is not relevant. We therefore expect our result to hold for arbitrary two-

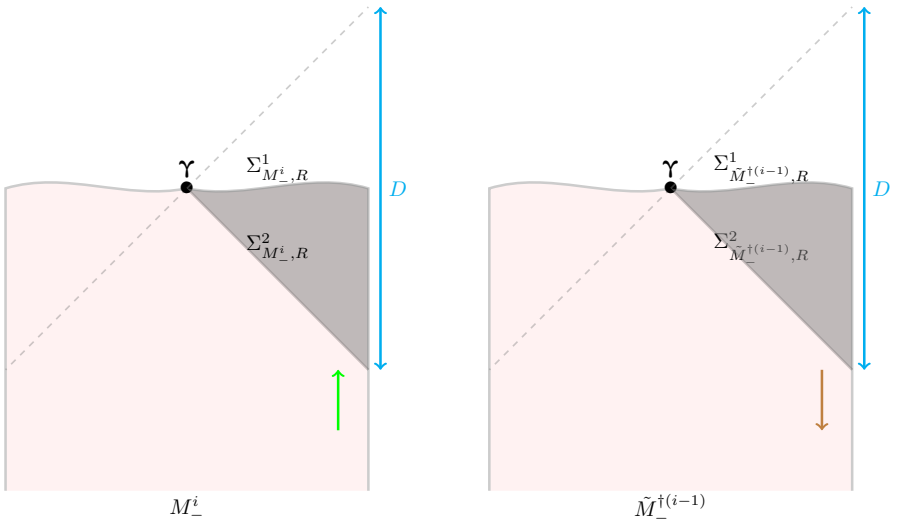

Figure 7.4: In every saddle, the sheets M^i_- and $\tilde{M}^{\dagger(i-1)}_-$ are sewn together by identifying an achronal surface $\Sigma_{M^i_-,R}$ in M^i_- with an achronal surface $\Sigma_{\tilde{M}^{\dagger(i-1)}_-,R}$ in $M^{\dagger(i-1)}_-$. These surfaces have boundaries consisting of $\boldsymbol{\gamma}$ and Σ_D; i.e., $\partial\Sigma_{M^i_-,R} = \partial\Sigma_{\tilde{M}^{\dagger(i-1)}_-,R} = \boldsymbol{\gamma} \cup \Sigma_D$. However, the action of saddles with replica and conjugation symmetry is independent of the choice of this achronal surface, and the action is also independent of the choice of Cauchy surface Σ_D for D. As a result, without changing the action we may deform any such $\Sigma^1_{M^i_-,R}$ and $\Sigma^1_{\tilde{M}^{\dagger(i-1)}_-,R}$ to surfaces $\Sigma^2_{M^i_-,R}$ and $\Sigma^2_{\tilde{M}^{\dagger(i-1)}_-,R}$ on the past lightcone of $\boldsymbol{\gamma}$. This makes manifest that the contribution of our saddle is independent of any choices within D.

derivative theories of matter minimally-coupled to Einstein-Hilbert gravity for which the matter sector satisfies the null energy condition. However, we leave a detailed proof of this generalization for future work.

7.3 Time independence of quantum-corrected (annealed) swap Rényis

Having established time-independence of gravitational annealed swap Rényis at leading order in G_N, it is of interest to consider quantum corrections. We focus here on corrections associated with matter fields, leaving aside subtleties associated with quantum corrections from gravitons. We expect that such subtleties can be dealt with using the techniques of [35], but we will not attempt to do so here.

In the classical case, we found that we could use a smooth real Lorentz signature 'shadow spacetime' to describe the area of any surface in $\mathcal{M}_n$ that was causally inaccessible from $\boldsymbol{\gamma}$. Moreover, replica symmetry of the classical replica saddle $\mathcal{M}_n$ led to a power series expansion of this area near $\boldsymbol{\gamma}$ which showed $\boldsymbol{\gamma}$ to be extremal. The null curvature condition on $\mathcal{M}_n$ then required D to be contained in the maximal AdS-Cauchy development of $\Sigma_{M_-^i}$, a situation that we summarize by saying that D is causally inaccessible from $\boldsymbol{\gamma}$.

We would like to simply extend this argument to include quantum corrections, replacing the null curvature condition with the quantum focussing condition (QFC) of [189]. This condition involves the entropy S_{QFT} of quantum fields on $\mathcal{M}_n$, which may be subtle in regions where the metric is complex. But it should have familiar properties in the regions where $\mathcal{M}_n$ is real and Lorentz signature.

Let us begin by studying the first-order quantum corrections about a classical saddle

replica $\mathcal{M}_n$. Then since the smooth shadow $\mathcal{S}_R$ is related by Cauchy evolution to a subset of a single sheet of $\mathcal{M}_n$., we may again describe the desired matter entropy S_{QFT} as a function on $\mathcal{S}_R$.

The remaining steps in the classical argument then followed from properties of power series expansions near $\boldsymbol{\gamma}$. These expansions were motivated by requiring the relevant quantities to satisfy the classical equations of motion. But to apply analogous reasoning in the quantum case we would need to understand the power series expansion for S_{QFT}. Since we do not have classical equations of motion to solve for S_{QFT}, we will need to pursue another approach.

We describe two such approaches below in section 7.3.1 and 7.3.2. Each alone addresses only special cases. The first explicitly assumes that $\mathcal{M}_n$ can be Wick-rotated to define a smooth Euclidean (or perhaps complex) manifold, while the second works directly in Lorentz signature but assumes the QFT to be holographic and works in the approximation where S_{QFT} can be computed using the classical Hubeny-Rangamani-Takayanagi prescription in the associated higher-dimensional spacetime. However, after presenting these arguments, we will show in section 7.3.3 that they can be combined to argue for general Lorentz-signature matter QFTs that the entropy S_{QFT} is in fact extremal on $\boldsymbol{\gamma}$, and thus that D is causally inaccessible from $\boldsymbol{\gamma}$ as desired. We then comment briefly on how the argument extends to higher order quantum corrections.

7.3.1 Argument via Wick rotation

As stated above, for our first approach we explicitly assume that $\mathcal{M}_n$ can be analytically continued to define a smooth Euclidean (or perhaps complex) manifold $\mathcal{M}_n^E$ by Wick rotating $\tilde{x}^{\pm}$ to complex coordinates $v, \bar{v}$ and defining the smooth coordinate $z = v^n, \bar{z} = \bar{v}^n$, with the understanding that we rotate the timelike coordinate $\tilde{x}^+ - \tilde{x}^-$

into the lower half plane in the ket spacetime and that we rotate $\tilde{x}^+ - \tilde{x}^-$ into the upper half plane in the bra spacetime. Indeed, the coordinates $z, \bar{z}$ are just the analogous Wick rotation of $\tilde{X}^\pm$. As a result, the metric (7.7) and the expansions (7.9), (7.10), (7.11) show that – if the spacetime is sufficiently analytic for the Wick rotation to be defined – the result will be smooth at the origin $z, \bar{z} = 0$.

Furthermore, since Wick rotation preserves the replica symmetry that was assumed for the real-time saddle $\mathcal{M}_n$, the resulting $\mathcal{M}_n^E$ is replica-invariant. This is clearly compatible with the Wick-rotation of the expansions (7.9), (7.10), (7.11), which are manifestly invariant under $z \to e^{\frac{2\pi i}{n}} z$ after the above rotation of $\tilde{X}^\pm$ to $z, \bar{z}$.

We may thus proceed to discuss the analytic continuation of S_{QFT} to $\mathcal{M}_n^E$. Let us begin by further discussing S_{QFT} in the real-time saddle $\mathcal{M}_n$. Recall that $S_{QFT}[\gamma]$ is the entropy on an achronal surface Σ_γ stretching from γ to a Cauchy surface Σ_D for some replica of D on the boundary. Furthermore, the notion of achronal surface is nominally defined only in region where the metric is real and Lorentz signature. We will call this replica D_1 below and take it to lie on the boundary of M_-^1. As a result, with our conventions for sewing together bra and ket spacetimes to make $\mathcal{M}_n$, this D_1 also lies on the boundary of $\tilde{M}_-^{\dagger n}$ (and not on the boundary of $\tilde{M}_-^{\dagger 1}$). Given this choice, one can generally find achronal surfaces Σ_γ of the above form when γ in the domain of dependence of $\Sigma_{M_-^1,R}$ or $\Sigma_{\tilde{M}_-^{\dagger n},R}$, but not when it lies in the domain of dependence of $\Sigma_{M_-^i,R}$ for $i \neq 1$ or $\Sigma_{\tilde{M}_-^{\dagger j},R}$ for $j \neq n$; see figure 7.5.

On the other hand, analytic continuation is trivial when z is real and positive, as $z = \bar{z} > 0$ is the surface $\Sigma_{M_-^1,R}$ on which the time coordinate $\tilde{x}^+ - \tilde{x}^-$ vanishes. Thus the surface lies in both $\mathcal{M}_n$ and $\mathcal{M}_n^E$.

Furthermore, on $\Sigma_{M_-^1,R}$ we may compute $S_{QFT}[\gamma]$ by using a second replica trick. By this we mean that we take m copies of the Euclidean spacetime $\mathcal{M}_n^E$ on which we wish to define the matter entropy S_{QFT}, cut them open, and then sew them back together

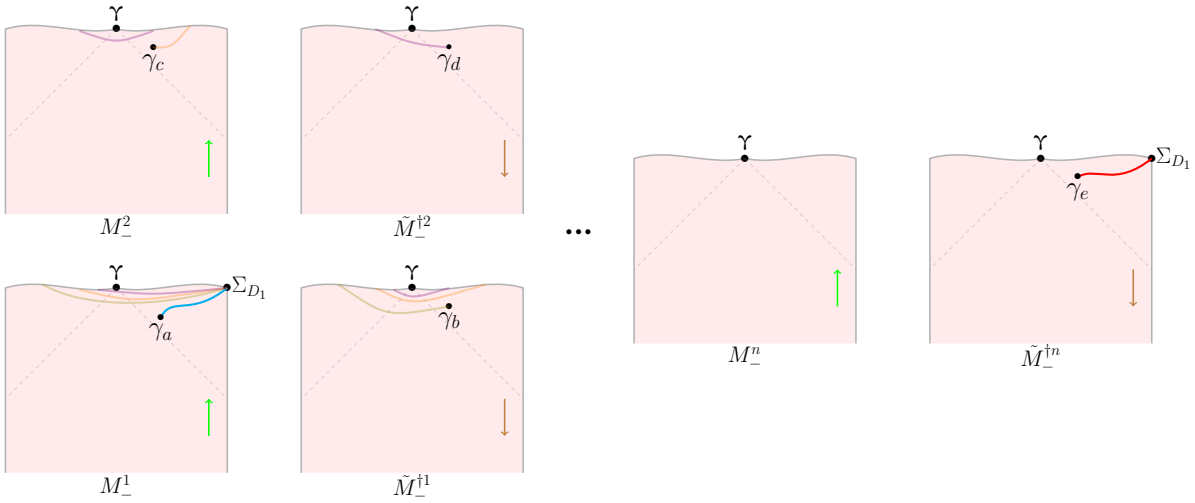

Figure 7.5: After choosing a particular replica D_1 of D and an associated Cauchy surface Σ_{D_1}, one can find an achronal surface Σ_γ from some codimension-2 surface γ to Σ_{D_1} only when γ is in the domain of dependence of $\Sigma_{M_-^1,R}$ or $\Sigma_{\tilde{M}_-^{\dagger n},R}$, but not in the domain of dependence of $\Sigma_{M_-^i,R}$ for $i \neq 1$ or $\Sigma_{\tilde{M}_-^{\dagger j},R}$ for $j \neq n$. The blue and red surfaces are such Σ_γ in the successful cases. We also show typical surfaces (orange, brown, and magenta) that would connect other regions to Σ_D. These latter surfaces must pass through regions with complex metric where achronality is not defined. Here the $M_-^i, \tilde{M}_-^{\dagger j}$ are sewn together as in figure 7.2. Thus, for example, the orange surface can be traced from $\gamma_c \subset M_-^2$ across the seam at the upper right of this sheet into $M_-^{\dagger 1}$, across that sheet moving to the left through the complex region to the past of $\boldsymbol{\gamma}$, across the seam at the upper left of $M_-^{\dagger 1}$ into M_-^1, and finally across M_-^1 moving to the right through the complex region to the past of $\boldsymbol{\gamma}$ to reach Σ_D.

using replica boundary conditions. This introduces a conical singularity at γ, but since we are only using this second replica trick to compute the matter entropy of a QFT on a fixed background we do not otherwise alter the metric (i.e., there is no 'backreaction' from this new conical singularity). Computing the matter QFT path integral over the m-replica spacetimes and taking an appropriate $m \to 1$ limit gives S_{QFT}. Furthermore this second replica trick calculation can be performed for any γ in $\mathcal{M}_n^E$ satisfying the homology constraint and so can be used to extend the definition of S_{QFT} to all of $\mathcal{M}_n^E$. Indeed, since there is no obstacle to the replica-trick computation giving an analytic result, we take it to be the desired analytic extension.

Note that this new replica trick explicitly preserves the $\mathbb{Z}_n$ replica-symmetry of the original $\mathcal{M}_n^E$. We have thus defined S_{QFT} as an analytic replica-symmetric function on $\mathcal{M}_n^E$. As a result, given any codimension-2 surface γ about which this $\mathbb{Z}_n$ acts as a rotation, first-order variations of $S_{QFT}[\gamma]$ must be invariant under such rotations and must thus vanish.

Applying this argument to the replica-invariant splitting surface $\boldsymbol{\gamma}$ shows that S_{QFT} is extremal on $\boldsymbol{\gamma}$ as desired. Returning to Lorentz signature and assuming the quantum focussing condition[16] [189] on the shadow $\mathcal{S}_R$, it immediately follows that this closed inequality holds on the closure of $\mathcal{S}_R$, and thus on the relevant outgoing null congruences from $\boldsymbol{\gamma}$. As a result, the generalized second law must hold on this null congruence [189]. We may then use the argument of [192] that, as in the classical case, $\boldsymbol{\gamma}$ must be causally separated from D.

Unitarity of the bulk QFT then allows us to again deform each $\Sigma_{M_-^i,R}$ to the past light cone of $\boldsymbol{\gamma}$ without changing $S_n(D)$. As before, this makes manifest that $S_n(D)$ is

[16]Since we consider only first-order backreaction to Einstein-Hilbert gravity, one might think that one need only assume the quantum null energy condition (QNEC) of [189]. This is true when $\mathcal{M}_n$ spacetime dimension 3 or less. But in higher dimensions the QNEC is not generally well-defined in curved space due to curvature-dependent UV divergences that depend on the choice of renormalization scheme [190, 191].

independent of the choice of either Σ_D or any sources within D.

7.3.2 Argument for holographic matter

We argued in section 7.3.1 above that, when $\mathcal{M}_n$ can be appropriately Wick-rotated to a Euclidean spacetime $\mathcal{M}_n^E$, our matter entropy S_{QFT} is stationary to first-order variations about $\boldsymbol{\gamma}$. We now give a different argument that works directly in the original real-time saddle $\mathcal{M}_n$ when the matter QFT happens to be holographic and S_{QFT} is computed using the classical Hubeny-Rangamani-Takayanagi (HRT) prescription in the associated higher-dimensional asymptotically-AdS spacetime $\mathcal{N}_n$ having boundary $\mathcal{M}_n$. For simplicity we also assume that it is sufficient to treat $\mathcal{N}_n$ as a solution to the vacuum Einstein equations (with a cosmological constant). See appendix F.1 for a simple example that illustrates the discussion below.

Let us discuss relevant features of $\mathcal{N}_n$ and the associated HRT prescription. Recall that $\mathcal{M}_n$ had an asymptotically-AdS boundary. But if $\mathcal{M}_n$ were the boundary of a smooth bulk spacetime $\mathcal{N}_n$, then of course $\partial\mathcal{M}_n$ would be empty. The resolution was explained in [193], which is to understand that the boundary of $\mathcal{M}_n$ must extend into the bulk as a dynamical object on which the bulk spacetimes can in some sense be said to end as well. For example, in simple cases this internal 'boundary' may be a string-theoretic orbifold or orientifold. More generally, at a phenomenological level one can simply model the object (whatever it may be) as an 'end-of-the-world brane' [194].

The key point for our purposes is the implication for the form of the homology constraint that should be satisfied by HRT surfaces $\gamma_{\mathcal{N}}$ for $S_{QFT}[\gamma]$. Recall that this is the entropy in $\mathcal{M}_n$ on a partial Cauchy surface Σ_γ stretching from γ to Σ_D. Although one may still say that $\gamma_{\mathcal{N}}$ must be homologous to Σ_γ, if one thinks of the bulk as containing an end-of-the-world brane this is now homology in the sense of manifolds with boundary.

In other words, one requires only that there be a bulk surface $\Sigma_{\mathcal{N}}$ for which $\partial\Sigma_{\mathcal{N}}$ is $\gamma_{\mathcal{N}} \cup \Sigma_\gamma$ up to additional contributions that coincide with the end-of-the-world brane. In certain microscopic descriptions this is clear from the fact that the end-of-the-world brane is really just a place where the bulk spacetime pinches off smoothly, but dualities require it to be true more generally. Perhaps the more fundamental point is that the end-of-the-world brane is dynamical, so that points on its world-volume behave in much the same way as other points in the bulk.

Let us now discuss the form of $\mathcal{N}_n$ in more detail. Note that the relationship of $\mathcal{N}_n$ to $\mathcal{M}_n$ is directly analogous to that of $\mathcal{M}_n$ to $\mathcal{B}_n$. It is true that the metric on $\mathcal{M}_n$ is complex in regions that we might say lie to the past of $\boldsymbol{\gamma}$ while the metric on $\mathcal{B}_n$ is real, but this point will not affect the discussion. In particular, we have taken $\mathcal{M}_n$ to preserve all of the symmetries of $\mathcal{B}_n$, so we will assume $\mathcal{N}_n$ to preserve these symmetries as well. The same argument as in section 7.2.3 then requires the metric on $\mathcal{N}_n$ to be real and Lorentz signature in regions causally inaccessible from $\boldsymbol{\gamma}_{\mathcal{N}}$, and the asymptotic form of the metric near $\boldsymbol{\gamma}_{\mathcal{N}}$ will be again follow (7.7), (7.7). We may thus construct a shadow $\mathcal{S}_R^{\mathcal{N}}$ and an extended shadow $\hat{\mathcal{S}}_R^{\mathcal{N}}$ of $\mathcal{N}_n$ using the recipe for $\mathcal{S}_R$ and $\hat{\mathcal{S}}_R$ from section 7.2.4. We may also note that $\boldsymbol{\gamma}_{\mathcal{N}}$ is homologous to Σ_γ for $\gamma = \boldsymbol{\gamma}$ in the sense defined above (since the relation between these surfaces is analogous to the relation between $\boldsymbol{\gamma}$ and Σ_D).

As a result, by the same logic as was to discuss $\boldsymbol{\gamma}$ in that section 7.2.4, we find that the replica-invariant surface $\boldsymbol{\gamma}_{\mathcal{N}}$ in $\mathcal{N}_n$ must be extremal in $\mathcal{S}_R^{\mathcal{N}}$. Using this argument in the bulk of $\mathcal{N}_n$ tells us that $\boldsymbol{\gamma}_{\mathcal{N}}$ is extremal under bulk variations. So since it is homologous to Σ_γ for $\gamma = \boldsymbol{\gamma}$, it is a candidate HRT surface for $\Sigma_{\boldsymbol{\gamma}}$ (i.e., for the surface Σ_γ with $\gamma = \boldsymbol{\gamma}$). Let us thus follow section 7.2.4 in assuming it to be the smallest such surface, in which case it must be the actual HRT surface for $\Sigma_{\boldsymbol{\gamma}}$.

However, since the extremality argument used only properties of $\mathcal{N}_n$ that are also true of $\mathcal{M}_n$ – an in particular properties of $\mathcal{M}_n$ that were already used in section 7.2.4

– we may also conclude $\boldsymbol{\gamma}_{\mathcal{N}}$ to be extremal with respect to variations of its boundary $\boldsymbol{\gamma} \subset \mathcal{S}_R$. Since we work in the approximation where $S_{QFT}[\gamma]$ is proportional to the area of the associated HRT surface in $\mathcal{N}_n$, it follows that $S_{QFT}[\gamma]$ is stationary to first order about the surface $\gamma = \boldsymbol{\gamma}$. But this $\boldsymbol{\gamma}$ was also a classical extremal surface, so this tells us that it is in fact a quantum extremal surface. If we assume the quantum focussing condition we may thus again repeat precisely the arguments at the end of section 7.3.1 to conclude that $\boldsymbol{\gamma}$ is causally inaccessible from D.

7.3.3 General Argument

The holographic argument in section 7.3.2 served mainly to illustrate the general point made at the very beginning of our discussion of quantum corrections. In particular, once some control was obtained over the asymptotic form of $S_{QFT}[\gamma]$ near the surface $\gamma = \boldsymbol{\gamma}$, we were able to show stationarity of S_{QFT} at $\boldsymbol{\gamma}$ using precisely the same argument given for stationarity of the area at $\boldsymbol{\gamma}$ in section 7.2.4. The assumption that the QFT was holographic served only to allow us to extract the desired asymptotic expansion from the existing literature.

Furthermore, in both sections 7.2.4 and 7.3.2, the desired asymptotic expansion was obtained by finding a self-consistent power series solution to the appropriate equations of motion. And in fact this was done by noting that Wick rotation is straightforward to any order in a series expansion, so that it was sufficient to transcribe the series solutions described for the Euclidean context in [73]. Despite the use of this Wick rotation, the resulting series should provide a good asymptotic expansion for the desired quantity in any Lorentz-signature theory, even in the presence of non-analytic sources.

We thus wish to now implement the analogous steps in a general quantum field theory. In that context the (variational) derivatives of S_{QFT} may again be said to be described

by 'equations of motion' which related them to certain correlation functions defined by the appropriate modular Hamiltonian and the stress tensor; see e.g. [195]. In principle, it should be possible to use this structure together with stress tensor conservation to construct the desired power series description of variations of S_{QFT} about $\boldsymbol{\gamma}$. In practice, of course, this is a highly non-trivial task.

Luckily, as described above, the general form of this expansion must be the same whether or not the theory admits a Wick rotation to Euclidean signature. Let us therefore assume that it does, and the rotation can be taken to have the form described in 7.3.1 above. Then the expansion can be Wick rotated as well, and as in section 7.3.1 it must be the series expansion of some analytic replica-invariant functional S_{QFT} on an analytic Euclidean (or complex) spacetime. In particular, in this case both S_{QFT} and the spacetime are analytic functions of the $z, \bar{z}$ obtained from Wick rotation of $\tilde{X}^{\pm}$. Analyticity and replica symmetry then require S_{QFT} to be stationary under first variations of $z, \bar{z}$ about $\boldsymbol{\gamma}$, and thus also require S_{QFT} to be stationary under first variations of $\tilde{X}^{\pm}$ about $\boldsymbol{\gamma}$. But since such variations are determined by the series expansion, and since we argued this expansion to have the same form in the general case as in the analytic case, S_{QFT} will be stationary on $\boldsymbol{\gamma}$ for any QFT. By assuming the quantum focussing condition, we may then again argue as above that $\boldsymbol{\gamma}$ will remain causally inaccessible from D under back-reaction from first-order quantum corrections.

7.3.4 Higher order quantum corrections

The argument given above clearly extends to higher order quantum corrections. Working out the detailed expansions will become more cumbersome at higher orders, as one must take into account higher and higher levels of back-reaction of the quantum fields on the bulk geometry. But expansions of both the area and S_{QFT} near the splitting

surface of such back-reacted saddles must nevertheless exist, and they will satisfy the same replica symmetry and compatibility with Euclidean expansions described above. So again both must be extremal at $\boldsymbol{\gamma}$ in saddles preserving both replica and conjugation symmetry.

7.4 Discussion

Our work above studied saddle points of real-time gravitational path integrals associated with the (annealed swap) Rényi entropy $S_n(D)$ for domains of dependence D on some asymptotically anti-de Sitter boundary for integer $n > 1$. For simplicity we considered pure Einstein-Hilbert gravity (in any dimension), but many other cases follow by dimensional reduction. In addition, footnote 11 describes how it may be generalized to gravity theories with perturbative higher derivative corrections by making use of further results from [73]. So long as the full system satisfies an appropriate analogue of the GSL, extending the arguments to any theory of matter governed by a local two-derivative action with perturbative higher-derivative terms appears to be merely a technical exercise.

We first worked at the level of the leading order terms in the stationary phase approximation, but we then included quantum corrections to all orders. We explicitly assumed our theory to satisfy the quantum focussing condition. When the saddle preserves replica and conjugation symmetries, we then showed under a certain technical assumption that the splitting surface $\boldsymbol{\gamma}$ to be causally inaccessible from D. As a result, we could deform the saddle without changing $S_n(D)$ to make manifest that $S_n(D)$ is independent of both the choice of any sources on D and the choice of any Cauchy surface Σ_D for D. One may thus say that (annealed swap) Rényi entropies are time-independent in the sense associated with unitary quantum theories living on the asymptotic boundary. However, this argument involved a technical assumption (see the end of section 7.2.3) about so-

lutions to the gravitational initial value problem for which the induced metric on the initial surface may fail to be positive definite. This assumption deserves to be better understood.

Recall then that unitarity is a key property of quantum mechanics, and that the study of quantum gravity has long sought to understand whether and in what sense unitarity might hold. In particular, in a baby universe scenario one should distinguish between unitary evolution of the full quantum gravity Hilbert space and unitarity 'from the perspective of an asymptotic observer,' by which we mean unitarity on each superselection sector for the algebra of asymptotic observables.

Now, it is natural for the above notions of unitarity to be closely related in a theory of quantum gravity. After all, one expects the gravitational Hamiltonian to be a boundary term, and thus to lie in any algebra of asymptotic observables. But this then immediately implies that it preserves the associated superselection sectors [196, 197].

In particular, a full proof of this unitarity follows if one adopts the axiomatic framework for gravitational path integrals described in [54]. The axioms of that reference are stated in terms of Euclidean path integrals, so we should in fact add the additional axiom that Lorentzian time-evolution is given by a Wick rotation of that framework. Under such assumptions, section 4.1 of [54] shows that the gravitational Hamiltonian is self-adjoint and lives in the algebra of boundary observables, so that e^{iHt} is unitary and preserves superselection sectors. In fact, section 4.1 of [54] also shows the density of states in each superselection sector to be bounded by $e^{S_{BH}}$. So then BH unitarity holds whenever this bound is saturated.

On the other hand, the current understanding of quantum gravity path integrals is sufficiently poor that such formal arguments are naturally regarded with suspicion. Furthermore, the conformal factor problem of Euclidean gravity [32, 198] then amplifies such concerns when Euclidean path integrals appear to play a fundamental role (though

there are good reasons to suspect that this is not a serious issue in the end [199, 200, 201, 202, 203]). As a result, more concrete tests of unitarity – such as the derivations of the Page curve and the tests described here – provide important pieces of evidence that the above formal arguments are physically meaningful. It thus remains of great interest to move beyond the limitations of the current work to address more general situations.

One extension turns out to be straightforward. This is the generalization to the case of non-integer replica numbers $n > 1$. At some level, time-independence of Rényi entropies for non-integer n must follow by analytic continuation from the integer n result derived here. But one may also give a more direct argument using the Lewkowycz-Maldacena trick of describing a replica-invariant saddle $\mathcal{M}_n$ by its $\mathbb{Z}_n$ quotient $\tilde{\mathcal{M}}_n = \mathcal{M}_n/\mathbb{Z}_n$. In terms of $\tilde{\mathcal{M}}_n = \mathcal{M}_n/\mathbb{Z}_n$, the boundary conditions for $\tilde{\mathcal{M}}_n$ do not depend on n, but $\tilde{\mathcal{M}}_n$ has a conical singularity whose strength does depend on n. While Lewkowycz and Maldacena worked in Euclidean signature, the analogous trick can also be used directly in Lorentz signature using the associated notion of 'conical singularity' (see e.g. [6]). This description is then straightforward to analytically continue to non-integer n. Furthermore, all of the power series expansions used in our work continue to hold on such $\tilde{\mathcal{M}}_n$ in the obvious way. For $2 > n > 1$ one finds that the Riemann tensor can be singular at $\tilde{X}^{\pm} = 0$ but, for vacuum Einstein-Hilbert gravity with cosmological constant, the equations of motion require the Ricci tensor to be proportional to the metric. In particular, $R_{ab}k^a k^b = 0$ for any null vector k^a, so one may continue to use the Raychaudhuri equation as in [78, 127]. With this understanding one may repeat our arguments verbatim for non-integer $n > 1$. Once again, the conclusion is that $S_n(D)$ depends only on D and not on the choice of a particular Cauchy surface $\Sigma_D \subset D$.

On the other hand, new input will clearly be required to generalize the symmetry-based arguments of this work to address saddles in which replica symmetry is broken. And while replica-invariant saddles appear to dominate in many situations, it has recently

been shown [38, 72, 7, 101] that replica-breaking saddles have important effects near HRT phase-transitions. Furthermore, even a small sub-dominant effect that violates unitarity would be of great interest. We will therefore return to the question of replica-breaking saddles in a forthcoming work.

Part III

Algebras from the Gravitational Path Integral

Chapter 8

A trace inequality for Euclidean gravitational path integrals (and a new positive action conjecture)

8.1 Introduction

The Anti-de Sitter/Conformal Field theory correspondence (AdS/CFT) [15] predicts exact equivalence between appropriate conformal field theories and their dual bulk string theories. Using the bulk to reproduce detailed properties of specific CFTs typically requires using intricate properties of the stringy description. However, it is often the case that fundamental properties of CFTs can already be seen in the approximation where the bulk theory is described by semiclassical gravity, perhaps coupled to appropriate matter fields. Important examples of such properties include CFT microcausality, strong subadditivity of entropy, and the fact that larger regions of the CFT define larger algebras of observables. In particular, these features are associated with results for asymptotically locally anti-de Sitter (AlAdS) bulk spacetimes satisfying the null energy condition. The

corresponding bulk results are, first, that any causal bulk curve between boundary points is deformable to a causal curve lying entirely within the boundary [204], second that strong subadditivity holds for HRT surfaces [78], and third that entanglement wedges nest appropriately [78, 205, 206]. Quantum effects in the bulk typically preserve such properties so long as they satisfy the quantum focussing conjecture [189].

The goal of the present work is to use the semiclassical bulk approximation to study the dual bulk implementation of the CFT inequality

$$\mathrm{Tr}_{\mathcal{D}}(BC) \leq \mathrm{Tr}_{\mathcal{D}}(B)\,\mathrm{Tr}_{\mathcal{D}}(C), \tag{8.1}$$

which relates traces of positive operators B, C on any Hilbert space $\mathcal{H}$. For positive $B = b^\dagger b$, $C = c^\dagger c$, some readers may prefer to write this in the form

$$\mathrm{Tr}_{\mathcal{D}}(bc^\dagger cb^\dagger) \leq \mathrm{Tr}_{\mathcal{D}}(b^\dagger b)\,\mathrm{Tr}_{\mathcal{D}}(c^\dagger c), \tag{8.2}$$

so that the argument of the trace on the left-hand-side is also a positive operator. Recall that positive operators are self-adjoint by definition [207], and that 'positivity' requires the eigenvalues to be non-negative. In (8.1) and (8.2), we use the symbol $\mathcal{D}$ to denote the non-gravitational CFT dual of a bulk theory, and we write $\mathrm{Tr}_{\mathcal{D}}$ to emphasize that the trace is the standard trace on the $\mathcal{D}$ side of the duality. In particular, $\mathrm{Tr}_{\mathcal{D}}$ denotes the familiar operation computed by introducing any orthonormal basis $|i\rangle_{\mathcal{D}}$ on the $\mathcal{D}$ Hilbert space and performing the sum

$$\mathrm{Tr}_{\mathcal{D}}(\mathcal{O}) := \sum_i {}_{\mathcal{D}}\langle i|\mathcal{O}|i\rangle_{\mathcal{D}}. \tag{8.3}$$

For simplicity of presentation we confine ourselves to the AdS/CFT context below, but similar discussions clearly apply to other gauge/gravity dualities as well, such as those

described in e.g. [208, 209]. To avoid infrared divergences, we assume $\mathcal{D}$ to be defined on a spatially compact spacetime. Since we consider path integrals dual to some $\mathrm{Tr}_{\mathcal{D}}\, B$, we may then take all of our Euclidean boundaries to be compact.

The inequality (8.1) is easily proven using standard Hilbert space operations in $\mathcal{D}$. One first notes that the inequality is trivial when $\mathrm{Tr}_{\mathcal{D}}(B) = +\infty$, so this leaves only the case of finite $\mathrm{Tr}_{\mathcal{D}}(B)$. One then observes that, when $\mathrm{Tr}_{\mathcal{D}}(B)$ is finite, the positivity of B requires the operator B to have a largest eigenvalue B_{max}. We then simply choose the $\{|i\rangle\}$ in (8.3) to be eigenstates of C with eigenvalues $C_i \geq 0$ and write

$$\mathrm{Tr}_{\mathcal{D}}(BC) = \sum_i C_i \, {}_{\mathcal{D}}\langle i|B|i\rangle_{\mathcal{D}} \leq \sum_i B_{max} C_i = B_{max}\, \mathrm{Tr}(C) \leq \mathrm{Tr}_{\mathcal{D}}(B)\, \mathrm{Tr}_{\mathcal{D}}(C). \tag{8.4}$$

Indeed, this argument also shows that the bound (8.1) is quite weak, and that it is saturated only when B, C are both proportional to a common projection of rank one. For $B = C$, this latter observation is equivalent to the familiar statement that the purity of a density matrix is 1 only when the density matrix is pure, and thus when it is proportional to a projection of rank one.

While the bound (8.1) may be weak, stronger bounds typically involve further details of the spectrum of B, C and are thus more difficult to study. One example is the bound $B_{max}\, \mathrm{Tr}(C)$ also derived in (8.4). Another is the even stronger von Neumann trace inequality $\mathrm{Tr}(BC) \leq \sum_i B_i C_i$, where we have now introduced the full set of eigenvalues B_i of B, and both C_i and B_i have been ordered so that $C_i \geq C_j$ and $B_i \geq B_j$ when $i \geq j$. These more intricate bounds on the CFT trace are correspondingly more awkward to study on the gravitational side of the AdS/CFT duality.

However, despite its weakness, the bound (8.1) can be used to derive fundamental consequences. One example is the fact that the algebra $B(\mathcal{H})$ of bounded operators on any Hilbert space is a type I von Neumann factor. This can be shown by first noting

that the commutant of $B(\mathcal{H})$ is trivial, so that $B(\mathcal{H})$ must be a factor of some type. One then considers any projection P and sets $C = B = P$. Since $P^2 = P$, the bound (8.1) requires $\mathrm{Tr}(P) \geq 1$ for any P. In contrast, when factors of some type other than I are present in a von Neumann algebra, any faithful normal semi-finite trace on the algebra will always assign arbitrarily small traces to some family of projections having arbitrarily small trace [210]. This result is a key motivation for our study.

Our goal here is to show how (8.1) arises from the bulk point of view. In doing so we will work at the level of the semiclassical approximation to the Euclidean path integral for a low-energy bulk effective theory. The semiclassical bulk description will necessarily involve gravity, but our analysis will not depend on the details of any UV completion.

Now, in fact, gravitational path integrals that include sums over topology are generally *not* dual to single CFTs as they fail to factorize over disconnected boundaries (see e.g. the classic discussion of [49]. However, if a non-factorizing bulk path integral makes sense, we expect it to behave like those discussed in [54, 211] where the path integral decomposes into a sum over so-called baby universe α-sectors in which factorization holds; see also [146, 147] for earlier discussions of this idea. We then expect (8.1) to be satisfied separately in each α-sector.

Furthermore, if an inequality of the form (8.33) holds in each member of an ensemble then, so long as the ensemble has non-negative probabilities to realize each of its members, a similar inequality will hold for ensemble averages. We might write this averaged inequality in the form

$$\langle \mathrm{Tr}_{\mathcal{D}}(bc^\dagger cb^\dagger)\rangle \leq \langle \mathrm{Tr}_{\mathcal{D}}(b^\dagger b)\,\mathrm{Tr}_{\mathcal{D}}(c^\dagger c)\rangle. \tag{8.5}$$

Here it will of course be important that the right-hand side is a single ensemble correlation function and *not* a product of ensemble averages.

It is therefore interesting to understand if a given bulk theory satisfies a corresponding inequality, which we might write in the form

$$\zeta\left(\tilde{M}_{bc^\dagger cb^\dagger}\right) \leq \zeta\left(\tilde{M}_{b^\dagger b} \sqcup \tilde{M}_{c^\dagger c}\right), \tag{8.6}$$

where $\sqcup$ denotes disjoint union and $\tilde{M}_{bc^\dagger cb^\dagger}$ is a smooth closed manifold specifying boundary conditions for our bulk theory on a Euclidean Asymototically locally Anti-de Sitter boundary that can be broken into four pieces $M_b, M_{b^\dagger}, M_c, M_{c^\dagger}$ such that connecting M_b and $M_{b^\dagger}$ gives a new smooth closed manifold $M_{bb^\dagger}$ that is invariant under a reflection-symmetry that exchanges the b and $b^\dagger$ pieces (and which complex-conjugates any complex boundary conditions) and similarly for $M_{cc^\dagger}$. (This notation will be explained in more detail in the sections below.) Note that, in general, the right-hand side may involve spacetime wormholes, and we should expect there to be cases where such wormholes are important in enforcing the inequality (8.6). In (8.6), we are allowed to the case where $\tilde{M}_{bc^\dagger cb^\dagger}$, though when $\tilde{M}_{bc^\dagger cb^\dagger}$ is a disjoint union of its $bb^\dagger$ and $cc^\dagger$ parts, those parts are precisely $\tilde{M}_{b^\dagger b}$, $\tilde{M}_{c^\dagger c}$ and (8.6) becomes a trivial equality. We will thus not consider that case further.

There is, however, an important issue of a normalization that remains to be addressed. The reader will immediately note that equations (8.1) and (8.6) fail to be invariant under rescaling the trace or the bulk path integral by a constant factor λ. This failure arises because the left-hand-side scales with λ while the right-hand-side scales with λ^2. As a result, if we are to compute $\mathrm{Tr}_{\mathcal{D}}\, B$ via a gravitational path integral, it is important to fix the overall normalization. We do so by requiring the path integral over all compact Euclidean spacetimes (with no boundaries) to be 1. This is, of course, equivalent to first allowing an arbitrary normalization and then dividing the result by the norm of the Hartle-Hawking no boundary state [212]. It is thus also equivalent to simply defining

our path integral to sum *only* over Euclidean spacetimes in which every bulk point is connected by some path to a point on the (asymptotically locally AdS) boundary at which boundary conditions are specified. This coincides with the traditional treatment of the gravitational path integral in AdS/CFT [17].

Our discussion begins with an analysis of simple cases and simple bulk theories in section 8.2. We first show that, in the context of black hole thermodynamics, standard results for either Jackiw-Teitelboim (JT) [163, 164] or Einstein-Hilbert gravity imply the bulk version of the inequality (8.6) to hold at all orders in the semiclassical expansion and at all orders in any perturbative higher-derivative corrections. By referring to the black hole thermodynamics context above, we mean that the operators B, C in (8.6) are both functions of the Hamiltonian H and that relevant path integrals are dominated by Euclidean black hole saddles. We focus on the simple case of pure Jackiw-Teitelboim (JT) gravity, where there are no other operators to consider and where all bulk saddles contain black holes. However, the arguments in 8.2.1 also apply to black hole thermodynamics more generally. We then also show that, due to the simplicity of JT gravity, for any UV completion where the path integral can be studied in the manner described by Saad, Shenker, and Stanford [51], we can show in interesting semiclassical limits that (8.6) holds even when the theory is coupled to matter (so long as the matter coupling is dilaton-free and the matter satisfies a positive action condition).

In Section 8.3, we then proceed to discuss (8.6) for operators B, C in more general theories and more general phases (perhaps not dominated by black holes). Since the inequality (8.6) holds for any quantum theory, it will be enlightening to look again at the $\mathcal{D}$ side of the duality to see how the standard non-gravitatioanl Euclidean path integral for $\mathcal{D}$ can be used to provide an alternate derivation of (8.6) at leading order in the semiclassical approximation (without yet invoking any possible gravitating bulk dual). This is done in section 8.3.1, where we assume only that each member of the relevant

class of Hamiltonians for the theory is bounded below and that the theory is 2nd order in derivatives. Higher derivative corrections can then be incorporated perturbatively. We do not study quantum corrections in this context since we will treat such corrections by a different argument in our discussion of gravitating bulk duals.

This sets the stage for us to address the general derivation of (8.6) from the gravitational side of the duality. We open this discussion in section 8.3.2 by showing that the basic outline of the non-gravitational argument of section 8.3.1 can be easily adapted to the gravitational context. However, a crucial ingredient in this argument turns out to be the fact that the non-gravitational Euclidean action is bounded below. This property is of course well-known to fail off-shell in gravitational theories; see e.g. [40]. We deal with this issue in stages by phrasing the argument of section 8.3.2 in terms of a series of assumptions about the gravitational path integral which will turn out to be plausible (and, in some cases, provably true) despite the fact that the gravitational action is unbounded below. The main discussion focuses on two-derivative theories of gravity (like Einstein-Hilbert or JT), though arbitrary higher derivative corrections are allowed so long as they are treated perturbatively. When our assumptions are satisfied, the argument establishes (8.6) at all orders in the semiclassical expansion.

We then separate out discussion of the status of those assumptions (and the associated issues surrounding the conformal factor problem of Euclidean gravity), placing this material in section 8.3.3. These assumptions imply a new positive action conjecture that generalizes the original conjecture of Hawking [40] in several ways. We prove this conjecture to hold in JT gravity minimally-coupled to positive-action matter, and we also motivate the conjecture more generally. Finally, we close in section 8.5 with a summary and brief discussion of future directions.

8.2 Simple cases and simple theories

Asymptotically Anti-de Sitter Jackiw-Teitelboim gravity is a simple $2d$ toy model of gravitational systems in which many explicit computations are possible. Section 8.2.1 considers the theory of "pure" JT gravity which contains only a metric g and a dilaton ϕ, with no additional matter fields. The addition of matter fields will be discussed in section 8.2.2 using ideas from [51]. We use conventions in which the pure JT action on a disk takes the form

$$\begin{aligned} I &= -\phi_0 \left[\int_{\mathcal{M}} \sqrt{g} R + 2 \int_{\partial_{as}\mathcal{M}} \sqrt{h} K + 2 \int_{\partial_f \mathcal{M}} \sqrt{h} K - 2 \sum_i \alpha_i \right] \\ &- \left[\int_{\mathcal{M}} \sqrt{g} \phi (R+2) + 2 \int_{\partial \mathcal{M}} \sqrt{h} \phi (K-1) \right]. \end{aligned} \tag{8.7}$$

Here ϕ_0 is a constant, h is the induced metric on a boundary, and K is the extrinsic curvature (a scalar, since the boundary is one-dimensional) defined by the outward-pointing normal. The detailed boundary conditions to be used will be described in appendix G.1.1.

8.2.1 The Trace Inequality in gravitational thermodynamics: Jackiw-Teitelboim gravity and beyond

Pure JT gravity has no local degrees of freedom, and in fact there is very little to compute. In particular, our 2-dimensional bulk must have a 1-dimensional boundary, so the only compact connected boundary is a circle. The JT path integral is then specified by the constant ϕ_0 in (8.7), a function ϕ_b on this circle having dimensions of length and prescribing boundary conditions for the dilaton, and the length β of the circle (as defined using a rescaled unphysical metric). However, one may change the conformal frame at infinity without changing the path integral and, by doing so, one can reduce the general

computation to the case where ϕ_b is any given positive constant $\bar{\phi}_b$ [213]. This result is reviewed in appendix G.1.4. As a result, in the rest of this section we simply choose some fixed value of this constant $\bar{\phi}_b$ and consider all circles to be labelled only by their length β in the corresponding conformal frame.

If one were to treat JT gravity non-perturbatively at a level where it is equivalent to a theory of a single matrix (see e.g. [211]), then (8.6) would follow by using this equivalence to transcribe into bulk language the quantum mechanics derivation given in section 8.1. Here we instead wish to focus on semiclassical treatments of JT gravity. The idea is to gain insight into calculations we can also hope to control in higher dimensional gravitational theories.

In higher dimensions, the semiclassical limit can be characterized by taking $G \to 0$. However, in JT gravity *two* of the above-mentioned parameters, ϕ_0 and $\bar{\phi}_b$, each take on aspects of the role played by G in higher dimensions. As a result, JT gravity admits many notions of semiclassical limit. One of these is given by taking ϕ_0 large with $\bar{\phi}_b$ fixed while another is the limit of large $\bar{\phi}_b$ with fixed ϕ_0. Establishing (8.6) in both cases then clearly also establishes the desired result in any limit where both ϕ_0 and $\bar{\phi}_b$ become large.

As one can see from (8.7), the entire affect of ϕ_0 is to weight spacetimes in the path integral by $e^{4\pi\phi_0\chi}$, where χ is the Euler character of the spacetime. As a result, since we use the normalization described in the introduction in which disconnected compact universes do not contribute, the limit $\phi_0 \to \infty$ with all other parameters held fixed is dominated by disk contributions. Furthermore, there is a factor of $e^{4\pi\phi_0}$ for each disk. The number of disks is determined by the number of circular boundaries for the path integral, which is necessarily *larger* on the right-hand-side of (8.6) (where $M_{bc^\dagger cb}$ has been split into $M_{b^\dagger b}$ and $M_{c^\dagger c}$) than on the left (where $M_{bc^\dagger cb}$ remains intact). The right-hand-side is thus clearly larger than the left-hand-side in the limit where ϕ_0 is taken large with all else fixed. This establishes the desired inequality (8.6) in this context.

However, as mentioned above, we can instead choose to keep ϕ_0 finite and to study the limit $\bar{\phi}_b \to \infty$ (with all else fixed, including the inverse temperature β, which we henceforth require to be finite). Let us use $Z(\beta)$ to denote the path integral defined by a circular boundary of length β. In the dual quantum mechanical system one would write

$$Z(\beta) = \mathrm{Tr}_{\mathcal{D}}(e^{-\beta H}). \tag{8.8}$$

Since the only objects we can compute are linear combinations of (8.8) with different values of β, the only operators in $\mathcal{D}$ that we can study are functions of H, where H is the Hamiltonian of $\mathcal{D}$. The change of conformal frame mentioned above that removes the dependence on general functions ϕ_b is sufficiently local that no further operators would have been found for more general (position-dependent) choices ϕ_b. For later use we note that at leading semiclassical order (with the above normalization of the action) one finds [213]

$$Z(\beta) \approx e^{4\pi\phi_0} e^{4\pi^2 \bar{\phi}_b/\beta}. \tag{8.9}$$

We will first discuss the trace inequality (8.6) for the simple case where $B = e^{-\beta_1 H}$ and $C = e^{-\beta_2 H}$. In doing so, it will be useful to recall that a partition function $Z(\beta)$ allows one to compute an associated entropy $S(\beta)$ using

$$S(\beta) := -\beta^2 \frac{d}{d\beta}\left(\beta^{-1} \ln Z(\beta)\right) \approx 4\pi(\phi_0 + 2\pi\bar{\phi}_b/\beta). \tag{8.10}$$

It turns out that the condition $S \geq 0$ is sufficient to derive the trace inequality (8.6) in the current context. To see this note that, for B, C as above, our (8.6) is equivalent to

$$\ln Z(\beta_1 + \beta_2) \leq \ln Z(\beta_1) + \ln Z(\beta_2). \tag{8.11}$$

In other words, (8.6) is equivalent to the requirement that $\ln Z(\beta)$ be a superadditive function of β. However, since $\beta > 0$, non-negativity of (8.10) is equivalent to stating that $\beta^{-1} \ln Z(\beta)$ decreases monotonically for $\beta \in (0, \infty)$. We may thus derive (8.11) from such non-negativity as follows:

$$\begin{aligned} \ln Z(\beta_1 + \beta_2) &= \beta_1 \frac{\ln Z(\beta_1 + \beta_2)}{\beta_1 + \beta_2} + \beta_2 \frac{\ln Z(\beta_1 + \beta_2)}{\beta_1 + \beta_2} \\ &\leq \beta_1 \frac{\ln Z(\beta_1)}{\beta_1} + \beta_2 \frac{\ln Z(\beta_2)}{\beta_2} = \ln Z(\beta_1) + \ln Z(\beta_2). \end{aligned} \tag{8.12}$$

Furthermore, for $S > 0$ we see that (8.6) becomes a strict inequality.

Since (8.10) is in fact positive, it follows that (8.6) is satisfied at this order for $B = e^{-\beta_1 H}$, $C = e^{-\beta_2 H}$. Indeed, we see that the inequality cannot be saturated for any β_1, β_2. As a result, when treated perturbatively, higher order corrections cannot lead to violations of (8.1).

Now, as described in [214], negative entropies *do* arise in non-perturbative regimes if one takes the path integral for the no boundary baby universe state to compute the entropy (8.10). But the entropies in individual super-selection sectors (which are dual to entropies of individual CFTs) should be positive even at the non-perturbative level; see again the discussion of superselection sectors, ensembles, and factorization in section 8.1. Furthermore, as described there, we would still expect the trace inequality to hold in the form (8.6), which requires us to include contributions from spacetime wormholes on the right-hand-side. Including simple such wormholes did indeed ameliorate the negative entropy issues discussed in [214]. Consistency with the dual matrix ensemble of [51] then requires that the remaining issue to be resolved by the inclusion of higher topologies and the appropriate non-perturbative completion, though this remains to be explicitly analyzed.

The simple argument given above for the case $B = e^{-\beta_1 H}$, $C = e^{-\beta_2 H}$ can be extended

to general functions of H constructed as linear combinations of the $e^{-\beta H}$. A straightforward way to do so is to realize that, in any dual quantum-mechanics theory, we may first analytically continue $e^{-\beta H}$ in β to construct the operators e^{itH}, whence for each real E one may define the operators

$$\delta(H-E) := \frac{1}{2\pi}\int_\Gamma dt\, e^{itH} e^{-itE}. \tag{8.13}$$

In (8.13), since we wish $\delta(H-E)$ to be the inverse Laplace transform of $e^{-\beta H}$, we should take the contour of integration Γ to be *above* any singularities that may arise. This is equivalent to choosing the contour for $\beta = -it$ to be to the *right* of any singularities. Linearity then implies the traces of the operators (8.13) to be given by the Fourier transform of $Z(-it) := \mathrm{Tr}_{\mathcal{D}}\, e^{itH}$, which we take to be given by the continuation of (8.9); i.e.

$$Z(-it) \approx Z(\beta) \approx e^{4\pi\phi_0} e^{i4\pi^2\bar{\phi}_b/t}. \tag{8.14}$$

Combining these results yields

$$\mathrm{Tr}_{\mathcal{D}}\ \delta(H-E) := \frac{1}{2\pi}\int dt\, Z(-it) e^{-itE} \approx \frac{e^{4\pi\phi_0}}{2\pi}\int dt\, e^{i4\pi^2\bar{\phi}_b/t} e^{-itE}, \tag{8.15}$$

where as in (8.13) the contour is taken to lie above the singularity at $t=0$, though we may otherwise choose it to run along the real t-axis.

For fixed real $E>0$, in the limit of large $\bar{\phi}_b$, we may then evaluate the remaining integral using the leading-order stationary phase approximation. The exponent is stationary at $t = \pm i\sqrt{4\pi^2\ \bar{\phi}_b/E}$, where the integrand on the far right of (8.15) takes the values $e^{\pm 4\pi\sqrt{\bar{\phi}_b E}}$. Since our contour lies above the singularity at $t=0$, it is then clear that the contour can be deformed to run through the saddle at $t = i\sqrt{4\pi^2\ \bar{\phi}_b/E}$, which would in any case give the larger saddle-point contribution. A more detailed analysis also shows

that the steepest ascent curve from this saddle lies along the positive t-axis and thus intersects the contour of integration as desired[1]. As a result, the leading semiclassical approximation gives

$$\mathrm{Tr}_{\mathcal{D}}\ \delta(H-E) \approx e^{4\pi\phi_0} e^{4\pi\sqrt{\bar{\phi}_b E}}\theta(E) = e^{S(E)}\theta(E), \tag{8.16}$$

where in the first step we have dropped a factor of $1/2\pi$ since it is subleading at leading semiclassical order. In (8.16) we have used the symbol $\theta(E)$ denotes the usual Heaviside step function and $S(E)$ is defined as

$$S(E) := S(\beta)\big|_{\beta=2\pi\sqrt{\bar{\phi}_b/E}}. \tag{8.17}$$

As usual the definition (8.17) is made because, at leading semiclassical order, the expectation value of E in the ensemble defined by $e^{-\beta H}$ is given by

$$E = \beta^{-1}(S - \ln Z) \approx 4\pi^2\ \bar{\phi}_b/\beta^2, \tag{8.18}$$

and because solving (8.18) for β yields the relation $\beta = 2\pi\sqrt{\bar{\phi}_b/E}$ used in (8.17).

Given any function f on the real line, we can now define an operator $f(H)$ via

$$f(H) := \int dE\, f(E)\delta(H-E). \tag{8.19}$$

Let us do so for two functions f_1, f_2, and let $f_1 f_2$ denote the product of these functions.

[1]For a more detailed discussion of steepest descent and ascent curves, see e.g. [181]. Interestingly, in this case the steepest descent curve is just the circle $tt^* = \frac{4\pi^2\ \bar{\phi}_b}{E}$, which can be thought of as running from the upper saddle at $t = i\sqrt{4\pi^2\ \bar{\phi}_b/E}$ to the lower saddle at $t = -i\sqrt{4\pi^2\ \bar{\phi}_b/E}$. But the part of the axis inside the circle can nevertheless be deformed to pass through the above saddle.

As a consequence of (8.13) one finds

$$\delta(H-E_1)\delta(H-E_2)=\delta(H-E_1)\delta(E_1-E_2), \tag{8.20}$$

which further implies that we have

$$f_1(H)f_2(H)=(f_1f_2)(H), \tag{8.21}$$

where $(fg)(H)$ is again defined as in (8.19) but using the function $(fg)(E):=f(E)g(E)$ in the integral over E.

Linearity and (8.15) then require

$$\begin{aligned}\mathrm{Tr}_{\mathcal{D}}\ f_1(H) &= \int_{E>0} dE\, f_1(E)e^{S(E)}, \quad \mathrm{Tr}_{\mathcal{D}}\ f_2(H)=\int_{E>0} dE\, f_2(E)e^{S(E)}, \quad \text{and}\\ \mathrm{Tr}_{\mathcal{D}}\ (f_1f_2)(H) &= \int_{E>0} dE\ (f_1(E)f_2(E))\, e^{S(E)}.\end{aligned} \tag{8.22}$$

Furthermore, for fixed f_1, f_2 in the limit of large $\bar{\phi}_b$, these integrals can be performed in the saddle point approximation. Since each integral is real, it must be dominated by the largest saddle on the positive real axis. Denoting the relevant values of E as E_1, E_2, E_{12}, we then have

$$\begin{aligned}\mathrm{Tr}_{\mathcal{D}}\ [f_1(H)] &\approx f_1(E_1)e^{S(E_1)}, \quad \mathrm{Tr}_{\mathcal{D}}\ [f_2(H)]\approx f_2(E_2)e^{S(E_2)},\\ \mathrm{Tr}_{\mathcal{D}}\ [(f_1f_2)(H)] &\approx (f_1(E_{12})f_2(E_{12}))\, e^{S(E_{12})}.\end{aligned} \tag{8.23}$$

But since E_1 dominates the first integral, we have $f_1(E_1)e^{S(E_1)} \geq f_1(E_{12})e^{S(E_{12})}$, and similarly $f_2(E_2)e^{S(E_2)} \geq f_2(E_{12})e^{S(E_{12})}$. Thus we find

$$\mathrm{Tr}_{\mathcal{D}}\ [(f_1f_2)(H)] \leq (f_1(E_1)f_2(E_2))\, e^{S(E_1)+S(E_2)-S(E_{12})}$$

$$\approx \quad e^{-S(E_{12})} \left(\mathrm{Tr}_{\mathcal{D}} \left[f_1(H)\right]\right) \left(\mathrm{Tr}_{\mathcal{D}} \left[f_2(H)\right]\right). \tag{8.24}$$

Finally, we note that in our semiclassical limit the quantity $S(E_{12})$ will be large and positive for any fixed $E_{12} > 0$. Thus we have $e^{-S(E_{12})} \ll 1$. In particular, this factor will be much more important than any subleading terms in our approximations.

This then establishes the trace inequality (8.6) for arbitrary f_1, f_2 at leading order in the limit of large $\bar{\phi}_b$. In fact, we have shown the inequality to hold strictly in this limit, in the sense that it cannot be saturated. As a result, quantum corrections cannot violate the trace inequality (8.6) when they are treated perturbatively. The same is true for any perturbative higher-derivative corrections one may wish to add.

While the above discussion was phrased in terms of JT gravity, the only properties we actually used were that B, C were chosen to be functions of H and that $S(E) > 0$ for all E. As a result, the same arguments also apply verbatim to such B, C when $\mathcal{D}$ is dual to a higher-dimensional gravity theory so long as each path integral is dominated by a black hole saddle (so that $S = A/4G > 0$). The one subtlety is that, due to the Hawking-Page transition, if one wishes to see the fact that $S(E) > 0$ at small E one will need to appropriately analytically continue to low energies the large-energy saddles that dominate the high-temperature phase; see e.g. the discussion of microcanonical entropy from the gravitational path integral in [103].

In this section we have considered choice of B, C that each define connected parts of the boundary. For example, the operators $B = e^{-\beta_1 H}$ and $C = e^{-\beta_2 H}$ are each associated with a single line-segment. As described in the introduction, when e.g. B instead contains several disconnected components, it may be important to include spacetime wormholes in the analysis. Since such cases quickly become cumbersome, we will not attempt treat them via explicit calculations of the form described above. However, such cases are readily included in the analysis of section 8.2.2 below.

8.2.2 Adding matter using the Saad-Shenker-Stanford pardigm

Jackiw-Teitelboim gravity turns out to be a simple enough theory that we can also establish (8.6) for the case where it has a dilaton-free coupling to positive-action matter. Here we require only that the theory admit a UV-completion in which the JT path integral can be treated in the manner described by Saad, Shenker, and Stanford in [51] and in which a semiclassical treatment remains valid. By a 'dilaton-free coupling,' we simply mean that the matter action depends *only* on the JT metric and does *not* depend on the dilaton. Furthermore, the specific positive-action matter requirement is that the classical matter action should be bounded below by zero on all asymptotically AdS_2 Euclidean spacetimes with arbitrary topology and arbitrary number of boundaries.

The present discussion will require certain details regarding the formulation and properties of JT gravity. In order not to distract from the main thrust of this work, we relegate the more technical analyses to appendix G.1. However, we recall here that the action for pure JT gravity on an asymptotically AdS_2 spacetime takes the form

$$\begin{aligned} I &= -\phi_0 \left[\int_{\mathcal{M}} \sqrt{g} R + 2 \int_{\partial \mathcal{M}} \sqrt{h} K \right] \\ &- \int_{\mathcal{M}} \sqrt{g} \phi (R+2) + 2 \int_{\partial \mathcal{M}} \sqrt{h} \phi (K-1). \end{aligned} \tag{8.25}$$

We refer the reader to appendix G.1 for a discussion of the boundary conditions under which (8.25) can be used, though in this section we will refer to the associated conditions as the requirement that the AdS_2 boundary be "smooth."

As in section 8.2.1, there are various possible notions of a semiclassical limit for this theory. And, again as in section 8.2.1, the effect of ϕ_0 is to weight topologies by a factor of $e^{4\pi\phi_0\chi}$ so that taking ϕ_0 large with all else fixed immediately yields (8.6). We will thus follow section 8.2.1 in showing that (8.6) *also* holds when we take $\bar{\phi}_b$ large while holding

all other parameters fixed (including both ϕ_0 and the inverse temperature β).

If one examines the action (8.25), one sees that it is strictly linear in ϕ. This remains true in the presence of our dilaton-free matter couplings. Following [51], it is then natural to define the "Euclidean" JT path integral by integrating ϕ over strictly *imaginary* values, so that the integrals over ϕ give delta-functions of $R+2$. The path integral then reduces to an integral over (real) $R=-2$ constant curvature Euclidean spacetimes and over any matter fields.

The bulk term in (8.25) vanishes for such spacetimes, so the JT action becomes a sum of boundary terms – one for each S^1 connected component of the boundary – each of which that can be written in terms of a Schwarzian action [213]. We will assume the remaining integrals to have a good semiclassical limit in the sense that, when $\bar{\phi_b} \to \infty$ with all else fixed, the result of the integrals is well approximated by e^{-I_0} where I_0 is the minimum-action configuration of metrics and matter fields that satisfy the boundary conditions.

Due to the simplicity of JT gravity, with this assumption one can again quickly see that (8.6) holds as $\bar{\phi_b} \to \infty$. The point is that, as shown in appendix G.1.4, in this context the action is bounded below by $-4\pi\phi_0\chi - \sum_j 4\pi^2\bar{\phi_b}/\beta_j$ where χ is the spacetime's Euler character and β_j is the preiod of the jth circular boundary. Since $\chi \leq n$ for any $2d$ manifold with n circular boundaries, we thus find a topology-independent lower bound $-\sum_j \left(4\pi\phi_0 + 4\pi^2\bar{\phi_b}/\beta_j\right)$. It should be no surprise that this is just the action of the Euclidean black hole with inverse temperature β.

Furthermore, since the matter action is non-negative, the full coupled matter-plus-gravity action is also bounded below by $-\sum_j \left(4\pi\phi_0 + 4\pi^2\bar{\phi_b}/\beta_j\right)$. It turns out that this is also a good estimate of the actual minimum of the action at large $\bar{\phi_b}$. To see this, let us use g_{min} to denote the Poincaré disk metric (representing Euclidean JT black holes with periods β_j) that saturates this bound. We then choose any matter field configuration that

satisfies the required boundary conditions when taken together with g_{min}. Since $\bar{\phi}_b$ is just an overall coefficient in front of the Schwarzian action (G.36), our g_{min} cannot depend on $\bar{\phi}_b$. Our full field configuration thus has action $I = -\sum_j \left(4\pi\phi_0 + 4\pi^2\bar{\phi}_b/\beta_j\right) + I_{matter,0}$ where the last term is manifestly independent of $\bar{\phi}_b$. But the true minimum I_0 of the full action must be less than or equal to this result, showing that I_0 satisfies

$$-\sum_j \left(4\pi\phi_0 + 4\pi^2\bar{\phi}_b/\beta_j\right) \leq I_0 \leq -\sum_j \left(4\pi\phi_0 + 4\pi^2\bar{\phi}_b/\beta_j\right) + I_{matter,0}. \tag{8.26}$$

In particular, in the limit of large $\bar{\phi}_b$ we see that I_0 will scale linearly in $\bar{\phi}_b$ with coefficient $-\sum_j 4\pi^2\bar{\phi}_b/\beta_j$. The inequality (8.6) then follows immediately by noting that if $\beta_B, \beta_C, \beta_{BC}$ are the lengths of the relevant boundaries then we must have $\beta_{BC} = \beta_B + \beta_C$, and thus also

$$\frac{1}{\beta_{BC}} = \frac{1}{\beta_B + \beta_C} < \frac{1}{\beta_B} + \frac{1}{\beta_C}. \tag{8.27}$$

Again, since this also forbids saturation of the trace inequality at this order, (8.6) must continue to hold in the presence of both higher-order semiclassical corrections or perturbative higher-derivative corrections.

8.3 The trace inequality in general semiclassical gravity theories

The remainder of this work is devoted to arguing that the bulk analog (8.6) of the trace inequality (8.6) should hold in general semiclassical theories of gravity and for general operators B, C. After the discussion of sections 8.1 and 8.2, this should not be a surprise. When the path integrals are dominated by black holes, it is natural to expect the behavior seen in section 8.2 where very general computations are semiclassically controlled by black

hole thermodynamics whence (as described in section 8.2.1) the trace inequality follows from positivity of the microcanonical entropy $S(E)$. Furthermore, when the gravitational path integrals are *not* dominated by black holes, it is natural for the bulk to behave like a standard quantum system so that the argument in (8.4) should apply. Putting these together should be expected to yield an argument for general theories of gravity.

What makes this discussion subtle is our lack of understanding of the Euclidean gravitational path integral, as well as the associated conformal factor problem that makes the Euclidean action unbounded below (see e.g. [40]). We therefore address these issues in stages below. We first return to the non-gravitational setting in section 8.3.1 and find a path integral derivation of our trace inequality in the semiclassical limit. We then show in section 8.3.2 that the broad outline of this non-gravitational path-integral argument can be transcribed to the gravitational case, so long as one makes a number of assumptions concerning both the gravitational action and the treatment of the conformal factor problem. We take care, however, to formulate such assumptions in such a manner that they remain plausible despite the above-mentioned fact that the gravitational action is *not* bounded below. This plausibility argument is then made in section 8.3.3, which in particular shows these assumptions to imply a new positive-action conjecture that extends the original positive-action conjecture of Hawking [32, 40] in several ways. The conjecture can then be verified for JT gravity with minimal (or, more generally, dilaton-free) couplings to positive-action matter. Furthermore, in simple contexts, for more general theories it can be related to positivity of the Hamiltonian with general boundary conditions.

8.3.1 Trace Inequality from the Semiclassical Euclidean Path Integral: The non-gravitational case

We now return to the non-gravitational context to describe a Euclidean path integral derivation of (8.6) in the semiclassical limit. We will restrict to the case where both B and C are defined by real sources. We will also assume that, with any fixed set of allowed real-valued sources, the corresponding Euclidean action is both real and bounded below.

We will also assume that each such path integral is dominated by a saddle (or by a set of saddles) in the semiclassical limit, and in particular that the action of any configuration is always greater than or equal to the action of the dominant saddle. The latter will be true under assumptions that prevent the action from being minimized on the boundaries of the space of allowed field configurations. Such assumptions are reasonable since regions near such boundaries typically have infinite measure, so that minimizing the action on such boundaries typically causes the path integral to diverge. We leave the exceptional cases open for future study.

Our restriction to real sources means that our path integrals are manifestly real. Such integrals can only be dominated in the semiclassical limit by real saddles corresponding to global minima of the action over the contour of integration. In particular, all saddles (as well as more general configurations) discussed below will lie on the contour of integration that defines the path integral. This means that no issues of contour deformations can be relevant to our discussion.

We will also consider only cases where the right side of (8.6) is dominated by a *single* saddle. Contexts with more than one equally-dominant saddle typically describe phase transitions; see e.g. the classic discussion of Hawking and Page [215]. Close to such a phase transition one typically finds that formally non-perturbative effects associated with addition saddles and/or mixing between saddles are more important than perturbative

corrections; see e.g. recent discussions in [67, 216] for condensed matter analogues and in [38, 7, 72, 206]. We thus save further consideration of this case for future study.

It will be enough for our purposes to work at leading order in the semi-classical expansion, so that the path integral is approximated by e^{-I}, where I is the Euclidean action of the dominant saddle. This is to be a model for the leading-order analysis of (gravitating) bulk duals in section 8.3.2, though in that section we will use a rather different method to include quantum corrections.

We have already mentioned that we are interested in quantum field theories with sources, say in d Euclidean spacetime dimensions. In quantum field theories, the UV structure of the Hilbert space can be sensitive to the choice of sources, and in fact to various time-derivatives of such sources when d is large. We will therefore further restrict discussion to the case where the Hilbert space of interest can be thought of as being defined by a set of time-translation-invariant boundary conditions that define an associated "cylindrical" Euclidean manifold $\mathcal{C}_\infty = \mathcal{B} \times \mathbb{R}$ with translation-invariant sources and where $\mathcal{B}$ is an appropriate $(d-1)$-dimensional manifold and $\times$ denotes the Cartesian product of metrics as well as of the underlying manifolds.

The equivalent definition in Lorentz signature would thus restrict us to considering Hilbert spaces defined by static metrics[2]. In particular, note that the $\mathbb{Z}_2$ relection symmetry of the $\mathbb{R}$ factor implies that $\mathcal{C}_\infty$ also admits a $\mathbb{Z}_2$ "time-reversal" symmetry. We refer to $\mathcal{C}_\infty$ as the infinite cylinder. It will be useful to define corresponding finite cylinders $\mathcal{C}_\epsilon = \mathcal{B} \times [0, \epsilon]$, and to define $\mathcal{B}_0$ to be the boundary of $\mathcal{C}_\epsilon$ at the zero of the interval.

[2] While it is also of interest to discuss time-dependent Lorentz-signature QFTs, upon analytic continuation to Euclidean signature such time-dependence is generally associated with complex-valued Euclidean sources. Complex sources raise further issues for the saddle-point approximation associated with the possible existence of saddles at points in the complex plane away from the original contour of integration. Such issues are beyond the scope of the current work, so we save that setting for future investigation. The same comment applies to stationary but non-static background metrics, to vector-valued sources with non-trivial time-components, and to other boundary conditions not naturally described as being of the form $B \times \mathcal{R}$ due to breaking time-reversal symmetry.

Due to the time reversal symmetry of $\mathcal{C}_\infty$, we will need this definition only for positive values of ϵ.

We emphasize that this is a restriction on the background fields that define the Hilbert space and not on the background fields used to construct any particular state. Of course, the two must be compatible, so in practice we will consider only states that are prepared by manifolds-with-boundary where a neighborhood of each boundary contains a *rim* diffeomorphic to a finite cylinder $\mathcal{C}_\epsilon$ (or, more properly, to the part of this cylinder associated with the half-open interval $[0, \epsilon)$).

In most of this section we will also assume that the Euclidean action I for our theory is the integral of a local Lagrangian L, with L built from fields and their *first* derivatives only. In particular, on a manifold M with boundary we assume that $I = \int_M L$ without additional boundary terms. Of course, many potential such boundary terms can be absorbed into L by the addition of a total divergence (so long as this divergence is again built from fields and their first derivatives). We note that the above condition implies that the equations of motion are of no more than 2nd order. However, at the end of this section we will see that perturbative higher derivative corrections can be easily included as well.

We begin by considering positive operators B and C. Such operators may always be written $B = b^\dagger b$, $C = c^\dagger c$ for appropriate b, c. We wil l assume that the operators b and c are each computed by some (perhaps complex) linear combination of Euclidean path integrals with real sources. For simplicity, we begin with the case where each operator b, c is computed by a single Euclidean path integral and save for later the study of non-trivial linear combinations. However, in contrast to section 8.2.1, we now include the case where the boundary associated with $\mathrm{Tr}_{\mathcal{D}}(BC)$ may be disconnected.

We use the notation M_b, M_c, M_B, M_C to denote the manifolds over which the path integrals for b, c, B, C are performed, together with the appropriate set of sources. To re-

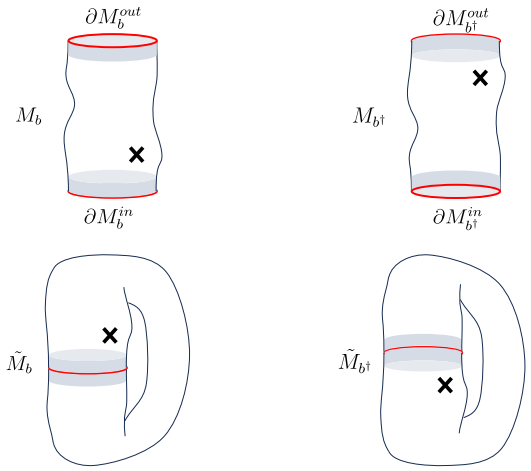

Figure 8.1: **Upper left panel:** A source-manifold with boundary M_b is shown with its input and output boundaries $\partial M_b^{in}, \partial M_b^{out}$ and the associated rims (grey shading). Each boundary (red) has a C_ϵ rim (grey). The $\times$ symbol indicates a localized feature of a source. **Upper right panel:** $M_{b\dagger}$ is constructed from M_b by interchanging the labels $\partial M_b^{in}, \partial M_b^{out}$ but keeping all sources unchanged. If one always draws ∂M_b^{in} at the bottom and ∂M_b^{out} at the top, one can think of this as acting with a reflection in the vertical direction. **Lower panels:** The closed source manifolds $\tilde{M}_b$ and $\tilde{M}_{b\dagger}$ (which are diffeomorphic for real sources).

mind the reader of this, we will sometimes refer to M_b, M_c, M_B, M_C as *source manifolds*. In particular, we take such source manifolds to specify the full set of background structures (e.g., spin-structures, etc.) which are required to define the theory[3]. A graphical representation of such a source manifold is provided on the upper left panel of figure 8.1.

Since b is an operator on a given Hilbert space, we may take the boundary ∂M_b to be the disjoint union of two parts ∂M_b^{in}, ∂M_b^{out} describing the input and output of b, and where the sources near both ∂M_b^{in} and ∂M_b^{out} are associated with the same Hilbert space that defines the theory. In particular, we assume that M_b may be chosen to be some C_ϵ in some neighborhood of each of ∂M_b^{in} and ∂M_b^{out} so that, in particular, the boundary ∂M_b^{in} (or ∂M_b^{out}) agrees with $\mathcal{B}_0$. As mentioned above, we refer to this as requiring M_b to have *rims*, and we make analogous requirements for the source-manifolds with boundary

[3]The restrictions imposed above, and in particular the implicit assumption that the theory be invariant under time-reversal, imply that our theory cannot depend on a choice of orientation. See related comments in footnote 2.

associated with any operator discussed below. Since the theory is non-gravitational, one should regard points on M_b and C_ϵ as being labelled. The agreement of ∂M_b^{in}, ∂M_b^{out} with $\mathcal{B}_0$ thus defines a particular diffeomorphism $\phi_b : \partial M_b^{in} \to \partial M_b^{out}$. We then define a closed source manifold $\tilde{M}_b$ (without boundary, so that $\partial \tilde{M}_b = \emptyset$) by using ϕ_b to identify ∂M_b^{in} with ∂M_b^{out}. The trace of b ($\mathrm{Tr}(b)$) is then computed by the path integral over the resulting $\tilde{M}_b$; see figure 8.1.

It is useful to take the definition of M_b to include the partition of ∂M_b into ∂M_b^{in} and ∂M_b^{out}. We may then describe $b^\dagger$ as being computed by the path integral over $M_{b^\dagger}$, where (since we restrict to real sources) $M_{b^\dagger}$ is constructed from M_b by interchanging the labels ∂M_b^{in}, ∂M_b^{out} but keeping all sources unchanged; see again figure 8.1.

Corresponding assumptions and definitions will also be made for any other operator c and the associated M_c, ∂M_c, and $\tilde{M}_c$. In particular, since b and c both act on the same Hilbert space $\mathcal{H}$, the inputs of b must be identical to those of c, and similarly for the outputs. As a result, the labelling of points on $\mathcal{B}_)$ also defines source-preserving diffeomorphisms $\phi_{bc} : \partial M_b^{in} \to \partial M_c^{out}$ and $\phi_{cb} : \partial M_c^{in} \to \partial M_b^{out}$. We may then use ϕ_{bc} (or ϕ_{cb}) to define the source manifold M_{bc} (or M_{cb}) by identifying the input of M_b with the output M_c (or vice versa). The path integral over M_{bc} then clearly computes the operator bc. Using both ϕ_{bc} and ϕ_{cb} to make identifications allows us to further construct the closed source manifold $\tilde{M}_{bc}$, over which the path integral computes $\mathrm{Tr}(bc)$. Note that swapping b and c would define the source manifold M_{cb} associated with the operator cb, but that $\tilde{M}_{cb} = \tilde{M}_{bc}$ so that $\mathrm{Tr}(bc) = \mathrm{Tr}(cb)$ as expected; see figure 8.2.

In order to derive (8.6), we will thus need to compare the Euclidean path integrals over $\tilde{M}_B$, $\tilde{M}_C$, and $\tilde{M}_{BC}$. Recall that we require $B = b^\dagger b$, $C = c^\dagger c$ where b, c can again be written as Euclidean path integrals, say over M_b, M_c. In direct parallel with the above construction of M_{bc} from M_b, M_c, we may also choose M_B to take the form $M_{b^\dagger b}$. The trace $\mathrm{Tr}(B)$ is then the path integral over the corresponding closed source manifold $\tilde{M}_{b^\dagger b}$.

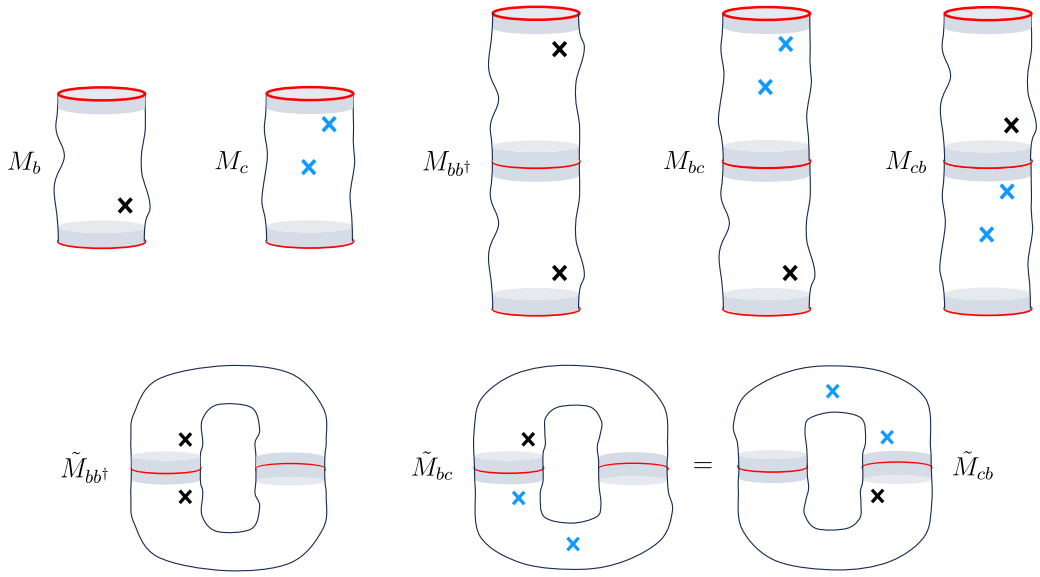

Figure 8.2: The source manifolds with boundary M_b, M_c can be used to construct M_{bc} , M_{cb}, and $M_{bb^\dagger}$ as well as the closed source manifolds $\tilde{M}_{bc} = \tilde{M}_{cb}$ as shown. In all cases the output boundaries are drawn at the top and the input boundaries are at the bottom. Note that $M_{bb^\dagger}$ and $\tilde{M}_{bb^\dagger}$ are both symmetric under reflections of the vertical direction.

Since the sources on M_b are real, they must agree with those on $M_{b^\dagger}$ up to an appropriate diffeomorphism. Thus M_B admits a $\mathbb{Z}_2$ symmetry that exchanges the b and $b^\dagger$ regions of $M_B = M_{b^\dagger b}$; see again figure 8.2.

Before proceeding, we pause to comment on our depiction in the figures of the source manifolds M_b, etc. Below, we will wish to show features of individual configurations of fields that appear in the path integral (in addition so the source features shown thus far). Such information makes the figures correspondingly more complicated, so that it is useful to make our illustrations more clean, even at the expense of making them more abstract. See figure 8.3 for the dictionary relating figures thus far to those that will appear below.

At leading semi-classical order, comparing path integrals over $\tilde{M}_B$, $\tilde{M}_C$, and $\tilde{M}_{BC}$ is equivalent to comparing the dominant saddles σ_B, σ_C, and σ_{BC} on these source manifolds. We begin with an observation, which we codify as a lemma to facilitate future reference:

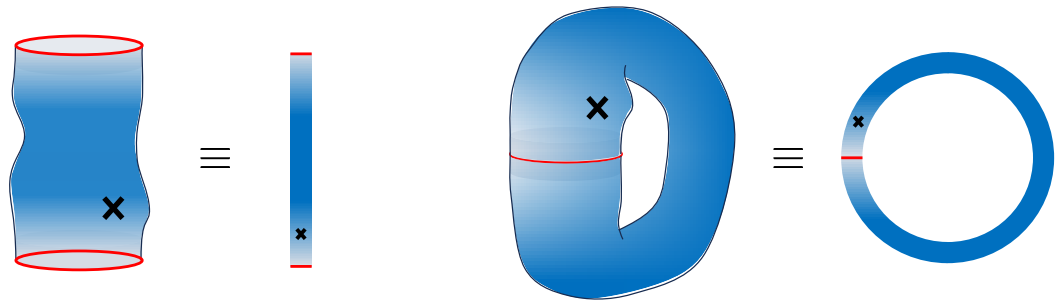

Figure 8.3: This figure illustrates the scheme that we adopt below to depict source manifolds along with particular configurations on such manifolds that arise in the associated path integrals. It also shows the connection to the old scheme. **Left panel:** A configuration for the path integral performed over a source-manifold M_b will be described by the coloration assigned to that manifold. The left hand side of the equivalence uses the old scheme with a two-dimensional depiction of the source manifold, but now with the coloration added. The right hand side uses the new scheme in which the source manifold is drawn as one-dimensional and the $\times$ is the only indication of structure associated with the sources. **Right panel:** A configuration for the path integral performed over the closed source-manifold $\tilde{M}_b$ is shown using both schemes.

Lemma 1 *Consider an operator $D = d^\dagger d$, where d is computed by a Euclidean path integral over a source manifold M_d. The source manifold $\tilde{M}_D = \tilde{M}_{d^\dagger d}$ then clearly enjoys a $\mathbb{Z}_2$ reflection symmetry as discussed above. This symmetry is in fact preserved by any saddle σ_D that dominates the path integral over $\tilde{M}_D$. In cases where the minimum value of the action is shared by several saddles, the symmetry is preserved by at least one such σ_D.*

To prove Lemma 1, we begin by considering an arbitrary saddle σ_D^0 for $\mathrm{Tr}_{\mathcal{D}}\, D$. Let σ_d^0 be the part of this saddle on M_d, and let $\sigma_{d^\dagger}^0$ be the part on $M_{d^\dagger}$. Furthermore, let $\Phi_d : M_d \to M_{d^\dagger}$ be the map that defines the $\mathbb{Z}_2$ symmetry of $\tilde{M}_D$.

If the saddle σ_D^0 breaks the $\mathbb{Z}_2$ symmetry of the background fields, then σ_d^0 and $\sigma_{d^\dagger}^0$ will not be related by Φ_d. In this case we can use σ_d^0 and $\sigma_{d^\dagger}^0$ to build new configurations for the path integral over $\tilde{M}_D$. In particular, as illustrated in figure 8.4, the action of Φ_d on σ_d^0 defines a new configuration $\sigma_d^R =: \Phi_d(\sigma_d^0)$ on $M_{d^\dagger}$, and gluing this to σ_d^0 defines a new

configuration σ_D^d for the path integral over $\tilde{M}_D$. We can also define a corresponding $\sigma_D^{d^\dagger}$ by gluing $\sigma_{d^\dagger}^0$ to its image under the inverse of Φ_d. Note that σ_D^d, $\sigma_D^{d^\dagger}$ will not generally solve the equations of motion at the surface where M_d meets $M_{d^\dagger}$, and in fact that derivatives of fields in σ_D^d, $\sigma_D^{d^\dagger}$ will not generally be continuous at these surfaces.

By construction, both σ_D^d and $\sigma_D^{d^\dagger}$ are invariant under Φ_d. The key observation needed to prove our Lemma is then that the action S is additive, in the sense that

$$I(\sigma_D^0) = I(\sigma_d^0) + I(\sigma_{d^\dagger}^0), \text{ while} \tag{8.28}$$

$$I(\sigma_D^d) = I(\sigma_d^0) + I(\Phi_d[\sigma_d^0]) = 2I(\sigma_d^0) \text{ and} \tag{8.29}$$

$$I(\sigma_D^{d^\dagger}) = I(\sigma_{d^\dagger}^0) + I(\Phi_d^{-1}[\sigma_{d^\dagger}^0]) = 2I(\sigma_{d^\dagger}^0). \tag{8.30}$$

This additivity follows from the fact that $S = \int L$, together with the requirement that L depend only on fields and their first derivatives. The point is that σ_D^0 must be smooth since it solves the Euclidean equations of motion with smooth boundary conditions. (We assume these equations to be elliptic.) Furthermore, by construction, the values of fields at the boundaries of σ_d^0 will agree with those at the boundaries of $\Phi_d[\sigma_d^0]$, and similarly for $\sigma_{d^\dagger}^0$ and $\Phi_d^{-1}[\sigma_{d^\dagger}^0]$. This means that the fields defined by either σ_D^d or $\sigma_D^{d^\dagger}$ are continuous. And while the first derivatives may not be continuous at the boundaries of M_d and $M_{d^\dagger}$, they have well-defined limits from each side; i.e., the first-derivatives have at worst step-function discontinuities. This means that L is bounded, and in particular has no delta-function contributions at the boundaries between the M_d and $M_{d^\dagger}$ regions of M_D.

It follows that the action does indeed satisfy (8.28)-(8.30). Comparing these equations shows that the smaller of $I(\sigma_D^d)$ and $I(\sigma_D^{d^\dagger})$ must be less than or equal to $I(\sigma_D^0)$, and that it is strictly less if $I(\sigma_d^0) \neq I(\sigma_{d^\dagger}^0)$. Furthermore, if the final σ_D^d, $\sigma_D^{d^\dagger}$ are not saddles then they cannot minimize the action and the action of the dominant saddle must be even

smaller; i.e.,

$$I(\sigma_D^{\rm dom}) \leq \min\{I(\sigma_D^d), I(\sigma_D^{d^\dagger})\} \leq I(\sigma_D^0). \tag{8.31}$$

As a result, if σ_D^0 is a dominant saddle, then σ_D^d, $\sigma_D^{d^\dagger}$ are also saddles with $I(\sigma_D^d) = I(\sigma_D^{d^\dagger}) = I(\sigma_D^0)$. Noting that σ_D^d, $\sigma_D^{d^\dagger}$ are invariant under the $\mathbb{Z}_2$ symmetry then establishes Lemma 1.

We are now in a position to prove our main result (8.6) at leading semi-classical order. As stated above, at this order, comparing path integrals over $\tilde{M}_B$, $\tilde{M}_C$, and $\tilde{M}_{BC}$ is equivalent to comparing the dominant saddles σ_B, σ_C, and σ_{BC} on these source manifolds. In particular, at this order we have

$$\operatorname{Tr} B = e^{-I(\sigma_B)}, \quad \operatorname{Tr} C = e^{-I(\sigma_C)}, \quad \text{and} \quad \operatorname{Tr} BC = e^{-I(\sigma_{BC})}. \tag{8.32}$$

We are interested in the case $\tilde{M}_B = \tilde{M}_{b^\dagger b}$, $\tilde{M}_C = \tilde{M}_{c^\dagger c}$, so that we may also write $\tilde{M}_{BC} = \tilde{M}_{d^\dagger d}$ using $d = bc^\dagger$ and the fact that $\tilde{M}_{b^\dagger bc^\dagger c} = \tilde{M}_{cb^\dagger bc^\dagger}$ (which in turn follows from the fact that our gluing operation is invariant under cyclic permutations). Applying Lemma 1 to $\tilde{M}_{BC} = \tilde{M}_{d^\dagger d}$, we may take σ_{BC} to have a $\mathbb{Z}_2$ conjugation symmetry that exchanges $d = cb^\dagger$ and $d^\dagger = bc^\dagger$. We may then cut the saddle σ_{BC} into the 4 pieces $k_b, k_{b^\dagger}, k_c, k_{c^\dagger}$ associated with the $M_b, M_{b^\dagger}, M_c, M_{c^\dagger}$ regions of $\tilde{M}_{BC}$. Here we use the symbol k (with subscripts) for configurations that are not given to us as saddles of the original path integrals.

We may now glue the resulting k_b and $k_{b^\dagger}$ together to define a $\mathbb{Z}_2$-symmetric configuration $\tilde{k}_B = k_{bb^\dagger}$ for the path integral over $\tilde{M}_B$; see figure 8.5. Note that $\mathbb{Z}_2$ symmetry requires the fields on k_B to be continuous at the boundaries between k_b and $k_{b^\dagger}$. Thus the action $I(k_B)$ is well-defined. We may also define the analogous configuration $k_C = k_{cc^\dagger}$ for the path integral over $\tilde{M}_C$, whose action $I(k_C)$ is again well-defined.

Furthermore, as in the proof of Lemma 1 we have $I(k_B)+I(k_C) = I(\sigma_{BC})$. And since the dominant saddles σ_B, σ_C must have actions no larger than $I(k_B)$, $I(k_C)$, using the leading semiclassical approximation (8.32) we find

$$\mathrm{Tr}(BC) \leq \mathrm{Tr}(B)\,\mathrm{Tr}(C) \tag{8.33}$$

as desired.

However, so far we have required each operator b, c to be given by a single path integral. We would also like to discuss operators given by a linear combination of path integrals. I.e., we wish to allow $b = \sum_i b_i$, and $c = \sum_i c_i$, where each of the b_i, c_j are single path-integrals as above. This generalization is straightforward when there is a single dominant saddle σ_{BC} for $\langle \mathrm{Tr}_{\mathcal{D}}(BC)$, which we as usual assume to be the case.

To proceed, we first write $B = \sum_{ij} b_i b_j^\dagger$, $C = \sum_{ij} c_i c_j^\dagger$, and $BC = \sum_{i,j,k,l} b_i b_j^\dagger c_k c_l^\dagger$. We then note that a dominant saddle σ_{BC} for $\mathrm{Tr}_{\mathcal{D}}\, BC$ will be associated with some particular term $b_i b_j^\dagger c_k c_l^\dagger$ (and also with its equally-dominant conjugate if this term is not real) . As in the proof of Lemma 1 we may then cut this saddle into two pieces corresponding to $M_{b_j^\dagger c_k}$ and $M_{c_l^\dagger b_i}$. Gluing each of these to its reflection then defines $\mathbb{Z}_2$-symmetric configurations for the diagonal terms given by path integrals over $\tilde{M}_{b_j b_j^\dagger c_k c_k^\dagger}$ and for $\tilde{M}_{b_i b_i^\dagger c_l c_l^\dagger}$. Since the original saddle σ_{BC} was dominant (with some action $I(\sigma_{BC})$) and our saddles are real, additivity again requires that the pieces corresponding to $M_{b_j^\dagger c_k}$ and $M_{c_l^\dagger b_i}$ both have actions $\frac{1}{2} I(\sigma_{BC})$, and that the new $\mathbb{Z}_2$-symmetric configurations are saddles with actions equal to $I(\sigma_{BC})$. (This follows from the analogue of (8.31) when σ_D^0 is dominant so that the left and right hand sides are equal.) As a result, the new saddles may be used as dominant saddles. Using either saddle in this way then reduces us to consideration of a single $\mathbb{Z}_2$-symmetric saddle, whence the rest of the argument follows as above.

It now remains to study higher-derivative corrections about a saddle σ_{BC}. We will use I_0 to denote the original action without such corrections. We will treat corrections to I_0 perturbatively, which means that at each order the saddles are found by solving a 2nd derivative equation of motion with sources determined by the lower-order parts of the solution.

At the off-shell level needed for our argument, at each order n in perturbation theory we may treat the action as being a 2nd order polynomial functional I_n of the fields. The coefficients of the quadratic terms in this functional are given by the second variations of I_0 about the lower order saddle. The action is thus positive semi-definite for perturbations about a dominant saddle. The coefficients in the linear term are given by varying the higher derivative corrections at linear order. We shall assume that any zero-modes of the linearized theory about σ_{BC} are associated with symmetries of I_0 that are preserved by the higher-derivative terms, and thus in particular that they are preserved by the linear term in I_n. It then follows that I_n is bounded from below, and that it is in fact minimized at the desired saddle.

Furthermore, in a perturbative treatment there can be no danger of violating (8.33) unless it is saturated by the classical 2-derivative theory. As a result, if we again suppose that the dominant 2-derivative saddle for each path integral is unique[4], then we need only consider perturbations around saddles $\tilde{\sigma}_B, \tilde{\sigma}_C, \sigma_{BC}$, where $\tilde{\sigma}_B, \tilde{\sigma}_C$ are constructed from σ_{BC} by using the above cut-and-paste procedure. In particular, at any point p_B on the B side of $\tilde{M}_{BC}$, the sources for the first correction will precisely match those at a corresponding point p_B on $\tilde{M}_B$, and similarly on any point p_C on the C side. It follows that the setting for computing the first-order corrections is of precisely the same form as

[4]In particular, it is unclear how to control the possibility that two a priori unrelated saddles might have precisely the same action at the two-derivative level, but might then have this degeneracy lifted by higher derivative corrections in a manner unfavorable to our argument. We leave consideration of this interesting-but-finely-tuned possibility open for future study.

the zero-order problem defined above, where the sources for this problem on $\tilde{M}_{BC}$ may again be reproduced by gluing $\tilde{M}_B$ to $\tilde{M}_C$. We may thus argue in exactly the same way that (8.33) also holds at first order in higher derivative corrections, and in fact iteratively at every higher order as well.

8.3.2 The trace inequality for semiclassical gravity

We now turn our attention to bulk gravity theories. For convenience of notation we continue to suppose that the bulk theory is dual to a hypothetical non-gravitational theory $\mathcal{D}$, or to an ensemble of such theories, though in the end our arguments will be entirely in the bulk. In particular, the arguments apply even to bulk theories for which dual non-gravitational boundary theories are not known to exist.

On the $\mathcal{D}$ side of the duality, the path integrals for $\langle \mathrm{Tr}_{\mathcal{D}}(B), \mathrm{Tr}_{\mathcal{D}}(C)\rangle$, and $\langle \mathrm{Tr}_{\mathcal{D}}(BC)\rangle$ may be formulated as path integrals over source manifolds $\tilde{M}_B, \tilde{M}_C$, and $\tilde{M}_{BC}$ just as in section 8.3.1, and in particular with $\tilde{M}_B = \tilde{M}_{b^\dagger b}$, $\tilde{M}_C = \tilde{M}_{c^\dagger c}$ and $\tilde{M}_{BC} = \tilde{M}_{d^\dagger d}$ for $d = cb^\dagger$. We again confine the discussion to the case where the boundary conditions defined by any such source manifold are real. By this we mean that, if the formalism allows complex bulk configurations k to be considered, then if k_B satisfies the boundary conditions defined by $\tilde{M}_B$, so does the complex conjugate k_B^*. We also again require each of the associated source-manifolds-with-boundary M_b, M_c to have $\mathcal{C}_\epsilon$ rims for some $\epsilon > 0$ as described in section 8.3.1.

The AdS/CFT dictionary of [17] (or its extrapolation to ensembles) then states that $\langle \mathrm{Tr}_{\mathcal{D}}(B)\,\mathrm{Tr}_{\mathcal{D}}(C)\rangle$, and $\langle \mathrm{Tr}_{\mathcal{D}}(BC)\rangle$ may equivalently be computed as bulk path integrals that sum over all bulk spacetimes with boundary conditions determined by the above source manifolds $\tilde{M}_B, \tilde{M}_C$, and $\tilde{M}_{BC}$. As stated in the introduction, we take this bulk path integral to be normalized by dividing by the no-boundary state or, equivalently,

we take the bulk path integral with boundary conditions set by some $\tilde{M}$ to sum *only* over bulk spacetimes in which every point can be connected to the boundary at $\tilde{M}$. Disconnected closed universes are *not* included in our sum.

At leading semiclassical order the basic structure of our arguments will closely follow those of section 8.3.1. In particular, we will again restrict to situations far from phase transitions by requiring the bulk path integral for $\langle \mathrm{Tr}_{\mathcal{D}}(B)\,\mathrm{Tr}_{\mathcal{D}}(C)\rangle$ to have a single dominant saddle. However, we will need to deal with two new inter-related further complications. The first is that gravitational actions are generally not bounded below on the space of real Euclidean fields. The second is that, as a result of the issue just described, the so-called "Euclidean" gravitational path integral cannot actually be taken to be defined as the integral over real Euclidean fields.

To allow the casual reader to focus on the big picture, the present section presents an overview of the argument for (8.6) and deals with the above issues by simply making assumptions about the gravitational path integral as needed. We then return to address those assumptions in section 8.3.3.

We begin by discussing the leading-order result, in which we take each path integral to be dominated by a smooth bulk saddle. Higher order corrections will be discussed later, at the end of this section.

We are free to call the dominant bulk saddles for each path integral σ_B, σ_C, and σ_{BC} in direct analogy with section 8.3.1. We thus have

$$\mathrm{Tr}_{\mathcal{D}}\, B = e^{-I(\sigma_B)}, \quad \mathrm{Tr}_{\mathcal{D}}\, C = e^{-I(\sigma_C)}, \quad \text{and} \quad \mathrm{Tr}_{\mathcal{D}}\, BC = e^{-I(\sigma_{BC})}. \tag{8.34}$$

In particular, we suppose that the semiclassical approximation to our path integral satisfies the following assumption:

Assumption 1 *For a bulk path integral specified by boundary conditions defined by a*

(compact) closed source manifold $\tilde{M}$ with real sources, we assume that there is a class of configurations $\mathcal{K}_{\tilde{M}}$ such that i) the bulk fields described by any $k \in \mathcal{K}_{\tilde{M}}$ are continuous, ii) the bulk action I is a real-valued functional on $\mathcal{K}_{\tilde{M}}$ and iii) in the semiclassical limit, the path integral is dominated by a real saddle $\sigma \in \mathcal{K}_{\tilde{M}}$ that minimizes the action I over $\mathcal{K}_{\tilde{M}}$. In particular, we have $I(\sigma) = \min_{k \in \mathcal{K}_{\tilde{M}}} I(k)$. Furthermore, if $\mathcal{K}_{\tilde{M}}$ includes a complex configuration k, then the complex conjugate k^* also lies in the same $\mathcal{K}_{\tilde{M}}$. We similarly assume that the class $\mathcal{K}_{\tilde{M}}$ is invariant under a corresponding action of any symmetry of $\tilde{M}$.

As described in section 8.3.1, this assumption is naturally satisfied in contexts where the Euclidean path integral over real fields converges. In that case, $\mathcal{K}_{\tilde{M}}$ is just the class of real field configurations. But this is not generally the case in gravitational theories. We thus emphasize that Assumption 1 does not require $\mathcal{K}_{\tilde{M}}$ to contain *all* real configurations, and in fact does not generally require configurations $k \in \mathcal{K}_{\tilde{M}}$ to be real at all (except for the dominant saddle in the semiclassical limit). Instead, it requires only that $I(k)$ be real-valued on $\mathcal{K}_{\tilde{M}}$. This flexibility will be useful in later sections where we discuss several different possible choices of $\mathcal{K}_{\tilde{M}}$ associated with different approaches to defining the path integral.

Since the present section addresses a general theory of gravity, we will make no attempt to write down an explicit action. However, we do require the action to satisfy the following additivity property which can be checked in any particular theory (and which will be discussed for familiar examples in section 8.3.3):

Assumption 2 *Consider two boundary source manifolds $\tilde{M}_{bc}$, $\tilde{M}_{c^\dagger d}$, where $\tilde{M}_{bc}$ is given by cyclicly gluing together the input and output boundaries of some M_b, M_c, and where $\tilde{M}_{c^\dagger d}$ is similarly constructed from $M_{c^\dagger}, M_d$. Given any real saddles $\sigma_{bc} \in \mathcal{K}_{\tilde{M}_{bc}}$, $\sigma_{c^\dagger d} \in \mathcal{K}_{\tilde{M}_{c^\dagger d}}$, we assume there is a prescription for slicing σ_{bc} into two pieces k_b, k_c, and of*

similarly slicing $\sigma_{c^\dagger d}$ into two pieces $k_{c^\dagger}, k_d$ which satisfy

$$I(\sigma_{bc}) = I(k_b) + I(k_c), \quad \text{and} \quad I(\sigma_{c^\dagger d}) = I(k_{c^\dagger}) + I(k_d). \tag{8.35}$$

We emphasize that this condition needs only be satisfied by real saddles and not by general configurations in $\mathcal{K}_{\tilde{M}_{bc}}$ and $\mathcal{K}_{\tilde{M}_{c^\dagger d}}$. We also assume that the slicing prescription preserves any symmetries of the bulk saddle σ_{bc}.

As shown in figure 8.6, the cutting of σ_{bc} into k_b, k_c generally creates new boundaries not restricted by properties of $\tilde{M}_{bc}$. As a result, we require the action I to be defined on such bulk configurations. This may require the specification of appropriate boundary terms at the new boundaries, as well as possible corner terms where the new boundaries intersect $\tilde{M}_{bc}$; see related discussions in [183, 217, 218].

Furthermore, suppose that there is a diffeomorphism Φ from the new boundaries of k_c to the new boundaries of $k_{c^\dagger}$ that preserves the values of all bulk fields (though which need not preserve normal derivatives of bulk fields). Then we can glue the new boundaries of k_b to those of k_d to create a new configuration $k_{bd} \in \mathcal{K}_{\tilde{M}_{bd}}$ whose actionwe assume to be

$$I(k_{bd}) = I(k_b) + I(k_d); \tag{8.36}$$

see again figure 8.6.

As in section 8.3.1, we first consider the case where each object in (8.6) is computed by a single path integral, returning later to cases that involve linear combinations of path integrals. We will need the analogue of Lemma 1 for the gravitational context:

Lemma 2 *Consider an operator $D = d^\dagger d$ in $\mathcal{D}$, where d is computed in $\mathcal{D}$ by a Euclidean path integral over a source manifold M_d with real sources. The source manifold $\tilde{M}_D = \tilde{M}_{d^\dagger d}$ then clearly enjoys a $\mathbb{Z}_2$ symmetry as discussed above. This symmetry is in fact*

preserved by any bulk saddle σ_D that dominates the bulk path integral for $\mathrm{Tr}_{\mathcal{D}}\,\tilde{M}_D$. *In cases where several allowed bulk saddles share this minimum value of the action, the symmetry is preserved by at least one such σ_D.*

Using assumptions 1 and 2, we can give a proof of Lemma 2 that directly parallels the proof of Lemma 1 in section 8.3.1. The argument is depicted in figure 8.7. We first consider an arbitrary saddle σ_D^0 that lies in $\mathcal{K}_{\tilde{M}_D}$ and use assumption 2 to divide it into $k_{d^\dagger}^0$, k_d^0. Note that the values of the bulk fields on the new boundaries of $k_{d^\dagger}^0$ agree with those on the new boundaries of k_d^0 by continuity on Σ_D^0; see again Assumption 1. But we can use the reflection symmetry of $\tilde{M}_D$ to construct a reflected saddle σ_D^R that again lies in $\mathcal{K}_{\tilde{M}_D}$, and which we then divide into $k_{d^\dagger}^R$, k_d^R. Because k_d^0 and $k_{d^\dagger}^R$ are related by the reflection symmetry, the field values on their new boundaries agree. We may thus paste these pieces together to form a new configuration $k_D^d \in \mathcal{K}_{\tilde{M}_D}$ with an explicit bulk reflection symmetry, and we may also construct the analogous $k_D^{d^\dagger} \in \mathcal{K}_{\tilde{M}_D}$ from σ_d^R and $\sigma_{d^\dagger}^0$. As in section 8.3.1, the additivity properties (8.35), (8.36) applied to the current pieces then imply that either $I(k_D^d) \leq I(\sigma_D^0)$ or $I(k_D^{d^\dagger}) \leq I(\sigma_D^0)$. As a result, if σ_D^0 is a dominant saddle, then either k_D^d or $k_D^{d^\dagger}$ must be an equally-dominant saddle that preserves the desired symmetry.

Lemma 2 will soon allows us to prove the trace inequality (8.6) at leading semi-classical order. As stated above, at this order we have

$$\mathrm{Tr}_{\mathcal{D}}\, B = e^{-I(\sigma_B)}, \quad \mathrm{Tr}_{\mathcal{D}}\, C = e^{-I(\sigma_C)}, \quad \text{and} \quad \mathrm{Tr}_{\mathcal{D}}\, BC = e^{-I(\sigma_{BC})}. \tag{8.37}$$

We are interested in the case $\tilde{M}_B = \tilde{M}_{b^\dagger b}$, $\tilde{M}_C = \tilde{M}_{c^\dagger c}$, so that we may also write $\tilde{M}_{BC} = \tilde{M}_{d^\dagger d}$ using $d = bc^\dagger$ and the fact that $\tilde{M}_{b^\dagger bc^\dagger c} = \tilde{M}_{cb^\dagger bc^\dagger}$. (This follows from the fact that our gluing operation is invariant under cyclic permutation of the parts to be glued). Applying Lemma 2 to $\tilde{M}_{BC} = \tilde{M}_{d^\dagger d}$, we may take σ_{BC} to have a $\mathbb{Z}_2$ symmetry

that exchanges $d = bc^\dagger$ and $d^\dagger = cb^\dagger$. We may then cut the saddle σ_{BC} into the two pieces k_B, k_C associated with the M_B, M_C source manifolds. Furthermore, since Assumption 2 required the slicing prescription to preserve symmetries of the original bulk saddle, the boundaries ∂k_B, ∂k_C will be invariant under corresponding reflection symmetries. This will in particular be true for the new boundaries created by slicing σ_{BC} into parts.

We now make a final monotonicity assumption regarding our action.

Assumption 3 *Consider again the setting of assumption 2 and the pieces k_b, k_c described there. Let $\partial_{new} k_b$ denote the new boundaries of k_b created by slicing σ_{bc} in two; i.e., these are the boundaries of k_b that were not boundaries in σ_{bc}. We assume that when k_b is invariant under a $\mathbb{Z}_2$ symmetry, we may use this symmetry to glue any point of $\partial_{new} k_b$ to its image to define a configuration $\tilde{k}_b \in \mathcal{K}_{\tilde{M}_b}$ associated with the bulk path integral for $\mathrm{Tr}_{\mathcal{D}}(b)$; see figure 8.8. We further assume that this gluing operation does not increase the action. In other words, we assume*

$$I(\tilde{k}_b) \leq I(k_b). \tag{8.38}$$

Before using this assumption, it is important to explain why the relation (8.38) is natural, and in particular why it is not generally an equality. In the nongravitational discussion of section 8.3.1, the topology of any saddle was always that of the corresponding source manifold $\tilde{M}$ that defined the relevant path integral. As a result, the equivalent of $\partial_{new} k_b$ always separated cleanly into input and output boundaries. In particular, in the non-gravitational case the reflection symmetry that acted on $\partial_{new} k_b$ had no fixed points. Thus the equivalent of $\tilde{k}_b$ was always smooth.

In the gravitational context, we may indeed expect that $I(\tilde{k}_b) = I(k_b)$ when $\tilde{k}_b$ is smooth. However, the dimensionality of the bulk saddle is typically greater than that of the source manifold. In particular, the topology of source manifold no longer dictates

the topology of the bulk. As a result, the construction of $\tilde{k}_b$ from k_b will introduce a conical deficit of π at any fixed points of the reflection symmetry that lie on the new boundary $\partial_{new} k_b$ of k_b; see again figure 8.8. In such cases, the monotonicity assumption (8.38) amounts to the condition that conical deficits give a non-positive contribution to the Euclidean gravitational action. This is consistent with the standard sign choices for the Euclidean Einstein-Hilbert and Jackiw-Teitelboim actions (see e.g. [40]). In fact, for later purposes it is useful to add a further assumption which essentially states that the contribution of conical deficits is strictly negative:

Assumption 4 *Consider again the context of Assumption 3. If the reflection symmetry of k_b has fixed points on $\partial_{new} k_b$, then we in fact have*

$$I(\tilde{k}_b) < I(k_b). \tag{8.39}$$

Assumption 4 will be of use when we consider perturbative corrections, though we will set it aside for now.

Returning to the main argument, we may use the above procedure to construct configurations $\tilde{k}_B, \tilde{k}_C$ for $\mathrm{Tr}_{\mathcal{D}}(B)$, $\mathrm{Tr}_{\mathcal{D}}(C)$ from the pieces k_B, k_C that were cut from σ_{BC}. We then apply Assumption 3, replacing b in (8.38) by either B or C. Finally, we apply the minimization assumption (Assumption 1) to find that the dominant saddles σ_B, σ_C for $\mathrm{Tr}_{\mathcal{D}}(B)$, $\mathrm{Tr}_{\mathcal{D}}(C)$ satisfy

$$I(\sigma_{BC}) = I(k_B) + I(k_C) \geq I(\tilde{k}_B) + I(\tilde{k}_C) \geq I(\sigma_B) + I(\sigma_C) \tag{8.40}$$

By (8.37), this is then equivalent to the desired trace inequality (8.6). The important steps of the above argument are illustrated in figure 8.9.

The above reasoning suffices for the case where B, C each represent a single boundary

condition. The remaining case where they are linear combinations of boundary conditions then follows just as at the end of section 8.3.1. Starting with a general saddle for any term in the sum associated with $\mathrm{Tr}_{\mathcal{D}}(BC)$, Assumptions 1 and 2 imply that there is another saddle with equal or lesser action that is associated with one of the diagonal terms in the sum. And this diagonal term can then be used as above to construct saddles σ_B, σ_C for $\mathrm{Tr}_{\mathcal{D}}\, B, \mathrm{Tr}_{\mathcal{D}}\, C$ that satisfy (8.40). So, again, the desired result holds.

We may also address perturbative quantum corrections to (8.6). This turns out to be straightforward since we take the path integral for $\langle \mathrm{Tr}_{\mathcal{D}}(BC) \rangle$ to be dominated by a *single* saddle. A key point is that perturbative quantum corrections are explicitly given by quantum field theory in the curved spacetime backgrounds defined by our saddles. In particular, they are computed by *non-gravitational* path integrals, or by path integrals that include only perturbative gravitons, of the general form described in section 8.3.1, but where the leading-order bulk saddles $\sigma_{BC}, \sigma_B, \sigma_C$ now play the role of $\tilde{M}_{BC}, \tilde{M}_B, \tilde{M}_C$ from section 8.3.1.

A second key point is that, in any strict perturbative framework, quantum corrections can lead to violations of (8.6) only if this inequality is saturated at leading semi-classical order. Since we assume unique saddles $\sigma_{BC}, \sigma_B, \sigma_C$ for, respectively, $\mathrm{Tr}_{\mathcal{D}}(BC)$, $\mathrm{Tr}_{\mathcal{D}}(B)$, and $\mathrm{Tr}_{\mathcal{D}}(C)$, our arguments above require that σ_B, σ_C can be obtained by slicing σ_{BC} into two pieces, each of which is separately invariant under a reflection symmetry. The saddle σ_B is then obtained by using the reflection symmetry of the B piece to glue together any new boundaries created by the slicing operation. The saddle σ_C is also constructed in the analogous fashion.

Furthermore, the above argument also shows that strict saturation of (8.6) at leading semiclassical order requires one to be able to reconstruct σ_{BC} from σ_B, σ_C by a procedure directly analogous to that building $\tilde{M}_{BC}$ from $\tilde{M}_B$, $\tilde{M}_C$ (shown previously in figure 8.5); i.e., $\sigma_B = k)B$ and $\sigma_C = k_C$. Moreover, the objects k_B, k_C used to construct $\tilde{k}_B =$

$\sigma_B, \tilde{k}_C = \sigma_C$ now play the roles of M_B, M_C from section 8.3.1. Thus, for example, the quantum correction to $\mathrm{Tr}_{\mathcal{D}} B$ is precisely $\mathrm{Tr}_{pert\ bulk} B_{pert\ bulk}$ where this is a trace over the perturbative bulk Hilbert space and where $B_{pert\ bulk}$ is an operator on that Hilbert space. Furthermore, the reflection symmetry of σ_B implies the operator $B_{pert\ bulk}$ to be positive. Indeed, since the analogous statements hold for C and BC, the simple quantum-mechanical argument given by (8.4) can be used to write

$$\mathrm{Tr}_{pert\ bulk}(B_{pert\ bulk} C_{pert\ bulk}) \leq (\mathrm{Tr}_{pert\ bulk} B_{pert\ bulk})(\mathrm{Tr}_{pert\ bulk} C_{pert\ bulk}). \tag{8.41}$$

Thus we see that, at each order in the semiclassical expansion, quantum corrections cannot induce violations of (8.6).

Since we have not specified the gravitational theory, it is not natural at this stage to separate out discussions of higher derivative terms. We will instead address related issues in section 8.3.3 when we discuss the status of our assumptions in various classes of theories.

8.3.3 The status of our assumptions in general gravitational theories

We now turn to a discussion of assumptions 1-4 from section 8.3.2 for general theories of gravity. These assumptions require the semiclassical approximation to Euclidean quantum gravity to be determined by minimizing an action functional over appropriate classes $\mathcal{K}_{\tilde{M}}$ of spacetimes satisfying boundary conditions given by some $\tilde{M}$. At first glance, this idea may appear to be famously false in Euclidean Einstein-Hilbert gravity due to the conformal factor problem [40]. In particular, one can find smooth Euclidean bulk spacetimes satisfying arbitrary boundary conditions that make the Euclidean Einstein-Hilbert

action arbitrarily negative, so that minimal action configurations do not exist.

Any attempt to establish the assumptions used in section 8.3.2 must thus begin with some viewpoint on how the conformal factor problem is to be addressed. We have already discussed the Saad-Shenker-Stanford paradigm for JT gravity (with dilaton-free matter couplings) in section 8.2.2, where we showed that it leads to the desired trace inequality in the semiclassical limit. While we see no simple argument that such a paradigm satisfies our assumption 3 or assumption 4, we argue below that our assumptions *are* in fact satisfied within two other (perhaps overlapping) paradigms for dealing with the conformal factor issue. The first, which we call the Gibbons-Hawking-Perry paradigm, is a hypothetical non-linear generalization of the contour rotation prescription described in [40] for linearized fluctuations about Euclidean Schwarzschild. The second follows [46] in taking the Lorentzian path integral to be fundamental, evaluating the Lorentzian path integral with "fixed-area boundary conditions," and arguing that the result reduces to an integral over Euclidean spacetimes that are on-shell up to the presence of conical singularities.

We discuss each of these paradigms in turn below. The first discussion (section 8.3.3) is necessarily brief and schematic due to the hypothetical nature of the supposed extension of known results. More details will be provided when considering the second paradigm in section 8.3.3. This will allow key elements of the assumptions either to be proven or to be reformulated as precise conjectures concerning the classical action which should be amenable to future mathematical and numerical studies.

The Gibbons-Hawking-Perry Contour Rotation Paradigm

As shown long ago by Gibbons, Hawking, and Perry [40], at the linearized level for familiar cases one can obtain physically reasonable results (see also [219, 41, 42, 43, 220, 221, 222, 223, 224, 44, 45]) by 'rotating the contour of integration.' This in fact

means that one defines the path integral to integrate over some non-trivial contour Γ in the space of complex metrics. In the linearized cases mentioned above, the action is real and bounded-below on the Γ chosen in [225]. This last point contrasts with the Saad-Shenker-Stanford paradigm which also uses a non-real contour, but on which the action is manifestly complex. In the case considered by Gibbons, Hawking and Perry, the action also diverges to $+\infty$ in all asymptotic regions of Γ. As a result, the action on Γ is necessarily minimized at some finite smooth saddle-point that dominates the path integral in the semi-classical limit. If this same structure persists in the non-linear theory, then Assumption 1 is clearly satisfied if we simply redefine configurations on Γ to be 'real' for the purposes of that assumption. See also the discussions of contour rotation for the full theory in [200, 226].

Now, Assumptions 3 and 4 require the full space $\mathcal{K}_{\tilde{M}}$ to admit configurations with conical singularities. If the saddles are known to be smooth, and if the construction of Γ respects symmetries of the boundary conditions, then we can take $\mathcal{K}_{\tilde{M}}$ to be given by those spacetimes lying on Γ which can be formed from smooth spacetimes by applying a single cut-and-paste operation of the type described in Assumption 2. This choice allows us to restrict attention to spacetimes that are 'not too wild' and on which we can hope to have some control over the action as a function on $\mathcal{K}_{\tilde{M}}$. Furthermore, if the specification of the desired contour Γ is sufficiently local in spacetime, then cutting spacetimes $\gamma_1, \gamma_2 \in \Gamma$ into pieces and pasting them together to build a new configuration γ will also naturally yield $\gamma \in \Gamma$. As a result, the above definition of $\mathcal{K}_{\tilde{M}}$ would then be manifestly invariant under such operations. So long as the spacetimes satisfy appropriate boundary conditions, Assumption 2 will then be satisfied if our action includes appropriate boundary terms. Explicit discussions of such boundary conditions and boundary terms for JT and Einstein-Hilbert gravity will appear in section 8.3.3 below.

It thus remains only to discuss Assumptions 3 and 4. As described between (8.38)

and (8.39), for Euclidean geometries in Einstein-Hilbert gravity the two sides of (8.38) differ only by contributions from the conical singularities. A standard calculation shows that this gives an extra factor of $e^{-A/4G}$ on the left hand side, where A is the area of the conical singularity. Similarly, in JT gravity (normalized as in (8.25)), the difference is a factor of $e^{-4\pi\phi}$ evaluated at the singularity. As a result, in either of these theories, so long as A (or ϕ) is positive on the contour Γ, these assumptions will be satisfied as well.

As a final comment on this paradigm, let us address the question of perturbative higher derivative corrections to either JT gravity or Einstein-Hilbert gravity. Rather than attempt to discuss Assumptions 1-4 for the full path integral with higher-derivative corrections, we will instead take perturbative treatment of such terms to mean that their corrections to the two-derivative theory are computed by first finding saddles that would dominate the semiclassical computation in the two-derivative theory, and then using the higher derivative terms to compute perturbative corrections to the relevant actions. So long as we suppose that the dominant 2-derivative saddle for each path integral is unique, we may then argue that the trace inequality (8.6) is preserved by higher derivative corrections in direct analogy with the non-gravitational discussion at the end of section 8.3.1. The only comment needed to promote that argument to the gravitational context is to again note that assumption 3 (applied at the level of the two-derivative theory) means that we may indeed confine discussion of higher derivative corrections to perturbation theory about saddle points for $\mathrm{Tr}_{\mathcal{D}}(B)$, $\mathrm{Tr}_{\mathcal{D}}(C)$ in the two-derivative theory that are constructed from the two-derivative saddle for $\mathrm{Tr}_{\mathcal{D}}(BC)$ using the cut-and-paste procedure above. As in the non-gravitational discussion at the end of section 8.3.1, we leave open for future study the more general but finely-tuned case where the saddles fail to be unique.

Euclidean path integrals from fixed-area Lorentzian path integrals

While the discussion of the Gibbons-Hawking-Perry paradigm in section 8.3.3 was straightforward, it also relied on the conjectured existence of a hypothetical contour Γ with certain properties. Furthermore, since the form of the presumed Γ is not known, it is difficult to perform further checks within that approach. In contrast, we shall see that the paradigm described in [46] allows a more detailed discussion of assumptions 1-4 and also presents more well-defined opportunities for further consistency checks.

The treatment of [46] considered the special case of computing partition functions $Z(\beta) = \mathrm{Tr}(e^{-\beta H})$ for time-independent gravitational systems. However, it did so by taking the Lorentz-signature path integral to be fundamental, and to be defined as an integral over spacetimes that were both real and Lorentz-signature up to the presence of certain codimension-2 singularities that one may call "Lorentzian conical singularities" following [6, 4]; see also [227, 228, 229, 230, 231, 232], as well as [200, 226] and [233, 234, 235] for earlier arguments that treating the Lorentzian formalization as fundamental is essential to resolving the Euclidean conformal factor problem. As a result, much as in section 8.2.1, $Z(\beta)$ was first written as an integral transform of distributional quantities that one may call $\mathrm{Tr}(e^{itH})$. Due to their distributional nature, the quantities $\mathrm{Tr}(e^{itH})$ are generally not well-defined for any fixed t, though integrating over t gives a well-defined result.

The suggestion of [46] was to first integrate over the real Lorenz-signature metrics while holding fixed the areas of the codimension-2 conical singularities. In practice, this was done using the stationary phase approximation. It is an interesting point that the Jackiw-Teitelboim and Einstein-Hilbert actions define good variational principles with such fixed-area boundary conditions [73], and that the associated saddles may have arbitrary conical singularities at the fixed-area surface (as suggested in [48, 47]); similar

statements also hold in the presence of perturbative higher derivative corrections [73]. Evaluating the above-mentioned integral transform then led to a result that could be expressed as a final integral over *Euclidean*-signature metrics that satisfied the Euclidean equations of motion everywhere away from the fixed-area codimension-2 conical singularities, and which were thus known as Euclidean fixed-area saddles. Since the saddles were parameterized by the here-to-fore-fixed areas of the conical singularities, the final integral was simply an integral over the associated areas. For simple gravitational partition functions, this process was shown in [46] to yield the standard results.

Let us therefore imagine that, in the semiclassical limit, a similar paradigm can be applied to any Euclidean path integral. In particular, given any operator B in the dual theory $\mathcal{D}$, we imagine that $\mathrm{Tr}_{\mathcal{D}}\, B$ can be computed semiclassically as

$$\mathrm{Tr}_{\mathcal{D}}\, B \approx \int_{A\in\mathbb{R}^+} dA\, e^{-\tilde{I}_A(s_A)}, \tag{8.42}$$

where $A \geq 0$ parameterizes the possible codimension-2 areas of a set of conical singularities, $\tilde{I}_A$ is an action that gives a good variational principle when the area A is fixed, and the argument s_A denotes the real Euclidean saddle of $\tilde{I}_A$ having the lowest action $\tilde{I}_A(s_A)$ for the given value of A that is consistent with satisfying the boundary condition at infinity. This paradigm can also be applied to JT gravity with matter (where a codimension-2 surface is a discrete set of points) by replacing the area A by the value of the dilaton ϕ summed over conical singularies. Here we assume $\phi_0 + \phi \geq 0$ at each singularity.

In writing (8.42), it is assumed that the integral on the right-hand-side converges and that no further contour rotations are required. This is not at all obvious from a cursory study of the gravitational action. However, as argued in [47] (see also [48]), the quantities $e^{\tilde{I}_A(s_A)}/\,\mathrm{Tr}_{\mathcal{D}}\, B$ are expected to represent the probabilities $p(A)$ of finding an extremal

surface with area A in a quantum gravity state with boundary conditions determined by the operator B. Since probabilities sum to unity, this would then require the right-hand-side of (8.42) to converge as desired. This idea has by now been investigated in a variety of contexts which appear to support this conclusion; see e.g. [38, 7, 236, 1, 46, 62, 237, 238].

For clarity, we formalize this assumption as follows:

Assumption 5 *We assume that, in the UV-completion of either JT gravity or Einstein-Hilbert gravity with minimally-coupled matter, the integral over fixed-area-saddles on the right-hand-side of* (8.42) *converges and gives a good approximation to the left-hand-side in the semiclassical limit.*

Assumption 5 is now *almost* sufficient to allow us derive assumptions 1-4 for both JT and Einstein-Hilbert gravity. However, recall that – just as in the non-gravitational setting of section 8.3.1 – the cut-and-paste operations of section 8.3.2 can produce surfaces on which certain equations of motion do not hold, and in particular at which first derivatives of fields fail to be continuous (though such derivatives admit well-defined limits when approaching the surface from either side).

As a result, we will need to further strengthen Assumption 5. We motivate the final version using an idea similar to the motivation for Assumption 5 itself. In particular, let us note that there is a set of diffeomorphism-invariant observables defined by the conformal geometry of a minimal surface anchored to particular cuts of the asymptotically AdS boundary. Furthermore, the same is true for the minimal surface that is anchored to both the fixed-area surface *and* to particular cuts of the asymptotically AdS boundary, and it is again true when the surface is minimal only within any given homotopy class. Similarly, as will be discussed further in the next paragraph, one would expect states to be orthogonal when they have distinct such conformal geometries. One therefore expects that one can assign a probability to each possible conformal geometry in this context,

and that the full path integral is given by integrating over such conformal geometries in analogy with (8.42). (As we will see below, it will be convenient to take the slicing prescription of Assumption 2 to be defined by minimal surfaces.)

Here we have restricted discussion to conformal geometries on the minimal surface since requiring the surface to be minimal is a form of gauge-fixing. After such gauge-fixing, the full induced metric will not form a set of commuting observables. Instead, one component of the induced metric becomes a function of the other coordinates and momenta by solving the Hamiltonian constraint. Since it is canonically conjugate to the trace of the extrinsic curvature (which has been fixed to zero), one solves this constraint for the conformal factor of the induced metric. The remaining conformal geometry on the minimal surface continues to define a set of commuting observables.

The above comments then motivate the following assumption, which is a generalization of Assumption 1:

Assumption 6 *Let $\mathcal{K}_{\tilde{M},A}$ be the class of spacetimes that i) satisfy asymptotic boundary conditions specified by $\tilde{M}$, ii) satisfy fixed-area boundary conditions at A, iii) have fields that are continuous everywhere, and iv) satisfy the conditions to be a fixed-area saddle everywhere except on a single codimension-1 minimal surface Σ anchored both to the fixed-area surface and to some cut of the boundary. As usual, we restrict to the case where the sources on $\tilde{M}$ are real. In this case we assume that the fixed-area action on $\mathcal{K}_{\tilde{M},A}$ is minimized by real saddles; i.e., every $k \in \mathcal{K}_{\tilde{M},A}$ has action equal to or greater than that of some real saddle $k_s \in \mathcal{K}_{\tilde{M},A}$ of the fixed-area action $\tilde{I}_A$.*

Note that minimal surfaces in Euclidean signature are often well-defined even when the spacetime is not smooth. We assume that this is the case in the above context though, if needed, we could further elaborate on this definition by requiring the spacetime to be built from smooth spacetimes using cut-and-paste along minimal surfaces.

Now, as discussed recently in both [239, 63] in the context of JT gravty, there are various subtleties and possible choices involved in using minimal surfaces to construct observables (or, equivalently in the language of those references, to fully fix a gauge in the Euclidean path integral). Such subtleties may in the end require further refinements to assumption 6. But it is also plausible that such issues are not important at the level of our current discussion. We have thus formulated assumption 6 without taking such issues into account. Similarly, while minimal surfaces are smooth when the bulk spacetime dimension satisfies $D \leq 7$ [240], they can be singular for $D \geq 8$ [241]. This is another reason why a useful conjecture for $D \geq 8$ could require further modification and/or additional work to describe a useful notion of the Einstein-Hilbert action on $\mathcal{K}_{\tilde{M},A}$. However, at least for $10 \geq D \geq 8$ it turns out that such singularities are non-generic [242, 243].

Returning to the discussion of Assumption 6, and in order to both gather further supporting evidence for it, let us note that a particular consequence of this assumption is a new positive action conjecture:

Assumption 7 *Let $\mathcal{K}_{\tilde{M},A}$ be as in Assumption 6. Then the fixed-area action $\tilde{I}_A$ is bounded below on $\mathcal{K}_{\tilde{M},A}$.*

This remains to be proven in general. However, we will argue in section 8.4 that this assumption should hold for any gravitational theory when the gravitational Hamiltonian is bounded below in an appropriate sense. We will also show there that it is equivalent to what is naturally called a positive-action conjecture for gravitational wavefunctions.

Furthermore, the results of appendix G.1 show explicitly that this conjecture holds for JT gravity with dilaton-free couplings to matter. In JT gravity, the value of the dilaton at a point plays the same role as the area of a codimension-2 surface in higher dimensional gravitational theories; see e.g [213, 182]. Furthermore, in the same way that

we might fix the area of a disconnected codimension-2 surface in higher dimensions, in JT we should allow the specification of a fixed-dilaton (fixed-ϕ) set, in the sense that we fix the sum $\phi_{total} = \sum_i \phi_i$ where ϕ_i are the dilaton values at each of the singular points. In discussing JT gravity we thus write $\mathcal{K}_{\tilde{M},\phi_{total}}$ instead of $\mathcal{K}_{\tilde{M},A}$.

The important point in the JT argument is that, since the bulk spacetime dimension is $D = 2$, the minimality of a codimension-1 surface Σ implies that its extrinsic curvature tensor vanishes. As a result, for any $k \in \mathcal{K}_{\tilde{M},A}$ the spacetime metric is in fact C^1 (except at the fixed-dilaton conical singularity) and the Ricci scalar cannot contain codimension-1 delta-functions localized on Σ. Since $R = -2$ on each side of Σ, we then find $R = -2$ on Σ as well (again, except at the fixed-dilaton conical singularity). Furthermore, as reviewed in appendix G.1.3, if we ignore the conical singularities then the JT action on $\mathcal{K}_{\tilde{M},\phi_{total}}$ would be given by the Schwarzian action. It would thus be bounded below by the analysis of appendix G.1.4.

But it is also easy to include the contribution from the conical singularities. This is just $I_{sing} = -2\pi \sum_i \phi_i \delta_i$, where δ_i is the conical deficit at each singularity. Conical excesses are also allowed, but those are just deficits with $\delta_i < 0$. Since each deficit must satisfy $\delta_i \leq 2\pi$ we have the bound

$$I_{sing} \geq -4\pi \sum_i \phi_i = -4\pi \phi_{total}. \tag{8.43}$$

Combining this with the bound on the Schwarzian action and the positivity of the matter action then establishes Assumption 7 in this context.

Having motivated Assumptions 5 and 6, we now turn to the issue of showing that – together with known results for JT and Einstein-Hilbert gravity – they imply Assumptions 1-4. Note that Assumptions 5 and 6 immediately imply Assumption 1, as they were designed to do. Furthermore, assumptions 3 and 4 were already shown to be true for

JT and Einstein-Hilbert gravity by the discussion of section 8.3.2 (between (8.38) and (8.39)).

This then leaves only Assumption 2. There are two parts to showing that this assumption holds. The first is to specify a cutting rule for Assumption 2 so that pasting the various pieces together yields a spacetime that satisfies the desired asymptotic boundary conditions and, in particular, for which the new spacetime has a sufficiently smooth asymptotic boundary for which the action is finite and for which the action defines a good variational principle. As noted above, for either JT or Einstein-Hilbert gravity, it will be convenient to take the cuts to be defined by minimal surfaces. For JT gravity, appendix G.1.1 then shows that the associated cut-and-paste construction preserves the boundary conditions of the variational principle (which were also shown to imply finiteness in appendix G.1.3). For Einstein-Hilbert gravity, this property is even easier to verify and is established in appendix G.2.

The second task is then to establish the additivity property (8.36). This is again straightforward for both JT and Einstein-Hilbert gravity. The main point is that, since the boundaries we sew together are now taken to have $K = 0$, there can be no delta-function contribution to the Ricci scalar at the seam where the sewing occurs – though, as described in appendix G.1.2, in JT gravity it turns out that even when the slicing surfaces are *not* minimal the delta-function in the Ricci scalar is such that it does not spoil (8.36).

Furthermore, the matter action is additive for the reasons explained in section 8.3.1. It thus remains only to show additivity for the boundary terms at asymptotic boundaries. One such term is always the Gibbons-Hawking term, while the rest are boundary counter-terms. Due to the condition that each operator have an appropriate "rim", the boundary metric and other analogous boundary conditions are manifestly smooth. Thus the boundary counter terms are integrals of smooth functions and their additivity is also

manifest.

The final term to consider is then the Gibbons-Hawking term. For a regulated version of the spacetime where the boundary has been moved inward to a finite value ϵ of the appropriate Fefferman-Graham coordinate (or of the defining function of the conformal frame in the language used for JT gravity in appendix G.1), the extrinsic curvature of the regulated boundary generally has a delta-function at the seam; see figure 8.10. But since the strength of this delta-function is always determined by the angles at which the asymptotic boundary meets the seam, we can render this part of the action additive by simply adding an appropriate 'corner term' to the definition of the action for the cut space.

This procedure is discussed in great detail for JT gravity in appendix G.1.2. The Einstein-Hilbert case is then discussed in appendix G.2. Appendix G.2 in fact shows that, with the usual boundary conditions and the choices we have made, the above delta-function turns out to make no contribution to the action in the limit $\epsilon \to 0$. Thus the corner terms also vanish in the $\epsilon \to 0$ limit and are not strictly needed in the Einstein-Hilbert case. As a result, for JT and Einstein-Hilbert gravity we have now shown that Assumptions 5 and 6 do in fact imply Assumptions 1-4.

8.4 On a positive-action conjecture for quantum gravity wavefunctions

As a slight aside from the main discussion, this section elaborates further on the status of Assumption 7 in Einstein-Hilbert and other theories of gravity. We will first describe how it is equivalent to what is naturally called a positive-action conjecture for quantum gravity wavefunctions. We then point out that, at least when the the surface Σ is a slice

of a foliation of the bulk spacetime that is smooth away from Σ and which also smoothly foliates a compact AlAdS boundary, the conjecture is implied by the requirement that the gravitational Hamiltonian H is bounded-below. While the known asymptotically AdS positive energy theorems [244, 245, 246] are not sufficient to prove positivity of H at this level, the connection nevertheless provides additional physical reasons to believe that Assumption 7 will hold.

Recall that Assumption 7 referred to bulk spacetimes $\mathcal{M}$ which have only asymptotic boundaries, but which may contain a surface Σ on which derivatives of fields are not continuous. Furthemore, away from Σ the Euclidean equations of motion are satisfied. As a result, if we cut the spacetime along Σ then each piece gives a smooth extremum of the standard Euclidean action so long as an appropriate boundary term is included at the cutting surface Σ and corresponding boundary conditions are imposed at Σ. In particular, even though $\mathcal{M}$ may have a conical singularity, the resulting pieces do not (though the boundaries of these pieces at Σ may contain 'corners' at which the extrinsic curvature of Σ contains delta-functions; see figure 8.11).

For Einstein-Hilbert gravity, it is convenient to take this boundary term to be a Gibbons-Hawking term at Σ, and thus to think of the resulting action as defining a variational principle for the space of configurations defined by fixing the induced metric on Σ to its value in $\mathcal{M}$. Note that such pieces are precisely the spacetimes that appear as saddles in Euclidean path integral computations of gravitational wavefunctions in the metric representation, where for a $(d+1)$-dimensional bulk, one thinks of the state as a functional $\Psi(g^{(d)})$ of the d-dimensional (Riemannian-signature) metric induced on a Cauchy surface. Furthermore, the induced metric $g^{(d)}$ on Σ that minimizes this action will correspond to the peak of that wavefunction, which one expects to be finite in the semiclassical limit. As a result, one could also motivate Assumption 7 from the belief that semiclassical Euclidean path integral calculations of such wavefunctions should give

sensible answers.

Now, much as in the discussion of section 8.3.2, if Σ divides $\mathcal{M}$ into two pieces $\mathcal{M}_1$ and $\mathcal{M}_2$, we can also glue $\mathcal{M}_1$ to a reflected manifold $\mathcal{M}_1^R$ with the same action to define a new member $\mathcal{M}_1^{double}$ of an appropriate space $\mathcal{K}_{\tilde{M},A}$. Moreover, as argued in section 8.3.3, Einstein-Hilbert gravity satisfies the additivity condition (8.36), so that

$$I(\mathcal{M}_1^{double}) = 2I(\mathcal{M}_1). \tag{8.44}$$

In particular, having a lower bound for $I(\mathcal{M}_1^{double})$ is equivalent to having a lower bound for the action $I(\mathcal{M}_1)$ of the piece $\mathcal{M}_1$. Furthermore, using

$$I(\mathcal{M}) = I(\mathcal{M}_1) + I(\mathcal{M}_2), \tag{8.45}$$

having a uniform lower bound for all such pieces would imply a lower bound for the action on $\mathcal{K}_{\tilde{M},A}$.

In fact, we can also drop the requirement that Σ be minimal. The reason for this is explained in detail for JT gravity in appendix G.1.3, though it holds equally well for general theories of gravity. As described there, if one thinks of each piece $\mathcal{M}_1, \mathcal{M}_2$ as being part of a larger saddle that extends beyond Σ, then the Hamiltonian constraint requires the on-shell action to be invariant under continuous deformations of Σ that do not move the anchor set $\partial\Sigma$ on the asymptotic boundary. More specifically, the previous statement is true so long as the action includes sufficient 'corner terms' so that it defines a good variational principle under boundary conditions for Σ consistent with the desired deformation.

It thus follows that Assumption (7) is in fact equivalent to the following conjecture which, due to the above-mentioned connection with $\Psi(g^{(d)})$, we call the positive-action

conjecture for quantum gravity wavefunctions:

Conjecture 1 *Consider the space of smooth Euclidean spacetimes having both an Asymptotically locally AdS (AlAdS) boundary (associated with some cosmological constant* $\Lambda < 0$*) and an additional finite-distance boundary at some surface* Σ*. In the usual way, we use a Fefferman-Graham expansion to fix a 'boundary metric' at the AlAdS boundary. We also impose some class of boundary conditions at the 'corners' where* Σ *meets the AlAdS boundary. We require that the boundary conditions allow* Σ *to be deformed to a minimal surface. Note, however, that we impose no boundary conditions on* Σ*.*

Let us now further restrict to such spacetimes that solve the vacuum Euclidean Einstein equations with cosmological constant Λ*. On such solutions we consider the Euclidean Einstein-Hilbert action with cosmological constant* Λ*, together with the standard Gibbons-Hawking term on all smooth parts of the boundary, the standard boundary counter-terms on the AlAdS boundary, and 'corner terms' appropriate to the above-chosen boundary conditions at the corners. For fixed such boundary conditions we require the above action functional is bounded below.*

Here the qualification that the corner boundary conditions must allow Σ to be deformed to a minimal surface is needed in order to preserve equivalence with Assumption 7, but is not obviously critical for the existence of a lower bound. We also emphasize that we have *not* fixed a particular induced metric on Σ, so that our lower bound is required to be independent of that induced metric. Furthermore, if conjecture 1 holds then one can clearly also couple the system to positive-action matter with similar results.

This conjecture generalizes Hawking's original positive action conjecture [40] from asymptotically flat to AlAdS spacetimes, and also by introducing the finite boundary Σ (appropriate to thinking of the spacetime as a Euclidean saddle for $\Psi(g^{(d)})$ instead of a partition function). Such generalizations are natural in the spirit of the original

conjecture. The above conjecture is also weaker than that of [40] in the sense that we require only that each set of boundary conditions lead to a lower bound, but we allow this lower bound to depend on the choice of boundary conditions and, in particular, we allow the possibility that for some boundary conditions the greatest lower bound is less than zero.

The positive action conjecture for asymptotically Euclidean spacetimes was proven by realizing that the Euclidean action in that context is equal to the Hamiltonian for a higher-dimensional Lorentzian-signature theory of gravity evaluated on a Riemannian-signature Cauchy surface [247]. This trick fails in the asymptotically AdS context, so a new proof strategy is needed.

While it is unclear to us how to give a complete proof in general, there is a simple context in which the conjecture follows from having a lower bound for the gravitational Hamiltonian. To see the connection, consider a bulk spacetime $\mathcal{M}$ subject to boundary conditions as stated in the conjecture, and suppose that $\mathcal{M}$ admits a smooth foliation such that $\Sigma = \Sigma_1 \cup \Sigma_2$ with Σ_1 diffeomorphic to Σ_2 and with both Σ_1, Σ_2 being limiting cases of the slices in the foliation. We will refer to Σ_1 as the time t_1 and to Σ_2 as the time t_2 with slices in the foliation labeled by $t \in (t_1, t_2)$. Consider then the action $I_{[t_1,t]}$ of for the region defined by slices with $t \in [t_1, t]$. Clearly the zero-volume region $[t_1, t_1]$ has $I_{[t_1,t_1]} = 0$. Furthermore, the usual Hamilton-Jacobi argument gives $\partial_{t_2} I_{[t_1,t_2]} = H(t_2)$, where $H(t_2)$ is the standard (time-dependent) gravitational Hamiltonian defined by the boundary conditions on the asymptotic boundary and evaluated on the initial data defined by the surface Σ_{t_2}. As a result, if the boundary Hamiltonian $H(t)$ has a t-independent lower bound E_0, then the action will satisfy

$$I_{[t_1,t_2]} \geq |t_2 - t_1| E_0. \tag{8.46}$$

For any given t it is natural to believe the corresponding $H(t)$ to be bounded below so, since we consider a case in which the range of t is compact, it is also natural to expect this lower bound to be uniform[5].

However, there are many situations which are not of the above form. Consider, for example, Euclidean AdS_3 in the conformal frame where the boundary metric is that of S^2. Slicing the S^2 along surfaces of constant polar angle θ, the boundary anchor sets $\partial\Sigma_t$ are then circles of time-dependent size that pinch off at the poles. Furthermore, due to the Casimir energy of AdS_3 [249, 250], the lower bound on the Hamiltonian diverges as the size of the circle shrinks to zero.

While spherical AdS_3 gives an example where $H(t)$ has no uniform bound, it is nevertheless a context where the total action is finite and, moreover, where one very much expects the given spacetime to minimize the action. We are therefore hopeful that further study of this example may suggest how the above sketch of a proof might be improved to deal with more general contexts. We may also hope to learn to deal with the loci where the bulk topology forces the above foliations break down. However, we leave such investigations for future work.

8.5 Discussion

The above work discussed the trace inequality

$$\mathrm{Tr}_{\mathcal{D}}(BC) \leq \mathrm{Tr}_{\mathcal{D}}(B)\,\mathrm{Tr}_{\mathcal{D}}(C), \tag{8.47}$$

[5]However, it should be noted that due to issues related to footnote 2 in section 8.3.1, the boundary conditions on certain slices of a Euclidean solution may not be simply related to boundary conditions for any Lorentz-signature gravitational Hamiltonian. Stability of the Lorentz-signature theory is thus insufficient to motivate the above belief. Furthermore, the known AlAdS positive-energy theorems address only a limited set of AlAdS boundary conditions. Indeed, techniques that follow [248] are likely limited to contexts that allow supersymmetry.

which applies to positive operators B, C on any Hilbert space $\mathcal{H}$. The symbol $\mathcal{D}$ denotes the non-gravitational CFT dual of a bulk theory, and we write $\mathrm{Tr}_{\mathcal{D}}$ to emphasize that the trace is the standard trace on the $\mathcal{D}$ side of the duality. In particular, $\mathrm{Tr}_{\mathcal{D}}$ denotes the familiar operation computed by introducing any orthonormal basis $|i\rangle_{\mathcal{D}}$ on the $\mathcal{D}$ Hilbert space and performing the sum (8.3). Averaging over an ensemble gives

$$\langle \mathrm{Tr}_{\mathcal{D}}(BC)\rangle \leq \langle \mathrm{Tr}_{\mathcal{D}}(B)\,\mathrm{Tr}_{\mathcal{D}}(C)\rangle. \tag{8.48}$$

Our goal was to understand the status of the above inequality on the bulk side of the AdS/CFT duality. In particular, we studied the conjectured inequality

$$\zeta\left(\tilde{M}_{bc^\dagger cb^\dagger}\right) \leq \zeta\left(\tilde{M}_{b^\dagger b} \sqcup \tilde{M}_{c^\dagger c}\right), \tag{8.49}$$

where $\sqcup$ denotes disjoint union. Here $\tilde{M}_{bc^\dagger cb^\dagger}$ is a smooth closed manifold specifying boundary conditions for our bulk theory on a Euclidean Asymototically locally Anti-de Sitter boundary that can be broken into four pieces $M_b, M_{b^\dagger}, M_c, M_{c^\dagger}$. Furthermore, we require that connecting M_b and $M_{b^\dagger}$ gives a new smooth closed manifold $M_{bb^\dagger}$ that is invariant under a reflection-symmetry that exchanges the b and $b^\dagger$ pieces (and which complex-conjugates any complex boundary conditions) and similarly for $M_{cc^\dagger}$.

At the level of the semiclassical expansion, and when the operators B, C define Eucldean bulk path integrals with connected boundaries, we argued that the natural bulk dual of (8.49) was in fact satisfied to all orders in the semiclassical expansion in two important contexts. The first is the case of JT gravity with a dilaton-free coupling to two-derivative matter, with the possible further addition of perturbative higher derivative terms. The second is given by Einstein-Hilbert gravity minimally coupled to two-derivative matter, where again higher derivative terms can also be included perturba-

tively.

In all cases we assumed the bulk path integral defined by $\tilde{M}_{bc^\dagger cb^\dagger}$ (dual to $\langle \mathrm{Tr}_{\mathcal{D}}(BC)\rangle$) to be dominated by a single bulk saddle. When several bulk saddles are equally dominant, formally non-perturbative effects associated with addition saddles and/or mixing between saddles can be more important than perturbative corrections and are subtle to analyze; see e.g. recent discussions in [67, 216] for condensed matter analogues and in [38, 7, 72, 206]. We thus save further consideration of this case for future study.

For pure JT gravity, much can be said using explicit calculations based on standard Euclidean saddles. In addition, the non-perturbative definition of the Euclidean path integral described by Saad, Shenker, and Stanford [51] can be used to give a general derivation of (8.49).

For more general cases the Euclidean path integral is sufficiently poorly understood that we cannot use the term "proofs" to refer to our arguments. Instead, we proceeded by stating various assumptions that we argued were plausibly true in regimes where a Euclidean gravitational path integral emerges from a more UV-complete theory. In particular, we considered three rather distinct paradigms for such path integrals. One of these was the possible extension of the Saad-Shenker-Stanford approach mentioned above [51] to (some UV-completion of) JT gravity coupled to positive action matter. Another paradigm a nonlinear generalization of the Gibbons-Hawking-Perry contour rotation prescription [40]. The third was the paradigm described in [46] that took a real-time formulation as fundamental but then described a procedure for transforming semiclassical computations into what were often sums over Euclidean saddles. We argued that all three paradigms lead to a bulk version of (8.47) in the semiclassical context described above.

A significant restriction in our arguments was that we considered only boundary conditions which are real in Euclidean signature, and which thus cannot include Lorentzian

components. There is a sense in which extending our analysis of general gravitational theories to complex boundary conditions would be trivial, since we need only suitably extend the various assumptions we made along the way. This, however, would miss an important point that arise for both the non-gravitational path integrals studied in section 8.3.1 and the JT case analyzed semiclassically in section 8.2.1. Once the sources are complex, the relevant saddles will generally not lie on the original contour of integration. In that context, the most direct analogue of the argument given here would attempt to show that cutting and pasting a valid complex saddle (through which the integration can be deformed to pass) for the left-hand-side of (8.49) yields a configuration k that lies on the steepest descent curve Γ_{ds} through the dominant saddle for the right-hand-side (so that dominant saddle then has lower action). Since it is not at all clear to us why that k should lie on the relevant Γ_{sd}, we have not attempted to formulate a gravitational argument in this language. Instead, we leave further consideration of complex sources for future work.

While it may be difficult to verify our assumptions about the Euclidean path integral, such assumptions imply other properties of the *classical* Euclidean action that are more amenable to study in the near future, and which in particular might be investigated numerically. The most tangible prediction is the positive action conjecture for gravitational wavefunctions described in section 8.4. This conjecture generalizes Hawking's original positive action conjecture [40] to the AdS context, and also generalizes it further by allowing spacetimes with an extra finite-distance boundary. However, we require only that the action be bounded below for each set of AlAdS bondary conditions, and not that the action be strictly non-negative. As some evidence in support of this conjecture, we *were* able to prove that the corresponding result holds in the simpler case of JT gravity (with general dilaton-free couplings to positive-action matter).

Let us now return to the discussion of (8.49). The main physical lesson from our

investigations appears to be that this inequality is closely associated with positivity of entropy in the sense of having a positive density of states. To be more precise, we saw in various ways that the right-hand-side of (8.47) tends to be *much* larger than the left when the spectral densities of B and C are large. This is manifest from the CFT-side argument surrounding equation (8.4), as well as from the thermodynamic discussion in section 8.2.1. However, a corresponding feature also appeared in our gravitational arguments where in the Einstein-Hilbert case we found the left-hand-side to be suppressed relative to the right by a factor of $e^{-A/4G}$ associated with the area of an extremal surface. Similarly, in the JT context with the action (8.25) we found a similar suppression by $e^{-4\pi\phi_0}$. These expressions are readily recognized as being associated with the RT/HRT entropy [26, 66, 27] of a boundary region.

While the inequality (8.47) is not at all highly constraining for familiar quantum mechanical operators, we noted in the introduction that it can have fundamental implications. For example, it is deeply associated with the fact that the algebra of bounded operators on a Hilbert space is a type I von Neumann algebra. We will return both to this connection and to the fundamental status of (8.47) in bulk gravitational theories in a forthcoming work [251].

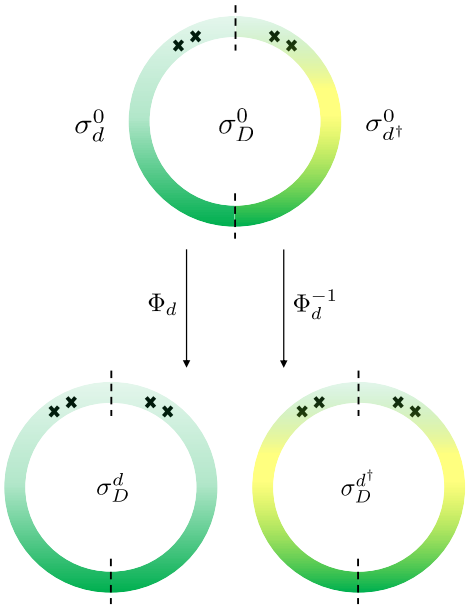

Figure 8.4: For $D = dd^\dagger$, and when considering the path integral that computes $\mathrm{Tr}_{\mathcal{D}}\, D$, a saddle σ_D^0 with no reflection symmetry can be used to construct two reflection symmetric saddles. The top figure shows such a situation where the background fields (denoted by the $\times$ symbols) are left-right symmetric but the saddle (described by the colorations) is not. The background fields for the top figure define $\mathrm{Tr}_{\mathcal{D}}\, D$, and the background fields on the left and right halves define respectively d, $d^\dagger$. To construct the new saddles, one simply cuts σ_D^0 into pieces $\sigma_d^0, \sigma_{d^\dagger}^0$, operates on each with the reflection maps Φ_d or Φ_d^{-1}, and forms new saddles $\sigma_D^d, \sigma_D^{d^\dagger}$ by sewing together each such reflection with the corresponding $\sigma_d^0, \sigma_{d^\dagger}^0$. Here the vertical arrows indicate the actions of Φ_d and Φ_d^{-1}, each of which acts as a left/right reflection on its argument (which is then glued to another copy of the corresponding $\sigma_d^0, \sigma_{d^\dagger}^0$). The resulting reflection-symmetric saddles are called $\sigma_D^d, \sigma_D^{d^\dagger}$. Equations (8.28)-(8.30) then require one of $\sigma_D^d, \sigma_D^{d^\dagger}$ to have action no greater than that of the original saddle σ_D^0.

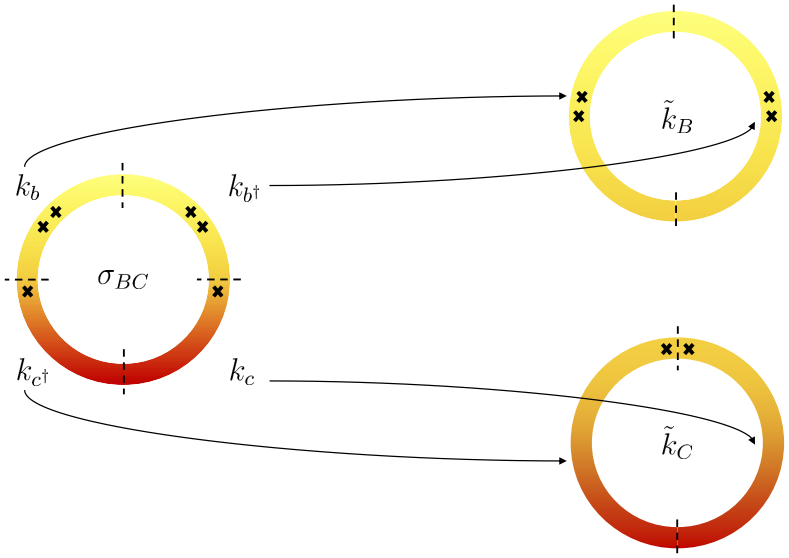

Figure 8.5: For $B = bb^\dagger, C = cc^\dagger$, a $\mathbb{Z}_2$-symmetric saddle σ_{BC} for $\mathrm{Tr}_{\mathcal{D}}\, BC$ (shown at left) can be cut into four pieces $k_c, k_{c^\dagger}, k_b, k_{b^\dagger}$. The pieces can then be recombined to make a pair of $\mathbb{Z}_2$-symmetric configurations $\tilde{k}_B$ and $\tilde{k}_C$ (shown at right) that contribute to the path integrals for, respectively, $\mathrm{Tr}_{\mathcal{D}}\, B$ and $\mathrm{Tr}_{\mathcal{D}}\, C$.

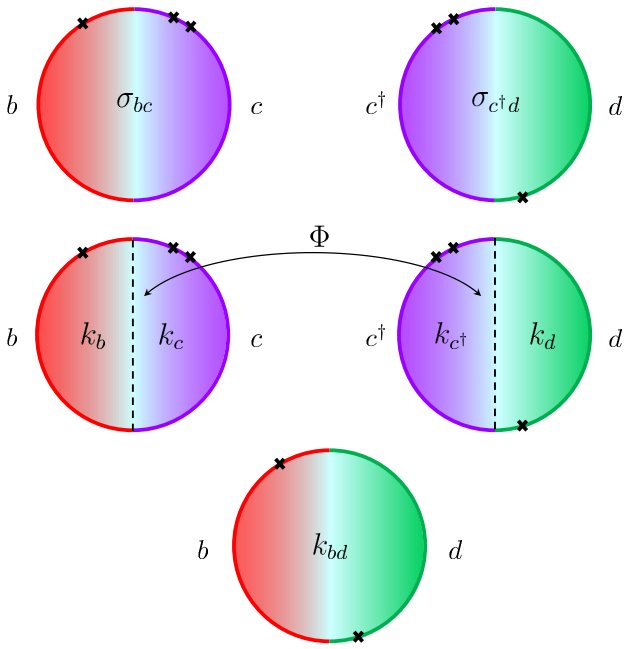

Figure 8.6: Real bulk saddles σ_{bc} and $\sigma_{c^\dagger d}$ for $\mathrm{Tr}_{\mathcal{D}}\, bc$ and $\mathrm{Tr}_{\mathcal{D}}\, c^\dagger d$ can be cut into pieces. Note that the cutting step generally creates new boundaries (dashed lines) not restricted by the asymptotically AdS boundary conditions. When the data on the two new boundaries are related by a diffeomorphism Φ, the pieces can be pasted together to make a bulk configuration k_{bd} for $\mathrm{Tr}_{\mathcal{D}}\, bd$.

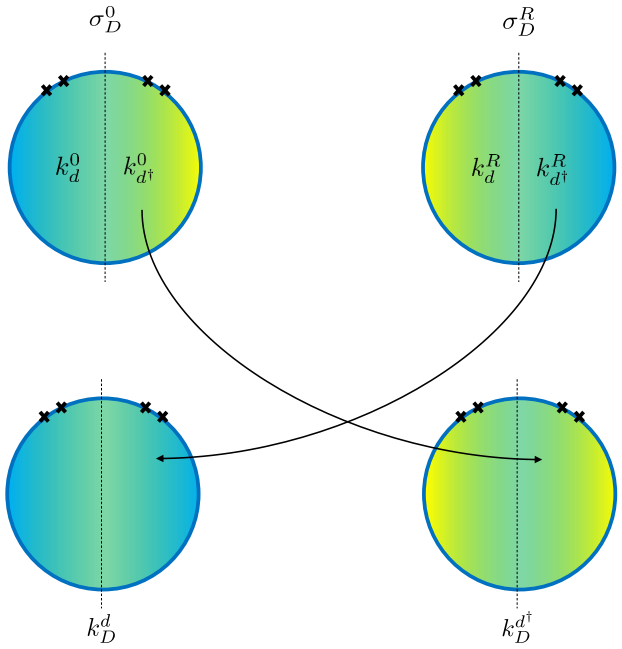

Figure 8.7: When $D = d^\dagger d$, an arbitrary bulk saddle σ_D^0 for $\mathrm{Tr}_{\mathcal{D}}\, D$ can be reflected to give another saddle σ_D^R for the same bulk path integral. We can cut σ_D^0 into parts $k_d^0, k_{d^\dagger}^0$, and we can similarly cut σ_D^R into $k_d^R, k_{d^\dagger}^R$. Gluing k_d^0 to $k_{d^\dagger}^R$ defines a $\mathbb{Z}_2$-symmetric configuration k_D^d for $\mathrm{Tr}_{\mathcal{D}}\, D$, and similarly gluing k_d^R to $k_{d^\dagger}^0$ defines a $\mathbb{Z}_2$-symmetric $k_D^{d^\dagger}$. One of these must have action less than or equal to that of the original saddle σ_D^0. If σ_D^0 was dominant, Assumption 1 would imply that we have now constructed two $\mathbb{Z}_2$-symmetric saddles both having precisely the same action as σ_D^0.

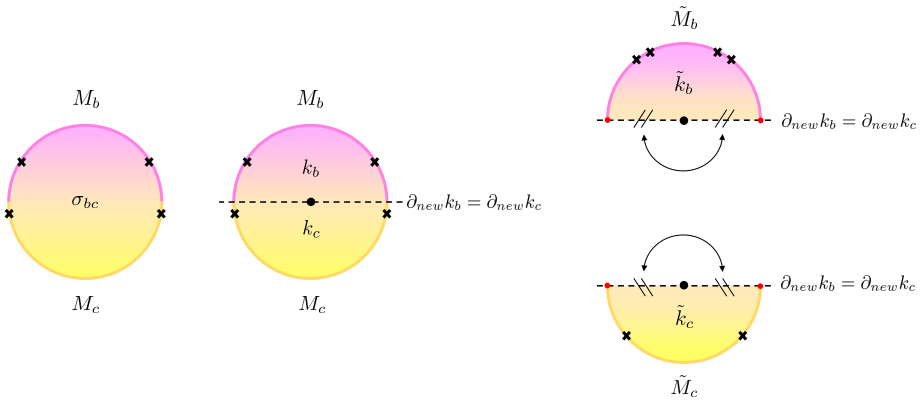

Figure 8.8: We consider a bulk saddle σ_{bc} with a $\mathbb{Z}_2$ reflection symmetry that preserves both M_b and M_c. Such a saddle can be cut into two reflection-symmetric pieces k_b and k_c. This creates new boundaries but, in each piece, the reflection symmetry allows one to remove the new boundaries by making identifications. The results define configurations $\tilde{k}_b \in \mathcal{K}_{\tilde{M}_b}, \tilde{k}_c \in \mathcal{K}_{\tilde{M}_c}$ that satisfy boundary conditions appropriate to computing $\mathrm{Tr}_{\mathcal{D}}(b)$, $\mathrm{Tr}_{\mathcal{D}}(c)$. If the reflections have fixed points on the new boundaries of k_b, k_c, then $\tilde{k}_b, \tilde{k}_c$ will have conical singularities with deficit angle π.

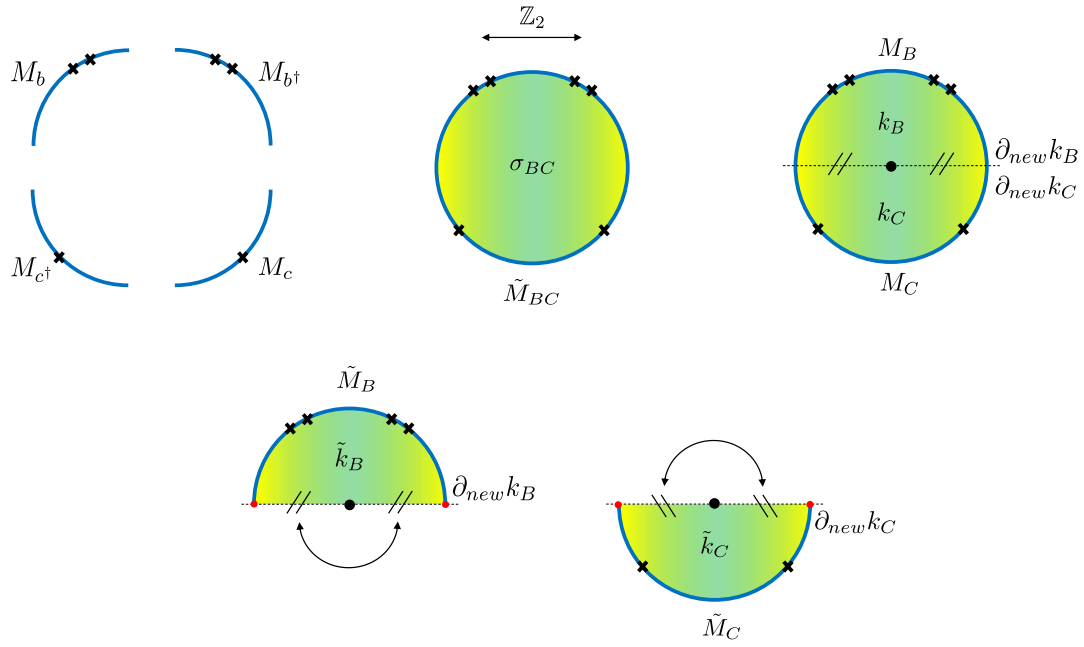

Figure 8.9: This diagram depicts a bulk version of the CFT argument shown in figure 8.5. **Upper left panel:** The boundary source manifolds M_b, $M_{b^\dagger}$, M_c and $M_{c^\dagger}$ which are glued together to form $\tilde{M}_{BC}$. **Upper middle panel:** By Lemma 2 we can consider a dominant bulk saddle σ_{BC} for the bulk path integral with boundary conditions $\tilde{M}_{BC}$ such that σ_{BC} has a $\mathbb{Z}_2$ reflection symmetry. **Upper right panel:** The saddle σ_{BC} can be cut into two pieces k_B, k_C. These pieces are *not* generally related by any symmetry. Instead, by Assumption 2, the new boundaries $\partial_{new}k_B = \partial_{new}k_C$ created by the cut are invariant under the $\mathbb{Z}_2$ reflection symmetry and $I(\sigma_{BC}) = I(k_B)+I(k_C)$. **Lower panel:** By gluing every point of $\partial_{new}k_B$ to its image under the $\mathbb{Z}_2$ symmetry we define a configuration $\tilde{k}_B$ for the bulk path integral with boundary conditions $\tilde{M}_B$. In particular, this operation identifies pairs of red dots to construct $\tilde{M}_B$. The configuration $\tilde{k}_C$ is also constructed in the same way from k_C. Assumptions 3 and 1 then imply$I(\sigma_{BC}) = I(k_B) + I(k_C) \geq I(\tilde{k}_B) + I(\tilde{k}_C) \geq I(\sigma_B) + I(\sigma_C)$, where σ_B, σ_C are the dominant saddles for $\mathrm{Tr}_{\mathcal{D}}\, B, \mathrm{Tr}_{\mathcal{D}}\, C$.

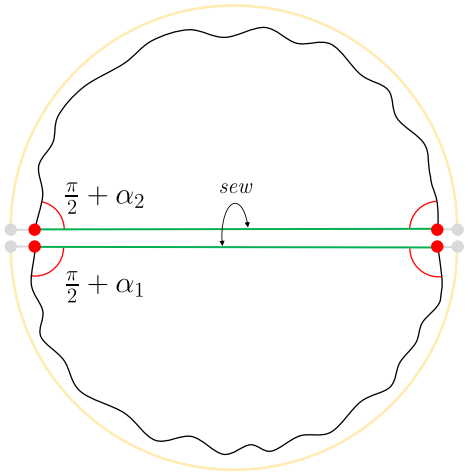

Figure 8.10: Our cut-and-paste construction can join pieces of the asymptotic boundary together in a way that is not smooth. We illustrate this here for a two-dimensional example (e.g., as appropriate to JT gravity). In particular, when two pieces are sewn together, two corners (with, say, associated interior intersection angles $\pi/2 + \alpha_1, \pi/2 + \alpha_2$) of the individual pieces can merge. When this occurs, the extrinsic curvature density $\sqrt{h}K$ of the resulting $\partial\mathcal{M}$ will contain a delta-function of strength $\alpha_1 + \alpha_2$.

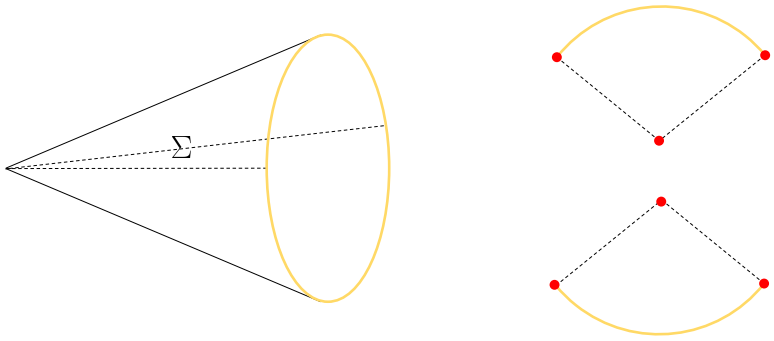

Figure 8.11: A cone is shown along with a minimal surface Σ anchored both to the conical defect and to the asymptotic boundary. Slicing the cone open along Σ gives a spacetime without conical defects, but where the new boundary may contain 'corners' (represented a red dots) at which the extrinsic curvature contains delta-functions.

Chapter 9

Algebras of boundary observables from gravitational path integrals: Understanding Ryu-Takayanagi/HRT as entropy without invoking holography

9.1 Introduction

The last few years have seen significant progress in our understanding of gravitational entropy. An important step forward was the discovery of non-trivial quantum-extremal surfaces in the context of black hole evaporation [37, 36] and their relation to gravitational replica calculations [39, 38]. These results in turn relied on the general connections between gravitational replicas and (quantum) extremal surfaces derived in [33, 34, 35]. As is by now well-known, these observations led to gravitational computations consistent

with the so-called Page curve [252, 253] expected from the idea that black holes are unitary quantum systems with a finite number of internal states that is well-approximated by $e^{S_{BH}}$, where S_{BH} is the appropriate Bekenstein-Hawking entropy.

The analysis of Hawking radiation is particularly clean in settings where the emitted Hawking radiation is transferred from an asymptotically anti-de Sitter (AdS) gravitational system to a quantum mechanical system in which gravity is completely non-dynamical. Such systems have often been called 'baths' in the recent literature. In this context, and in appropriate semiclassical limits following [33, 34], the above results imply that the usual von Neumann entropy of the bath can be studied using what [92] termed 'the Island Formula,' which is a special case of the quantum-corrected Ryu-Takayanagi/Hubeny-Rangamani-Takayanagi (RT/HRT) formula [26, 66, 27] (with quantum corrections understood in the sense of [29]).

While such arguments were motivated by considerations related to the AdS/CFT correspondence [15] (or equivalently from gauge/gravity duality or gravitational holography), the final versions of the arguments rely only on properties of the gravitational path integral. In particular, at least for bath entropies described by the Island Formula, one may safely interpret the result in terms of standard von Neumann entropies *without* assuming the gravitational bulk system to admit a holographic field theory dual. The only subtlety here is that (see e.g. [51, 54, 55]) the semiclassical bulk gravitational theory appears to allow baby-universe superselection sectors (often called α-sectors) of the form described in [146, 147], and that the Island Formula in fact describes an average over such bulk α-sectors that characterizes the von Neumann entropy S_α of the bath state ρ_α in a typical α-sector [54, 55]. This explains the observation of [188] that the computation fails to take the form expected for the von Neumann entropy of the bath computed in the total bath state $\oplus_\alpha \rho_\alpha$.

The fact that one need not assume a holographic dual field theory in order to interpret

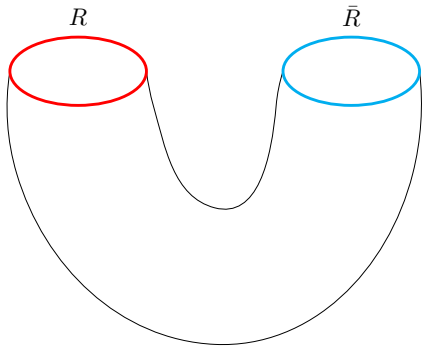

Figure 9.1: We consider boundary regions $R, \bar{R}$ associated with 'complete boundaries' in the sense that $\partial R = \emptyset = \partial \bar{R}$. We also require $R, \bar{R}$ to be compact.

QES computations for a bath in terms of standard bath entropies suggests that this lesson may hold more generally. In particular, in order to avoid divergences, let us take the boundary region R to be compact and without boundary $\partial R = \emptyset$; see figure 9.1. In this context we might expect that purely-bulk arguments can be used to construct a Hilbert space $\mathcal{H}_R$ associated with R, or perhaps a set of Hilbert spaces $\mathcal{H}_R^i$ associated with R, such that the associated RT/HRT formula can be understood in terms of $-Tr_i \rho_R^i \ln \rho_R^i$, where ρ_R^i is the density matrix describing the bulk quantum state on $\mathcal{H}_R^i$ and Tr_i is the standard Hilbert space trace on $\mathcal{H}_R^i$. Here the label set index for the index i may include both continuous and discrete subsets.

In certain limiting cases, related results were recently established by Chandrasekaran, Penington, and Witten [62], and especially by Penington, and Witten [63]. However, the fact that their von Neumann algebras were type II rather than type I meant that their results were not given directly by standard Hilbert space traces. A related comment is that the results of [62, 63] were valid only in a bulk semiclassical limit in which Hilbert space densities of states diverge.

In contrast, we wish to consider a context in which Hilbert space densities of states are finite so that the above entropies will not require renormalization. This then requires appropriate couplings to be finite as well. We wish to define entropies in this setting

which, if we later take an appropriate limit, will be well approximated by RT/HRT entropies. In our finite-coupling regime, a primary question will be how the choice of boundary regions $R, \bar{R}$ can define the desired Hilbert spaces $\mathcal{H}^i_R$. In particular, we will be far from the semiclassical regime in which entanglement wedges are well-defined; see e.g. the discussion in the final paragraph of [25].

Of course, the bulk path integral at finite coupling is poorly understood. Rather than attempt to find and study a UV-completion for any specific model, we instead proceed by simply supposing that we are given a UV-complete finite-coupling bulk AlAdS theory with an object that can be called a 'Euclidean path integral' that satisfies a simple set of axioms[1]. Most of our axioms are commonly assumed for asymptotically-AdS gravitational theories, and were in particular used in [54]. However, we also include a separate axiom enforcing the trace inequality recently discussed in [256]. This inequality will play a critical role in our work below.

This framework allows us to answer the above challenge by constructing von Neumann algebras $\mathcal{A}_R$, $\mathcal{A}_{\bar{R}}$ of observables associated with the regions R and $\bar{R}$ and by showing these algebras to contain only type I or II factors. The elements of these algebras may be called 'boundary observables' in the sense of [196], though we again emphasize that they are defined without assuming the existence of a dual field theory. Indeed, it seems natural to expect the required axioms to hold for successful ultraviolet (UV) completions of general asymptotically-AdS gravitational systems, whether the completion be called string field theory, spin-foam loop quantum gravity, or by some other name.

Our construction also leads to an associated von Neumann entropy on R which can be studied using a standard gravitational replica trick. As usual, in appropriate semiclassical settings, this entropy is given by the RT/HRT formula with corrections from both quan-

[1]The Euclidean setting is convenient, but need not be fundamental. We are hopeful that Euclidean path integrals can generally be derived from Lorentzian path integrals using arguments along the lines of those described in [46]; see e.g. [254] and [255] for recent comments on such ideas.

tum [28] and higher-derivative effects (see e.g. [111, 112, 257]). Furthermore, $\mathcal{A}_R, \mathcal{A}_{\bar{R}}$ decompose into direct sums/integrals of type I or II von Neumann factors. The corresponding Hilbert space on which these algebras act must decompose into a sum/integral of terms $\mathcal{H}^i$ (say, labelled by an index i), and for the type I factors, each of the sectors is a tensor product $\mathcal{H}^i_{\bar{R}} \otimes \mathcal{H}^i_R$ such that $\mathcal{A}^i_R$ acts only on $\mathcal{H}^i_R$ and $\mathcal{A}^i_{\bar{R}}$ acts only on $\mathcal{H}^i_{\bar{R}}$. We also show that $\mathcal{A}_R$ and $\mathcal{A}_{\bar{R}}$ are commutants. It will then follow that the RT/HRT prescription computes appropriate semiclassical limits of

$$\sum_i \tilde{p}_i S_{vN}(\rho_i) - \sum_i \tilde{p}_i \ln \tilde{p}_i + \sum_i \tilde{p}_i S^i_0, \tag{9.1}$$

where p_i is the probability to find the system in the subspace $\mathcal{H}_i$, ρ_i is the (normalized) density matrix induced on $\mathcal{H}^i_R$ by the projection of the full state to $\mathcal{H}_i$, the S^i_0 are a set of positive constants, and we have defined the quantities

$$\tilde{p}_i = \frac{e^{S^i_0} p_i}{\sum_j e^{S^i_0} p_i}. \tag{9.2}$$

In (9.1), the sums should be understood as also including integrals over any continuous subsets of the label set for the index i. Further simplifications of (9.1) will appear in [258].

Our work below begins in section 9.2 with an overview of relevant axioms for a (UV-completion of a) Euclidean gravitational path integral and the construction of the relevant sectors of the gravitational Hilbert space. The von Neumann algebras $\mathcal{A}_R$, $\mathcal{A}_{\bar{R}}$ are then defined in section 9.3 for the case where each of R, $\bar{R}$ are a union of spatially-compact asymptotically AdS boundaries with, for simplicity, R diffeomorphic to $\bar{R}$. The type I/II structure and the associated decomposition of appropriate sectors of the bulk Hilbert space are then derived in section 9.4.

9.2 The Path Integral and the Hilbert Space

The goal of this section is to write down a set of axioms for an object that we will call the Euclidean path integral for a UV-completion of some AlAdS theory of gravity, and to then use those axioms to construct the sectors of the Hilbert space that we will study in sections 9.3 and 9.4 below. We emphasize that we will require *only* that such axioms hold, and that any object satisfying the axioms may be called a Euclidean path integral, regardless of whether it is in fact computed as an integral over anything resembling Euclidean geometries. We also emphasize that there may well be many other properties that a good bulk theory should satisfy and which are not captured by our axioms; i.e., we suggest our axioms to be necessary, though probably not sufficient, for a theory to be satisfactory. What we find to be of most interest below is just how much can be derived from the above simple Axioms 1-6.

Section 9.2.1 briefly motivates and then records the desired axioms. The relevant Hilbert space sectors are then constructed in section 9.2.2. Much of the analysis below follows [54].

9.2.1 Motivation and axioms

While in the end we will not strictly require that our path integral be formulated as a sum over geometries, we would like our axioms to apply to any such cases that exist. Let us thus briefly consider a path integral that actually integrates over a set of fields, among which the (Euclidean-signature) metric, in order to motivate a reasonable set of axioms below. We will take the metric-integral to include a sum over all possible topologies. The bulk fields will be collectively denoted ϕ, for which the corresponding Euclidean action will be $S[\phi]$. To every smooth *closed* (i.e., $\partial M = \emptyset$) AlAdS boundary M at which appropriate (potentially complex) boundary conditions are specified, a Euclidean path

integral would then assign the complex number

$$\zeta(M) \coloneqq \int_{\phi \sim M} \mathcal{D}\phi e^{-S[\phi]}. \tag{9.3}$$

Here we use the symbol M to denote not just the boundary manifold, but also the relevant boundary conditions for the bulk field ϕ. The notation $\phi \sim M$ in (9.3) indicates that we integrate only over bulk fields ϕ satisfying such conditions.

In order to avoid overuse of terms involving the word 'boundary,' we henceforth refer to the boundary conditions on bulk fields as *sources*, and we refer to M as a (boundary) *source manifold* to remind the reader of our inclusive terminology. This terminology will seem natural to practitioners of AdS/CFT, though long experience in that context has established that, even without invoking such a duality, the boundary conditions for bulk fields play precisely the same role as sources for familiar non-gravitational quantum field theories. In the AlAdS_d context with d even, the appropriate notion of sources/boundary conditions will typically be given by equivalence classes under Weyl transformations.

It is reasonable to expect $\zeta(M)$ to be finite for smooth M, and for $\zeta(M)$ to enjoy some degree of continuity under appropriately-small deformations of the boundary conditions described by M. For the present purposes we allow the sources described by M to be complex, though one can also restrict the discussion to real boundary conditions (or to complex linear combinations thereof). For complex sources, expression (9.3) suggests that $[\zeta(M)]^* = \zeta(M^*)$ where * denotes complex conjugation and, in particular, M^* is the same manifold as M but with complex-conjugated sources.

Let us imagine that we cut the path integral (9.3) into two parts along a slice Σ_{bulk} through the bulk spacetime. By this we mean that we slice each configuration ϕ that enters into the path integral into two parts, and that in all cases we call the cut Σ_{bulk} even though the geometry of Σ_{bulk}, and in fact the topology of Σ_{bulk}, will depend on ϕ.

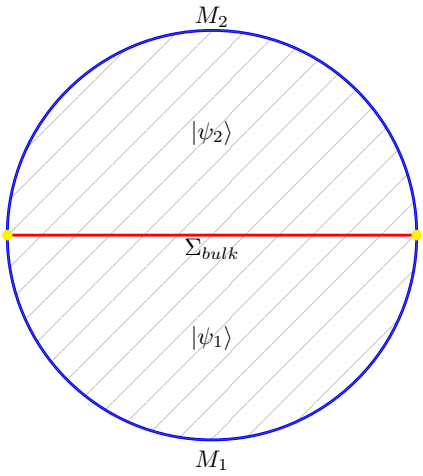

Figure 9.2: A slice Σ_{bulk} (red line) of the path integral intersects the AlAdS boundary M (blue line) at a codimension-2 surface $\partial\Sigma_{bulk}$ (yellow points) which splits M into two parts denoted by M_1, M_2. Each half of the path integral defines a quantum state ψ_i by computing the wavefunction of ψ_i on Σ_{bulk}. These wavefunctions can be thought of as the result of Euclidean evolution from the boundary conditions M_i, and the path integral can then be regarded as computing the transition amplitude $\langle\psi_2|\psi_1\rangle$.

We will, however, require the intersection $\partial\Sigma_{bulk}$ of Σ_{bulk} with the AlAdS boundary M to be independent of ϕ. In the usual way, it is natural to take each of the two resulting pieces of the path integral to compute the wavefunction (or the complex conjugate of a wavefunction) of a state in a Hilbert space $\mathcal{H}_{\partial\Sigma}$ defined by the choice of $\partial\Sigma$. The original (uncut) path integral then computes the inner product in $\mathcal{H}_{\partial\Sigma}$ of the two states thus defined. In particular, when the states are identical, the original uncut path integral computes the norm of the state and thus should give a non-negative result.

Furthermore, it natural to generalize the above discussion by replacing M with a finite formal linear combination of source manifolds

$$M := \sum_{I=1}^{n} \gamma_I M_I, \tag{9.4}$$

for some $n \in \mathbb{Z}^+$ with $\gamma_I \in \mathbb{C}$, in which case we simply use linearity to define

$$\zeta(M) := \sum_I \gamma^n_{I=1} \zeta(M_I). \tag{9.5}$$

In this case we also define

$$M^* := \sum_{I=1}^{n} \gamma_I^* M_I^*. \tag{9.6}$$

In particular, some such formal sums can again be 'sliced' into two pieces, and when the two pieces are isomorphic (up to the appropriate complex conjugation), we again expect $\zeta(M)$ to compute a non-negative norm. Below, we will use the notation X^d to denote the set of *smooth* d-dimensional source manifolds M (without boundaries) appropriate to some given theory. We then use the notation $\underline{X}^d$ to denote formal finite linear combinations of such manifolds with coefficients in $\mathbb{C}$ as in (9.4) (with $M_I \in X^d$). Members of both X^d and $\underline{X}^d$ will be denoted M to avoid cumbersome notation. As above, we will extend any function $\zeta : X^d \to \mathbb{C}$ to $\underline{X}^d$ via (9.5).

This brief discussion motivates us to require the following four axioms for the UV-completion of any $(d+1)$-dimensional AlAdS[2] Euclidean quantum gravity path integral $\zeta(M)$:

Axiom 1 Finiteness: *For some space of d-dimensional source manifolds X^d, we are given a function $\zeta : X^d \to \mathbb{C}$; i.e., $\zeta(M)$is well-defined and finite for every $M \in X^d$. Although we do not specify the detailed nature of the allowed sources, the sources should be given by fields on an underlying manifold and X^d should include any smooth manifold with smooth sources fields of the allowed types.*

[2]We also expect our axioms to apply to UV-completions of bulk gravitational theories of spacetimes asymptotic to $\mathcal{M}_{d+1} \times X$ where $\mathcal{M}_{d+1}$ is AlAdS_{d+1} and X is a fixed compact manifold of arbitrary dimension, as well as to other asymptotic structures such as those described in [209].

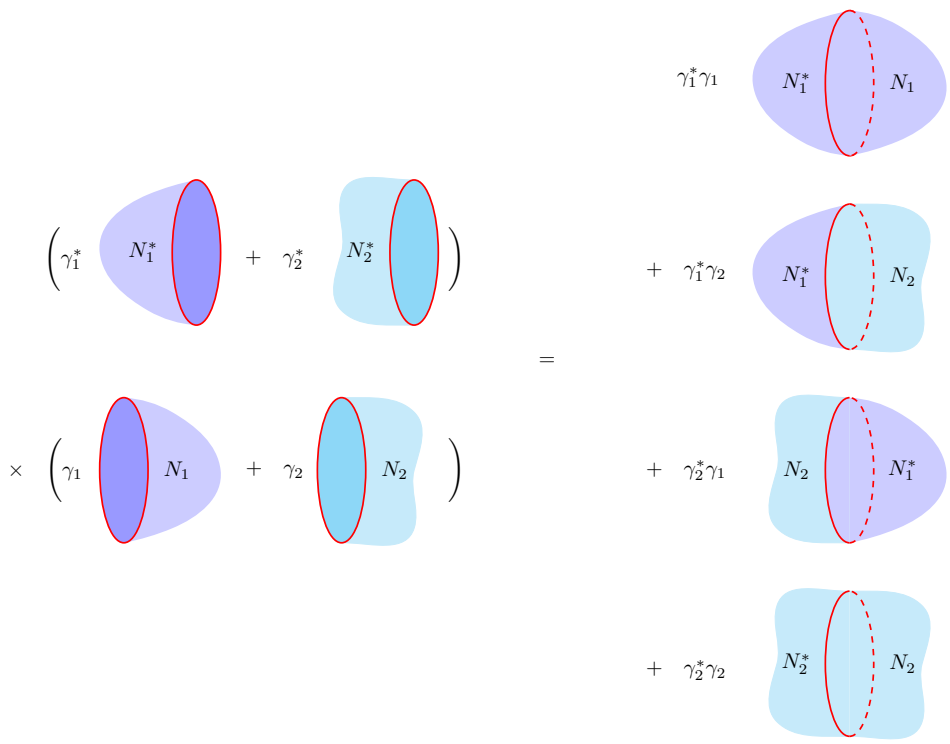

Figure 9.3: A reflection-symmetric $M \in \underline{X}^d$ is shown for a case where M is a sum of 4 terms.

Axiom 2 Reality: *For every $M \in \underline{X}^d$, we have both $M^* \in \underline{X}^d$ and $[\zeta(M)]^* = \zeta(M^*)$, where M^* is defined by* (9.6).

Axiom 3 Reflection Positivity: *Suppose for some $n \in \mathbb{Z}^+$ that $M \in \underline{X}^d$ can be written in the form $M = \sum_{I,J=1}^n \gamma_I^* \gamma_J M_{I,J}$ where $\gamma_I \in \mathbb{C}$, γ_I^* denotes the complex conjugate of γ_I, and where each $M_{I,J}$ can be sliced into two parts N_I^*, N_J; see figure 9.3 By such a slicing, we mean that there is a smooth codimension-1 hypersurface $\Sigma_{I,J}$ in $M_{I,J}$ that partitions $M_{I,J}$ into N_I^* and N_J, so that N_I^* and N_J are source manifolds with boundaries. In particular, the above notation requires that the same source manifold-with-boundary N_I^* is obtained from slicing $M_{I,J}$ for each J, and the same source manifold-with-boundary N_J is obtained by slicing $M_{I,J}$ for each I. In particular, slicing the diagonal closed manifold $M_{I,I}$ along $\Sigma_{I,I}$ yields N_I^* and N_I. The notation N_I^* indicates that each diagonal source*

manifold $M_{I,I}$ admits a diffeomorphism $\phi_{I,I}$ that both acts as a reflection about $\Sigma_{I,I}$ and which complex-conjugates all sources. When these conditions hold, $\zeta(M)$ is a non-negative real number.

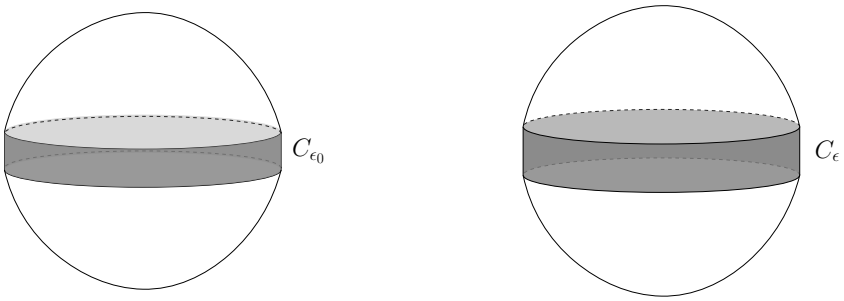

Figure 9.4: The source manifold $M = M_{\epsilon_0}$ contains a cylinder C_{ϵ_0} of length ϵ_0. Changing the length of this cylinder to ϵ defines a new source manifold M_ϵ.

Axiom 4 Continuity: *Suppose that a source manifold $M \in X^d$ contains a region diffeomorphic to an (orthogonal) cylinder source manifold-with-boundary C_{ϵ_0} of some length ϵ_0; see figure 9.4. The term (orthogonal) cylinder source manifold-with-boundary indicates C_{ϵ_0} is topologically of the form $B \times [0, \epsilon_0]$ and that C_{ϵ_0} admits a Killing field ξ which generates a local symmetry of C_{ϵ_0} and the sources it represents, with ξ orthogonal to ∂C_{ϵ_0}. By a local symmetry, we mean that at each point in the interior of C_{ϵ_0} the flow along ξ is well-defined for at least some finite values of the Killing parameter, though of course the boundaries ∂C_{ϵ_0} prohibit C_{ϵ_0} from enjoying a translational symmetry along these flows. The statement that C_{ϵ_0} has length ϵ_0 means that the two copies of B in ∂C_{ϵ_0} are related by flow through a Killing parameter ϵ_0, though the actual value of ϵ_0 is not meaningful since we have not fixed a preferred normalization for the Killing field ξ. For simplicity we will drop the qualifier 'orthogonal' when discussing cylinders C_ϵ below.*

Let us now write $M = M_{\epsilon_0}$ and define a related family of manifolds M_ϵ by replacing the C_{ϵ_0} contained in M_{ϵ_0} with the analogous cylinder C_ϵ. The resulting $\zeta(M_\epsilon)$ is then required to be a continuous function of ϵ.

The reader will note that our continuity condition is extremely weak, and that one generally expects rather stronger continuity conditions to hold. However, axiom 4 has the benefit of being simple to state for general boundary dimension d, and it will turn out to be sufficient for our purposes below.

Axioms 1, 2, and 3 are requirements explicitly stated in [54]. However, [54] also implicitly used additional assumptions to deal with spacetime wormholes. In particular, as explained in [54], axioms 1-3 imply that the set of real source manifolds $M \in X^d$ are associated with a collection of symmetric operators defined on a common dense domain in a natural quantum gravity Hilbert space, and that any two such operators commute on this domain. Ref [54] then suggested that each of these symmetric operators had a unique self-adjoint extension (i.e., that each was essentially self-adjoint) and that these extensions were again mutually commuting. This outcome will seem natural to many physicists, though the above results are not sufficient to prove that it actually occurs[3]. However, if this suggestion holds then the self-adjoint extensions can be simultaneously diagonalized on the full quantum gravity Hilbert space. The simultaneous eigenspaces of these operators are then called "baby universe superselection sectors," and have the property that closed manifolds define operators proportional to the identity on each such sector. As a result, each sector is associated with a modified path integral that exhibits the following factorization property for closed source manifolds $M_1, M_2 \in X^d$:

$$\zeta(M_1 \sqcup M_2) = \zeta(M_1)\zeta(M_2), \tag{9.7}$$

where the symbol $\sqcup$ denotes the disjoint union of source manifolds-without-boundary. Such superselection sectors are often called α-sectors, and play the role of the α-states

[3]See in particular [259] for an example where symmetric operators that commute on a common invariant dense domain are essentially self-adjoint but where their self-adjoint extensions nevertheless fail to commute.

described in [146, 147]. Once this structure is established, it is then sufficient to deal with each baby universe superselection sector individually.

It is tempting to expect that the bulk path integrals of UV-complete theories generally lead to a framework of the above form. Note that this form allows the case suggested in [260] where there is only one such superselection sector, so that each $M \in X^d$ defines an operator proportional to the identity on the entire Hilbert space. However, we emphasize that in the presence of multiple such superselection sectors, it would be natural to simply work with each such sector separately and thus to frame arguments in terms of path integrals satisfying (9.7). As a result, rather than introduce further complicated axioms which would imply the general sum over superselection sectors described above, we will simply assume that we start with a path integral satisfying the factorization property (9.7). In particular, we include the following axiom:

Axiom 5 Factorization: *For source manifolds $M_1, M_2 \in X^d$, the function ζ satisfies* (9.7).

Finally, in certain contexts (which will be clarified below) it was recently argued in [256] that a certain so-called trace-inequality (equation 9.8 below) holds for any gravitational path integral to all orders in the semiclassical approximation (and to all orders in perturbative higher dervative terms). It is therefore natural to suppose this inequality to hold non-perturbatively as well[4]. In our present notation, this assumption takes the following form:

Axiom 6 Trace Inequality: *Suppose that some $M \in \underline{X}^d$ can be cut into two pieces, N_1, N_2, with boundaries $\partial N_1 = \partial N_2$ of the form $B \sqcup B$, where $\sqcup$ denotes disjoint union and where the notation B again includes a specification of sources at B. When M is a*

[4]The skeptical reader may wish to know that the trace inequality (Axiom 6) actually follows from axioms 1-5. This will be explained in [258].

linear combination of manifolds, we require B to be the same for every term in the linear combination. Suppose further that by gluing together the two copies of B bounding N_1 we can form a smooth closed source manifold M_1, and that we can similarly form a smooth M_2 from N_2. In such cases we require that

$$\zeta(M) \leq \zeta(M_1)\zeta(M_2). \tag{9.8}$$

We emphasize that, due to axiom 5, in a theory with baby universe superselection sectors we would in fact be assuming that the inequality (9.8) holds in each such sector separately. Indeed, it is worth remarking that the analogue of (9.8) generally *fails* in a superposition of such superselection sectors. To see this, consider a family ζ_α of functions on X^d satisfying the above axioms, and define $\zeta_{sup} = \int d\alpha\, \zeta_\alpha$ for some normalized probability measure $d\alpha$. For simplicity, let us consider the case where B is empty so that N_1, N_2 are already closed manifolds that we may call M_1, M_2, and let us further consider the special case $M_1^* = M_2$. Then by axiom 5 we have

$$\zeta_{sup}(M) = \int d\alpha\, \zeta_\alpha(M) = \int d\alpha\, |\zeta_\alpha(M_2)|^2. \tag{9.9}$$

But for any probability measure $d\alpha$ the variance of $\zeta_\alpha(M_2)$ must be non-negative:

$$\int d\alpha\, |\zeta_\alpha(M_2)|^2 - |\int d\alpha\, \zeta_\alpha(M_2)|^2 \geq 0. \tag{9.10}$$

Furthermore, (9.10) can be saturated only when $\zeta_\alpha(M_2)$ is independent of α for almost every α, in which case the superposition is effectively trivial. For non-trivial superpositions we thus find

$$\zeta_{sup}(M) = \int d\alpha |\zeta_\alpha(M_2)|^2 > |\int d\alpha \zeta_\alpha(M_2)|^2 = \zeta_{sup}(M_1)\zeta_{sup}(M_2), \tag{9.11}$$

which would violate (9.8).

We also comment that (9.11) is consistent with the analysis of [256], as [256] considered only cases in which the source manifold M is connected. In the context of connected source manifolds M, [256] argued in that, when the bulk path integral admits a semi-classical limit defined by Einstein-Hilbert or Jackiw-Teitelboim gravity with perturbative corrections, the inequality (9.8) should hold to all orders in the relevant expansions.

9.2.2 Sectors of The Quantum Gravity Hilbert Space

As noted at the beginning of this section, one expects to be able to obtain states of any quantum gravity theory by 'cutting open' the associated path integral. The details of this construction will be described below. As remarked in the introduction, our approach will be to remain agnostic about the inner workings of the path integral, and simply to view it as a function $\zeta : X^d \to \mathbb{C}$ satisfying axioms 1-6.

We refer the reader to [54] for further discussion of what it means to cut open a quantum gravity path integral. However, at an abstract level it is clear that doing so requires that we cut any closed AlAdS boundary M into two pieces N_1, N_2 with $\partial N_1 = \partial N_2$. We should then associate quantum gravity states with these two pieces such that the inner product of the two states is $\zeta(M)$.

However, there are several subtleties in this process that merit discussion. The first such subtlety arises when there are open sets in N_1, N_2 that contain $\partial N_1 = \partial N_2$ and which admit non-trivial symmetries. In that case, there is more than one way to glue the pieces N_1, N_2 back together to obtain a smooth manifold. Furthermore, each such gluing g generally leads to a different closed manifold M_g, only one of which can be the original M from which the pieces N_1, N_2 were cut. As a result, it is not sufficient to think of N_1, N_2 as diffeomorphsim equivalence classes of source manifolds with boundaries. Instead, we

see that we should think of the points on $\partial N_1 = \partial N_2$ as being labelled, so that M can be reconstructed by gluing N_1 to N_2 along their boundaries in the manner dictated by matching identical labels. As a result, we will henceforth use the notation N to denote a manifold with boundary ∂N, together with a labelling of points on ∂N.

Now, suppose that we are given two manifolds N_1, N_2 with labelled boundaries $\partial N_1, \partial N_2$, such that the boundary labels define a diffeomorphism $\phi : \partial N_1 \to \partial N_2$. (Recall that diffeomorphisms are required to be surjective.) We can then use this ϕ to glue N_1 to N_2 to define a closed manifold M without boundary. However, there is no guarantee that the resulting boundary fields on M will be smooth, or indeed that they will even be continuous. As a result, $\zeta(M)$ may not be well-defined.

We will deal with this issue by using the following simple expedient: Rather than attempting to construct the entire quantum gravity Hilbert space, we will instead construct only sectors that are associated with certain types of data on the codimension-2 boundaries ∂N. In particular, we will consider only source manifolds-with-boundary N that are *rimmed* in the following sense:

Definition 1 *A source manifold N with boundary ∂N will be said to be rimmed when there is a neighborhood N_ϵ of ∂N on which the sources are real and such that N_ϵ is diffeomorphic to some cylinder source manifold C_ϵ of the form defined in Axiom 4. The region N_ϵ is then called a rim of N.*

We also make the following definitions:

Definition 2 *We will say that two rimmed source-manifolds N_1, N_2 with boundaries $\partial N_1, \partial N_2$ agree on their boundaries when they admit rims $N_{1\epsilon}, N_{2\epsilon}$ that are related by a diffeomorphism that preserves both sources and the labels on $\partial N_1, \partial N_2$. By the local translation symmetry, the data on all of $N_{1\epsilon}, N_{2\epsilon}$ is determined by data at $\partial N_1, \partial N_2$, so we will write $\partial N_1 = \partial N_2$ to denote the above agreement on the rims $N_{1\epsilon}, N_{2\epsilon}$. We will*

Figure 9.5: Gluing N_1 to N_2 and then N_1^* to N_2^* defines source manifolds-without-boundary $M_{N_1^* N_2}$ and $M_{N_1 N_2^*}$ that are related by a diffeomorphism that complex–conjugates sources. As depicted here, the relevant diffeomorphism acts as a reflection about the plane indicated by the dashed line. Thus $(M_{N_1^* N_2})^* = M_{N_1 N_2^*}$, where "=" means that the two are related by a diffeomorphism.

similarly use the symbol ∂N to denote the manifold at the boundary of source manifold-with-boundary N together with enough information about the sources on N to reconstruct sufficiently small rims N_ϵ.

The utility of restricting to rimmed source-manifolds is that, when two rimmed source-manifolds N_1, N_2 admit agree at their boundary ($\partial N_1 = \partial N_2$), it is then clear that they can be glued together to define a smooth source manifold-without-boundary that we may call $M_{N_1 N_2}$, so that $\zeta(M_{N_1 N_2})$ is well-defined. And since definition 1 required sources on the rim-regions to be real, we can similarly construct a smooth source-manifold $M_{N_1^* N_2}$. For future use we note that since this gluing operation acts symmetrically on N_1, N_2, we have

$$M_{N_1 N_2} = M_{N_2 N_1}. \tag{9.12}$$

Due to this symmetry, we also have

$$(M_{N_1 N_2})^* = M_{N_1^* N_2^*}; \tag{9.13}$$

see figure 9.5. Here we recall that the action of * on a source manifold-with-boundary N was defined in Axiom 3 to include a reflection as well as complex-conjugation of sources.

In particular, for a given such choice of ∂N (in the sense of Definition 2) we can

define a sector $\mathcal{H}_{\partial N}$ of the quantum gravity Hilbert space by considering the space $Y^d_{\partial N}$ of rimmed source manifolds N having the given boundary ∂N. From $Y^d_{\partial N}$, we can then construct the space $\underline{Y}^d$ of finite formal linear combinations $N = \sum_{I=1}^n \gamma_I N_I$ with $\gamma_I \in \mathbb{C}$ and $N_I \in Y^d_{\partial N}$. We then associate a (not necessarily distinct) state $|N\rangle$ with each $N \in \underline{Y}^d_{\partial N}$. Two such states $|N_1\rangle, |N_2\rangle$ are defined to have (pre-)inner product

$$\langle N_1 | N_2 \rangle := \zeta(M_{N_1^* N_2}), \tag{9.14}$$

where $M_{N_1^* N_2} \in \underline{X}^d$ is defined by using the distributive law $M_{N_1(\alpha N_2 + \beta N_3)} = \alpha M_{N_1 N_2} + \beta M_{N_1 N_3}$ and similarly for $M_{(\alpha N_1^* + \beta N_3^*) N_2}$. The inner product is Hermitian due to (9.12), (9.13), and Axiom 2, and the inner product is positive semi-definite by Axiom 3. We may then say that (9.14) defines a pre-Hilbert space $H_{\partial N}$. Taking the quotient by the space $\mathcal{N}_{\partial N}$ of any null vectors and completing the result then yields a Hilbert space $\mathcal{H}_{\partial N}$ that we call the ∂N-sector of the full quantum gravity Hilbert space. Below, we will use the notation $|N\rangle$ to denote both elements of the pre-Hilbert space $H_{\partial N}$ and the associated equivalence class in $\mathcal{H}_{\partial N}$, though the distinction should always be clear from the context. Indeed, since $\underline{Y}^d_{\partial N}$ allows only finite linear combinations, it may often be the case that $\mathcal{N}_{\partial N}$ is empty and the quotient is trivial.

The above expedient will allow us to proceed quickly to constructing and studying algebras of operators on $\mathcal{H}_{\partial N}$ without characterizing in detail either the degree of differentiability of sources on M required for $\zeta(M)$ to be finite or the manner in which divergences arise when such conditions fail. If our goal is to construct those states which are associated with static Lorentz-signature boundary conditions, then one may expect that our restriction to rimmed surfaces gives the full such Hilbert space. One argument for this comes from AdS/CFT, in which case the rims correspond to insertions of $e^{-\epsilon H}$ for some ϵ. Since $e^{-\epsilon H}$ is invertible, even at fixed finite ϵ the rimmed surfaces will generate a

complete set of states. However, even without relying on AdS/CFT, since we allow the rim N_ϵ to be arbitrarily small, and since we require the path integral to be continuous in ϵ, the restriction to rimmed surfaces should still allow full information to be obtained about the sector of the theory associated with a given ∂N of the type described above.

There are, however, two shortcomings to our approach. The first is that we obtain no information about inner products $\langle N_1|N_2\rangle$ when $\partial N_1 \neq \partial N_2$. Such inner products do not necessarily vanish, especially in low dimensions. Indeed, for $d = 1$ both AdS/CFT and the associated semiclassical bulk computations suggest that the inner product can be non-zero even when the sources on $M_{N_1^* N_2}$ are discontinuous (so long as $M_{N_1^* N_2}$ is a well-defined toplogical manifold).

The second shortcoming is that, while we expect to construct all states associated with static Lorentz-signature boundaries, at least in high dimensions we expect to miss sectors of the quantum gravity Hilbert space associated with non-static boundaries. Based on both the AdS/CFT context and the divergences that manifest themselves in the associated semiclassical bulk computations, we expect this issue to be related to what one finds when studying quantum fields on curved spacetime, where in high dimensions the space of states on a given Cauchy slice Σ (say, specified by the correlation functions of fields and their derivatives on Σ) can depend not only on the metric induced on Σ but also on various normal derivatives of background fields (sources) evaluated at Σ. It would be interesting to return to both of these issues in the future, though a full analysis of the second issue seems likely to require a Lorentz-signature analysis.

9.3 Algebras of boundary observables

We have thus far described how our path integral ζ can be used to construct sectors $\mathcal{H}_{\partial N}$ of the quantum gravity Hilbert space. But it can also be used to construct operators,

and this construction will be useful in understanding the further structure of $\mathcal{H}_{\partial N}$ and the relation to RT entropy. To understand such operators, let us again consider the space of rimmed surfaces $Y^d_{\partial N}$ for some choice of codimension-2 boundary ∂N. We will now further suppose that ∂N is the disjoint union of two pieces, $\partial N = B_1 \sqcup B_2$, with both B_1, B_2 being compact and closed (in the sense that $\partial B_1 = \partial B_2 = \emptyset$). Then any $N \in Y^d_{\partial N}$ defines an operator from $\mathcal{H}_{B_1}$ to $\mathcal{H}_{B_2}$ by gluing surfaces along B_1.

We may thus construct operators that preserve a given sector $\mathcal{H}_B$ by considering the case $B_1 = B_2 = B$. In this case, we may endow the surfaces $Y^d_{B\sqcup B}$ with a multiplication operation which then promotes the space of formal linear combinations $\underline{Y}^d_{B\sqcup B}$ to an algebra. In fact, we introduce two such algebras below that we call A^B_L and A^B_R in section 9.3.1 below. After defining these surface algebras, we will show that they admit representations on $\mathcal{H}_{B\sqcup B}$ in section 9.3.2 and that they lead to associated von Neumann algebras $\mathcal{A}^B_L$ and $\mathcal{A}^B_R$ whose properties will be studied in section 9.4.

9.3.1 Surface algebras and a trace

To understand the difference between A^B_L and A^B_R, recall that points on $B \sqcup B$ are labelled, which in particular means that the two copies of B are distinguished. We will refer to the first copy as the 'left boundary' and the second copy as the 'right boundary.' The two algebras A^B_L and A^B_R then differ according to whether multiplication is defined by gluing As a result, as a shorthand we will use the notation $\mathcal{H}_{LR}$ below to refer to $\mathcal{H}_{B\sqcup B}$.

On the set $Y^d_{B\sqcup B}$ we may define the *left product* $(\cdot_L)$ as the operation that takes as input an ordered pair of rimmed surfaces a and b, and which constructs the surface $a \cdot_L b$ that results from gluing the *left* boundary of b to the right boundary of a (see figure 9.6).

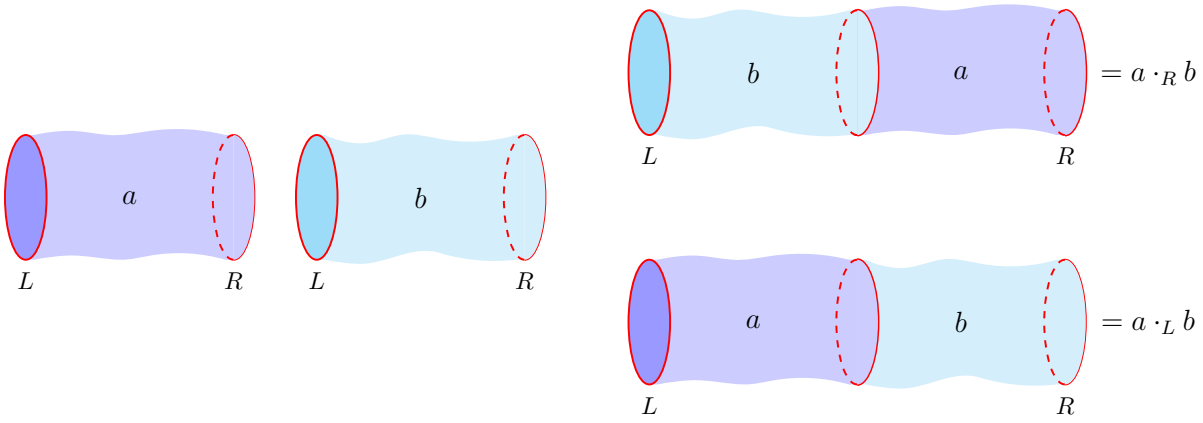

Figure 9.6: For two elements $a, b \in Y^d_{B \sqcup B}$ (shown on the left), we define the left and right products $a \cdot_L b$ and $a \cdot_R b$ by the gluing procedures shown above.

For simplicity, we will adopt the notation

$$ab \coloneqq a \cdot_L b \quad . \tag{9.15}$$

We similarly define the *right product* $(\cdot_R)$ as the operation that, given an ordered pair of surfaces a and b, glues the *right* boundary of b to the left boundary of a. Note that

$$a \cdot_R b = b \cdot_L a = ba \tag{9.16}$$

We can also extend this product to linear combinations $a, b \in \underline{Y}^D_{B \sqcup B}$ by defining it to satisfy the distributive law. The set $\underline{Y}^d_{B \sqcup B}$ equipped with the left product then forms an algebra A^B_L which we call the *left surface algebra*. Similarly, the right product on $\underline{Y}^d_{B \sqcup B}$ leads to the *right surface algebra* A^B_R. Since every element of $\underline{Y}^d_{B \sqcup B}$ has a finite rim at each boundary, gluing two surfaces a, b together always results in a surface larger than either a or b, so that neither of these algebras can contain an identity element.

However, the algebras A^B_L and A^B_R do admit a natural involution $\star$ satisfying

$$(a \cdot_L b)^\star = b^\star \cdot_L a^\star = a^\star \cdot_R b^\star, \tag{9.17}$$

so that $\star$ defines an anti-linear isomorphism between the left and right algebras. To define the operation $\star$, recall that Axiom 3 introduced a complex conjugation operation $*$ on $N \in Y^d_{B\sqcup B}$. In particular, N^* was defined so that M_{N^*N} has a reflection symmetry that complex conjugates all sources. This means that N^* is the same manifold as N (with the same labels on ∂N), and that $*$ acts on scalar sources by standard complex-conjugation (though the operation on vector, tensor, and spinor sources is more complicated).

In addition, $Y^d_{B\sqcup B}$ admits a natural transpose operation ^{t} that simply swaps the left and right boundaries of any $N \in Y^d_{B\sqcup B}$ while preserving all sources and leaving the labels on ∂N otherwise unchanged. The transpose and complex conjugation operations commute, and for any a in either algebra we may then define

$$a^\star := a^{t*}. \tag{9.18}$$

Due to the inclusion of the transpose operation, we then immediately find (9.17).

A final consequence of the labelling of points on B is that, by writing $\partial N = B \sqcup B$ we also mean that the labels on the two copies of B agree up to the distinction between the left and right boundaries. To be precise, we mean that these labels define a diffeomorphism ϕ_{LR} from the left boundary to the right boundary that preserves enough information about sources near each boundary to reconstruct infinitesimal rims at each B. This ϕ_{LR} can then be used to identify the left and right boundaries of any $a \in Y^d_{B\sqcup B}$, and thus to define a source manifold[5] $M(a) \in X^d$ (i.e., without boundary) from any $a \in Y^d_{B\sqcup B}$. We can also extend this operation to linear combinations $a \in \underline{Y}^d_{B\sqcup B}$ by linearity, so that we then find $M(a) \in \underline{X}^d$.

This observation allows the path integral to define a useful trace operation tr on both

[5]Though there are similarities, this is a different gluing operation than the one used to construct $M_{N_1N_2}$, so we use a correspondingly similar-but-different notation $M(a)$.

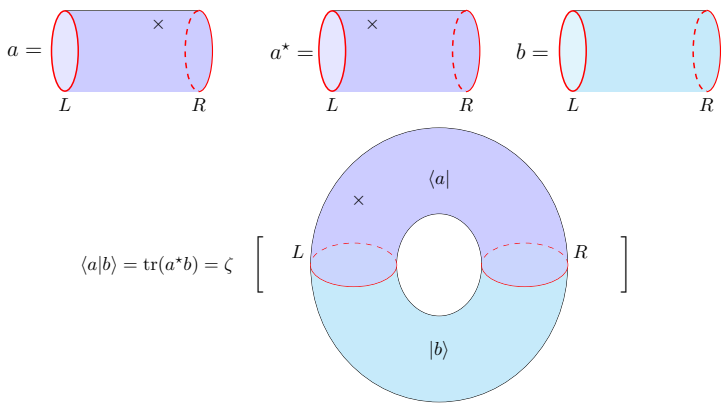

Figure 9.7: For the operators $a, a^\star$ and b shown on the top, $\mathrm{tr}(a^\star b)$ is computed on the bottom. This is equal to the inner product $\langle a|b\rangle$ for corresponding states $|a\rangle$ and $|b\rangle$.

A_L^B and A_R^B, which associates to any $a \in \underline{Y}_{LR}^d$ the finite number

$$\mathrm{tr}(a) := \zeta\left(M(a)\right). \tag{9.19}$$

Note that since $M(ab) = M(ba)$, we clearly have

$$\mathrm{tr}\ ab = \mathrm{tr}\ ba, \tag{9.20}$$

and similarly for the right product. While the trace operation is defined directly for any $a \in \underline{Y}_{LR}^d$ (without using properties of either the left or right algebras), the result (9.20) makes it reasonable to refer to this operation as a trace on both A_L^B and A_R^B.

Before proceeding to the next step of our analysis it will also be useful to note that, for $a, b \in \underline{Y}_{LR}^d$, as shown in figure 9.7 we have

$$\langle a|b\rangle = \zeta\left(M(a^\star b)\right) = \mathrm{tr}(a^\star b). \tag{9.21}$$

This relation will be used to translate certain Hilbert space statements into operator

statements and vice versa. In particular, for $a = b$ we have

$$\mathrm{tr}(a^\star a) = \zeta\left(M(a^\star a)\right) = \langle a|a\rangle \geq 0, \tag{9.22}$$

where we remind the reader that the inequality on the right was a consequence of axiom 3.

9.3.2 Representation of the surface algebras on $\mathcal{H}_{LR}$

Our axioms can also be used to define a representation $\hat{A}_L^B$ of the algebra A_L^B from section 9.3.1 that acts on the Hilbert space $\mathcal{H}_{LR}$. The first step in this construction is to consider $a, b \in \underline{Y}_{LR}^d$ and to define the action of an operator $\hat{a}_L$ on $|b\rangle$ in the pre-Hilbert space H_{LR} by

$$\hat{a}_L\,|b\rangle = |ab\rangle\,, \quad \forall\,|b\rangle \in \mathcal{H}_{LR}; \tag{9.23}$$

see figure 9.8 Here we have used the condensed notation $ab \coloneqq a \cdot_L b$ defined above. When a is a simple surface $a \in Y_{LR}^d$, this $\hat{A}_L^B$ acts on $|b\rangle \in H_{LR}$ by just gluing the surface a to the left boundary of b. Note that, consistently with the definition of a representation, we find

$$(\hat{a}_L\hat{b}_L)\,|c\rangle = |abc\rangle = \hat{a}_L(\hat{b}_L\,|c\rangle). \tag{9.24}$$

The next step is to show that $\hat{a}_L$ annihilates any null space $\mathcal{N}_{LR} = \mathcal{N}_{B\sqcup B}$ of any pre-Hilbert space states with vanishing norm, so that $\hat{a}_L$ yields a well-defined operator on $H_{LR}/\mathcal{N}_{LR}$. We will also need to extend the definition of $\hat{a}_L$ to the full Hilbert space $\mathcal{H}_{LR}$ in a manner consistent with (9.24). Both of these steps are straightforward due to the trace inequality. To see this, recall that for $a, b \in \underline{Y}_{LR}^d$ we have $\hat{a}_L|b\rangle = |ab\rangle$, and thus

$$|\hat{a}_L|b\rangle|^2 = \langle ab|ab\rangle = \mathrm{tr}(b^\star a^\star ab) = \mathrm{tr}(bb^\star a^\star a) \leq \mathrm{tr}(bb^\star)\,\mathrm{tr}(a^\star a) = \mathrm{tr}(a^\star a)\langle b|b\rangle. \tag{9.25}$$

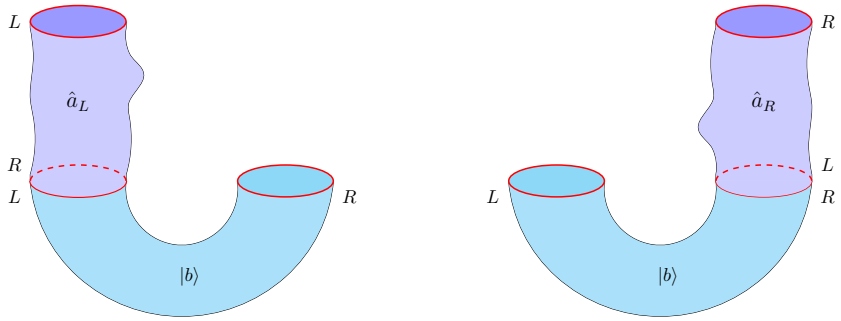

Figure 9.8: For surfaces a, b, the left panel shows the action $\hat{a}_L$ (in the representation $\hat{A}_L^B$ of the left algebra) on $|b\rangle \in \mathcal{H}_{LR}$, while the right panel shows the associated action of $\hat{a}_R$ (in the right representation $\hat{A}_R^B$ of the right algebra).

In the second step of (9.25) we have used (9.21) with a and b both replaced by ab. The third step then used cyclicity of the trace ((9.20)), and the fourth and fifth steps then follow directly from axiom (9.8) and another use of (9.21). The result is that a is bounded by $\sqrt{\text{tr } a^\star a}$ on H_{LR}.

In particular, if $|b\rangle \in \mathcal{N}_{LR}$ then $\langle b|b\rangle = 0$. The result (9.25) then clearly requires $\hat{a}_L|b\rangle$ to have zero norm as well. Thus $\hat{a}_L$ preserves $\mathcal{N}_{LR}$ and induces an operator on the quotient $\mathcal{H}_{LR}/\mathcal{N}_{LR}$. We can then apply (9.25) on this quotient to show that the operator $\hat{a}_L$ is bounded by $\sqrt{\text{tr } a^\star a}$ on the dense subspace $\mathcal{H}_{LR}/\mathcal{N}_{LR}$ of $\mathcal{H}_{LR}$. It thus admits a unique continuous extension to the entire space $\mathcal{H}_{LR}$, which is again bounded by $\sqrt{\text{tr } a^\star a}$; see e.g. [259]. We will continue to use the symbol $\hat{a}_L$ for this extension. Continuity implies that such extensions also satisfy (9.24), which makes clear that we have constructed a representation of A_L^B on $\mathcal{H}_{LR}$ as desired. We call this representation $\hat{A}_L^B$.

Since the operators in $\hat{A}_L^B$ are bounded, it is easy to discuss their adjoints. Any such operator is defined by some $a \in \underline{Y}_{LR}^d$, and for $b, c \in \underline{Y}_{LR}^d$ we must have

$$\langle b|\hat{a}_L^\dagger|c\rangle = (\langle c|\hat{a}_L|b\rangle)^* = \text{tr}\,(c^\star a b)^* = \text{tr}\,(b^\star a^\star c) = \langle b|\widehat{a^\star}_L|c\rangle. \tag{9.26}$$

Here the 3rd step follows from(9.21) and the relation $(\langle c|d\rangle)^* = \langle d|c\rangle$ with $d = ab$. Since (9.26) holds on a dense set of states and both $\widehat{a^\star}_L$ and $\hat{a}_L^\dagger$ are bounded, we must in fact have $\widehat{a^\star}_L = a_L^\dagger$ on all of $\mathcal{H}_{LR}$.

The right algebra A_R^B admits a similar representation $\hat{A}_R^B$ in $\mathcal{H}_{LR}$ defined by gluing surfaces to the *right* boundary of $\mathcal{H}_{LR}$. For $a, b \in \underline{Y}_{LR}^d$ we have

$$\hat{a}_R \, |b\rangle = |a \cdot_R b\rangle = |b \cdot_L a\rangle = |ba\rangle \,, \quad \forall \, |b\rangle \in \mathcal{H}_{LR}. \tag{9.27}$$

This action satisfies

$$(\hat{b}_R \hat{c}_R) \, |a\rangle = |(b \cdot_R c) \cdot_R a\rangle = |a \cdot_L (b \cdot_R c)\rangle = |a \cdot_L c \cdot_L b\rangle = \hat{b}_R(\hat{c}_R \, |a\rangle) \tag{9.28}$$

as required. The extension to the full space $\mathcal{H}_{LR}$ then proceeds precisely as above. The discussion of adjoints is analogous to the left case and we again find $\widehat{a^\star}_R = a_R^\dagger$. Perhaps the most interesting point to mention is that operators in the right representation $\hat{A}_R^B$ always commute with operators in the left-representation $\hat{A}_L^B$. In particular, for $a \in A_R^B$, $b \in A_L^B$, and $c \in \underline{Y}_{B \sqcup B}^d$ we clearly have

$$\hat{a}_R \hat{b}_L |c\rangle = |bca\rangle = \hat{b}_L \hat{a}_R |c\rangle. \tag{9.29}$$

Furthermore, the operators $\hat{a}_R$, $\hat{b}_L$ are bounded (and thus continuous) on $\mathcal{H}_{LR}$ and the above states $|c\rangle$ are dense in $\mathcal{H}_{LR}$. We may thus take limits to conclude that (9.29) in fact holds for $|c\rangle \in \mathcal{H}_{LR}$.

It will also be useful to note that our trace operation tr on A_L^B defines a trace on the representation $\hat{A}_L^B$. We of course wish to declare that

$$\text{tr } \hat{a}_L := \text{tr } a. \tag{9.30}$$

The important property of the definition (9.30) (which we show below) is that it satisfies tr a = tr b whenever $\hat{a}_L = \hat{b}_L$. This is equivalent to saying that the trace is faithful in the sense that tr $a = 0$ when $\hat{a}_L = 0$.

This property can be established using the continuity axiom 4. In particular, let $C_\beta \in \underline{Y}^d_{LR}$ be the cylinder of length β defined by B as in Axiom 4, and consider $aC_{2\beta} \in \underline{Y}^d_{LR}$. Since $C_{2\beta} = C_\beta C_\beta$, and since our C_β is real, we have

$$\mathrm{tr}\,(aC_{2\beta}) = \mathrm{tr}\,(C_\beta a C_\beta) = \langle C_\beta | \hat{a}_L | C_\beta \rangle. \tag{9.31}$$

Clearly the right-hand side vanishes for all β if $\hat{a}_L = 0$. However, axiom 4 requires the $\beta \to 0$ limit of (9.31) to give tr(a):

$$\mathrm{tr}(a) = \lim_{\beta \downarrow 0} \langle C_\beta | \hat{a}_L | C_\beta \rangle, \tag{9.32}$$

where the notation $\beta \downarrow 0$ emphasizes that C_β is defined only for $\beta > 0$ so that the limit is necessarily taken from above. Thus, as desired, we find tr$(a) = 0$ when $\hat{a}_L = 0$.

9.3.3 The von Neumann algebras $\mathcal{A}^B_L$ and $\mathcal{A}^B_R$

We are now ready to use the representation $\hat{A}^B_L$ to define a von Neumann algebra $\mathcal{A}^B_L$ (and to similarly construct a related von Neumann algebra $\mathcal{A}^B_R$ from the right representation $\hat{A}^B_R$). Much as in the construction of $\mathcal{H}_{LR}$ from the pre-Hilbert space H_{LR}, this will involve two steps. The first is to take the quotient of $\hat{A}^B_L$ by the null space $\mathcal{N}_L$ of $a \in A^B_L$ that act on $\mathcal{H}_{LR}$ as the zero operator. The second is then to complete the quotient $\hat{A}^B_L/\mathcal{N}_L$ by taking its closure in the weak operator topology or, what is known to be equivalent in the context, the strong operator topology[6] Due to the von Neumann

[6]The weak operator topology means that for a net of operators T_α, $T_\alpha \to T$ if and only if $\langle x\,|T_\alpha|\,y\rangle \to \langle x|T|y\rangle$ for every $|x\rangle, |y\rangle \in \mathcal{H}$. In contrast, the strong operator topology means that $T_\alpha \to T$ if and only

bicommutant theorem (see e.g. section 0.4 of [262]), we can also equivalently define $\mathcal{A}_L^B$ as the double commutant of $\hat{A}_L^B/\mathcal{N}_L$ within the algebra $\mathcal{B}(\mathcal{H}_{LR})$ of bounded operators on our Hilbert space. This in particular means that each operator in the resulting von Neumann algebra $\mathcal{A}_L^B$ is again bounded. Of course, corresponding statements hold for the right algebras as usual.

For every operator a in a von Neumann algebra, the adjoint $a^\dagger$ also lies in the von Neumann algebra. So the adjoint operation continues to act as an involution on $\mathcal{A}_L^B$.

We also introduced a trace operation tr on the operators in $\hat{A}_L^B$ in (9.30), which we in particular showed is well-defined and finite on the quotient $\hat{A}_L^B/\mathcal{N}_L$. In the theory of von Neumann algebras one generally allows traces of some operators to diverge. One thus defines a trace as a function taking values in the closed interval $[0, +\infty]$ (i.e., one allows some traces to be $+\infty$). Nevertheless, even in this sense, a trace is usually well-defined only on postive elements of the von Neumann algebra. This restriction is closely related to the familiar fact that the quantity $\sum_i A_i^i$ is manifestly well-defined for a finite-dimensional square matrix A_j^i, and that for infinite-dimensional positive matrices A_j^i the fact that each A_i^i is non-negative means that if $\sum_i A_i^i$ does not converge to a finite number, then we may say that it 'converges' to $+\infty$. But when A_j^i is not positive, an infinite sum of the form $\sum_i A_i^i$ can be oscillatory and need not converge in any sense.

We will thus attempt to extend our notion of tr only to positive elements $a \in \mathcal{A}_L^B$, which in this context means that a is a positive operator on $\mathcal{H}_{LR}$. To define a useful such extension, we need to find a function from the positive elements $a \in \mathcal{A}_L^B$ to $[0, +\infty]$ that agrees with our previous definition of tr for $a \in \hat{A}_L^B$ and which satisfies other properties to be discussed below.

It will thus be productive to consider alternative representations of the operation tr

if $T_\alpha|y\rangle \to T|y\rangle$ for every $|y\rangle \in \mathcal{H}$. The two associated notions of closure agree for convex sets bounded operators; see e.g. theorem 5.1.2 of [261].

on $\hat{A}_L^B$. We begin by returning to the relation (9.32), which was argued above to hold for all $a \in \underline{Y}_{LR}^d$. This will turn out to be a step toward the definition of our trace on $\mathcal{A}_L^B$, though we will now pause briefly to further rewrite the identity (9.32) in order to make certain properties manifest.

Let us first introduce the normalized cylinders $\tilde{C}_\beta \in \underline{Y}_{LR}^d$ defined by

$$\tilde{C}_\beta \equiv C_\beta / ||C_\beta||, \tag{9.33}$$

where $||C_\beta||$ denotes the operator norm on $\mathcal{H}_{LR}$. One may expect that the continuity axiom (Axiom 4) requires $||C_\beta|| \to 1$ as $\beta \to 0$. This is correct, but the proof is somewhat technical and we relegate it to appendix H.1. As a further remark, note that $\tilde{C}_\beta$ is normalized so as to have operator norm 1, but that the state $|\tilde{C}_\beta\rangle$ is typically still *not* normalized with respect to the Hilbert space inner product. In fact, the norm of $|\tilde{C}_\beta\rangle$ generally diverges as $\beta \to 0$.

For $a \in \underline{Y}_{LR}^d$, we may replace C_β on the right-hand-side of (9.32) with $\tilde{C}_\beta$ and use the above observation to write

$$\lim_{\beta \downarrow 0} \langle \tilde{C}_\beta | \hat{a}_L | \tilde{C}_\beta \rangle = \lim_{\beta \downarrow 0} \frac{\langle C_\beta | \hat{a}_L | C_\beta \rangle}{||C_\beta||^2} = \mathrm{tr}(\hat{a}_L). \tag{9.34}$$

In particular, the second step uses the fact that both $||C_\beta||^2$ and $\langle C_\beta | \hat{a}_L | C_\beta \rangle$ have limits that converge to finite values, and that $||C_\beta||^2 \to 1$.

The formulation in terms of $\tilde{C}_\beta$ is useful because the operator norm of $\tilde{C}_\beta$ is clearly 1. We show below that for positive $\hat{a}_L$ this requires $\langle \tilde{C}_\beta | \hat{a}_L | \tilde{C}_\beta \rangle$ to be a decreasing function of β, which means that for positive $\hat{a}_L$ we can also write (9.34) as a supremum over β:

$$\mathrm{tr}(\hat{a}_L) = \sup_{\beta > 0} \langle \tilde{C}_\beta | \hat{a}_L | \tilde{C}_\beta \rangle. \tag{9.35}$$

This is an improvement over (9.32) because the supremum operation is better behaved than taking general limits.

To show that $\langle \tilde{C}_\beta | \hat{a}_L | \tilde{C}_\beta \rangle$ is a decreasing function of β, note that for $\beta' > 0$ we may write

$$|\tilde{C}_{\beta+\beta'}\rangle = |\tilde{C}_\beta \tilde{C}_{\beta'}\rangle = \widehat{\tilde{C}_{\beta'}}_R |\tilde{C}_\beta\rangle. \tag{9.36}$$

Let us also recall from (9.29) that $\widehat{\tilde{C}_{\beta'}}_R$ commutes with any $\hat{a}_L$. Furthermore, both $\hat{a}_L$ and $\widehat{\tilde{C}_{\beta'}}_R$ are positive, so in particular they are both self-adjoint. We may then use the fact that commuting self-adjoint operators can be diagonalized to introduce a set of common eigenstates $|\lambda, \kappa\rangle$ where $\lambda \geq 0$ is the eigenvalue of $\widehat{C_{\beta'}}_R$ and $\kappa \geq 0$ is the eigenvalue of $\hat{a}_L$. Since the operator norm of $\widehat{\tilde{C}_{\beta'}}_R$ is 1, the parameter λ takes values only in the interval $[0, 1]$. We will also define a measure $d\mu(\lambda, \kappa)$ that gives a resolution of the identity $\mathbb{1} = \int d\mu(\lambda, \kappa) |\lambda, \kappa\rangle\langle\lambda, \kappa|$.

The argument is now straightforward as we may use self-adjointness of $\widehat{\tilde{C}_{\beta'}}_R$ to write

$$\begin{aligned}
\langle \tilde{C}_{\beta+\beta'} | \hat{a}_L | \tilde{C}_{\beta+\beta'} \rangle &= \langle \tilde{C}_\beta | \widehat{\tilde{C}_{\beta'}}_R \hat{a}_L \widehat{\tilde{C}_{\beta'}}_R | \tilde{C}_\beta \rangle \\
&= \int d\mu(\lambda, \kappa) \langle \tilde{C}_\beta | \widehat{\tilde{C}_{\beta'}}_R \hat{a}_L \widehat{\tilde{C}_{\beta'}}_R | \lambda, \kappa \rangle \langle \lambda, \kappa | \tilde{C}_\beta \rangle \\
&= \int d\mu(\lambda, \kappa) \lambda^2 \kappa |\langle \tilde{C}_\beta | \lambda, \kappa \rangle|^2 \\
&\leq \int d\mu(\lambda, \kappa) \kappa |\langle \tilde{C}_\beta | \lambda, \kappa \rangle|^2 = \langle \tilde{C}_\beta | \hat{a}_L | \tilde{C}_\beta \rangle,
\end{aligned} \tag{9.37}$$

where we pass from the 3rd to the 4th line by using $\lambda^2 \leq 1$.

This shows that $\langle \tilde{C}_\beta | \hat{a}_L | \tilde{C}_\beta \rangle$ increases monotonically as β decreases and thus that (9.35) holds for positive elements of $\hat{A}_L^B$. We may then extend tr to any positive element in the left von Neumann algebra via the analogous expression

$$\mathrm{tr}(a) := \sup_{\beta > 0} \langle \tilde{C}_\beta | a | \tilde{C}_\beta \rangle \quad \text{for } a \in \mathcal{A}_L, \tag{9.38}$$

and similarly for $\mathcal{A}_R^B$. In particular, the limit on the right-hand-side in fact exists for all positive bounded operators a. To see this, we note that the quantity $\langle\tilde{C}_\beta|a|\tilde{C}_\beta\rangle$ is positive for all β, so taking the supremum necessarily yields a value in $[0,+\infty]$ as desired.

Now, in the theory of von Neumann algebras, what we have shown thus far is sufficient to qualify tr as what is called a *weight* on $\mathcal{A}_L^B$. For tr to qualify as what is usually called a trace requires an additional property, which is that it give identical results for both $a^\dagger a$ and $aa^\dagger$ for any $a \in \mathcal{A}_L^B$. T

To show this, it will be useful to find yet another characterization of our trace on $\mathcal{A}_L^B$. We begin by again recalling that $\mathbb{1} - \tilde{C}_{2\beta'}$ is positive, so that $a^\dagger a - a^\dagger \tilde{C}_{2\beta'} a$ is also positive. Thus for any $|b\rangle \in \mathcal{H}_{LR}$ we have

$$\langle b|a^\dagger a|b\rangle - \langle b|a^\dagger \tilde{C}_{2\beta'} a|b\rangle \geq 0. \tag{9.39}$$

Taking $|b\rangle = |\tilde{C}_\beta\rangle$ then gives

$$\langle\tilde{C}_\beta|a^\dagger a|\tilde{C}_\beta\rangle \geq \langle\tilde{C}_\beta|a^\dagger \tilde{C}_{2\beta'} a|\tilde{C}_\beta\rangle \tag{9.40}$$

for all β, β'. In particular, taking supremums yields

$$\mathrm{tr}(a^\dagger a) = \sup_{\beta>0} \langle\tilde{C}_\beta|a^\dagger a|\tilde{C}_\beta\rangle \geq \sup_{\beta,\beta'>0} \langle\tilde{C}_\beta|a^\dagger \tilde{C}_{2\beta'} a|\tilde{C}_\beta\rangle. \tag{9.41}$$

We can in fact show that (9.41) is an equality using Axiom 4 and the fact that $\mathcal{A}_L^B$ can be characterized as the closure of $\hat{A}_L^B$ in the *strong* operator topology. This will then give the desired reformulation of our trace that will allow us to prove $\mathrm{tr}\,(ab) = \mathrm{tr}\,(ba)$.

The above characterization of $\mathcal{A}_L^B$ means that for fixed β and any $\epsilon > 0$ there is an operator $\hat{a}_L \in \hat{A}_L^B$ such that $a|\tilde{C}_\beta\rangle - \hat{a}_L|\tilde{C}_\beta\rangle$ has magnitude less than ϵ. Using $||\tilde{C}_{2\beta'}|| = 1$

we then find

$$|\langle\tilde{C}_\beta|a^\dagger\tilde{C}_{2\beta'}a|\tilde{C}_\beta\rangle - \langle\tilde{C}_\beta|\hat{a}_L^\dagger\tilde{C}_{2\beta'}\hat{a}_L|\tilde{C}_\beta\rangle| \leq 2\epsilon||a||\sqrt{\langle\tilde{C}_\beta|\tilde{C}_\beta\rangle} + \epsilon^2. \tag{9.42}$$

Furthermore, since Axiom 4 requires $\langle\tilde{C}_\beta|\hat{a}_L^\dagger C_{2\beta'}\hat{a}_L|C_\beta\rangle$ to be continuous in β', for small enough β' we have

$$|\langle\tilde{C}_\beta|\hat{a}_L^\dagger C_{2\beta'}\hat{a}_L|C_\beta\rangle - \langle\tilde{C}_\beta|\hat{a}_L^\dagger\hat{a}_L|C_\beta\rangle| \leq \epsilon. \tag{9.43}$$

Combining (9.42) (both as written and for $\beta' = 0$) with (9.43) for small enough β' then yields

$$\begin{aligned}
|\langle\tilde{C}_\beta|a^\dagger\tilde{C}_{2\beta'}a|\tilde{C}_\beta\rangle - \langle\tilde{C}_\beta|a^\dagger a|\tilde{C}_\beta\rangle| \;&\leq\; |\langle\tilde{C}_\beta|a^\dagger\tilde{C}_{2\beta'}a|\tilde{C}_\beta\rangle - \langle\tilde{C}_\beta|\hat{a}_L^\dagger\tilde{C}_{2\beta'}\hat{a}_L|\tilde{C}_\beta\rangle| \\
&+\; |\langle\tilde{C}_\beta|a^\dagger a|\tilde{C}_\beta\rangle - \langle\tilde{C}_\beta|\hat{a}_L^\dagger\hat{a}_L|\tilde{C}_\beta\rangle| \\
&+\; |\langle\tilde{C}_\beta|\hat{a}_L^\dagger\tilde{C}_{2\beta'}\hat{a}_L|\tilde{C}_\beta\rangle - \langle\tilde{C}_\beta|\hat{a}_L^\dagger\hat{a}_L|\tilde{C}_\beta\rangle| \\
&\leq\; 4\epsilon||a||\sqrt{\langle\tilde{C}_\beta|\tilde{C}_\beta\rangle} + 2\epsilon^2 + \epsilon,
\end{aligned} \tag{9.44}$$

which clearly vanishes as $\epsilon \to 0$. This shows that $\sup_{\beta'>0}\langle\tilde{C}_\beta|a^\dagger\tilde{C}_{2\beta'}a|\tilde{C}_\beta\rangle$ cannot be smaller than $\langle\tilde{C}_\beta|a^\dagger a|\tilde{C}_\beta\rangle$, and thus that the inequality in (9.41) is saturated. We have thus established that for all $a \in \mathcal{A}_L^B$ (or correspondingly $\mathcal{A}_R^B$) our trace may be written in the form

$$\mathrm{tr}(a^\dagger a) = \sup_{\beta,\beta'>0}\langle C_\beta|a^\dagger C_{2\beta'}a|C_\beta\rangle. \tag{9.45}$$

To establish cyclicity, we again use that a is a strong operator topology limit of a sequence $a_n \in \hat{A}_L^B$. This means that $a_n|\psi\rangle$ converges in the Hilbert space norm to $a|\psi\rangle$ for all $|\psi\rangle$, and in particular for $|\psi\rangle = |\tilde{C}_\beta\rangle$. Thus we may write

$$\langle\tilde{C}_\beta|a^\dagger\tilde{C}_{2\beta'}a|\tilde{C}_\beta\rangle \;=\; \left(\lim_{n\to\infty}\langle\tilde{C}_\beta|\widehat{(a_n)}_L^\dagger\right)\tilde{C}_{2\beta'}\left(\lim_{m\to\infty}\widehat{(a_m)}_L|\tilde{C}_\beta\rangle\right)$$

$$\begin{aligned} &= \left(\lim_{n\to\infty} \langle a_n \tilde{C}_\beta|\right) \tilde{C}_{2\beta'} \left(\lim_{m\to\infty} |a_m \tilde{C}_\beta\rangle\right) \\ &= \lim_{n\to\infty} \lim_{m\to\infty} \langle a_n \tilde{C}_\beta | \tilde{C}_{2\beta'} | a_m \tilde{C}_\beta\rangle. \end{aligned} \tag{9.46}$$

In passing to the final line we have used the fact that bounded operators and normalizable states define continuous functions on the Hilbert space to take the limits outisde the inner product, and to write them in an arbitrary order (i.e., this observation also shows that the limits written in this way commute). Furthermore, we may also write

$$\langle a_n \tilde{C}_\beta | \tilde{C}_{2\beta'} | a_m \tilde{C}_\beta\rangle = \text{tr}\, \left(\tilde{C}_\beta a_n^\star \tilde{C}_{2\beta'} a_m \tilde{C}_\beta\right) = \text{tr}\, \left(\tilde{C}_{\beta'} a_m \tilde{C}_{2\beta} a_n^\star \tilde{C}_{\beta'}\right) = \langle a_m \tilde{C}_{\beta'} | \tilde{C}_{2\beta} | a_n^\star \tilde{C}_{\beta'}\rangle. \tag{9.47}$$

This shows that we can exchange $a_n^\star$ and a_m in (9.46) if we also exchange β with β'. In other words, we have shown

$$\langle \tilde{C}_\beta | a^\dagger \tilde{C}_{2\beta'} a | \tilde{C}_\beta\rangle = \langle \tilde{C}_{\beta'} | a \tilde{C}_{2\beta} a^\dagger | \tilde{C}_{\beta'}\rangle \tag{9.48}$$

for all β, β' and all $a \in \mathcal{A}_L^B$. Combining this result with (9.45) then establishes the desired cyclic identity

$$\text{tr}\; a^\dagger a = \text{tr}\; a a^\dagger. \tag{9.49}$$

We emphasize that our trace will generally give $+\infty$ for some positive elements of $\mathcal{A}_L^B$. In particular, the identity operator lies in $\mathcal{A}_{L/R}^B$ since it can be written in the form

$$\mathbb{1} = \lim_{\beta\to 0} C_\beta. \tag{9.50}$$

But we also see that

$$\text{tr}\; \mathbb{1} = \lim_{\beta_1,\beta_2\to 0} \langle \tilde{C}_{\beta'} | C_\beta | \tilde{C}_{\beta'}\rangle = \lim_{\beta_1,\beta_2\to 0} ||C_{\beta'}||^{-2}\, \text{tr}\, (C_{\beta+\beta'})\,. \tag{9.51}$$

Using the result $\lim_{\beta' \to 0} ||C_{\beta'}|| = 1$ from appendix H.1 then makes it clear that right-hand-side diverges in familiar semiclassical theories of gravity.

9.3.4 An Alternative Definition?

In the above, we used the Hilbert space $\mathcal{H}_{LR}$ to construct the von Neumann algebras $\mathcal{A}_L^B$ and $\mathcal{A}_R^B$. But $\mathcal{H}_{LR}$ is just a sector of the full quantum gravity Hilbert space $\mathcal{H}_{QG}$. It is thus interesting to ask if a different result might be obtained by using $\mathcal{H}_{QG}$, even if our axioms do not suffice to characterize this space in detail.

The natural analogue of our construction above would be to fix a B and then define a representation of A_L^B on every sector of the form $\mathcal{H}_{B \sqcup B'}$ for any B', where we include the case $B' = B$. This representation will again defined operators $\hat{a}_L$ by gluing any $a \in A_L^B$ to the left boundary of states in $\mathcal{H}_{B \sqcup B'}$. We then quotient by the null space $\mathcal{N}_L$ of elements $a \in A_L^B$ that annihilate *every* $|b\rangle \in \mathcal{H}_{B \sqcup B'}$. Since $\hat{a}_L$ is again bounded, it suffices to act with $\hat{a}_L$ on the dense subspace of states $|b\rangle$ defined by linear combinations of surfaces. And, in fact, it suffices to check whether any matrix element of the form $\langle b|\hat{a}_L|c\rangle$ is non-zero for any two rimmed surfaces b, c. Since c has a rim, we can always write $c = C_\beta c'$ for some $\beta > 0$. As a result, we have

$$\langle b|\hat{a}_L|c\rangle = \langle b|\hat{a}_L|C_\beta c'\rangle = \mathrm{tr}(b^\star a C_\beta c') = \mathrm{tr}(c' b^\star a C_\beta) = \langle bc'^\star|\hat{a}_L|C_\beta\rangle, \tag{9.52}$$

where the right-hand side is now a matrix element in the sector $\mathcal{H}_{LR}$ studied above. As a result, the null space $\mathcal{N}_L$ defined by considering the full Hilbert space $\mathcal{H}_{QG}$ is identical to that defined by studying only $\mathcal{H}_{LR}$.

It then remains to take the closure of $\mathcal{A}_L^B/\mathcal{N}_L$ in the weak operator topology. Here it is not enough to work with a dense set of states, as the w.o.t. closure defined by a dense set of states is typically much larger than that defined by a Hilbert space. This is

like when one considers a dense set of states $\mathcal{D}$, and then realized that each such state defined a linear functional on $\mathcal{D}$, which is thus a member of $\mathcal{D}'$. Taking the w.o.t. closure then gives all of $\mathcal{D}' \supset \mathcal{H}$, while using $\mathcal{D} = \mathcal{H}$ gives $\mathcal{D}' = \mathcal{H}$.

This means that there is a difference between working on $\mathcal{H}_{LR}$ and all of $\mathcal{H}_{QG}$. In particular, there may not be a common C_β that we can factor out to write (9.52).

It thus seems like the completion defined by $\mathcal{H}_{QG}$ may be larger than that defined by $\mathcal{H}_{LR}$, in that a sequence that converges in the latter may in fact have multiple limit points in the former. However, it also appears that if we take the resulting multiple operators on $\mathcal{H}_{QG}$ and restrict them all to act on $\mathcal{H}_{LR}$ that they will all act in the same way. So in that sense we will not lose anything by using just $\mathcal{H}_{LR}$ if we want to describe algebras on $\mathcal{H}_{LR}$. Probably this is only worth a very brief comment in the final version of the paper.

9.4 Type I or II von Neumann factors, Hilbert space structure, and entropy

9.4.1 Properties of the trace

It follows immediately from our work above that tr has the following 3 useful properties on $\mathcal{A}_L^B$:

1. Linearity: $\mathrm{tr}(a+b) = \mathrm{tr}(a) + \mathrm{tr}(b)$, and $\mathrm{tr}(\lambda a) = \lambda\,\mathrm{tr}(a)$ for any positive $a, b \in \mathcal{A}_L$ and $\lambda \geq 0$.

2. Invariance under unitaries: $\mathrm{tr}(U^\dagger a U) = \mathrm{tr}\, a$ for any positive $a \in \mathcal{A}_L$ and any unitary $U \in \mathcal{A}$. Since $U^\dagger U = \mathbb{1}$, this clearly follows from the cyclic property $\mathrm{tr}(aa^\dagger) = \mathrm{tr}(a^\dagger a)$. In fact, given property 1, this invariance can be shown to be

equivalent to the cyclic property.

3. Faithfulness: $\mathrm{tr}(a) = 0$ if and only if $a = 0$.

We can also establish two further properties:

5. Semifiniteness: for any positive operator $a \in \mathcal{A}$, there exists a nonzero positive operator $b \in \mathcal{A}$ with $b < a$ and $\mathrm{tr}(b) < \infty$. The notation $b < a$ means that $a - b$ is positive.

6. Normality: For an increasing bounded sequence of positive operators ρ_α in $\mathcal{A}_L$ with supremum $\rho = \sup_\alpha \rho_\alpha$, we have $\mathrm{tr}\ \rho = \sup_\alpha \mathrm{tr}\ \rho_\alpha$.

The proofs of properties 4 and 5 are short, but they are somewhat technical. To avoid distraction from the main results we thus relegate them to appendix H.2.

The first two properties are actually the minimal requirements for the map tr to be a trace on a von Neumann algebra. The faithfulness property gives a sense in which our trace is non-degenerate. Semifiniteness guarantees that not all operators have infinite trace, and the normality condition describes a sense in which the trace is continuous.

The latter properties are important since there is no normal semifinite trace on a type III von Neumann factor. Establishing 4 and 5 above thus tells us that our von Neumann algebra contains only Type I and Type II factors. Furthermore, for such factors there is a unique faithful, normal, semifinite trace up to an overall factor about which more will be said below. See e.g. .

According to the commutation theorem for semifinite traces, a von Neumann algebra $\mathcal{A}$ with a semifinite trace tr is the commutant of its opposite algebra $\mathcal{A}^{op}$ ($\mathcal{A}$ with reversed multiplication rule) when acting on the Hilbert space $\mathcal{H} = \left\{a \in \mathcal{A} : \mathrm{tr}\, a^\dagger a < \infty\right\}$. The algebras $\mathcal{A}_L^B$ and $\mathcal{A}_R^B$ are opposite algebras of each other, and $\mathcal{H}_{LR}$ is just the Hilbert space whose norm is defined by tr. Thus we proved $\mathcal{A}_L^B$ and $\mathcal{A}_R^B$ are commutants of

each other. Alternately one can check that our algebras satisfy the conditions for the commutation theorems in [263], and thus are each others commutants.

9.4.2 $\mathcal{A}^B_{L/R}$ only contains Type I or II factors

In general, our algebra has a direct sum structure,

$$\mathcal{A}^B_{L/R} = \bigoplus_\beta \left(\mathcal{A}^B_{L/R}\right)^\beta, \tag{9.53}$$

where each $\left(\mathcal{A}^B_{L/R}\right)^\beta$ is a factor, and this direct sum could also be an integral when the parameter β is continuous. The reason why the algebra has a direct sum structure is because although $\mathcal{A}^B_L$ and $\mathcal{A}^B_R$ are commutants, there could still be non-trivial center operators. Different eigenvalues of the center operators correspond to different superselection sectors of the algebra. For the same reason, the Hilbert space takes the form

$$\mathcal{H}_{LR} = \bigoplus_\beta \mathcal{H}^\beta_{LR}, \tag{9.54}$$

and for any type I factor in this direct sum, the corresponding Hilbert space takes the form

$$\mathcal{H}^\beta_{LR} = \mathcal{H}^\beta_L \otimes \mathcal{H}^\beta_R. \tag{9.55}$$

For any type I or II factor, the faithful, normal, semifinite trace is unique up to an overall constant. For every sector β, the Hilbert space trace Tr is given by $\mathrm{Tr}\, O = \sum_i \langle i|O|i\rangle$ for any orthonormal complete basis $|i\rangle$. For every sector β, the trace defined by the von Neumann algebra is related to the Hilbert space trace via

$$\mathrm{tr} = e^{S^\beta_0}\, \mathrm{Tr}_\beta\,. \tag{9.56}$$

9.4.3 Entropies from algebras

For any positive operator ρ, we can define the Renyi entropies $S_n(\rho) = \frac{1}{1-n} \ln \operatorname{tr} \rho^n$, which gives the von Neumann entropy $S_{vN}(\rho) = -\operatorname{tr} \rho \ln \rho$ after analytic continuation as $n \to 1$. In the semiclassical limit, Lewkowycz and Maldacena showed that the above procedure gives the Ryu-Takayanagi formula as the von Neumann entropy. In terms of the Hilbert space, for a density operator ρ, the von Neumann entropy is given by

$$\sum_\beta \tilde{p}_\beta S_{vN}\left(\rho_\beta\right) - \sum_\beta \tilde{p}_\beta \ln \tilde{p}_\beta + \sum_\beta \tilde{p}_\beta S_0^\beta \tag{9.57}$$

where p_i is the probability to find the system in the subspace $\mathcal{H}_{LR}^\beta$, ρ_β is the (normalized) density matrix by the projection of the full state to $\mathcal{H}_{LR}^\beta$, the S_0^β are a set of positive constants, and we have defined the quantities

$$\tilde{p}_\beta = \frac{e^{S_0^\beta} p_\beta}{\sum_\beta e^{S_0^\beta} p_\beta}.$$

Thus we have given a bulk Hilbert space interpretation of the Ryu-Takayanagi formula, without making reference to holography.

Appendix A

Appendix to Chapter 2

A.1 Action calculations for one interval case

This appendix derives the Euclidean action (2.35) for the one-interval case. The action contains three parts: the Einstein-Hilbert term, the Gibbons-Hawking term and the counterterms. The action also depends on the choice of cutoff δ introduced in section 2.4.

While one could calculate the bulk action using the metric (2.24), it turns out to be easier to use the cylindrical coordinates in which the metric takes the form

$$ds^2 = (1+r^2)dx^2 + \frac{dr^2}{1+r^2} + \alpha^2 r^2 d\phi^2 \tag{A.1}$$

Our cutoff spacetime is then bounded by the extremal surfaces $x = -\frac{1}{2}\alpha L_0$ and $x = \frac{1}{2}\alpha L_0$, which in the Poincaré ball coordinates are anchored to the boundary cutoff surfaces described in section 2.4. In order to arrive at a description where the coordinate ranges

are independent of α, we introduce $\tilde{x} = x/\alpha \in [-L_0/2, L_0/2]$ which yields

$$ds^2 = \frac{dr^2}{1+r^2} + \alpha^2 \left[(1+r^2)d\tilde{x}^2 + r^2 d\phi^2\right]. \tag{A.2}$$

The metric (A.2) can be written in the Fefferman-Graham form by defining

$$z := \frac{2}{\alpha} \frac{1}{r + \sqrt{1+r^2}}, \tag{A.3}$$

which yields

$$ds^2 = \frac{1}{z^2}\left(dz^2 + (1+\alpha^2 z^2/4)^2 d\tilde{x}^2 + (1-\alpha^2 z^2/4)^2 d\phi^2\right). \tag{A.4}$$

Here $z = 0$ is the AdS boundary and $z = 2/\alpha$ is the ϕ-axis. The associated boundary metric is just a cylinder of length L_0 and circumference 2π. For convenience, we may now identify the extremal surfaces $\tilde{x} = \pm L_0/2$ so that the boundary becomes a torus. While actions I computed in this conformal frame may differ from those computed in the round conformal frame, the difference arises only from the conformal anomaly. Since the anomaly is the same for each state (i.e., for each α), this contributes only an overall normalization constant (which might depend on δ and λ) to our probabilities $P(\alpha) \sim e^{-I}$, and in any case the normalization must be later fixed to yield $\int d\alpha P(\alpha) = 1$.

We are thus free to use the above toroidal frame for any value of λ. The action consists of an Einstein-Hilbert term (with a cosmological constant), a Gibbons-Hawking term, and a counter-term. Since $R - 2\Lambda = -4 + 16\pi\mu G\delta(x^\mu - x^\mu_{\text{string}})$, the Einstein-Hilbert term may be further divided into two parts. The contribution from string itself is clearly

$$I_{\text{string}} = -\mu\alpha L_0 = \frac{(\alpha-1)\alpha L_0}{4G}. \tag{A.5}$$

Since a radial cutoff at $z = \epsilon$ yields $r = \frac{1}{\alpha\epsilon}(1 - \alpha^2\epsilon^2/4 + O(\epsilon^4))$, the Einstein-Hilbert (with cosmological constant) contribution from the region away from the string is

$$\begin{aligned} I_{EH1} &= -\frac{1}{16\pi G}\int d^3x\sqrt{g}(-4) \\ &= \frac{\alpha L_0}{2G}\int_0^{r(\epsilon)} \alpha r dr = \frac{\alpha^2 L_0}{4G}\left(\frac{1}{\alpha^2\epsilon^2} - \frac{1}{2}\right). \end{aligned} \tag{A.6}$$

To calculate the Gibbons-Hawking term, we first need to calculate the extrinsic curvature on the surface $r = r(\epsilon)$. The unit normal to that surface is

$$n^\mu \partial_\mu = \sqrt{1 + r^2}\partial_r, \tag{A.7}$$

so the trace of the extrinsic curvature is

$$\begin{aligned} K &= n^\rho \partial_\rho \ln\sqrt{g} + \partial_\rho n^\rho \\ &= \sqrt{1+r^2}\partial_r \ln(\alpha r) + \partial_r\sqrt{1+r^2} = 2 + O(r^{-4}) = 2 + O(\epsilon^4) \end{aligned} \tag{A.8}$$

Since a constant r surface has area $2\pi\alpha^2 L_0 r\sqrt{1+r^2} = 2\pi\alpha^2 L_0 r^2\sqrt{1+r^{-2}} = \frac{2\pi}{\epsilon^2}L_0 + O(\epsilon^2)$, the Gibbons-Hawking term is

$$\begin{aligned} I_{GH} &= -\frac{1}{8\pi G}\int d^2x\sqrt{h}K \\ &= -\frac{L_0}{2G\epsilon^2} + O(\epsilon^2), \end{aligned} \tag{A.9}$$

where $\sqrt{h}$ is the area element of the induced metric on the surface $r = \textit{constant}$. Finally, the counterterm is

$$\begin{aligned} I_{CT} &= \frac{1}{8\pi G}\int d^2x\sqrt{h} \\ &= \frac{L_0}{4G\epsilon^2} + O(\epsilon^2). \end{aligned} \tag{A.10}$$

Summing these terms and taking $\epsilon \to 0$ gives the total action (2.35).

Appendix B

Appendix to Chapter 3

B.1 Scalar field solution via Fourier expansion

B.1.1 Massless Field

Let us now take a moment to construct the solutions in Eqs. (3.17), (3.18) directly, without recourse to analytic continuation. As is well-known, the space of solutions to the Klein-Gordon equation in 1+1 dimensional Minkowski space has a basis given by plane waves. A general solution $\phi(T, X)$ may thus be written in the form

$$\phi(T,X) = \int_{-\infty}^{+\infty} a(\zeta) e^{i(|\zeta|T - \zeta X)} d\zeta + \int_{-\infty}^{+\infty} a^*(\zeta) e^{-i(|\zeta|T - \zeta X)} d\zeta. \tag{B.1}$$

The initial condition is given by Eq. (3.12):

$$\phi_0(X) = 2X^{k/m}\Theta(X) + 2(-1)^k(-X)^{k/m}\Theta(-X), \qquad \partial_T \phi|_{T=0} = 0, \tag{B.2}$$

which yields

$$a^*(\zeta) = a(-\zeta), \tag{B.3}$$

and

$$a(\zeta) = \frac{\Gamma\left(\frac{k+m}{m}\right)|\zeta|^{-\frac{k+m}{m}}\left(-\left((-1)^k+1\right)\sin\left(\frac{\pi k}{2m}\right)+(-i)\left((-1)^k-1\right)\mathrm{sgn}(\zeta)\cos\left(\frac{\pi k}{2m}\right)\right)}{2\pi}. \tag{B.4}$$

This result simplifies for even and odd k:

$$a(\zeta) = -\frac{\Gamma(1+k/m)\sin\left(\frac{\pi k}{2m}\right)}{\pi}|\zeta|^{-k/m-1}, \qquad k \in 2\mathbb{Z} \tag{B.5}$$

$$a(\zeta) = i\frac{\Gamma(1+k/m)\cos\left(\frac{\pi k}{2m}\right)}{\pi}\mathrm{sign}(\zeta)|\zeta|^{-k/m-1}, \qquad k \in 2\mathbb{Z}+1. \tag{B.6}$$

Here in finding Eq. (B.5) and Eq. (B.6), we rotated the contour of integration to make the integrals convergent. For $k \in 2\mathbb{Z}$, the field $\phi(U,V)$ is given by

$$\begin{aligned}\phi(U,V) &= \int_{-\infty}^{+\infty}\left(-\frac{\Gamma(1+k/m)\sin\left(\frac{\pi k}{2m}\right)}{\pi}|\zeta|^{-k/m-1}\right)\left(e^{i(|\zeta|T-\zeta X)}+e^{-i(|\zeta|T-\zeta X)}\right)d\zeta \\ &= |V|^{k/m}+|U|^{k/m},\end{aligned} \tag{B.7}$$

where we used

$$\int_0^{+\infty} d\zeta\zeta^{-k/m-1}(e^{i\zeta V}+e^{-i\zeta V}) = 2|V|^{k/m}\cos\left(\frac{\pi k}{2m}\right)\Gamma(-k/m). \tag{B.8}$$

In Eq. (B.8), an analytic continuation in k/m is needed to make sense of the integral. Similarly for odd k we find

$$\phi(T,X) = \int_{-\infty}^{+\infty} \left(i\frac{\Gamma(1+k/m)\cos\left(\frac{\pi k}{2m}\right)}{\pi}\text{sign}(\zeta)|\zeta|^{-k/m-1} \right) \left(e^{i(|\zeta|T-\zeta X)} - e^{-i(|\zeta|T-\zeta X)}\right) d\zeta$$
$$= \text{sign}(V)|V|^{k/m} - \text{sign}(U)|U|^{k/m}. \tag{B.9}$$

Thus, we see that both solutions agree with the solution we found previously by using appropriate analytic continuations.

B.1.2 Massive Field

In Sec. 3.3.2, we guessed the solution in the future wedge for the massive scalar field theory using the separation of variables and continuity of the solution. Here we derive the same solution directly by performing a Fourier transform.

Doing the Fourier transform directly on the initial data is not easy in this case. One way to go around this is to use the integral representation of the Bessel function,

$$I_\nu(x) = -i2^{-\nu-1}x^\nu \int \frac{\Gamma(s)}{\Gamma(s+1/2)\Gamma(1/2-s)\Gamma(1+\nu-s)} \left(\frac{x^2}{4}\right)^{-s} ds, \tag{B.10}$$

where the integral runs over the imaginary line with a positive real part.

Using this representation, the calculation is almost the same as the massless case. For simplicity, let's set k to be even, although the analysis is quite similar for odd k. Defining $V = T + X, U = T - X, \nu \equiv k/m$, we have

$$\phi(T=0,X) = 2I_{k/m}(\mu|X|) = -i \int \frac{\Gamma(s)}{\Gamma(s+1/2)\Gamma(1/2-s)\Gamma(1+\nu-s)} 2^{2s-\nu}|\mu X|^{\nu-2s} ds. \tag{B.11}$$

As a result,the Fourier coefficients are given by

$$\begin{aligned} a(\zeta) &= \frac{1}{4\pi}\int_{-\infty}^{+\infty}\phi(T=0,X)e^{-i\zeta X}dX \\ &= -\frac{i}{2\pi}\int ds\,\frac{\Gamma(s)2^{2s-\nu}\mu^{\nu-2s}}{\Gamma(s+1/2)\Gamma(1/2-s)\Gamma(1+\nu-s)} \\ &\qquad\qquad \left(-\Gamma(1+\nu-2s)\sin\left(\frac{\pi(\nu-2s)}{2}\right)|\zeta|^{-\nu+2s-1}\right) \qquad \text{(B.12)} \\ &= \int ds\, b(s)|\zeta|^{2s-\nu-1}, \qquad \text{(B.13)} \end{aligned}$$

where $b(s) \equiv i\frac{\Gamma(1+\nu-2s)2^{2s-\nu}\sin\left(\frac{\pi(\nu-2s)}{2}\right)\Gamma(s)}{2\pi\Gamma(s+1/2)\Gamma(1/2-s)\Gamma(1+\nu-s)}\mu^{\nu-2s}$. Therefore, the field is given by

$$\phi(T,X) = \int ds\, b(s)\int |\zeta|^{2s-\nu-1}\left(e^{i\left(\sqrt{\zeta^2+\mu^2}T-\zeta X\right)} + e^{-i\left(\sqrt{\zeta^2+\mu^2}T-\zeta X\right)}\right)d\zeta. \qquad \text{(B.14)}$$

This integral is hard to do in general, so for a simpler case, we instead check that Eq. (B.14) reduces to Eq. (3.23) when $X = 0$. In this case we have

$$\begin{aligned} \phi(T,0) &= \int b(s)ds\int |\zeta|^{2s-\nu-1}\left(e^{i\left(\sqrt{\zeta^2+\mu^2}T\right)} + e^{-i\left(\sqrt{\zeta^2+\mu^2}T\right)}\right)d\zeta \\ &= \int b(s)ds\int \mu^{2s-\nu}|\sinh(y)|^{2s-\nu-1}\left(e^{i\mu T\cosh(y)} + e^{-i\mu T\cosh(y)}\right)\cosh(y)dy \\ &= 2\int b(s)ds\int \mu^{2s-\nu}2^{s-\nu/2-1/2}\frac{\Gamma(s-\nu/2)}{\sqrt{\pi}}\times \\ &\times\left(-K_{s-\nu/2+1/2}(-i\mu T)(-i\mu T)^{-s+\nu/2+1/2} - K_{s-\nu/2+1/2}(i\mu T)(i\mu T)^{-s+\nu/2+1/2}\right) \\ &= -2\int b(s)ds\int \mu^{2s-\nu}\frac{\Gamma(s-\nu/2)}{\sqrt{\pi}}\int d\tilde{s}\frac{1}{4\pi i}\Gamma(\tilde{s})\Gamma(\tilde{s}-s+\nu/2-1/2)\times \\ &\qquad\qquad \times\left[\left(\frac{i\mu T}{2}\right)^{1-2\tilde{s}} + \left(\frac{-i\mu T}{2}\right)^{1-2\tilde{s}}\right]. \end{aligned} \qquad \text{(B.15)}$$

The first simplification is that

$$\sqrt{\pi}\Gamma(1+\nu-2s)2^{2s-\nu} = \Gamma(\nu/2+1/2-s)\Gamma(\nu/2+1-s), \qquad \text{(B.16)}$$

and

$$\Gamma(\nu/2+1-s)\Gamma(s-\nu/2)=\pi/\sin(\pi(s-\nu/2)). \tag{B.17}$$

Using these identities and integrating over s (and wrapping poles to the left), we find

$$-\int b(s)\mu^{2s-\nu}\Gamma(s-\nu/2)\Gamma(\tilde{s}-s+\nu/2-1/2)=-i\frac{\Gamma(1-\tilde{s})\Gamma(\tilde{s}+\nu/2-1/2)}{\Gamma(3/2-\tilde{s}+\nu/2)}.$$

Defining $s_1=\tilde{s}-1/2$, and using $\Gamma(1/2-s_1)\Gamma(1/2+s_1)=\pi/\cos(\pi s_1)$ we have

$$\begin{aligned}\phi(T,0)&=-\int ds_1\frac{i}{2\pi}\frac{\Gamma(1/2-s_1)\Gamma(1/2+s_1)\Gamma(s_1+\nu/2)}{\Gamma(1+\nu/2-s_1)}2\cos(\pi s_1)\left(\frac{\mu T}{2}\right)^{-2s_1}\\&=-\int ds_1\frac{i}{\pi}\frac{\Gamma(s_1+\nu/2)}{\Gamma(1+\nu/2-s_1)}\left(\frac{\mu T}{2}\right)^{-2s_1}=2J_{k/m}(\mu T),\end{aligned} \tag{B.18}$$

as expected from by Eq. (3.23) by setting $V=T, U=T$ and considering even k.

B.2 Finding Solutions by Analytic Continuation in JT gravity

This appendix illustrates how the Lorentz signature solutions can be found by first regularizing the Euclidean conical singularities in a way that splits it (symmetrically) into two such singularities as in figure 3.2, and then analytically continuing the region between them.

For a Euclidean JT gravity solution with a conical defect, we have

$$ds^2=m^2(r^2-r_s^2)d\tau^2+\frac{dr^2}{r^2-r_s^2}, \tag{B.19}$$

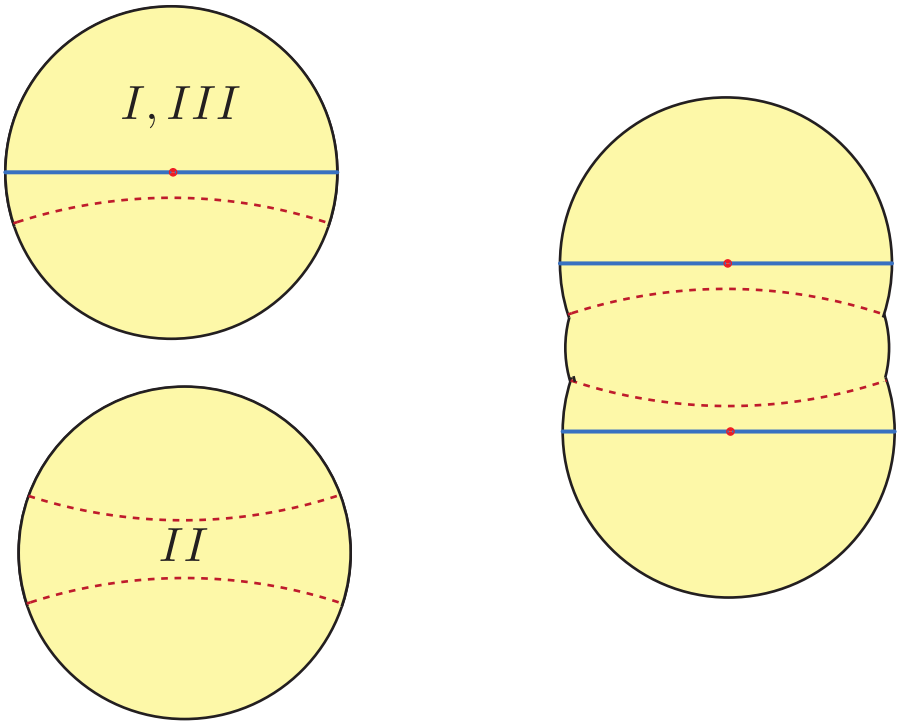

Figure B.1: Left: We take solutions corresponding to a conical defect of opening angle $2\pi m$ and cut pieces of it, denoted I and III, slightly greater than half so as to avoid the defect. We then patch it onto a portion of the smooth AdS_2 solution, labelled II, by imposing matching conditions on the geodesic and at the asymptotic boundary. This leads to a regularized split solution which can be analytically continued to a Lorentzian spacetime. In the limit $\delta \to 0$, we obtain the same solution that we expect from initial data evolution.

$$\Phi = m\Phi_b r, \tag{B.20}$$

where the periodicity of τ is $2\pi/r_s$. When $m = 1$, the solution is smooth, so $r_s = \frac{2\pi}{\beta}$.

The boundary condition is that the boundary length is $\frac{\beta}{\epsilon}$. This means that we should put the cutoff at $r = r_c = \frac{1}{m\epsilon}$, and the dilaton value there is $\frac{\Phi_b}{\epsilon}$.

We cut the solution at the following geodesic:

$$\begin{aligned} r(\lambda) &= \frac{1}{m}\sqrt{\delta^2 + (mr_s)^2}\cosh\lambda, \\ \tau(\lambda) &= \frac{1}{r_s}\arctan\left(\frac{mr_s}{\delta}\tanh\lambda\right), \end{aligned} \tag{B.21}$$

where δ indicates how far the geodesic is from the center of the disk. At $r = \frac{1}{m\epsilon}$, the affine parameter is

$$\lambda_c = \cosh^{-1}\frac{1/\epsilon}{\sqrt{\delta^2 + (mr_s)^2}}. \tag{B.22}$$

In the middle region, we have a JT solution without a defect:

$$ds^2 = (\bar{r}^2 - \bar{r}_s^2)d\bar{\tau}^2 + \frac{d\bar{r}^2}{\bar{r}^2 - \bar{r}_s^2}, \tag{B.23}$$

$$\Phi = \bar{\Phi}_b\bar{r}, \tag{B.24}$$

where the periodicity of $\bar{\tau}$ is $2\pi/\bar{r}_s$. We cut it at the geodesic

$$\begin{aligned} \bar{r}(\bar{\lambda}) &= \sqrt{\bar{\delta}^2 + \bar{r}_s^2}\cosh\bar{\lambda}, \\ \bar{\tau}(\bar{\lambda}) &= \frac{1}{\bar{r}_s}\arctan\left(\frac{\bar{r}_s}{\bar{\delta}}\tanh\bar{\lambda}\right). \end{aligned} \tag{B.25}$$

At the cutoff $\bar{r} = \bar{r}_c = \frac{1}{\epsilon}$, the affine parameter is

$$\bar{\lambda}_c = \cosh^{-1}\frac{1/\epsilon}{\sqrt{\bar{\delta}^2 + \bar{r}_s^2}}. \tag{B.26}$$

We now glue these solutions together to regularize the conical defect solution to have a neighbourhood of a smooth solution near the $\mathbb{Z}_2$ symmetric slice. The first matching condition is that the affine parameters are the same:

$$\lambda_c = \bar{\lambda}_c, \tag{B.27}$$

from which we get

$$\bar{\delta} = \sqrt{m^2 r_s^2 - \bar{r}_s^2 + \delta^2}. \tag{B.28}$$

The second matching condition is that the total boundary length is $\frac{\beta}{\epsilon}$:

$$4\left(\frac{\pi}{r_s} - \tau(\lambda_c)\right) + 4\left(\frac{\pi}{2\bar{r}_s} - \bar{\tau}(\bar{\lambda}_c)\right) = \beta. \tag{B.29}$$

To leading order in ϵ, we know that the relation between r_s and $\bar{r}_s$ can be solved from

$$\pi(r_s + \bar{r}_s) - 2\bar{r}_s \tan^{-1}\left(\frac{m r_s}{\delta}\right) - 2 r_s \tan^{-1}\left(\frac{\bar{r}_s}{\bar{\delta}}\right) = 0. \tag{B.30}$$

This is in general hard to solve, but we can see that in the limit $\delta \to 0$, we have $\bar{r}_s = m r_s$.

The last matching condition is that, the dilaton values should be the same at the boundary. Thus, we have

$$\bar{\Phi}_b = \Phi_b. \tag{B.31}$$

If we now analytically continue the middle region to Lorentzian signature, we obtain a smooth black hole with $\bar{r}_s = m r_s$, which means $\bar{\beta} = \frac{\beta}{m}$. The boundary dilaton is $\bar{\Phi}_b = \Phi_b$. Note that for this kind of spacetime that we constructed, the dilaton field only matches along the geodesic when we take $\delta \to 0$ limit. This is of course, as we expect from fixed-area state in pure JT gravity with $U(1)$ symmetry, identical to the microcanonical TFD at the temperature $\bar{\beta}$.

More generally, this technique of regularizing the conical defect solution and analytically continuing from the neighbourhood of the $\mathbb{Z}_2$ symmetric slice might be useful. In certain situations, it may be simpler than solving the initial value problem.

B.3 Solving the AdS_3 metric perturbatively

In Sec. 3.4.3, we solved for the scalar field in AdS_3 and described the solution for the backreacted metric. In this appendix, we write down all the equations for the metric components explicitly and show that they can be solved perturbatively as claimed in Sec. 3.4.3.

The solution for the scalar field to leading order is

$$\phi = 2\eta\cos(k\theta)\frac{f_{m,k}(r)}{f_{m,k}(r_c)}, \qquad f_{m,k}(r) = r^{k/m}{}_2F_1\left(\frac{k}{2m}, \frac{k}{2m}+1, \frac{k}{m}+1, -r^2\right). \tag{B.32}$$

From this solution, the stress tensor is decomposed into Fourier modes as

$$T_{\mu\nu} = \nabla_\mu\phi\nabla_\nu\phi - \frac{g_{\mu\nu}}{2}(\nabla\phi)^2 = T^-_{\mu\nu}e^{-2ik\theta} + T^+_{\mu\nu}e^{2ik\theta} + T^0_{\mu\nu}. \tag{B.33}$$

Following [33], the ansatz for the metric to first order in η^2 is

$$ds^2 = \frac{dr^2}{1+r^2+g(r,\theta)} + m^2r^2d\theta^2 + m^2(1+r^2)\left(1+v(r,\theta)\right)dy^2, \tag{B.34}$$

where $g(r,\theta), v(r,\theta)$ are the metric perturbation, and have the following Fourier expansion,

$$g(r,\theta) = g^+(r)e^{2ik\theta} + g(r)^0 + g^-(r)e^{-2ik\theta}, \qquad v(r,\theta) = v^+(r)e^{2ik\theta} + v^0(r) + v^-(r)e^{-2ik\theta} \tag{B.35}$$

Plugging the stress tensor in the Einstein's equation (we set $8\pi G = 1$)

$$R_{\mu\nu} - \frac{g_{\mu\nu}}{2}(R+2) = T_{\mu\nu}, \tag{B.36}$$

one finds that Fourier modes decouple to the first order. For the yy-components, we have

$$4k^2 g^-(r) + m^2 r(1+r^2) g^{-\prime}(r) = 2r^2 T^-_{yy} = \frac{\eta^2}{f^2_{m,k}(r_c)}(1+r^2)\left(k^2 f_{m,k}(r)^2 - m^2 r^2 (1+r^2) f'^2_{m,k}\right), \tag{B.37}$$

$$g^{0\prime}(r) = \frac{2r}{m^2(1+r^2)} T^0_{yy} = \frac{\eta^2}{f^2_{m,k}(r_c)} \partial_r \left(r(1+r^2) f_{m,k}(r) f'_{m,k}(r)\right), \tag{B.38}$$

$$4k^2 g^+(r) + m^2 r(1+r^2) g^{+\prime}(r) = 2r^2 T^+_{yy} = \frac{\eta^2}{f^2_{m,k}(r_c)}(1+r^2)\left(k^2 f_{m,k}(r)^2 - m^2 r^2 (1+r^2) f'^2_{m,k}\right), \tag{B.39}$$

where in Eq. (B.38), the equation of motion for the scalar field is used. These equations are all first order differential equations and therefore, the solutions can be written in terms of integrals involving $f_{m,k}(r)$ and its derivatives. Using the solutions for $g^{\pm}(r), g^0(r)$, the rr components of Einstein's equations give the differential equations for $v^{\pm}, v^0$,

$$-4k^2(1+r^2)v^- + 2m^2 r^2 g^-(r) + m^2 r(1+r^2)^2 v^{-\prime}(r) = 2m^2 r^2 (1+r^2)^2 T^-_{rr}, \tag{B.40}$$

$$2r g^0(r) + (1+r^2)^2 v^{0\prime}(r) = 2T^0_{rr} r (1+r^2)^2, \tag{B.41}$$

$$-4k^2(1+r^2)v^+ + 2m^2 r^2 g^+(r) + m^2 r(1+r^2)^2 v^{+\prime}(r) = 2m^2 r^2 (1+r^2)^2 T^+_{rr}, \tag{B.42}$$

where

$$T^0_{rr} = \frac{\eta^2}{m^2 r^2(1+r^2) f^2_{m,k}(r_c)}(-k^2 f_{m,k}(r)^2 + m^2 r^2(1+r^2) f'_{m,k}(r)^2), \tag{B.43}$$

$$T^-_{rr} = \frac{\eta^2}{2m^2 r^2(1+r^2) f^2_{m,k}(r_c)}(k^2 f_{m,k}(r)^2 + m^2 r^2(1+r^2) f'_{m,k}(r)^2), \tag{B.44}$$

$$T^+_{rr} = \frac{\eta^2}{2m^2 r^2(1+r^2) f^2_{m,k}(r_c)}(k^2 f_{m,k}(r)^2 + m^2 r^2(1+r^2) f'_{m,k}(r)^2). \tag{B.45}$$

Therefore, the equations for $v^{\pm}(r), v^0(r)$ are also first order and the solutions can be written in terms of integrals of the stress tensor or power series expansions. We also checked that the power series solutions of $g^{\pm,0}, v^{\pm,0}$ satisfy other components of Einstein's equations and therefore, the verified the consistency of the metric ansatz. The form of the power series expansions have been listed in Eq. (3.74).

Appendix C

Appendix to Chapter 4

C.1 An alternate accounting scheme

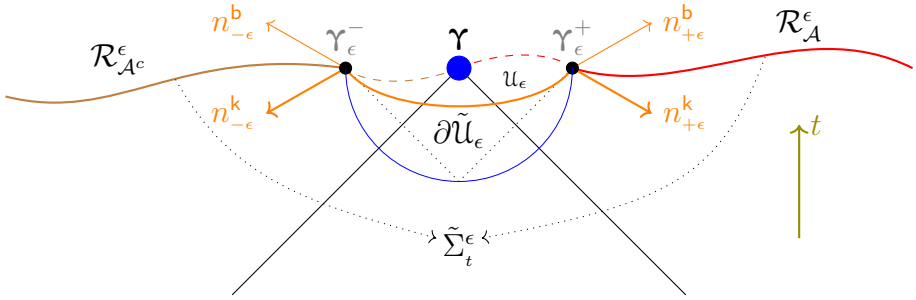

Figure C.1: A choice of $\partial\tilde{\mathcal{U}}_\epsilon$ (orange curve) whose intersection with $\tilde{\Sigma}_t$ is not orthogonal. We have indicated its timelike normal at the locus where the regulating surface intersects the bulk Cauchy slice both into the ket part of the spacetime, as well as the corresponding normal from the bra side. The latter has been reflected up into the future to make clear that in the limit of the smooth join the inner product is between anti-parallel vectors owing to the opposite time-orientation on M^{b} relative to that on M^{k}.

As described at the end of section 4.3.2, it is sometimes useful to absorb the brane contribution S_γ into the contributions from the ket and bra parts of the spacetime. For

instance, one can redefine the terms in (4.2) to

$$S = \left(S^k_{\rm gr} + \frac{1}{2}S_{\boldsymbol{\gamma}}\right) - \left(S^b_{\rm gr} - \frac{1}{2}S_{\boldsymbol{\gamma}}\right) \equiv \tilde{S}^k_{\rm gr} - \tilde{S}^b_{\rm gr}\,. \tag{C.1}$$

In order that (C.1) agree precisely with (4.2), we take $\tilde{S}^k_{\rm gr} = \lim_{\epsilon\to 0}\tilde{S}^{k,\epsilon}_{\rm gr}$ with

$$\begin{aligned}
\tilde{S}^{k,\epsilon}_{\rm gr} &= \frac{1}{16\pi G_N}\int_{\mathsf{M}^{\mathsf{k}}_\epsilon} d^{d+1}x\,\sqrt{-g}\left[R + \frac{d(d-1)}{\ell^2_{\rm AdS}}\right] + S^\epsilon_{\rm bdy} + S^\epsilon_{\rm corner}\,,\\
S^\epsilon_{\rm bdy} &= \frac{1}{8\pi G_N}\int_{\mathcal{B}} d^dx\,\sqrt{|\gamma|}\,K + \frac{1}{8\pi G_N}\int_{\tilde{\Sigma}^\epsilon_t\cup\partial\mathcal{U}_\epsilon}\sqrt{|h|}\,K\\
S^\epsilon_{\rm corner} &= \frac{1}{16\pi G_N}\int_{\boldsymbol{\gamma}^+_\epsilon\cup\boldsymbol{\gamma}^-_\epsilon} dA\,\cosh^{-1}\left(n^{\mathsf{k}}_\epsilon\cdot n^{\mathsf{b}}_\epsilon\right)\,,
\end{aligned} \tag{C.2}$$

with a complex-conjugate prescription for $\tilde{S}^b_{\rm gr}$. Here $\gamma_{\mu\nu}$ is the induced metric on the boundary $\mathcal{B}$ and h_{ij} that on the interior boundary. K is the trace of the extrinsic curvature defined using the appropriate normal. We have also allowed for possible 'corner' terms associated with choosing $\partial\mathcal{U}_\epsilon$ to have non-orthogonal intersection with the bulk timefold $\tilde{\Sigma}_t$ as shown in fig. C.1 (the orange curve).

We consider the case where the regulating surface $\partial\mathcal{U}_\epsilon$ is everywhere spacelike. By doing so we no longer pick up the poles in the boost angle at the past light cone. The contribution (4.13) now instead can be attributed to this corner term (cf., for instance [152] where this was discussed earlier). The explicit expression for the corner contribution is given in terms of the inner product (or relative boost) between the unit normals n^{k}_ϵ and n^{b}_ϵ to the regulator surfaces $\mathcal{U}_\epsilon$ on the ket and the bra geometries, respectively. Though we integrate the corner contribution over the regulated codimension-2 fixed point loci $\boldsymbol{\gamma}^\pm_\epsilon$, the essential contribution can be understood from the $1+1$ dimensional example, where each corner contributes $\frac{i}{16G_N}$ to $\tilde{S}^{k,\epsilon}_{\rm gr}$. We could also consider a more general non-orthogonal intersection as mentioned in footnote 14, where the final result works out

albeit with a slightly modified accounting of the contributions.

The boundary terms and the corner terms are written out here in the standard metric formulation above. The corner terms were derived in [150] using the differential formulation of the action (using a non-holonomic tetrad basis) which has the added advantage of seeing quite explicitly that they are essential to having a well-defined variational principle. As in section 4.3.2, the extrinsic curvature terms $S^{\epsilon}_{\text{bdy}}$ receive subtle contributions when the boundary transitions from being spacelike to timelike, though these again have a simple universal form in the differential formalism [150].

C.2 Smoothing the bra-ket gluing via excursions into the complex plane

In this appendix we recall a particularly clean example from [141, 142, 143] of the gluing of the bra and ket branches of a saddle-point. In this case the gluing is performed by making a smooth excursion into the space of complex metrics, which smooths out both the timefolds and the cosmic brane splitting surface described in the main text. As discussed in the aforementioned references, the fact that the construction solves the field equations with the correct boundary conditions is critical for obtaining the proper physics for boundary correlators. This example also gives a very explicit illustration of the reality of the weight e^{iS} associated with replica-symmetric saddles.

We will borrow from the example discussed in [141, 142, 143] which corresponds to the case of replica number $n = 1$. The context there involved computing boundary correlation functions of light fields in a thermal state in the limit of vanishing bulk Newton constant G_N. As a result, back-reaction from the quantum fields could be neglected. The problem thus reduced to studying quantum fields on a fixed bulk background that (for $n = 1$)

was just the $(d+1)$-dimensional AdS-Schwarzschild black hole with specified inverse temperature β. For a thermal problem, one may think of starting with the Euclidean solution, constructing the full complex black hole geometry by analytic continuation, and then choosing to deform the original Euclidean slice of this complex geometry as desired into an arbitrary contour of real bulk dimension $d+1$. For the purposes of studying boundary correlation functions of light fields at general Lorentzian times $t > 0$, it was useful in [143] to take the resulting slice at the AdS boundary to extend to $t = +\infty$ along the positive real Lorentzian axis as shown in the left panel of fig. C.2. The right panel shows the generalization of the boundary geometry to $n = 3$. In both cases, we can think of the boundary conditions as forcing t to follow a certain contour in the complex time-plane.

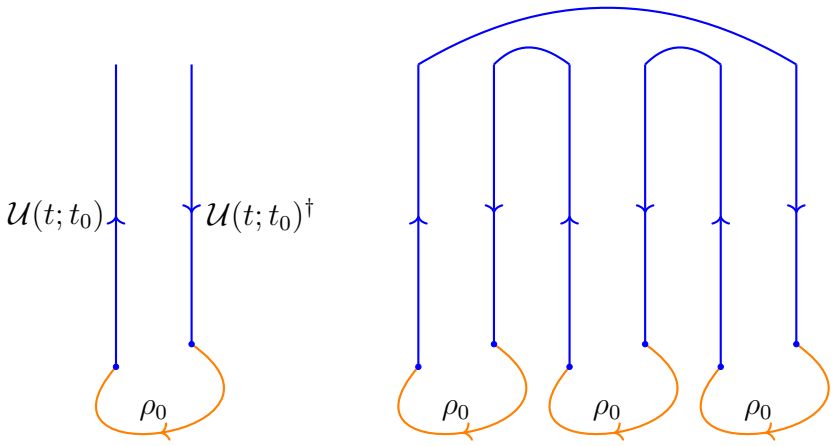

Figure C.2: The thermal density matrix of a field theory can be prepared from a Euclidean path integral on a $\mathcal{B} = \mathbf{S}^1_{t_{\rm E}} \times \Sigma_t$ with $t_{\rm E} = \beta + it$. Its time evolution $\rho(t)$ in real-time is indicated on the left. On the right we depict the gluing of three copies of this real-time density matrix to compute the third moment $\mathrm{Tr}(\rho(t)^3)$. Since there are no sources in the Lorentzian evolution the forward backward evolution legs of this real-time contour cancel pairwise leaving behind a path integral that is localized on the Euclidean section, now on a thermal circle that it three times larger. This is a consequence of the standard collapse rules of real-time path integral contours.

If we are interested only in the computation of the moments $\mathrm{Tr}(\rho(t)^n)$, then the real-

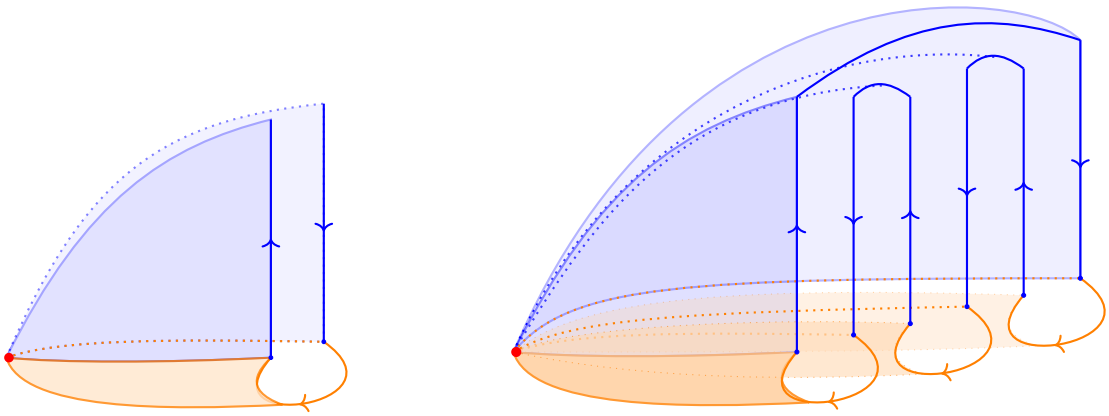

Figure C.3: Gravity dual of the field theory computation illustrated in fig. C.2. The bulk thermal density matrix $\rho(t)$ is obtained by slicing open the Euclidean black hole spacetime, with suitable real-time evolution ending on the cuts thus created. The cuts are pinned at the tip of the Euclidean cigar, which corresponds to the bifurcation surface of the black hole. Lorentzian sections are the time-evolution of the initial state, which geometrically gives rise to the domain of outer communication This is a particularly convenient choice. One can also include part of the real-time black hole interior. This does not matter as the unitary evolution cancels between the bra and ket pieces as described. For our choice we have two such copies one for the ket and another for the bra as indicated on the left panel. On the right we illustrate the ansatz for the computation of $\mathrm{Tr}(\rho(t)^3)$; we have copies of the density matrix constructed gravitationally sewn together capturing the kinematic data. Dynamics dictated by the gravitational equations of motion, will ensure the absence of any singularity at the splitting surface $\boldsymbol{\gamma}$ as discussed in the text.

time evolution pieces between the bras and kets of neighbouring copies of $\rho(t)$ cancel pairwise using unitarity of the evolution in the form $\mathcal{U}(t,0)\mathcal{U}^\dagger(t,0) = 1$. This leaves behind a path integral contour that is localized on the Euclidean section alone. However, now the Euclidean thermal circle is n-times larger, and indeed we recover the fact that the moments of the thermal density matrix are simply partition functions at a rescaled temperature.[1]

Let us now turn to the holographic description of this example. We first consider the saddle-point spacetime that computes Tr $\rho(t)$ as described in the papers referenced above. The above cancellations imply that it is related to the Euclidean AdS-Schwarzschild black hole. However, in order to allow the insertion of operators at non-zero real times t, it is useful to describe the saddle using a different contour through the complexified AdS-Schwarzschild spacetime that also has real Lorentz-signature pieces.

Indeed, a key part of the geometry of [143] may represented by a two-sheeted Lorentz-signature spacetime where the sheets are respectively associated with the bra and ket parts of $\rho(t)$. Rather than terminate the Lorentzian evolution at the time t of interest along the boundary, we choose to extend the spacetime to future timelike infinity along both the ket and the bra segments. In the bulk, we similarly take the bra and ket spacetimes to be sewn to each other long the future event horizon, so that the Lorentzian part of each sheet corresponds to the $t > 0$ part of the AdS-Schwarzschild domain of outer-communication; see fig. C.3 (Figure 2 of [143]). As we discuss below, this allows for a simple presentation of the bra-to-ket sewing using a complexified coordinate chart. This two-sheeted Lorentzian geometry is then glued at $t = 0$ onto the Euclidean black hole solution, which is the familiar Gibbons-Hawking cigar spacetime of [32].

[1]Note that these statements are a simple consequence of unitary evolution and an important consistency requirement of the real-time path integral contours. In Schwinger-Keldysh computations they are usually referred to as collapse rules, see [117, 118] for a general discussion and implications in the context of Schwinger-Keldysh and out-of-time-order observables.

The sewing of bra to ket along the future horizon can be performed cleanly and explicitly using ingoing Eddington-Finkelstein coordinates (which are regular in this part of the complexified geometry). We promote the radial coordinate r to be complex and take the Lorentzian bra and ket spacetimes to lie on the edges of a branch cut along the positive real r-axis. We then sew the branches together by choosing a curve in the complex r-plane that circles the branch point at $r = r_+$ as shown in fig. C.4. This is conveniently described by introducing a new coordinate ζ that is sensitive to the branch cut, taking values in $1 + i\mathbb{R}$ along the ket piece and values $0 + i\mathbb{R}$ along the bra piece.

Focusing on the thermal state defined by the Rindler patch of AdS_2 for simplicity[2] we can write the spacetime metric for the Lorentzian part of the evolution as

$$ds^2 = -r_+^2 \csc^2(\pi\zeta) \left(dt^2 + \frac{2\pi i}{r_+} dt\, d\zeta \right) , \tag{C.4}$$

where we have chosen $\zeta = \frac{1}{2\pi i} \log\left(\frac{r-r_+}{r+r_+}\right)$ which makes explicit the placement of the aforementioned logarithmic branch cut. On the individual ket and bra copies we could revert to the standard Rindler coordinates and write the metric as

$$ds^2 = -(r^2 - r_+^2)\, dt^2 + 2\, dt\, dr\, . \tag{C.5}$$

The metric here is written in ingoing coordinates which is convenient for gluing the bra and ket copies across the future horizon.

The fact that geometry is a saddle point to the Einstein-Hilbert action follows im-

[2]In higher dimensions we have for the Schwarzschild-AdS_{d+1} geometries from [143]

$$\begin{aligned} ds^2 &= -r(\zeta)^2\, f(r)\, dt^2 + i\,\beta\, r(\zeta)^2\, dt\, d\zeta + r^2(\zeta)\, d\mathbf{x}_{d-1}^2\, , \qquad f(r) = 1 - \frac{r_+^d}{r^d}\, , \\ \zeta &= \frac{i\, d}{2\pi(d-1)} \left(\frac{r}{r_+}\right)^{d-1} {}_2F_1\left(1, 1 - \frac{1}{d}, 2 - \frac{1}{d}; \frac{r^d}{r_+^d}\right) . \end{aligned} \tag{C.3}$$

where the branch-cut of the hypergeometric function has been placed to run from r_+ to ∞.

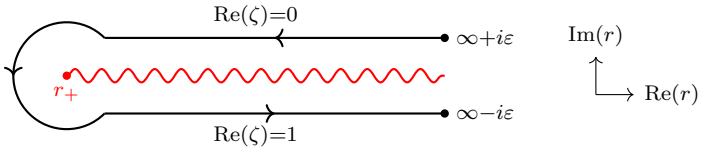

Figure C.4: The complex r plane with the locations of the two boundaries and the horizon marked. The grSK contour is a codimension-1 surface in this plane (drawn at fixed v). The direction of the contour is as indicated counter-clockwise encircling the branch point at the horizon.

mediately from the fact that the local equations of motion are satisfied everywhere. In particular, the smoothness of the gluing ensures that the space has no (complex) conical singularities. In (C.4) we have exploited a set of complex coordinates to go around the location of the cosmic brane. The gluing along the future horizons is essentially passing from one sheet to another smoothly.[3] We also make use of the fact that, while our coordinates (v, r) are not in fact smooth at $\boldsymbol{\gamma}$ (the bifurcation surface), one expects (as motivated in [143]) that the complexified domains of outer communication described by fig. C.4 can be smoothly glued onto the Euclidean cigar. Intuitively, one imagines the Lorentzian evolution on the ket (bra) part starting (terminating) at the $t_{\text{E}} = 0 - \varepsilon$ ($t_{\text{E}} = 0 + \varepsilon$). The Euclidean cigar smoothly connects up these initial and final Cauchy slices. However, as written our coordinate chart (C.4) does not explicitly include the Euclidean section – it would be useful to tighten the argument to exhibit the entire spacetime including the initial state preparation as a complex curve in the complex (v, r) space.

To compute the on-shell action we follow the contour integral prescription of [143] for the Lorentzian part ($t > 0$). One should also include the contribution from the initial state ρ_0, which, as we know, is just the Gibbons-Hawking computation of the black hole

[3]Note that the passage to the complex coordinates enables us to see smoothness explicitly. One can also choose to work with real sections gluing the bra and ket copies in a replica symmetric manner along the future horizon. This is the viewpoint originally advocated in [159].

entropy and follows from the Euclidean path integral on the cigar. We will include this in the final answer.

Focusing for the present on the real-time section (defined using the above complex regulator), we upgrade the Einstein-Hilbert action to

$$S_{\rm gr} = \frac{1}{16\pi G_N}\left[\oint_{\mathcal{C}} d\zeta \int d^dx\,\sqrt{-g}\,R + 2\oint_{\mathcal{C}} d\zeta \int d^dx\,\sqrt{|h|}\,\left(K - 2(d-1) - \frac{1}{d-2}\,{}^hR\right)\right] \tag{C.6}$$

where we have separated out the radial integral from the other directions and have explicitly included the boundary counter-terms (the boundary cosmological constant and the Einstein-Hilbert term). The contour $\mathcal{C}$ we integrate over runs counterclockwise from the bra boundary to the ket boundary encircling the branch point at the horizon, see fig. C.4. The contour integral picks up the discontinuity across the cut. However, for the metric functions in (C.4) there is none as the metric enjoys periodicity under $\zeta \to \zeta + 1$. So the on-shell action receives no contribution from the Lorentzian sections and collapses completely onto the initial state.[4]

Since the initial state path integral coincides with the usual thermal path integral, we correctly obtain the usual thermal partition sum $\mathrm{Tr}(e^{-\beta H}) = e^{-I_1}$

$$\log \mathrm{Tr}(\rho(t)) = \log \mathrm{Tr}(\rho_0) = \log \mathrm{Tr}(e^{-\beta H}) = 4\pi\, c_{\rm eff}\, \mathrm{V}_{d-1}\left(\frac{4\pi}{d\,\beta}\right)^d \tag{C.7}$$

as indeed expected from the Schwinger-Keldysh collapse rules (note that $\beta = \frac{4\pi}{dr_+}$ for the Schwarzschild-AdS$_{d+1}$ black hole).

This construction readily generalizes to the computation of the replica geometries $\mathcal{M}_n$ which compute spectral moments of the thermal density matrix for the entire CFT in real-time. We simply lay out n-copies of the bra and ket geometries described above

[4]This cancellation would be obstructed if we turn on sources in the Lorentzian evolution as can be seen from the correlation function calculations in [143].

(with r_+ arbitrary) and glue them in a replica symmetric manner as shown at right in fig. C.3. This describes the kinematics of the construction as in the main text – the explicit geometry will be determined by the imposing the Einstein-Hilbert dynamics. In particular, the parameter r_+ should chosen to make the resulting complex geometry smooth.

Heuristically, the replica spacetime including the Lorentzian sections should resemble the following. The ket and bra segments of the geometry are confined to $t \geq 0$ and $r \geq r_+$, respectively and the homology surface is the $t = 0$ (ingoing slice) with the homology wedge being the future half of domain of outer communication. The cyclic gluing of the replica copies should be accompanied by suitable smoothing out of the seams along the future horizons by excursions into the complex domain. The non-trivial part is again localized on the splitting surface, which here is the bifurcation surface $r = r_+$. While the full solution is not yet available in closed form, one can argue how the computation of the on-shell action works.

In the current example, the variational problem is completely specified by (4.4). The only boundary terms are those that are needed for the usual AdS asymptotics which we included in (C.6). Now we simply upgrade the contour integral prescription to cover the n-fold replica geometry. The crucial point is once again the observation that the on-shell action receives no contribution from the Lorentzian sections and collapses completely onto the initial state. For the Rényi entropies one will find pairwise cancellations between bra and ket pieces leaving behind n-copies of the thermal boundary conditions, making it clear that r_+ should take the value appropriate to a black hole of inverse temperature $n\beta$. This then results correctly in the n^{th} moment of the thermal density matrix giving

$$e^{-I_n} = \log \mathrm{Tr}(\rho(t)^n) = \log \mathrm{Tr}(\rho_0^n) = \log \mathrm{Tr}(e^{-n\,\beta H}) = 4\pi\, c_{\text{eff}}\, \mathrm{V}_{d-1} \left(\frac{4\pi}{n\,\beta\,d}\right)^d . \qquad \text{(C.8)}$$

Appendix D

Appendix to Chapter 5

D.1 A Rindler regulator for on-shell action of the semi-infinite interval

In this appendix we provide an alternate calculation to that given in section 5.3.3 for the Rényi entropy of a semi-infinite interval from the Lorentzian on-shell action in a single fundamental domain. The calculation in the main text used a small polygonal cut-off around the branch point with an $i\varepsilon$ prescription. The imaginary part of the action then came from the principal value prescription. Here we will instead evaluate the Lorentzian action in Rindler coordinates with cut-off surfaces of constant Rindler radius. The imaginary part of the action now comes from the excursion into the Euclidean time direction as we pass between the different wedges.

We start with the Lorentzian action after integration over the bulk coordinates which is given by (5.60) and (5.61). In particular, we want to evaluate $\mathfrak{I}_{\text{half-line}}$ which we rewrite

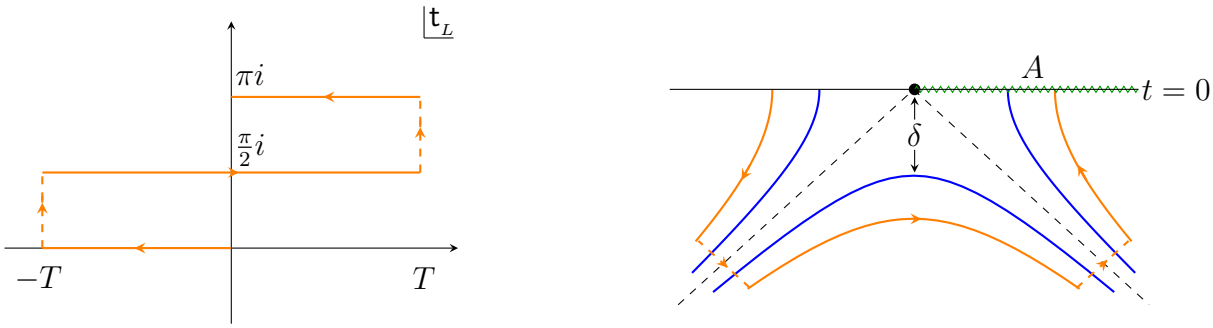

Figure D.1: Left: integration contour in the complex t_L-plane. Right: boundary spacetime $\mathbb{R}^{1,1}$ for $t < 0$ with cut-offs (blue) at Rindler radius $r = \delta$. The t_L contour (orange) has an excursion into the Euclidean time domain (dashed) as it passes between wedges.

here for the reader's convenience:

$$\mathfrak{I}_{\text{half-line}} = \int_{t<0} \frac{d\tilde{x}^+ \, d\tilde{x}^-}{\tilde{x}^+ \, \tilde{x}^-}. \tag{D.1}$$

We transform to Rindler coordinates (t, ρ) and impose cut-offs at some very small Rindler radius $\rho = \delta$. Recall that to pass between wedges we shift t in the imaginary direction by $i\frac{\pi}{2}$. We require that the time contour be continuous so we must include the integration along this imaginary direction from 0 to $i\frac{\pi}{2}$. Therefore, the time contour for t_L is given by

$$C_T = [0, -T] \cup \left[-T, -T + i\frac{\pi}{2}\right] \cup \left[-T + i\frac{\pi}{2}, T + i\frac{\pi}{2}\right] \cup \left[T + i\frac{\pi}{2}, T + i\pi\right] \cup [T + i\pi, i\pi]\,, \tag{D.2}$$

where we have put in some large time cut-off T. The contour is depicted in fig. D.1.

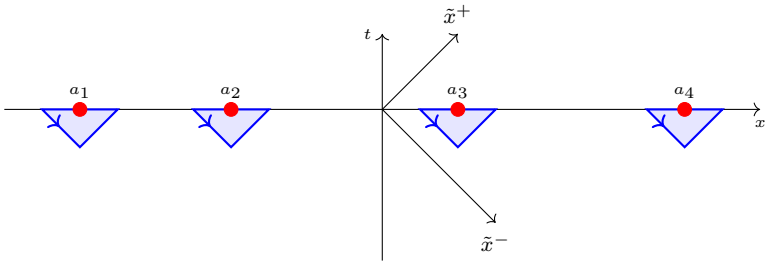

Figure D.2: The domain of integration $\mathcal{R}$ for (5.95) is the lower half space $t < 0$ with triangular regions $\mathcal{U}_i^\epsilon$ around each a_i removed. This choice is particularly convenient for the light-cone like coordinates $\tilde{x}^\pm$ that we work with, since the boundaries of the region $\mathcal{R}$ lie at constant $\tilde{x}^\pm = a_i \mp \delta$.

The integral giving $\mathfrak{I}_{\text{half-line}}$ is now trivial:

$$\mathfrak{I}_{\text{half-line}} = 2 \lim_{T\to\infty} \int_{C_T} d\mathsf{t}_L \int_\delta^L \frac{dr}{r} = 2\pi i \log\left(\frac{L}{\delta}\right). \tag{D.3}$$

This agrees with the result from section 5.3.3. In particular, it verifies that there is a missing factor of 2 if one only considers the branch point at the origin. This way of doing the calculation makes it manifest how the imaginary part of the Lorentzian action gives the Euclidean action because the imaginary part comes from an explicit integration over Euclidean time.

D.2 Lorentzian action for disjoint interval Rényi entropies

To evaluate the integral in (5.95) directly we consider the lower half of the (x, t) plane $(t < 0)$ and use the past directed light-rays from $x = a_i \pm \delta$ to carve out little triangular

regions which we excise, see fig. D.2. Thus,

$$\begin{aligned}\mathcal{R} &= \left(\mathbb{R}^{1,1} \cap \{(x,t)|t<0\}\right) \backslash \bigcup_{i=1}^{2N} \mathcal{U}_i^\delta \\ \mathcal{U}_i^\delta &= \left\{(\tilde{x}^+,\tilde{x}^-)\Big|\ \tilde{x}^+ \in (a_i-\delta, a_i+\delta)\ \ \&\ \ \tilde{x}^- < a_i+\delta\ \ \&\ \ \tilde{x}^+ - \tilde{x}^- < 0\right\}.\end{aligned} \tag{D.4}$$

For future use let us also define the boundaries of $\mathcal{U}_i^\delta$ as

$$\begin{aligned}\partial\mathcal{U}_i^+ &= \{\tilde{x}^+ = a_i - \delta\,,\ \tilde{x}^- \in [a_i-\delta, a_i+\delta]\} \\ \partial\mathcal{U}_i^- &= \{\tilde{x}^- = a_i + \delta\,,\ \tilde{x}^+ \in [a_i+\delta, a_i-\delta]\}\end{aligned} \tag{D.5}$$

where we have specified the ranges consistent with the orientation of the boundaries.

To compute the integral we will introduce a function $\mathfrak{T}(\tilde{x}^+,\tilde{x}^-)$ whose light-cone derivatives give the two terms in the integrand

$$\partial_-\mathfrak{T}(\tilde{x}^+,\tilde{x}^-) = \sqrt{T_{--}}\,, \qquad \partial_+\mathfrak{T}(\tilde{x}^+,\tilde{x}^-) = \sqrt{T_{++}}\,. \tag{D.6}$$

We will content ourselves with local behaviour near the sources a_i which are given by the Lorentzian analog of (5.82)

$$\begin{aligned}\mathfrak{T}(\tilde{x}^+,\tilde{x}^-) &= s_i\left[\sqrt{\Delta_n}\log\left[(\tilde{x}^- - a_i)(\tilde{x}^+ - a_i)\right] - C_i + \frac{p_i}{2\sqrt{\Delta_n}}(\tilde{x}^- + \tilde{x}^+ - 2\,a_i) + \cdots\right] \\ \partial_\pm\mathfrak{T}(\tilde{x}^+,\tilde{x}^-) &= s_i\left[\frac{\sqrt{\Delta_n}}{\tilde{x}^\pm - a_i} + \frac{p_i}{2\sqrt{\Delta_n}} + \cdots\right] \\ \frac{\partial}{\partial a_j}\mathfrak{T}(\tilde{x}^+,\tilde{x}^-) &= -s_i\left[\sqrt{\Delta_n}\left(\frac{1}{\tilde{x}^- - a_i} + \frac{1}{\tilde{x}^+ - a_i}\right) + \frac{p_i}{\sqrt{\Delta_n}}\right]\,\delta_{ij} - s_i\ \frac{\partial C_i}{\partial a_j} + \cdots\,,\end{aligned} \tag{D.7}$$

where the ellipses denote higher order terms in the local expansion about $\tilde{x}^+ = \tilde{x}^- = a_i$.

We therefore have to evaluate

$$\begin{aligned}\frac{\partial}{\partial a_i} S^k_{\text{gr,fund}} &= \frac{c}{24\pi}\left[\mathfrak{I}_{\text{bulk}} + \mathfrak{I}_{\text{bdy}}\right] \\ \mathfrak{I}_{\text{bulk}} &= \int_{\mathcal{R}} d\tilde{x}^- \, d\tilde{x}^+ \, \frac{\partial}{\partial a_i}(\partial_- \mathfrak{T} \, \partial_+ \mathfrak{T}) \\ \mathfrak{I}_{\text{bdy}} &= \int_{\partial \mathcal{U}_i^+} d\tilde{x}^- \partial_- \mathfrak{T} \, \partial_+ \mathfrak{T}\Big|_{\tilde{x}^+ = a_i - \delta} + \int_{\partial \mathcal{U}_i^-} d\tilde{x}^+ \partial_- \mathfrak{T} \, \partial_+ \mathfrak{T}\Big|_{\tilde{x}^- = a_i + \delta}\end{aligned} \tag{D.8}$$

Let us first evaluate the boundary integral which is straightforward as we have to compute contributions of the form

$$\begin{aligned}\mathfrak{I}_{\text{bdy}} = &\int_{a_i-\delta}^{a_i+\delta} d\tilde{x}^- \left[\frac{\sqrt{\Delta_n}}{\tilde{x}^- - a_j} + \frac{p_j}{2\sqrt{\Delta_n}} + \cdots\right]\left[\frac{\sqrt{\Delta_n}}{-\delta} + \frac{p_i}{2\sqrt{\Delta_n}} + \cdots\right] \\ &+ \int_{a_i+\delta}^{a_i-\delta} d\tilde{x}^+ \left[\frac{\sqrt{\Delta_n}}{\delta} + \frac{p_i}{2\sqrt{\Delta_n}} + \cdots\right]\left[\frac{\sqrt{\Delta_n}}{\tilde{x}^+ - a_j} + \frac{p_j}{2\sqrt{\Delta_n}} + \cdots\right].\end{aligned} \tag{D.9}$$

We see that the only part that contributes is the one where the terms align, i.e., only from $i = j$, since this is the only situation when the integral has a non-vanishing imaginary part from the principal value prescription. Therefore, keeping track of the orientation of the boundary we find the two terms add to give

$$\text{Im}(\mathfrak{I}_{\text{bdy}}) = -\pi\left[\frac{\Delta_n}{-\delta} + \frac{p_i}{2}\right] - \pi\left[\frac{\Delta_n}{\delta} + \frac{p_i}{2}\right] = -\pi\, p_i\,. \tag{D.10}$$

The bulk terms can be evaluated along similar lines. We first exchange the order of integration and use the fact that $\partial_+\partial_-\mathfrak{T}$ has no support in the region of integration: it is localized at the branch points following the same chain of logic that led to the first line

of (5.44). Hence,

$$\begin{aligned}\mathfrak{I}_{\text{bulk}} &= \int_{\mathcal{R}} d\tilde{x}^- \, d\tilde{x}^+ \partial_- \left(\partial_{a_i}\mathfrak{T} \, \partial_+\mathfrak{T}\right) + \partial_+ \left(\partial_{a_i}\mathfrak{T} \, \partial_-\mathfrak{T}\right) \\ &= \sum_{j=1}^{2N} \left[\int_{\partial\mathcal{U}_j^-} d\tilde{x}^+ \, \partial_{a_i}\mathfrak{T} \, \partial_+\mathfrak{T} + \int_{\partial\mathcal{U}_j^+} d\tilde{x}^- \, \partial_{a_i}\mathfrak{T} \, \partial_-\mathfrak{T} \right]\end{aligned} \tag{D.11}$$

It is now straightforward to use (D.7) and compute each of the terms in the above. For instance we have to compute integrals of the form:

$$\begin{aligned}&-\int_{a_j+\delta}^{a_j-\delta} d\tilde{x}^+ \left[\left(\frac{\sqrt{\Delta_n}}{\delta} + \frac{\sqrt{\Delta_n}}{\tilde{x}^+ - a_j} + p_j\right)\delta_{ij} + \frac{\partial C_j}{\partial a_i} + \cdots\right]\left[\frac{\sqrt{\Delta_n}}{\tilde{x}^+ - a_j} + \frac{p_j}{2\sqrt{\Delta_n}} + \cdots\right] \\ &\qquad = i\pi\left[\frac{3p_i}{2}\,\delta_{ij} + \frac{\partial C_j}{\partial a_i} + \frac{\Delta_n}{\delta}\,\delta_{ij}\right] + \cdots \\ &-\int_{a_j-\delta}^{a_j+\delta} d\tilde{x}^- \left[\left(-\frac{\sqrt{\Delta_n}}{\delta} + \frac{\sqrt{\Delta_n}}{\tilde{x}^- - a_j} + p_j\right)\delta_{ij} + \frac{\partial C_j}{\partial a_i} + \cdots\right]\left[\frac{\sqrt{\Delta_n}}{\tilde{x}^- - a_j} + \frac{p_j}{2\sqrt{\Delta_n}} + \cdots\right] \\ &\qquad = i\pi\left[\frac{3p_i}{2}\,\delta_{ij} + \frac{\partial C_j}{\partial a_i} - \frac{\Delta_n}{\delta}\,\delta_{ij}\right] + \cdots\end{aligned} \tag{D.12}$$

where we have only indicated explicitly the imaginary parts that arise from the principal value prescription. The terms combine nicely together to give

$$\text{Im}(\mathfrak{I}_{\text{bulk}}) = 2\pi\left(\frac{3p_i}{2} + \sqrt{\Delta_n}\sum_{j=1}^{2N}\frac{\partial C_j}{\partial a_i}\right) = -\pi\, p_i \tag{D.13}$$

where we finally used (5.90).

Putting it all together we have the expected result from the Lorentzian replica computation, viz., (5.97). As noted earlier this was to be expected owing to the contributions arising from the regions where the metric becomes complex.

D.3 The second Rényi entropy for two intervals: Geometry

In this appendix we give explicit details for the 2-interval second Rényi entopy. We focus on the Schottky construction on the boundary and the determination of the bulk handlebody geometries. We will use these results in appendix D.4 to compute the on-shell action of the gravitational dual.

D.3.1 The boundary geometry

The boundary manifold has a complex structure

$$z^2 = \frac{(v-a_1)(v-a_3)}{(v-a_2)(v-a_4)} \implies z^2 = \frac{v(v-1)}{(v-\chi)}\,, \tag{D.14}$$

where we have used a Möbius transformation to set $a_1 = 0$, $a_2 = \chi$, $a_3 = 1$, and $a_4 \to \infty$, respectively. In particular, we have

$$\chi = \frac{(a_1-a_2)(a_3-a_4)}{(a_1-a_3)(a_2-a_4)}\,. \tag{D.15}$$

The modulus of the torus is given in terms of the elliptic integral, cf., (D.28),

$$\tau(\chi) = i\,\frac{K(1-\chi)}{K(\chi)}\,, \tag{D.16}$$

which implies that a modular transform $\tau \leftrightarrow -\frac{1}{\tau}$ corresponds to the exchange $\chi \leftrightarrow 1-\chi$.

Note however, that the Rényi entropy is not invariant under $\mathrm{SL}(2,\mathbb{C})$ transformations which we used to gauge fix a_i. On the contrary the mutual Rényi information defined by

$$I^{(2)}_{\mathcal{A}_1\cup\mathcal{A}_2} = S^{(2)}_{\mathcal{A}_1} + S^{(2)}_{\mathcal{A}_2} - S^{(2)}_{\mathcal{A}_1\cup\mathcal{A}_2}\,, \tag{D.17}$$

is invariant under $\mathrm{SL}(2,\mathbb{C})$. Using the purity of the vacuum state one can relate $I^{(n)}(1-\chi)$ to $I^{(n)}(\chi)$. The swap $\chi \leftrightarrow 1-\chi$ which is achieved by $a_2 \leftrightarrow a_4$ exchanges the two choices of cycles, $\mathfrak{C}_d \leftrightarrow \mathfrak{C}_c$. One can use Schottky uniformization[1] to directly determine [126]

$$\begin{aligned} I^{(2)}(\chi) &= \max\left\{ I^{(2)}_{\mathfrak{C}_d}(\chi), I^{(2)}_{\mathfrak{C}_c}(\chi) \right\} \\ &= \max\left\{ -\frac{c}{12}\,\log\left(2^8\,\frac{1-\chi}{\chi^2}\right) - i\,\frac{\pi}{6}\,c\,\tau(\chi), -\frac{c}{12}\,\log\left(2^8\,\frac{1-\chi}{\chi^2}\right) + i\,\frac{\pi}{6}\,c\,\frac{1}{\tau(\chi)} \right\}. \end{aligned} \tag{D.18}$$

This result was first derived in [123] and leads to the aforesaid phase transition since $I^{(2)}_{\mathfrak{C}_d}(\chi)$ dominates for $\chi < \frac{1}{2}$.

As explained above, one could construct directly the covering space handlebody, and recover from it the on-shell action for the geometry. A direct evaluation of on-shell action turns out to be formidable even for the case of the 2^{nd} Rényi entropy for two-intervals. We were however able to derive (D.18) directly by computing the gravitational action in Euclidean signature. As this computation has not been reported in the literature we present it in appendix D.4. However, we found it somewhat cumbersome to manipulate for the real-time analysis, so we resorted to a different approach in the main text.

D.3.2 The Euclidean handlebodies

For $N = 2$ and $n = 2$ the monodromy problem relies on the following differential equation

$$\psi''(v) + \frac{1}{2}\left[\Delta_2\left(\frac{1}{v^2} + \frac{1}{(v-1)^2} + \frac{1}{(v-\chi)^2} - \frac{2}{v(v-\chi)}\right) - \frac{p_\chi\,\chi\,(\chi-1)}{v(v-1)(v-\chi)}\right]\psi(v) = 0\,. \tag{D.19}$$

[1] We explain the elements underlying the Schottky uniformization calculation in section 5.4.1 and derive the result by explicitly evaluating the on-shell gravitational action in Euclidean signature in appendix D.4.

In writing this expression we have gauge fixed the branch points using (D.15) and set $p_\chi = -p_2$ and set $n = 2$ after using the relations in (5.75). While the natural map on the cover is (D.14), for solving (D.19) it will be useful to introduce a new elliptic coordinate $\eta(v)$; see (D.26) and rewrite (D.19) using the conformal transformation properties of $\psi(v)$ and $T(v)$. Under $v \to \mathfrak{f}(v)$ one has

$$\psi(v) = \left(\frac{\partial \mathfrak{f}}{\partial v}\right)^{-\frac{1}{2}} \psi(\mathfrak{f}(v))\,, \qquad T_{vv} = \left(\frac{\partial \mathfrak{f}}{\partial v}\right)^{2} T_{\mathfrak{f}\mathfrak{f}} + \{\mathfrak{f}, v\}\,. \tag{D.20}$$

This implies that the monodromy equation can be brought to the form of a standard differential equation

$$\frac{\mathrm{d}^2\psi(\eta)}{\mathrm{d}\eta^2} - \frac{2K(\chi)^2}{\pi^2}\left(\frac{\chi-2}{4} + p_\chi\,\chi(\chi-1)\right)\psi(\eta) = 0\,. \tag{D.21}$$

This has solutions in terms of simple exponentials if we also reparameterize the accessory parameter as

$$p_\chi = \frac{1}{\chi(\chi-1)}\left[\frac{2-\chi}{4} + \frac{\pi^2}{2\,K(\chi)^2}\,\mathfrak{p}^2\right]\,. \tag{D.22}$$

Altogether we find that the desired solution to the inverse map $\tilde{y}(v)$ is given by

$$\tilde{y}(v) = e^{2\,\mathfrak{p}\,\eta(v)}\,. \tag{D.23}$$

To complete the solution we need to fix p_χ by computing the monodromies around the two possible choices of cycles: the disconnected one $\mathfrak{C}_d$ and the connected one $\mathfrak{C}_c$ in fig. 5.6.

For two intervals the second Rényi entropy computation leads to the following stress

energy on a single sheet (using $\Delta_2 = \frac{3}{8}$):

$$T_{vv}(v) = \frac{3}{8}\left(\frac{1}{v^2} + \frac{1}{(v-1)^2} + \frac{1}{(v-\chi)^2} - \frac{2}{v(v-\chi)}\right) - \frac{p_\chi\,\chi\,(\chi-1)}{v(v-1)(v-\chi)}. \tag{D.24}$$

To complete its specification we fix p_χ by computing the monodromies around the two possible choices of cycles $\mathfrak{C}_d$ and $\mathfrak{C}_c$ in fig. 5.6. One finds:

$$\begin{aligned} \mathfrak{p}_d = -\frac{i}{2} \quad &\Longrightarrow \quad p_\chi\big|_{\mathfrak{C}_d} = \frac{1}{4\chi(\chi-1)}\left[2-\chi-\frac{\pi^2}{2\,K(\chi)^2}\right], \\ \mathfrak{p}_c = \frac{i}{2\,\tau(\chi)} \quad &\Longrightarrow \quad p_\chi\big|_{\mathfrak{C}_c} = \frac{1}{4\chi(\chi-1)}\left[2-\chi+\frac{\pi^2}{2\,K(1-\chi)^2}\right], \end{aligned} \tag{D.25}$$

where $\tau(\chi)$ is the modulus of the torus and is defined in (D.16).

These are given in (D.25) as a function of the cross-ratio χ.

The torus elliptic map: The elliptic map from the complex v plane to the torus is

$$\eta(v) = \frac{\pi}{2K(\chi)}\int_0^v \frac{d\zeta}{\sqrt{\zeta(\chi-\zeta)(1-\zeta)}}\,. \tag{D.26}$$

We can either invoke Legendre integral definition of the incomplete elliptic function[2] or the inverse Jacobi elliptic sine (denoted $\mathrm{sn}(z,m)$) amplitude, and write

$$\eta(v) = \frac{\pi}{K(\chi)}\,F\left(\arcsin\left(\sqrt{\frac{v}{\chi}}\right),\chi\right) = \frac{\pi}{K(\chi)}\,\mathrm{sn}^{-1}\left(\arcsin\left(\sqrt{\frac{v}{\chi}}\right),\chi\right) \tag{D.27}$$

which fixes the function in the principal domain $v \in [0,\chi]$. For the other domains we analytically continue past the cuts which are at $(0,\chi)$ and $(1,\infty)$. The normalization

[2]We define $K(x)$ to be the incomplete elliptic integral of the first kind as in (D.28). The definition differs from some traditional forms, which define the integral in (D.28) as $F(\frac{\pi}{2},\sqrt{x})$; see for example [264, Eq. 19.2.4].

factor is the complete elliptic integral of the first kind

$$K(x) = \int_0^{\frac{\pi}{2}} \frac{d\theta}{\sqrt{1 - x\,\sin^2\theta}} \equiv F\left(\frac{\pi}{2}, x\right). \tag{D.28}$$

D.4 The second Rényi entropy for two intervals: Euclidean on-shell action

In this appendix we evaluate the on-shell gravitational action in Euclidean signature for the second Rényi entropy for two intervals. We will compute the action of the covering space $\mathcal{M}_2$ using the Schottky construction outlined in section 5.4.1. The action was evaluated numerically for higher Rényi entropies ($n > 2$) in [126] and here we will evaluate it analytically for $n = 2$. From this we can extract the second mutual Rényi information and thus derive (D.18).

For definiteness we will focus on the choice of cycles $\mathfrak{C}_c$, but the other choice of cycles follows similarly. We previously obtained the coordinate $\tilde{y}(v)$ for the Schottky domain of the boundary torus (D.23). For the purposes of evaluating the action, it is nicer to use a different coordinate for the Schottky domain which is related to $\tilde{y}(v)$ in (D.23) by a $\mathrm{PSL}(2,\mathbb{C})$ transformation.[3] We choose our new coordinate $y(v)$ to diagonalize the monodromy around a_1 which gives

$$y(v) = \tanh(\pi\mathfrak{p}_c)\tanh\left(\mathfrak{p}_c\eta(v)\right). \tag{D.29}$$

To keep future expressions legible we also introduce a parameter χ_S encoding the complex

[3]This is not strictly a $\mathrm{PSL}(2,\mathbb{C})$ transformation because the determinant is not equal to 1, but the Schottky construction is only defined up to an overall scaling, which we have chosen such that $y(1) = 1$.

structure via

$$\chi_S \equiv y(\chi) = \tanh^2(\pi \mathfrak{p}_c), \tag{D.30}$$

where we have used $\eta(\chi) = \pi$. The fundamental domain $\mathcal{D}_{\text{bdy}}$ of the Schottky quotient is the exterior of the two discs bounded by the circles $\mathfrak{C}_1, \tilde{\mathfrak{C}}_1$ which we have illustrated in fig. D.3. The generator of the Schottky group identifies these two circles as discussed previously. The replica symmetry acts simply on the fundamental domain described by the $y(v)$ coordinate: $y(v) \to -y(v)$.

We construct the bulk geometry by filling in the cycles $\mathfrak{C}_c$. The bulk geometry has the standard Poincaré metric

$$ds^2 = \frac{d\xi^2 + dy\, d\bar{y}}{\xi^2} \tag{D.31}$$

with the fundamental domain in the bulk obtained by extending the boundary circles, whose radius is $\ell = \frac{1-\chi_S}{2}$, into hemispheres and identifying these hemispheres by the action of the Schottky group, as illustrated in fig. D.4.

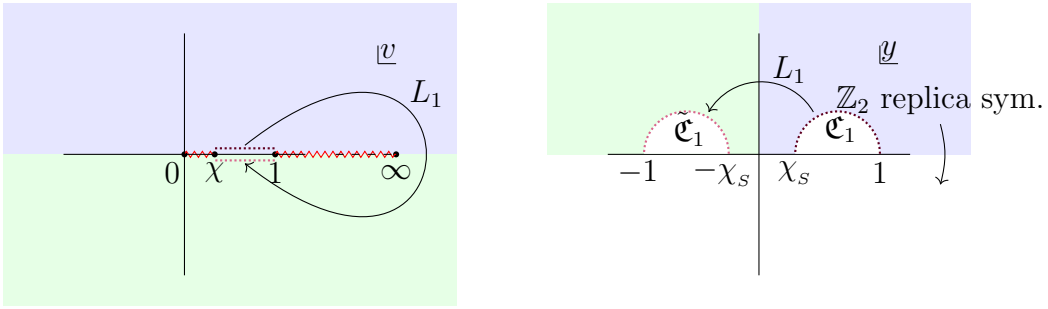

Figure D.3: Left: one sheet of the boundary geometry $\mathcal{B}_{2,2}$ with the generator L_1 of the Schottky group corresponding to non-trivial monodromy around the cycle containing one of the branch cuts. Right: the image of $\mathcal{B}_{2,2}$ in the y-plane with the two circles $\mathfrak{C}_1, \tilde{\mathfrak{C}}_1$ identified by the action of the Schottky group and their interiors removed to give the fundamental domain. The upper and lower y-plane are related by the $\mathbb{Z}_2$ replica symmetry with each corresponding to a sheet of $\mathcal{B}_{2,2}$.

D.4.1 On-shell gravitational action

We now proceed to evaluate the Euclidean gravitational action for the metric (D.31) on the bulk fundamental domain $\mathcal{D}_{\text{bulk}}$. We need to evaluate the action

$$S^E_{\text{gr}}[\mathcal{M}_2] = -\frac{1}{16\pi G_N}\left[\int_{\mathcal{M}_2} d^3x\,\sqrt{g}\,(R+2) + 2\int_{\mathcal{B}_c}\sqrt{\gamma}\,K - 2\int_{\mathcal{B}_c}\sqrt{\gamma}\right]. \tag{D.32}$$

The boundary curvature counterterm in (5.49) is absent here since the torus is flat.

We will use Fefferman-Graham coordinates $(\rho, v, \bar{v})$ to define the cut-off surface because these give a simple way to extract the contribution from the branch points. The contribution comes from the conformal factor between the $(\xi, y, \bar{y})$ coordinates and the Fefferman-Graham coordinates, cf., (5.36). The transformation between the coordinates is given by

$$\xi = \frac{\sqrt{\rho}\,e^{-\varphi}}{1+\rho\,e^{-2\varphi}\,|\partial_z\varphi|^2}\,, \qquad y = w + \frac{\rho\,e^{-2\varphi}\,\partial_{\bar{z}}\varphi}{1+\rho\,e^{-2\varphi}\,|\partial_z\varphi|^2}\,, \tag{D.33}$$

where we set $\Omega \equiv e^{-\varphi}$ in (5.42) and have

$$\varphi = -\log\left[\frac{\pi\sqrt{\chi_S}\,\mathfrak{p}_c}{2K(\chi)}\frac{1}{\sqrt{|v(v-1)(v-\chi)|}}\,\text{sech}(\mathfrak{p}_c\eta(v))\,\text{sech}(\mathfrak{p}_c\bar{\eta}(\bar{v}))\right]. \tag{D.34}$$

We define the cut-off surface by $\rho = \rho_c$ which describes a non-trivial cut-off surface $\mathcal{B}_c$ in Poincaré coordinates described by $\xi = \xi_c(y, \bar{y})$ restricted to $\mathcal{D}_{\text{bulk}}$.

The three contributions to the action can be evaluated directly. We find

$$\begin{aligned}
S_{\text{EH}}[\mathcal{M}_2] &= \int_{\mathcal{M}_2} d^3x\,\sqrt{g}\,(R+2) = -2\int_{\mathcal{M}_2} dy\,d\bar{y}\,\frac{d\xi}{\xi^3}\,,\\
S_{\text{GH}}[\mathcal{M}_2] &= 2\int_{\mathcal{B}_c}\sqrt{\gamma}\,K = 2\int_{\mathcal{B}_c} dy\,d\bar{y}\,\left(\frac{e^{2\varphi}}{\rho_c} + 2|\partial_y\varphi|^2 - 2\partial_y\partial_{\bar{y}}\varphi\right)\,,\\
S_{\text{ct}}[\mathcal{M}_2] &= 2\int_{\mathcal{B}_c}\sqrt{\gamma} = \int_{\mathcal{B}_c} dy\,d\bar{y}\,\left(\frac{e^{2\varphi}}{\rho_c} + 4|\partial_y\varphi|^2\right).
\end{aligned} \tag{D.35}$$

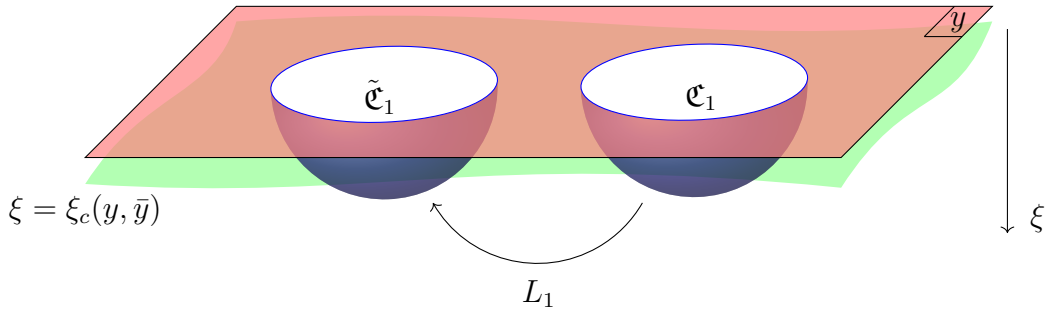

Figure D.4: The bulk fundamental domain of the Schottky construction consisting of two hemispheres excised from AdS_3 with their boundaries identified by the action of the Schottky group. The bulk coordinate ξ is cut off by the surface $\xi = \xi_c(y, \bar{y})$ (green).

In deriving the boundary quantities we used

$$\begin{aligned} &\gamma_{yy} = \frac{1}{\xi_c^2}\left(\partial_y \xi_c\right)^2 , \qquad \gamma_{\bar{y}\bar{y}} = \frac{1}{\xi_c^2}\left(\partial_{\bar{y}} \xi_c\right)^2 , \qquad \gamma_{y\bar{y}} = \frac{1}{\xi_c^2}\left(\left|\partial_y \xi_c^2\right| + \frac{1}{2}\right) , \\ &K = 2\left(2\xi_c \partial_y \partial_{\bar{y}} \xi_c - 4|\partial_y \xi_c|^2 + 1\right) \end{aligned} \tag{D.36}$$

The boundary integrals above are straightforward, but the bulk integral in $S_{\rm EH}$ has two distinct contributions: one contribution comes from the region of the bulk below the cut-off surface and the other comes from the region below the hemispheres. Picking θ to be the azimuthal coordinate around the hemisphere (whose radius we recall is $\frac{1-\chi_S}{2}$) we can evaluate the two contributions and obtain

$$\begin{aligned} S_{\rm EH}[\mathcal{M}_2] &= -2\int_{\mathcal{M}_2} dy\, d\bar{y}\, \frac{d\xi}{\xi^3} = -\left[\int_{\mathcal{B}_c} dy\, d\bar{y}\, \frac{1}{\xi_c(y,\bar{y})^2} + 2\int_{\rm hemi} dy\, d\bar{y}\, \frac{1}{\xi_{\rm hemi}(y,\bar{y})^2}\right] \\ &= -\left[\int_{\mathcal{B}_c} dy\, d\bar{y}\left(\frac{e^{2\varphi}}{\rho_c} + 2|\partial_y \varphi|^2\right) + 2\int_0^{2\pi} d\theta \int_0^{r_{\rm cut-off}(\theta)} dr\, \frac{r}{\ell^2 - r^2}\right] \\ &= -\left[\int_{\mathcal{B}_c} dy\, d\bar{y}\left(\frac{e^{2\varphi}}{\rho_c} + 2|\partial_y \varphi|^2\right) + 2\int_0^{2\pi} d\theta\, \left(2\varphi - \log\left(\frac{\rho_c}{\ell^2}\right)\right)\right] , \end{aligned} \tag{D.37}$$

Putting all of the pieces in (D.35) together we see that the leading divergences cancel

as they must and the Euclidean action (D.32) becomes

$$S^E_{\rm gr}[\mathcal{M}_2] = \frac{1}{8\pi G_N}\left[\int_{\mathcal{B}_c} dy\, d\bar{y}\, \left(|\partial_y\varphi|^2 + 2\partial_y\partial_{\bar{y}}\varphi\right) + 2\int_0^{2\pi} d\theta\, \varphi + 4\pi\log(\ell) - 2\pi\log(\rho_c)\right]. \tag{D.38}$$

We will evaluate each of these terms in turn.

The first term in (D.38) can be computed very similarly to the one interval case (5.56) where we integrate by parts to reduce the integral to the contributions from the boundaries of the domain. There are boundary terms from the circles $\{\mathfrak{C}_1, \tilde{\mathfrak{C}}_1\}$ in the y-plane and boundary terms from the discs D_i^δ of radius δ that we cut out around each branch point a_i in the v-plane. Finally, there are boundary terms from the IR cut-offs in the y- and v-planes. We thus find:

$$\begin{aligned}\int_{\mathcal{B}_c} dy\, d\bar{y}\, |\partial_y\varphi|^2 &= \delta\sum_{i=1}^{3}\oint_{a_i}\varphi\partial_{|v|}\varphi + \int_0^{2\pi} d\theta\, \ell\varphi\partial_r\varphi|_{r=\ell} + S_{\rm IR} \\ &= -\pi\log\left[\left(\frac{\pi\,\mathfrak{p}_c\,\sqrt{\chi_S}}{2\,K(\chi)\sqrt{\delta}}\right)^3 \frac{\mathrm{sech}^2(\pi\,\mathfrak{p}_c)\,\mathrm{csch}^2(\pi\,\mathfrak{p}_c)}{\chi(1-\chi)}\right] - \int_0^{2\pi} d\theta\,\varphi + S_{\rm IR}\,,\end{aligned} \tag{D.39}$$

where the contribution from the boundaries in the v-plane has a factor of 2 owing to the two sheets of $\mathcal{B}_{2,2}$ and in the last line we have used the fact that $\partial_r\varphi|_{r=\ell} = -1/\ell$. The term labeled $S_{\rm IR}$ is the contribution from large radius region in the y or v-planes, and in particular includes the contribution from the branch point a_4. We evaluate these separately in appendix D.4.3 as they are involved, but quote here the final result:

$$S_{\rm IR} = \pi\left[\log\left(\frac{K(\chi)\,\sqrt{\delta\,\chi_S}}{2^5\pi\,\mathfrak{p}_c}\right) + 2\,\log(\rho_c) + 3\log(a_4) - 8\,\log(R_v)\right], \tag{D.40}$$

where we are meant to take the limit $R_v, a_4 \to \infty$.

The second term in (D.38) reduces to a sum of localized delta functions as in the

one-interval case and thus vanishes,

$$\begin{aligned}&\int_{\mathcal{B}_c} d\bar{y}\, dy\, \partial_y \partial_{\bar{y}} \varphi \\ &= 2\int_{\widehat{\mathbb{C}}\setminus \cup_i D_i^\delta} d\bar{v}\, dv\, \partial_v \partial_{\bar{v}} \varphi \quad = \frac{\pi}{4}\int_{\widehat{\mathbb{C}}\setminus \cup_i D_i^\delta} d\bar{v}\, dv\, \delta\left(|v|\right) + \delta\left(|v-1|\right) + \delta\left(|v-\chi|\right) \\ &= 0.\end{aligned} \tag{D.41}$$

The third term in (D.38) turns out to be formidable. We use various elliptic function identities to evaluate it in appendix D.4.2 and find when all the dust settles the result

$$\int_0^{2\pi} d\theta\, \varphi = 4\pi \log\left(\frac{2^{\frac{3}{2}}\,\pi\,\mathfrak{p}_c}{K(\chi)}\cosh(\pi\,\mathfrak{p}_c)\right) - 4\pi^2 \mathfrak{p}_c. \tag{D.42}$$

Plugging all of these pieces into (D.38), we arrive at our final answer for the Euclidean action:

$$S^E_{\rm gr}[\mathcal{M}_2] = -\frac{\pi\, c}{3}\mathfrak{p}_c + \frac{c}{12}\log\left(\delta^2\chi(1-\chi)\right) + \frac{c}{4}\log(a_4) - \frac{2c}{3}\log(R_v). \tag{D.43}$$

To obtain the Rényi entropy, we need to normalize by the gravitational action of the sphere $S^E_{\rm gr}[\mathcal{M}_1]$. However, one needs to be careful because we have chosen a particular IR regularization scheme to deal with the fact that we placed one of the branch points at infinity (this is the same as the regularization scheme used in [265]). As a result, the action on the sphere is no longer unity like in the single interval case, instead one finds

$$S^E_{\rm gr}[\mathcal{M}_1] = \frac{c}{6}\log\left(\frac{\rho_c}{R_v^2}\right) - \frac{c}{3}. \tag{D.44}$$

The second Rényi entropy for two intervals is thus (using $\mathfrak{p}_c$ from (D.25))

$$\begin{aligned} S^{(2)}_{\mathcal{A}_1\cup\mathcal{A}_2} &= S^E_{\rm gr}[\mathcal{M}_2] - 2S^E_{\rm gr}[\mathcal{M}_1] \\ &= -i\frac{\pi c}{6\tau(\chi)} + \frac{c}{12}\log\left(\delta^2\chi(1-\chi)\right) + \frac{2c}{3} + \frac{c}{4}\log(a_4) - \frac{c}{3}\log(\rho_c). \end{aligned} \tag{D.45}$$

We emphasize that this only gives the second Rényi entropy for the connected phase $1/2 \leq \chi < 1$. For the second mutual Rényi information $I^{(2)}$ we need the second Rényi entropy for the single interval using our choice of regularization and thus it will differ from (5.57). It is given by

$$S^{(2)}_{\mathcal{A}_i} = \frac{c}{4}\log\left(\delta^{\frac{1}{3}}|a_{2i} - a_{2i-1}|\right) - \frac{c}{3}\log(2) - \frac{c}{6}\log(\rho_c) + \frac{c}{3}. \tag{D.46}$$

We thus arrive at the second mutual Rényi information (with the regulators δ, a_4, ρ_c canceling)

$$I^{(2)}(\chi) = -\frac{c}{12}\,\log\left(2^8\,\frac{1-\chi}{\chi^2}\right) + i\,\frac{\pi}{6}\,c\,\frac{1}{\tau(\chi)}. \tag{D.47}$$

This is in complete agreement with the result (D.18) obtained from the accessory parameter (in the connected phase). The disconnected case proceeds along similar lines with $\mathfrak{p}_c \to \mathfrak{p}_d$.

D.4.2 Hemisphere integral

We now turn to the calculation of the integral of $\varphi = -\log\Omega$ along the azimuthal angle of the hemisphere appearing in (D.38). To do this, we first need to rewrite the coordinate y along the semi-circles given by the intersection of the circles $\mathfrak{C}_1, \tilde{\mathfrak{C}}_1$ with the upper-half y-plane. These semi-circles are the images of the intervals $[\chi + i\epsilon, 1 + i\epsilon]$ and $[\chi - i\epsilon, 1 - \epsilon]$ in the v-plane, respectively; see fig. D.3. In the interval $v \in [\chi, 1]$, the torus

elliptic map[4] is given by continuing (D.27) outside the principal domain,

$$\eta(v \pm i\epsilon) = \pm\pi + i\frac{\pi}{K(\chi)}\,\mathrm{sn}^{-1}\left(\Theta(v), 1-\chi\right)\,, \tag{D.48}$$

with

$$\sin\Theta = \sqrt{\frac{(v-\chi)}{(1-\chi)v}}\,, \qquad v = \frac{\chi}{1-(1-\chi)\sin^2\Theta}. \tag{D.49}$$

Using this the map $y(v)$ in the interval $v \in [\chi, 1]$ then takes the form

$$y(v \pm i\epsilon) = \tanh(\pi\,\mathfrak{p}_c)\tanh\left(\mathfrak{p}_c\eta(v)\right) = \frac{\pm\chi_{_S} + i\zeta(v)}{1 \pm i\zeta(v)}, \tag{D.50}$$

where we have defined a new map $\zeta(v)$ using the addition formula, viz.,

$$\zeta(v) = \tanh(\pi\,\mathfrak{p}_c)\tan\left(i\mathfrak{p}_c(\pi - \eta(v))\right) = \tanh(\pi\,\mathfrak{p}_c)\tan\left(\frac{\pi\,\mathfrak{p}_c}{K(\chi)}\,\mathrm{sn}^{-1}\left(\Theta(v), 1-\chi\right)\right). \tag{D.51}$$

This gives the desired description of the semi-circle. Note that we can invert $\Theta(\zeta)$ and write

$$\sin\Theta = \mathrm{sn}(w, 1-\chi)\,, \qquad w = \frac{2K(1-\chi)}{\pi}\coth(\pi\,\mathfrak{p}_c)\,\zeta(v)\,. \tag{D.52}$$

Armed with these definitions we can evaluate $\varphi(v)$ in the interval $v \in [\chi, 1]$ to be

$$\varphi(v) = -\frac{1}{2}\log\left(\frac{dy}{dv}\frac{d\bar{y}}{d\bar{v}}\bigg|_{v=\bar{v}}\right) = -\log\left(\frac{(1-\chi_{_S})\zeta'(v)}{\zeta(v)^2+1}\right). \tag{D.53}$$

Likewise, the azimuthal angle as a function of v is

$$\theta(v) = \tan^{-1}\left(\frac{2\zeta(v)}{\zeta(v)^2-1}\right). \tag{D.54}$$

[4]We find it useful to employ Jacobian notation cf., [264, Sec. 22.1], to avail of various identities. A useful reference for elliptic function properties is [266].

The desired integral thus becomes

$$\int_0^{2\pi} d\theta\, \varphi = 2\int_0^{\pi} d\theta\, \varphi = -4\int_\chi^1 dv\, \left(\frac{\zeta'(v)}{\zeta(v)^2+1}\right) \log\left(\frac{(1-\chi_S)\,\zeta'(v)}{\zeta(v)^2+1}\right). \tag{D.55}$$

Evaluating the argument of the logarithm we find it convenient to split integral into two pieces, one of which can be integrated directly, leading to

$$\int_0^{2\pi} d\theta\, \varphi = 2\pi \log\left(\frac{8K(\chi)\cosh^3(\pi\,\mathfrak{p}_c)\sinh(\pi\,\mathfrak{p}_c)}{\pi\,\mathfrak{p}_c}\right) - 4\pi^2\,\mathfrak{p}_c + \mathcal{I}(\chi), \tag{D.56}$$

with

$$\mathcal{I}(\chi) = 4\int_\chi^1 dv\, \frac{\zeta'}{1+\zeta^2}\, \log\left(\sqrt{v(1-v)(v-\chi)}\right). \tag{D.57}$$

To evaluate $\mathcal{I}(\chi)$ we evaluate the integrand in terms of Jacobi elliptic functions:

$$\sqrt{v(1-v)(v-\chi)} = \frac{\chi(1-\chi)\cos\Theta\sin\Theta}{\left(1-(1-\chi)\sin^2\Theta\right)^{\frac{3}{2}}} = \frac{\chi(1-\chi)\ \mathrm{sn}(w,1-\chi)\ \mathrm{cn}(w,1-\chi)}{\mathrm{dn}^3(w,1-\chi)}, \tag{D.58}$$

where we have used the relations $\mathrm{sn}^2(z,m)+\mathrm{cn}^2(z,m)=1$ and $m\ \mathrm{sn}^2(z,m)+\mathrm{dn}^2(z,m)=1$, and w is defined above in (D.52). The integral changing variables to w, with $\tilde{w}=\frac{\pi w}{2K(x)}$, is

$$\begin{aligned}\mathcal{I}(\chi) &= 2\pi\log\left(\chi(1-\chi)\right) + \mathcal{J}(1-\chi)\\ \mathcal{J}(x) &= \frac{2\pi\ \coth(\pi\,\mathfrak{p}_c)}{K(x)}\int_0^{K(x)} dw\, \frac{\sec^2\tilde{w}}{\coth^2(\pi\,\mathfrak{p}_c)+\tan^2\tilde{w}}\log\left(\frac{\mathrm{sn}(w,x)\ \mathrm{cn}(w,x)}{\mathrm{dn}^3(w,x)}\right).\end{aligned} \tag{D.59}$$

We can now exploit the fact that Jacobian elliptic functions have an infinite product

representation:

$$\begin{aligned}
\mathrm{sn}(w,x) &= 2\left(\frac{q_x}{x}\right)^{\frac{1}{4}} \sin\tilde{w} \prod_{n=1}^{\infty} \frac{1-2\,q_x^{2n}\,\cos(2\tilde{w})+q_x^{4n}}{1-2\,q_x^{2n-1}\,\cos(2\tilde{w})+q_x^{4n-2}} \\
\mathrm{cn}(w,x) &= 2\left(\frac{(1-x)\,q_x}{x}\right)^{\frac{1}{4}} \cos\tilde{w} \prod_{n=1}^{\infty} \frac{1+2\,q_x^{2n}\,\cos(2\tilde{w})+q_x^{4n}}{1-2\,q_x^{2n-1}\cos(2\tilde{w})+q_x^{4n-2}} \\
\mathrm{dn}(w,x) &= (1-x)^{\frac{1}{4}} \prod_{n=1}^{\infty} \frac{1+2\,q_x^{2n-1}\,\cos(2\tilde{w})+q_x^{4n-2}}{1-2\,q_x^{2n-1}\,\cos(2\tilde{w})+q_x^{4n-2}}.
\end{aligned} \tag{D.60}$$

where $q_x = e^{\pi i \tau(x)}$ is the elliptic nome. These products inside the logarithm become an infinite sum of logarithms and a change of variables to $\tan(\tilde{w})$ allows for a straightforward evaluation of the resulting integrals. Once the dust settles, we arrive at

$$I(\chi) = \pi \log\left(\frac{16\,q_{1-\chi}\,\chi(1-\chi)\,\coth^2(\pi\,\mathfrak{p}_c)}{(\coth(\pi\,\mathfrak{p}_c)+1)^4}\right) + 4\pi \sum_{n=1}^{\infty} \log\left(\frac{1+q_{1-\chi}^{2n+1}}{1-q_{1-\chi}^{2n}}\,\frac{1-q_{1-\chi}^{2n+1}}{1-q_{1-\chi}^{2n}}\,\frac{1+q_{1-\chi}^{2n}}{1-q_{1-\chi}^{2n}}\right) \tag{D.61}$$

which can be simplified using (D.60) evaluated at special values of w to give

$$\mathcal{I}(\chi) = 2\pi \log\left(\frac{\pi^3\,\mathfrak{p}_c^3\,\mathrm{sech}(\pi\,\mathfrak{p}_c)\,\mathrm{csch}(\pi\,\mathfrak{p}_c)}{K(\chi)^3}\right). \tag{D.62}$$

Inserting this result into (D.56) gives the result (D.42) quoted earlier.

D.4.3 IR divergences

The final ingredient in our computation is the evaluation of the long-distance contributions encoded in S_{IR}, which originate from several different places and we will discuss each of them in turn.

- Firstly, the integration by parts of the 'kinetic term' for φ in (D.39) contributes. Imposing large radius cut-offs R_y and R_v in the y- and v-planes, respectively, we

obtain the following boundary contributions to (D.39)

$$\begin{aligned}&\lim_{R_v,R_y\to\infty}\int_0^{2\pi}d\theta\, R_v\varphi\partial_r\varphi|_{r=R_v}+\frac{1}{2}\int_0^{2\pi}d\theta\, R_y\varphi\partial_r\varphi|_{r=R_y}\\&=\lim_{R_v,R_y\to\infty}2\int_0^{2\pi}d\theta\,\varphi(R_v,\theta)-\int_0^{2\pi}d\theta\,\varphi(R_y,\theta)=\lim_{R_v,R_y\to\infty}4\pi\varphi(R_v)-2\pi\varphi(R_y)\,,\end{aligned}\tag{D.63}$$

using the fact that $\partial_r\varphi|_{r=R_v}=2/R_v$ and $\partial_r\varphi|_{r=R_y}=-2/R_y$. Furthermore, φ becomes angle independent in the infinite radius limit (as we shall see later).

- The second contribution comes from working in Poincaré coordinates which misses an extra term coming from the curvature of the y sphere (which is pushed off to infinity in these coordinates). To find this extra term, we pass to global coordinates with metric

$$ds^2=\frac{d\xi^2}{\xi^2}+R_y^2\left(\frac{R_y}{\xi}-\frac{\xi}{R_y}\right)^2\frac{dy\,d\bar{y}}{(R_y^2+|y|^2)^2},\tag{D.64}$$

which recovers the Poincaré metric for $R_y\to\infty$. One finds the extra contribution by computing the Einstein-Hilbert action with this metric in global coordinates and comparing to Einstein-Hilbert action in Poincaré coordinates (D.35). One thus finds the missing term to be

$$\begin{aligned}&\lim_{R_y\to\infty}\frac{1}{8\pi G_N}\int dy\,d\bar{y}\,\frac{R_y^2}{(R_y^2+|y|^2)^2}\left(\log\left(\frac{\rho_c}{R_y^2}\right)-2\varphi\right)\\&=\lim_{R_y\to\infty}\frac{1}{4G_N}\log\left(\frac{\rho_c}{R_y^2}\right)-\frac{1}{2G_N}\varphi(R_y)\end{aligned}\tag{D.65}$$

- The third and final contribution, requires careful analysis of the contribution to the action from the branch point a_4 which we have sent to infinity. This was discussed in Appendix D of [126] for the case $n>2$. The main challenge with obtaining this contribution is that when we set $a_4=\infty$, we have $y(a_4=\infty)=\infty$ so we cannot

distinguish the contribution of the branch point from the contribution of the sphere curvature at $y = \infty$ discussed above. We give an analytic estimate for $n = 2$ below.

To understand the a_4 contribution, we deform the map y slightly so that a_4 does not map to infinity, instead $y(a_4) = y_4 \gg 1$ with some point $v_\infty \approx a_4$ on one sheet such that $y(v_\infty) = \infty$. This will allow us to separately find the contribution from a_4 and from the sphere curvature (D.65). We will then take the limits $y_4 \to \infty$ followed by $a_4 \to \infty$.

Now that a_4 is finite, we can use that $y(v)$ is a power series in $(v - a_4)^{\frac{1}{2}}$ near a_4 by the Schottky construction to write

$$y(v) = y_4 + \mu_4 (v - a_4)^{\frac{1}{2}} + \mathcal{O}(v - a_4) . \tag{D.66}$$

Therefore, the contribution of a_4 to the integral of the 'kinetic term' for φ evaluated in (D.39) is given by

$$- \oint_{a_4} \varphi \partial_{|v|} \varphi = \pi \log \left(\frac{|\mu_4|}{2\epsilon^{\frac{1}{2}}} \right) . \tag{D.67}$$

We next find the behavior of y and φ at R_y and R_v. Since we only put v_∞ on one sheet, $y(v)$ must have an order one pole at this point so near v_∞ (with residue ν_∞), we have

$$y(v) \approx \frac{\nu_\infty}{v - v_\infty} \implies \lim_{R_y \to \infty} \varphi(R_y) = \lim_{R_y \to \infty} \log \left(\frac{|\nu_\infty|}{R_y^2} \right) . \tag{D.68}$$

Recall that the accessory parameters are chosen such that y is regular at $v = \infty$. It is not branched at this point since a_4 is finite, thus near $v = \infty$

$$y(v) = y_\infty + \frac{\mu_\infty}{v} \implies \lim_{R_v \to \infty} \varphi(R_v) = \lim_{R_v \to \infty} \log \left(\frac{R_v^2}{|\mu_\infty|} \right) . \tag{D.69}$$

Having extracted all the necessary contributions from a_4, R_v, and R_y, we can now take the desired limits $y_4 \to \infty$ and then $a_4 \to \infty$. From (D.67) and plugging (D.68) and

(D.69) into (D.63) and (D.65), one finds that the contribution to the action from the newly defined parameters is

$$\mathfrak{S} = -\frac{1}{4G_N} \log \left(\frac{|\nu_\infty| \, |\mu_4|^{\frac{1}{2}}}{|\mu_\infty|^2} \right). \tag{D.70}$$

We need to understand the behavior of these three parameters when we take the desired limits. To take the limit $y_4 \to \infty$ (or equivalently $a_4 \to v_\infty$), we use that y is 2-branched at a_4 to write the inverse function $v(y)$ near y_4 as

$$v(y) \approx a_4 + \frac{y_4^4}{\mu_4^2} \left(\frac{1}{y} - \frac{1}{y_4} \right)^2, \tag{D.71}$$

where we fixed the coefficient of the quadratic term by comparison with (D.66). One can then extract from (D.71) the relation between ν_∞ and y_4, μ_4 by taking y large and then $y_4 \to \infty$ with the result

$$v - v_\infty = \lim_{y_4 \to \infty} (v - a_4) \quad \Longrightarrow \quad \nu_\infty = -2\frac{y_4^3}{\mu_4^2}. \tag{D.72}$$

Furthermore, observe that in the limit $y_4 \to \infty$ the behavior of y near a_4 is given by

$$\lim_{y_4 \to \infty} y(v) \approx -\frac{|y_4|^2}{|\mu_4| \, (v - a_4)^{\frac{1}{2}}}. \tag{D.73}$$

Taking the limit $a_4 \to \infty$ we can find the relationship between $\frac{y_4^2}{\mu_4}$ and μ_∞ as follows. We compute the residue at $v = \infty$ of $y(v)^2$ using (D.69) and equate it to the limit $a_4 \to \infty$ of the residue at $v = a_4$ of $y(v)^2$ using (D.73). We repeat the same procedure for the function $y(v)^2/v$ and then plug the latter equation into the former. The final result is

$$\lim_{a_4 \to \infty} |\mu_\infty| = \lim_{a_4 \to \infty} \frac{\sqrt{a_4} \, |y_4|^2}{2 \, |\mu_4|}. \tag{D.74}$$

This completes the analysis of the parameters in $\mathfrak{S}$ in the desired sequence of limits, in particular we can write the argument of the logarithm in terms of a_4, y_4, and μ_4. We want to compute the latter two parameters from the analytic solution for $y(v)$ (D.29). However, this was obtained by solving the monodromy problem which assumed that $a_4 = \infty$. The function $y(v)$ is regular at $v = \infty$ for finite a_4, but this is no longer the case when $a_4 = \infty$ so that the map is 2-branched at $v = \infty$ with the following behavior

$$y(v) \approx \hat{\mu}_4 \, v^{\frac{1}{2}}. \tag{D.75}$$

Taking the limit $a_4 \to \infty$ and then $v \to \infty$ in (D.73) and comparing to (D.75) gives

$$\hat{\mu}_4 = \lim_{a_4 \to \infty} \frac{|y_4|^2}{a_4 \, |\mu_4|} \, . \tag{D.76}$$

Finally, it remains to find an explicit expression for $\hat{\mu}_4$ from (D.29). Using (D.26), one finds for small δ

$$\eta\left(\frac{1}{\delta}\right) = \pi\,\tau - \frac{\pi}{K(\chi)}\sqrt{\delta} + \mathcal{O}\left(\delta^{\frac{3}{2}}\right) \implies \lim_{\delta \to 0} y\left(\frac{1}{\delta}\right) = -\frac{K(\chi)\sqrt{\chi_S}}{\pi\,\mathfrak{p}_c\sqrt{\delta}} \implies \hat{\mu}_4 = -\frac{K(\chi)\sqrt{\chi_S}}{\pi\,\mathfrak{p}_c}. \tag{D.77}$$

Therefore,

$$\mathfrak{S} = -\frac{1}{4G_N}\log\left(\frac{8}{a_4^{\frac{3}{2}}|\widehat{\mu}_4|^{\frac{1}{2}}}\right) = \frac{1}{8G_N}\,\log\left(\frac{a_4^3\,K(\chi)\sqrt{\chi_S}}{2^6\,\pi\,\mathfrak{p}_c}\right). \tag{D.78}$$

Putting all of this together, we find the total contribution from the long-distance pieces:

$$S_{\rm IR} = \pi\left[\log\left(\frac{K(\chi)\sqrt{\delta\,\chi_S}}{2^5\pi\,\mathfrak{p}_c}\right) + 2\,\log(\rho_c) + 3\log(a_4) - 8\,\log(R_v)\right]. \tag{D.79}$$

D.5 Actions, signs, and all that

We collect here some useful facts about actions and signs that the reader might find helpful in checking various details of the paper.

D.5.1 Signs of gravitational action

The Lorentzian gravitational action S which enters in the path integral measures as $e^{iS_{\rm gr}}$ for standard time-ordered scattering computations, or as $e^{i(S^k_{\rm gr}-S^b_{\rm gr})}$ is given by

$$S_{\rm gr} \equiv S^k_{\rm gr} = \frac{1}{16\pi G_N}\left[\int d^{d+1}x\,\sqrt{-g}\,(R+d(d-1)) + 2\int d^dx\,\sqrt{-\gamma}\,K + S_{\rm ct}\right] \qquad \text{(D.80)}$$

The Euclidean path integral on the other hand is defined to be one with a real measure $e^{-S^E_{\rm gr}}$ which in turn can be obtained by analytic continuation. When we Wick rotate $t \to -i\,t_{\rm E}$ we pick end up picking a factor of $-i$ from the integration measure, which combined with the i in the quantum weighting, gives $+1$. A more straightforward statement is that the Euclidean action should correspond to the Euclidean Hamiltonian and generically be positive definite. This is why one defines:

$$S^E_{\rm gr} = -\frac{1}{16\pi G_N}\left[\int d^{d+1}x\,\sqrt{g}\,(R+d(d-1)) + 2\int d^dx\,\sqrt{\gamma}\,K + S_{\rm ct}\right] \qquad \text{(D.81)}$$

The evaluation of the functional integral is supposed to give a generating function (or a partition function), Z which in turn is expressed as a free energy (to pick up the connected components). We usually define therefore

$$Z = e^{-I} = \int_L [Dg]\,e^{iS_{\rm gr}}\,, \qquad Z = e^{-I} = \int_E [Dg]\,e^{-S^E_{\rm gr}} \qquad \text{(D.82)}$$

In thermodynamic systems $I = \beta F$ where F is the free energy, which for sensible

thermal systems is negative $F = E - TS$. This is necessary for positivity of entropy and for the usual intuition that systems with lower free energy dominate the canonical ensemble (since $S = -\frac{\partial F}{\partial T}$ using $dF = -S\,dT$). This implies $I < 0$ (it is negative of the pressure). A saddle point or stationary phase evaluation of the above path integrals then gives:

$$I = S^E_{\rm gr}\big|_{\text{on-shell}}\,, \qquad I = -i\,S_{\rm gr} = -i(S^k_{\rm gr} - S^b_{\rm gr}) = 2\,{\rm Im}(S^k_{\rm gr}) \tag{D.83}$$

These statements can be checked for the planar-Schwarzschild-AdS$_5$ black hole which does define a sensible thermodynamic system for the dual CFT plasma. With a UV cut-off at $r = r_c$ in Schwarzschild coordinates one finds:

$$\begin{aligned} \int d^5x\,\sqrt{g}\,(R+12) &= -2(r_c^4 - r_+^4) \\ 2\int d^4x\,\sqrt{\gamma}\,K &= 8\,r_c^4 - 4r_+^4 \\ S_{\rm ct} &= -6r_c^4 + 3\,r_+^4 \end{aligned} \tag{D.84}$$

giving $S^E_{\rm gr}\big|_{\text{on-shell}} = I = -r_+^4$ which is the expression that correctly reproduces the pressure of the dual plasma.

D.5.2 Complex integral identities

In our evaluation of the $\hat{I}_n$ in Euclidean signature for N-intervals we made use of two identities which we quote here in generality. First, consider an integral $\mathcal{I}$

$$\mathcal{I} = \int_{\mathcal{R}_\epsilon} dv d\bar{v}\,\mathfrak{F}(v,\bar{v}) = i\int_{\mathcal{R}_\epsilon} \mathfrak{F}(v,\bar{v})\,dv\wedge d\bar{v} \tag{D.85}$$

over a domain $\mathcal{R}_\epsilon$ of the complex plane defined by excising discs $\mathcal{D}^\epsilon_i$ centered at a_i

$$\mathcal{R}_\epsilon = \mathbb{C}\backslash\left(\cup_j \mathcal{D}^\epsilon_j\right) \tag{D.86}$$

If one wishes to consider the variations of the integral with respect to the locations a_i then not only should one consider the explicit variation of the integrand but also account for the variation of the domain $\mathcal{R}_\epsilon$. The latter is a boundary integral and the general result we need is

$$\frac{\partial}{\partial a_i}\mathcal{I} = i\int_{\mathcal{R}_\epsilon}\frac{\partial}{\partial a_i}\mathfrak{F}(v,\bar{v})\,dv\wedge d\bar{v} + i\oint_{\partial\mathcal{D}_i^\epsilon}\mathfrak{F}(v,\bar{v})\,d\bar{v} - i\oint_{\partial\mathcal{D}_i^\epsilon}\mathfrak{F}(v,\bar{v})\,dv \tag{D.87}$$

Another relation we have employed is the Stokes' theorem on the Dolbeault complex ($d=\partial+\bar{\partial}$). For a holomorphic $\mathfrak{f}(v)$ we have

$$i\int_{\mathcal{R}}\left(\partial_v\mathfrak{f}(v)+\partial_{\bar{v}}\bar{\mathfrak{f}}(\bar{v})\right)\,dv\wedge d\bar{v} = i\int_{\mathcal{R}} d\left(\mathfrak{f}\,d\bar{v}-\bar{\mathfrak{f}}\,dv\right) = i\int_{\partial\mathcal{R}}\left(\mathfrak{f}\,d\bar{v}-\bar{\mathfrak{f}}\,dv\right) \tag{D.88}$$

Appendix E

Appendix to Chapter 6

E.1 Calculation of the Corner Terms

In this appendix, we calculate the contribution to the action from the corners using the expression in [183].

Without loss of generality, let us assume $\tilde{t} < \delta$, where $\tilde{t}$ is the new time coordinate corresponding to the Cauchy slice with constant global time T. The corners where this Cauchy slice meets the asymptotic cutoff surface $r = r_c = \frac{1}{\epsilon}$ contribute corner terms to our gravitational action. First we compute the normal vectors for the surfaces. For the spacelike Cauchy slice, its normal vector is

$$n_a = \sqrt{1 + X^2} dT_a \tag{E.1}$$

In global coordinates, the cutoff surface $r = r_c$ is

$$X^2 - \frac{r_c^2}{r_s^2 \cos^2 T} + 1 = 0, \tag{E.2}$$

with the normal vector

$$m_a = \frac{1}{\sqrt{N}} \left(-\frac{2r_c^2 \tan T}{r_s^2 \cos^2 T} dT_a + 2X dX_a \right), \tag{E.3}$$

where N is the normalization factor.

Finally, the corner term is given by

$$S_{\rm c} = 2 \times 2 \int_{\rm corner} \Phi K dx = 4\phi_b r_c \sinh^{-1}(n \cdot m) = 4\phi_b r_s \sin T + \mathcal{O}(r_c^{-2}) \tag{E.4}$$

where we have included an extra factor of 2 to account for two corners.

Appendix F

Appendix to Chapter 7

F.1 Replica symmetry and the entropy of a holographic theory on $\mathcal{M}_n$: an example

This appendix provides a simple example illustrating the discussion in section 7.3.2 of S_{QFT} for holographic field theories on $\mathcal{M}_n$. For simplicity, we consider Jackiw-Teitelboim gravity with two boundaries, and we focus on the Renyi problem associated with the entropy of a single boundary in the vacuum state. The classical real-time replica wormholes $\mathcal{M}_n$ for this problem were constructed in [4], which found that they may be built from $2n$ manifolds $M_-^i, \tilde{M}_-^j$ each with the identical metric

$$ds^2 = \frac{4(\tilde{x}^+\tilde{x}^-)^{\frac{1}{n}-1}d\tilde{x}^+d\tilde{x}^-}{n^2(1-(\tilde{x}^+\tilde{x}^-)^{\frac{1}{n}})^2}. \tag{F.1}$$

The AdS boundaries are located at $\tilde{x}^+\tilde{x}^- = 1$. We take the splitting surface $\boldsymbol{\gamma}$ to lie at $\tilde{x}^+ = \tilde{x}^- = 0$ and we sew the replicas together in the usual way along arbitrary spacelike surfaces connecting $\boldsymbol{\gamma}$ to the right AdS boundary (where $\tilde{x}^\pm > 0$).

We now couple our JT-gravity system to a holographic quantum field. To make the

example non-trivial, we will allow the quantum field to be in any member of a one-parameter family of states labelled by an amplitude A, with $A = 0$ being the vacuum state. In general, we would expect there to be some back-reaction on the metric (F.1) for $A \neq 0$. But for simplicity we will choose a model for which this back-reaction vanishes at the order where S_{QFT} is given by the classical HRT entropy.

In particular, we take our holographic QFT to be dual to gravity on an AdS_3 spacetime with boundary metric given by (F.1). Since the boundary metric itself has a boundary, we also take the bulk to be truncated by a dynamical EOW brane anchored to the AdS boundaries of (F.1).

As described in section 7.3.2, the relevant HRT surfaces $\gamma_{\mathcal{N}}$ will stretch from some point γ in the 2-d JT-gravity spacetime (F.1) to this end-of-the world brane.

It will be convenient to define our model so that the bulk spacetime $\mathcal{N}$ is always described by the same bulk metric and such that it always has vanishing boundary stress tensor. We can do so while still allowing non-trivial fluctuations in the bulk HRT entropy by including a dynamical field ϕ that lives on the EOW brane. We take this ϕ to be a massless scalar on the brane so that the bulk action takes the form

$$I = -\frac{1}{16\pi G}\int_{\mathcal{N}_n} d^3x(R - 2\Lambda) - \frac{1}{8\pi G}\int_{EOW} d^2x\sqrt{h}K - \int_{EOW} d^2x\sqrt{h}h^{ij}\partial_i\phi\partial_j\phi \quad \text{(F.2)}$$

with appropriate counterterms. Here h_{ij} is the induced metric on the EOW brane.

Our one-parameter family of states will then be defined by imposing the boundary condition

$$\phi_b = A\left(\tilde{x}^+ + \tilde{x}^-\right) \quad \text{(F.3)}$$

on every M^i_-, $\tilde{M}^i_-$. As we can see, this boundary condition has the $\mathbb{Z}_n$ replica symmetry. We now solve for the backreaction caused by the EOW-brane scalar field. The equation

of motion for h_{ij} gives

$$K_{ij} - h_{ij}K = 8\pi G T_{ij} \tag{F.4}$$

where

$$T_{ij} = \frac{2}{\sqrt{h}}\frac{\delta I_\phi}{\delta h^{ij}} = \partial_i\phi\partial_j\phi - \frac{1}{2}h_{ij}h^{kl}\partial_k\phi\partial_l\phi. \tag{F.5}$$

The equation of motion for the scalar field gives

$$\partial_i(\sqrt{h}h^{ij}\partial_j\phi) = 0 \tag{F.6}$$

The boundary metric (F.1) suggests that we describe the bulk using the hyperbolic slicing of AdS_3 and replace each hyperbolic slice with the $R = -2$ metric (F.1) so that the bulk metric takes the form

$$ds^2 = d\rho^2 + \cosh^2\rho\left(\frac{4(\tilde{x}^+\tilde{x}^-)^{\frac{1}{n}-1}d\tilde{x}^+d\tilde{x}^-}{n^2(1-(\tilde{x}^+\tilde{x}^-)^{\frac{1}{n}})^2}\right). \tag{F.7}$$

Without an EOW brane the coordinate ρ would range over the entire real line: $-\infty < \rho < \infty$. However, we take the boundary metric (F.1) to live at $\rho = -\infty$, and the EOW brane will cut off the bulk at some $\rho = \rho_{EOW}(\tilde{x}^+, \tilde{x}^-)$. When no matter field is present, the brane lies at $\rho_{EOW} = 0$, where the extrinsic curvature vanishes.

We wish to solve the equations of motion to find ρ_{EOW} perturbatively in A. At zeroth order we have $\rho = 0$ on the brane. We may thus choose boundary conditions in the far past (or on a Euclidean piece of an appropriate Schwinger-Keldysh contour) so that at this order we have

$$\phi = \phi_0 := A\left(\tilde{x}^+ + \tilde{x}^-\right), \tag{F.8}$$

Its stress tensor on the brane is $T_{++} = T_{--} = A^2$, and the trace vanishes, $T_{+-} = 0$.

To compute backreaction, we take the brane to be located at $\rho = \rho_1(\tilde{x}^+, \tilde{x}^-)$, whose

normal is

$$n_\mu dx^\mu = \frac{1}{N}\left(d\rho + \partial_+\rho_1 d\tilde{x}^+ + \partial_-\rho_1 d\tilde{x}^-\right). \tag{F.9}$$

To leading order in ρ_1, the EOW brane extrinsic curvature $K_{\mu\nu} = \nabla_\mu n_\nu$ has components

$$K_{++} = \frac{1}{n\tilde{x}^+}\left(\frac{2}{1-(\tilde{x}^+\tilde{x}^-)^{\frac{1}{n}}} - n - 1\right)\partial_+\rho_1 - \partial_+^2\rho_1 \tag{F.10}$$

$$K_{--} = \frac{1}{n\tilde{x}^-}\left(\frac{2}{1-(\tilde{x}^+\tilde{x}^-)^{\frac{1}{n}}} - n - 1\right)\partial_-\rho_1 - \partial_-^2\rho_1 \tag{F.11}$$

$$K_{+-} = -\frac{2(\tilde{x}^+\tilde{x}^-)^{\frac{1}{n}-1}}{n^2\left(1-(\tilde{x}^+\tilde{x}^-)^{\frac{1}{n}}\right)^2}\rho_1 - \partial_+\partial_-\rho_1 \tag{F.12}$$

Solving the equations of motion

$$K_{ij} = 8\pi G T_{ij}, \tag{F.13}$$

one finds that the position of the EOW brane is

$$\rho_1(\tilde{x}^+,\tilde{x}^-) = -\frac{8\pi G A^2 n}{4n^2-1}\frac{(1+2n-(2n-1)(\tilde{x}^+\tilde{x}^-)^{\frac{1}{n}})}{2(1-(\tilde{x}^+\tilde{x}^-)^{\frac{1}{n}})}\left((\tilde{x}^+)^2+(\tilde{x}^-)^2\right). \tag{F.14}$$

The entanglement entropy of Σ_γ is given by the length of the HRT surface (geodesic) that goes from γ to the EOW brane. For our choice of coordinates, the geodesics of interest are given by $(\tilde{x}^+,\tilde{x}^-) = const$, $-\infty < \rho < \rho_1$. Thus the entanglement entropy of Σ_γ is given by

$$S_{QFT}[\gamma] = \frac{1}{4G_N}\int_{-1/\epsilon}^{\rho_1(\tilde{x}^+,\tilde{x}^-)} d\rho = \frac{\rho_1(\tilde{x}^+,\tilde{x}^-)+1/\epsilon}{4G_N}. \tag{F.15}$$

where we have introduced a cutoff at $\rho = -1/\epsilon$. Rewriting the above formulae in terms of the coordinates $\tilde{X}^\pm \equiv (\tilde{x}^\pm)^{\frac{1}{n}}$, it is then easy to see that first derivatives of S_{QFT} with

respect to $\tilde{X}^{\pm}$ vanish at the splitting surface $\boldsymbol{\gamma}$ ($\tilde{x}^{+} = \tilde{x}^{-} = 0$):

$$\frac{dS_{QFT}[\boldsymbol{\gamma}]}{d\tilde{X}^{\pm}} = 0. \tag{F.16}$$

F.2 The shadow as a Wick rotation

This appendix illustrates how, when the real-time saddle $\mathcal{M}_n$ is a Wick rotation of some $\mathcal{M}_n^E$, the extended shadow $\hat{\mathcal{S}}_R$ can be taken to be defined by a different (and smoother!) Wick rotation of $\mathcal{M}_n^E$.

As mentioned in footnote 15, any such $\mathcal{M}_n^E$ must have a $\mathbb{Z}_2$ symmetry that acts simultaneously by a reflection across a fixed-point set $\mathcal{F}$ and by complex-conjugating all sources. This symmetry is a consequence of hermiticity for each copy of the density matrix employed in the replica trick. The set $\mathcal{F}$ thus partitions $\mathcal{M}_n^E$ pieces, each containing $n/2$ replicas (whether n is odd or even). The extended shadow $\hat{\mathcal{S}}_R$ can then be defined by introducing a Euclidean time τ for which $\mathcal{F}$ is $\tau = 0$ and then performing the standard Wick rotation in terms of τ. For even n, both the of $\mathcal{F}$ to the left and right of $\boldsymbol{\gamma}$ coincide with surfaces $\Sigma_{M_-^i,R}, \Sigma_{M_-^j,R}$ so that $\hat{\mathcal{S}}_R$ has a $\mathbb{Z}_2$ reflection symmetry, while for odd n the left part of $\mathcal{F}$ instead coincides with some $\Sigma_{M_-^j,L}$ (which by replica symmetry has the same geometry as $\Sigma_{M_-^i,L}$). See figure F.1.

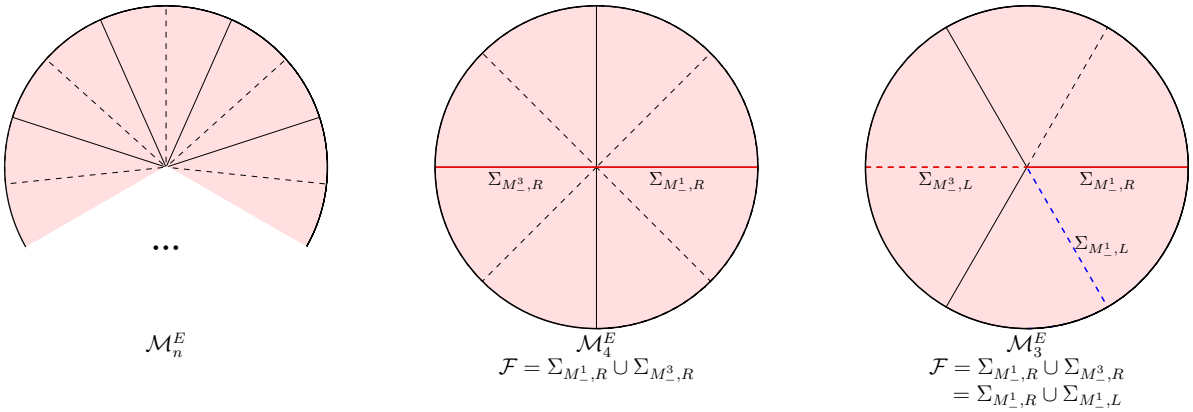

Figure F.1: **All panels:** Examples for various n of the Euclidean manifolds $\mathcal{M}_n^E$ that can be Wick rotated to obtain the real-time saddle $\mathcal{M}_n$. We take these to have replica and conjugation symmetries. Each conjugation symmetry leaves invariant some combination of dashed and solid black surfaces. As a result, the induced metric is real on these surfaces and the Euclidean-signature extrinsic curvature is imaginary. Thus Wick rotation to Lorentz signature gives real Cauchy data on these surfaces. **Center and Right:** For the cases $n = 4$ and $n = 3$, we may consider symmetries that act simultaneously by complex conjugation and by reflection across the red surfaces $\mathcal{F}$ shown. In each case, we may take $\mathcal{F}$ to be the surface $\tau = 0$ and then Wick rotate τ to define a Lorentz signature spacetime. The result is not $\mathcal{M}_n$ (which is given by a different Wick rotation). Instead, it gives a valid extended right shadow $\hat{\mathcal{S}}_R$. In the even case (center), this shadow $\hat{\mathcal{S}}_R$ has a right/left $\mathbb{Z}_2$ reflection symmetry that for swaps the isometric surfaces $\Sigma_{M_-^{n/2+1},R}$ and $\Sigma_{M_-^1,R}$. But in the odd case the fact that all dashed surfaces are related by replica symmetry means that $\hat{\mathcal{S}}_R$ is a smooth manifold whose initial data on $\mathcal{F}$ matches that of any M_-^i on $\Sigma_{M_-^i}$.

Appendix G

Appendix to Chapter 8

G.1 Properties of the JT action

This appendix discusses a number of details regarding asymptotically AdS_2 Jackiw-Teitelboim gravity. After defining the theory by stating the action and boundary conditions in section G.1.1, additivity of the JT action in the sense of (8.36) is shown in section G.1.2. The relation to the Schwarzian action is then reviewed in section G.1.3, and the Schwarzian form is then shown to be bounded below in section G.1.4.

G.1.1 Action and Boundary conditions for JT gravity

Much of the later analysis in this appendix will involve study of the boundary conditions for asymptotically AdS_2 JT gravity. The purpose of this section is to describe such boundary conditions in detail. We consider here the pure JT gravity theory consisting of only a dilaton ϕ and a metric g on a 2d spacetime $\mathcal{M}$, without additional matter fields. While our boundary conditions are just those of e.g. [51] (which are the Euclidean versions of those of [213]), we take this opportunity to rewrite them in a form more similar to that commonly used to describe asymptotically locally Anti-de Sitter spacetimes in

higher dimensional theories of gravity. For use with our cut-and-paste constructions, we also allow a slight extension of the usual boundary conditions to in which certain fields can be non-smooth on a codimension-1 surface. Below, we set the AdS_2 scale ℓ to 1.

The first step in defining configurations of our theory is to consider 2-dimensional compact manifolds $\widehat{\mathcal{M}}$ with boundaries. These are perhaps most simply defined as the spaces obtained from S^2 by i) removing n open disks, which creates n circular boundaries that we label $i = 1, \ldots, n$, ii) choosing $g < n/2$ and then for $i \leq g$ identifying the ith circular boundary with the $(i + g)$th circular boundary, iii) perhaps filling in one of the remaining circular boundaries with a cross-cap in order to obtain the non-orientable cases. Examples are shown in the left panel of figure G.1.

However, in order to accommodate the cut-and-paste constructions described in the main text, we also consider certain 2d manifolds with corners at their boundaries. In practice, it will be sufficient to define these by starting with one of the above 2d manifolds $\widehat{\mathcal{M}}$ with boundary (and without corners), choosing any smooth $1d$ surface Σ in that manifold that divides $\widehat{\mathcal{M}}$ into two parts, and removing one of the parts. We call what is left a manifold $\mathcal{M}$ with boundaries and corners; see the right panel of figure G.1.

The boundary of the final $\mathcal{M}$ now consists of two types of segments. The first type, whose union we we call the asymptotic boundary $\partial_{as}\mathcal{M}$, consists of those segments in $\partial\mathcal{M}$ which also lie on the boundary of the parent space $\widehat{\mathcal{M}}$ from which $\mathcal{M}$ was cut: $\partial_{as}\mathcal{M} = \partial\mathcal{M} \cap \partial\widehat{\mathcal{M}}$. The second type, whose union we call the finite boundary $\partial_f\mathcal{M}$, consists of the remainder which we see must in fact form the slicing surface Σ (so that $\partial_f\mathcal{M} = \Sigma$). In general, $\partial_{as}\mathcal{M}$ and $\partial_f\mathcal{M}$ will intersect at a finite number of points.

We wish to consider metrics g on $\mathcal{M}$ which are the restriction of metrics $\hat{g}$ on the parent space $\widehat{\mathcal{M}}$ and which in some region near $\partial_{as}\widehat{\mathcal{M}}$ can be written in the form

$$ds^2 = \frac{dz^2 + h(\theta, z)d\theta^2}{z^2}, \tag{G.1}$$

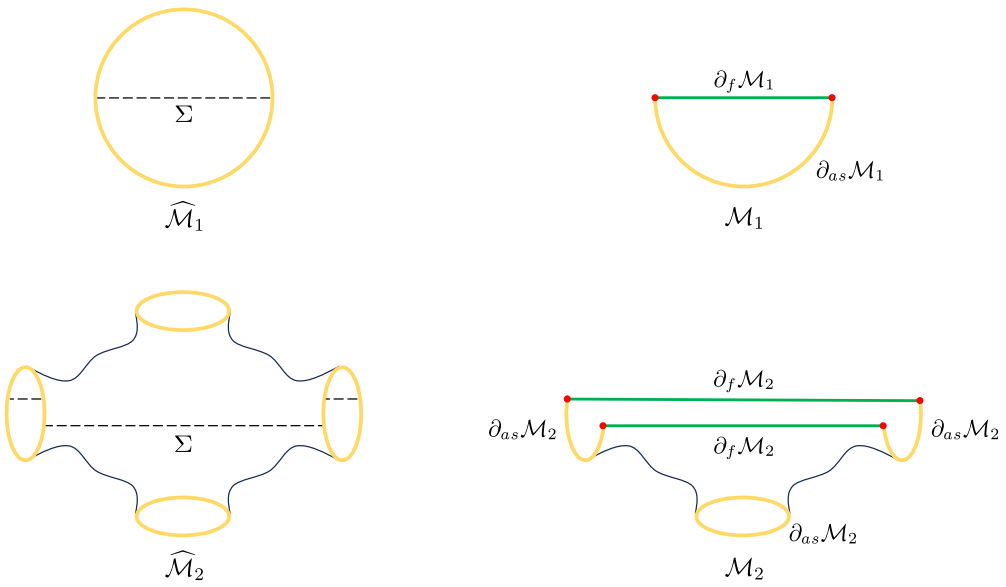

Figure G.1: Two examples of parent spaces $\widehat{\mathcal{M}}$ are shown at left. These $\widehat{\mathcal{M}}$ have only asymptotic boundaries (yellow). Cutting away the part beyond a surface Σ gives a manifold with boundaries and corners that we call $\mathcal{M}$. Such $\mathcal{M}$ generally still have asymptotic boundaries $\partial_{as}\mathcal{M}$ (yellow) inherited from $\widehat{\mathcal{M}}$, but also have finite boundaries $\partial_f\mathcal{M}$ (green) created by the cut. The two types of boundaries will generally meet at corners (red).

where both the function h and the coordinates z, θ are smooth on $\widehat{\mathcal{M}}$, where z has a first-order zero at $\partial_{as}\widehat{\mathcal{M}}$, and where both $\partial_z h$ and $\partial_z^2 h$ vanish at $z = 0$. Similarly, we consider dilaton fields of the form

$$\phi = \frac{f(\theta, z)}{z}, \tag{G.2}$$

with f smooth on $\widehat{\mathcal{M}}$. Note that, for a given metric and dilaton, the form of (G.1) and (G.2) are preserved by appropriate smooth coordinate transformations which satisfy

$$z \;\to\; a(\theta) z + O(z^3), \tag{G.3}$$

$$\theta \;\to\; b(\theta) + O(z^2), \tag{G.4}$$

and under which we find that the associated h on the boundary transforms as $h|_{z=0} \to (h[\frac{1}{a}\frac{db}{d\theta}]^2)|_{z=0}$. As a result, the coordinates (z, θ) that give the form (G.1) and (G.2) are far from unique.

We also wish to impose further boundary conditions. To do so, we endow each of our manifolds with a special preferred scalar function Ω which will be used to translate between the physical metric and dilaton (which diverge at $\partial_{as}\mathcal{M}$) and an unphysical rescaled metric and dilaton that will be used to specify the additional boundary conditions. It is convenient to define Ω to be a function on the parent space $\widehat{\mathcal{M}}$ such that Ω vanishes on $\partial\widehat{\mathcal{M}} = \partial_{as}\widehat{\mathcal{M}}$ but has $d\Omega$ nowhere vanishing on $\partial\widehat{\mathcal{M}} = \partial_{as}\widehat{\mathcal{M}}$. We require Ω to be smooth on most of the spacetime, though – for use with our cut-and-paste constructions – we also allow the existence of a finite number of smooth codimension-1 surfaces Σ on which Ω is continuous and limits of first derivatives from either side are well-defined, but where $d\Omega$ can have discontinuities across the surface. The various such surfaces Σ are allowed to intersect at a finite number of points. We will refer to Ω as the defining function of the conformal frame, or simply as the conformal factor. In terms of any given set of coordinates (z, θ) satisfying the conditions above, we may write

$$\Omega = z\omega(z, \theta) \tag{G.5}$$

for some smooth positive function ω that does not vanish anywhere on $\partial\widehat{\mathcal{M}} = \partial_{as}\widehat{\mathcal{M}}$. We then use Ω to define rescaled (unphysical) fields

$$d\tilde{s}^2 := \Omega^2 ds^2, \quad \text{and} \quad \tilde{\phi} := \Omega\phi. \tag{G.6}$$

We may thus introduce a coordinate u on each connected component of $\partial_{as}\mathcal{M}$ such that u measures the unphysical proper distance defined by $d\tilde{s}^2$, and we may then require $\tilde{\phi}$ on

$\partial_{as}\mathcal{M}$ to be some fixed function $\phi_b(u)$; i.e., we impose

$$\tilde{ds}^2\big|_{\partial_{as}\mathcal{M}} = du^2, \quad \tilde{\phi}|_{\partial_{as}\mathcal{M}} = \phi_b(u). \tag{G.7}$$

We note for future reference that (G.7) implies

$$\omega^{-1}|_{z=0} = \sqrt{h|_{z=0}}\frac{d\theta}{du}. \tag{G.8}$$

Since (G.7) are coordinate invariant, they are in particular preserved by coordinate transformations of the form (G.3).

Finally, as a further boundary condition, on every piece of $\partial_f\mathcal{M}$ we require $\theta(z)$ to have an expansion of the form

$$\theta = \theta_0 + \theta_2 z^2 + ... \tag{G.9}$$

near $\partial_{as}\mathcal{M}$ in terms of coordinates in which the metric takes the form (G.1). Since the $O(z)$ term in (G.9) vanishes, this in particular requires all intersections between the finite and asymptotic boundaries to be orthogonal as defined by the unphysical metric $\tilde{g}$. Note that this condition is again preserved by coordinate transformations of the form (G.3).

In the above we take each point on $\partial_{as}\widehat{\mathcal{M}}$ to be assigned a value of u as a boundary condition, so that we in particular fix the range of u, and thus the unphysical proper length of each segment of the asymptotic boundary. This completes our discussion of (asymptotic) boundary conditions for JT gravity. Note that, since we allowed discontinuities in $d\Omega$, these boundary conditions are manifestly invariant under the cut-and-paste construction associated with Assumption 2 of section 8.3.2.

G.1.2 Additivity and the JT action

Having stated the dilaton and metric boundary conditions above, we can now proceed to discuss the JT action. Here we focus on the additivity property (8.36). We now include possible (dilaton-free) couplings to matter, meaning that the dilaton should not appear in the matter action. However, we will not spell out the details of the matter action or boundary conditions. We will simply (and implicitly) assume that the matter action for a given metric is of the form described in section 8.3.1 (so that the matter action is separately additive), and that the matter fields fall-off sufficiently quickly at infinity that they do not affect the leading behavior of the dilaton given in (G.7) even when the equations of motion are satisfied.

Since the metric and dilaton diverge at the asymptotic boundaries $z = 0$, the JT action will be defined as the $\epsilon \to 0$ limit of actions for regulated manifolds $\mathcal{M}_\epsilon$, each given by the region of $\mathcal{M}$ with $\Omega \geq \epsilon$ for some $\epsilon > 0$. The boundary $\partial\mathcal{M}_\epsilon$ of the regulated spacetime can again be decomposed into two parts, $\partial_f\mathcal{M}_\epsilon$ and $\partial_{as}\mathcal{M}_\epsilon$, the first of which is just the part of $\partial_f\mathcal{M}$ that remains in $\mathcal{M}_\epsilon$, and the second is the closure of the remainder:

$$\partial_f\mathcal{M}_\epsilon := \mathcal{M}_\epsilon \cap \partial_f\mathcal{M}, \quad \text{and} \quad \partial_{as}\mathcal{M}_\epsilon := \overline{\partial\mathcal{M}_\epsilon \setminus \partial_f\mathcal{M}_\epsilon}. \tag{G.10}$$

Again, the two parts generally intersect in a finite number of points, though the intersections are no longer strictly orthogonal at finite ϵ. For a given intersection point i, we thus let $\pi/2 + \alpha_i > 0$ denote the (interior) angle at which the finite and asymptotic boundaries meet; see figure G.2.

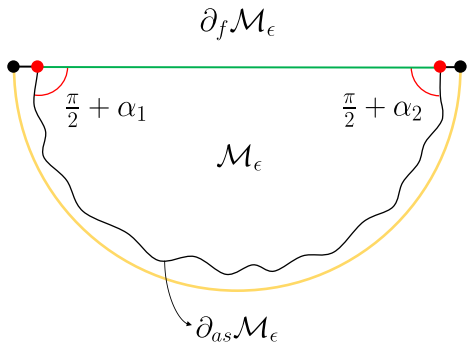

Figure G.2: A regulated manifold $\mathcal{M}_\epsilon$ is shown with its finite boundary $\partial_f \mathcal{M}_\epsilon$ and asymptotic boundary $\partial_{as} \mathcal{M}_\epsilon$ intersecting at angles $\pi/2 + \alpha_1$ and $\pi/2 + \alpha_2$.

We now take the action to be $I := \lim_{\epsilon \to 0} I_\epsilon$ with

$$\begin{aligned} I_\epsilon &= -\phi_0 \left[\int_{\mathcal{M}_\epsilon} \sqrt{g} R + 2 \int_{\partial_{as} \mathcal{M}_\epsilon} \sqrt{h} K + 2 \int_{\partial_f \mathcal{M}_\epsilon} \sqrt{h} K - 2 \sum_i \alpha_i \right] \\ &- \left[\int_{\mathcal{M}_\epsilon} \sqrt{g} \phi (R+2) + 2 \int_{\partial_{as} \mathcal{M}_\epsilon} \sqrt{h} \phi (K-1) + 2 \int_{\partial_f \mathcal{M}_\epsilon} \sqrt{h} \phi K - 2 \sum_i \alpha_i \phi_i \right] \\ &+ I_{matter}. \end{aligned} \tag{G.11}$$

Here ϕ_0 is a constant, h is the induced metric on a boundary, K is the extrinsic curvature (a scalar, since the boundary is one-dimensional) defined by the outward-pointing normal, i ranges over all points where $\partial_f \mathcal{M}_\epsilon$ meets $\partial_{as} \mathcal{M}_\epsilon$, and ϕ_i are the values of ϕ at such meeting points. Note that in the first line we have included separate terms at $\partial_{as} \mathcal{M}_\epsilon$ and $\partial_f \mathcal{M}_\epsilon$, neither of which will include effects from corners where they intersect. The natural delta-function contributions from K at corners have instead been written explicitly in terms of the α_i (up a $\pi/2$ offset for each corner that we now discuss).

The usual calculation then shows (G.11) to be a good variational principle when the induced metric and dilaton are fixed on the finite boundaries $\partial_f \mathcal{M}$ and the boundary conditions of (G.1.1) are imposed at the asymptotic boundary, and of course when boundary

conditions appropriate to I_{matter} are imposed on matter fields. In particular, while the fact that we allowed $d\Omega$ to be discontinuous across a surface introduces delta-functions in the extrinsic curvature of $\mathcal{M}_\epsilon$ at some values of θ, these delta-functions give finite results when integrated over θ. The discontinuities in $d\Omega$ then have no further impact on the computation. In particular, they do not change any powers of ϵ.

Note that, since we require the matter action to be dilaton-free, the equation of motion obtained by varying ϕ in (G.11) is just $R + 2 = 0$ for any allowed matter. In particular, the matter field can have no effect on the asymptotics of the metric. This also means that the only positivity property of the matter that we will need is that I_{matter} be bounded below (say, by zero) for any asymptotically AdS_2 constant curvature $R = -2$ Euclidean metric g.

We now make a number of comments about the action (G.11), in particular regarding its additivity properties. It is convenient to begin by discussing the first line in (G.11), which turns out to purely topological. Let us denote these terms by I_{top}. Since the interior angles at each intersection point i are $\pi/2 + \alpha_i$, the Gauss-Bonnet theorem requires

$$I_{top} = -4\pi\phi_0\chi + \pi\phi_0 \sum_i (1) = -\pi\phi_0(4\chi - n_{int}), \tag{G.12}$$

where χ is the Euler character of $\mathcal{M}_\epsilon$ and n_{int} is the number of points where $\partial_f\mathcal{M}_\epsilon$ and $\partial_{as}\mathcal{M}_\epsilon$ intersect. The ϵ-dependence of I_{top} is manifestly trivial, so we will drop ϵ labels when discussing it below.

Furthermore, given disjoint configurations $\mathcal{M}_1$ and $\mathcal{M}_2$, we see that I_{top} satisfies

$$I_{top}(\mathcal{M}_1 \sqcup \mathcal{M}_2) = I_{top}(\mathcal{M}_1) + I_{top}(\mathcal{M}_2). \tag{G.13}$$

Here we use $\mathcal{M}$ to denote both the underlying manifold with boundaries and corners and

the fields carried by that manifold. We will continue this abuse of notation below. The symbol $\sqcup$ denotes disjoint union.

The term I_{top} also satisfies a second more interesting identity. To describe this identity, consider a configuration $\mathcal{M}$ for which $\partial_f \mathcal{M}$ has n_f connected components $\partial_{f,j}\mathcal{M}$ for $j = 1, \dots n_f$. We wish to form a new configuration $\overline{\mathcal{M}}$ by identifying pairs of components $\partial_{f,j}\mathcal{M}$. In particular, for some $m_f < n_f/2$, suppose we have (surjective) diffeomorphisms $\eta_j : \partial_{f,j}\mathcal{M} \to \partial_{f,j+m_f}\mathcal{M}$ for $j = 1, \dots m_f$ that preserve both the induced metric[1] and the conformal factor Ω. We define $\overline{\mathcal{M}}$ by using each η_j to identify its domain with its range, so that

$$n_f(\overline{\mathcal{M}}) = n_f(\mathcal{M}) - 2m_f. \tag{G.14}$$

The configuration $\overline{\mathcal{M}}$ is not generally smooth, but we can nevertheless evaluate $I_{top}(\overline{\mathcal{M}})$ as in (G.12) to find

$$I_{top}(\overline{\mathcal{M}}) = -\pi\phi_0(4\bar{\chi} - \bar{n}_{int}), \tag{G.15}$$

where $\bar{\chi}$ and $\bar{n}_{int}$ are respectively the Euler character of $\overline{\mathcal{M}}$ and the number of intersections of $\partial_{as}\overline{\mathcal{M}}$ with $\partial_f\overline{\mathcal{M}}$. Now, since the components $\partial_{f,j}\mathcal{M}$ of $\partial_f\mathcal{M}$ are one-dimensional, each component is either a line segment or a circle. We may thus divide the m_f identifications into m_s that identify pairs of line segments and m_c that identify circles (with $m_f = m_c + m_s$). Identifying circles does not change the number of points where $\partial_f\mathcal{M}_\epsilon$ and $\partial_{as}\mathcal{M}_\epsilon$ intersect, but identifying two line segments removes 4 intersections (two on each segment); see figure G.3. Thus

$$\bar{n}_{int} = n_{int} - 4m_s. \tag{G.16}$$

[1]Since the conformal factor is also preserved, it does not matter whether we state this definition in terms of g or $\tilde{g}$. We also note that we have excluded the possibility of identifying some component of $\partial_{f,j}\mathcal{M}$ with itself. When the component is an S^1, nontrivial such identifications do exist that yield smooth results, and our analysis below could be generalized to include them, but we will have no need of them.

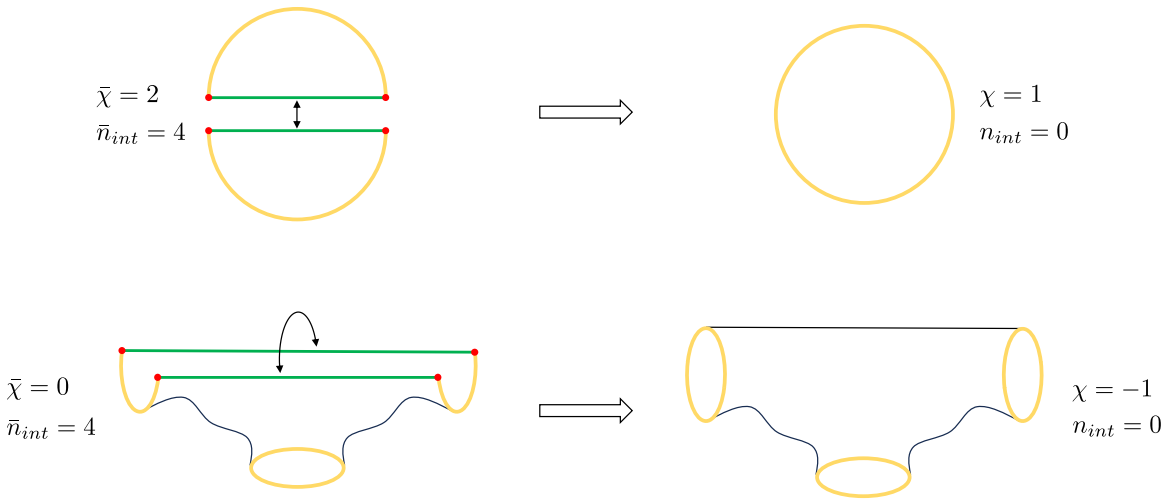

Figure G.3: Examples of the gluing operation that constructs $\overline{\mathcal{M}}$ from $\mathcal{M}$. While the gluing changes both χ and n_{int}, it does not change $4\bar{\chi} - \bar{n}_{int}$. Indeed, we find $4\bar{\chi} - \bar{n}_{int} = 4\chi - n_{int} = 4$ on the top line and $4\bar{\chi} - \bar{n}_{int} = 4\chi - n_{int} = -4$ on the bottom.

Similarly, identifying pairs of circles is well-known to leave the Euler character unchanged. However, identifying a pair of line segments lowers χ by 1; see again figure G.3. Thus we have

$$\bar{\chi} = \chi - m_s, \tag{G.17}$$

and

$$4\bar{\chi} - \bar{n}_{int} = 4\chi - n_{int}, \tag{G.18}$$

we thus find

$$I_{top}(\overline{\mathcal{M}}) = I_{top}(\mathcal{M}). \tag{G.19}$$

Because it satisfies (G.13) and (G.19), we say that I_{top} is sewing-additive. This in particular means that it satisfies (8.36). We will use the same term below for any other

functional satisfying analogous identities. (Note that this as yet says nothing about the operations associated with the yet-to-be-discussed monotonicity relations (8.38) and (8.39).)

In fact, the entire regulated Euclidean action I_ϵ defined by (G.11) is sewing-additive. It is already manifest that I_ϵ satisfies

$$I_\epsilon(\mathcal{M}_1 \sqcup \mathcal{M}_2) = I_\epsilon(\mathcal{M}_1) + I_\epsilon(\mathcal{M}_2), \tag{G.20}$$

so we may focus on the analog of (G.19) for the new manifold $\overline{\mathcal{M}}$ formed from any $\mathcal{M}$. Below, we also focus on the remaining terms $I - I_{top}$, since we have already established (G.19) for I_{top}.

There are now two effects to consider in order to show $I_\epsilon(\overline{\mathcal{M}}) = I_\epsilon(\mathcal{M})$. The first is that, as in the discussion of I_{top} above, intersections between the finite and asymptotic boundaries can disappear in pairs, so that there are contributions $\alpha_i\phi_i$ to $I_\epsilon(\mathcal{M})$ that do not appear in $I_\epsilon(\overline{\mathcal{M}})$. However, such a disappearance is associated with the joining of two asymptotic boundary segments as shown in figure 8.10 from section 8.3.3. The result is generally not smooth, so that the extrinsic curvature density $\sqrt{h}K$ of $\partial_{as}\overline{\mathcal{M}}$ contains a new delta-function of a strength defined by the angles α_i associated with the disappearing pair of intersections. In fact, for disappearing interior intersection angles α_1, α_2, the delta-function is of strength $\alpha_1 + \alpha_2$. This relation can be derived from the Gauss-Bonnet theorem. In particular, $\sqrt{h}K$ remains smooth when both of the disappearing intersections are orthogonal ($\alpha_1 = \alpha_2 = 0$). See again figure 8.10 in section 8.3.3.

The second effect is that, when two boundaries are sewn together, the seam is smooth only when the extrinsic curvatures K match appropriately on the two surfaces. More generally, the sewing leads to a singularity on the seam which gives a delta-function in $\sqrt{g}R$ related to the discontinuity in extrinsic curvatures. This phenomenon is well-known

from the Israel junction conditions; see e.g. [267]. The particular relation again follows by applying the Gauss-Bonnet theorem to a disk of infinitesimal size (and perhaps strong curvature) bounded by the two surfaces to be sewn together and then taking the limit where the surfaces coincide. In this way one sees that the contribution to $I_\epsilon(\overline{\mathcal{M}})$ from the delta-function in R on $\overline{\mathcal{M}}$ precisely compensates for the fact that $I_\epsilon(\overline{\mathcal{M}})$ no longer includes explicit contributions from the boundaries of $\mathcal{M}$ that have been sewn together.

Since the remaining contributions to (G.11) take identical forms in $\overline{\mathcal{M}}$ and $\mathcal{M}$, this establishes the desired relation

$$I_\epsilon(\overline{\mathcal{M}}) = I_\epsilon(\mathcal{M}). \tag{G.21}$$

In particular, we see that the regulated action I_ϵ is already sewing-additive at finite ϵ. Taking the limit $\epsilon \to 0$ then shows that corresponding property again holds for the unregulated action I.

G.1.3 Relation to the Schwarzian Action

As shown in [213] (see [51] for a Euclidean-signature treatment), the on-shell action for pure JT gravity takes a so-called Schwarzian form, which has proved to be extremely useful. We very briefly review this below, though most of the present section is a slight aside that generalizes the above result to our class of manifolds-with-boundaries-and-corners $\mathcal{M}$. The extension is not of critical use in the main text, but may be enlightening to some readers.

We also comment briefly on the off-shell extension of this result. The only equation of motion used to derive the Schwarzian action below is $R + 2 = 0$. Since the first line of (G.11) is topological, deviations from the on-shell result are controlled by the term involving $\sqrt{g}\phi(R+2)$. In the usual way (see e.g. [268] for a review) since we took the asymptotically locally AdS_2 boundary conditions to require both $\partial_z h$ and $\partial_z^2 h$ vanish at

$z = 0$, we find $R + 2 = O(z^3)$. Thus $\sqrt{g}\phi(R + 2) = O(1)$ and the discrepancy from the on-shell result is finite.

This discussion is often phrased in terms of a coordinate system in which the function h (defined by (G.1)) satisfies $h|_{z=0} = 1$, with θ taking values in $[0, 2\pi]$. As noted above, this can always be achieved via coordinate transformations of the form (G.3), which are indeed gauge redundancies of our system. The essential point is then that the extrinsic curvature scalar K of the family of surfaces $\Omega = \epsilon$ satisfies the asymptotic expansion

$$K = 1 + \epsilon^2 \, \mathrm{Sch}(\tan \frac{\theta(u)}{2}, u), \tag{G.22}$$

where

$$\mathrm{Sch}(f(u), u) = \frac{d}{du}\left(\frac{f''(u)}{f'(u)}\right) - \frac{1}{2}\left(\frac{f''(u)}{f'(u)}\right)^2, \tag{G.23}$$

and prime $'$ denotes $\frac{d}{du}$ so that

$$Sch(\tan \frac{\theta(u)}{2}, u) = \frac{1}{2}(\theta')^2 - \frac{1}{2}\left(\frac{\theta''}{\theta'}\right)^2 + \frac{d}{du}\left(\frac{\theta''}{\theta'}\right). \tag{G.24}$$

As a result, when $\mathcal{M}$ has only asymptotic boundaries (G.11) yields

$$I = I_{top} - 2\int \phi_b(u)\left(\frac{1}{2}(\theta')^2 - \frac{1}{2}\left(\frac{\theta''}{\theta'}\right)^2 + \frac{d}{du}\left(\frac{\theta''}{\theta'}\right)\right) du. \tag{G.25}$$

We now wish to obtain analogous results for our manifolds $\mathcal{M}$ with general finite boundaries and corners where the finite and asymptotic boundaries intersect. This in particular means that we will need to take due care to include all of the terms in (G.11) that did not appear in [51]. These are the terms that involve $\partial_f \mathcal{M}$, including the α_i terms associated with the intersection $\partial_f \mathcal{M} \cap \partial_{as} \mathcal{M}$. Importantly, we will again take $\mathcal{M}$ to be on-shell, which in particular means that it was cut from an on-shell parent configuration

$\widehat{\mathcal{M}}$.

The above-mentioned terms at first appear to depend strongly on the choice of $\partial_f \mathcal{M}$, or equivalently on the choice of the surface Σ used to cut the parent space $\widehat{\mathcal{M}}$ to form $\mathcal{M}$. However, as usual for gravitational systems, this is not in fact the case. This is most easily seen by writing the action in the standard Hamiltonian form (see e.g. [269] and references therein)

$$I = \int_{\mathcal{M}} (p_i \dot{q}^i - N^{\perp} \tilde{\mathcal{H}}_{\perp} - N^{||} \tilde{\mathcal{H}}_{||})) - \int_{\partial_{as} \mathcal{M}} N^{\perp} H_{\partial} + I_{degen}, \tag{G.26}$$

where, p_i, q^i are an appropriate set of coordinates and momenta, $N^{\perp}, N^{||}$ are the usual lapse and shift, and I_{degen} denotes additional potential contributions from any locus where the foliation used to define the Hamiltonian formalism degenerates.

In (G.26), we choose the coordinates q^i to be whatever quantities are to be held fixed on $\partial_f \mathcal{M}$ for (G.11) to define a good variational principle. Indeed, it is perhaps useful to recall that the form (G.26) must hold for any action, and in particular that the above condition on q^i requires any additional boundary term on $\partial_f \mathcal{M}$ to be independent of the momenta p_i. Furthermore, any such boundary terms can then be absorbed into the bulk by an appropriate redefinition of the momenta p_i, leaving us with an action of the form (G.26) as claimed.

The usual Hamilton-Jacobi argument then shows that variations of I with respect to infinitesimal changes in the location of the surface Σ used to cut $\mathcal{M}$ from $\widehat{\mathcal{M}}$ must involve two contributions. Here we restrict attention to variations that preserve the boundary conditions stated above for I, and which also preserve the points where Σ intersects $\partial_{as} \mathcal{M}$. The first contribution is given by varying the location of Σ while holding each q^i fixed on Σ, and the second is given by leaving Σ fixed within the manifold by varying that values of q^i on Σ as dictated by the appropriate evolution under the equations of motion (in

accord with the would-be motion of Σ through $\widehat{\mathcal{M}}$). So long as the intersection of Σ with $\partial_{as}\mathcal{M}$ does not change, combining the two terms gives a result in which contributions of the $p_i\dot{q}^i$ term cancel completely. The remainder is simply linear in the constraints $\mathcal{H}_\perp$ and $\mathcal{H}_{||}$. But the constraints vanish since $\mathcal{M}$ is on-shell, and we see that the desired variation vanishes as well.

In other words, the action of $\mathcal{M}$ is in fact invariant under smooth deformations of the surface Σ used to slice it from an on-shell $\widehat{\mathcal{M}}$, so long as the deformations both leave fixed the intersections of Σ with the asymptotic boundary $\partial_{as}\widehat{\mathcal{M}}$ and respect the boundary conditions associated with the action I. In particular, this requires that the α_i remain of whatever order in ϵ is specified by the boundary conditions.

This result then allows us to evaluate the action $I(\mathcal{M})$ by choosing any convenient surface Σ related to $\partial_f\mathcal{M}$ via smooth boundary-condition preserving deformations within $\mathcal{M}$. One choice we can always make is to minimize the physical length of Σ (after subtracting the appropriate universal divergence from the region near the boundary). In two Euclidean dimensions, doing so necessarily results in a smooth surface with vanishing extrinsic curvature [240]; i.e., in a geodesic.

Having thus set $K = 0$ on Σ, inspection of (G.11) shows that all boundary terms on the interior of $\partial_f\mathcal{M}$ now vanish. The only remaining contributions to I from Σ are then those associated with the angles α_i. These are straightforward to compute using the well-known fact that geodesics in spacetimes of the form given by (G.1) are asymptotically of the form $\theta = \theta_0 + \theta_2 z^2 + \ldots$, while the proper distance s along the geodesic is $s = \ln z + O(z^2)$. This fact follows from using (G.1) and expanding the geodesic equation in powers of z (say, by taking z as a non-affine parameter along the geodesic). Note that the above expansion shows that taking $K = 0$ on $\partial_f\mathcal{M}$ is consistent with (G.9).

At $\Omega = \epsilon$ the unit-normalized tangent to the inward-directed geodesic is of the form

$$(\frac{d\theta}{ds}, \frac{dz}{ds}) = (\frac{d\theta}{dz}, 1)\frac{dz}{ds} = (2\theta_2\epsilon/\omega, 1)\frac{\epsilon}{\omega}(1 + O(\epsilon)). \tag{G.27}$$

On the other hand, defining $\omega_0(\theta) = \omega|_{z=0}$ and noting that $\Omega = z\omega_0 + O(z^2)$, we see that at $\Omega = \epsilon$ the regulated version of the asymptotic boundary $\partial_{as}\mathcal{M}$ has (in the direction of increasing θ) the unit-normalized tangent

$$(1, \frac{dz}{d\theta})\frac{d\theta}{ds} = (1, -\epsilon\frac{d}{d\theta}\omega^{-1})\frac{\epsilon}{\omega}. \tag{G.28}$$

Since we chose the tangent along the asymptotic boundary to be in the direction of increasing θ, combining these with (G.1) yields

$$\begin{aligned} \cos(\alpha + \pi/2) &= \pm\frac{\epsilon}{\omega}\left(2\theta_2 + \frac{d}{d\theta}\ln\omega^{-1}\right) + O(\epsilon^2) \\ &= \pm\frac{2\pi\epsilon}{\beta}\left(2\theta_2 + \frac{\theta''}{(\theta')^2}\right) + O(\epsilon^2), \end{aligned} \tag{G.29}$$

where the $+$ $(-)$ sign corresponds to an intersection point at the large-θ (small-θ) end of an asymptotic boundary segment; see figure G.4. Applying (G.8) with $h = 1$ then yields

$$\alpha = \mp\epsilon\left(2\theta_2\theta' + \frac{\theta''}{\theta'}\right) + O(\epsilon^2), \tag{G.30}$$

and

$$\phi\ \alpha = \mp\phi_b(u)\left(2\theta_2\theta' + \frac{\theta''}{(\theta')}\right) + O(\epsilon), \tag{G.31}$$

where now the $(-)$ sign is correct for an intersection point at the large-θ end of an asymptotic boundary segment and the $(+)$ sign holds at the small-θ end.

As a result, we find

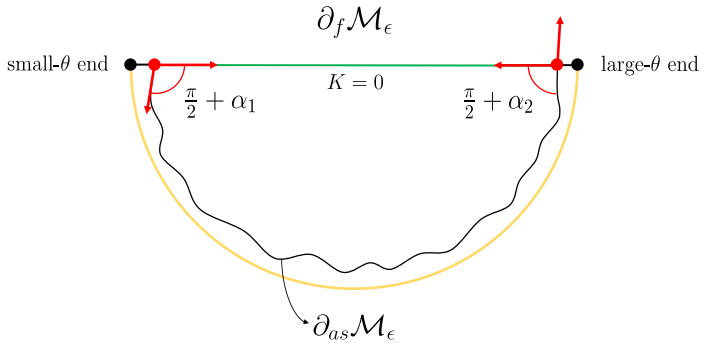

Figure G.4: The figures shows tangent vectors to $\partial_{as}\mathcal{M}$ in the direction of increasing θ and inward-directed tangents to $\partial_f \mathcal{M}$. When the finite boundaries are geodesics, the indicated angles α_i satisfy (G.29) and (G.31) with the signs stated in the text.

$$I = I_{top} - 2\int \phi_b(u)\left(\frac{1}{2}(\theta')^2 - \frac{1}{2}\left(\frac{\theta''}{\theta'}\right)^2\right) du + 4\sum_i \phi_b(u_i)\theta_{2,i}\theta'(u_i), \tag{G.32}$$

where $u_i, \theta_{2,i}$ are the u-value and θ_2-value of the ith intersection point between the finite and asymptotic boundaries. The natural boundary term in (G.25) has been cancelled by the $\phi_i\alpha_i$ contributions, but a new boundary term involving θ_2 remains. This is related to the fact that, as discussed in the main text, sewing together two boundaries may not result in an asymptotic boundary that is smooth at finite ϵ. In other words, the sewn-together manifold may not be associated with a smooth conformal factor Ω. We have seen, however, that the extension to conformal factors that allow $\sqrt{h}K$ to contain delta-functions causes no significant issues.

G.1.4 Positivity of the Schwarzian action

We now establish the positivity result needed in the main text. In particular, we consider manifolds $\mathcal{M}$ satisfying the above boundary conditions and which have *only* asymptotic boundaries (i.e., $\partial_f \mathcal{M} = \emptyset$.). Positivity of α, ϕ and the above-noted fact that we can freely choose any finite boundaries to be geodesics then immediately also imply a similar lower bound for the case of non-empty $\partial_f \mathcal{M}$.

As noted previously, we require I_{matter} to be minimally-coupled to the metric g. In particular, the dilaton ϕ should not appear in I_{matter}. We also require that I_{matter} be bounded below by zero when the metric g satisfies $R + 2 = 0$ and is locally asymptotically AdS_2. Since the topological term is minimized by taking the spacetime to be a disconnected union of disks, for fixed boundary conditions the full action will be bounded below if we can derive a lower bound for the Schwarzian action (G.25) for each disk; i.e., on each circular boundary. This is certainly to be expected since the Schwarzian action arises [270] (see also [167]) as an effective description of the low energy limit of (a limit of) the Sachdev-Ye-Kitaev model (first introduced in [271]), which is a standard quantum mechanical system. However, it is reassuring to see a direct argument[2].

For general $\phi_b(u)$, we would like to simplify (G.25) by defining a new coordinate $\tilde{u}$ such that

$$d\hat{u} = \frac{\hat{\phi}_b}{\phi_b} du. \tag{G.33}$$

We can think of this $\hat{u}$ as being associated with a different choice of conformal frame defined by $\hat{\Omega} := \frac{\hat{\phi}_b}{\phi_b}\Omega$, in which we see that the new boundary dilaton profile would be given by $\hat{\phi}_b$. Since we have required that Ω be specified as part of the definition of the system, it would not be correct to say that the coordinate transformation (G.33) actually

[2]It seems likely that this result is already somewhere in the vast literature concerning the Schwarzian action. The authors would be happy to receive references to earlier published versions of this result.

changes the boundary values of ϕ, but it nevertheless allows us to rewrite any function of the original ϕ_b boundary conditions in terms of another JT system with boundary conditions specified by $\hat{\phi}_b$. The Schwarzian action correspondingly becomes

$$\begin{aligned} I_{Schwarz} &:= -2\int du\, \phi_b(u)\, \mathrm{Sch}(\tan(\theta/2), u) \\ &= -2\int d\hat{u}\, \hat{\phi}_b(\hat{u})\, \mathrm{Sch}(\tan(\theta/2), \hat{u}) - \int du \left(\left(\partial_{\hat{u}} \frac{\hat{\phi}_b}{\phi_b} \right)^2 + 2\frac{\hat{\phi}_b}{\phi_b} \partial_{\hat{u}}^2 \frac{\hat{\phi}_b}{\phi_b} \right). \end{aligned} \tag{G.34}$$

The last term becomes manifestly non-negative after integrating by parts. Thus we only need to show that the first term is bounded below for any convenient $\hat{\phi}_b(u)$ (and with the period of $\hat{u}$ dictated by this choice via (G.33) andwith any convenient the period of $\hat{u}$). For simplicity, we choose $\hat{\phi}_b(u)$ to be a constant (which we again call $\bar{\phi}_b$). We also choose the period of $\hat{u}$ to be 2π, which then sets the value of $\bar{\phi}_b$ for a given $\phi_b(u)$.

To clean up the notation, we will henceforth write $\hat{u}$ as simply u so that the simplified action (dropping the final term in (G.34)) becomes

$$\begin{aligned} \bar{I}_{Schwarz} &= -2\int du\, \bar{\phi}_b(\hat{u})\, \mathrm{Sch}(\tan(\theta/2), u) \\ &= -\int du\, \bar{\phi}_b(\hat{u}) \left[(\theta')^2 - \left(\frac{\theta''}{\theta'} \right)^2 + 2\frac{d}{du} \left(\frac{\theta''}{\theta'} \right) \right]. \end{aligned} \tag{G.35}$$

Since we consider only circular boundaries, we can ignore the total derivative that gives the final term of (G.35). It is also convenient to write $\eta(u) = \theta'(u)$, so that $\bar{I}_{Schwarz}$ becomes

$$\bar{I}_{Schwarz} = -\bar{\phi}_b \int du \left(\eta^2 - \left(\frac{\eta'}{\eta} \right)^2 \right). \tag{G.36}$$

The expression (G.36) is to be evaluated on functions η that satisfy an important con-

straint, since θ must increase by 2π when u increases by 2π. In other words, we require

$$\int_0^{2\pi} du\, \eta = 2\pi. \tag{G.37}$$

We can take this constraint into account by adding a Lagrange multiplier to the action:

$$\bar{I}_{Schwarz} = -\bar{\phi}_b \left[\int du \left(\eta^2 - \left(\frac{\eta'}{\eta} \right)^2 \right) - \lambda \left(\int du\, \eta - 2\pi \right) \right]. \tag{G.38}$$

There is an obvious saddle of this action at $\eta = 1, \lambda = 2$. Perturbations around this saddle point may be studied by writing $\eta = 1 + \Upsilon$. Expanding (G.38) to quadratic order yields

$$\Delta \bar{I}_{Schwarz} = -\int du\, \bar{\phi}_b \left(\Upsilon^2 - (\Upsilon')^2 \right) = -\int du\, \bar{\phi}_b \left(\Upsilon^2 + \Upsilon\Upsilon'' \right) + \text{bdy terms}. \tag{G.39}$$

The eigenfunctions of the operator $\partial_u^2 + 1$ are

$$\Upsilon = e^{iku}, \quad k \in \mathbb{Z}, \tag{G.40}$$

with eigenvalues $-k^2 + 1$. The $k = 0$ mode thus has negative action, but it is forbidden the constraint

$$\int_0^{2\pi} du\, \Upsilon = 0. \tag{G.41}$$

The modes $k = \pm 1$ have vanishing action, and they turn out to correspond to the SL(2,$\mathbb{R}$) symmetries of the Schwarzian action. These are in fact gauge symmetries of JT gravity, though they appear as global symmetries of $\bar{I}_{Schwarz}$ due to the partial gauge-fixing used in deriving $\bar{I}_{Schwarz}$ [213]. Other modes all have positive quadratic action $\Delta \bar{I}_{Shcw}$.

The above analysis shows $\eta = 1$ to be a local minimum of the action over the space of allowed configurations. Importantly (and as we will see explicitly below), the same

must be true for all of the saddles that can be reached by following the flat directions associated with the SL(2,$\mathbb{R}$) symmetries. These of course share the same minimum value of $\bar{I}_{Schwarz}$.

However, we wish to show that this value is in fact a *global* minimum. One way to proceed is to note that (since we have fixed the winding number) the space of configurations is connected. As a result, if any configuration has lower action than $\eta = 1$, there is a path through configuration space that connects it to $\eta = 1$. Furthermore, starting at the $\eta = 1$ end of the path, the analysis above shows that the action must first increase before it can decrease. This is the case even if the path starts by following some path in the space $\mathcal{Z}$ of saddles related to $\eta = 1$ by SL(2,$\mathbb{R}$) zero modes, as it must clearly leave the space $\mathcal{Z}$ at some point and since we have shown that all paths leaving $\mathcal{Z}$ must first increase the action before the action can decrease.

As a result, along any given such path p there must be a point P_0 at which the action reaches a local maximum $\mu(p)$. Let us now attempt to minimize $\mu(p)$ over all paths p. So long there are no directions in which $\mu(p)$ remains finite at the edge of space of allowed configurations (i.e., when η diverges at some u), then the minimal $\mu(p)$ must in fact be a saddle s for the action $\bar{I}_{Schwarz}$ which satisfies $\bar{I}_{Schwarz}(s) > \bar{I}_{Schwarz}(\eta = 1)$; i.e., it must be a new saddle for the Schwarzian action.

While we will not exclude the runaway possibility with complete rigor, if the divergence in η admits any kind of asymptotic expansion at large λ it would certainly require the first two terms to cancel against each other at leading order. But such cancelation requires

$$\eta = \pm\eta'/\eta + \dots, \tag{G.42}$$

where $\dots$ represents lower order terms. Solving (G.42) yields $\pm\eta = \frac{1}{u+\Delta}$ where Δ is a function whose derivative Δ' vanishes vanishes as $\eta \to \infty$. Without loss of generality we

can take the point at which η diverges to be $u = 0$, in which case Δ is approximately constant near $u = 0$. As a result, the integral $\int \eta$ must diverge and the constraint (G.37) cannot be satisfied.

Thus, if the action were to be unbounded below, there must be a new saddle point. However, we will now seek such new saddles directly and show that they do not exist. To do so, note that the action can be equivalently written as the action of a particle in a potential by defining $\chi = \ln \eta$ to write

$$\bar{I}_{Schwarz} = \bar{\phi}_b \int du \, \left((\chi')^2 - (e^{2\chi} - \lambda e^{\chi} + \lambda) \right). \tag{G.43}$$

The solutions to saddle-point equations of motion can of course be labelled by the total energy E which we normalize as

$$(\chi')^2 + e^{2\chi} - \lambda e^{\chi} + \lambda = E. \tag{G.44}$$

Note further that the potential $V(\chi) = e^{2\chi} - \lambda e^{\chi} + \lambda$ always approaches λ as $u \to -\infty$, but that it does so in different ways depending on the value of λ. For $\lambda \leq 0$ the potential increases monotonically and all orbits are unbound. Here we use the term 'orbit' to refer to some $\chi(u)$ that solves the equation of motion obtained from (G.43) by varying χ, but which does not necessarily satisfy either the periodicity condition $\chi(u) = \chi(u + 2\pi)$ or the constraint (G.37). In contrast, for $\lambda > 0$ the potential has a single critical point at $\chi = \ln \lambda/2$ and at which $V = \lambda - \lambda^2/4$. This critical point is in fact a global minimum of the potential. Thus the case $\lambda > 0$ admits both unbound orbits (with $E \geq \lambda$) and bound orbits (with $E < \lambda$).

The potential remains finite in the asymptotic region of large negative χ, so the velocity in this region is finite. Since the unbound orbits all run to large negative χ, they

must thus take infinite time to reach $\chi = -\infty$. This means that there is no sense in which they can be periodic, and such orbits are not allowed.

We can therefore focus on the bound orbits. Let us first consider the special cases that sit at the global minimum for all time. Such solutions are clearly periodic with any period. However, they satisfy the constraint (G.37) only for $\chi = 0$, which then requires $\lambda = 2$, $E = 1$. For future reference we note that $E - \lambda = -1$.

Finally, we can investigate the constraints for the other bound states. The first constraint is that χ is periodic with period 2π,

$$\begin{aligned} 2\pi &= \int_0^{2\pi} du\, \chi' = 2\int_{\chi_-}^{\chi_+} \frac{d\chi}{\sqrt{E-\lambda-e^{2\chi}+\lambda e^{\chi}}} \\ &= 2\int_{\eta_-}^{\eta_+} \frac{d\eta}{\eta\sqrt{-(\eta-\eta_+)(\eta-\eta_-)}} = 2\pi i \frac{1}{\sqrt{E-\lambda}}, \end{aligned} \tag{G.45}$$

which again requires $E-\lambda = -1$. Here the second step in (G.45) used equation (G.44) and the quantities $\eta_\pm$ are defined by first defining $\chi_\pm$ to be the two roots of the denominator of the integrand and then setting $\eta_\pm = e^{\chi_\pm} = \frac{\lambda \pm \sqrt{\lambda^2+4E-4\lambda}}{2}$. The final answer on the right-hand-side was obtained by noting that the integral over η can be expressed as a contour integral around a branch cut from η_- to η_+. Since the contour integral for large η vanishes, the final answer is given by the residue of the pole at $\eta = 0$.

The second constraint turns out to be trivially satisfied for any E and λ since we find

$$\int du\, \eta = 2\int_{\eta_-}^{\eta_+} \frac{\eta}{\eta'} = 2\int_{\eta_-}^{\eta_+} \frac{1}{\sqrt{-(\eta-\eta_+)(\eta-\eta_-)}} = 2\pi. \tag{G.46}$$

Again, in the final step the integration is performed using complex contour integration techniques. Thus we see that all saddles have $E - \lambda = -1$, but that there is a saddle for each $\lambda \in \mathbb{R}$ (or, equivalently, for each real E). The original $\eta = 1$ saddle lies in this family with $\lambda = 2$, which corresponds to the case where $\eta_+ = \eta_-$.

All of these solutions turn out to have the same action, consistent with the earlier statement that there is a family of solutions related by an SL(2,$\mathbb{R}$) symmetry. To see this, note that the Schwarzian action is given by

$$\begin{aligned}\bar{I}_{Schwarz} &= \bar{\phi}_b \int_0^{2\pi} du\ \left((\chi')^2 - (e^{2\chi} - \lambda e^{\chi} + \lambda)\right) \\ &= \bar{\phi}_b \int_0^{2\pi} du\ \left(E - 2(e^{2\chi} - \lambda e^{\chi} + \lambda)\right) \\ &= 2\bar{\phi}_b \int_{\eta_-}^{\eta_+} d\eta\, \frac{E - 2\eta^2 + 2\lambda\eta - 2\lambda}{\eta'} \\ &= 2\bar{\phi}_b \int_{\eta_-}^{\eta_+} d\eta\, \frac{E - 2\eta^2 + 2\lambda\eta - 2\lambda}{\eta\sqrt{E - \eta^2 + \lambda\eta - \lambda}},\end{aligned} \tag{G.47}$$

where still need to set $E - \lambda = -1$. This integral can once again be tackled by the methods of complex methods. The integrand has poles at $\eta = 0, \infty$, so this integral can be evaluated using their residues to find

$$\bar{I}_{Schwarz} = \bar{\phi}_b 2\pi i\sqrt{E - \lambda} = -2\pi\bar{\phi}_b, \tag{G.48}$$

which is a constant independent of λ. Note that this corresponds to the action in section 8.2 with $\beta = 2\pi$.

As also expected from the SL(2,$\mathbb{R}$) symmetry, linearizing about any such saddle gives identical results to linearizing about $\eta = 1$. This observation completes the argument that (G.48) is in fact the minimum value of $\bar{I}_{Schwarz}$, and thus that the Schwarzian action is bounded below.

Allowing a general β, multiple S^1 boundaries labelled by j, and restoring the topological term would yield the general bound

$$I = I_{top} + I_{Schwarz} \geq -\sum_j \left(4\pi\phi_0 + 4\pi^2\bar{\phi}_b/\beta_j\right). \tag{G.49}$$

G.2 Cut-and-paste Asymptotically locally AdS boundary conditions for the Einstein-Hilbert action with boundary counterterms

The standard treatments of Asymptotically locally AdS (AlAdS) boundary conditions, and in particular standard discussions of boundary counterterms, typically assume that all structures should be smooth (see e.g. [196] for a review and references). However, as described in detail for JT gravity in appendix G.1, our cut-and-paste constructions generally lead to some lack of differentiability. The purpose of this section is thus to extend such boundary conditions and to establish the various properties of the action needed for section 8.3.3.

The form of our cut-and-paste construction will make this straightforward. The conical singularities required were already addressed thoroughly in [73] (and in any case do not affect the asymptotic boundary conditions). In addition, as argued in section 8.3.3, the bulk terms in the action remain finite and well-defined under our operations. We thus need only consider the effects of these operations on the asymptotic region of the spacetime.

Since section 8.3.3 chooses to slice the smooth spacetimes along minimal surfaces, our study of the asymptotics will be facilitated by understanding the asymptotics of codimension-1 minimal surfaces Σ in smooth AlAdS spacetimes. We are interested in surfaces that are anchored on the asymptotic boundary, in the sense that $\partial\Sigma$ is a smooth codimension-1 submanifold of $\partial\mathcal{M}$. These anchor sets are always boundaries of the form $\partial M_a = \partial M_b$ at which two source manifolds-with-boundaries M_a, M_b are sewn together

to form some closed manifold $\tilde{M}_{ab}$. Furthermore, by the rim requirement of section 8.3.2, such boundaries always lie in cylinders $\mathcal{C}_\epsilon$ of the form discussed in section 8.3.1.

It is thus convenient to define a Euclidean "time" coordinate t_E on the AlAdS boundary $\tilde{M}$ such that t_E is constant on each cut on which our extremal surface is to be anchored, and for which the (unphysical) AlAdS boundary metric has $g^{(0)}_{t_E t_E} = 1$. We make take any connected component of the anchor set to be of the form $t_E = t_0$.

Consider in particular the part of the extremal surface near this anchor set. When the bulk AlAdS spacetime has dimension $d+1$, we may introduce $d-1$ coordinates dx^i on the $t = t_0$ slice and use these (along with t) to construct a Fefferman-Graham coordinate system near $\tilde{M}$. The codimension-1 minimal surface can of course be found by minimizing the volume functional

$$V[\Sigma] = \int_\Sigma \sqrt{g_\Sigma} = \int_\Sigma dz dx^{d-1} z^{-d} \sqrt{g^{(0)}_{\partial\Sigma}} \sqrt{1 + (\partial_z t_E)^2} (1 + \dots), \tag{G.50}$$

where g_Σ is the determinant of the induced metric on Σ, $g^{(0)}_\Sigma$ is the determinant of the metric induced on $\partial\Sigma$ by the (unphysical) AlAdS boundary metric $g^{(0)}$, and $\dots$ denotes terms that are subleading as $z \to 0$.

The Euler-Lagrange equation associated with extremizing (G.50) is then proportional to

$$0 = \partial_z \frac{1}{z^d \sqrt{1 + (\partial_z t_E)^2}} \partial_z t_E (1 + \dots), \tag{G.51}$$

which for some constant C yields

$$C z^d \sqrt{1 + (\partial_z t_E)^2} = \partial_z t_E (1 + \dots), \tag{G.52}$$

whence we find

$$\partial_z t_E = O(z^d), \quad \text{and thus} \quad t_E = t_0 + O(z^{d+1}). \tag{G.53}$$

As a result, our cut-and-paste construction using minimal surfaces clearly defines spacetimes in which the usual Fefferman-Graham expansion holds up to possible corrections at order z^{d+1} relative to the leading terms. Since all divergences in the gravitational action are associated with terms that are at most of order z^{d-1}, an action defined using the standard boundary counter-terms will remain finite on such spacetimes. In particular, the traced extrinsic curvature K of a $z = constant$ surface will contain a delta-function $\delta(t-t_0)$, but with a coefficient of order z^{d+1}. Since the volume element on the asymptotic boundary is only $O(z^{-d})$, this means that such a delta-function makes no contribution to the Gibbons-Hawking term at $z = 0$.

Furthermore, since the boundary stress tensor T^{IJ}_{bndy} is associated with the term of order z^d in the Fefferman-Graham expansion of the bulk metric, it remains well-defined as well. Here we use I, J to denote $\{t_E, x^i\}$. Thus by the usual computation we may write the variation of the action as

$$\delta I = \int_{\partial \mathcal{M}} T^{ij}_{bndy} \delta g^{(0)}_{ij} + \text{EOM terms}, \tag{G.54}$$

where EOM terms denotes terms proportional to the usual bulk equations of motion. In particular, from this we see that the standard action continues to give a good variational principle for our cut-and-paste spacetimes. As a result, we are free to extend the domain of the usual action to include the above non-smooth spacetimes without further modifications.

Appendix H

Appendix to Chapter 9

H.1 The operator norm of the unnormalized cylinder operator C_β approaches 1 at small β.

We now provide the proof of the following lemma:

Lemma 3 *The operator norm $||C_\beta||$ of the (unnormalized) cylinder operator satisfies $||C_\beta|| \to 1$ as $\beta \to 0$.*

To show that this is the case, recall that since $C_\beta \in Y^d_{B \sqcup B}$ it defines a bounded operator. Furthermore, since $C_\beta = C^*_\beta$ and $C^t_\beta = C_\beta$, we have $C^\dagger_\beta = C^\star_\beta = C_\beta$, so that C_β is self-adjoint and can be diagonalized. Furthermore, since $C_\beta = C^\dagger_{\beta/2} C_{\beta/2}$, the eigenvalues of C_β are non-negative.

Now consider the family of operators $C_{\beta/n}$ for $n \in \mathbb{Z}^+$ and some fixed value of β. The norm $||C_{\beta/n}||$ is the supremum of the set of eigenvalues of $C_{\beta/n}$. But the operators $C_{\beta/n}$ have a common set of eigenstates $|\lambda\rangle$ with eigenvalues $\lambda^{1/n}$ for some bounded set of

positive real numbers λ. In particular, we have

$$||C_{\beta/n}|| = \sup_{\lambda} \lambda^{1/n} = (\sup_{\lambda} \lambda)^{1/n} = ||C_{\beta}||^{1/n}. \tag{H.1}$$

Thus

$$\lim_{n\to\infty} ||C_{\beta/n}|| = 1. \tag{H.2}$$

This establishes that we can find sequences of C_β with $\beta \to 0$ for which $||C_\beta|| \to 1$. However, it remains to show that this convergence is sufficiently uniform that $||C_\beta||$ converges for an arbitrary sequence of C_β with $\beta \to 0$.

Suppose first that $||C_\beta|| \leq 1$ for all β. Then since $C_{\beta_1+\beta_2} = C_{\beta_1}C_{\beta_2}$ for $\beta_1, \beta_2 > 0$, we have

$$||C_{\beta_1+\beta_2}|| \leq ||C_{\beta_1}||||C_{\beta_1}|| \leq ||C_{\beta_1}||. \tag{H.3}$$

In particular, in this case for all β we find that $||C_\beta||$ is monotonically increasing as β decreases. Thus (H.2) for any fixed β implies $\lim_{\beta\to 0} ||C_\beta|| = 1$.

The remaining case occurs when $||C_{\beta_0}|| \geq 1$ for some β_0. We will now show both that this requires $||C_\beta|| > 1$ for all small enough β, and that small enough $||C_\beta||$ are bounded above by a quantity that tends to 1. This will then establish $\lim_{\beta\to 0} ||C_\beta|| = 1$ for this final case.

The condition $||C_{\beta_0}|| \geq 1$ means that there is some state $|\psi\rangle$ for which $\langle\psi|C_{2\beta_0}|\psi\rangle \geq \langle\psi|\psi\rangle$. Now, recall that states of the form $|a\rangle$ for $a \in \underline{Y}^d_{B\sqcup B}$ are dense in $\mathcal{H}_{LR}$, so that any state $|\psi\rangle$ can be approximated by such $|a\rangle$. Since $C_{2\beta_0}$ is bounded, the expectation value of $C_{2\beta_0}$ is a continuous function of $|\psi\rangle$. Thus there must also be some $|a\rangle$ for which $\langle a|C_{2\beta_0}|a\rangle = \lambda\langle a|a\rangle$ with $\lambda > 1$.

Let us now consider some small β and write $\beta_0 = \lfloor \frac{\beta_0}{\beta} \rfloor \beta + \Delta$. Here we use the notation $\lfloor \beta_0/\beta \rfloor$ to denote the greatest integer less than β_0/β. Thus $0 \leq \Delta \leq \beta$. As a result, the

continuity axiom (Axiom 4) requires

$$\langle a|C_{2\Delta}|a\rangle \to \langle a|a\rangle \tag{H.4}$$

as $\beta \to 0$. Since we have

$$\lambda\langle a|a\rangle = \langle a|C_{2\beta}|a\rangle = \langle a|C_\Delta C_{2n\beta'} C_\Delta|a\rangle \leq ||C_\beta||^{2n}\langle a|C_{2\Delta}|a\rangle, \tag{H.5}$$

equation (H.4) tells us that for any $\epsilon > 0$ we can find a β_1 such that for $\beta < \beta_1$ we have $\langle a|C_{2\Delta}|a\rangle \leq (1+\epsilon)\langle a|a\rangle$, and thus

$$\langle a|a\rangle \leq ||C_{\beta'}||^{2n}(1+\epsilon). \tag{H.6}$$

Let us now choose $1+\epsilon < \lambda$. Then from (H.6) we see that there must be a β_1 such that $||C_\beta|| \geq \left(\frac{\lambda}{1+\epsilon}\right)^{1/2n} \geq 1$ for all $\beta < \beta_1$.

On the other hand, we can also show that $||C_\beta||$ is bounded above by a quantity that tends to 1 as $\beta \to 0$. To do so recall that

$$||C_\beta|| \leq \text{tr } C_\beta, \tag{H.7}$$

and that tr C_β is a continuous function of β for $\beta > 0$. As a result, on any fixed interval $[\beta_2, 2\beta_2]$ we find tr $C_\beta \leq \mathcal{C}$ for some constant $\mathcal{C} > 0$. Thus (H.7) requires $||C_\beta|| \leq \mathcal{C}$ on this interval as well.

Furthermore, as discussed above, for any β we have $||C_{\beta/n}|| = ||C_\beta||^{1/n}$. Since any $\beta > 0$ with $\beta < \beta_2$ can be written as β'/n for some $\beta' \in [\beta_2, 2\beta_2]$, this gives us an upper bound $\mathcal{C}^{1/n}$ on such $||C_\beta||$, where $n = \lfloor 2\beta_2/\beta \rfloor$. Combining this with the above

observation yields

$$1 \leq ||C_\beta|| \leq \mathcal{C}^{1/n}. \tag{H.8}$$

And since $\mathcal{C}^{1/n} \to 1$ as $\beta \to 0$, we must have $||C_\beta|| \to 1$ as claimed.

H.2 The trace is normal and semifinite

This appendix establishes that the traces (9.38) on the von Neumann algebras $\mathcal{A}_L^B$, $\mathcal{A}_R^B$ are both normal and semifinite. We call these properties Lemmas 1 and 2 below. Recall that normality and semifiniteness were defined in properties 5 and 6 of section 9.4.1.

Lemma 4 *The trace* tr *defined by* (9.38) *is normal on both* $\mathcal{A}_L^B$ *and* $\mathcal{A}_R^B$.

We will give the proof for $\mathcal{A}_L^B$. The argument for $\mathcal{A}_R^B$ is directly analogous.

Proof: Consider an increasing sequence of positive operators $a_n \in \mathcal{A}_L^B$. For each a_n we have

$$\text{tr } a_n := \sup_{\beta>0} \langle \tilde{C}_\beta | a_n | \tilde{C}_\beta \rangle. \tag{H.9}$$

Furthermore, for an increasing sequence of positive operators, the expectation value in any state $|\psi\rangle$ is also an increasing sequence; i.e., $a_n + 1 \geq a_{n+1}$ implies $\langle\psi|a_{n+1}|\psi\rangle \geq \langle\psi|a_n|\psi\rangle$ (where it is possible that both sides diverge). Thus

$$\langle\psi| \left(\sup_n a_n \right) |\psi\rangle \geq \sup_n \langle\psi|a_n|\psi\rangle = \lim_{n\to\infty} \langle\psi|a_n|\psi\rangle. \tag{H.10}$$

In fact, proposition 4.64 of shows that the above is actually an equality:

$$\langle\psi| \left(\sup_n a_n \right) |\psi\rangle = \sup_n \langle\psi|a_n|\psi\rangle = \lim_{n\to\infty} \langle\psi|a_n|\psi\rangle. \tag{H.11}$$

Combining these results gives

$$\begin{aligned} \mathrm{tr}\left(\sup_n a_n\right) &= \sup_\beta \left(\langle \tilde{C}_\beta | (\sup_n a_n) | \tilde{C}_\beta \rangle \right) = \sup_\beta \sup_n \langle \tilde{C}_\beta | a_n | \tilde{C}_\beta \rangle \\ &= \sup_{n,\beta} \langle \tilde{C}_\beta | a_n | \tilde{C}_\beta \rangle = \sup_n \sup_\beta \langle \tilde{C}_\beta | a_n | \tilde{C}_\beta \rangle = \sup_n (\mathrm{tr}\ a_n)\,. \end{aligned} \tag{H.12}$$

The key point in (H.12) is that taking the supremum over n always commutes with taking the supremum over β since taking both supremums (in either order) is equivalent to taking the supremum over all pairs (n, β). This result is the desired normality property.

■

Lemma 5 *The trace* tr *defined by* (9.38) *is semifinite on both* $\mathcal{A}_L^B$ *and* $\mathcal{A}_R^B$.

We will give the proof for $\mathcal{A}_L^B$. The argument for $\mathcal{A}_R^B$ is directly analogous.

Proof: We need only show that every positive $a \in \mathcal{A}_L^B$ satisfies $a > b$ for some positive $b \in \mathcal{A}_L^B$ with finite trace, where the notation $a > b$ means that $a - b$ is positive.

Let us begin by recalling that the normalized cylinder operator $\tilde{C}_{2\beta}$ has operator norm 1 but is not the identity. Thus $\mathbb{1} - \tilde{C}_{2\beta}$ is positive. It then follows that $\gamma^\dagger(\mathbb{1} - \tilde{C}_{2\beta})\gamma$ is also positive for any γ, since the expectation value in any state $|\psi\rangle$ will satisfy

$$\langle \psi | \gamma^\dagger (\mathbb{1} - \tilde{C}_{2\beta}) \gamma | \psi \rangle = \langle \gamma\psi | (\mathbb{1} - \tilde{C}_{2\beta}) | \gamma\psi \rangle \geq 0, \tag{H.13}$$

where we have momentarily defined $|\gamma\psi\rangle := \gamma|\psi\rangle$ even for γ not in $\hat{A}_L^B$. The positivity of $\gamma^\dagger(\mathbb{1} - \tilde{C}_{2\beta})\gamma$ is then equivalent to the statement

$$\gamma^\dagger \gamma > \gamma^\dagger \tilde{C}_{2\beta} \gamma. \tag{H.14}$$

Next recall that since a is positive it is in fact of the form $\gamma^\dagger\gamma$ for $\gamma \in \mathcal{A}_L^B$. The above result then implies that our trace is semifinite if we can show that $b = \gamma^\dagger \tilde{C}_{2\beta} \gamma$ has finite

trace. We have

$$\begin{aligned} \mathrm{tr}(\gamma^\dagger \tilde{C}_{2\beta}\gamma) &= \sup_{\beta'} \langle \tilde{C}_{\beta'}|\gamma^\dagger \tilde{C}_{2\beta}\gamma|\tilde{C}_{\beta'}\rangle \\ &= \sup_{\beta'} \langle \tilde{C}_{\beta}|\gamma \tilde{C}_{2\beta'}\gamma^\dagger|\tilde{C}_{\beta}\rangle < \langle \tilde{C}_{\beta}|\gamma\gamma^\dagger|\tilde{C}_{\beta}\rangle. \end{aligned} \tag{H.15}$$

Here we have used (9.48) to pass from the first line to the second, and the final step follows from the fact that $\langle \tilde{C}_\beta|\gamma\tilde{C}_{2\beta'}\gamma^\dagger|\tilde{C}_\beta\rangle$ is the expectation value of $\tilde{C}_{2\beta'}$ in the state $\gamma^\dagger|\tilde{C}_\beta\rangle$ together with the above observation that $||C_{2\beta'}|| \leq 1$. The right-hand side is clearly finite, so this establishes that our $b < a$ has finite trace, so that tr is semifinite as claimed. ■

Bibliography

[1] X. Dong, D. Marolf, P. Rath, A. Tajdini, and Z. Wang, *The spacetime geometry of fixed-area states in gravitational systems*, *JHEP* **08** (2022) 158, [arXiv:2203.0497].

[2] H. Maxfield and Z. Wang, *Gravitating spinning strings in AdS_3*, *JHEP* **07** (2022) 075, [arXiv:2203.0249].

[3] D. Marolf and Z. Wang, *Time-independence of gravitational Rényi entropies and unitarity in quantum gravity*, *JHEP* **10** (2021) 196, [arXiv:2106.0783].

[4] S. Colin-Ellerin, X. Dong, D. Marolf, M. Rangamani, and Z. Wang, *Real-time gravitational replicas: Low dimensional examples*, *JHEP* **08** (5, 2021) 171, [arXiv:2105.0700].

[5] A. Al Balushi, Z. Wang, and D. Marolf, *Traversability of Multi-Boundary Wormholes*, *JHEP* **04** (2021) 083, [arXiv:2012.0463].

[6] S. Colin-Ellerin, X. Dong, D. Marolf, M. Rangamani, and Z. Wang, *Real-time gravitational replicas: Formalism and a variational principle*, *JHEP* **05** (12, 2020) 117, [arXiv:2012.0082].

[7] D. Marolf, S. Wang, and Z. Wang, *Probing phase transitions of holographic entanglement entropy with fixed area states*, *JHEP* **12** (6, 2020) 084, [arXiv:2006.1008].

[8] D. Marolf, A. C. Wall, and Z. Wang, *Restricted Maximin surfaces and HRT in generic black hole spacetimes*, *JHEP* **05** (2019) 127, [arXiv:1901.0387].

[9] Z. Fu, A. Maloney, D. Marolf, H. Maxfield, and Z. Wang, *Holographic complexity is nonlocal*, *JHEP* **02** (2018) 072, [arXiv:1801.0113].

[10] R. L. Arnowitt, S. Deser, and C. W. Misner, *The Dynamics of general relativity*, *Gen. Rel. Grav.* **40** (2008) 1997–2027, [gr-qc/0405109].

[11] S. W. Hawking, *Particle Creation by Black Holes*, *Commun. Math. Phys.* **43** (1975) 199–220. [Erratum: Commun.Math.Phys. 46, 206 (1976)].

[12] J. D. Bekenstein, *Black holes and entropy*, *Phys. Rev. D* **7** (1973) 2333–2346.

[13] G. 't Hooft, *Dimensional reduction in quantum gravity*, *Conf. Proc. C* **930308** (1993) 284–296, [gr-qc/9310026].

[14] L. Susskind, *The World as a hologram*, *J. Math. Phys.* **36** (1995) 6377–6396, [hep-th/9409089].

[15] J. M. Maldacena, *The Large N limit of superconformal field theories and supergravity*, *Adv. Theor. Math. Phys.* **2** (1998) 231–252, [hep-th/9711200].

[16] S. S. Gubser, I. R. Klebanov, and A. M. Polyakov, *Gauge theory correlators from noncritical string theory*, *Phys. Lett. B* **428** (1998) 105–114, [hep-th/9802109].

[17] E. Witten, *Anti-de Sitter space and holography*, *Adv. Theor. Math. Phys.* **2** (1998) 253–291, [hep-th/9802150].

[18] O. Aharony, S. S. Gubser, J. M. Maldacena, H. Ooguri, and Y. Oz, *Large N field theories, string theory and gravity*, *Phys. Rept.* **323** (2000) 183–386, [hep-th/9905111].

[19] J. M. Maldacena, *Eternal black holes in anti-de Sitter*, *JHEP* **04** (2003) 021, [hep-th/0106112].

[20] D. Harlow and D. Stanford, *Operator Dictionaries and Wave Functions in AdS/CFT and dS/CFT*, arXiv:1104.2621.

[21] A. Hamilton, D. N. Kabat, G. Lifschytz, and D. A. Lowe, *Holographic representation of local bulk operators*, *Phys. Rev. D* **74** (2006) 066009, [hep-th/0606141].

[22] T. Banks, M. R. Douglas, G. T. Horowitz, and E. J. Martinec, *AdS dynamics from conformal field theory*, hep-th/9808016.

[23] A. Almheiri, X. Dong, and D. Harlow, *Bulk Locality and Quantum Error Correction in AdS/CFT*, *JHEP* **04** (2015) 163, [arXiv:1411.7041].

[24] X. Dong, D. Harlow, and A. C. Wall, *Reconstruction of Bulk Operators within the Entanglement Wedge in Gauge-Gravity Duality*, *Phys. Rev. Lett.* **117** (2016), no. 2 021601, [arXiv:1601.0541].

[25] D. Harlow, *The Ryu–Takayanagi Formula from Quantum Error Correction*, *Commun. Math. Phys.* **354** (2017), no. 3 865–912, [arXiv:1607.0390].

[26] S. Ryu and T. Takayanagi, *Holographic derivation of entanglement entropy from AdS/CFT*, *Phys. Rev. Lett.* **96** (2006) 181602, [hep-th/0603001].

[27] V. E. Hubeny, M. Rangamani, and T. Takayanagi, *A Covariant holographic entanglement entropy proposal*, *JHEP* **07** (2007) 062, [arXiv:0705.0016].

[28] T. Faulkner, A. Lewkowycz, and J. Maldacena, *Quantum corrections to holographic entanglement entropy*, *JHEP* **11** (2013) 074, [arXiv:1307.2892].

[29] N. Engelhardt and A. C. Wall, *Quantum Extremal Surfaces: Holographic Entanglement Entropy beyond the Classical Regime*, *JHEP* **01** (2015) 073, [arXiv:1408.3203].

[30] J. D. Bekenstein, *Black holes and the second law*, *Lett. Nuovo Cim.* **4** (1972) 737–740.

[31] J. D. Bekenstein, *Generalized second law of thermodynamics in black hole physics*, *Phys. Rev. D* **9** (1974) 3292–3300.

[32] G. W. Gibbons and S. W. Hawking, *Action Integrals and Partition Functions in Quantum Gravity*, *Phys. Rev.* **D15** (1977) 2752–2756.

[33] A. Lewkowycz and J. Maldacena, *Generalized gravitational entropy*, *JHEP* **08** (2013) 090, [arXiv:1304.4926].

[34] X. Dong, A. Lewkowycz, and M. Rangamani, *Deriving covariant holographic entanglement*, *JHEP* **11** (2016) 028, [arXiv:1607.0750].

[35] X. Dong and A. Lewkowycz, *Entropy, Extremality, Euclidean Variations, and the Equations of Motion*, *JHEP* **01** (2018) 081, [arXiv:1705.0845].

[36] A. Almheiri, N. Engelhardt, D. Marolf, and H. Maxfield, *The entropy of bulk quantum fields and the entanglement wedge of an evaporating black hole*, *JHEP* **12** (2019) 063, [arXiv:1905.0876].

[37] G. Penington, *Entanglement Wedge Reconstruction and the Information Paradox*, *JHEP* **09** (5, 2019) 002, [arXiv:1905.0825].

[38] G. Penington, S. H. Shenker, D. Stanford, and Z. Yang, *Replica wormholes and the black hole interior*, *JHEP* **03** (11, 2019) 205, [arXiv:1911.1197].

[39] A. Almheiri, T. Hartman, J. Maldacena, E. Shaghoulian, and A. Tajdini, *Replica Wormholes and the Entropy of Hawking Radiation*, *JHEP* **05** (11, 2019) 013, [arXiv:1911.1233].

[40] G. Gibbons, S. Hawking, and M. Perry, *Path Integrals and the Indefiniteness of the Gravitational Action*, *Nucl. Phys. B* **138** (1978) 141–150.

[41] T. Prestidge, *Dynamic and thermodynamic stability and negative modes in Schwarzschild-anti-de Sitter*, *Phys. Rev. D* **61** (2000) 084002, [hep-th/9907163].

[42] B. Kol, *The Power of Action: The Derivation of the Black Hole Negative Mode*, *Phys. Rev. D* **77** (2008) 044039, [hep-th/0608001].

[43] M. Headrick and T. Wiseman, *Ricci flow and black holes*, *Class. Quant. Grav.* **23** (2006) 6683–6708, [hep-th/0606086].

[44] D. Marolf and J. E. Santos, *The Canonical Ensemble Reloaded: The Complex-Stability of Euclidean quantum gravity for Black Holes in a Box*, arXiv:2202.1178.

[45] D. Marolf and J. E. Santos, *Stability of the microcanonical ensemble in Euclidean Quantum Gravity*, arXiv:2202.1236.

[46] D. Marolf, *Gravitational thermodynamics without the conformal factor problem: Partition functions and Euclidean saddles from Lorentzian Path Integrals*, *JHEP* **07** (3, 2022) 108, [arXiv:2203.0742].

[47] X. Dong, D. Harlow, and D. Marolf, *Flat entanglement spectra in fixed-area states of quantum gravity*, *JHEP* **10** (2019) 240, [arXiv:1811.0538].

[48] C. Akers and P. Rath, *Holographic Renyi Entropy from Quantum Error Correction*, *JHEP* **05** (2019) 052, [arXiv:1811.0517].

[49] J. M. Maldacena and L. Maoz, *Wormholes in AdS*, *JHEP* **02** (2004) 053, [hep-th/0401024].

[50] P. Saad, S. H. Shenker, and D. Stanford, *A semiclassical ramp in SYK and in gravity*, arXiv:1806.0684.

[51] P. Saad, S. H. Shenker, and D. Stanford, *JT gravity as a matrix integral*, arXiv:1903.1111.

[52] A. Maloney and E. Witten, *Averaging over Narain moduli space*, *JHEP* **10** (2020) 187, [arXiv:2006.0485].

[53] N. Afkhami-Jeddi, H. Cohn, T. Hartman, and A. Tajdini, *Free partition functions and an averaged holographic duality*, *JHEP* **01** (2021) 130, [arXiv:2006.0483].

[54] D. Marolf and H. Maxfield, *Transcending the ensemble: baby universes, spacetime wormholes, and the order and disorder of black hole information*, *JHEP* **08** (2020) 044, [arXiv:2002.0895].

[55] D. Marolf and H. Maxfield, *Observations of Hawking radiation: the Page curve and baby universes*, *JHEP* **04** (10, 2020) 272, [arXiv:2010.0660].

[56] M. Takesaki, *Theory of Operator Algebras I, II, III.* Springer, 1979.

[57] S. Balakrishnan, T. Faulkner, Z. U. Khandker, and H. Wang, *A General Proof of the Quantum Null Energy Condition*, *JHEP* **09** (2019) 020, [arXiv:1706.0943].

[58] T. Faulkner, R. G. Leigh, O. Parrikar, and H. Wang, *Modular Hamiltonians for Deformed Half-Spaces and the Averaged Null Energy Condition*, *JHEP* **09** (2016) 038, [arXiv:1605.0807].

[59] S. Leutheusser and H. Liu, *Causal connectability between quantum systems and the black hole interior in holographic duality*, arXiv:2110.0549.

[60] S. Leutheusser and H. Liu, *Emergent times in holographic duality*, arXiv:2112.1215.

[61] E. Witten, *Gravity and the Crossed Product*, arXiv:2112.1282.

[62] V. Chandrasekaran, G. Penington, and E. Witten, *Large N algebras and generalized entropy*, arXiv:2209.1045.

[63] G. Penington and E. Witten, *Algebras and States in JT Gravity*, arXiv:2301.0725.

[64] V. Chandrasekaran, R. Longo, G. Penington, and E. Witten, *An algebra of observables for de Sitter space*, *JHEP* **02** (2023) 082, [arXiv:2206.1078].

[65] C. Murthy and M. Srednicki, *Structure of chaotic eigenstates and their entanglement entropy*, *Phys. Rev.* **E100** (2019), no. 2 022131, [arXiv:1906.0429].

[66] S. Ryu and T. Takayanagi, *Aspects of Holographic Entanglement Entropy*, *JHEP* **08** (2006) 045, [hep-th/0605073].

[67] L. Vidmar and M. Rigol, *Entanglement Entropy of Eigenstates of Quantum Chaotic Hamiltonians*, *Phys. Rev. Lett.* **119** (2017), no. 22 220603, [arXiv:1708.0845].

[68] C. T. Asplund, A. Bernamonti, F. Galli, and T. Hartman, *Holographic Entanglement Entropy from 2d CFT: Heavy States and Local Quenches*, *JHEP* **02** (2015) 171, [arXiv:1410.1392].

[69] N. Bao and H. Ooguri, *Distinguishability of black hole microstates*, *Phys. Rev.* **D96** (2017), no. 6 066017, [arXiv:1705.0794].

[70] M. Banados, C. Teitelboim, and J. Zanelli, *The Black hole in three-dimensional space-time*, *Phys. Rev. Lett.* **69** (1992) 1849–1851, [hep-th/9204099].

[71] M. Banados, M. Henneaux, C. Teitelboim, and J. Zanelli, *Geometry of the (2+1) black hole*, *Phys. Rev. D* **48** (1993) 1506–1525, [gr-qc/9302012]. [Erratum: Phys.Rev.D 88, 069902 (2013)].

[72] X. Dong and H. Wang, *Enhanced corrections near holographic entanglement transitions: a chaotic case study*, *JHEP* **11** (6, 2020) 007, [arXiv:2006.1005].

[73] X. Dong and D. Marolf, *One-loop universality of holographic codes*, *JHEP* **03** (2020) 191, [arXiv:1910.0632].

[74] X. Dong, *The Gravity Dual of Renyi Entropy*, *Nature Commun.* **7** (2016) 12472, [arXiv:1601.0678].

[75] D. L. Jafferis, A. Lewkowycz, J. Maldacena, and S. J. Suh, *Relative entropy equals bulk relative entropy*, *JHEP* **06** (2016) 004, [arXiv:1512.0643].

[76] S. Fischetti and D. Marolf, *Complex Entangling Surfaces for AdS and Lifshitz Black Holes?*, *Class. Quant. Grav.* **31** (2014), no. 21 214005, [arXiv:1407.2900].

[77] M. Headrick and T. Takayanagi, *A Holographic proof of the strong subadditivity of entanglement entropy*, *Phys. Rev. D* **76** (2007) 106013, [arXiv:0704.3719].

[78] A. C. Wall, *Maximin Surfaces, and the Strong Subadditivity of the Covariant Holographic Entanglement Entropy*, *Class. Quant. Grav.* **31** (2014), no. 22 225007, [arXiv:1211.3494].

[79] N. Bao, G. Penington, J. Sorce, and A. C. Wall, *Beyond Toy Models: Distilling Tensor Networks in Full AdS/CFT*, *JHEP* **19** (2020) 069, [arXiv:1812.0117].

[80] J. Brown and M. Henneaux, *Central Charges in the Canonical Realization of Asymptotic Symmetries: An Example from Three-Dimensional Gravity*, *Commun. Math. Phys.* **104** (1986) 207–226.

[81] P. Calabrese and J. L. Cardy, *Entanglement entropy and quantum field theory*, *J. Stat. Mech.* **0406** (2004) P06002, [hep-th/0405152].

[82] P. Calabrese and J. Cardy, *Entanglement entropy and conformal field theory*, *J. Phys.* **A42** (2009) 504005, [arXiv:0905.4013].

[83] V. E. Hubeny, H. Maxfield, M. Rangamani, and E. Tonni, *Holographic entanglement plateaux*, *JHEP* **08** (2013) 092, [arXiv:1306.4004].

[84] I. A. Morrison and M. M. Roberts, *Mutual information between thermo-field doubles and disconnected holographic boundaries*, *JHEP* **07** (2013) 081, [arXiv:1211.2887].

[85] K. Krasnov, *Holography and Riemann surfaces*, *Adv. Theor. Math. Phys.* **4** (2000) 929–979, [hep-th/0005106].

[86] K. Krasnov, *Black hole thermodynamics and Riemann surfaces*, *Class. Quant. Grav.* **20** (2003) 2235–2250, [gr-qc/0302073].

[87] K. Skenderis and B. C. van Rees, *Holography and wormholes in 2+1 dimensions*, *Commun. Math. Phys.* **301** (2011) 583–626, [arXiv:0912.2090].

[88] D. Marolf and J. Wien, *Adiabatic corrections to holographic entanglement in thermofield doubles and confining ground states*, *JHEP* **09** (2016) 058, [arXiv:1605.0280].

[89] S. Bhattacharyya, V. E. Hubeny, S. Minwalla, and M. Rangamani, *Nonlinear Fluid Dynamics from Gravity*, *JHEP* **02** (2008) 045, [arXiv:0712.2456].

[90] V. E. Hubeny, S. Minwalla, and M. Rangamani, *The fluid/gravity correspondence*, in *Theoretical Advanced Study Institute in Elementary Particle Physics: String theory and its Applications: From meV to the Planck Scale*, pp. 348–383, 2012. arXiv:1107.5780.

[91] M. Rangamani, *Gravity and Hydrodynamics: Lectures on the fluid-gravity correspondence*, *Class. Quant. Grav.* **26** (2009) 224003, [arXiv:0905.4352].

[92] A. Almheiri, R. Mahajan, J. Maldacena, and Y. Zhao, *The Page curve of Hawking radiation from semiclassical geometry*, *JHEP* **03** (2020) 149, [arXiv:1908.1099].

[93] W. Donnelly, S. Timmerman, and N. Valdés-Meller, *Entanglement entropy and the large N expansion of two-dimensional Yang-Mills theory*, *JHEP* **04** (2020) 182, [arXiv:1911.0930].

[94] W. Donnelly and G. Wong, *Entanglement branes in a two-dimensional string theory*, *JHEP* **09** (2017) 097, [arXiv:1610.0171].

[95] W. Donnelly and V. Shyam, *Entanglement entropy and $T\overline{T}$ deformation*, *Phys. Rev. Lett.* **121** (2018), no. 13 131602, [arXiv:1806.0744].

[96] M. Taylor and W. Woodhead, *Renormalized entanglement entropy*, *JHEP* **08** (2016) 165, [arXiv:1604.0680].

[97] W. Donnelly, B. Michel, D. Marolf, and J. Wien, *Living on the Edge: A Toy Model for Holographic Reconstruction of Algebras with Centers*, *JHEP* **04** (2017) 093, [arXiv:1611.0584].

[98] F. Pastawski, B. Yoshida, D. Harlow, and J. Preskill, *Holographic quantum error-correcting codes: Toy models for the bulk/boundary correspondence*, *JHEP* **06** (2015) 149, [arXiv:1503.0623].

[99] P. Hayden, S. Nezami, X.-L. Qi, N. Thomas, M. Walter, and Z. Yang, *Holographic duality from random tensor networks*, *JHEP* **11** (2016) 009, [arXiv:1601.0169].

[100] D. Marolf, *CFT sewing as the dual of AdS cut-and-paste*, *JHEP* **02** (2020) 152, [arXiv:1909.0933].

[101] C. Akers and G. Penington, *Leading order corrections to the quantum extremal surface prescription*, *JHEP* **04** (8, 2021) 062, [arXiv:2008.0331].

[102] A. Goel, L. V. Iliesiu, J. Kruthoff, and Z. Yang, *Classifying boundary conditions in JT gravity: from energy-branes to α-branes*, *JHEP* **04** (2021) 069, [arXiv:2010.1259].

[103] D. Marolf, *Microcanonical Path Integrals and the Holography of small Black Hole Interiors*, *JHEP* **09** (2018) 114, [arXiv:1808.0039].

[104] R. Bousso, V. Chandrasekaran, P. Rath, and A. Shahbazi-Moghaddam, *Gravity dual of Connes cocycle flow*, *Phys. Rev. D* **102** (2020), no. 6 066008, [arXiv:2007.0023].

[105] M. Kaplan and D. Marolf, *The action of HRT-areas as operators in semiclassical gravity*, arXiv:2203.0427.

[106] X. Dong, D. Marolf, and P. Rath, *Geometric entropies and their geometric flow: the power of Lorentzian methods*, to appear.

[107] A. Almheiri and J. Polchinski, *Models of AdS_2 backreaction and holography*, *JHEP* **11** (2015) 014, [arXiv:1402.6334].

[108] S. Klainerman, I. Rodnianski, and J. Szeftel, *The Bounded L2 Curvature Conjecture*, arXiv:1204.1767.

[109] S. Klainerman, I. Rodnianski, and J. Szeftel, *Overview of the proof of the Bounded L^2 Curvature Conjecture*, arXiv:1204.1772.

[110] N. D. Birrell and P. C. W. Davies, *Quantum Fields in Curved Space*. Cambridge Monographs on Mathematical Physics. Cambridge Univ. Press, Cambridge, UK, 2, 1984.

[111] X. Dong, *Holographic Entanglement Entropy for General Higher Derivative Gravity*, *JHEP* **01** (2014) 044, [arXiv:1310.5713].

[112] J. Camps, *Generalized entropy and higher derivative Gravity*, *JHEP* **03** (2014) 070, [arXiv:1310.6659].

[113] A. Belin and S. Colin-Ellerin, *Bootstrapping quantum extremal surfaces. Part I. The area operator*, *JHEP* **11** (2021) 021, [arXiv:2107.0751].

[114] J. S. Schwinger, *Brownian motion of a quantum oscillator*, *J. Math. Phys.* **2** (1961) 407–432.

[115] L. Keldysh, *Diagram technique for nonequilibrium processes*, *Zh. Eksp. Teor. Fiz.* **47** (1964) 1515–1527.

[116] I. L. Aleiner, L. Faoro, and L. B. Ioffe, *Microscopic model of quantum butterfly effect: out-of-time-order correlators and traveling combustion waves*, *Annals Phys.* **375** (2016) 378–406, [arXiv:1609.0125].

[117] F. M. Haehl, R. Loganayagam, and M. Rangamani, *Schwinger-Keldysh formalism. Part I: BRST symmetries and superspace*, *JHEP* **06** (2017) 069, [arXiv:1610.0194].

[118] F. M. Haehl, R. Loganayagam, P. Narayan, and M. Rangamani, *Classification of out-of-time-order correlators*, *SciPost Phys.* **6** (2019), no. 1 001, [arXiv:1701.0282].

[119] M. Rangamani and T. Takayanagi, *Holographic Entanglement Entropy*, vol. 931. Springer, 2017.

[120] P. Calabrese and J. L. Cardy, *Evolution of entanglement entropy in one-dimensional systems*, *J. Stat. Mech.* **0504** (2005) P04010, [cond-mat/0503393].

[121] P. Calabrese and J. Cardy, *Quantum Quenches in Extended Systems*, *J. Stat. Mech.* **0706** (2007) P06008, [arXiv:0704.1880].

[122] D. V. Fursaev, *Proof of the holographic formula for entanglement entropy*, *JHEP* **09** (2006) 018, [hep-th/0606184].

[123] M. Headrick, *Entanglement Renyi entropies in holographic theories*, *Phys. Rev. D* **82** (2010) 126010, [arXiv:1006.0047].

[124] H. Casini, M. Huerta, and R. C. Myers, *Towards a derivation of holographic entanglement entropy*, *JHEP* **05** (2011) 036, [arXiv:1102.0440].

[125] T. Hartman, *Entanglement Entropy at Large Central Charge*, arXiv:1303.6955.

[126] T. Faulkner, *The Entanglement Renyi Entropies of Disjoint Intervals in AdS/CFT*, arXiv:1303.7221.

[127] M. Headrick, V. E. Hubeny, A. Lawrence, and M. Rangamani, *Causality & holographic entanglement entropy*, *JHEP* **12** (2014) 162, [arXiv:1408.6300].

[128] A. Almheiri, R. Mahajan, and J. Maldacena, *Islands outside the horizon*, arXiv:1910.1107.

[129] D. N. Page, *Average entropy of a subsystem*, *Phys. Rev. Lett.* **71** (1993) 1291–1294, [gr-qc/9305007].

[130] A. Almheiri, T. Hartman, J. Maldacena, E. Shaghoulian, and A. Tajdini, *The entropy of Hawking radiation*, arXiv:2006.0687.

[131] F. F. Gautason, L. Schneiderbauer, W. Sybesma, and L. Thorlacius, *Page Curve for an Evaporating Black Hole*, *JHEP* **05** (2020) 091, [arXiv:2004.0059].

[132] T. Anegawa and N. Iizuka, *Notes on islands in asymptotically flat 2d dilaton black holes*, arXiv:2004.0160.

[133] K. Hashimoto, N. Iizuka, and Y. Matsuo, *Islands in Schwarzschild black holes*, *JHEP* **06** (2020) 085, [arXiv:2004.0586].

[134] T. Hartman, E. Shaghoulian, and A. Strominger, *Islands in Asymptotically Flat 2D Gravity*, *JHEP* **07** (2020) 022, [arXiv:2004.1385].

[135] X. Dong, X.-L. Qi, Z. Shangnan, and Z. Yang, *Effective entropy of quantum fields coupled with gravity*, *JHEP* **10** (2020) 052, [arXiv:2007.0298].

[136] Y. Chen, V. Gorbenko, and J. Maldacena, *Bra-ket wormholes in gravitationally prepared states*, arXiv:2007.1609.

[137] C. Krishnan, *Critical Islands*, *JHEP* **01** (2021) 179, [arXiv:2007.0655].

[138] T. Hartman, Y. Jiang, and E. Shaghoulian, *Islands in cosmology*, arXiv:2008.0102.

[139] K. Skenderis and B. C. van Rees, *Real-time gauge/gravity duality*, *Phys. Rev. Lett.* **101** (2008) 081601, [arXiv:0805.0150].

[140] K. Skenderis and B. C. van Rees, *Real-time gauge/gravity duality: Prescription, Renormalization and Examples*, *JHEP* **05** (2009) 085, [arXiv:0812.2909].

[141] P. Glorioso, M. Crossley, and H. Liu, *A prescription for holographic Schwinger-Keldysh contour in non-equilibrium systems*, arXiv:1812.0878.

[142] B. Chakrabarty, J. Chakravarty, S. Chaudhuri, C. Jana, R. Loganayagam, and A. Sivakumar, *Nonlinear Langevin dynamics via holography*, *JHEP* **01** (2020) 165, [arXiv:1906.0776].

[143] C. Jana, R. Loganayagam, and M. Rangamani, *Open quantum systems and Schwinger-Keldysh holograms*, *JHEP* **07** (2020) 242, [arXiv:2004.0288].

[144] D. Marolf, *States and boundary terms: Subtleties of Lorentzian AdS / CFT*, *JHEP* **05** (2005) 042, [hep-th/0412032].

[145] J. Louko and R. D. Sorkin, *Complex actions in two-dimensional topology change*, *Class. Quant. Grav.* **14** (1997) 179–204, [gr-qc/9511023].

[146] S. R. Coleman, *Black Holes as Red Herrings: Topological Fluctuations and the Loss of Quantum Coherence*, *Nucl. Phys. B* **307** (1988) 867–882.

[147] S. B. Giddings and A. Strominger, *Loss of Incoherence and Determination of Coupling Constants in Quantum Gravity*, *Nucl. Phys. B* **307** (1988) 854–866.

[148] S. B. Giddings and A. Strominger, *Baby Universes, Third Quantization and the Cosmological Constant*, *Nucl. Phys. B* **321** (1989) 481–508.

[149] F. M. Haehl, T. Hartman, D. Marolf, H. Maxfield, and M. Rangamani, *Topological aspects of generalized gravitational entropy*, *JHEP* **05** (2015) 023, [arXiv:1412.7561].

[150] I. Jubb, J. Samuel, R. Sorkin, and S. Surya, *Boundary and Corner Terms in the Action for General Relativity*, *Class. Quant. Grav.* **34** (2017), no. 6 065006, [arXiv:1612.0014].

[151] E. Farhi, A. H. Guth, and J. Guven, *Is It Possible to Create a Universe in the Laboratory by Quantum Tunneling?*, *Nucl. Phys. B* **339** (1990) 417–490.

[152] Y. Neiman, *The imaginary part of the gravity action and black hole entropy*, *JHEP* **04** (2013) 071, [arXiv:1301.7041].

[153] W. G. Unruh, G. Hayward, W. Israel, and D. Mcmanus, *Cosmic String Loops are Straight*, *Phys. Rev. Lett.* **62** (1989) 2897–2900.

[154] R. P. Geroch and J. H. Traschen, *Strings and Other Distributional Sources in General Relativity*, *Phys. Rev. D* **36** (1987) 1017.

[155] T. Faulkner, F. M. Haehl, E. Hijano, O. Parrikar, C. Rabideau, and M. Van Raamsdonk, *Nonlinear Gravity from Entanglement in Conformal Field Theories*, *JHEP* **08** (2017) 057, [arXiv:1705.0302].

[156] M. Botta-Cantcheff, P. Martínez, and G. A. Silva, *On excited states in real-time AdS/CFT*, *JHEP* **02** (2016) 171, [arXiv:1512.0785].

[157] D. Marolf, O. Parrikar, C. Rabideau, A. Izadi Rad, and M. Van Raamsdonk, *From Euclidean Sources to Lorentzian Spacetimes in Holographic Conformal Field Theories*, *JHEP* **06** (2018) 077, [arXiv:1709.1010].

[158] F. M. Haehl, E. Mintun, J. Pollack, A. J. Speranza, and M. Van Raamsdonk, *Nonlocal multi-trace sources and bulk entanglement in holographic conformal field theories*, *JHEP* **06** (2019) 005, [arXiv:1904.0158].

[159] B. C. van Rees, *Real-time gauge/gravity duality and ingoing boundary conditions*, *Nucl. Phys. Proc. Suppl.* **192-193** (2009) 193–196, [arXiv:0902.4010].

[160] K. Goto, T. Hartman, and A. Tajdini, *Replica wormholes for an evaporating 2D black hole*, arXiv:2011.0904.

[161] A. Anderson and B. S. DeWitt, *Does the Topology of Space Fluctuate?*, *Found. Phys.* **16** (1986) 91–105.

[162] C. Manogue, E. Copeland, and T. Dray, *The trousers problem revisited*, *Pramana* **30** (1988) 279–292.

[163] R. Jackiw, *Lower Dimensional Gravity*, *Nucl. Phys. B* **252** (1985) 343–356.

[164] C. Teitelboim, *Gravitation and Hamiltonian Structure in Two Space-Time Dimensions*, *Phys. Lett. B* **126** (1983) 41–45.

[165] T. Azeyanagi, T. Nishioka, and T. Takayanagi, *Near Extremal Black Hole Entropy as Entanglement Entropy via AdS(2)/CFT(1)*, *Phys. Rev. D* **77** (2008) 064005, [arXiv:0710.2956].

[166] A. Sen, *Entropy Function and AdS(2) / CFT(1) Correspondence*, *JHEP* **11** (2008) 075, [arXiv:0805.0095].

[167] J. Maldacena and D. Stanford, *Remarks on the Sachdev-Ye-Kitaev model*, *Phys. Rev. D* **94** (2016), no. 10 106002, [arXiv:1604.0781].

[168] J. Lin, *Entanglement entropy in Jackiw-Teitelboim Gravity*, arXiv:1807.0657.

[169] T. G. Mertens and G. J. Turiaci, *Defects in Jackiw-Teitelboim Quantum Gravity*, *JHEP* **08** (2019) 127, [arXiv:1904.0522].

[170] D. L. Jafferis and D. K. Kolchmeyer, *Entanglement Entropy in Jackiw-Teitelboim Gravity*, arXiv:1911.1066.

[171] C. Holzhey, F. Larsen, and F. Wilczek, *Geometric and renormalized entropy in conformal field theory*, *Nucl. Phys. B* **424** (1994) 443–467, [hep-th/9403108].

[172] K. Skenderis and S. N. Solodukhin, *Quantum effective action from the AdS / CFT correspondence*, *Phys. Lett. B* **472** (2000) 316–322, [hep-th/9910023].

[173] L.-Y. Hung, R. C. Myers, M. Smolkin, and A. Yale, *Holographic Calculations of Renyi Entropy*, *JHEP* **12** (2011) 047, [arXiv:1110.1084].

[174] K. Krasnov, *On holomorphic factorization in asymptotically AdS 3-D gravity*, *Class. Quant. Grav.* **20** (2003) 4015–4042, [hep-th/0109198].

[175] P. Calabrese, J. Cardy, and E. Tonni, *Entanglement entropy of two disjoint intervals in conformal field theory*, *J. Stat. Mech.* **0911** (2009) P11001, [arXiv:0905.2069].

[176] P. G. Zograf and L. A. Takhtadzhyan, *On uniformization of riemann surfaces and the weil-petersson metric on teichmüller and schottky spaces*, *Mathematics of the USSR-Sbornik* **60** (1988), no. 2 297.

[177] Y. Kusuki, T. Takayanagi, and K. Umemoto, *Holographic Entanglement Entropy on Generic Time Slices*, *JHEP* **06** (2017) 021, [arXiv:1703.0091].

[178] T. Anous, T. Hartman, A. Rovai, and J. Sonner, *Black Hole Collapse in the 1/c Expansion*, *JHEP* **07** (2016) 123, [arXiv:1603.0485].

[179] M. Kontsevich and G. Segal, *Wick Rotation and the Positivity of Energy in Quantum Field Theory*, *Quart. J. Math. Oxford Ser.* **72** (2021), no. 1-2 673–699, [arXiv:2105.1016].

[180] E. Witten, *A Note On Complex Spacetime Metrics*, arXiv:2111.0651.

[181] E. Witten, *Analytic Continuation Of Chern-Simons Theory*, *AMS/IP Stud. Adv. Math.* **50** (2011) 347–446, [arXiv:1001.2933].

[182] D. Harlow and D. Jafferis, *The Factorization Problem in Jackiw-Teitelboim Gravity*, *JHEP* **02** (2020) 177, [arXiv:1804.0108].

[183] G. Hayward, *Gravitational action for space-times with nonsmooth boundaries*, *Phys. Rev. D* **47** (1993) 3275–3280.

[184] S. D. Mathur, *The Information paradox: A Pedagogical introduction*, *Class. Quant. Grav.* **26** (2009) 224001, [arXiv:0909.1038].

[185] D. Harlow, *Jerusalem Lectures on Black Holes and Quantum Information*, *Rev. Mod. Phys.* **88** (2016) 015002, [arXiv:1409.1231].

[186] D. Marolf, *The Black Hole information problem: past, present, and future*, *Rept. Prog. Phys.* **80** (2017), no. 9 092001, [arXiv:1703.0214].

[187] W. F. Stinespring, *Functions on C *-Algebras*, *Proc. Amer. Math. Soc.* **6** (1955) 211.

[188] S. B. Giddings and G. J. Turiaci, *Wormhole calculus, replicas, and entropies*, *JHEP* **09** (2020) 194, [arXiv:2004.0290].

[189] R. Bousso, Z. Fisher, S. Leichenauer, and A. C. Wall, *Quantum focusing conjecture*, *Phys. Rev. D* **93** (2016), no. 6 064044, [arXiv:1506.0266].

[190] Z. Fu, J. Koeller, and D. Marolf, *The Quantum Null Energy Condition in Curved Space*, *Class. Quant. Grav.* **34** (2017), no. 22 225012, [arXiv:1706.0157]. [Erratum: Class.Quant.Grav. 35, 049501 (2018)].

[191] C. Akers, V. Chandrasekaran, S. Leichenauer, A. Levine, and A. Shahbazi Moghaddam, *Quantum null energy condition, entanglement wedge nesting, and quantum focusing*, *Phys. Rev. D* **101** (2020), no. 2 025011, [arXiv:1706.0418].

[192] N. Engelhardt and A. C. Wall, *Coarse Graining Holographic Black Holes*, *JHEP* **05** (2019) 160, [arXiv:1806.0128].

[193] O. Aharony, D. Marolf, and M. Rangamani, *Conformal field theories in anti-de Sitter space*, *JHEP* **02** (2011) 041, [arXiv:1011.6144].

[194] T. Takayanagi, *Holographic Dual of BCFT*, *Phys. Rev. Lett.* **107** (2011) 101602, [arXiv:1105.5165].

[195] V. Rosenhaus and M. Smolkin, *Entanglement Entropy for Relevant and Geometric Perturbations*, *JHEP* **02** (2015) 015, [arXiv:1410.6530].

[196] D. Marolf, *Unitarity and Holography in Gravitational Physics*, *Phys. Rev.* **D79** (2009) 044010, [arXiv:0808.2842].

[197] D. Marolf, *Black Holes, AdS, and CFTs*, *Gen. Rel. Grav.* **41** (2009) 903–917, [arXiv:0810.4886].

[198] G. W. Gibbons and M. J. Perry, *Quantizing Gravitational Instantons*, *Nucl. Phys. B* **146** (1978) 90–108.

[199] J. B. Hartle and K. Schleich, *THE CONFORMAL ROTATION IN LINEARIZED GRAVITY*, .

[200] A. Dasgupta and R. Loll, *A Proper time cure for the conformal sickness in quantum gravity*, *Nucl. Phys. B* **606** (2001) 357–379, [hep-th/0103186].

[201] D. Anninos, F. Denef, and D. Harlow, *Wave function of Vasiliev's universe: A few slices thereof*, *Phys. Rev. D* **88** (2013), no. 8 084049, [arXiv:1207.5517].

[202] J. Cotler, K. Jensen, and A. Maloney, *Low-dimensional de Sitter quantum gravity*, *JHEP* **06** (2020) 048, [arXiv:1905.0378].

[203] N. Benjamin, S. Collier, and A. Maloney, *Pure Gravity and Conical Defects*, *JHEP* **09** (2020) 034, [arXiv:2004.1442].

[204] S. Gao and R. M. Wald, *Theorems on gravitational time delay and related issues*, *Class. Quant. Grav.* **17** (2000) 4999–5008, [gr-qc/0007021].

[205] B. Czech, J. L. Karczmarek, F. Nogueira, and M. Van Raamsdonk, *The Gravity Dual of a Density Matrix*, *Class. Quant. Grav.* **29** (2012) 155009, [arXiv:1204.1330].

[206] C. Akers, J. Koeller, S. Leichenauer, and A. Levine, *Geometric Constraints from Subregion Duality Beyond the Classical Regime*, arXiv:1610.0896.

[207] B. Blackadar, *Operator algebras: Theory of C*-algebras and von Neumann algebras*. Springer, 2006.

[208] T. Banks, W. Fischler, S. H. Shenker, and L. Susskind, *M theory as a matrix model: A Conjecture*, *Phys. Rev. D* **55** (1997) 5112–5128, [hep-th/9610043].

[209] N. Itzhaki, J. M. Maldacena, J. Sonnenschein, and S. Yankielowicz, *Supergravity and the large N limit of theories with sixteen supercharges*, *Phys. Rev. D* **58** (1998) 046004, [hep-th/9802042].

[210] R. V. Kadison and J. R. Ringrose, *Fundamentals of the Theory of Operator Algebras. Volume II: Advanced Theory.* American Mathematical Society, 1997.

[211] A. Blommaert, L. V. Iliesiu, and J. Kruthoff, *Alpha states demystified — towards microscopic models of AdS_2 holography*, *JHEP* **08** (2022) 071, [arXiv:2203.0738].

[212] J. B. Hartle and S. W. Hawking, *Wave Function of the Universe*, *Phys. Rev. D* **28** (1983) 2960–2975.

[213] J. Maldacena, D. Stanford, and Z. Yang, *Conformal symmetry and its breaking in two dimensional Nearly Anti-de-Sitter space*, *PTEP* **2016** (2016), no. 12 12C104, [arXiv:1606.0185].

[214] N. Engelhardt, S. Fischetti, and A. Maloney, *Free energy from replica wormholes*, *Phys. Rev. D* **103** (2021), no. 4 046021, [arXiv:2007.0744].

[215] S. W. Hawking and D. N. Page, *Thermodynamics of black holes in anti-de Sitter space*, *Communications in Mathematical Physics* **87** (1982), no. 4 577 – 588.

[216] C. Murthy and M. Srednicki, *Structure of chaotic eigenstates and their entanglement entropy*, *Phys. Rev. E* **100** (Aug, 2019) 022131.

[217] S. W. Hawking and C. J. Hunter, *The Gravitational Hamiltonian in the presence of nonorthogonal boundaries*, *Class. Quant. Grav.* **13** (1996) 2735–2752, [gr-qc/9603050].

[218] J. D. Brown, S. R. Lau, and J. W. York, Jr., *Action and energy of the gravitational field*, gr-qc/0010024.

[219] B. Allen, *Euclidean Schwarzschild negative mode*, *Phys. Rev. D* **30** (1984) 1153–1157.

[220] R. Monteiro and J. E. Santos, *Negative modes and the thermodynamics of Reissner-Nordstrom black holes*, *Phys. Rev. D* **79** (2009) 064006, [arXiv:0812.1767].

[221] R. Monteiro, M. J. Perry, and J. E. Santos, *Thermodynamic instability of rotating black holes*, *Phys. Rev. D* **80** (2009) 024041, [arXiv:0903.3256].

[222] R. Monteiro, M. J. Perry, and J. E. Santos, *Semiclassical instabilities of Kerr-AdS black holes*, *Phys. Rev. D* **81** (2010) 024001, [arXiv:0905.2334].

[223] D. Marolf and J. E. Santos, *AdS Euclidean wormholes*, *Class. Quant. Grav.* **38** (1, 2021) 224002, [arXiv:2101.0887].

[224] J. Cotler and K. Jensen, *Wormholes and black hole microstates in AdS/CFT*, arXiv:2104.0060.

[225] G. W. Gibbons and M. J. Perry, *Black Holes and Thermal Green's Functions*, *Proc. Roy. Soc. Lond. A* **358** (1978) 467–494.

[226] J. Ambjorn, A. Dasgupta, J. Jurkiewicz, and R. Loll, *A Lorentzian cure for Euclidean troubles*, *Nucl. Phys. B Proc. Suppl.* **106** (2002) 977–979, [hep-th/0201104].

[227] J. B. Hartle and K. Schleich, *The Conformal Rotation in Linearised Gravity*, in *Quantum Field Theory and Quantum Statistics* (C. J. I. I. A. Batalin and G. A. Vilkovisky, eds.), pp. 67–87, 4, 1987. arXiv:2004.0663.

[228] K. Schleich, *Conformal Rotation in Perturbative Gravity*, *Phys. Rev. D* **36** (1987) 2342–2363.

[229] P. O. Mazur and E. Mottola, *The Gravitational Measure, Solution of the Conformal Factor Problem and Stability of the Ground State of Quantum Gravity*, *Nucl. Phys. B* **341** (1990) 187–212.

[230] S. B. Giddings, *The Conformal Factor and the Cosmological Constant*, *Int. J. Mod. Phys. A* **5** (1990) 3811–3830.

[231] S. B. Giddings, *Wormholes, the conformal factor, and the cosmological constant*, in *International Colloquium on Modern Quantum Field Theory*, 5, 1990.

[232] D. Marolf, *Path integrals and instantons in quantum gravity: Minisuperspace models*, *Phys. Rev. D* **53** (1996) 6979–6990, [gr-qc/9602019].

[233] J. Feldbrugge, J.-L. Lehners, and N. Turok, *Lorentzian Quantum Cosmology*, *Phys. Rev. D* **95** (2017), no. 10 103508, [arXiv:1703.0207].

[234] J. Feldbrugge, J.-L. Lehners, and N. Turok, *No smooth beginning for spacetime*, *Phys. Rev. Lett.* **119** (2017), no. 17 171301, [arXiv:1705.0019].

[235] J. Feldbrugge, J.-L. Lehners, and N. Turok, *No rescue for the no boundary proposal: Pointers to the future of quantum cosmology*, *Phys. Rev. D* **97** (2018), no. 2 023509, [arXiv:1708.0510].

[236] X. Dong, X.-L. Qi, and M. Walter, *Holographic entanglement negativity and replica symmetry breaking*, *JHEP* **06** (2021) 024, [arXiv:2101.1102].

[237] J. Kudler-Flam and P. Rath, *Large and small corrections to the JLMS Formula from replica wormholes*, *JHEP* **08** (2022) 189, [arXiv:2203.1195].

[238] A. Blommaert, J. Kruthoff, and S. Yao, *The power of Lorentzian wormholes*, arXiv:2302.0136.

[239] D. Stanford and Z. Yang, *Firewalls from wormholes*, arXiv:2208.0162.

[240] H. Fédérer, *The singular sets of area minimizing rectifiable currents with codimension one and of area minimizing flat chains modulo two with arbitrary codimension*, *Bulletin of the American Mathematical Society* **76** (1970) 767–771.

[241] J. Simons, *Minimal varieties in riemannian manifolds*, *Annals of Mathematics* **88** (1968) 62.

[242] Y. Li and Z. Wang, *Generic regularity of minimal hypersurfaces in dimension 8.*, *arXiv: Differential Geometry* (2020).

[243] O. Chodosh, C. Mantoulidis, and F. Schulze, *Generic regularity for minimizing hypersurfaces in dimensions 9 and 10*, 2023.

[244] L. F. Abbott and S. Deser, *Stability of Gravity with a Cosmological Constant*, *Nucl. Phys. B* **195** (1982) 76–96.

[245] G. W. Gibbons, C. M. Hull, and N. P. Warner, *The Stability of Gauged Supergravity*, *Nucl. Phys. B* **218** (1983) 173.

[246] G. T. Horowitz and R. C. Myers, *The AdS / CFT correspondence and a new positive energy conjecture for general relativity*, *Phys. Rev. D* **59** (1998) 026005, [hep-th/9808079].

[247] G. W. Gibbons and C. N. Pope, *The positive action conjecture and asymptotically Euclidean metrics in quantum gravity*, *Communications in Mathematical Physics* **66** (1979), no. 3 267 – 290.

[248] E. Witten, *A Simple Proof of the Positive Energy Theorem*, *Commun. Math. Phys.* **80** (1981) 381.

[249] V. Balasubramanian and P. Kraus, *A Stress tensor for Anti-de Sitter gravity*, *Commun. Math. Phys.* **208** (1999) 413–428, [hep-th/9902121].

[250] S. de Haro, S. N. Solodukhin, and K. Skenderis, *Holographic reconstruction of space-time and renormalization in the AdS / CFT correspondence*, *Commun. Math. Phys.* **217** (2001) 595–622, [hep-th/0002230].

[251] E. Colafranceschi, D. Marolf, and Z. Wang, *???, To Appear*, . To Appear.

[252] D. N. Page, *Information in black hole radiation*, *Phys. Rev. Lett.* **71** (1993) 3743–3746, [hep-th/9306083].

[253] D. N. Page, *Time Dependence of Hawking Radiation Entropy*, *JCAP* **09** (2013) 028, [arXiv:1301.4995].

[254] A. Blommaert, J. Kruthoff, and S. Yao, *An integrable road to a perturbative plateau*, arXiv:2208.1379.

[255] M. Usatyuk, *Comments on Lorentzian topology change in JT gravity*, arXiv:2210.0490.

[256] E. Colafraceschi, D. Marolf, and Z. Wang, *A trace inequality for the semiclassical Euclidean gravitational path integral*, .

[257] R.-X. Miao and W.-z. Guo, *Holographic Entanglement Entropy for the Most General Higher Derivative Gravity*, *JHEP* **08** (2015) 031, [arXiv:1411.5579].

[258] X. Dong and D. Marolf, *Reflection-positivity quantizes the Gibbons-Hawking density of states, To Appear*, . To Appear.

[259] M. Reed and B. Simon, *Methods of Modern Mathematical Physics. Vol. I Functional Analysis*. Academic Press, 1972.

[260] J. McNamara and C. Vafa, *Baby Universes, Holography, and the Swampland*, arXiv:2004.0673.

[261] R. V. Kadison and J. R. Ringrose, *Fundamentals of the Theory of Operator Algebras. Volume II: Elementary Theory*. American Mathematical Society, 1983.

[262] V. Sunder, *An Invitation to von Neumann Algebras*. Springer-Verlag, 1986.

[263] M. A. Rieffel, *Commutation theorems and generalized commutation relations*, *Bulletin de la Société Mathématique de France* **104** (1976) 205–224.

[264] "NIST Digital Library of Mathematical Functions." http://dlmf.nist.gov/, Release 1.0.28 of 2020-09-15. F. W. J. Olver, A. B. Olde Daalhuis, D. W. Lozier, B. I. Schneider, R. F. Boisvert, C. W. Clark, B. R. Miller, B. V. Saunders, H. S. Cohl, and M. A. McClain, eds.

[265] O. Lunin and S. D. Mathur, *Correlation functions for M**N / S(N) orbifolds*, *Commun. Math. Phys.* **219** (2001) 399–442, [hep-th/0006196].

[266] P. F. Byrd and M. D. Friedman, *Handbook of elliptic integrals for engineers and physicists*, vol. 67. Springer, 2013.

[267] E. Poisson, *A Relativist's Toolkit: The Mathematics of Black-Hole Mechanics*. Cambridge University Press, 12, 2009.

[268] D. Marolf, W. Kelly, and S. Fischetti, *Conserved Charges in Asymptotically (Locally) AdS Spacetimes*, pp. 381–407. 2014. arXiv:1211.6347.

[269] S. Carlip and C. Teitelboim, *The Off-shell black hole*, *Class. Quant. Grav.* **12** (1995) 1699–1704, [gr-qc/9312002].

[270] A. Kitaev, "A simple model of quantum holography." `http://online.kitp.ucsb.edu/online/entangled15/kitaev/`,`http://online.kitp.ucsb.edu/online/entangled15/kitaev2/`. Talks at KITP, April 7, 2015 and May 27, 2015.

[271] S. Sachdev and J. Ye, *Gapless spin-fluid ground state in a random quantum heisenberg magnet*, *Phys. Rev. Lett.* **70** (May, 1993) 3339–3342.